ECOLOGICAL IMPACTS OF PHOTOAUTOTROPHIC EUENDOLITHS ON SOUTH AFRICAN MUSSEL BEDS

A THESIS SUBMITTED IN FULFILMENT OF THE REQUIREMENTS FOR THE

DEGREE OF

DOCTOR OF PHILOSOPHY

OF

RHODES UNIVERSITY

(MARINE BIOLOGY)

BY

ALEXIA M. DIEVART

ORCID: 0000-0003-3989-4120

FINAL SUBMISSION: JANUARY 2024

DECLARATION

I declare that this thesis, done after registration for the degree of PhD at Rhodes University, was composed by myself and that the work has not been submitted for any other degree or professional qualification except as specified. I confirm that the work submitted is my own, except where work has formed part of jointly-authored publications has been included. My contribution and those of the other authors to this work have been explicitly indicated below. The experimental work is almost entirely my own work, the collaborative contributions being indicated clearly and acknowledged below. I confirm that appropriate credit has been given within this thesis where reference has been made to the work of others.

The work presented in Chapter 2 was previously published in *Diversity* as Photoautotrophic Euendoliths and Their Complex Ecological Effects in Marine Bioengineered Ecosystems by Alexia M. Dievart (PhD student and author of this declaration), Christopher D. McQuaid, Gerardo I. Zardi, Katy R. Nicastro and Pierre W. Froneman (supervisor). Author contributions for this publication were as follow: conceptualization, A.M.D., C.D.M., G.I.Z., K.R.N.; funding acquisition, C.D.M.; project administration, A.M.D.; supervision, C.D.M., G.I.Z., K.R.N., P.W.F.; visualization, A.M.D.; writing—original draft, A.M.D.; writing—review and editing, A.M.D., C.D.M., G.I.Z., K.R.N., P.W.F. I specifically carried out the conceptualization, project administration, visualization, writing of the original draft, and the review and editing of the final draft.

The work presented in Chapter 3 was previously published in *Diversity* as Euendolithic Infestation of Mussel Shells Indirectly Improves the Thermal Buffering Offered by

Mussel Beds to Associated Molluscs, but One Size Does Not Fit All by Alexia M. Dievart (PhD student and author of this declaration), Christopher D. McQuaid, Gerardo I. Zardi, Katy R. Nicastro and Pierre W. Froneman (supervisor). Author contributions for this publication were as follow: conceptualization, G.I.Z., K.R.N. and A.M.D.; methodology, C.D.M., G.I.Z., K.R.N. and A.M.D.; fieldwork, A.M.D.; formal analysis, A.M.D.; data collection, A.M.D.; data curation, A.M.D.; writing—original draft preparation, A.M.D.; writing—review and editing, A.M.D., C.D.M., G.I.Z., K.R.N. and P.W.F.; visualization, A.M.D.; supervision, P.W.F., C.D.M. and G.I.Z.; project administration, A.M.D.; funding acquisition, P.W.F. and C.D.M. I specifically carried out the conceptualization, project administration, methodology, fieldwork, formal analysis, data collection and curation, visualization, writing of the original draft and the review and edition of the final draft.

The experimental work conducted for this thesis was almost entirely my own work. Collaborative contributions were made as follow: conceptualization, C.D.M., G.I.Z., and K.R.N. for Chapter 4 and 5; fieldwork, Tristan A. Van Rooyen (external) for Chapter 3, 4 and 5; formal analysis and writing—review and editing, Guy F. Sutton (Research entomologist, CBC, Rhodes University) for Chapter 3; laboratory work, Masibonge F. Nsibande (Honours student) and Lutendo F. Thomo (3rd year Bachelor student) for Chapters 4 and 5. I specifically played a major role in the preparation and execution of the experiment, and the data analysis and interpretation are entirely my own work.

Date: 01/06/2023

ABSTRACT

Ecosystem engineers are organisms that create, modify, maintain and/or destroy habitats *via* their own physical structures or by transforming resources from one state to another. Ecosystem engineer's often sustain and facilitate the survival of organisms in physically stressful environments, including rocky shores. Parasites can modify a wide range of physiological, behavioural, and morphological traits in their hosts, thus potentially altering the hosts' ecosystem engineering capabilities. On intertidal rocky shores, mussel beds provide an important habitat for a large number of associated intertidal species and alleviate environmental stresses, mainly temperature and desiccation. Photoautotrophic euendoliths are shell-boring microscopic parasites that colonize mussel shells worldwide. Euendoliths have both negative lethal and sub-lethal effects, as well as conditional positive effects, on individual mussels or mussel beds. Here, I explore the influence of euendolithic infestation of the mussel shell on the associated infaunal and epibiotic communities of the native brown mussel, *Perna perna*, at selected sites along the South African coastline using a combination of laboratory and field-based experiments. Photoautotrophic euendoliths can be considered as conditionally helpful parasites of mussels, as their corroding activity increases the albedo of the mussel shell through the whitening of its surface, thus reducing mussels' body temperatures and increasing their survival rates under extremely stressful environmental conditions. The beneficial effects of euendolithic infestation on mussels' body temperatures and selected associated molluscs were investigated using infrared thermography. Euendolith-infested mussel beds and their associated infauna displayed significantly lower body temperatures than non-infested mussel beds. The thermal

benefits offered to the associated infauna were, however, dependent on their body colour with dark-coloured individuals deriving no thermal benefits.

Infaunal communities associated with either euendolith-infested and non-infested manipulated mussel beds were described in terms of abundances and biomass (expressed as dry weight), after a 6-month exposure *in situ* at several sites along the south and east coasts of South Africa. It was anticipated that the infaunal communities associated with infested mussel beds would be less diverse, and have lower biomass, but include unique species vulnerable to thermal and desiccation stress as euendolithic infestation, while altering byssal thread production, may provide an improved microclimate. Not only was the structural complexity of the mussel bed unaltered by euendolithic infestation but also the anticipated euendolith-induced improvements in temperatures and humidities within mussel beds did not influence infaunal communities at the end of the experiment. However, there was site-specific differences in both the number of byssal threads per mussel and infaunal community structure. As the thermal mitigation provided by euendolithic infestation in mussel beds is conditional, and mobile species are the most likely to migrate from a stressful to a more benign habitat under stressful environment conditions, the length of the exposure period and the time of sampling at the end of the experiment could explain these results. Finally, the corrosive activity of euendolithic infestation destroys the antifouling properties of the mussel shell, increasing its roughness and thus promoting epibiosis. Using natural mussel beds, epibiotic communities found on individual mussel shells were described in terms of abundance, cover, and biomass (expressed as dry weight). The degree of mussel shell degradation covaried with mussel shell length. Prevalence and abundances in epibionts increased with increasing levels of euendolith-induced shell degradation and were significantly higher on the infested (i.e., degraded) portion of the mussel shell. The percentage cover

and biomass of the epibionts, although variable, tended to decrease with shell degradation. Sessile epibionts, including barnacles and encrusting algae (i.e., ochrophytes and rhodophytes) were the main drivers of differences between epibiotic communities found on infested and non-infested mussel shells. Euendolithic infestation of the mussel shell tended to favour the settlement of epibionts, but the continuous degradation of the mussel ultimately impeded epibiotic survival and growth. This complex trade-off was further influenced by species interactions within the epibiotic community found on mussel shells.

In summary, euendolithic infestation has the potential to influence the ecosystem engineering capabilities of mussel beds in intertidal ecosystems, by extending mussels' phenotype beyond the range of natural plasticity. Euendolith-infested mussel beds provide a better thermal refuge to associated infaunal communities than non-infested mussel beds, although this advantage is limited to stressful environmental conditions. However, euendolithic infestation did not influence the mussel bed structural complexity. While euendolithic infestation appeared to promote the settlement of epibionts on the mussel shell, the continuous degradation of the mussel shell likely impedes the development of epibiotic communities in the longer term. As euendolithic infestation is anticipated to increase in prevalence and intensity with global climate change and ocean acidification, disentangling the influence of these shell-boring parasites on mussel beds is critical for the conservation of critical intertidal ecosystems.

TABLE OF CONTENTS

DECLARATION iii

ABSTRACT v

TABLE OF CONTENTS viii

ACKNOWLEDGEMENTS xiii

CHAPTER 1 1

General introduction and thesis overview 1

1.1. Ecosystem engineering in a changing natural world 1

1.2. Parasitism and ecosystem engineering 4

1.3. South African intertidal rocky shores as an open laboratory 6

1.4. Shell-boring microscopic parasites in mussel beds 11

1.5. Thesis objectives and overview 13

CHAPTER 2 15

Photoautotrophic euendoliths and their complex ecological effects in marine bioengineered ecosystems 15

2.1. Introduction 16

2.2. What are euendoliths and how are they observed? 18

2.3. How do euendoliths erode calcium carbonate? 24

2.4. Incidence of photoautotrophic euendoliths in marine ecosystems 30

2.4.1. Light availability 30

2.4.2. Nature of the substrate 33

2.4.3. Biotic and abiotic environmental factors 35

2.4.4. Photoautotrophic euendoliths as bioindicators 39

2.5. Photoautotrophic euendoliths in marine bioengineered ecosystems 41

2.5.1. Corals and crustose coralline algae 44

2.5.2. Bivalves 51

2.5.3. Other groups 57

2.6. Photoautotrophic euendoliths in the Anthropocene 58

2.7. Conclusions 62

CHAPTER 3 64

Euendolithic infestation of mussel shells indirectly improves the thermal buffering offered by mussel beds to associated molluscs, but one size does not fit all 64

3.1. Introduction 65

3.2. Materials and Methods 68

3.2.1. Focal species and experimental setting 68

3.2.2. Body temperature assessment 71

3.2.3. Desiccation assessment 72

3.2.4. Data analyses 73

3.3. Results 74

3.3.1. Body temperature assessment 74

3.3.2. Desiccation assessment 78

3.4. Discussion 78

3.5. Conclusions 82

CHAPTER 4 84

Shell-boring microscopic parasites in an ecosystem engineer do not influence infaunal community structure 84

4.1. Introduction 85

4.2. Materials and Methods 90

4.2.1. Focal species 90

4.2.2. Transplant experiments 91

4.2.3. Data analyses 96

4.3. Results 99

4.3.1. Within-bed structural complexity 99

4.3.2. Infaunal communities 103

4.4. Discussion 116

4.4.1. Within-bed structural complexity 117

4.4.2. Infaunal communities 119

4.5. Conclusions 124

CHAPTER 5 126

Life on collapsing shells: the relationship between euendolithic infestation and epibiosis 126

5.1. Introduction 127

5.2. Materials and Methods 132

5.2.1. Collection procedure 132

5.2.2. Laboratory analyses 133

5.2.3. Data analyses 135
5.3. Results 139
5.3.1. Relationship between mussel shell condition and epibiosis 139
5.3.2. Epibiotic communities 143
5.4. Discussion 185
5.4.1. General relationship between mussel shell condition and epibiosis 185
5.4.2. Epibiotic communities associated with the mussel shell.....189
5.4.3. Interactions between euendolithic infestation and epibiosis 198
5.5. Conclusions 201
CHAPTER 6.....202
Synthesis and conclusion 202
6.1. Ecosystem engineering mediated by euendolithic infestation in mussels.....203
6.1.1. Shell colour polymorphism and indirect thermal benefits 204
6.1.2. Architectural complexity of the mussel bed habitat to associated communities 210
6.1.3. An evaluation of the methodologies 216
6.2. How can parasites become your ally? 219
6.2.1. Photoautotrophic euendoliths as conditionally helpful parasites 219
6.2.2. From parasitism to mutualism: a continuum.....220
6.3. Parasite-mediated ecosystem engineering, present and future 221
6.3.1. Photoautotrophic euendoliths and mussels: a contribution to the field 221

6.3.2. Predicting the influence of euendolithic infestation on mussel beds in the future 224

Supplementary Materials 227

Chapter 3.....227

Chapter 4.....235

Chapter 5.....245

5.3.1. Relationship between mussel shell condition and epibiosis 245

5.3.2. Epibiotic communities 248

References.....345

ACKNOWLEDGEMENTS

I would like to thank my first supervisor, Distinguished Professor Christopher D. McQuaid, and my co-supervisor Dr Gerardo I. Zardi, for giving me the opportunity to realize a PhD project in South Africa after a successful collaboration during my MSc. Thank you to Dr Katy R. Nicastro for your contribution throughout this project and your invaluable insight. While several obstacles have been encountered along the way, particularly due to COVID and the difficulty to provide financial and logistical support during the first year of the PhD, the relationship we established nonetheless allowed us to continue working together in a fruitful manner. I have learnt more from you that I could have asked for, as a scientist and as a person. This was, and still is, a true privilege.

I should express my particular thanks to my current supervisor, Professor William Froneman, for allowing me to complete my PhD project to its end. Your support has been invaluable. I don't have enough words to express my gratitude. I hope I have proved myself worthy of this opportunity, and that you are proud of my hard work. Working with you and your team again in the future would be amazing!

This thesis would have not been successful without the help from Ms Ticia Swanepoel and her incredible administrative and technical skills. Your love and kindness made me feel at home, though I have been far away from home for so many years.

If I had to thank but only a single person, this would be my partner, Tristan Van Rooyen. After only a few months, and a difficult resignation, you did not hesitate a second and gave your best for the success of my fieldwork and laboratory work. In less than six months, we added more than 30 000 km to your bakkie's odometer and offered it a technical visit nearly every month. You went head on in this adventure, during

which I dragged you to the most beautiful, and some truly ghastly, places along the coast of South Africa. You drove for hours, for several consecutive days, every second week, from the dangerous roads of the Transkei to the well-maintained roads of the Western Cape. We walked kilometers on the beach to get to the rocky shores where I wanted to sample. We carried kilograms of mussels, caught many invertebrates and mussel predators, and drilled hundreds of holes to set up experiments. On a rather safe rocky shore, but during terrible weather, a big wave pushed us right into a gulley, heads in the water. Without you, anything could have happened, but you brought us back to safety in the blink of an eye. Once fieldwork was over, you spent days in the laboratory with me to weigh all the little critters found in the mussel beds. Your family became my family while I was away from home, and I never felt alone. You have been my rock throughout my PhD, and I hope I will be able to bring you as much support for your own projects.

Finally, I would like to thank the close friends I made at Rhodes University and in Grahamstown. Thank you to the members of the Organelle, the amazing digs I was part of for a whole year, for making the COVID time a bliss: Dr Megan Reid, Dr Chad Keats, David Taylor, Ariana Watkins, Bruce Roestof, Garyn Townsend, and Dr Abby Gilson. Let us not forget the many colleagues at the Department: Dr Natanah Molline Gusha, for your good advice and your support; Dr Kevin C. K. Ma, for your unstoppable drive when science projects are concerned; Chipo Mungenge, to whom I wish to continue being brave to process her samples in the laboratory while I am not here to keep her company; Clarke van Steenderen, for your cheerful spirit; and the two amazing students I had the chance to supervise, Masibonge F. Nsibande (Honours student) and Lutendo F. Thomo (3rd year Bachelor student), for helping me process all these samples in the last capital months of the PhD. Thank you to the Rhodes Taekwondo club and its members, for keeping me in great physical and mental shape,

and being a place where I could push beyond my limits and achieve great deeds, like obtaining my green belt. All our hard work was rewarded with many medals at tournament, and you keep going strong! Thank you to the Manleys Flat Cricket club, to which I have been introduced by Chad, for being a place to unwind and have fun while holding the bar, and to the STAG Shooting Club, and particularly Andrew Kirk, which I frequented thanks to Tristan, to allow me to discover shooting as a sport and the kind and caring people that practice it. Last but not least, I wish to thank Christo and Robyn Nel, for being such a good company, always!

The success of this thesis goes further than the frontiers of South Africa. I am extending my deepest gratitude to my parents that always supported me, through my BSc and MSc in Reunion Island, and now my PhD in South Africa. You were always present, and I am glad you are also fulfilling your dreams back in France.

I am thankful to Rhodes University for the facilities provided, especially at the Department of Zoology and Entomology, and to the National Research Foundation for funding this PhD.

Lastly, I am grateful to myself, for the hard work I put to complete my PhD, against difficult odds, and for my personal growth during these last three years. This was both the most terrible and the most beautiful years of my life so far. I am excited to see what I will achieve in the future!

CHAPTER 1

GENERAL INTRODUCTION AND THESIS OVERVIEW

1.1. Ecosystem engineering in a changing natural world

Physical ecosystem engineering refers to an ecological process in which an organism, the ecosystem engineer, directly or indirectly modulates the availability (i.e., quality, quantity, and distribution) of resources to other species by causing physical state changes in biotic or abiotic materials (Jones et al., 2010, 1997, 1994; Jones and Gutiérrez, 2007). Ecosystem engineers thus create, modify, maintain and/or destroy habitats. Two types of ecosystem engineer are recognised, autogenic and allogenic engineers. *Autogenic engineers* change the environmental *via* their own physical structures (e.g., trees, scleractinian corals, bivalves; Gutiérrez et al., 2003; Wild et al., 2011), whereas *allogenic engineers* do so by transforming living and non-living materials from one physical state to another, *via* mechanical or other means, such as biodeposition or by-products of trophic behaviours (e.g., beaver dams, rabbit burrows, bulldozing by marine snails; Bertness, 1984a; Naiman et al., 1988). The ecosystem engineering process comprises four criteria: (1) An engineer causes structural change; (2) Structural change causes abiotic change; (3) Structural and abiotic change cause biotic change; (4) Structural, abiotic, and biotic change can feedback to the engineer, but not necessarily (Jones et al., 2010). Physical resources which may be affected by ecosystem engineers include living space (Gutiérrez et al., 2003), local environmental conditions, such as humidity and temperature (Badano and Cavieres, 2006; Jurgens and Gaylord, 2018), and biogeochemical processes (Caraco et al., 2006; Gutiérrez and Jones, 2006). Building

on the example provided in Gutiérrez et al. (2003), the pathways through which ecosystem engineering can affect physical resources can be illustrated using molluscan shells. In an intertidal benthic habitat, imagine a molluscan shell occurring on a flat soft substratum. Either live or dead, the presence of the shell increased the spatial heterogeneity and complexity, by adding a 3D-structure on an otherwise flat substratum. The shell itself became a substratum for both boring and epibiotic organisms that cannot settle on the soft subtrastum. Moreover, the shell presence, as well as the molluscan feeding or attachment behaviour, may cause changes in near-bed flow and infiltration of water, thus altering the particle and solute transport in the benthic habitat. Finally, the internal shell cavity of a dead mollusc may become a more favorable microhabitat that organisms may exploit to evade environmental stress (such as temperature extremes, desiccation, hydrodynamic forces) and predators, or even as a living space (e.g., hermit crabs). Although ecosystem engineering takes place at both small and large spatial scales, relative to the size of the ecosystem engineer, and on time scales from the nearly instantaneous to the extraordinarily protracted (Hastings et al., 2007; Jones et al., 1994), the most obvious ecosystem engineering is mainly attributed to species with large *per capita* effects (i.e., large impacts for each individual), living at high densities, over large areas for a long time, and giving rise to structures that persist for millennia and which affect many resource flows (Hastings et al., 2007; Jones et al., 1994). While their effects can be positive and negative depending on the context (Crooks, 2002; Gribben et al., 2013; Jones et al., 1997; Yeakel et al., 2020), ecosystem engineers ultimately provide a different physical habitat from the unmodified surrounding environment, allowing for colonization by new species and influencing the performance of others, thus increasing local species richness and diversity (Badano and Marquet, 2008; Bangert and Slobodchikoff, 2006; Wright et al., 2002).

Positive interactions (i.e., facilitation) through ecosystem engineering are essential in physically stressful environments, such as arid or intertidal habitats, where harsh physical conditions often limit the presence and survival of organisms (Bertness and Callaway, 1994; Bruno et al., 2003; Crain and Bertness, 2006). In such environments, ecosystem engineers mitigate environmental stress through their presence and activity, effectively supporting ecosystem functioning. Variable in space and time, the magnitude of stress mitigation provided by ecosystem engineers is mostly relevant when abiotic stress is high (Cartwright and Williams, 2014; Lathlean and McQuaid, 2017; Wright et al., 2006; Wright and Gribben, 2017). Habitat destruction, over-exploitation, biological invasions, and anthropogenic global climate change are driving rapid changes in environmental conditions worldwide, leading to dramatic shifts in ecological communities and loss of biodiversity (Barnosky et al., 2011; Bellard et al., 2012; Cardinale et al., 2012; Hooper et al., 2012; Nagelkerken and Connell, 2022; Parmesan, 2006; Parmesan and Yohe, 2003; Tilman et al., 2001; UNCED, 1993). Global climate change and habitat modification will thus challenge the roles that ecosystem engineers play in ecosystem functioning (Coggan et al., 2018; Wernberg et al., 2016; Wild et al., 2011). Nevertheless, ecosystem engineers could act as critical refuges from increasing abiotic stress for a wide array of associated organisms, in addition to their role in the provision of habitat (Cartwright and Williams, 2014; Jurgens and Gaylord, 2018; Lathlean and McQuaid, 2017; Wright et al., 2006; Wright and Gribben, 2017). In this context, ecosystem engineers constitute key conservation targets for the preservation of natural habitats and their functions (Boogert et al., 2006).

1.2. Parasitism and ecosystem engineering

Not only do impacts of ecosystem engineers vary in space and time, but the population or individual traits of ecosystem engineers can affect how they modify the environment (Kuppler et al., 2016; Nicastro et al., 2020; Wieters, 2005; Zardi et al., 2015). In this way, intraspecific genotypic and phenotypic diversity, including age, sex, colour, size, shape, densities or behaviour, influence the quality of the habitat provided by ecosystem engineers (Cole and McQuaid, 2010; Hughes et al., 2008; Hughes and Stachowicz, 2004; Lourenço et al., 2017; Nicastro et al., 2020). Indeed, in marine mussels, different bed configurations or distinct genetic lineages support different infaunal abundance and biomass (Cole, 2010; Nicastro et al., 2020; Zardi et al., 2015), while in mangroves, the height and density of pneumatophores influence their colonization by algae, which in turn facilitate epifaunal colonization (Bishop et al., 2013). Intraspecific trait variation might be stochastic (Fox and Kendall, 2002), genetic (Bangert et al., 2008; Hughes and Stachowicz, 2004; Zardi et al., 2015) or induced by abiotic and biotic factors (Adler and Harvell, 1990; Emery and Rudgers, 2014; Garner and Litvaitis, 2013; Lourenço et al., 2017). For example, in dune grass, climate factors such as temperature and precipitation influence plant size (Emery and Rudgers, 2014). In mussel beds, byssal thread production and mussel growth are influenced by a combination of abiotic (i.e., wave exposure, temperature) and biotic factors (i.e., presence of fouling organisms on the mussel) (Garner and Litvaitis, 2013). Finally, in southern Australia, the presence of invasive seaweed influences the ecosystem engineering traits of native clams (i.e., burial depth), thus indirectly facilitating community diversity by increasing clam shell surface available for epibiotic colonization (Gribben et al., 2009).

Parasites have the ability to modify a wide range of physiological, behavioural, and morphological traits in their hosts, often altering more than one specific host trait (Calvo-Ugarteburu and McQuaid, 1998; Poulin and Thomas, 1999; Thomas et al., 2010; Zardi et al., 2016). Subject to debate (Bush et al., 2001; Goff, 1982; Price, 1977), parasitism is considered through an ecological lens in this thesis as an exploitative relationship between an organism (i.e., the parasite) living strictly in or on another individual living organism (i.e., the host), from which part or all of the parasite's trophic or non-trophic resource requirements are obtained and where the parasite exhibits some degree of adaptive structural modification and causes some degree of real damage and trait alterations in the host. In the case of ecosystem engineers, parasitism can indirectly interfere with the engineering capacities of the host if the altered traits directly correspond, or are related, to the trait involved in the engineering process (Thomas et al., 1999). In autogenic engineers, parasites that alter the growth or shape of their hosts can affect the corresponding engineering trait (i.e., host size or shape) and thus the amount of living space provided to associated organisms (Ndhlovu et al., 2021a). For instance, live mollusc shells are a well-known substratum for epibionts, such as algae and sessile invertebrates (Bell, 2013; Gutiérrez et al., 2003; Marquet et al., 2013). Infestation by endoparasites (e.g., trematodes) or ectoparasites (e.g., shell-boring microorganisms) have been demonstrated to affect the shell growth of molluscs (Minchella, 1985; Ndhlovu et al., 2021a), thus impacting the amount of available space for epibiotic settlement. Similarly, the influence of parasites on the behaviour of ecosystem engineers (e.g., molting, habitat selection, burrowing) can be reflected by the degree to which they modify the environment, with variable consequences on the associated organisms (Pascal et al., 2020; Thomas et al., 1998). For example, infestation of crabs by parasitic crustaceans (e.g., *Sacculina granifera*

Boschma, 1973) impedes moulting (Shields, 1992), turning the cuticle of infested crabs into a more permanent substratum for epibionts, thereby favouring the emergence of a new engineering trait (Thomas et al., 1999). Likewise, cockles infested by trematodes are unable to bury themselves in the sediment, which increase the risk of desiccation during low tide and influences the presence and abundance of associated organisms (Thomas et al., 1998). Finally, mud shrimps infested by bopyrid ectoparasites have been demonstrated to reduce the time allocated to burrowing and ventilating activities, which leads to strong reductions in bioturbation rates and biogeochemical fluxes in the environment they modify (Pascal et al., 2020).

1.3. South African intertidal rocky shores as an open laboratory

At the southern tip of Africa, the conjunction of the Atlantic Ocean in the west and the Indian Ocean in the east gives rise to a hydrographically complex area. The South African marine environment is subjected to the influence of two major current systems: the cold Benguela Current along the west coast (Hutchings et al., 2009) and the warm Agulhas Current along the east coast (Gründlingh, 1983; Schumann, 1987), which overlap on the south coast (Lutjeharms, 1998). The South African coastline spans 3,650 km in length, with contrasting local levels of wave exposure and a wide variety of habitats (e.g., boulder shore, sandy coast, exposed rocky shore) (Sink et al., 2012), and is divided into several biogeographic regions, mainly the cool-temperate west coast, the warm-temperate south coast, and the subtropical east coast (Lombard et al., 2004). Along the cool-temperate west coast, coastal fauna includes relatively few species when compared to the warm-temperate south and subtropical east coasts, but each species is highly abundant, and individuals grow much larger (Bustamante and Branch, 1996; Day, 1969). Due to its unique situation, South Africa is recognized as a biodiversity

hotspot, with approximately 13,000 recorded marine species and many taxa comprising of smaller organisms (e.g., Platyhelminthes, Nematodes) still being underestimated (Griffiths et al., 2010).

Intertidal rocky shores, which represent the interface between land and sea, are open ecosystems subject to extreme natural environmental fluctuations, often occurring at small spatial and time scales (Helmuth et al., 2006a; Helmuth and Hofmann, 2001; Lathlean et al., 2011). Among environmental stresses experienced by intertidal organisms (Raffaelli and Hawkins, 1996), sand burial, temperature and desiccation are the most important abiotic determinants of zonation patterns, directly influencing the physiological performance of organisms and the structure of ecological communities (Helmuth et al., 2006a; Somero, 2002; Zardi et al., 2008). Sporadic sand inundation and burial is often responsible for the mass mortality of several intertidal species, and often entire communities (Roleda and Dethleff, 2011; Yáñez et al., 2008; Zardi et al., 2008). Meanwhile, intertidal organisms are exposed daily to fluctuating solar irradiation and temperatures (Helmuth et al., 2010; Helmuth and Hofmann, 2001), reaching extremes during warm, sunny, midday low tides, with little to no overcast and low wind speeds (Helmuth et al., 2011; Mislan et al., 2009). Intertidal organisms often live at the edge of their physiological thermal tolerances (Somero, 2002; Stillman and Somero, 1996; Stillman, 2002). Triggered by anomalously weak wind speeds and increased solar irradiation (Gupta et al., 2020; Schlegel et al., 2017), heatwaves are expected to increase in intensity, duration and frequency in response to global climate change (Oliver et al., 2021, 2019). Because organisms suffer more from extremes than slow changes in their environment (Gaines and Denny, 1993), marine heat waves have been associated with mass mortalities, large-scale shifts in species location, and changes in species phenology and ecosystem structures in intertidal ecosystems

(Helmuth et al., 2002; Lima et al., 2007; Sanford et al., 2019; White et al., 2023). Intertidal organisms have evolved a wide range of thermal adaptations, including specific behaviours (e.g. 'mushrooming' in limpets; Williams et al., 2005), and more importantly, the use of microhabitats which serve as thermal refuges (Cartwright and Williams, 2014; Lathlean et al., 2016a). It is important to note that such behaviours are mostly relevant when the organism suffers from temperature or desiccation stress (Muñoz et al., 2005). Thus, the vertical pattern of species' distributions on rocky shores commonly reflects a combination of abiotic stress gradients, such as hydrodymanic stress (e.g., wave height and force, topography), sand accumulation, and the above-mentioned temperature and desiccation, with species resistant to high air temperatures dominating the upper intertidal and more sensitive species thriving closer to the water mark (McMahon, 1990; Somero, 2002), and biotic stress gradients (i.e., predation, competition). Along the South African coastline, the vertical zonation on rocky shores is summarized, with the dominant species present for each zone, in Figure 1.1.

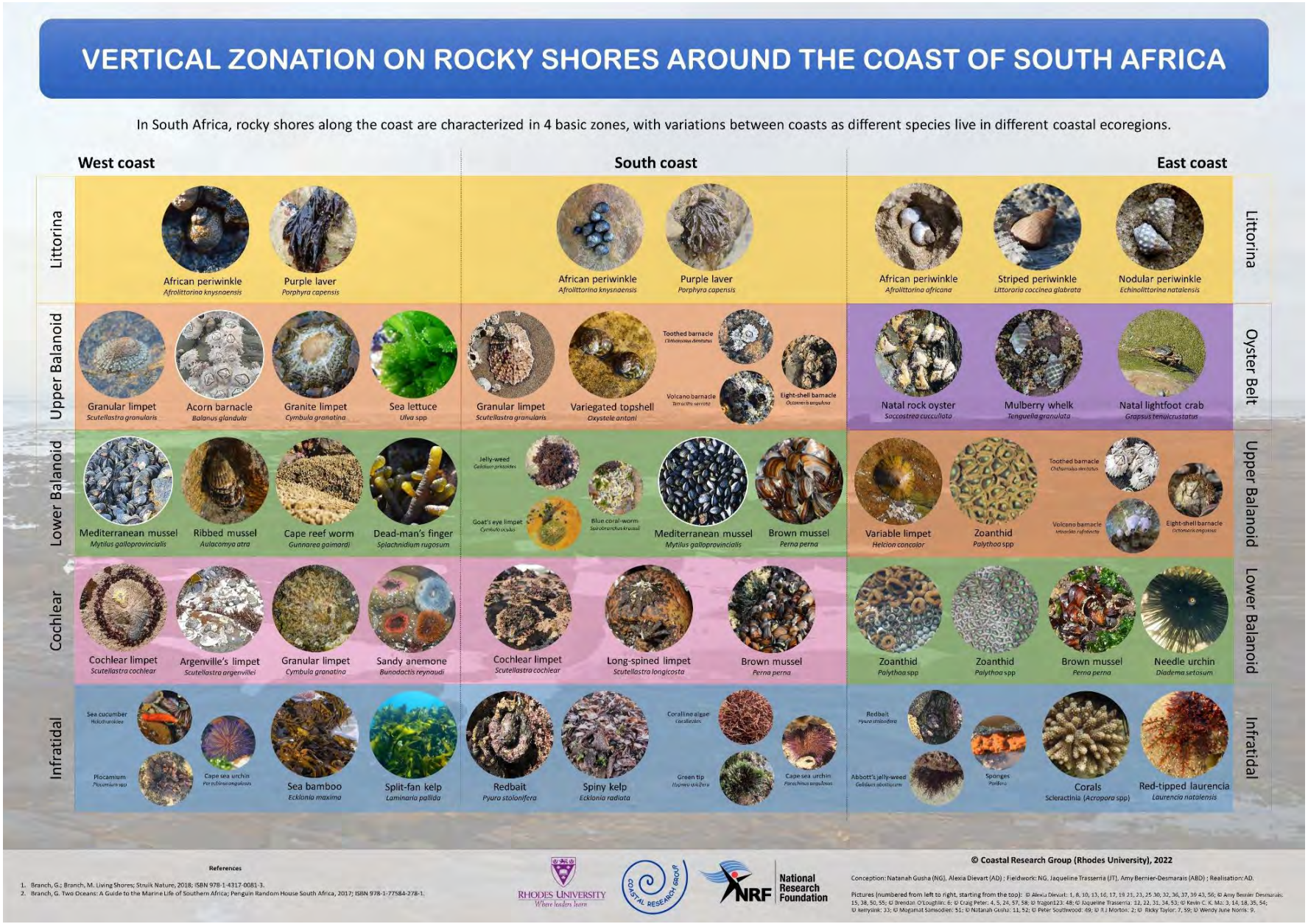

Figure 1.1. Vertical zonation on rocky shores along the coast of South Africa (Coastal Research Group, 2022).

Mussel beds form an important intertidal matrix in the mid-intertidal, also referred to as the 'mussel zone', that support many associated species and are thus essential to the function of intertidal ecosystems worldwide (Hammond and Griffiths, 2006, 2004). On the west coast of South Africa, the 'mussel zone' is dominated by two invasive mussels, the blue mussel *Mytilus galloprovincialis* Lamarck, 1819 and the bisexual mussel *Semimytilus patagonicus* (Hanley, 1843), where they replaced two native mussels, the ribbed mussel *Aulacomya atra* (Molina, 1782) and the black mussel *Choromytilus meridionalis* (Krauss, 1848) (De Greef et al., 2013; Grant and Cherry, 1985). The native brown mussel *Perna perna* (Linnaeus, 1758) dominates on the east coast, and co-occurs with *M. galloprovincialis* on the south coast (Bownes and McQuaid, 2006). On the south coast, the 'mussel zone' can be further divided into the high 'mussel zone' dominated by *M. galloprovincialis*, the low 'mussel zone' dominated by *P. perna*, and the mid 'mussel zone' where the two species overlap and coexist (Bownes and McQuaid, 2009). Among the associated species that characterise the high 'mussel zone' are toothed (*Chthamalus dentatus* Krauss, 1848) and volcano barnacles (*Tetraclita serrata* Darwin, 1954), gastropod snails (e.g., *Afrolittorina* spp S. T. Williams, D. Reid & Littlewood, 2003, *Oxystele* spp R. A. Philippi, 1847), dwarf cushion stars (*Parvulastra exigua* (Lamarck, 1816)) and limpets (e.g., *Scutellastra granularis* (Linnaeus, 1758)). In the mid 'mussel zone', the eight-shelled barnacle (*Octomeris angulosa* (Sowerby, 1825)) is commonly found on wave-exposed rocky shores, as well as foliose red algae (e.g., *Gelidium pristoides* (Turner) Kützing, 1843). Finally, communities in the low 'mussel zone' include sensitive species to thermal and desiccation stress, such as the cochlear limpet (*Scutellastra cochlear* (Born, 1778)), branching red algae (e.g., *Plocamium* spp J.V.Lamouroux, 1813), as well as encrusting

(e.g., *Spongites yendoi* (Foslie) Y.M.Chamberlain, 1993, Corallinales) and articulated coralline algae (Branch and Branch, 2018; Branch et al., 2016; Day, 1969).

In addition to the provision of a physical habitat for both infaunal and epibiotic species (Gutiérrez et al., 2003; Palomo et al., 2007; Suchanek, 1985), mussel beds mitigate both temperature and desiccation stress under extreme environmental conditions (Gutiérrez et al., 2019; Helmuth, 1998; Jurgens and Gaylord, 2018; Nicastro et al., 2020; Stephens and Bertness, 1991), act as a refuge against predators, especially for juveniles (Lintas and Seed, 1994; Thiel and Dernedde, 1994; Witman, 1985), and participate in the transport of solutes and organic particles (Crooks and Khim, 1999; Tsuchiya and Nishihira, 1985). The engineering properties of mussel beds are affected by intraspecific trait variation at the individual and patch levels, such as the size (as a proxy of age; Lathlean et al., 2016b; Tsuchiya and Nishihira, 1986) and density of mussels (Cole, 2010), distinct genetically-based behaviours between lineages (Nicastro et al., 2020; Zardi et al., 2015) or the structure of the mussel beds (Palomo et al., 2007). Moreover, engineering traits of mussels (e.g., survival, byssal thread production, gaping behaviour) are influenced by abiotic and biotic factors, such as wave exposure, temperature and ocean acidification (Garner and Litvaitis, 2013; Hicks and McMahon, 2003; O'Donnell et al., 2013), the presence of predators, parasites and epibionts (Garner and Litvaitis, 2017; Kaehler and McQuaid, 1999; Nicastro et al., 2019; Reimer and Tedengren, 1997; Tummon Flynn et al., 2020).

1.4. Shell-boring microscopic parasites in mussel beds

Colonizing intertidal bivalves around the world, independently of their location or the nature of the shore, photoautotrophic euendoliths are shell-boring microscopic parasites comprising cyanobacteria (blue algae), rhodophytes (red microalgae) and chlorophytes

(green microalgae) (Cerrano et al., 2001; Kaehler, 1999; Mao Che et al., 1996; Ndhlovu et al., 2021b). In live and dead bivalves, photoautotrophic euendoliths colonize the shell as soon as the periostracum, the well-defined external layer of the shell that protects the shell against both boring and fouling organisms, is damaged (Akpan, 1990; Kaehler, 1999; Kaehler and McQuaid, 1999; Raghukumar et al., 1991). Infestation by photoautotrophic euendoliths increases in prevalence and intensity as bivalves age, reaching between 25 and 95% incidence depending on the location and the bivalve species (Ćurin et al., 2014; Gehman and Harley, 2019; Kaehler, 1999; Ndhlovu et al., 2019; Zardi et al., 2009). Photoautotrophic euendoliths have both negative lethal and sub-lethal effects, as well as surprising conditional positive effects, on the individual bivalves (Kaehler and McQuaid, 1999; Marquet et al., 2013; Monsinjon et al., 2021; Ndhlovu et al., 2022, 2021a; Zardi et al., 2021, 2016, 2009).

The boring activities of euendoliths into the shells of bivalves adversely affect their overall fitness (Kaehler and McQuaid, 1999; Marquet et al., 2013; Ndhlovu et al., 2022, 2021a; Zardi et al., 2009). For instance, infestation by photoautotrophic euendoliths in mussels reduces survival, by decreasing shell strength and thickness and thus increasing vulnerability to predation, wave action, or trampling (Kaehler and McQuaid, 1999; Nicastro et al., 2019), as well as the perennity of mussel beds, by decreasing reproductive output (Kaehler and McQuaid, 1999; Ndhlovu et al., 2022). Infested mussels display a reduced scope for growth (Ndhlovu et al., 2021a), and lower attachment strength, imputed to a lower production of byssal threads (Kaehler and McQuaid, 1999; Ndhlovu et al., 2022; Zardi et al., 2009). Moreover, shell microtopography and its antifouling properties (Bers et al., 2010; Scardino et al., 2003) can be altered by the corrosive activity of euendoliths, which can influence the amount and quality of space available for the settlement of epibionts, such as barnacles (Ma et al., 2023;

Marquet et al., 2013). In the same way, infested mussels present a rougher surface which influences the complexity of mussel beds and thus their hydrodynamic properties, through the deceleration of near-bed flow velocities which leads to greater ingestion rates and retention of microplastics (Nicastro et al., 2022). However, as a by-product of their erosive activity, photoautotrophic euendoliths have surprising beneficial effects on mussels, individually and in aggregation, although restricted in space and time to extremely stressful environmental conditions (Lourenço et al., 2017; Monsinjon et al., 2021; Zardi et al., 2021, 2016). Infested mussel shells are lighter in colour, and thus reflect more light, which reduces the body temperatures of infested mussels and increases their survival rates during extreme conditions (Monsinjon et al., 2021; Zardi et al., 2021, 2016). The beneficial effect of photoautotrophic euendoliths can extend to neighbouring mussels, creating a more benign microclimate within infested mussel beds (Lourenço et al., 2017). Ultimately, euendolithic infestation becomes so severe that bivalves fracture their own shells with the force applied by their adductor muscles (Kaehler, 1999; Kaehler and McQuaid, 1999). On rocky shores, infestation of mussels by shell-boring microscopic parasites have thus the potential to influence the ecosystem engineering capabilities of mussel beds, in terms of structure, architectural complexity and stress-mitigating microclimate (e.g., Zardi et al., 2023), with complex ecological consequences on the associated invertebrate communities.

1.5. Thesis objectives and overview

Given the unique ecological engineering roles of mussel beds on the environmentally stressful rocky shores, the main objective of this thesis was to explore the influence of euendolithic infestation of the mussel shells on the associated infaunal and epibiotic

communities. The study, therefore, aims to contribute towards the current understanding on how parasites influence ecosystem engineering, focusing on the engineer role of the native brown mussel, *Perna perna*, at selected sites in the extremely variable and stressful rocky shore environments along the South African coastline. Using a combination of manipulative *in situ* and laboratory-based experiments, the current study assessed : (i) if the beneficial effects of euendolithic infestation on the body temperatures of mussels extends to the associated invertebrates, (ii) the influence of euendolithic infestation on mussel bed structural complexity and how this cascades to associated infaunal communities along a biogeographic gradient, and (iii) evaluate the influence of euendolithic infestation on the associated epibiotic communities.

The thesis comprises six chapters. **Chapter 1** is the general introduction which sets the context and framework of the thesis. **Chapter 2** provides and in-depth review of the nature and diversity of marine photoautotrophic euendoliths, and discusses how environmental conditions influence their incidence, the ecological consequences of their infestation in various marine calcifiers (i.e., corals and crustose coralline algae, bivalves), their likely response to global climate change and ocean acidification. **Chapter 3** presents the main findings of a laboratory-based study that investigated the potential thermal benefits of infested mussels for selected associated invertebrates. **Chapter 4** of the thesis presents the main findings of a common-garden experiments across bioregions that investigated the influence of euendolithic infestation of mussels on associated infauna. **Chapter 5** evaluates the influence of photoautotrophic euendoliths on the mussel shell as a habitat for epibionts. Finally, a general synthesis of the overall findings in the context of the methods used and the existing literature is provided in **Chapter 6**.

CHAPTER 2

PHOTOAUTOTROPHIC EUENDOLITHS AND THEIR COMPLEX ECOLOGICAL EFFECTS IN MARINE BIOENGINEERED ECOSYSTEMS

Published on September 7th, 2022, as: Dievart, A.M.; McQuaid, C.D.; Zardi, G.I.; Nicastro, K.R.; Froneman, P.W. Photoautotrophic Euendoliths and Their Complex Ecological Effects in Marine Bioengineered Ecosystems. *Diversity* 2022, *14*, 737. https://doi.org/10.3390/d14090737

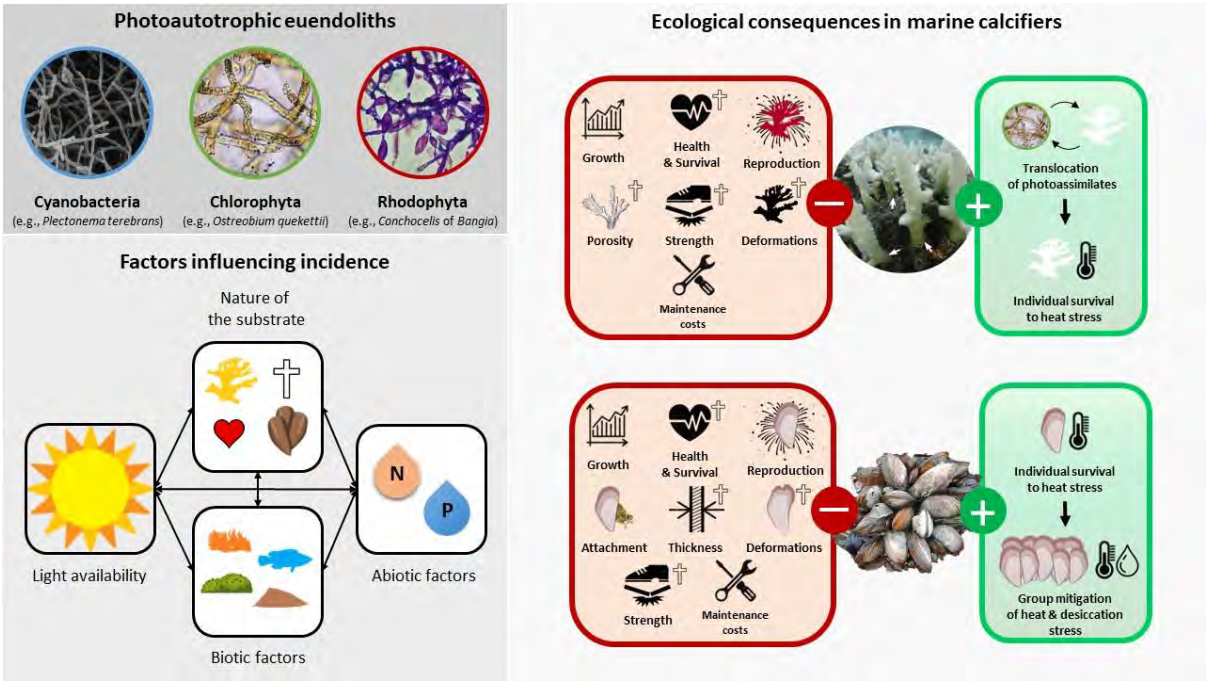

Figure 2.0. Graphical abstract published in Dievart et al. (2022). **Top left, darker grey panel**: main taxonomical groups of photoautotrophic euendoliths represented by their most common euendolithic species; **bottom left, lighter grey panel**: principal factors influencing the incidence of euendolithic infestation around the world; and **right panel**: summary of the negative (in red) and positive (in green) consequences of euendolithic infestation on live corals and mussels.

2.1. Introduction

Autotrophic (cyanobacteria, and red and green microalgae) and heterotrophic (fungi) euendolithic microorganisms, discovered in the 19th century (Carpenter, 1845), actively penetrate the hard substrates in which they live (Golubic et al., 1981). Euendolithic organisms have been present on Earth since the Proterozoic, 2 500 to 541 million years ago (Zhang and Golubic, 1987), coinciding with the appearance of oxygen in Earth's atmosphere, and are thus thought to have played a major role in the development and evolution of life, as well as in the production and destruction of carbonates (Knoll, 2008; Sánchez-Baracaldo et al., 2022; Schneider and Le Campion-Alsumard, 1999). Euendoliths are ubiquitous, as they can be found in almost every environment, geographical location, or depth, where the appropriate substratum (e.g., relatively soluble carbonate and phosphate substrates) is available and their biological requirements are met (Frémy, 1945; Friedmann et al., 1988; Gaylarde et al., 2006; Golubic et al., 1975; Golubic and Schneider, 2003; Schneider and Le Campion-Alsumard, 1999). For example, photoautotrophic euendoliths are restricted to the photic zone, where there is sufficient light to carry out photosynthesis, and are particularly diverse and ecologically significant in marine environments (Frémy, 1945; Golubic et al., 1975). They colonize a wide variety of carbonate substrates, from inanimate and dead carbonates to the calcified structures of live animals, such as the skeletons of hard corals, bivalve shells, and the thalli of crustose coralline algae (Ghirardelli, 2002; Kaehler, 1999; Le Campion-Alsumard et al., 1995a; Musso, 1994; Tribollet and Payri, 2001). Since their discovery, numerous studies have been conducted on the euendoliths colonizing inanimate and dead calcium carbonates (Chazottes et al., 1995; Glaub et al., 2001; Golubic et al., 1975; Golubic and Schneider, 1979; Kiene and Hutchings, 1994). Initially, researchers speculated that the bioerosive

activities of euendoliths had little to no effect on infested live calcifying organisms (Lauckner, 1983). However, an increasing number of more recent studies suggest that euendolithic infestation has both negative and, surprisingly, beneficial effects on live calcifying organisms (Fine and Loya, 2002; Hassenrück et al., 2013; Kaehler and McQuaid, 1999; Zardi et al., 2016). Bivalves, corals, and coralline algae create persistent physical structures that provide habitats for a wide array of associated species (Crooks and Khim, 1999; Knowlton et al., 2010). Thus, they are referred to as 'ecosystem engineers' and can form the basis of entire ecosystems (Jones et al., 1997, 1994). Such marine ecosystems are under multiple anthropogenic pressures, including overexploitation, chronic pollution, and population fragmentation, and their responses to ongoing global climate change and ocean acidification remain uncertain (Helmuth et al., 2006b; Wild et al., 2011). Under such circumstances, the negative and beneficial effects of euendolithic infestation on individual live calcifying organisms have the potential to reverberate at the population, community, or ecosystem level, with complex, and potentially unexpected, ecological outcomes (Lourenço et al., 2017; Tribollet, 2008a). Understanding how euendolithic infestation interacts with other environmental stressors, and how these interactions will change under future environmental conditions is critical to predicting the long-term fate of such ecosystems.

Here, this chapter focuses on photoautotrophic euendoliths in the marine environment and their complex ecological effects on live calcifying organisms and the bioengineered ecosystems they create. This review discusses: (1) the nature of marine euendoliths and the techniques used for their observation, (2) the mechanisms involved in their bioerosive activity, (3) their incidence and distribution in marine ecosystems, in relation to various environmental parameters, and their potential as ecological indicators (*sensu* Fedor and Spellerberg, 2013), (4) how they affect today's living calcifying organisms, with a focus

on corals, coralline algae, and bivalves, and (5) how euendoliths are anticipated to respond to global climate change, and particularly to ocean acidification.

2.2. What are euendoliths and how are they observed?

Initially thought to be part of the substrate morphology (Carpenter, 1845), microborings observed in calcium carbonate substrates were later correctly attributed to the activities of microorganisms, such as algae and fungi (Bornet and Flahault, 1889; Kölliker, 1860; Wedl, 1859), which became known as 'endoliths'. The term 'endolith' refers to a morphologically and physiologically heterogenous group of microorganisms living within a rock or other stony matter, such as coral skeletons or animal shells (Gary et al., 1973), and more specifically, to organisms that actively bore into relatively soluble substrates, such as phosphate and carbonate substrates (Couradeau et al., 2017; Golubic et al., 1981, 1975) (Figure 2.1).

While more detailed classifications exist (e.g., Amarelle et al., 2019), a broad distinction is made among:

1. Epiliths that live on the surface of the substrate;
2. Chasmoliths that adhere to the surface of fissures and cracks in the substrate;
3. Cryptoendoliths that adhere to the surface of pre-existing cavities within porous rocks, including spaces produced and vacated by euendoliths, with no dissolution action;
4. Euendoliths that actively penetrate carbonate (and phosphate) substrates and reside partially or completely inside cavities of their own making.

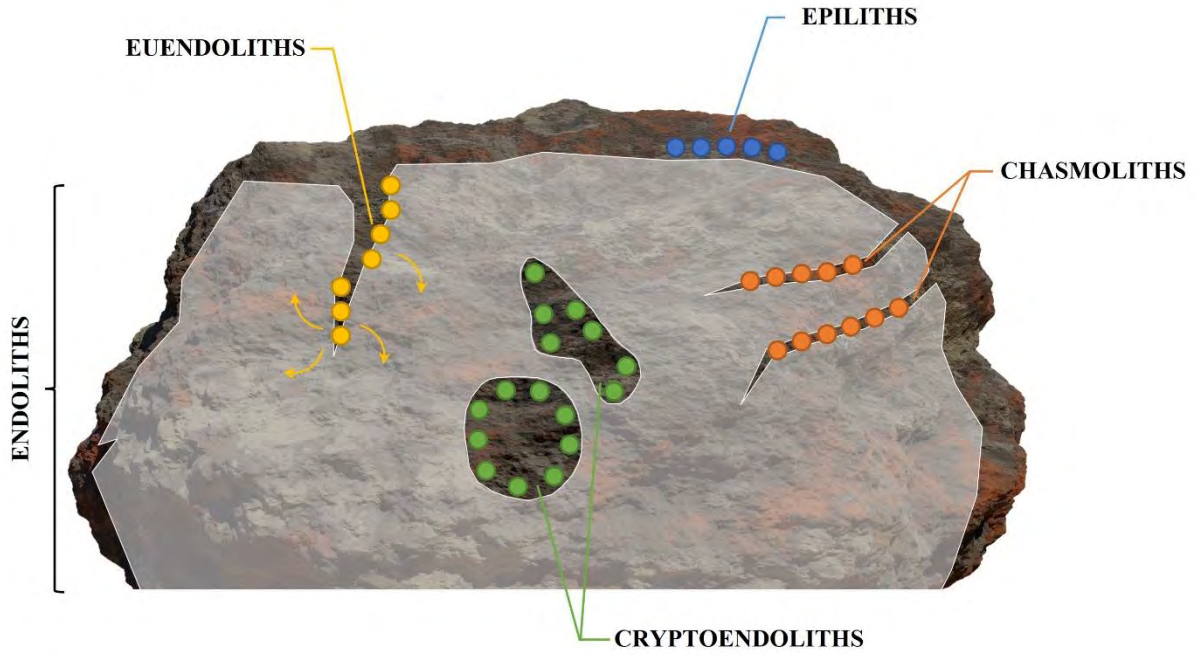

Figure 2.1. Types of endolithic organisms in relation to a hard rocky substrate (modified from Amarelle et al., 2019).

These distinctions are not mutually exclusive as some organisms can display more than a single boring habit or may alter their habits during their life cycles. For example, several boring algae mature on the surface of shells and penetrate the substrate with endolithic filaments, while part of their thallus remains epilithic (Ercegović, 1932; Wisshak, 2012). Endolithic green algae from the genus *Ostreobium* Bornet and Flahault, 1889 switch to a chasmolithic lifestyle after reaching larger cavities within the substrate (Schroeder, 1972). Some red algae from the genera *Porphyra* C. Agardh, 1824 and *Bangia* Lyngbye, 1819 can exhibit an endolithic lifestyle during the early stages of their life cycle, called the conchocelis phase, while occurring in a wide variety of habitats as adults (Drew, 1958, 1954).

The first descriptions of euendoliths were derived from dead mollusk shells gathered from the coast (Bornet and Flahault, 1889; Lagerheim, 1886). Euendolithic green algae were observed through a thin shell fragment, forming a horizontal layer parallel to the

surface, with an underlying network of ramifications into the substrate. Relatively inaccessible (Figure 2.1), euendolithic microorganisms and their microborings require basic but specific techniques to be studied (Golubic et al., 2019, 1975; Wisshak, 2012). These include:

1. **Isolation of endoliths**. After fixing the sample (substrate and euendoliths of interest) in formaldehyde solution to prevent structural damage to enclosed euendolithic organisms, the surrounding carbonate substrate is usually dissolved using dilute acid. The released endolithic filaments can then be observed and identified under light microscopy or transmission electron microscopy (TEM) (Golubic et al., 1975). As the hard matrix supporting the euendolithic filaments is dissolved, the organic components of the boring collapse, making spatial relationships and growth arrangements difficult to reconstruct. This technique only allows a qualitative assessment of euendolithic communities but is still widely used to detect and identify euendoliths of interest (Al-Thukair et al., 1994; Ndhlovu et al., 2021b; Tribollet and Payri, 2001).
2. ***In situ* observations**. Microborings can be studied in standard petrographic thin sections or sufficiently transparent fragments of shells using light microscopy (Rooney and Perkins, 1972) or scanning electron microscopy (SEM). The 2D visualization of microborings by petrographic thin sections is of limited use for the study of 3D objects, such as empty or filled euendolithic microborings, but allows their observation and the estimation of their true penetration depth in association with the surrounding matrix (Wisshak, 2012).
3. **Cast-embedding of microboring networks** (Golubic et al., 1975, 1970; Wisshak, 2012). Combined embedding and casting in polymerized resins preserves the spatial arrangements of boring tunnels (3D architecture) and the

euendolithic organisms in situ (Golubic et al., 1970), allowing proper examination after the dissolution of the surrounding substrate (routine protocol in Golubic et al., 1975, see Figure 2 in Wisshak, 2012). Such casts can then be observed using light microscopy or SEM. However, this technique is limited when microborings are filled by secondary carbonate precipitation following the death of the euendoliths (Wisshak, 2012).

4. **Cultivation** (Al-Thukair, 2011; Al-Thukair et al., 1994; Chacón et al., 2006). Natural samples (e.g., shell fragments, ooids) harboring euendoliths are used to inoculate agar plates containing a chemically defined culture medium. Once single colonies grow enough to be mechanically isolated, each colony is transferred into a liquid medium and stored under specific environmental conditions. While cultivation selects heavily for fast-growing microorganisms, it is a valuable tool to confirm taxonomic identification and to investigate the life history and physiology of euendoliths (Drew, 1958, 1954; Pasella et al., 2022). Cultivation also represents a necessary step to build the databases used for the identification of environmental DNA sequences (Chacón et al., 2006).
5. **X-ray computed tomography (CT) and micro-computed tomography (micro-CT)** (reviewed in Cunningham et al., 2014). These non-destructive 3D-visualization tools are firmly established for paleontological investigations, with their highest resolution encompassing the spatial magnitude of microborings (Silbiger et al., 2014; Sutton, 2008; Wisshak et al., 2017). They are, however, still relatively expensive and time-consuming, and require a high level of technical skill (Cunningham et al., 2014; Wisshak et al., 2017). More affordable micro-CT and associated analyses can underestimate the extent of bioerosion by photoautotrophic euendoliths (Silbiger et al., 2014), as microborings range

between 1 and 100 μm in diameter (Tribollet, 2008a). Micro-CT does, nonetheless, allow the investigation of microborings (empty or filled) within substrates that cannot be altered or dissolved (e.g., type material).

Most techniques used to observe euendoliths focus on the characteristic pattern of their microborings (i.e., form, diameter, direction, length, and pattern of the tunnel), which allows taxonomic identification even in the absence of the organism itself. Different euendolithic species boring into the same substrate and under uniform ecological conditions will produce distinctive boring patterns, in terms of size, shape, and mode of branching of tunnels (Golubic, 1969). Both biological and mineralogical factors should be considered in the characterization of microborings. While the size, frequency, and branching patterns of microborings are dictated by the size and properties of the euendolithic organism, the directions of growth and the fine sculpture of the inner surface of the microborings are influenced by the mineralogical properties of the substrate (Golubic, 1969; Golubic et al., 1975). Critically, a single euendolithic species can display a large variety of morphologically different patterns when boring into different substrates or under different ecological conditions of light and water supply, amongst others (Golubic, 1969). For example, the microborings produced by intertidal euendolithic cyanobacteria are shallower and composed of straight tunnels where desiccation is high, in the supratidal or upper intertidal, while being deeper and tortuous in areas with stagnant water or lower on the shore (Golubic, 1969). These factors reduce the accuracy of taxonomic identification using microborings. Moreover, euendolithic organisms often exhibit few distinguishing morphological features, making taxonomic identification via direct observation equally unreliable (Verbruggen, 2014). While morphological features of the organism or its traces (i.e., microborings) are useful in the initial discovery of unknown entities, taxonomic identification is best achieved using

genetic and molecular techniques (Verbruggen, 2014) and/or cultivation (Chacón et al., 2006).

Used as a complement to morphological descriptions, single- and multi-marker genetic approaches allow the identification of cryptic clades and/or species within euendolithic species complexes and provide tools to determine the composition of natural euendolithic communities. For example, two species within the green algal genus *Ostreobium* were described using morphological features (Bornet and Flahault, 1889; Lukas, 1974), whereas up to 95 delimited cryptic species have been identified within this genus using genetic and molecular techniques (Gonzalez-Zapata et al., 2018; Gutner-Hoch and Fine, 2011; Marcelino and Verbruggen, 2016; Ricci et al., 2021; Sauvage et al., 2016; Verbruggen et al., 2009). Environmental DNA (eDNA) metabarcoding allows the automated identification of multiple euendolithic species from a single sample, either containing entire organisms or a piece of substrate containing degraded DNA/RNA (e.g., coral skeleton, bivalve shell), by targeting the amplification and sequencing of one or several specific DNA/RNA regions using universal primers (Taberlet et al., 2012). The composition of euendolithic communities can be investigated using multiple markers, including 16S rRNA and 23S rDNA targeting bacteria and cyanobacteria (Marcelino and Verbruggen, 2016; Ricci et al., 2021; Roush et al., 2021; Yang et al., 2019), and 18S rRNA, rbcL, and tufA targeting chlorophytes (Gutner-Hoch and Fine, 2011; Pasella et al., 2022; Ricci et al., 2021; Sauvage et al., 2016; Tandon et al., 2023). Moreover, the use of eDNA metabarcoding, in combination with other techniques, such as microscopy, spectrophotometry, and cultivation, has revealed previously undisclosed diversity of prokaryotic and eukaryotic endolithic organisms (Chacón et al., 2006; Marcelino and Verbruggen, 2016; Ricci et al., 2021) and can help resolve their phylogenetic history (Marcelino and Verbruggen, 2016).

For example, euendolithic green algae almost exclusively belong to the class Ulvophyceae, in which the ability to bore evolved independently over 20 times (Marcelino and Verbruggen, 2016), while the cyanobacterium *Acaryochloris marina* H.Miyashita & M.Chihara, 2003 has been recorded for the first time in the skeleton of live corals using eDNA (Marcelino and Verbruggen, 2016) and produces chlorophyll-*d*, allowing it to use far-red light for photosynthesis and thus to occupy niches depleted of visible light (Behrendt et al., 2011). Finally, the correct identification of the euendolithic species is fundamental in the study of euendolithic communities and their impacts, as different strains within the same species complex (e.g., *Ostreobium queckettii* Bornet and Flahault, 1889) can differ in their physiology (Iha et al., 2021; Massé et al., 2020).

2.3. How do euendoliths erode calcium carbonate?

To understand biologically mediated carbonate dissolution, the basis of biotic carbonate precipitation in its simplest form needs to be revisited. Through their metabolic activity, small cells or organisms indirectly create a microenvironment where the concentrations in the chemical species present increase the local precipitation of carbonate, such as calcification by photosynthetic cyanobacterial communities (Golubic et al., 2000; Merz-Preiβ, 2000).

At slightly alkaline or neutral pH, oxygenic photosynthesis can be expressed as:

$$\boldsymbol{HCO_3^- + H^+ \rightarrow C(H_2O) + O_2} \qquad (2.1)$$

Protons effectively consumed by oxygenic photosynthesis can then drive the thermodynamic equilibrium of carbonate dissolution–precipitation (with the equilibrium constant expressed as K_{s0}) toward the solid phase (indicated by (s); here, calcium carbonate):

$$\boldsymbol{CaCO_3\,(s) + H^+ \leftrightarrow Ca^{2+} + HCO_3^-\,;\, K_{s0}} \tag{2.2}$$

The free energy of dissolution ΔG is given by:

$$\boldsymbol{\Delta G = RTln\left(\frac{IAP}{K_{s0}}\right)} \tag{2.3}$$

where R is the ideal gas constant (8.314 $J{\cdot}K^{-1}{\cdot}mol^{-1}$); T, the absolute temperature (in Kelvin); K_{s0}, the equilibrium constant of carbonate dissolution–precipitation; and IAP is the ion activity product (Stumm and Morgan, 1996). If $IAP > K_{s0}$, carbonate precipitation will be thermodynamically favoured whereas if $IAP < K_{s0}$, dissolution will be favoured. Through their autotrophic metabolism, cyanobacteria and microalgae promote the alkalinization of the medium, increasing local carbonate precipitation. Furthermore, in the case of marine euendoliths, seawater is supersaturated with respect to calcite and aragonite, making carbonate dissolution thermodynamically unfavourable (Garcia-Pichel, 2006). This leads to an apparent geomicrobial paradox in photoautotrophic euendolithic organisms (Garcia-Pichel, 2006): how do they achieve local carbonate dissolution, essential for boring, although their autotrophic nature and their surrounding environment should enhance local carbonate precipitation?

The exact mechanisms by which euendolithic organisms bore into carbonate substrates have long remained elusive (Alexanderson, 1975; Cockell and Herrera, 2007; Garcia-Pichel, 2006; Hatch, 1980; Lagerheim, 1886; Schneider and Le Campion-Alsumard, 1999), with several possible mechanisms being suggested for euendolithic cyanobacteria and later discarded (Garcia-Pichel, 2006; Garcia-Pichel et al., 2010). Indeed, suggested boring mechanisms in cyanobacteria need to be consistent with observations and physiological and geochemical principles (Garcia-Pichel, 2006).

Specifically, they need to fulfil three necessary conditions:

1. The dissolution process is thermodynamically unfavourable, as it mainly occurs in waters saturated with calcium carbonate (i.e., calcite and aragonite). Excavation then becomes an ATP-driven active process with an energetic cost;
2. The carbonate-dissolving mechanisms must be localized at the "head" of the microborer (i.e., apical cells) as dissolution produces true tunnels, with the typical "negative" shape of the borer (Golubic, 1969);
3. The proposed mechanisms must allow for the conservation of mass and electrical charge as in chemical reactions, the mass and the electrical charge of the components before the reaction must be equal to the mass and the electrical charge of the components after the reaction.

Previously proposed mechanisms included the excretion of weak organic acids, the separation of antagonistic photosynthetic and boring activities, and enzymatic dissolution (Alexanderson, 1975; Hatch, 1980; Stal and Krumbein, 1987), but none fulfil all three conditions listed above (Garcia-Pichel, 2006; Garcia-Pichel et al., 2010).

Garcia-Pichel (2006) subsequently proposed an alternative boring mechanism, coined 'The Calcium Pump', which relies on the active transport of Ca^{2+} through the cyanobacterial trichome, leading to low concentrations of free Ca^{2+} at the end of the borehole, which in turn decreases ion activity product below levels that would make dissolution thermodynamically favourable (i.e., $IAP < K_{s0}$; Figure 2.2). The participation of P-type Ca^{2+} ATPases and evidence for transcellular Ca^{2+} transport have been demonstrated for strains of one of the most common cyanobacterial euendoliths, *Mastigocoleus testarum* Lagerheim ex Bornet and Flahault, 1886 (Garcia-Pichel et al., 2010; Guida and Garcia-Pichel, 2016). Long-range Ca^{2+} transport

within the cyanobacterial filament is made possible through two unique cellular adaptations discovered in this cyanobacterium: active pumping of Ca^{2+} is orchestrated by the preferential localization of P-type Ca^{2+} ATPases at one pole of the cell, while specialized cells, called calcicytes, allow fast Ca^{2+} transport at low, nontoxic concentrations throughout undifferentiated cells (Figure 2.2). Calcicytes also act as a buffer against excessive, detrimental Ca^{2+} concentrations before final excretion from the borehole (Guida and Garcia-Pichel, 2016). Furthermore, 'The Calcium Pump' model fulfils the three necessary conditions enumerated earlier: it is an active process, localized at the end of the borehole, which allows for the conservation of mass and electrical charge (Garcia-Pichel, 2006). The model is also consistent with the observation of microetchings (Alexanderson, 1975; Fredd and Fogler, 1998), which, in the absence of hard or moving parts in cyanobacteria, points towards carbonate dissolution by cation removal, and with the range of bored substrates, which share Ca^{2+} as a common denominator (Garcia-Pichel, 2006). Finally, it alleviates reprecipitation of calcium carbonate within the borehole thanks to the intracellular transport of Ca^{2+} (Garcia-Pichel, 2006). While these studies have shed light on the boring mechanism for euendolithic cyanobacteria (Ramírez-Reinat and Garcia-Pichel, 2012), details regarding the boring mechanism carried out by other photoautotrophic euendoliths have still not been investigated in depth. However, Krause et al. (2019) have recently demonstrated the existence of active calcium uptake by the green alga *Ostreobium queckettii*, occurring at the apical tip of the siphonal thallus, in a process similar to that exhibited by cyanobacteria. All microborers exclusively use chemical bioerosion (Garcia-Pichel, 2006; Tribollet, 2008) and with regards to these latest findings, further studies are required to reveal the exact boring mechanism of endolithic green and red algae.

As to why euendoliths bore, Garcia-Pichel et al. (2010) suggested that they are metabolically dependent on the substrate for dissolved carbon dioxide CO_2 released during substrate excavation that can be used for photosynthesis. Euendoliths preferentially fix carbon from the most readily available source, either from the atmospheric pool of dissolved CO_2 or the mineral substrate they bore into (Guida et al., 2017). When dissolved CO_2 is limited, euendolithic microorganisms, such as *Mastigocoleus testarum*, grow preferentially as euendoliths and thus, derive most of their carbon from the mineral substrate they excavate (Guida et al., 2017). By doing so, euendoliths can complete their geomicrobial action on the substrate and potentially gain a competitive advantage over photosynthetic epiliths, which may suffer from limited dissolved CO_2 access as the epilithic biofilm thickens (Guida et al., 2017). Considering a variety of possible selection pressures (e.g., nutrient acquisition, protection from UV and/or predators), Cockell and Herrera (2007) suggested that the boring behaviours of euendoliths could also have originated as mechanisms against entombment by mineralization, especially in substrates with high mineralization rates.

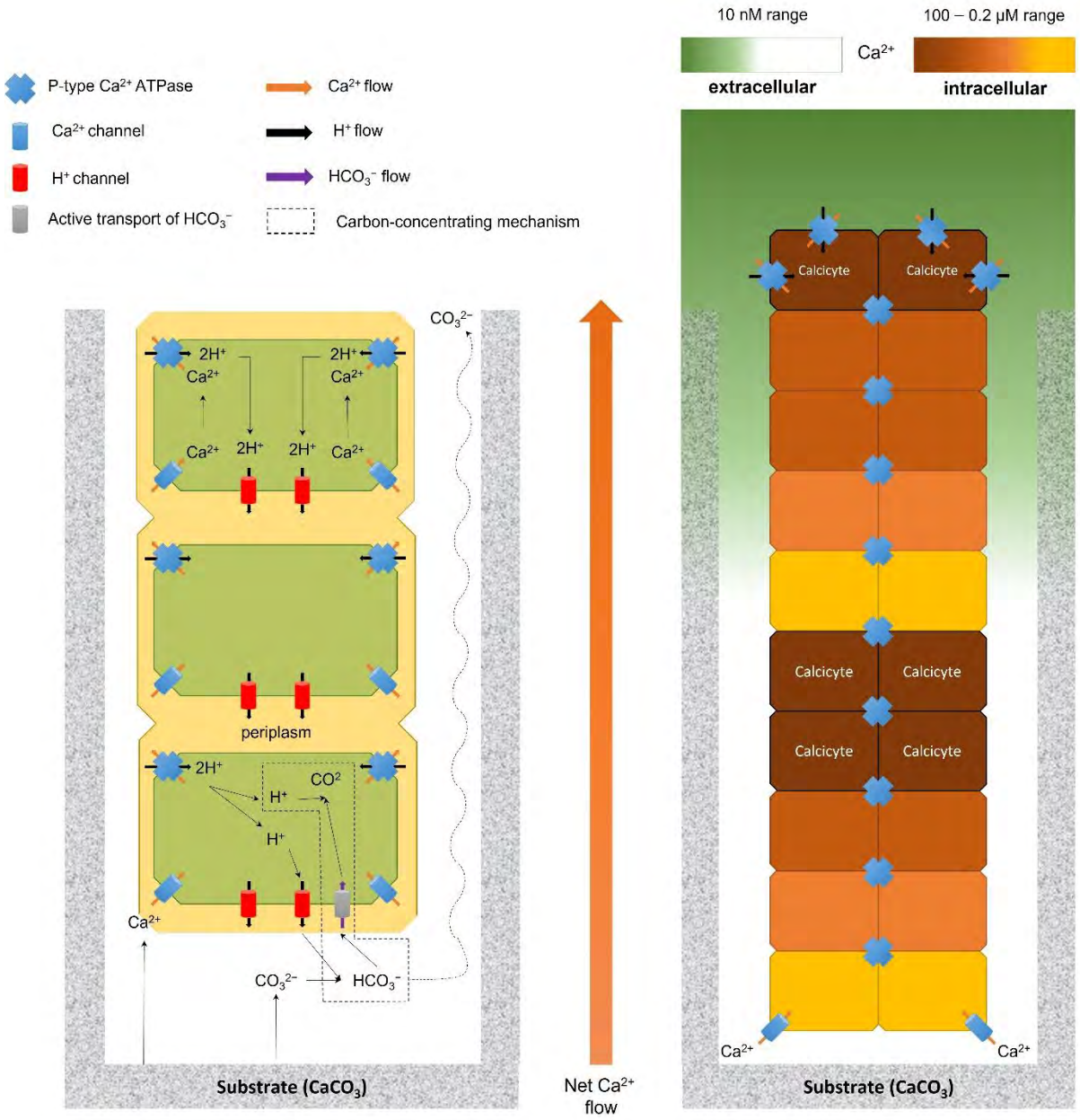

Figure 2.2. (Right panel). Proposed 'Calcium Pump' transport mechanism within the trichome of euendolithic cyanobacteria (both filamentous and pseudofilamentous), with the inferred distributions of transporter components (legend in the upper left corner) and the potential fates of the calcite dissolution products (Ca^{2+} and CO_3^{2-}). The calcium transport unit consists of repeating individual bipolar cells, where one pole is specialized for calcium uptake and the opposite for calcium extrusion. Conversion of carbonate ions CO_3^{2-} released from calcite into HCO_3^- is promoted by the counter-transported protons. This HCO_3^- is then actively transported within the cell, where it is converted into CO_2 through the carbon-concentrating mechanisms and can then be used in photosynthesis (Reinfelder, 2011). **(Left panel)** Holistic calcium ion localization during boring, with relative calcium concentrations within each compartment indicated. Calcicytes allow a higher proportion of cells within the trichome to remain photosynthetically active by controlling intrafilamentous calcium flow (modified from Guida, 2016).

2.4. Incidence of photoautotrophic euendoliths in marine ecosystems

Photoautotrophic euendoliths have a cosmopolitan geographical distribution and have been recorded in a variety of habitats, including terrestrial (Ascaso et al., 1998; Friedmann et al., 1988), freshwater and volcanic lakes (Gaylarde et al., 2006; Huber and Jadin, 1892), brackish (Akpan, 1990), and marine environments (Cerrano et al., 2001; Schneider and Le Campion-Alsumard, 1999). Euendoliths are ubiquitous in the marine environment, occurring in enclosed seas, such as the Adriatic Sea (Ghirardelli, 2002) and the Mediterranean Sea (Ćurin et al., 2014; Pantazidou et al., 2006), in cold-temperate (Akpan and Farrow, 1984; Försterra et al., 2005; Wilkinson and Burrows, 1972), tropical waters (Le Campion-Alsumard et al., 1995a; Mao Che et al., 1996; Perry, 1998; Tribollet, 2008b), as well as in the Arctic and Antarctic (Cerrano et al., 2001; Meyer et al., 2020). Present essentially anywhere there is sufficient light to allow for photosynthesis and a carbonate substrate to bore into; euendolithic communities play an important role in ecological processes in the marine environment (Campbell, 1983; Schneider and Le Campion-Alsumard, 1999).

Although they appear to erode virtually all suitable substrates, the distribution of euendoliths and the composition of euendolithic communities are extremely variable and depend on light availability, the nature of the substrate, and a variety of abiotic and biotic environmental factors acting in synergy (Chacón et al., 2006; Chazottes et al., 1995; Gektidis, 1999).

2.4.1. Light availability

As photosynthetic organisms, light availability is the major determinant of euendolithic activity and distribution and has a strong influence on the composition of euendolithic

communities (Gektidis, 1999), reflecting the specific light requirements of different species (Tribollet et al., 2011). In most marine habitats, light availability is highly variable and is influenced by the topography of the area, the presence of 3D structures, the nature of the substrate, and water depth.

Euendoliths are more abundant, and erosion more severe, in microhabitats with high light availability, such as sun-exposed surfaces in the intertidal, mostly horizontal, and moderately inclined surfaces high on the shore (Gehman and Harley, 2019; Kaehler, 1999; Monsinjon et al., 2021; Zardi et al., 2009), or in shallow waters (Gektidis, 1999), compared to microhabitats with low light availability, such as down-facing and shaded substrates (Gektidis et al., 2007; Wisshak et al., 2011; Zardi et al., 2009). Reduction of light availability at polluted sites (Le Bris et al., 1998; Tribollet and Golubic, 2005) or in habitats at greater depths (Gektidis, 1999; Perry, 1998) similarly reduces euendolith abundance. Geographically, photoautotrophic euendoliths are more abundant, and erosion more severe, at lower latitudes than higher latitudes, in both the intertidal and underwater (Lourenço et al., 2017; Wisshak et al., 2011, 2005; Zardi et al., 2021). As boring by euendoliths is an active mechanism, it is often restricted to environmental conditions optimal for growth (Ramírez-Reinat and Garcia-Pichel, 2012). As solar irradiance increases and cloud cover decreases, the depth of the photic zone increases towards lower latitudes (Wisshak et al., 2005). At higher latitudes, temperatures and light availability are generally low and highly seasonal (Zardi et al., 2021), with a prolonged night and ice cover towards the poles (Cerrano et al., 2001; Meyer et al., 2021, 2020) and a condensed photic zone (Wisshak et al., 2011, 2005). Combined, these unfavourable environmental conditions slow down euendolithic infestation and limit photoautotrophic euendolithic communities to a few specialist species capable of coping with such adverse conditions.

While the composition of euendolithic communities shifts as light availability decreases with increasing depth, their bathymetric distribution is consistent around the world (see Tables 1 and 2 in Wisshak, 2012) (Bentis et al., 2000; Chazottes et al., 2002, 1995; Gektidis, 1999; Gektidis et al., 2007; Golubic et al., 1975; Hutchings, 1986; Radtke and Golubic, 2005; Vogel et al., 2000; Wisshak et al., 2011, 2005). Euendoliths are ubiquitous in the supratidal, intertidal, and wave spray zones (Golubic et al., 1984), where assemblages are dominated by cyanobacteria and chlorophytes, referred to as the CyChlo-association (Gektidis, 1999), in sediments (Perry, 1998) as well as mollusk shells and coral skeletons (Akpan and Farrow, 1984; Gektidis, 1999; Kaehler, 1999). In the shallow photic zones, the additional conchocelis stages of rhodophytes can be observed (CyChloRho-association) in the early stages of colonization (Gektidis, 1999). In the dysphotic zone or in shaded microhabitats, where light availability is dramatically reduced, only heterotrophs and low-light specialists amongst the photoautotrophs occur, forming the so-called OstPleHet-association (Akpan and Farrow, 1984; Gektidis, 1999; Golubic and Schneider, 2003). These include the cyanobacterium *Leptolyngbya terebrans* (Bornet & Flahault ex Gomont) Anagnostidis & Komárek, 1988 (formerly *Plectonema terebans* Bornet and Flahault ex Gomont, 1892) and the chlorophyte *Ostreobium queckettii* that have been recorded down to about 300 m (Kiene et al., 1995; Le Campion-Alsumard et al., 1982; Lukas, 1978). Finally, heterotrophic organisms (i.e., fungi and bacteria) dominate the benthic assemblages of the deep, aphotic zone. At a finer scale, different clades within the same euendolithic species can be distributed along a depth gradient, suggesting different physiological traits (Gutner-Hoch and Fine, 2011). Not only does the composition of euendolithic communities change with depth, but also with time, as mature euendolithic communities, even in shallow, clear waters, are dominated by the OstPleHet-association (Gektidis, 1999).

2.4.2. Nature of the substrate

Photoautotrophic euendoliths colonize a wide range of carbonate substrates, from compact limestone and loose sediments to living calcifying organisms or their fragmented remains (Golubic et al., 1975). Euendoliths have been recorded in the skeletons of corals (Försterra and Häussermann, 2008; Le Campion-Alsumard et al., 1995a; Tribollet, 2008a) and coralline algae (Ghirardelli, 2002; Reyes-Nivia et al., 2014; Tribollet and Payri, 2001), in the shells of mollusks (Kaehler, 1999; Mao Che et al., 1996; Tribollet et al., 2008) and brachiopods (Gaspard, 2011), in the tests of foraminifera (Golubic et al., 1984), in the calcareous tubes of annelids (Wilkinson and Burrows, 1972) and the plates of barnacles (Meyer et al., 2020), and in sclerosponges (Lukas, 1973).

Colonization by and distribution of euendoliths is intrinsically influenced by the nature and physical properties of the substrate, such as its mineralogy, porosity, translucency, density, or architecture (Chacón et al., 2006; Couradeau et al., 2017; Perry, 1998). While most euendoliths appear to be generalists, substrate preferences are found in some, such as the cyanobacterium *Mastigocoleus testarum* that bores into calcium carbonate substrates but not into other carbonates (Couradeau et al., 2017; Ramírez-Reinat and Garcia-Pichel, 2012). Skeletal remains of calcifying organisms are more susceptible to euendolithic infestation than other carbonate substrates (Perkins and Halsey, 1971; Perry, 1998; Rooney and Perkins, 1972; Schroeder, 1972), with the highest levels of an infestation occurring in the densest and least porous substrates. Within skeletal remains, the high-Mg calcite skeleton of crustose coralline algae is more susceptible to dissolution than the skeletons of massive or branching corals or bivalve shells, which are mostly composed of aragonite (Diaz-Pulido et al., 2014; Nash et al., 2013). In shallow waters, the depth of penetration of euendoliths in dead coral skeletons nearly approximates that in live bivalve shells (Chazottes et al., 1995;

Mao Che et al., 1996; Perry, 1998; Tribollet, 2008b). This is a result of the higher porosity and translucency of the coral skeleton (Tribollet, 2008a), and the presence of organic lamellae (i.e., conchiolin) within bivalve shells that slow down excavation by photoautotrophic euendoliths (Rooney and Perkins, 1972). Only heterotrophic euendoliths, such as fungi, can penetrate and proliferate into organic lamellae, as they feed on the organic matter (Golubic et al., 2005; Mao Che et al., 1996; Rooney and Perkins, 1972).

In live calcifying hosts (e.g., corals, coralline algae, bivalves), a wide range of defences prevents the colonization of the calcified parts by euendoliths. Coral skeletons are protected by the polyp tissue (Bentis et al., 2000; Gutiérrez-Isaza et al., 2015; Le Campion-Alsumard et al., 1995a), while coralline algae have the capacity of sloughing their protective epithelial cells to prevent biofouling (Keats et al., 1993). Bivalve, brachiopod, and other mollusk shells have a protective layer, the periostracum, which deters fouling organisms (Bers et al., 2010; Owen and Williams, 1969; Prusina et al., 2015; Scardino et al., 2003; Scardino and de Nys, 2004). Nonetheless, the incidence of euendolithic infestation in live calcifying organisms is high around the world, independent of the location or the substrate. Nearly all corals around the world have been recorded as infested by euendoliths (Försterra and Häussermann, 2008; Le Campion-Alsumard et al., 1995a; Lukas, 1973), while up to 90% of bivalve shells are infested on rocky shores worldwide (Ćurin et al., 2014; Gehman and Harley, 2019; Kaehler, 1999; Zardi et al., 2009). After the death of the calcifying organisms, colonization becomes more intense, as euendoliths do not have to overcome the active or passive defence mechanisms of the host or adjust their boring performances to carbonate accretion rates of living organisms (Gutiérrez-Isaza et al., 2015; Le Campion-Alsumard et al., 1995a; Perry, 1998; Tribollet and Payri, 2001). In newly

available dead carbonate substrates, a succession of microborer communities can be observed, boring from the surface down into the substrate (Fine et al., 2006; Grange et al., 2015; Le Campion-Alsumard et al., 1995a; Odum and Odum, 1955): (i) pioneer species, such as the large chlorophyte *Phaeophila* sp. Hauck, 1876 and the cyanobacterium *Mastigocoleus testarum*, settle within the first three months, (ii) these are followed by an intermediate stage, between three and six months, where the chlorophyte *Ostreobium* sp. starts to dominate euendolithic communities, and (iii) the final stage, largely dominated by *Ostreobium*, after more than six months of exposure.

2.4.3. Biotic and abiotic environmental factors

In addition to light, biotic, and abiotic environmental factors can act in synergy to influence the composition and density of euendolithic communities, as well as their rates of microbioerosion. In the intertidal, the abrasive effects of sand and other sediments carried by the winds or the waves favour the initial colonization of the substrate by euendoliths, and ultimately increase the severity of infestation in mussels (Kaehler, 1999). Meanwhile, in shallow waters, nutrient concentration, epilithic cover, and the presence of macroborers and macrograzers interact to shape euendolithic communities (Chazottes et al., 1995; Fordyce et al., 2020; Le Campion-Alsumard, 1979; Tribollet and Golubic, 2011). This interaction operates through several mechanisms:

1. Photoautotrophic euendoliths penetrate the substrate until they reach their compensation depth, where photosynthesis balances respiration, after which boring either stops or proceeds parallel to the surface (Chazottes et al., 1995; Schneider and Torunski, 1983; Vogel et al., 2000);
2. Grazers are attracted to the substrate by the presence of photoautotrophic euendoliths, as these represent a renewable source of food (Chazottes et al., 1995; Nicholson and Clements, 2020; Tribollet and Payri, 2001). The boring activity of

euendoliths weakens the superficial layers of the substrate, which can facilitate the settlement of macroborers with their own bioerosive activity, as well as grazing;

3. On the one hand, macrograzers constantly remove the superficial layers of the substrate, thus extending the depth to which the light can penetrate and, therefore, the depth to which the endoliths can bore, increasing microboring rates (Schneider and Torunski, 1983; Zubia and Peyrot-Clausade, 2001). Grazing also reduces the settlement and growth of epilithic organisms that compete with euendoliths for space and diminish light availability (Golubic and Schneider, 1979). On the other hand, macroborers excrete different waste products within the infested substrate, such as ammonium, phosphates, or CO_2. Such waste products act as fertilizer for euendolithic communities, which increase in abundance, biomass, and productivity in the vicinity of macroborers (Fordyce et al., 2020; Rice et al., 2020; Zubia and Peyrot-Clausade, 2001).

Under intense grazing pressure, euendolithic growth and boring rates cannot keep pace with the rapid removal of the substratum by grazers, resulting in lower microboring rates (Chazottes et al., 2002). If grazing exceeds euendolithic boring rates, the food resource is eventually exhausted, and the denuded surface must be recolonized: intense grazing impedes the development of euendolithic communities so that they rarely reach maturity (Chazottes et al., 2002; Kiene and Hutchings, 1994). Different groups of organisms are more or less efficient at grazing (Tribollet and Golubic, 2005). Sea urchins are efficient grazers compared to fish, and remove a larger portion of the carbonate substrate, resulting in a lower measurable boring activity of euendoliths in sites with higher densities of sea urchins than of fish (Chazottes et al., 2002; Pari et al., 2002, 1998; Tribollet and Golubic, 2005).

Depending on its nature, the epilithic communities covering the bored substrate can also influence the abundance and composition of euendolithic communities, by diminishing light availability and attracting/deterring macrograzers (Carreiro-Silva et al., 2005; Chazottes et al., 2002; Gektidis, 1999; Tribollet and Golubic, 2005; Vogel et al., 2000). With time, epiliths start to colonize the surface of the bored substrate and become denser, filtering out light for the underlying euendolithic communities. Interactions between epilithic cover and euendolithic communities are generally reported for substrates exposed for long periods of time, usually greater than six months (Carreiro-Silva et al., 2012, 2009; Gektidis, 1999; Vogel et al., 2000). Under low grazing pressure, the pioneer species *Mastigocoleus testarum* dominates euendolithic communities on experimental substrates covered with algal turfs, joined by the low-light specialists *Leptolyngbya terebrans* and *Ostreobium queckettii* on shaded substrates covered with crustose coralline algae or macroalgae (Chazottes et al., 2002; Tribollet and Golubic, 2005). Depending on its nature, the epilithic cover can influence the intensity of macrograzing on the bored substrate: algal turfs attract macrograzers while crustose coralline algae and macroalgae, which are unpalatable or inedible for most grazers, act as a deterrent (Chazottes et al., 2002; Nicholson and Clements, 2020; Pari et al., 1998).

Nutrient concentrations in the surrounding environment influence the abundance, species composition, and microbioerosion rates of euendolithic communities, as well as the density and species composition of the epilithic communities (Chazottes et al., 2002; Le Bris et al., 1998). At sites subjected to eutrophication, microbioerosion rates by euendoliths are higher than in more oligotrophic waters, in association with either low (Chazottes et al., 2002) or high grazing pressure (Zubia and Peyrot-Clausade, 2001). Conversely, nutrient-enriched turbid inshore waters are characterized by lower microbioerosion rates compared to clear oligotrophic offshore waters at the Great Barrier

Reef, suggesting that increased turbidity resulting from the entrapment of sediments in the epilithic cover at inshore sites diminishes light availability and, thus, restricts euendolithic colonization, even at high nutrient concentrations (Tribollet and Golubic, 2005). Elevated concentrations of inorganic nutrients (e.g., nitrogen, phosphorus) drastically increase the severity of colonization, the depth of penetration, and ultimately the microbioerosion rates of euendolithic communities, especially in the absence of macrograzing (Carreiro-Silva et al., 2012, 2009, 2005). Different euendolithic taxa display variable responses to the addition of nutrients, depending on the nature of the nutrient and the specific limitations of the euendoliths; while heterotrophic euendoliths increase in abundance when exposed to increased levels of organic matter, euendolithic green algae and cyanobacteria react to higher levels of nitrogen and phosphate, respectively (Carreiro-Silva et al., 2012, 2009, 2005). In live calcifying substrates, the effects of nutrient addition on euendolithic communities can be mitigated by the host response to the same nutrients. For example, when phosphorus is added, the skeletal growth rates of hard corals increase and "dilute" euendolithic communities, as they are unable to keep up with increased coral growth (Godinot et al., 2012). Additionally, nutrient concentrations can influence the species composition and density of epilithic communities (Le Bris et al., 1998), with an indirect impact on the underlying euendolithic communities (Chazottes et al., 2002; Gektidis, 1999; Vogel et al., 2000). In coral reefs with low nutrient loads, the epilithic cover is dominated by algal turfs associated with pioneer euendolithic species that require high light intensities, while in reefs subjected to eutrophication, the dominance shifts to macroalgae and crustose coralline algae, diminishing light availability for an underlying euendolithic community abundant in low-light specialists (Chazottes et al., 2002).

2.4.4. Photoautotrophic euendoliths as bioindicators

With their specific niche specializations, in terms of nutrition, light, temperature, nutrient concentrations, and other physical parameters, and the characteristic microborings they produce, photoautotrophic and heterotrophic euendoliths can be used as present geographical, water quality, and paleobathymetric bioindicators at the species or community level (Golubic et al., 1984, 1975). Similarly, fossil euendoliths could potentially be used as indicators of past temperatures, salinity levels, or trophic dynamics, but more research is still needed (Wisshak, 2012). Some euendoliths, such as members of the genus *Ostreobium*, display a complex biogeographical distribution. *Ostreobium* has been found in abundance on temperate coasts but becomes rare in tropical waters (Perkins and Halsey, 1971; Rooney and Perkins, 1972), showing a clear latitudinal pattern. Within the genus, *Ostreobium queckettii* dominates endolithic assemblages in nearly all corals, while *O. constrictum* K.J. Lukas, 1974 and *O. brabantium* Weber Bosse, 1932 have only been found in the Atlantic and Pacific Oceans, respectively (Lukas, 1974). More recently, del Campo et al. (2017) revealed a complex biogeographical distribution of three identified clades within the genus *Ostreobium* across coral reefs. However, there is a need for more recent and detailed regional comparisons of the incidence of individual euendolithic species and the composition of euendolithic assemblages, as advances in molecular genetic techniques and the use of polyphasic approaches allow better detection and taxonomic identification of euendolithic specimens (Chacón et al., 2006; Marcelino and Verbruggen, 2016; Ricci et al., 2021).

Photoautotrophic euendoliths have the potential to be employed as indicators of water quality and/or pollution (Al-Thukair, 2002; Carreiro-Silva et al., 2012, 2009, 2005; Cherchi et al., 2012). The composition of euendolithic communities shifts depending on the concentrations of inorganic nutrients and organic matter in the surrounding

environment (Carreiro-Silva et al., 2012, 2009, 2005). In the Arabian Gulf, oil pollution is responsible for a dramatic decrease in the abundance of live euendoliths and microbioerosion rates on foraminifera (Al-Thukair, 2002), while in Italy, benthic foraminifera demonstrate increased levels of euendolithic infestation by photoautotrophic euendoliths in sites with heavy metal pollution (Cherchi et al., 2012, 2009).

Modern euendolithic bathymetric distribution can be reliably used as an indicator of the current depth, as it can be cross-checked by direct measurements of the physical parameters. Through their boring activity, microbial euendoliths leave traces, as an "instant fossil" in the sedimentary record, each with its own bathymetric range (Golubic et al., 1984) and remarkable constancy through time. While single fossil traces can be used for the identification of individual ichnotaxa, the study of euendolithic trace communities (or ichnocoenoses) within the substrate allows for paleobathymetric and paleoecological reconstructions over geological time scales (Glaub et al., 2001; Golubic et al., 1975). The light-dependence of photoautotrophic euendoliths thus reveals itself as a useful tool to determine the limit between past photic and aphotic zones (Glaub et al., 2001). The study of fossil trace assemblages in paleodepth reconstruction allows for a finer detection of past sea level variations than other commonly used methods (Chazottes et al., 2009), such as the analyses of the successive coralgal communities (Cabioch et al., 1999). However, fossil microborings should be compared with modern microborings from similar substrate types (Chazottes et al., 2009; Vogel et al., 2000) and the ichnocoenoses described must be directly compared with modern assemblages for interpretation (Golubic et al., 1975). Indeed, a bathymetric ichnocoenoses index could provide misleading paleobathymetric conclusions in shallow waters when 3D-underwater structures (e.g., reefs) create heterogeneous light conditions

on the infested substrate (i.e., illuminated, shaded, and cryptic habitats) at the same depth (Försterra et al., 2005; Gektidis et al., 2007; Perry and Macdonald, 2002). Similarly, the investigated substrate could have been translocated from shallow depths to its deposition site (Wisshak, 2012). Thus, fossil microborings should be viewed as semiquantitative rather than absolute indicators of paleophotic zones (Perry and Macdonald, 2002; Swinchatt, 1969).

2.5. Photoautotrophic euendoliths in marine bioengineered ecosystems

While numerous studies have assessed euendolith-induced biodegradation of carbonate skeletal materials, until recently, severe harm to living host organisms was understood to be limited to the erosive activity of invertebrates or fungal borers (Lauckner, 1983). Due to low light penetration within the substratum, photoautotrophic euendoliths were generally thought to be unable to inflict significant structural damage on live organisms, as they eroded only the uppermost layers of the carbonate substrate (Lauckner, 1983). Over the last three decades, mounting evidence has shown that the eroding activity of photoautotrophic euendoliths can be the source of severe, often lethal, damage to living calcifying organisms (Hassenrück et al., 2013; Kaehler and McQuaid, 1999; Zardi et al., 2009). However, the presence of euendoliths has also been observed to have beneficial effects (Fine and Loya, 2002; Gehman and Harley, 2019; Zardi et al., 2016).

Here, this study focuses on three groups of calcifying organisms, i.e., corals, crustose coralline algae, and bivalves, and describe the process of colonization by euendoliths in live hosts, their incidence, and their detrimental and beneficial effects on the individual host, as well as on the bioengineered ecosystem (summarized in Table 2.1), i.e., coral reefs, coralline algal mats, and bivalve beds (Diaz-Pulido et al., 2014; Reyes-Nivia et al., 2014).

Table 2.1. Summary of the negative and positive effects observed and suspected (underlined) of euendolithic infestation on the physiological parameters, calcified structures, biological interactions, and bioengineering qualities of main live calcifying hosts.
Symbols for effects: (=)—no effect; (↑)—positive effect, reinforcement; (↓)—negative effect, reduction; (↑↓)—variable responses depending on the host species and/or environmental conditions; (~)—alteration in the composition of the parameter; (✝)—mortality observed in the host species; (↔)—mutualistic relationship; (lim)—effect observed during unusual harsh environmental conditions (i.e., heatwaves). Please note that some effects presented in this table are based on observations of a single species or different life cycle stages of the host species. Other live calcifying hosts of photoautotrophic euendoliths include soft corals, other marine molluscs (i.e., limpets, snails), barnacles, brachiopods, and foraminifera.

Responses to Endolithic Infestation	Live Calcifying Hosts				References
	Corals	Coralline Algae	Bivalves	Others	
Physiological Parameters					
Growth	↓ =		↓	↓	Curry, 1983; Hassenrück et al., 2013; Kaehler and McQuaid, 1999; Massé et al., 2020; Ndhlovu et al., 2021a; Prusina et al., 2015
General condition	=		↓		Ćurin et al., 2014; Kaehler and McQuaid, 1999; Marquet et al., 2013; Massé et al., 2018; Schlichter et al., 1997, 1995; Zardi et al., 2009
Reproduction			↓	=	Goldberg et al., 1984; Kaehler and McQuaid, 1999; Ndhlovu et al., 2022, 2021a
Attachment strength			↓		Marquet et al., 2013; Ndhlovu et al., 2022; Zardi et al., 2009
General survival	↥ =		↓ ✝	↓	Kaehler, 1999; Kaehler and McQuaid, 1999; Massé et al., 2020; Ndhlovu et al., 2022; Nicastro et al., 2019; Nolan, 1991; Odum and Odum, 1955; Prusina et al., 2015; Schlichter et al., 1997, 1995
Individual survival to heat stress	↑ (lim)		↑ (lim)		Fine et al., 2005, 2004; Fine and Loya, 2002; Gehman and Harley, 2019; Lourenço et al., 2017; Monsinjon et al., 2021; Zardi et al., 2021, 2016
Calcified structures					
Microbioerosion	↑	↑↓	↑	↑	Curry, 1983; Gehman and Harley, 2019; Kaehler and McQuaid, 1999; Le Campion-Alsumard et al., 1995a; Prusina et al., 2015; Reyes-Nivia et al., 2013, 2014; Tribollet and Payri, 2001
Thickness	↑		↓ ✝	↓	Försterra et al., 2005; Hassenrück et al., 2013; Kaehler and McQuaid, 1999; Prusina et al., 2015

Table 2.1. (continued).

Responses to Endolithic Infestation	Live Calcifying Hosts				References
	Corals	Coralline Algae	Bivalves	Others	
Calcified structures (suite)					
Porosity	↑	↑	↥		Gehman and Harley, 2019; Hassenrück et al., 2013; Le Campion-Alsumard et al., 1995a; Tribollet and Payri, 2001
Deformations	↑		↑ ☩	↑	Ćurin et al., 2014; Goldberg et al., 1984; Hassenrück et al., 2013; Kaehler, 1999; Le Campion-Alsumard et al., 1995b; Morse et al., 1981, 1977
Maintenance costs	↥		↑	↥	Ćurin et al., 2014; Försterra et al., 2005; Hassenrück et al., 2013; Kaehler and McQuaid, 1999; Le Campion-Alsumard et al., 1995b; Ndhlovu et al., 2021a; Prusina et al., 2015
Mineralogy		~	≃		Ćurin et al., 2014; Diaz-Pulido et al., 2014
Biological interactions					
Epibionts			↥		Marquet et al., 2013
Predators	↥		↥		Zardi et al., 2009
Grazers	↥		↥	↑	Nicholson and Clements, 2020; Nolan, 1991
Photoautotrophic euendoliths	↔	↔	↔		Gehman and Harley, 2019; Hassenrück et al., 2013; Odum and Odum, 1955; Schlichter et al., 1997, 1995; Tribollet and Payri, 2001
Bioengineered ecosystems					
Architectural complexity		↑↓	↓		Diaz-Pulido et al., 2014; Reyes-Nivia et al., 2014
Coastal protection from waves and other stressors	↓	↑↓	↓	↓	Diaz-Pulido et al., 2014; Nicastro et al., 2019; Nolan, 1991; Reyes-Nivia et al., 2014, 2013; Zardi et al., 2009
Mitigation of environmental stressors for associated species			↥		Lourenço et al., 2017; Monsinjon et al., 2021; Zardi et al., 2021
Resistance to anthropogenic stressors			↓		Nicastro et al., 2022, 2019

2.5.1. Corals and crustose coralline algae

In live corals, the colonization of the skeleton by euendoliths from the water column is prevented by the polyp tissue (Bentis et al., 2000; Gutiérrez-Isaza et al., 2015; Le Campion-Alsumard et al., 1995b). In young coral recruits, the entire corallite (i.e., part of the skeleton elaborated by a single polyp) is tightly covered with polyp tissue (Försterra and Häussermann, 2008; Massé et al., 2018; Stolarski, 1996), which efficiently protects the underlying calcareous skeleton from infestation by other life stages of endolithic organisms (e.g., propagules, epilithic biofilms), thanks to its superficial mucus and cnidocysts. In some instances, the polyp tissue retracts towards the proximal portions of the coral colony, either temporarily when corals are under major thermal stress (Brown et al., 1991) or permanently in the case of solitary corals (Lazier et al., 1999), leaving the skeleton unprotected. Therefore, photoautotrophic euendoliths have the ability to colonize the coral skeleton from its base, as soon as the larvae settle on an already-infested substrate (Massé et al., 2018), or to enter through the exposed skeleton through lateral fissures or when the polyp tissue retracts (Brown et al., 1991; Lazier et al., 1999). In live crustose coralline algae (Corallinophycidae), colonization by photoautotrophic euendoliths from the surface is prevented by the presence of live cells (as for corals), capable of 'sloughing' as a defence against biofouling (Keats et al., 1993; Steneck, 1986). With crustose coralline algae (CCA) growing apically, the live tissue remains in the upper part of the thallus, giving it a red colour, leaving empty calcified cell walls at the basal layer of the thallus, which turns whitish-grey (Ghirardelli, 2002; Tribollet and Payri, 2001). Without the protective live tissue, euendoliths colonize CCA from its basal layer, which can be in direct contact with an already-infested substrate (Ghirardelli, 2002; Tribollet and Payri, 2001). Thereafter, photoautotrophic euendoliths have to match or exceed skeletal calcification

rates, by positive phototrophic growth orientation (i.e., growing from the inside of the skeleton towards the surface) and high rates of growth and carbonate penetration (Le Campion-Alsumard et al., 1995a; Tribollet and Payri, 2001). Only a few euendolithic organisms have adapted to low-light conditions, such as the cyanobacterium *Leptolyngbya terebrans*, the chlorophyte *Ostreobium queckettii*, and less frequently some conchocelis stages of Bangial rhodophytes, are known to keep pace with coral growth (Gutiérrez-Isaza et al., 2015; Gutner-Hoch and Fine, 2011; Laborel and Le Campion-Alsumard, 1979; Le Campion-Alsumard et al., 1995b, 1995a; Lukas, 1974; Ralph et al., 2007). In addition, the cyanobacterium *Mastigocoleus testarum* can be found in live CCA crusts (Försterra and Häussermann, 2008; Ghirardelli, 2002; Tribollet and Payri, 2001), and *L. terebrans* has been observed boring directly into CCA calcified cell walls (Ghirardelli, 1998). Areas of dense euendolithic growth are often correlated with areas of slower growth in corals, as shown by the patterns of coloured bands in massive, slow-growing corals (Delvoye, 1992; Duerden, 1902; Highsmith, 1981; Le Campion-AIsumard et al., 1995a). In fast-growing corals, such patterns are less clear (Tribollet et al., 2018), with euendoliths being more abundant in the middle part of the skeleton (Godinot et al., 2012). The distribution of euendolithic organisms is, however, not limited to the coloured bands as they can be present in most regions of the skeleton although in insufficient densities to be visible (Le Campion-Alsumard et al., 1995a). In the same fashion, euendolithic infestation in live CCA crusts forms a green band underneath the live tissue (Tribollet and Payri, 2001). Photoautotrophic euendoliths are ubiquitous in live zooxanthellate corals (Symbiodiniaceae (LaJeunesse et al., 2018)), with 100% of Atlantic, Indian, and Pacific corals being infested (Duerden, 1902; Highsmith, 1981; Le Campion-Alsumard et al., 1995a; Lukas, 1973; Odum and Odum, 1955). In the southern Chilean fjords, 83% of the colonies of the azooxanthellate

Desmophyllum dianthus (Esper, 1974) were infested in the euphotic zone (Försterra and Häussermann, 2008). Photoautotrophic euendoliths have been recorded from live crustose coralline algae in the Mediterranean Sea and the Pacific Ocean (Ghirardelli, 2002; Tribollet and Payri, 2001).

The negative effects of endolithic infestation on live corals have largely been demonstrated in azooxanthellate corals, which do not benefit from a symbiosis with zooxanthellae. However, given their similar calcification rates (Marshall, 1996), it is reasonable to expect that azooxanthellate and zooxanthellate corals will display similar negative effects to infestation by photoautotrophic euendoliths. Euendolithic infestation affects apical growth and skeletal structure of adult coral colonies (Hassenrück et al., 2013); however, it does not slow the extension rates and fitness of coral recruits (Massé et al., 2018). Heavily infested areas of the coral *Desmophyllum dianthus* display a thicker but more porous skeletal structure, reduced apical extension, and enhanced skeletal deformations (Hassenrück et al., 2013). Thus, euendolithic infestation alters the calcification pattern of the coral and unbalances the energetic budget towards the maintenance of skeletal integrity, at the expense of the vertical growth of the polyp and other essential biological processes, such as reproduction. Skeletal deformations, resulting from the secondary deposition of aragonite on the coral skeleton, can act as a mechanical barrier to endolithic infestation (Hassenrück et al., 2013; Le Campion-Alsumard et al., 1995b), but are linked to increased coral mortality and reduced coral growth and reproduction, thus reducing the overall fitness of the coral (Aeby et al., 2011; McClanahan et al., 2009). As a source of food for grazing organisms (Golubic et al., 1984), euendoliths attract excavating invertebrates and vertebrates, enhancing overall bioerosion activity in coral reefs and leading to deeper damage to the substrate (Chazottes et al., 1995; Tribollet and

Golubic, 2005). Finally, filamentous cyanobacteria associated with the Black Band Disease have been observed actively boring through both coral skeleton and tissue, indicating a potential relationship between endolithic organisms within the coral skeleton and coral diseases (Miller et al., 2011). As euendoliths accelerate internal bioerosion rates in CCA, their infestation is likely to increase CCA porosity (Tribollet and Payri, 2001), with consequences similar to those in corals. As microbioerosion is lower in CCA than in corals (7.9% vs. 25% of the bored substrate) (Le Campion-Alsumard et al., 1995a; Tribollet and Payri, 2001), its negative effects on CCA might also not be detectable or significant.

As early as the 1950s, Odum and Odum (1955) suspected another kind of relationship between photoautotrophic euendoliths and their live coral hosts, one that is positive and mutualistic rather than negative, which they termed 'ectosymbiosis'. Forty years later, Schlichter et al. (1995) first demonstrated the translocation of photoassimilates from the euendolithic algae living in the coral skeleton to the coral tissue via the uptake mechanisms for dissolved organic substances of cnidarians in the azooxanthellate coral *Tubastraea micranthus* (Ehrenberg, 1834). This interaction increases the polyp's fitness by increasing productivity and biomass, while in return, the metabolic end products of the coral can be used by the endolithic algae. Subsequently, Schlichter et al. (1997) highlighted the role of the green euendolithic alga *Ostreobium queckettii* in intra-colonial nutrient recycling in two zooxanthellate coral species, though this was considered to be minor compared to the contribution made by zooxanthellae.

In live coral skeletons, three main factors influence the availability of light to euendolithic organisms (Highsmith, 1981; Kanwisher and Wainwright, 1967):

1. Between 0.1 and 10% of the photosynthetically active radiation (PAR) penetrates and reaches the zone of the endolithic algae, the main part of PAR being absorbed by the zooxanthellae in the coral tissue (Halldal, 1968; Magnusson et al., 2007; Schlichter et al., 1997; Shibata and Haxo, 1969);
2. Light transmission is affected by the architecture of the coral's skeleton. Corallites on the top of coral colonies guide light deeper into the coral skeleton, while for corallites on the side of the colony, light enters at an angle, reducing its penetration into the skeleton (Highsmith, 1981);
3. Water depth.

Low light intensities within the coral skeleton suggest an adaptation to shaded environments for euendoliths and, thus, low euendolithic photosynthetic production and a low contribution to the metabolism of healthy zooxanthellate corals (Kanwisher and Wainwright, 1967; Ralph et al., 2007; Schlichter et al., 1997; Shashar and Stambler, 1992). For example, respiration and photosynthetic rates of endolithic algae in the zooxanthellate coral *Porites compressa* Dana (1846) represent, respectively, only 1.4% and 6% of those of the zooxanthellae, corresponding to the amount of PAR effectively reaching the endoliths (Schlichter et al., 1997; Shashar and Stambler, 1992). During bleaching events, however, corals lose their symbiotic zooxanthellae and their shading effect to the endolithic layer (Figure 2.3c,d). Photoautotrophic euendoliths then acclimate to the increased solar irradiance penetrating the skeleton (Fine et al., 2005) and start blooming (Galindo-Martínez et al., 2022). Two to three weeks after the onset of bleaching, characteristic greenish (*Ostreobium queckettii*) and reddish (*Leptolyngbya terebrans*) pigments of photoautotrophic euendoliths become visible through the now transparent coral tissue (Figure 2.3d) (Fine and Loya, 2002; Försterra et al., 2005; Försterra and Häussermann, 2008). Following this increase in

photosynthetic activity, increased quantities of photoassimilates are continuously translocated between the euendoliths and the coral tissue, thanks to the close contact between euendolithic filaments and coral tissue; the cytoplasmic compartments of corals and euendolithic algae are only separated by a cell membrane and by a cell wall and membrane, respectively (Schlichter et al., 1995). On the one hand, due to the capacity of coral cells to absorb dissolved organic substances, such as sugars and amino-acids (Schlichter, 1984), these photosynthetic products can be readily used by the coral tissue when released by euendoliths, and contribute to the metabolic demands of the coral, especially during bleaching events (Fine and Loya, 2002; Kühl et al., 2008; Schlichter et al., 1995). On the other hand, euendoliths may benefit from the internal CO_2 pool and nitrogen-containing metabolites of the coral, using these as a source of inorganic carbon for photosynthesis and nitrogen, respectively (Titlyanov et al., 2008). Although euendolithic sources of energy are nutritionally less important than those of zooxanthellae (Kühl et al., 2008; Schlichter et al., 1997) and insufficient to support sexual reproduction by the coral (Fine et al., 2001), the bloom of euendolithic organisms in the coral skeleton can promote the survival of zooxanthellate corals during bleaching events until new zooxanthellae are recruited (Galindo-Martínez et al., 2022). In the event of a rapid bleaching event, however, high light intensities coupled with high temperatures cause the photoinhibition of euendolithic activity (Fine et al., 2005). Moreover, the increased abundance of euendoliths in the coral skeleton during bleaching events can result in a corresponding increase in bioerosion rates, further increasing the porosity of the coral skeleton (Tribollet and Golubic, 2011). Thus, photoautotrophic euendolithic communities can sustain coral survival through a critical supply of organic carbon and nutrients during periods of environmental change but slowly weaken the structural integrity of the coral skeleton, increasing its vulnerability to mechanical

damage. Conversely, in live CCA crusts, euendolithic infestation can reduce the susceptibility of CCA skeletons to dissolution, especially under ocean acidification and global climate change (Diaz-Pulido et al., 2014; Reyes-Nivia et al., 2014). Through their boring activity, photoautotrophic euendoliths remove highly soluble magnesium calcite from the skeleton, indirectly increasing internal interstitial pH (Reyes-Nivia et al., 2013), thereby promoting internal secondary precipitation of minerals (Nothdurft and Webb, 2009) and increasing the relative abundance of dolomite in the skeleton (Diaz-Pulido et al., 2014). CCA skeletons rich in dolomite are less susceptible to dissolution and skeletal disruption (Diaz-Pulido et al., 2014; Nash et al., 2013), as dolomite is a more stable form of carbonate and some euendoliths (such as *Mastigocoleus testarum*) are unable to bore through it (Ramírez-Reinat and Garcia-Pichel, 2012). Because live CCA crusts are only moderately bored compared to corals, it appears that the beneficial effects of euendolithic infestation could largely outweigh their negative effects, even under heat and acidification stress.

Coral reefs are amongst the most diverse and complex marine ecosystems in the world, providing a habitat for countless associated species (Knowlton et al., 2010), as well as providing many services to mankind, such as commercial fishing, tourism, and coastal protection against storms and cyclones (Harmelin-Vivien, 1994; Knowlton et al., 2010). In tropical reefs, CCA are critical biological and geological components (Steneck, 1986), cementing together sand, dead corals, and debris to create a stable substratum (Littler and Littler, 1995). This substratum facilitates the settlement of coral larvae and other invertebrates of commercial value, such as abalone and sea urchins (Diaz-Pulido et al., 2014; Harrington et al., 2004; Hayakawa et al., 2008). Overall, the maintenance of healthy coral reef ecosystems is critically dependent on the balance between constructive forces, such as calcification by corals and encrusting coralline

algae, and destructive forces, including bioerosion (Scoffin et al., 1980). Severe euendolithic infestation of individual coral skeletons can fragilize whole coral reefs, increasing their susceptibility to damage by cyclones and storms (Harmelin-Vivien, 1994), El Niño events (Eakin, 1996; Glynn, 1994), and predators, such as the crown-of-thorns starfish (Musso, 1994), and diminishing the coastal protection they offer to other ecosystems and mankind. However, during extreme heat waves, euendolithic infestation of corals can mitigate the effects of bleaching and promote coral survival (Fine et al., 2005; Fine and Loya, 2002; Schlichter et al., 1997, 1995). In live CCA crusts, euendolithic infestation promotes long-term survival by altering the mineralogical composition of the skeleton (Diaz-Pulido et al., 2014; Nash et al., 2013). Finally, by affecting the inanimate substrates composing the ecosystem as well, endolithic infestation plays a role in shore bioerosion in interaction with grazers (Tribollet and Golubic, 2005). For more detail about the role of boring microflora in modern coral reef ecosystems, see Tribollet (2008a).

2.5.2. Bivalves

In live bivalves, the colonization of the shell by photoautotrophic euendoliths is prevented by the periostracum, a well-defined external proteinaceous coating of variable thickness that constitutes the outermost layer of the shell (Figure 2.3a) (Akpan, 1990; Kaehler, 1999; Kaehler and McQuaid, 1999; Raghukumar et al., 1991). The early developmental stages of bivalves are largely free of endoliths (Cerrano et al., 2001; Zardi et al., 2009), as their protective periostracum is still intact. Over time, the periostracum can be abraded, by contact with neighboring mussels within a bed and/or by sediment particles carried by waves (Kaehler, 1999; Zardi et al., 2009) or by the activity of macrograzers (Cerrano et al., 2001). Once the periostracum is removed, photoautotrophic euendoliths colonize the bivalve shell from the outside in, in a similar

fashion to dead substrates. This involves a succession of microboring species through time (Kaehler, 1999; Mao Che et al., 1996; Ndhlovu et al., 2021b): (i) pioneer species within the first months, such as the cyanobacteria *Mastigocoleus testarum* and *Leptolyngbya terebrans*, and the chlorophyte *Phaeophila* sp., (ii) an intermediate stage after the pioneer species are established, with the addition of the cyanobacterium *Solentia stratosa* Ercegovic, 1927, and (iii) a late successional stage, after more than six months of exposure, with the addition of the cyanobacteria *Hyella* sp. Bornet and Flahault, 1888 and/or *Pleurocapsa* sp. Thuret, 1885, and the chlorophyte *Ostreobium queckettii*, which replaces *Phaeophila*. In some instances, infested bivalve shells take a greenish colour when euendolithic infestation is dense (Akpan, 1990; Cerrano et al., 2001). The spatial distribution of cyanobacterial euendoliths in bivalve shells reflects this succession in time, as the last colonizers are only found towards the older parts of the shell, where they co-occur with pioneer species (Ndhlovu et al., 2021b). The succession of microborer communities does not necessarily involve the replacement of euendolithic species by others (Mao Che et al., 1996), but rather their addition (Kaehler, 1999; Ndhlovu et al., 2021b). Consequently, euendolithic infestation is stronger on the oldest parts of the shell (i.e., umbo and central shell), and with increasing shell length, as a proxy of age (Cerrano et al., 2001; Ćurin et al., 2014; Kaehler and McQuaid, 1999; Lourenço et al., 2017; Mao Che et al., 1996; Marquet et al., 2013). Most studies have focused on the succession of cyanobacterial euendolithic communities on bivalve shells (Kaehler, 1999; Ndhlovu et al., 2021b), so less detail is available for chlorophytes and other photoautotrophic euendoliths (Alfaro et al., 2008; Ćurin et al., 2014; Mao Che et al., 1996). Photoautotrophic euendoliths colonize intertidal bivalve shells around the world, independent of their location or the nature of the shore (Cerrano et al., 2001; Kaehler, 1999; Ndhlovu et al., 2019). On South African

rocky shores, the incidence of endolith-infested shells in the brown mussel *Perna perna* and the blue mussel *Mytilus galloprovincialis* varied between 23% and 95% on sheltered shores within bays and on shores exposed to the open ocean, respectively (Kaehler, 1999; Ndhlovu et al., 2019; Zardi et al., 2009). In California, between 60% and 90% of the shells of the Californian mussels, *Mytilus californianus* Conrad, 1837, were infested by euendoliths, depending on their position with respect to height on the shore (Gehman and Harley, 2019), while 93% of the shells of the bearded horse mussel, *Modiolus barbatus* Linnaeus (1758), were infested in the Adriatic Sea (Ćurin et al., 2014).

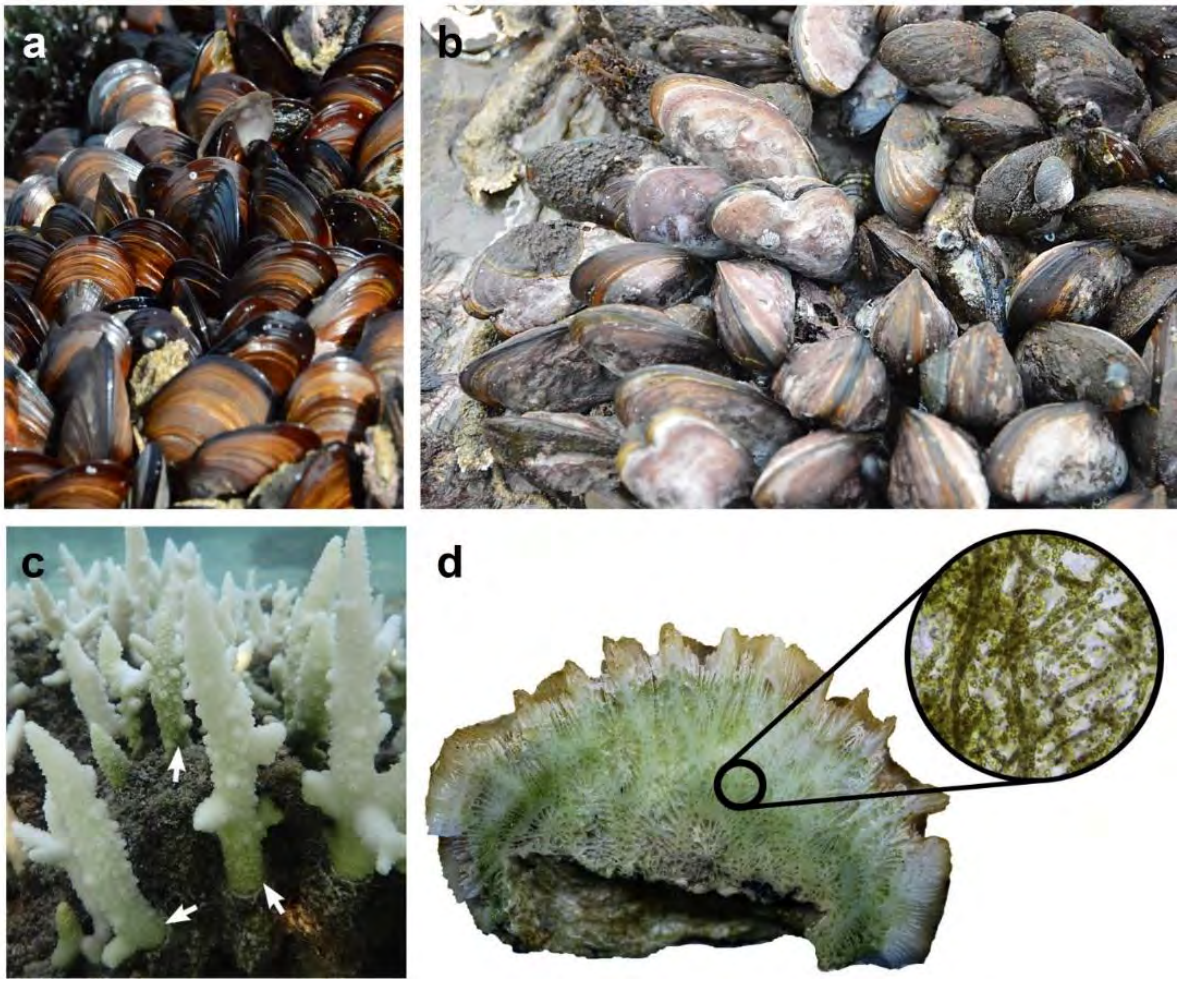

Figure 2.3. Signs of infestation by euendolithic microborers in live marine calcifiers. (a) Non-infested *Perna perna* bed. (b) *Perna perna* mussels showing extremely eroded shells due to the action of euendolithic cyanobacteria. (c) Bleached coral with evident *Ostreobium* bloom (indicated by white arrows). (d) Cross-section of *Paragoniastrea australensis* coral showing *Ostreobium* that inhabits the skeleton. The inset shows *Ostreobium* filaments after skeletal decalcification. Copyright: © Alexia DIEVART (a,b), © Alexander Fordyce (c). Images (c,d) from Iha et al. (2021).

As euendoliths bore into the shell, bivalves need to repair the shell and maintain carbonate structures through secondary carbonate deposition (Kaehler and McQuaid, 1999), an energetically demanding process requiring 25–50% of their energy budget (Gardner and Thomas, 1987; Griffiths and King, 1979). The bivalve's energetic budgeting then shifts towards self-repair with time, at the expense of growth, reproduction, attachment strength, and overall condition (Alfaro et al., 2008; Kaehler and McQuaid, 1999; Ndhlovu et al., 2022, 2021a; Zardi et al., 2009). The severity of euendolithic infestation and its negative effects on bivalves is, however, species-specific. In South Africa, the invasive blue mussel, *Mytilus galloprovincialis*, exhibits greater infestation levels and negative effects than the native brown mussel, *Perna perna* (Ndhlovu et al., 2019; Zardi et al., 2009). Regardless of the rate of shell deposition in infested bivalves (up to two times that of non-infested bivalves), it is never enough to compensate for the degradation caused by euendoliths (Kaehler and McQuaid, 1999). Ultimately, infestation becomes so severe that bivalves fracture their own shells with the force applied by their adductor muscles (Kaehler, 1999). Thus, endolithic infestation can at times account for more than 50% of total mortality in highly infested populations (Kaehler and McQuaid, 1999).

Moreover, damage to the individual bivalve exceeds simple structural damage and has critical consequences at the population and community levels. Through their boring activity, euendoliths reduce shell strength and thickness, increasing vulnerability to predation, wave action (Kaehler and McQuaid, 1999), or trampling (Nicastro et al., 2019). Similarly, shell microtopography and its antifouling characteristics (Bers et al., 2010) can be altered by euendoliths, which could lead to higher settlement of epibionts such as barnacles (as hypothesized in Marquet et al., 2013). Infestations by larger epibionts increase a bivalve's vulnerability to

drag forces and predators (Wahl, 2008), while these epibionts' boring actions could further enhance euendolithic infestation (Marquet et al., 2013; Thieltges and Buschbaum, 2007). In addition, by creating a more complex, rougher shell surface, euendolithic infestation influences the hydrodynamic properties of mussel beds, leading to greater ingestion rates of microplastics by mussels within infested mussel beds, and greater retention of microplastic on infested mussel shells and within infested mussel beds (Nicastro et al., 2022). Moreover, infested mussels produce fewer byssal threads for attachment to the substratum, making them more vulnerable to drag forces (Ndhlovu et al., 2022; Zardi et al., 2009) and creating an architecturally less complex mussel bed for the associated infauna. Gonad mass, and thus reproductive capacity, are also negatively affected by euendolithic infestation (Alfaro et al., 2008; Kaehler and McQuaid, 1999; Ndhlovu et al., 2022; Zardi et al., 2009). Larger mussels, responsible for the bulk of gamete output from the population, are the most susceptible to mortality through shell collapse and suffer the greatest decrease of gonad tissue due to endolithic infestation (Kaehler and McQuaid, 1999), thus reducing population reproductive output.

Shell-boring photoautotrophic euendoliths have, however, also been shown to have beneficial effects on the bivalve host under certain environmental conditions (Gehman and Harley, 2019; Lourenço et al., 2017; Zardi et al., 2016). Infested mussels lose their dark colour through the loss of the periostracum, which exposes the pale nacreous layer underneath and the deposition of excess calcium on the outside of the shell by euendoliths (Figure 2.3b) (Gehman and Harley, 2019; Kaehler, 1999; Ndhlovu et al., 2021b; Zardi et al., 2016). Infested mussel shells, being paler, absorb around 10% less sunlight energy than non-infested shells, resulting in lower body temperatures (up to 5°C lower) and greater water retention (Gehman and Harley, 2019; Zardi et al., 2016). During heat waves, infested mussels can experience lower short-term

mortality rates (Gehman and Harley, 2019; Zardi et al., 2016), as they warm up slower and reach lower body temperatures than non-infested mussels during aerial exposure (Zardi et al., 2021). The beneficial effects of endolithic infestation can extend to neighboring mussels within a bed: mussel beds mostly composed of infested mussels exhibit lower temperatures and higher humidity in the interstitial space (Lourenço et al., 2017; Zardi et al., 2021). The beneficial effects of euendoliths are regulated by particular topographic and meteorological conditions (Lourenço et al., 2017; Monsinjon et al., 2021; Zardi et al., 2021). Thermal buffering by euendoliths is greatest when bivalves occur on horizontal or moderately inclined, mostly sun-exposed, surfaces, and under conditions of high solar irradiance and air temperature, low wind speed, and moderate humidity (Monsinjon et al., 2021; Zardi et al., 2021). Thus, thermal buffering by euendoliths is the strongest and most ecologically significant when (and where) bivalves suffer from stressful environmental conditions, particularly in the summer and at lower latitudes (Lourenço et al., 2017; Monsinjon et al., 2021; Zardi et al., 2021). The protection offered to associated species by the bioengineering effects of mussel beds is thus likely to be enhanced by endolith-induced improvements in within-bed humidity and temperature, especially in the upper intertidal zone where mussel beds are typically mono-layered and thermal refuges are scarce (Gehman and Harley, 2019).

Worldwide, bivalves are the most prominent ecosystem engineers on intertidal rocky shores (Gutiérrez et al., 2003), providing a functional habitat and refuge to a wide array of associated species in a physiologically stressful environment characterized by high temperature and low humidity during emersion (Gutiérrez et al., 2003; Stephens and Bertness, 1991; Suchanek, 1985; Witman, 1985). Bivalve beds offer a refuge from thermal and desiccation stresses (Jurgens and Gaylord, 2018;

Stephens and Bertness, 1991), and predators (Thiel and Dernedde, 1994; Witman, 1985), a habitat for epibionts (Gutiérrez et al., 2003), and participate in the transport of solutes and organic particles in the near-shore environment (Crooks and Khim, 1999; Tsuchiya and Nishihira, 1985). Bivalve beds provide many ecosystem services, such as fishing, other resources, protection against the waves, and stabilization of the coastline (Borsje et al., 2011; Piazza et al., 2005). Euendolithic infestation of bivalve beds increases the susceptibility of these ecosystems to damage by waves and anthropogenic stressors, such as trampling and plastic pollution (Nicastro et al., 2022, 2019), while reducing their vulnerability to heat waves (Zardi et al., 2021, 2016).

2.5.3. Other groups

While limited information is available on the incidence and distribution of photoautotrophic euendoliths in calcifying organisms, the physiological, biological, and ecological impacts of endolithic infestation have not been documented outside of commercially or structurally important calcifiers, such as corals, CCA, and bivalves (see Tribollet, 2008a).

In soft corals, the chlorophytes *Ostreobium queckettii* and *Ulvella endozoica* (Goldberg, Makemson, and Colley) R. Nielsen, C.J. O'Kelly, and B.Wysor (2013) are associated with lower tensile strength and elasticity of the endoskeleton (Goldberg et al., 1984), and necrosis of the surrounding live tissue in two species of gorgonian corals (Morse et al., 1981, 1977). In brachiopods, the presence of conchocelis stages of the red algae *Porphyra* or *Bangia* recorded in the outer layer of the shell (Curry, 1983; Gaspard, 2011; Peck et al., 1987) was linked to the potential disruption of growth and shell weakening, as biomineralization processes are disturbed and 'blisters' appeared at the areas of shell repair, as in bivalves (Curry, 1983). Limpet and snail shells are infested by euendolithic cyanobacteria, such as *Mastigocoleus testarum* or

Hyella caespitosa Bornet and Flahault, 1888 (Prusina et al., 2015), and green and red algae, such as *Phaeophila* or *Porphyra* (Cerrano et al., 2001; Nolan, 1991; Walker, 1998), and become thinner and more fragile due to bioerosion (similar to bivalves). Infested limpets and snails suffer higher mortality rates, especially in adverse environments (i.e., open coast) (Day et al., 2000; Nolan, 1991). In barnacles, the chlorophyte *O. queckettii*, the cyanobacterium *M. testarum*, *Hyella* sp. and *Leptolyngbya terebrans*, and conchocelis stages of *Bangia* red algae were found in the plates (Drew, 1954; Meyer et al., 2021, 2020; Parke and Moore, 1935). Euendolithic infestation starts from the apex of the shell down to the base, weakening the barnacle shell and channelling its energy towards self-repair (Parke and Moore, 1935). In foraminifera, the shell is infested by the same euendolithic species as barnacles, which increases their susceptibility to mechanical breakage and fragmentation and can potentially attract grazers (Peebles and Lewis, 1988). By contrast, euendoliths at the test surface can promote the formation of a micritic crust around infested tests through secondary carbonate deposition (Kobluk and Risk, 1977), potentially increasing the potential of the test for preservation (Bathurst, 1966).

While the effects of euendolithic infestation on live calcifying organisms, such as foraminifera, limpets, brachiopods, or barnacles, could be simply underexplored, the sparsity of studies could also be an artifact of lower levels of euendolithic infestation in these organisms, which could translate in less detectable negative effects on the host.

2.6. Photoautotrophic euendoliths in the Anthropocene

Marine calcifiers, photoautotrophic euendoliths and their future relationship, will be influenced by global climate change (GCC) (Andersson, 2005; Raven, 2005; Schönberg et al., 2017; Tribollet, 2008a). GCC is caused by the increase in the emission

of anthropogenic greenhouse gases, such as CO_2, and manifests as an increase in air and sea surface temperatures (SST), and changes in rainfall regimes (Mendoza et al., 2021). As air temperatures rise, cloud cover is predicted to decrease at the planetary scale, which increases the amount of solar radiation reaching the surface, increasing temperatures even more (Mendoza et al., 2021). For the past 200 years, the world's oceans have absorbed about one-third of the CO_2 released into the atmosphere, which has led to ocean acidification (OA), with a reduction of the pH of surface seawater of 0.1 units (Caldeira and Wickett, 2003; Gruber et al., 1996; Sabine et al., 2004). If global anthropogenic CO_2 emissions continue to rise in line with current trends, the average pH of the ocean's surface could further decrease by 0.7 units in the next millennium, with a rate of change one hundred times greater than in the past 300 M years (Caldeira and Wickett, 2003; Key et al., 2004). For marine calcifiers, rising SST, ocean acidification, and the increase in solar radiation will negatively impact calcification, survival, growth, and reproduction, and diminish their resistance to other environmental stressors, such as pollution (Gattuso et al., 1999; Helmuth et al., 2006b; Hoegh-Guldberg, 1999; O'Donnell et al., 2013; Petes et al., 2007). With decreasing calcification and a weakening of existing calcified structures due to passive dissolution in a more acidic ocean, marine calcifying organisms will become more susceptible to bioerosion (Schönberg et al., 2017). Understanding how photoautotrophic euendoliths will behave in our changing world thus becomes important for understanding the fate of many bioengineered marine ecosystems (Schönberg et al., 2017; Tribollet, 2008a).

Euendolithic infestation by photoautotrophs of carbonate substrates, especially those of live calcifying organisms, is expected to increase in prevalence with increased SST, solar radiation, and OA (Enochs et al., 2016; Marcelino et al., 2017; Monsinjon et al., 2021; Reyes-Nivia et al., 2014, 2013; Zardi et al., 2021). Surveys at sites with natural pH

gradients, such as volcanic vents (Cherchi et al., 2012; Enochs et al., 2016; Marcelino et al., 2017), and a series of mesocosm experiments controlling SST and pH (Diaz-Pulido et al., 2014, 2012; Leggat et al., 2019; Reyes-Nivia et al., 2014; Tribollet et al., 2019, 2009, 2006) confirm this trend in experimental and dead substrates. The distribution of photoautotrophic euendoliths could expand towards higher latitudes where they are currently less abundant, as a result of the lowering calcium carbonate saturation caused by global climate change in these regions, which would facilitate the microbioerosive processes (Andersson, 2005). Photoautotrophic euendoliths are also expected to increase in biomass and cover, and to penetrate deeper and faster into the substrate, thus promoting microbioerosion, with a shift in communities under predicted future oceanic conditions of increased SST and reduced pH. Moreover, the increase in frequency and intensity of marine heat waves in response to GCC will likely be associated with mass mortality events in bivalves (Petes et al., 2007; Zardi et al., 2009), and coral and CCA reefs (Diaz-Pulido et al., 2014). Such mortality events ultimately increase the availability of dead carbonate substrates for photoautotrophic euendoliths. Although manipulative experiments are scarce (Diaz-Pulido et al., 2012), hypotheses can be formulated on the future of photoautotrophic euendoliths that colonize live marine calcifiers by capitalizing on the knowledge compiled in this review. In a similar fashion to dead substrates, photoautotrophic euendoliths are expected to increase in abundance and biomass in live calcifying organisms with increasing SST and solar radiation. Under OA and GCC, marine calcifiers are more vulnerable to microbioerosion (Raven, 2005) and heat waves (Diaz-Pulido et al., 2014; Petes et al., 2007). With favourable environmental change and the weakening of calcifying organisms, the negative effects of euendolithic infestation (Hassenrück et al., 2013; Kaehler and McQuaid, 1999; Massé et al., 2018; Zardi et al., 2009) are expected to be magnified in

the future. In the worst-case scenario, the combined influence of GCC and euendolithic infestation is expected to increase microbioerosion rates by up to 150% in reefs by 2100 (Carreiro-Silva et al., 2012, 2009, 2005; Reyes-Nivia et al., 2014, 2013). This equates to about two-thirds of reef carbonate deposited per year being dissolved by the action of microborers by 2100 (Tribollet et al., 2019).

As the negative effects of euendolithic infestation on live calcifying organisms are expected to increase in intensity under future oceanic conditions, so might the beneficial effects. Photoautotrophic euendoliths can contribute to host survival under OA and heat waves. In corals, photoassimilates are translocated directly from the euendoliths to the host until symbiotic zooxanthellae recolonize the coral tissue (Fine et al., 2001; Fine and Loya, 2002; Schlichter et al., 1997, 1995). However, this mutualistic relationship is limited in the case of rapid heat wave-induced bleaching events, as high light intensities coupled with high temperatures inhibit euendolithic photosynthetic activity (Fine et al., 2005). In bivalves, photoautotrophic euendoliths indirectly enhance the albedo of the shell, thus reducing the overall body temperature and the mortality rates experienced by infested bivalves (Gehman and Harley, 2019; Zardi et al., 2021, 2016). The beneficial effects of euendoliths can extend to neighbouring mussels, further increasing the thermal buffering provided by mussel beds to associated species on rocky shores (Lourenço et al., 2017; Zardi et al., 2021). In CCA crusts, photoautotrophic euendoliths preferentially remove the highly dissoluble fraction of the carbonate skeleton, thus increasing its resistance to bioerosion, either due to OA or photoautotrophic euendoliths themselves (Diaz-Pulido et al., 2014; Nash et al., 2013; Ramírez-Reinat and Garcia-Pichel, 2012; Reyes-Nivia et al., 2013). Both detrimental and beneficial effects of euendolithic infestation in live calcifying organisms are expected to increase in intensity with the ongoing GCC and OA. Nevertheless, in the long term,

euendolithic infestation is detrimental to its calcifying hosts, ultimately leading to their death.

2.7. Conclusions

As discussed, photoautotrophic euendoliths are significant biological components of marine ecosystems. Photoautotrophic euendoliths, which are relatively inaccessible without specific observational techniques, are ubiquitous, found wherever there is a calcium carbonate substrate and suitable environmental conditions for survival. Through their boring activity, they leave long-lasting traces in the substrate that allow their identification. As each species has its own ecological requirements, the presence and abundance of euendolithic species and the composition of euendolithic communities are influenced by abiotic (e.g., light availability, nature of the substrate, water quality) and biotic parameters (e.g., grazers, epibiotic communities). Therefore, euendolithic species or entire communities can be employed as geographical, water quality, or paleobathymetric indicators. Photoautotrophic euendoliths colonize both inanimate calcium carbonate substrates and the calcified structures of live organisms. In live calcifying organisms, endolithic infestation has both detrimental and beneficial effects: while euendoliths bore into the calcified structure, the host's energy is allocated to secondary structural repair at the expenses of growth, survival, and reproduction; but endolithic infestation can mitigate temperature stress of the host or provide an alternative source of nutrition in the case of corals. However, in the long term, endolithic infestation ultimately leads to the host's death. In the future, the prevalence and severity of endolithic infestation are predicted to increase, which could lead to higher levels of microbioerosion in marine carbonate substrates, either inanimate or alive, and thus profoundly modify the dynamics of ecosystems founded on marine calcifiers.

Infestation by photoautotrophic euendoliths in live calcifying ecosystem engineers can significantly influence the phenotype, physiology, and biology of individual host specimens, and thus the quality of the habitat they collectively provide (e.g., mussel beds, coral reefs). Research on photoautotrophic euendoliths, especially in live substrates, could beneficiate from the following directions in the future:

1. Update and standardize the taxonomy of known photoautotrophic euendolithic species, including morphological descriptions, ecological requirements, and molecular-based approaches to taxonomy;
2. Determine the boring mechanisms for euendolithic species, such as red and green algae, and how these processes may be affected by environmental change, including OA and GCC;
3. Investigate euendolithic communities (e.g., species composition, abundance, biomass), and the prevalence and severity of euendolithic infestation in less-investigated marine calcifiers (e.g., brachiopods, barnacles, limpets, snails), under different environmental conditions and timescales, and using a combination of approaches;
4. Develop a standardized experimental framework, including *ex situ* and *in situ* experiments, to evaluate and compare the modalities of euendolithic infestation and how infestation may be influenced by various abiotic and biotic parameters (e.g., nutrient concentrations, light availability, presence of grazers and predators);
5. Determine the detrimental and beneficial effects of euendolithic infestation on live marine calcifiers, using manipulative experiments when possible;
6. Centralize available information on euendoliths (including heterotrophs) in a publicly accessible database (e.g., Ocean Acidification International Coordination Centre).

CHAPTER 3

EUENDOLITHIC INFESTATION OF MUSSEL SHELLS INDIRECTLY IMPROVES THE THERMAL BUFFERING OFFERED BY MUSSEL BEDS TO ASSOCIATED MOLLUSCS, BUT ONE SIZE DOES NOT FIT ALL

Published on February 8th, 2023, as: Dievart, A.M.; McQuaid, C.D.; Zardi, G.I.; Nicastro, K.R.; Froneman, P.W. Euendolithic Infestation of Mussel Shells Indirectly Improves the Thermal Buffering Offered by Mussel Beds to Associated Molluscs, but One Size Does Not Fit All. *Diversity* **2023**, *15*, 239. https://doi.org/10.3390/d15020239

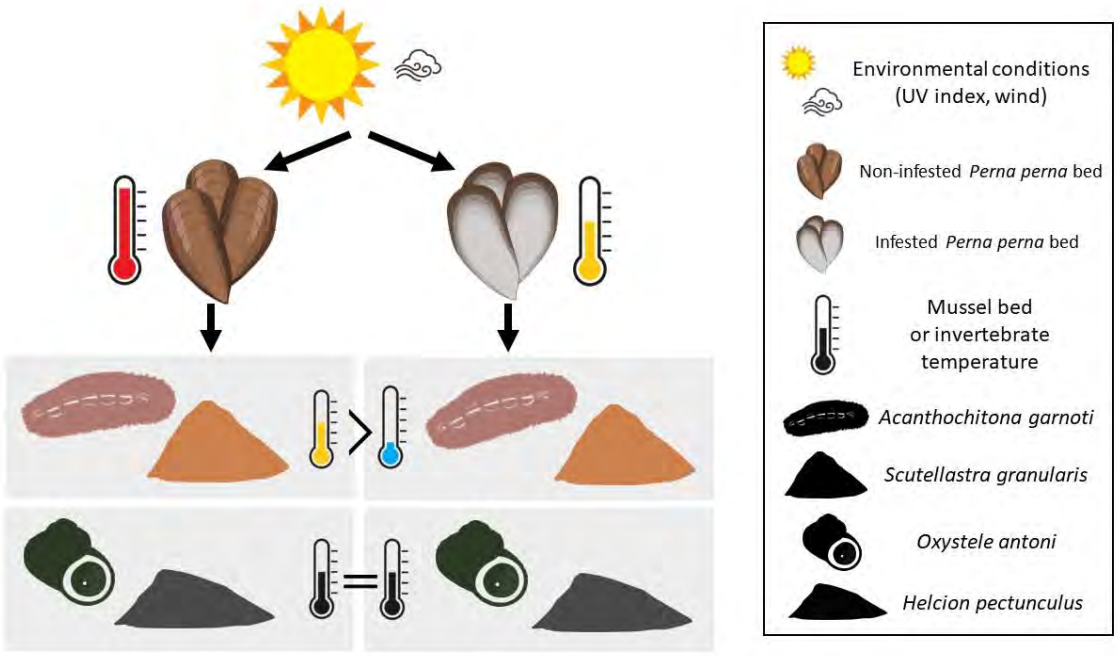

Figure 3.0. Graphical abstract published in Dievart et al. (2023) and illustrating the thermal buffering offered by euendolith-infested mussel beds to some associated molluscs and not others.

3.1. Introduction

Heatwaves are discrete periods of prolonged, abnormally warm air (i.e., atmospheric heatwave) or seawater temperature (i.e., marine heatwave) at a particular location (Oliver et al., 2021). The frequency, duration, and intensity of atmospheric and marine heatwaves have increased since the pre-industrial era (Marin et al., 2021; Meehl and Tebaldi, 2004; Oliver et al., 2018) and are expected to increase with global climate change (GCC), with many parts of the coast and ocean reaching a state of near-permanent heatwave by the end of the century (Frölicher et al., 2018; Mbokodo et al., 2020; Oliver et al., 2019). These events are triggered by anomalous weak wind speeds and increased solar radiation, amongst other environmental factors (Gupta et al., 2020; Schlegel et al., 2017). Since organisms suffer more from extremes than slow changes in their environment (Gaines and Denny, 1993), heatwaves have been implicated in large-scale shifts in species location, phenological changes, changes in ecosystem structure, and elevated levels of mortality in coastal ecosystems (Helmuth et al., 2002; Lima et al., 2007; Sanford et al., 2019; White et al., 2023). This is particularly true for rocky intertidal shores, where temperature and desiccation stress are extremely high during aerial exposure. This is especially the case on sunny days with little to no overcast and low to no wind (Helmuth et al., 2011). However, the effect is highly variable at small scales due to the complex topography of these shores (Helmuth et al., 2006b, 2002; Lathlean et al., 2017) and at larger scales due to the timing of tides and local weather patterns (Helmuth et al., 2011; Mislan et al., 2009). Intertidal organisms already live at, or close to, their upper thermal tolerance limits and are thus more susceptible to local extinction events (Helmuth et al., 2002; Somero, 2010, 2002). However, intertidal organisms can display behavioural thermal adaptations to reduce their temperatures, such as ‘mushrooming’ (Williams et al., 2005), changing the

orientation of the shell (Muñoz et al., 2005), or seeking thermal refuge in a more favourable microhabitat (Cartwright and Williams, 2014; Lathlean et al., 2016a; Van Rensburg et al., 2021), which are only effective if the organisms are under stress (Muñoz et al., 2005).

On rocky shores, mussel beds form an important intertidal habitat that mitigates both temperature and desiccation stress, creating a suitable microhabitat for many species, particularly under extreme environmental conditions (Gutiérrez et al., 2019; Helmuth, 1998; Jurgens and Gaylord, 2018; Nicastro et al., 2020). Not only do these ecosystem engineers (*sensu* Jones, Lawton & Shachak, 1994) provide a thermal refuge, but the properties of the mussel bed influence the quality of the habitat they provide (Lathlean et al., 2016b; Lourenço et al., 2017; Thomas et al., 1998). Worldwide, mussel shells are targeted by photoautotrophic euendolithic microorganisms, which can indirectly modify the mussel phenotype, thus influencing the thermal buffering provided by mussel beds (Kaehler, 1999; Lourenço et al., 2017; Zardi et al., 2016). Photoautotrophic euendoliths refer to a heterogeneous group of microorganisms (i.e., cyanobacteria, chlorophytes, and rhodophytes) that live and actively bore into relatively soluble substrates, such as phosphate and carbonate substrates (e.g., coral skeletons, bivalve shells) (Couradeau et al., 2017; Golubic et al., 1981, 1975). Present essentially anywhere there is sufficient light for photosynthesis and a suitable substratum to bore into, photoautotrophic euendoliths readily infest marine calcifiers (i.e., corals, bivalves, crustose coralline algae), with both negative and positive effects (Dievart et al., 2022). In addition to its negative sub-lethal and lethal effects on mussels (Dievart et al., 2022; Kaehler and McQuaid, 1999; Zardi et al., 2009), euendolithic infestation causes a distinctive discolouration of the mussel shell as a by-product of its corrosive activity, thereby increasing its albedo (Kaehler, 1999; Zardi et al., 2016).

Since they reflect more light, infested mussels display lower body temperature and greater survival rates than non-infested mussels during heatwaves (Zardi et al., 2021, 2016). This beneficial effect of euendolithic infestation extends to both infested and non-infested neighbouring mussels but is restricted to periods of intense heat and desiccation stress (Lourenço et al., 2017; Monsinjon et al., 2021; Zardi et al., 2021). It is anticipated that GCC and ocean acidification will coincide with increased rates, prevalence, and severity of euendolithic infestation of mussels (Dievart et al., 2022). Investigating the potential impacts of euendolithic infestation of mussel beds on the thermal buffering they provide to associated species is critical to predicting how intertidal ecosystems will react to GCC in the future.

To monitor the ecological responses of organisms to GCC, ecologists need to use tools and methodologies that can capture the actual conditions experienced by targeted species within their natural microhabitats, often at small scales (Lathlean et al., 2011; Stobart et al., 2016). Infrared thermography (IRT) is a non-invasive tool for the rapid detection and measurement of small-scale temperature variability *in situ* without disturbing the animals' behaviour or thermoregulatory capacities (Lathlean and Seuront, 2014; Lathlean et al., 2017). Previously restricted to terrestrial ecology, IRT has been successfully employed in intertidal ecosystems to investigate the role of small-scale temperature variability on the physiology and ecosystem functioning of intertidal communities (Caddy-Retalic et al., 2011; Chapperon and Seuront, 2011a; Helmuth et al., 2002; Muñoz et al., 2005). Shell temperatures of intertidal molluscs measured by IRT have been shown to be strongly correlated with internal body temperatures (Caddy-Retalic et al., 2011; Chapperon and Seuront, 2011b; Seuront et al., 2018). Body temperatures of intertidal invertebrates are determined by heat fluxes towards and from the organism (Denny and Harley, 2006;

Harley et al., 2009), which are dependent on the interaction between climatic heat sources at macroscales (e.g., air and water temperatures; Helmuth, 1998; Helmuth et al., 2002), non-climatic heat sources at the niche level (e.g., solar irradiance and re-radiation from the substratum; Marshall, McQuaid and Williams, 2010), and biotic factors at the organismal level (e.g., shell colour, morphology and size, behaviour, selection of thermally favourable microhabitats; Muñoz et al., 2005; Harley et al., 2009). Non-climatic heat sources appear to have primary control over body temperatures of intertidal ectotherms (Marshall et al., 2010), along with substratum temperature for organisms with a large foot that maintains a conductive, direct contact with the substratum (e.g., limpets, snails, chitons, barnacles; Wethey, 2002; Denny and Harley, 2006; Caddy-Retalic et al., 2011; Chapperon & Seuront, 2011b).

In this context, the present study investigated whether euendolithic infestation of mussel beds alters, during aerial exposure, the body temperatures and desiccation stress of selected molluscs known to inhabit mussel beds on South African rocky shores. I hypothesized that: (i) the body temperatures of key intertidal species would be lower, and warming rates slower, in beds formed by endolith-infested mussels than non-infested individuals, (ii) similarly, loss of water by key intertidal species would be lower, and their desiccation rates slower, in endolith-infested beds, and (iii) this would only be true under high temperature and desiccation stress (i.e., at midday on days with high solar irradiance and low wind speed).

3.2. Materials and Methods

3.2.1. Focal species and experimental setting

Four key intertidal invertebrate species were selected: the limpets *Scutellastra granularis* and *Helcion pectunculus* (Gmelin, 1791), the chiton *Acanthochitona garnoti*

(Blainville, 1825), and the top shell *Oxystele antoni*. These mobile molluscs were specifically selected as: (i) they are able to move between microhabitats during emersion and are commonly found in mussel beds, (ii) they have a rather large foot that maximizes conductive contact with the substratum, and (iii) they suffer differently from high solar irradiance because of differences in shell pigmentation and texture, as these both affect the absorption of solar radiation (McMahon, 1990). Invertebrates were collected on the rocky shores of Port Alfred (Shelly Beach – 33°36′49.0"S, 26°53′20.7"E). Prior to each experiment, invertebrates were kept in seawater (20 – 22 °C), with rocks colonized by microalgae collected from the rocky shores of origin, under a 12h/12h light/dark regime, for 48h.

The investigated molluscs present morphological differences in shape and colour. On the one hand, the chiton *Acanthochitona garnoti* and the limpet *Scutellastra granularis* are both light in colour, with a large foot relative to their height, and display little to no shell features. By contrast, the limpet *Helcion pectunculus* and the top shell *Oxystele antoni* are both dark in colour. While *H. pectunculus* has a similar shape and foot size to *S. granularis*, its shell is even more heavily sculpted. Conversely, *O. antoni* has a coiled smooth shell with a smaller aperture and can retract its foot inside its shell when stressed. All the chitons and *S. granularis* limpets used in this study displayed significant levels of shell erosion, which could not be directly imputed to euendolithic infestation. However, the alteration in their shell colour that could influence the recorded shell and/body temperatures were kept consistent between individuals.

Artificial mussel beds were created from shells of the brown mussel, *Perna perna*, a dominant ecosystem engineer on rocky shores on the South and East coasts of South Africa (Bownes and McQuaid, 2006; Zardi et al., 2007b). Artificial mussel beds consisted of two treatments: (a) 100% non-infested *P. perna* (n = 3) and (b) 100% infested

P. perna (n = 3). Mussels (shell length: 4 – 5 cm) were collected on the rocky shores of Port Alfred (Shelly Beach – 33°36′49.0"S, 26°53′20.7"E) and Kasouga (Ship Rock – 33°38′54.3"S, 26°45′31.6"E), with care taken to sample mussels displaying either low (stage A – B, for the purpose of this study classified as 100% non-infested) or high (stage D – E, classified here as 100% infested) levels of euendolithic infestation (Kaehler, 1999; Ndhlovu et al., 2021b). After collection, the mussel shells were cleaned of their epibionts, while the soft tissue was replaced with a silicone sealing compound (Bostik Marine Silicone Sealant) and left to dry at air temperature for at least 48 h before use. The sealant is known to mirror the temperature of mussel tissue closely in these circumstances (Helmuth and Hofmann, 2001). Between 70 and 80 biomimetic mussels were then arranged vertically, with the umbo towards the substrate to mimic their natural position on the shore, in each basket (diameter: 20 cm) made of semi-rigid, white PVC net (mesh size: 4 cm) to create artificial mussel beds (Lourenço et al., 2017; Nicastro et al., 2012; Zardi et al., 2016).

The series of experiments described below were conducted on a flat roof of the Zoology and Entomology Department of Rhodes University, in Grahamstown, between April and May 2021 and in February 2022, on sunny days, with little to no overcast and low wind speeds (Table 3.1) and high sun elevation (10 am – 3 pm) to maximize the likelihood of extreme temperature and desiccation stress. Prior to each experiment, artificial mussel beds were kept in the dark overnight in seawater (20 – 22°C) to ensure their exposure to the same environmental conditions (temperature and light). After emersion, artificial mussel beds were positioned in pairs (i.e., one non-infested bed and one infested bed) on previously soaked bathmats to simulate the matrix of a natural mussel bed, which is made up of byssal threads, pebbles, broken shells, and sediment, and retains moisture during aerial exposure. This also avoided direct contact with the

underlying concrete. Early trials demonstrated that, without the soaking process and the use of mats, artificial mussel beds would dry out in about 20 min, and the infaunal specimens subsequently died of desiccation after about 30 min.

All statistical analyses were performed in R (R Core Team, 2022).

Table 3.1. Meteorological conditions for our series of experiments investigating temperature stress with the corresponding infaunal species investigated.

Date	Infaunal species	Size range (mm) [1]	UV index [2]	Air temperature [3] (°C)	Humidity [3] (%RH)	Pressure [4] (x 10^3 Pa)	Wind speed [4] ($km.h^{-1}$)	Wind direction [4]
13/04/2021	*Helcion pectunculus*	18–23	7	26.11–27.78	38–43	96.2–96.5	7.88–8.69	S-E
	Oxystele antoni	13–16						
14/04/2021	*Scutellastra granularis*	20–30	6.5	22.78–25.00	45–55	96.2–96.5	13.68	S-W
15/04/2021	*Helcion pectunculus*	18–25	6	22.22–22.78	41–44	95.8	16.90–19.79	S-W
	Oxystele antoni	13–16						
18/04/2021	*Scutellastra granularis*	20–30	5.5	25.00–27.78	11	95.8	19.47–21.24	N-W
09/02/2022	*Acanthochitona garnoti*	19–25	13	25.00	47–49	95.2	19.47–21.24	S
10/02/2022	*Acanthochitona garnoti*	19–25	12	25.00–26.11	43	95.5	14.00–15.45	S

[1] Shell length range for *Scutellastra granularis* and *Helcion pectunculus*, shell diameter range for *Oxystele antoni*, and body length range for *Acanthochitona garnoti.*
[2] https://www.weatheronline.co.uk. Accessed on February 12th, 2022.
[3] Direct measurements using a thermocouple and a hygrometer for air temperature and relative humidity, respectively.
[4] https://world-weather.info/forecast/south_africa/grahamstown/. Accessed on February 12th, 2022.

3.2.2. Body temperature assessment

At the beginning of the experiment, 4 – 8 randomly chosen specimens of the invertebrate species investigated were transferred from their holding tank to each artificial mussel bed. Artificial mussel beds and their infauna were then exposed to the sun for 90 minutes, during which thermal images were captured every 5 minutes. All infrared pictures were taken at the height of approximately 1.5 m from ground level, following a consistent order, using a Testo 882 (Testo AG, Germany) hand-held infrared camera

with emissivity values set at 0.95 (Lathlean and Seuront, 2014), a thermal sensitivity of 50 mK, and an accuracy of ± 2°C or ± 2% of reading, whichever was greater. The experiment was run twice on different dates for each invertebrate species and concurrently in the case of *Oxystele antoni* and *Helcion pectunculus* (Table 3.1).

All infrared images (e.g., Figure 3.1) were analyzed using IRSoft 4.8. Within each bed, all infaunal specimens, and five random mussels, were selected at each time interval, and their shell temperatures were recorded using the one point-measure tool targeting the middle of each infaunal and mussel specimen.

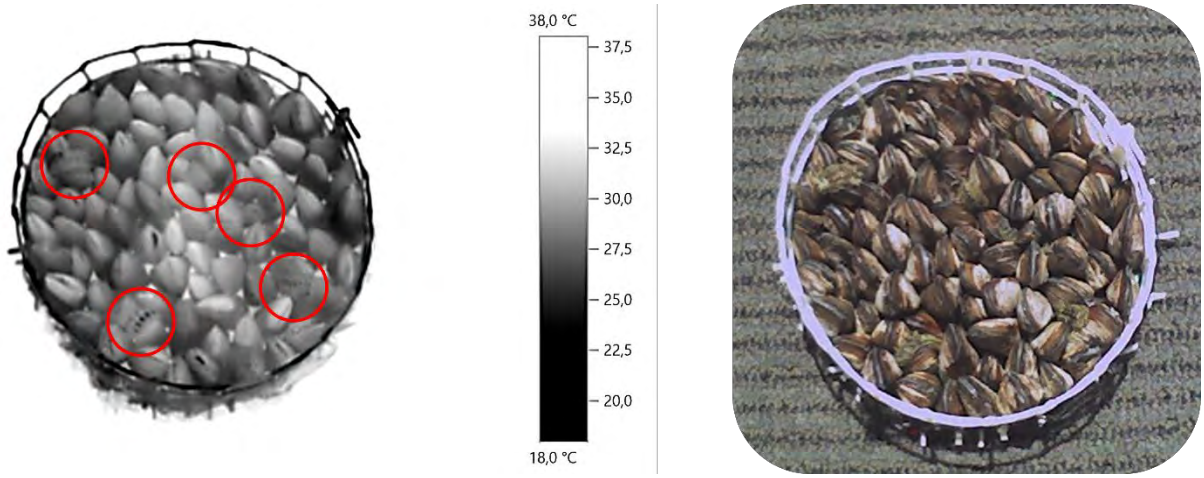

Figure 3.1. Example of infrared image obtained in this study with the position of *Acanthochitona garnoti* specimens (red circles) and the corresponding classic image.

3.2.3. Desiccation assessment

Our series of desiccation experiments were conducted on the following dates: 18 April 2021 (*Oxystele antoni*), 1 May 2021 (*Acanthochitona garnoti*), 2 May 2021 (*Scutellastra granularis*), and 17 May 2021 (*Helcion pectunculus*).

At the beginning of the experiment, 15 randomly selected specimens of each infaunal species were transferred from their holding tank to each artificial mussel bed. Artificial mussel beds and their infauna were then exposed to the sun for 90 minutes.

At selected time intervals (i.e., at the start of the experiment, then after 15, 30, 60, and 90 minutes), three random individuals for each species were selected from each mussel bed and stored in separate sealed tubes in the shade. At the end of the experiment, each specimen was weighed (wet weight), then dried at 60°C for 48h, and weighed again (dry weight). The experiment was run only once for each invertebrate species.

3.2.4. Data analyses

For both experiments, data did not fit the assumptions of normality and homogeneity of variances. We used a series of Generalized Additive Models (GAMs) to assess the effect of euendolithic infestation overtime on the shell temperatures of both biomimetic mussels and infaunal invertebrate species, as well as on the wet weight of infaunal invertebrate species. GAMs were selected to model these data due to the non-linear relationships present. For the body temperature assessment, either biomimetic mussel or infaunal species shell temperatures at each time step were specified as a continuous response variable and infestation status (infested/non-infested) as a categorical parametric fixed effect. For the desiccation assessment, the wet weight of individual invertebrates was log-transformed and specified as a continuous response variable and infestation status (infested/non-infested) and invertebrate species as categorical parametric fixed effects. A unique identifier code was given to each biomimetic mussel (for the body temperature assessment) or infaunal specimen measured (for both assessments). For all biomimetic mussels and infaunal invertebrate species (except *Acanthochitona garnoti*), a non-linear relationship between infestation and shell temperature was specified using a smoothed cubic regression spline with $k = 4$ knots. For *Acanthochitona garnoti* and the corresponding biomimetic mussels, a non-linear relationship between infestation and shell temperature was specified using a smoothed cubic regression spline with $k = 6$ knots. A non-linear relationship between infestation

and wet weight of invertebrates was specified using a smoothed cubic regression spline with $k = 5$ knots. A smoothed random effect term for each specimen nested within the mussel bed was specified to account for repeated shell temperature measurements on the same individual at different time intervals while allowing intercepts to vary between mussel beds. Model fits were assessed using residual diagnostics using the 'appraise' function from the 'gratia' R package (Simpson, 2022). To test for a significant effect of infestation on shell temperature or wet weight, parametric *F*-tests were computed ($P < 0.05$) using the 'anova.gam' function from the 'mgcv' R package (Wood, 2017). Wald's-like tests were used to assess whether the non-linear relationship between infestation and shell temperature over time (i.e., heating rates) differed between infested vs. non-infested infauna and whether the non-linear relationship between infestation and wet weight of invertebrates over time (i.e., desiccation rates) differed between infaunal species (Wood, 2013).

3.3. Results

3.3.1. Body temperature assessment

A general trend was observed among all experimental dates for biomimetic mussels. Regardless of the date or the time interval considered, infested biomimetic mussels exhibited lower shell temperatures (1.7 – 4.2°C lower) than non-infested mussels ($p < 0.001$, Table S3.1, Figure 3.2). Shell temperatures of biomimetic mussels increased with time, but mostly in the first 30 minutes, with infested mussels warming at a slower rate than non-infested mussels ($p < 0.001$, Table S3.2, Figure 3.2). By the end of the experiment, shell temperatures in non-infested and infested mussel beds had increased by 70.9 and 63.3%, respectively. Variations in mussel shell temperatures and warming rates

were observed between dates and were linked to variations in environmental conditions, especially in UV index and wind speed ($p < 0.05$, Tables 3.1 and S3, Figure 3.2).

For *Acanthochitona garnoti* and *Scutellastra granularis*, shell temperatures (averaged over all the time periods) were significantly lower on infested mussel beds than on non-infested mussel beds ($p < 0.001$, Tables S3.4 and S3.8, Figure 3.3). Although heating rates of *A. garnoti* were not statistically different (Table S3.5, Figure 3.3), heating rates of *S. granularis* were significantly slower on infested mussel beds than on non-infested mussel beds ($p < 0.05$, Table S3.9, Figure 3.3). Mollusc shell temperatures and heating rates were not significantly different between experimental dates for these two species (Tables 3.1, S3.6, and S3.10, Figure 3.3). Finally, for both *A. garnoti* and *S. granularis*, the shell temperatures of molluscs were always lower than the shell temperatures of the biomimetic mussels for each corresponding infestation condition and experimental date ($p < 0.001$, Tables S3.7 and S3.11, Figure 3.3).

For *Oxystele antoni* and *Helcion pectunculus*, their shell temperatures and those of biomimetic mussels, as well as their respective warming rates, were never significantly different between species or infestation status of the mussel bed (Tables S3.12 and S3.13, Figure 3.4). Variations in mollusc and biomimetic mussel shell temperatures were observed between experimental dates ($p < 0.05$, Tables 3.1 and S3.14, Figure 3.4) and were linked to variations in environmental conditions, especially in wind speed.

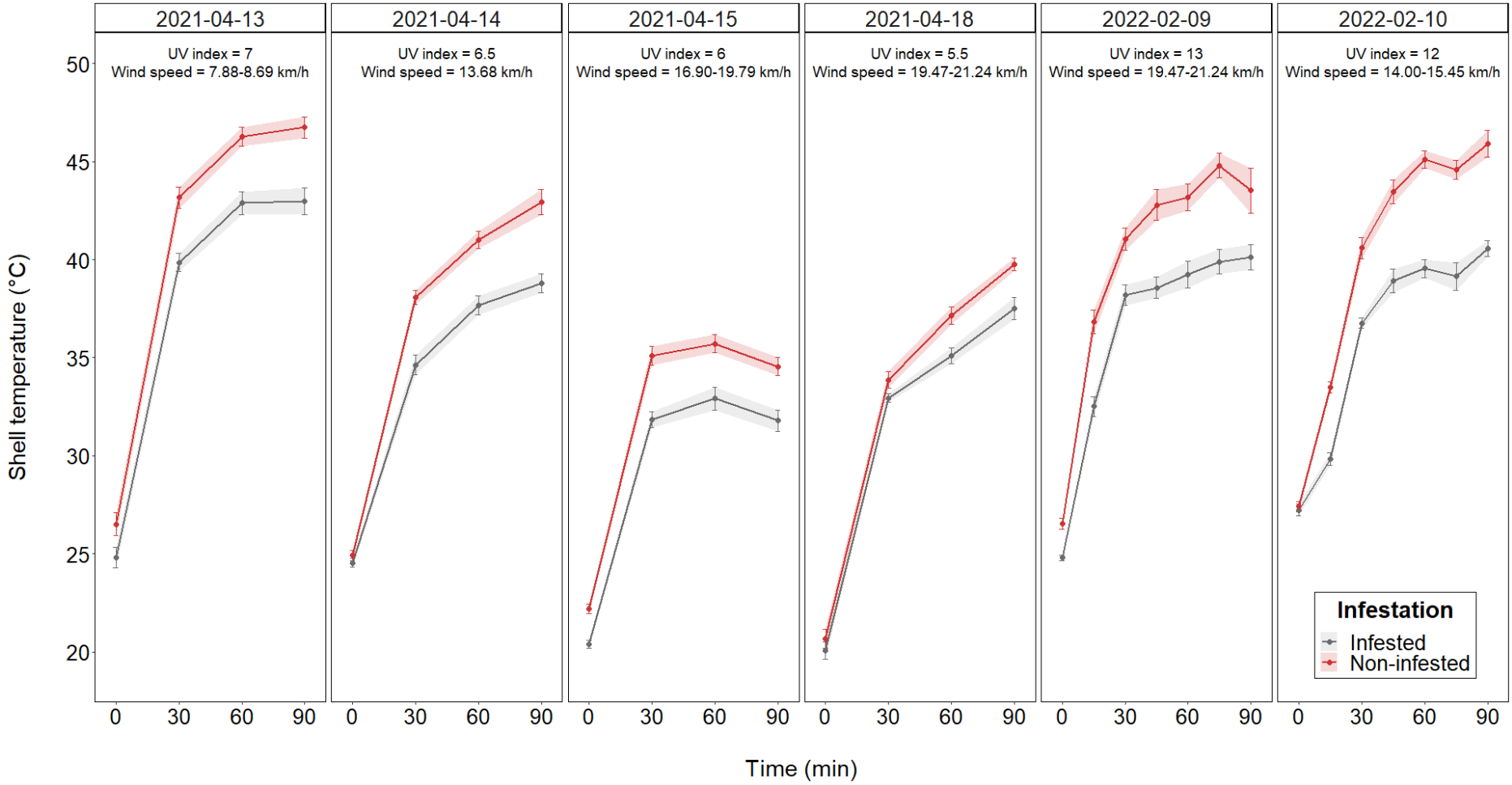

Figure 3.2. Changes in mean (± SE) shell temperatures (in °C) of infested and non-infested individual biomimetic mussels (*Perna perna*) for 90 min after emersion (n = 3 mussel beds) on each experimental date.

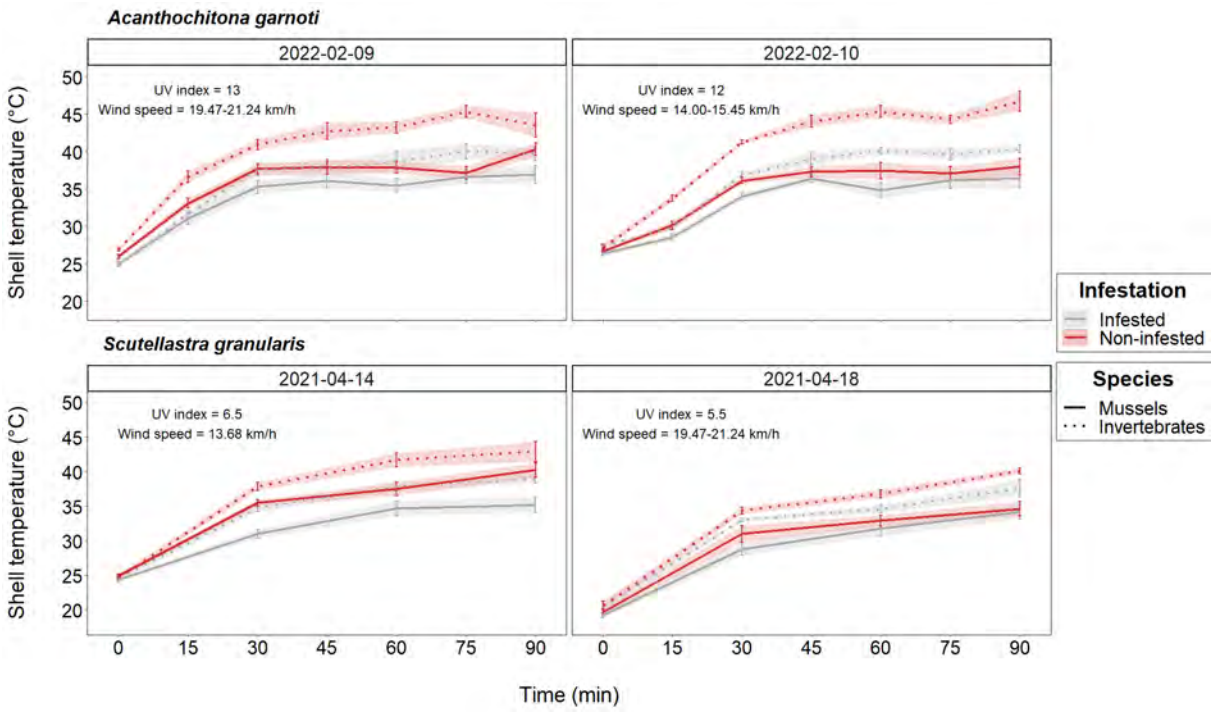

Figure 3.3. Changes in mean (± SE) shell temperatures (in °C) of the chiton (*Acanthochitona garnoti*) and the limpet (*Scutellastra granularis*), with the corresponding biomimetic mussels (*Perna perna*), in either infested or non-infested mussel beds (n = 3) for 90 min after emersion, on each corresponding experimental date.

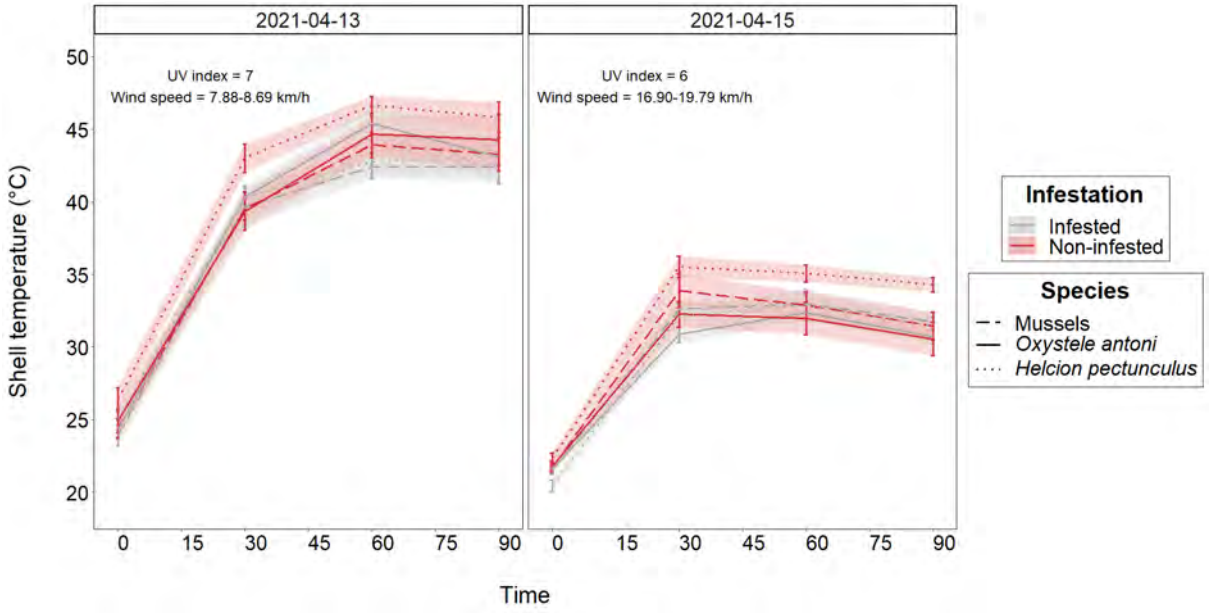

Figure 3.4. Changes in mean (± SE) shell temperatures (in °C) of the limpet (*Helcion pectunculus*), the top shell (*Oxystele antoni*), and biomimetic mussels (*Perna perna*) in either infested or non-infested mussel beds (n = 3) for 90 min after emersion, on each experimental date.

3.3.2. Desiccation assessment

No statistical differences in wet weight or desiccation rates of invertebrate specimens were detected between infested and non-infested mussel beds (Table S3.15). Variations in wet weight, but not in desiccation rates (Table S3.16), were detected between invertebrate species, regardless of infestation levels of the mussels ($p < 0.05$, Table S3.15).

3.4. Discussion

Rocky shores are amongst the most physically stressful environments on the planet. Despite the severity of physical gradients, mainly temperature and desiccation, rocky intertidal shores are biologically rich ecosystems. Global climate change (GCC) is likely to be associated with an increase in the physical gradients observed on rocky shores and an increased frequency of heat waves (Frölicher et al., 2018; Oliver et al., 2019). These changes will likely cause shifts in community structure and local extinctions (Helmuth et al., 2002; Lima et al., 2007; Sanford et al., 2019). However, under stressful conditions, intertidal organisms can display thermal behavioural adaptations, such as seeking refuge in mussel beds, which mitigate temperature and desiccation stress (Cartwright and Williams, 2014; Lathlean et al., 2016a; Muñoz et al., 2005; Williams et al., 2005). Numerous studies have investigated the effects of infestation by euendolithic shell-boring parasites on individual mussels and the mussel bed microclimate (reviewed in Dievart et al., 2022). This study is amongst the first attempts to assess the indirect thermodynamic benefits conferred by euendolithic infestation of mussel beds to their associated infauna (Zardi et al., 2023).

The results of the manipulative experiments indicated a buffering role of photoautotrophic shell-degrading euendoliths on the thermal stress experienced by

mussels. Infested biomimetic mussels displayed significantly lower shell temperatures and slower warming rates than non-infested biomimetic mussels, even when environmental conditions were not considered stressful (i.e., low solar irradiance and high wind speed, Figure 1). Since biomimetic mussels have been extensively used to record organismal body temperatures (Fitzhenry et al., 2004; Helmuth et al., 2016; Helmuth and Hofmann, 2001; Zardi et al., 2021) and avoid potential confounding factors (e.g., gaping behaviour, architectural complexity), these results effectively isolate a marked cooling effect of euendolithic infestation through the whitening of the mussel shell and of the mussel bed. This is in agreement with previous studies conducted with both live and biomimetic mussels with and without euendolithic infestation (Gehman and Harley, 2019; Lourenço et al., 2017; Monsinjon et al., 2021; Zardi et al., 2021, 2016).

Euendolithic infestation of mussel shells (i.e., substratum), at times, indirectly influenced the body temperatures of associated invertebrates but not their warming rates. In our study, the light-coloured invertebrates (i.e., *Acanthochitona garnoti* and *Scutellastra granularis*) displayed lower shell temperatures on euendolith-infested mussels compared to non-infested mussels and were always cooler than the substratum. In Portugal, Zardi et al. (2023) obtained similar results for the limpet *Patella vulgata* Linnaeus, 1758, the snail *Littorina littorea* (Linnaeus, 1758), and mussel recruits using artificial mussel beds made of blue mussels, *Mytilus galloprovincialis*. However, this was not the case for the dark-coloured invertebrates in this study (i.e., *Helcion pectunculus* and *Oxystele antoni*), for which shell temperatures did not differ significantly between infestation status and with the substratum. Body temperatures of intertidal ectotherms (including mussels) are primarily driven by non-climatic heat sources, either directly through solar irradiance or indirectly through re-radiation by the substratum

(Chapperon and Seuront, 2011b; Marshall et al., 2010). The latter is especially true for organisms with a large foot that maintains conducive contact with their substrate, such as limpets, snails, or chitons (Caddy-Retalic et al., 2011; Chapperon and Seuront, 2011b; Denny and Harley, 2006; Marshall et al., 2010; McQuaid et al., 1979; Wethey, 2002). Consequently, molluscs gain considerable heat from the substratum (McQuaid et al., 1979), often exhibiting the same temperature as the substratum (Chapperon and Seuront, 2011b; Denny and Harley, 2006), though they can sometimes become even warmer (Williams et al., 2005).

At a finer scale, the organism's morphology, such as the shell colour and shape, or behaviour, may also influence its thermal properties (Harley et al., 2009; McQuaid et al., 1979; Muñoz et al., 2005; Vermeij, 1973). This helps explain why euendolithic effects on the temperatures of mussels indirectly affect the temperatures of some animals but not others. Darker organisms absorb more heat from solar irradiance and do so faster (Etter, 1988) but also lose heat faster through convection (Geen and Johnston, 2014). Taller shells, with a more circular aperture, have a smaller contact area with the substratum, reducing heat gain through conduction (Harley et al., 2009; Hayworth and Quinn, 1990; Wethey, 2002), and, being taller, project into faster wind velocities, increasing heat loss through convection (Vermeij, 1973). Although the wind has a cooling effect on the mussels themselves (Lathlean et al., 2016b), because of the architectural complexity and intricate matrix of byssal threads within mussel beds, the effects of wind on the infauna would be negligible. Highly sculpted shells displaying heavy ridges, bumps, or other features, have a larger contact area with the atmosphere, thereby increasing heat loss through convection. This process is, however, only effective at high wind speeds (Harley et al., 2009; Vermeij, 1973) and, again, is not directly important within a mussel bed.

In addition, intertidal organisms can display a variety of behavioural adaptations to thermal and desiccation stress, including seeking thermal refuges (e.g., the underside of rocks, crevices, and mussel beds) for most invertebrates (Cartwright and Williams, 2014; Lathlean et al., 2016a), 'mushrooming' for limpets (Williams et al., 2005), or forming aggregations for snails (Chapperon and Seuront, 2011a).

We selected four intertidal invertebrates known to inhabit mussel beds commonly. On the one hand, the morphological differences between mollusc species could, in part, explain why an indirect effect of euendolithic infestation on body temperatures was only detected for *Acanthochitona garnoti* and *Scutellastra granularis*, for which heat transfer through conduction from the substratum (here, the mussel bed) is maximized. Indeed, *A. garnoti* and *S. granularis* (heavily eroded) are light in colour, with a large foot and little to no shell features, whereas *Helcion pectunculus* and *Oxystele antoni* are both dark in colour, the former having a heavily sculpted shell, while the latter has a coiled smooth shell. On the other hand, behavioural differences in the face of thermal and desiccation stress could have influenced the body temperatures of invertebrates. Most invertebrate specimens explored the substratum for a short time, between 5 and 10 minutes after the beginning of the experiments. Afterward, some specimens displayed thermoregulatory behaviours, such as seeking thermal refuges within the mussel beds for *A. garnoti* (Harper and Williams, 2001), 'mushrooming' for the two limpet species *S. granularis* and *H. pectunculus* (Williams et al., 2005), or adopting a standing position for *O. antoni* (Chapperon et al., 2017). However, this was not the case for all invertebrate specimens. Thermoregulatory behaviours were thus only sporadically observed during our experiment in both mussel bed infestation treatments. Moreover, invertebrates seeking refuge between or under the biomimetic mussels could not be captured by the infrared camera and were not integrated into this study. Finally, thermoregulatory behaviours are

often effective in the short term and represent high-risk strategies for invertebrates (Chapperon et al., 2017; Williams et al., 2005).

Our desiccation stress experiments did not detect an effect of euendolithic infestation of the mussel bed on water loss by infaunal invertebrates. This could be explained by the short exposure time of invertebrates to adverse environmental conditions (i.e., 90 minutes), the non-stressful conditions on the experimental dates (i.e., low solar irradiance and medium to high wind speeds), and the various behaviours displayed by invertebrates to minimize water loss under stress. It is also noted that the wet weight of each specimen used was not accounted for at the start of the experiment. Replicating the experiments while taking into account the initial wet weight, within species and between species, could potentially help to assess, with more accuracy, water loss.

3.5. Conclusions

This study shows that euendolith-induced corrosion enhances the quality of mussel beds as thermal refugia for selected invertebrate species. The beneficial effects of euendolithic corrosion on the mussel bed as a habitat are, however, highly variable at fine scales of space and time, which is true for the intertidal as a whole. Moreover, the colour phenotype of the species investigated is important in determining whether it benefitted from the indirect cooling effects of euendoliths. Thus, the additional thermal buffering provided by euendolithic infestation of mussel shells is only relevant if the organisms are thermally stressed, and its extent depends on the species in question. Under GCC, intertidal ecosystems are expected to greater suffering from extreme temperature and desiccation stress in the future, while euendolithic infestation of mussels will become more severe. In this context, euendolithic infestation may improve the chances of survival of mussels and the quality of mussel beds as thermal refuges for associated

invertebrates, which could, in turn, decrease their susceptibility to local extinctions. At the same time, euendolithic infestation also has negative impacts that could hinder the quality of habitat offered by mussel beds or its stability through time (Dievart et al., 2022). In addition, the bioerosive activities of photoautotrophic euendoliths and grazers can interact and result in increased levels of shell erosion (Schönberg and Wisshak, 2014). It is thus important to understand the ecological consequences of euendolithic infestation on mussel beds as a habitat and how this parasitic/mutualistic relationship will influence the wider ecosystem, that is, the rocky shore.

CHAPTER 4

SHELL-BORING MICROSCOPIC PARASITES IN AN ECOSYSTEM ENGINEER DO NOT INFLUENCE INFAUNAL COMMUNITY STRUCTURE

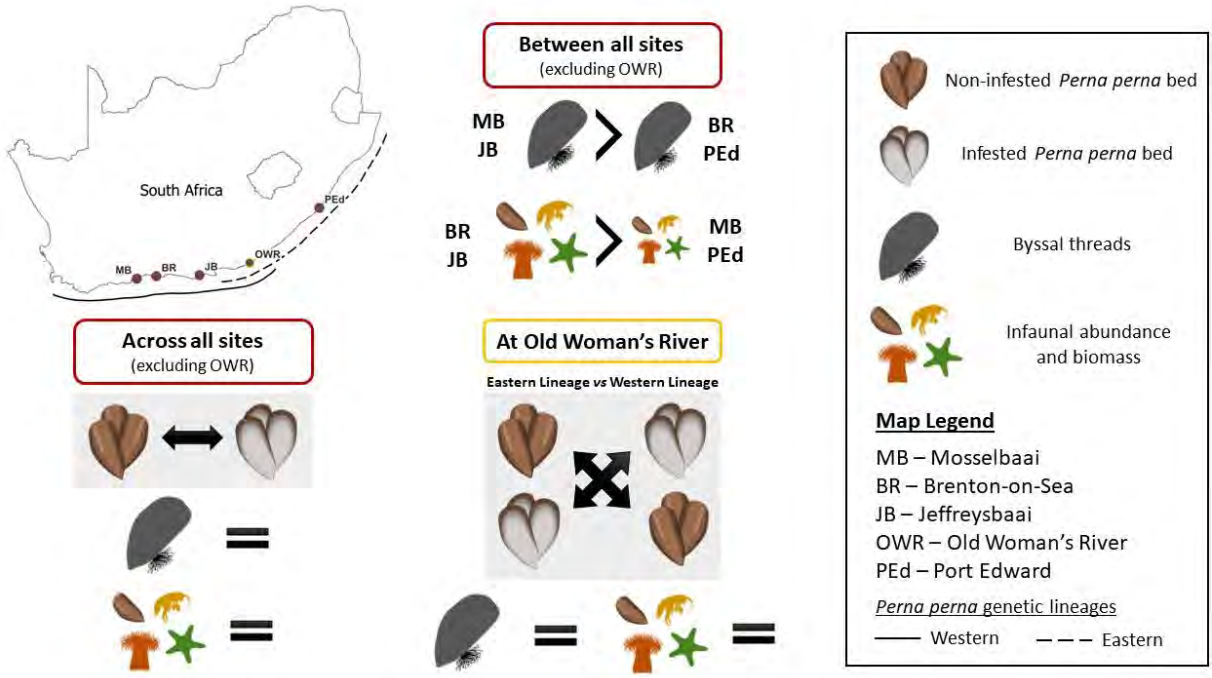

Figure 4.0. Graphical abstract summarizing the findings presented in Chapter 4. **Top left corner**: map of the experimental sites where artificial mussel bed transplants were made along the South African coastline and distribution of *Perna perna* genetic lineages (plain line: western; dashed line: eastern); **bottom left corner and right panel**: graphical presentation of the experimental results, comparing the number of byssal threads and the abundance and the biomass of infaunal communities associated with either non-infested and infested *Perna perna* beds.

4.1. Introduction

Since the late 1980's, unprecedent concern about biodiversity arose within the scientific community and public opinion (Brundtland, 1987; UNCED, 1993). As human activities increasingly threatened biodiversity worldwide, the need to conserve and maintain genetic diversity, species, and ecosystems was recognized internationally and has led to the development of national conservation strategies (UNCED, 1993). Habitat destruction and fragmentation, pollution, over-exploitation, biological invasions, and anthropogenic global climate change are triggering rapid changes in environmental conditions, leading to global biodiversity loss and changes in species distributions, thus influencing the composition of ecological communities (Barnosky et al., 2011; Bellard et al., 2012; Cardinale et al., 2012; Nagelkerken and Connell, 2022; Parmesan, 2006; Parmesan and Yohe, 2003; Tilman et al., 2001; UNCED, 1993). The increasing and accelerating loss of biodiversity (Myers and Knoll, 2001; Parmesan, 2006; Pimm, 1998; Thomas et al., 2004; Urban, 2015) is considered a major driver of ecosystem change (Hooper et al., 2012; Tilman et al., 2014, 2012). In this context, increased research has focused on estimating the magnitude and consequences of biodiversity loss to ecosystem structure and functioning (Balvanera et al., 2014; Hooper et al., 2012; Tilman et al., 2012), and the services that they provide (Isbell et al., 2017; Kremen, 2005). In most related studies, however, biodiversity has been estimated at the species level, which, while essential, is not necessarily representative of overall biodiversity (Mace et al., 2012; Thomas et al., 2004; Urban, 2015). Assuming that a species is a physiologically homogeneous unit is often misleading, as sex, ages classes, genotypes and phenotypes may differ in ecologically significant ways within a given species (Bolnick et al., 2011, 2003; Fraser and Bernatchez, 2001). More recently, intraspecific phenotypic trait variation has been

demonstrated to have large effects on ecological processes (Hughes et al., 2008), such as primary productivity (Gerstenmaier et al., 2016; Tomimatsu et al., 2014), population response to environmental stress and recovery from disturbance (Hughes and Stachowicz, 2004; Reusch et al., 2005; Reynolds et al., 2012), interspecific competition (Hughes, 2014), community structure (Bangert et al., 2008; Whitlock et al., 2007), and fluxes of energy and nutrients (Tomimatsu et al., 2014).

Intraspecific diversity may functionally supersede the role of species diversity (Cook-Patton et al., 2011; Nicastro et al., 2020; Whitham et al., 2003), with more genetically or phenotypically diverse populations displaying enhanced resilience to disturbances or recruitment success compared to less diverse populations (Ehlers et al., 2008; Hughes and Stachowicz, 2004; Reusch et al., 2005). Moreover, within a species' distributional range, different lineages or populations inhabiting distinct bioregions can retain unique genotypic and phenotypic diversity which can culminate in different ecological traits (Bolnick et al., 2003; Bruno et al., 2003; Denoël and Winandy, 2015; Hughes et al., 2008; Whitham et al., 2003), thus influencing the ecosystem structure. Beyond genetic causation, biotic interactions, such as predation or parasitism, can also modify individual phenotypes within a species, thus further increasing intraspecific diversity (Mouritsen and Poulin, 2002; Poulin and Thomas, 1999; Reimer and Tedengren, 1997; Zardi et al., 2023). This is particularly true for ecosystem engineers which are organisms that directly or indirectly control the availability of resources (other than themselves) to other organisms by causing physical state changes in biotic or abiotic materials, thus modifying, maintaining, creating and/or destroying habitats (Crooks, 2002; Jones et al., 2010, 1997, 1994).

Mussels are important ecosystem engineers in marine intertidal rocky shores where they form large, dense beds (Buschbaum et al., 2009; Gutiérrez et al., 2003; Suchanek, 1985).

Mussels modify their environment primarily through the physical structure of their aggregations (i.e., autogenic engineering) and behaviours that transform living or non-living materials from one physical state to another *via* mechanical or other means, such as biodeposition or by-products of feeding behaviours (i.e., allogenic engineering) (Jones et al., 2010, 1997, 1994). In doing so, mussel aggregations form important intertidal matrices that support associated infaunal and epibiotic communities, and are thus critical to the functioning of intertidal ecosystems (e.g., Buschbaum et al., 2009; Nicastro et al., 2012; Stephens and Bertness, 1991). Mussel beds provide a protection from thermal stress (Cole, 2010; Jurgens and Gaylord, 2018; Stephens and Bertness, 1991) and predators (Thiel and Dernedde, 1994; Witman, 1985), participate in the transport of solutes and organic particles (Crooks and Khim, 1999; Tsuchiya and Nishihira, 1985), and provide surfaces for the settlement of epibionts (Bell et al., 2015; Gutiérrez et al., 2003). The degree to which ecosystem engineers modify their environment is in part determined by the population or individual traits of these facilitators (Bruno et al., 2003; Wieters, 2005). In this way, the engineering capabilities of mussels are themselves affected by the properties of the mussel beds. Physical heterogeneity (i.e., architectural complexity) of a mussel bed is determined by shell size and microtopography (Lathlean et al., 2016b; Nicastro et al., 2022), geometry and packing (Hughes and Griffiths, 1988; Koivisto and Westerbom, 2010), individual age (Tsuchiya and Nishihira, 1986), as well as the structure of the mussel bed (i.e. single- or multi-layered) (Cole and McQuaid, 2010). Importantly, mussels secrete byssal threads that firmly attach to the underlying rocky substratum, which, combined with shell fragments, debris and sediments, create a matrix that further increases physical heterogeneity and retains humidity during aerial exposure (Seed and Suchanek, 1992). In addition, mussel beds alleviate environmental stress for associated communities by

modifying conditions of irradiance, temperature, wave force and humidity (Gutiérrez et al., 2019; Jurgens and Gaylord, 2018; Lathlean et al., 2016a, 2016b; Nicastro et al., 2010; Nicastro et al., 2012). Finally, as organisms with broad geographic ranges across variable environments, mussel beds display marked inter- and intra-specific genotypic and phenotypic diversity that likely induces variations in the ecosystem processed provided by mussel beds (Cunha et al., 2014; Nicastro et al., 2020; Oróstica et al., 2022; Zardi et al., 2007b, 2015).

Around the world, shell-boring microscopic parasites (i.e., photoautotrophic euendoliths) target mussel shells and indirectly modify the mussel phenotype (reviewed in Dievart et al., 2022). Amongst other effects, the corrosive of photoautotrophic euendoliths influences the architectural complexity of individual mussels and in aggregation (Ndhlovu et al., 2022; Nicastro et al., 2022; Zardi et al., 2009). Euendolithic infestation influences the shell microtopography of individual mussels (i.e., increase in rugosity), which increases by ca. 15 % the surface complexity of euendolith-infested mussel beds, and the subsequent ingestion and trapping of microplastics (Nicastro et al., 2022). However, infested mussels attach less strongly to the substratum, likely caused by a lower production of byssal threads (Ndhlovu et al., 2022; Zardi et al., 2009), which contributes to a less architecturally complex habitat. Euendolithic infestation negatively influences the quality of mussel bed habitat offered to a wide array of dependent species, by indirectly increasing the risks of microplastic moving up the food chain and providing a less complex habitat for infaunal species. By contrast, infested mussel shells become distinctively discoloured through the boring activity of euendoliths, thus increasing their albedo. In doing so, infested mussel shells reflect more sunlight, resulting in lower individual body temperatures and greater water retention under stressful conditions (Gehman and Harley, 2019; Zardi et al., 2021,

2016). The beneficial effect of euendolithic infestation can extend to neighbouring mussels, with infested mussel beds exhibiting lower interstitial temperatures and higher humidity than non-infested beds (Lourenço et al., 2017; Zardi et al., 2021).

On South African rocky shores, the native brown mussel, *Perna perna*, dominates the warm-temperature south coast and subtropical east coast (Bownes and McQuaid, 2006; Nicastro et al., 2010), with a strong genetic break on the south-east coast (Barker, 2021; Cunha et al., 2014; Zardi et al., 2007b, 2015) that demarcates two evolutionary distinct genetic lineages. The two lineages display fundamental differences in behaviour (i.e., attachment strength and production of byssal threads, and gaping), influencing survival rates along small- and large-scale environmental gradients (Nicastro et al., 2020; Zardi et al., 2015, 2011), as well as mussel bed microclimate, which in turn modify the quality of habitat they provide for associated species (Nicastro et al., 2020; Oróstica et al., 2022; Zardi et al., 2015). Using manipulative field experiments along this stretch of coast, the current study assessed the effects of intraspecific phenotypic diversity induced by photoautotrophic euendoliths on infaunal communities associated with *P. perna*, considering the two genetic lineages present in South Africa. I hypothesized that (1) euendolith-infested mussel beds would produce less byssal threads and thus be less structurally complex than non-infested mussel beds, (2) associated fauna would be less abundant and diverse, but unique species vulnerable to thermal and desiccation stress would be found, in infested mussel beds compared to non-infested mussel beds, as euendolithic infestation would reduce byssal thread production but sometimes improved mussel bed microclimate, (3) euendolithic infestation would interact with the genetically-based differences in behaviour between eastern and western *P. perna* lineages, with infested western mussels supporting similar infaunal communities that non-infested and infested eastern mussels.

4.2. Materials and Methods

4.2.1. Focal species

The genetic lineages of *Perna perna* show a clear geographic distribution on the coasts of South Africa (Figure 4.1). The South-African coastline can be divided into three main bioregions: the cool-temperate west coast, the warm-temperate south coast and the subtropical east coast (Emanuel et al., 1992). *Perna perna* dominates the warm-temperate and subtropical bioregions, becomes nearly absent from the cold waters of the west coast (Tagliarolo et al., 2016), and finally reappears from central Namibia to the Mediterranean (Cunha et al., 2014; Lourenço et al., 2012). Analyses of *P. perna* microsatellite (Zardi et al., 2015), mitochondrial (Barker, 2021; Zardi et al., 2007b) and nuclear markers (Cunha et al., 2014) revealed a sharp phylogenetic break at the warm-temperate/subtropical transition on the southeast coast, with distinct western and eastern genetic lineages overlapping in their distributions over a distance of approximately 300 km (Figure 4.1).

During aerial exposure, *P. perna* maintains aerobic respiration by alternatively opening and closing its valves (i.e., gaping behaviour), which leads to lower body temperatures and higher humidity within aggregations (Lathlean et al., 2016a, 2016b; Nicastro et al., 2012). The two lineages exhibit differences in gaping behaviour, as well as attachment strength (through the production of byssal threads), with the eastern lineage gaping more and producing more byssal threads than the western lineage (Zardi et al., 2015). There are no apparent phenotypic shell differences between the lineages (Zardi et al., 2006). Both lineages support distinct infaunal communities and mussel recruitment rates (Nicastro et al., 2020; Oróstica et al., 2022). While *P. perna* suffers from heavy euendolithic infestation across its distribution range (Kaehler, 1999;

Marquet et al., 2013; Ndhlovu et al., 2019), no difference in the prevalence of infestation has been observed between the two lineages (Ndhlovu et al., 2019).

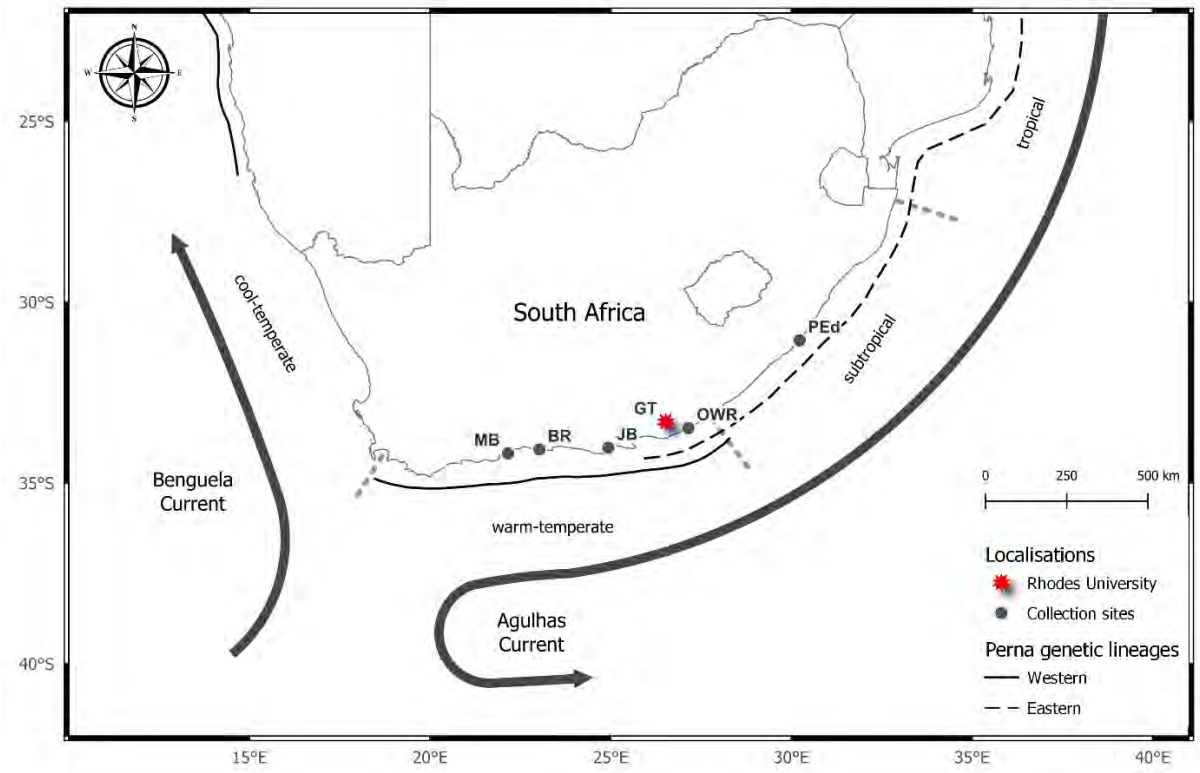

Figure 4.1. Map of the experimental sites on the South African coastline. Grey dots represent localities where the experiments were conducted (MB: Mosselbaai; BR: Brenton-on-Sea; JB: Jeffreysbaai; OWR: Old Woman's River; PEd: Port Edward; see Table 4.1). The distributional ranges of *Perna perna* lineages are represented by a continuous black line (western) and a dashed black line (eastern) (according to Barker, 2021; Zardi et al., 2007b, 2015). The three biogeographic regions along the South African coastline are delimited by grey dotted lines (according to Emanuel et al., 1992).

4.2.2. Transplant experiments

To assess the effects of euendolithic infestation on infaunal communities associated with the two lineages of *P. perna*, artificial mussel beds were deployed at six transplant sites along the South and East coasts (Table 4.1, Figure 4.1): for the western lineage, Mosselbaai (34°10'58.6"S, 22°09'29.2"E), Brenton-on-Sea (34°04'31.7"S 23°01'28.1"E) and Jeffreysbaai (34°01'33.2"S 24°55'50.4"E); in the overlapping area, Old Woman's River (33°28'55.7"S 27°09'08.2"E); and for the eastern lineage, Port Edward (31°03'23.5"S, 30°13'40.6"E). Artificial mussel beds were deployed at an additional transplant site for the eastern lineage, Cebe (32°32'33.2"S, 28°34'14.3"E), however all

quadrats were lost following intense storm episodes. Other potential transplant sites were investigated on the East coast (i.e., Haga Haga, Msikaba, Sharks Point, Port St Johns, Uhmlanga), but did not support the necessary mussel abundances to conduct this experiment.

The manipulative experiment deployed in the distribution area of pure genetic lineages (Barker, 2021; Cunha et al., 2014; Zardi et al., 2007b) consisted of two treatments: (a) 100% non-infested *P. perna* individuals, or (b) 100% infested *P. perna* individuals (Figure 4.2). For each site known to support pure genetic lineages (i.e., Mosselbaai, Brenton-on-Sea, Jeffreysbaai and Port Edward), each treatment was made up of mussels collected at the same site and deployed in the field the following day (Nicastro et al., 2020; Oróstica et al., 2022). After collection, mussels were allocated to a category of euendolithic infestation (as defined in Kaehler, 1999): A – shells with clean, intact periostracum and distinct outer growth lines, B – shells with central portion of surface eroding and turning pale purple with outer growth lines becoming indistinct, C – shells with erosion spreading past the central porting with grooves and pits appearing on shell surface, D – shells heavily pitted and becoming deformed with outer growth lines almost completely absent, and E – shells extremely pitted, deformed and brittle, eventually holed (e.g., Kaehler, 1999; Kaehler & McQuaid, 1999; Zardi et al., 2009; Marquet et al., 2013; Ndhlovu et al., 2019). Mussels affected to categories A and B were used to create non-infested mussel beds, while mussels from categories C and D were used to create infested mussel beds.

The common-garden experiment conducted within the overlapping area (i.e., Old Woman's River) consisted of four treatments: (a) 100% non-infested eastern *P. perna*, (b) 100% non-infested western *P. perna*, (c) 100% infested eastern *P. perna*, and (d) 100% infested western *P. perna* (Figure 4.2). For this site, mussels were collected

outside the overlapping area from locations known to support pure genetic lineages (i.e., Port Edward for the eastern lineage and Jeffreysbaai for the western lineage). After collection, mussels used in the common-garden experiment were kept in seawater tanks (salinity: 35‰), in a controlled environment (CE) room set at 20°C (± 0.5°C) under a 12:12h (light:dark) light regime for approximately two weeks before deployment in the field, following Nicastro et al. (2020) and Oróstica et al. (2022).

Table 4.1. Summary of the transplant experiments including dates of deployment in the field, dates of collection and missing quadrats.

Site	*Perna* lineage	Date of mussel sampling	Date of deployment	Date of collection	Missing quadrats at collection
Mosselbaai	Western	07/10/2021	08/10/2021	18/03/2022	None
Brenton-on-Sea	Western	05/10/2021	06/10/2021	17/03/2022	1 infested
Jeffreysbaai	Western	03/10/2021	04/10/2021	16/03/2022	1 infested, 1 non-infested
Old Woman's River	Western, Eastern	W: 18/10/2021, E: 22/10/2021	04/11/2021, 05/11/2021	16/05/2022	None
Port Edward	Eastern	18/11/2021	19/11/2021	02/03/2022	2 infested, 1 non-infested

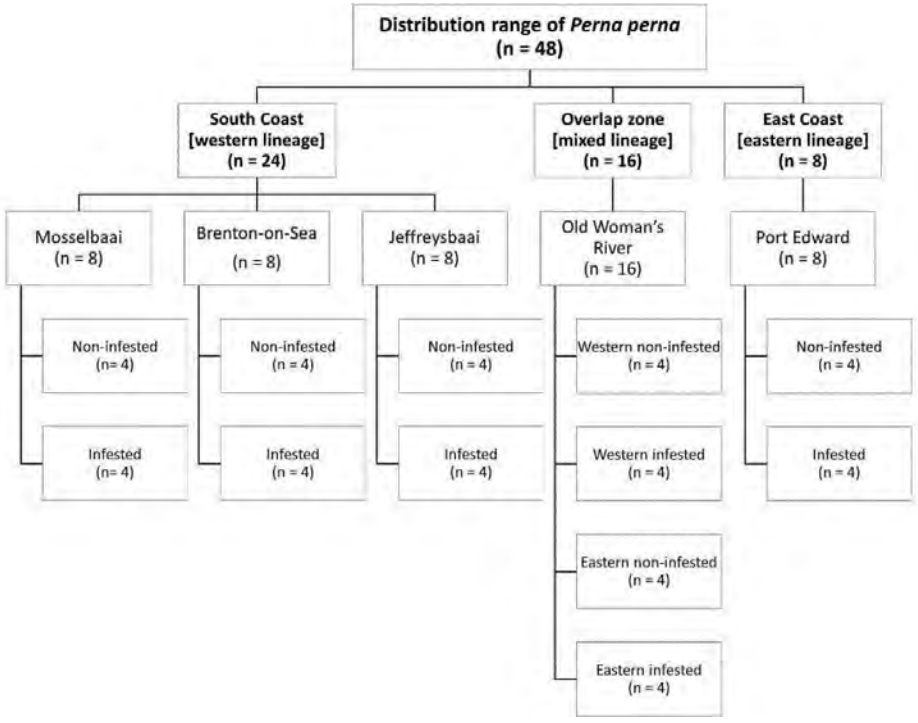

Figure 4.2. Experimental design of the transplantations for each site and each treatment. n = number of replicate plots.

For all sites, mussels (shell length: 4 – 5 cm) were gently scrubbed clean of all associated taxa with a scalpel, separated and randomly allocated across treatments before being deployed in the field. For each site and each treatment, mussels were then placed in 15 x 15 cm stainless steel quadrats (n = 4), in pairs (i.e., 1 infested and 1 non-infested), secured by washers and screws into rawlplugs, in previously drilled holes, and then covered with a strong nylon mesh (mesh size: 16 mm), so they could firmly re-attach to the substratum (Nicastro et al., 2020; Oróstica et al., 2022; Zardi et al., 2011) (Figure 4.3). Each artificial mussel bed was placed in a flat cleared area on the mid-shore, among, but not touching, existing mussel beds (Figure 4.3). Forty-five mussels were placed in each quadrat, which constitute 100% cover, at densities representative of co-occurring natural mussel beds (McQuaid and Mostert, 2010). To avoid losses of mussels due to wave action or storm events, the mesh was retained on the artificial mussel beds for the entire duration of the experiment which lasted from five to six months (Table 4.1). Previous, manipulative experiments showed that the presence of the mesh does not affect the temperatures experienced by mussels of the same colour (Zardi et al., 2011). However, as the beneficial thermal buffering provided by euendoliths is caused by the whitening of the mussel shell, shading by the mesh might mask such effects for the associated infaunal communities.

Figure 4.3. Configuration of the transplant experiments *in situ*, as set up on the rocky shores, for the common-garden experiment in Old Woman's River (a) and Port Edward (c). Quadrats were placed in a flat cleared area, on the mid-shore, among, but not touching, existing mussel patches, in Old Woman's River (b) and Port Edward (d).

To assess infaunal communities, all mussels and associated infauna were collected at the end of the experiment (Table 4.1). Samples were preserved in 70% ethanol in the field, then washed and separated through a sieve with 0.5 mm mesh in the laboratory. All invertebrate macrofauna (> 0.5 mm) were sorted, counted, and identified to the lowest taxonomic level possible (using Branch et al., 2016; Day, 1969, 1967; Griffiths, 1976; Kensley, 1978), before being dried for two days at 60°C for a minimum of two days, to assess their biomass (Hines and Comtois, 1985). To assess within-bed structural complexity, the number of live and dead mussels, as well as the number of broken shells were recorded for each artificial bed. Additionally, the total number of

byssal threads was counted for three mussels in each artificial mussel bed at the end of the experiment (Nicastro et al., 2010; Zardi et al., 2007a, 2006).

4.2.3. Data analyses

As site is intricately confounded with *Perna perna* lineage, separate analyses were conducted to test (1) the effect of euendolithic infestation and site, across all sites excluding Old Woman's River, and (2) the effect of euendolithic infestation and *P. perna* lineage in the common-garden experiment conducted at Old Woman's River, on both the structural complexity of the artificial mussel beds and the infaunal communities they hosted.

All datasets and R scripts can be accessed and downloaded using the following link: https://github.com/AlexiaDievart/endolith_infauna.

4.2.3.1. Within-bed structural complexity

Within-bed structural complexity was assessed using the total number of mussels (live and dead), as well as the number of broken shells (i.e., shell fragments presenting the hinge and pieces of both valves), and the average number of byssal threads per mussel for each treatment.

Across all sites (excluding Old Woman's River), a series of type II two-way ANOVAs were employed to assess the effect of euendolithic infestation (fixed factor, two levels: non-infested, infested) and site (fixed factor, four levels: Mosselbaai, Brenton-on-Sea, Jeffreysbaai, Port Edward) on the total number of mussels (live and dead), broken shells and byssal threads per mussel, as data fitted the assumptions of normality (Shapiro's test) and homogeneity of variances (Levene's test). When an effect was significant, pairwise comparisons using Tukey's HSD were conducted. At Old Woman's River, a series of two-way ANOVAs were employed to assess the effect of euendolithic infestation (fixed

factor, two levels: non-infested, infested) and *P. perna* lineage (fixed factor, two levels: eastern, western) on the total number of mussels, broken shells and byssal threads per mussel, as data fitted the assumptions of normality (Shapiro's test) and homogeneity of variances (Levene's test). When an effect was significant, pairwise comparisons using Tukey's HSD were conducted.

4.2.3.2. Infaunal communities

First, infaunal communities were described in terms of total abundance and biomass of infauna, species richness (S), species diversity, either calculated with Shannon-Wiener (*H'*) or Simpson (λ) diversity index, and species evenness, calculated with Pielou's evenness index (J), per quadrat. Species richness is the number of different species represented in an ecological community (Colwell, 2009). Shannon-Wiener diversity index emphasizes rare species, while Simpson diversity index emphasizes common species (Colwell, 2009; Fedor and Spellerberg, 2013; Nagendra, 2002). Pielou's evenness index indicates how evenly the individuals in an ecological community are distributed among the different species (Pielou, 1966).

Across all sites (excluding Old Woman's River), a series of type II two-way ANOVAs were employed to assess the effect of euendolithic infestation (fixed factor, two levels: non-infested, infested) and site (fixed factor, four levels: Mosselbaai, Brenton-on-Sea, Jeffreysbaai, Port Edward) on species richness, species diversity (Shannon-Wiener and Simpson indexes), and species evenness (Pielou's index), as data fitted the assumptions of normality (Shapiro's test) and homogeneity of variances (Levene's test). The effect of euendolithic infestation and site on total infaunal abundance and biomass was assessed using a Generalized Linear Model (GLM, family: Gamma), as the data did not fit the assumptions. Model fits were assessed using residual diagnostics using the 'appraise' function from the 'gratia' R package (Simpson, 2022). When an effect was significant,

pairwise comparisons using Tukey's HSD were conducted. At Old Woman's River, a series of two-way ANOVAs were employed to assess the effect of euendolithic infestation (fixed factor, two levels: non-infested, infested) and *Perna perna* lineage (fixed factor, two levels: eastern, western) on total infaunal abundance and biomass, species richness, species diversity (Shannon-Wiener and Simpson indexes), and species evenness (Pielou's index), as the data fitted the assumptions of normality (Shapiro's test) and homogeneity of variances (Levene's test).

Second, changes in infaunal communities between beds composed of different degree of euendolithic infestation across all sites (excluding Old Woman's River) and of different lineages and degree of infestation at Old Woman's River were compared in terms of abundance or biomass for each species and each quadrat using a series of multivariate analyses.

Across all sites (excluding Old Woman's River), two-way permutational multivariate analyses of variance (PERMANOVA) were performed with euendolithic infestation (two levels: infested, non-infested) and site (four levels: Mosselbaai, Brenton-on-Sea, Jeffreysbaai, Port Edward) as categorical parametric fixed effects for both species abundance and biomass. At Old Woman's River, two-way PERMANOVA were performed with infestation and *P. perna* lineages (two levels: eastern, western) as categorical parametric fixed effects. For each PERMANOVA analysis, a Bray-Curtis dissimilarity matrix for square root transformed multivariate data was used to reduce asymmetry and compress large values, as the raw data were heavily skewed (Lamy et al., 2015). Significance of F-ratios was determined from 9,999 randomizations (Anderson, 2005). Permutation tests of multivariate dispersion (PERMDISP; Anderson, 2004) were used to check the homogeneity in the average dissimilarities of samples from the central location of their group. Similarity percentage analyses

(SIMPER; Clarke and Ainsworth, 1993) were then used to determine the percentage contribution of each variable (species abundance or biomass) made to the Bray-Curtis dissimilarities. Species were ranked by their contribution to overall dissimilarity and included up to a cumulative total of 50% of average dissimilarity. Differences between assemblages were visualized using: (1) non-metric multidimensional scaling (nMDS) ordination plots, (2) dispersion plots, and (3) hierarchical cluster analysis using the Ward linkage method. Ward linkage method minimizes variances in hierarchically identified assemblages and performs well with Bray-Curtis measures (Dominik et al., 2017; Singh et al., 2011). All methods were based on Bray-Curtis similarity matrices of either species abundance or species biomass.

4.3. Results

4.3.1. Within-bed structural complexity

Across all sites (excluding Old Woman's River), the total number of mussels (live and dead) and the average number of byssal threads per mussel did not differ significantly between infested and non-infested mussel beds although significant differences were observed between the different sites (Figure 4.4a,b; Tables 4.2a,c). The number of broken shells did not differ significantly between the levels of euendolithic infestation or sites (Figure 4.4c; Table 4.2b).

The total number of mussels per quadrat at Mosselbaai was significantly higher than at Port Edward (Figure 4.4a; Table 4.3a, $p < 0.05$). The number of byssal threads per mussel at Jeffreysbaai was significantly higher than at Brenton-on-Sea ($p < 0.001$) and Port Edward ($p < 0.01$), and significantly higher in Mosselbaai compared to Brenton-on-Sea ($p < 0.01$) (Figure 4.4c; Table 4.3b).

Table 4.2. Type II two-way ANOVAs on the effect of euendolithic infestation and site on (a) the total number of mussels (live and dead), (b) the number of broken shells, and (c) the number of byssal threads, across all sites, excluding Old Woman's River. Significant p-values are underlined.
Models used in these analysese are as follow: (a) tot_mussels ~ infestation + site, (b) nb_broken ~ infestation + site, and (c) nb_byssal ~ infestation + site. Interactions were not significant in any of the models.

Source of variation	Type II Sum of Squares	df	*F*-value	p-value
(a) Total number of mussels				
Infestation	3.02	1	0.032	0.861
Site	1159.50	3	4.039	0.019
Residuals	2201.17	23		
(b) Number of broken shells				
Infestation	3.306	1	0.376	0.546
Site	20.028	3	0.758	0.529
Residuals	202.474	23		
(c) Number of byssal threads				
Infestation	254	1	0.074	0.787
Site	93523	3	9.034	3.668×10^{-5}
Residuals	251917	73		

Table 4.3. Results of the TukeySD post-hoc pairwise comparisons on the effect of site on (a) the total number of mussels and (b) the number of byssal threads, across all sites, excluding Old Woman's River. Significant p-values are underlined.

Site (a)	Site (b)	Estimate	Std Error	*t*-value	p-value
(a) Total number of mussels					
Mosselbaai	Brenton-on-Sea	3.547	5.070	0.700	0.896
	Jeffreysbaai	9.167	5.283	1.735	0.329
	Port Edward	– 16.690	5.070	– 3.292	0.015
Brenton-on-Sea	Jeffreysbaai	– 5.620	5.449	– 1.031	0.733
	Port Edward	– 13.143	5.229	– 2.513	0.084
Jeffreysbaai	Port Edward	– 7.523	5.449	– 1.381	0.523
(b) Number of byssal threads					
Mosselbaai	Brenton-on-Sea	58.33	17.58	3.318	0.008
	Jeffreysbaai	– 33.89	18.32	– 1.850	0.258
	Port Edward	– 35.26	19.38	– 1.819	0.272
Brenton-on-Sea	Jeffreysbaai	92.22	18.89	4.881	< 0.001
	Port Edward	23.07	19.86	1.161	0.652
Jeffreysbaai	Port Edward	– 69.15	20.58	– 3.360	0.007

At Old Woman's River, the total number of mussels (live and dead) and broken shells per quadrat, as well as the number of byssal threads per mussel, were not significantly different between euendolithic infestation levels and *Perna perna* lineages (Figure 4.4d,e,f; Tables 4.4a,b,c).

Table 4.4. Two-way ANOVAs (balanced design) on the effect of euendolithic infestation and *Perna perna* lineages on (a) the total number of mussels (live and dead), (b) the number of broken shells, and (c) the number of byssal threads, at Old Woman's River. No significant p-values were detected.
Models used in these analysese: (a) tot_mussels ~ infestation + lineage, (b) nb_broken ~ infestation + lineage, and (c) nb_byssal ~ infestation + lineage. Interactions were not significant in any of the models.

Source of variation	Sum of Squares	df	*F*-value	p-value
(a) **Total number of mussels**				
Infestation	138.06	1	2.827	0.117
Lineage	162.56	1	3.329	0.091
Residuals	634.81	13		
(b) Number of broken shells				
Infestation	189.06	1	1.335	0.269
Lineage	297.56	1	2.101	0.171
Residuals	1840.81	13		
(c) Number of byssal threads				
Infestation	4701	1	1.275	0.265
Lineage	7475	1	2.028	0.161
Residuals	165847	45		

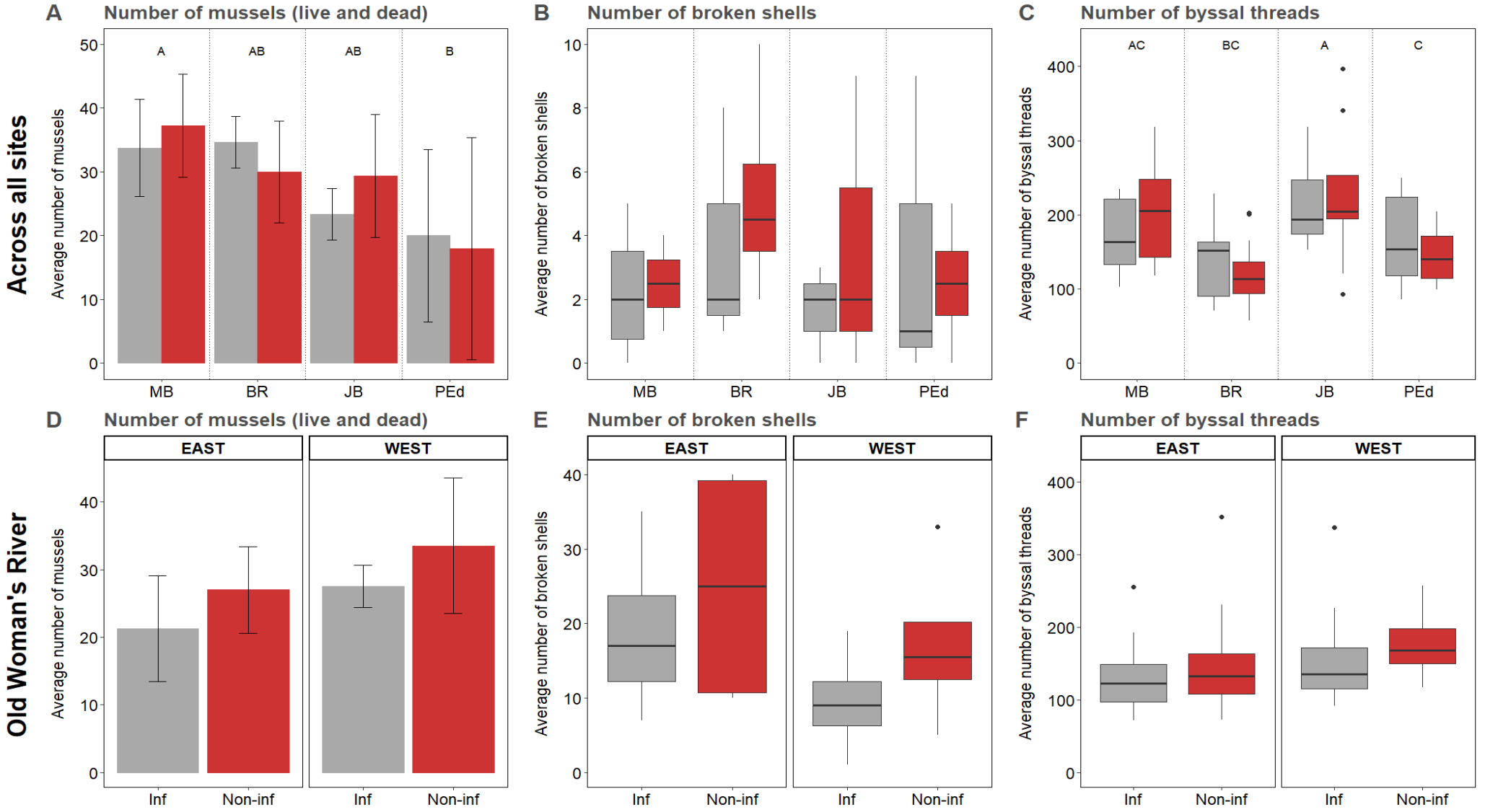

Figure 4.4. Barplot for (a, d) average number of mussels (live and dead) per quadrat (± SD), and boxplots for (b, e) average number of broken shells per quadrat (± SD), and (c, f) average number of byssal threads per mussels (± SD). Across all sites, excluding Old Woman's River (a, b, c), homogeneous groups are indicated by similar letters. MB: Mosselbaai; BoS: Brenton-on-Sea; JB: Jeffreysbaai; PEd: Port Edward. At Old Woman's River (d, e, f), no significant differences were detected between infestation levels or *Perna perna* lineages (East and West). Infested and non-infested mussel beds are represented in grey and red respectively.

4.3.2. Infaunal communities

A total of 115 invertebrate taxa were recorded within the experimental mussel beds across all treatments and sites (Table S4.1, Figure 4.5). Among the infauna, 14 taxa could only be identified to phylum, order, class, or family levels, while seven taxa could only be identified to the genus level. A total of 80 taxa were associated with the infested mussel beds and 80 taxa with the non-infested mussel beds across all sites (excluding Old Woman's River). At Old Woman's River, if both infestation levels and *Perna perna* genetic lineages are considered, 40 taxa were associated with the eastern infested mussel beds, 50 taxa with the western infested mussel beds, 53 taxa with the eastern non-infested mussel beds, and 43 taxa with the western non-infested mussel beds. Across all sites (excluding Old Woman's River), a total of 60 taxa were common at both infestation levels, while at Old Woman's River, 25 taxa were common to all treatment levels. It is to note that some shelled invertebrates recorded from the experimental mussel beds displayed significant levels of shell erosion (e.g., *Scutellastra granularis*, *Acanthochitona garnoti*), which was expected and could not be directly imputed to euendolithic infestation for this study.

Across all sites (excluding Old Woman's River), total infaunal abundance and biomass differed significantly between sites, but not between infestation levels of the mussels (Figure 4.6a,b; Table 4.5a,b). Species richness did not differ significantly between euendolithic infestation levels or sites (Figure 4.6c; Table 4.6a). Species diversity, calculated with either Shannon-Wiener (*H'*) or Simpson (λ) diversity index, and species evenness, calculated with Pielou's index, differed significantly between sites, but not between levels of euendolithic infestation (Figure 4.5d,e,f; Table 4.6b,c,d).

Table 4.5. Type II two-way ANOVAs (unbalanced design) on the Generalized Linear Model (GLM) of the effect of euendolithic infestation and site on (a) the total abundance and (b) the total biomass of infauna across all sites, excluding Old Woman's River. Significant p-values are underlined.
Models used in these analyses are as follow: (a) ab_total ~ infestation + site, family = "Gamma", (b) biom_total ~ infestation + site, family = "Gamma". Interactions were not significant in any of the models.

Source of variation	LR Chisq	df	P (> Chisq)
(a) **Total infaunal abundance**			
Infestation	0.597	1	0.440
Site	73.589	3	$\underline{7.269 \times 10^{-16}}$
Residuals	5.081	23	
(b) Total infaunal biomass			
Infestation	0.244	1	0.622
Site	35.414	3	$\underline{9.959 \times 10^{-8}}$
Residuals	13.607	23	

Table 4.6. Type II two-way ANOVAs (unbalanced design) on the effect of euendolithic infestation and site on (a) species richness, (b) species diversity, calculated with Shannon-Wiener index (*H'*), (c) species diversity, calculated with Simpson's index (λ), and (d) species evenness, calculated with Pielou's index (J) across all sites, excluding Old Woman's River. Significant p-values are underlined.
Models used in these analyses are as follow: (a) count ~ site + infestation , (b) shannon ~ site + infestation, (c) simpson ~ site + infestation, and (d) pielou ~ site + infestation. Interactions were not significant in any of the models.

Source of variation	Type II Sum of Squares	df	*F*-value	p-value
(a) **Species richness**				
Infestation	0.62	1	0.025	0.875
Site	172.95	3	2.365	0.097
Residuals	560.68	23		
(b) Shannon-Wiener index (*H'*)				
Infestation	0.0457	1	0.434	0.517
Site	1.289	3	4.078	<u>0.018</u>
Residuals	2.424	23		
(c) Simpson's index (λ)				
Infestation	0.010	1	1.688	0.207
Site	0.079	3	4.509	<u>0.013</u>
Residuals	0.134	23		
(d) Pielou's index (J)				
Infestation	0.008	1	1.086	0.308
Site	0.168	3	7.638	<u>0.001</u>
Residuals	0.169	23		

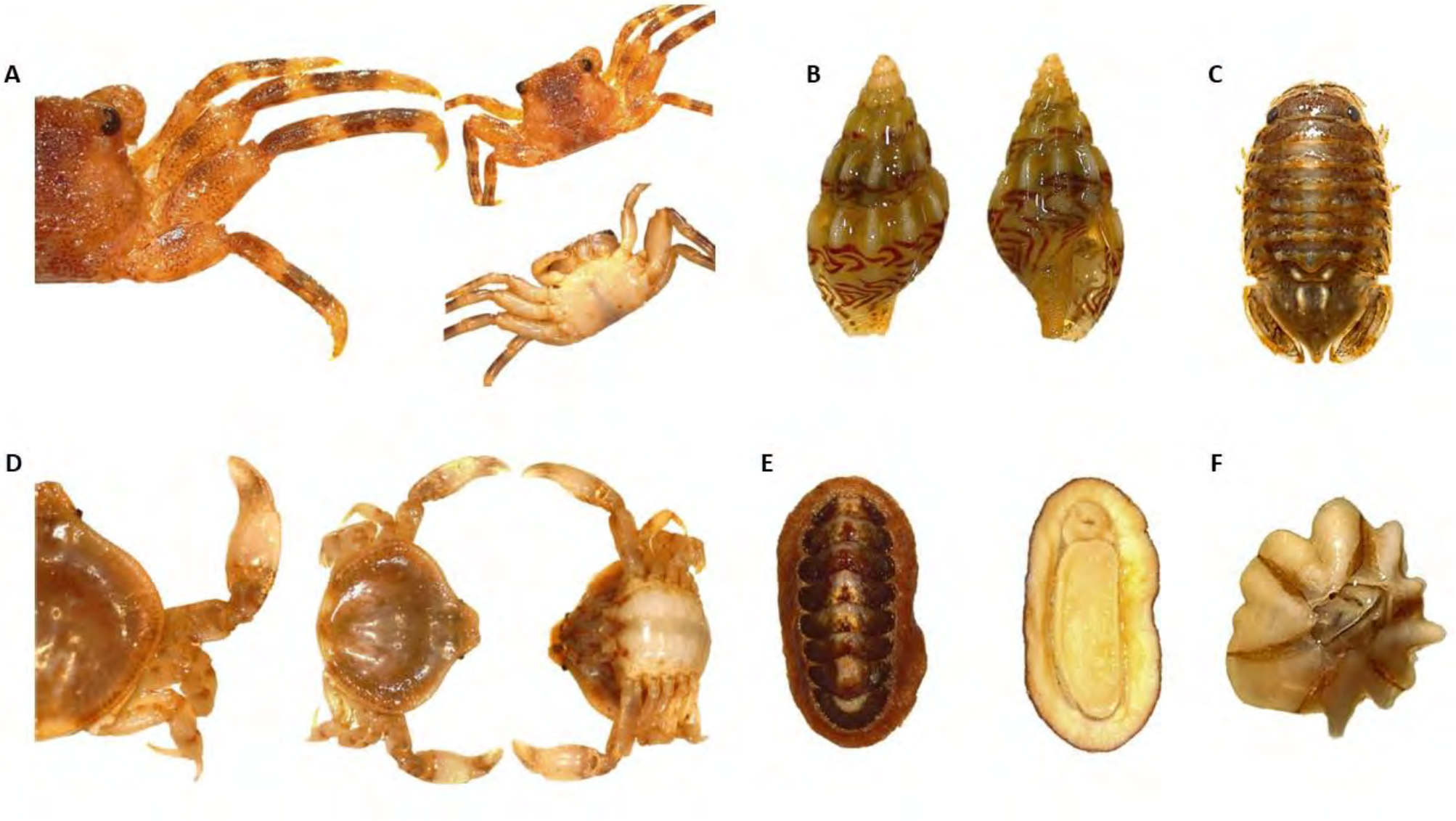

Figure 4.5. Pictures of infaunal invertebrates of interest found in the manipulated mussel beds set up on the rocky shores for this study: (a) Juvenile *Plagusia squamosa*, in non-infested mussel beds at Port Edward; (b) Juvenile *Anachis kraussi* subsp. *kraussi*, in non-infested mussel beds at Port Edward; (c) female *Parisocladus perforatus*, in non-infested mussel beds at Mosselbaai; (d) *Leucisca squalina*, in non-infested mussel beds at Port Edward; (e) *Onithochiton literatus*, in infested mussel beds at Port Edward; (f) *Chthamalus dentatus*, in non-infested mussel beds at Mosselbaai. For all pictures: © Alexia DIEVART.

Across all sites (excluding Old Woman's River), total infaunal abundances at Brenton-on-Sea and Jeffreysbaai were significantly higher than at Mosselbaai and Port Edward (Figure 4.6a; Table 4.7a). Similarly, the total infaunal biomass at Brenton-on-Sea was significantly higher than at Mosselbaai and Port Edward, while total infaunal biomass at Jeffreysbaai was significantly higher than at Port Edward (Figure 4.6b; Table 4.7b). Species diversity calculated with Shannon-Wiener index (*H'*) was significantly higher at Port Edward than at Mosselbaai (Figure 4.6d; Table 4.7c), while species diversity calculated with Simpson's index (λ) was significantly higher at Port Edward than at both Mosselbaai and Jeffreysbaai (Figure 4.6e; Table 4.7d). Species evenness, calculated with Pielou's index (J), at Port Edward was significantly higher than at all the other sites (Figure 4.6f; Table 4.7e).

At Old Woman's River, total infaunal abundance and biomass, species richness, species diversity, either calculated with Shannon-Wiener (*H'*) or Simpson (λ) diversity index, and species evenness, calculated with Pielou's index, were not significantly different between infestation levels and *Perna perna* lineages (Figure 4.6g,h,i,j,k,l; Table 4.8a,b,c,d,e,f).

Table 4.7. Results of the TukeySD post-hoc pairwise comparisons on the effect of site on the (a) total infaunal abundance, (b) total infaunal biomass, (c) species diversity, calculated with Shannon-Wiener index (*H'*), (d) species diversity, calculated with Simpson's index (λ), and (e) species evenness, calculated with Pielou's index (J), across all sites, excluding Old Woman's River. Significant p-values are underlined.

Site (a)	Site (b)	Estimate	Std Error	z-value	P (> z)
(a) Total infaunal abundance					
Mosselbaai	Brenton-on-Sea	4.110×10^{-3}	0.903×10^{-3}	4.553	< 0.001
	Jeffreysbaai	3.239×10^{-3}	0.968×10^{-3}	3.346	3.880×10^{-3}
	Port Edward	4.595×10^{-3}	1.836×10^{-3}	2.503	0.051
Brenton-on-Sea	Jeffreysbaai	0.872×10^{-3}	0.528×10^{-3}	1.650	0.322
	Port Edward	8.705×10^{-3}	1.646×10^{-3}	5.287	< 0.001
Jeffreysbaai	Port Edward	7.833×10^{-3}	1.684×10^{-3}	4.652	< 0.001
(b) Total infaunal biomass					
Mosselbaai	Brenton-on-Sea	3.474×10^{-4}	1.165×10^{-4}	2.983	0.013
	Jeffreysbaai	2.525×10^{-4}	1.270×10^{-4}	1.987	0.168
	Port Edward	5.254×10^{-4}	2.795×10^{-4}	1.880	0.209
Brenton-on-Sea	Jeffreysbaai	9.488×10^{-5}	6.681×10^{-5}	1.420	0.451
	Port Edward	8.728×10^{-4}	2.578×10^{-4}	3.385	0.003
Jeffreysbaai	Port Edward	7.779×10^{-4}	2.628×10^{-4}	2.960	0.013
(c) Shannon-Wiener index (*H'*)					
Mosselbaai	Brenton-on-Sea	– 0.311	0.168	– 1.850	0.277
	Jeffreysbaai	– 0.130	0.175	– 0.743	0.878
	Port Edward	0.562	0.168	3.342	0.014
Brenton-on-Sea	Jeffreysbaai	– 0.181	0.181	– 1.000	0.750
	Port Edward	0.251	0.174	1.447	0.484
Jeffreysbaai	Port Edward	0.432	0.181	2.389	0.107
(d) Simpson's index (λ)					
Mosselbaai	Brenton-on-Sea	– 0.069	0.040	– 1.743	0.325
	Jeffreysbaai	– 0.014	0.041	– 0.340	0.986
	Port Edward	0.134	0.040	3.384	0.013
Brenton-on-Sea	Jeffreysbaai	– 0.055	0.043	– 1.292	0.577
	Port Edward	0.065	0.041	1.591	0.403
Jeffreysbaai	Port Edward	0.120	0.043	2.819	0.045
(e) Pielou's index (J)					
Mosselbaai	Brenton-on-Sea	– 0.035	0.044	– 0.785	0.860
	Jeffreysbaai	0.036	0.046	0.777	0.864
	Port Edward	0.172	0.044	3.869	0.004
Brenton-on-Sea	Jeffreysbaai	– 0.071	0.048	– 1.484	0.463
	Port Edward	0.137	0.046	2.989	0.031
Jeffreysbaai	Port Edward	0.208	0.048	4.352	0.001

Table 4.8. Two-way ANOVAs (balanced design) on the effect of euendolithic infestation and *Perna perna* lineages on (a) the total infaunal abundance, (b) the total infaunal biomass, (c) species richness, (d) species diversity, calculated with Shannon-Wiener index (*H'*), (e) species diversity, calculated with Simpson's index (λ), and (f) species evenness, calculated with Pielou's index (J), at Old Woman's River. No significant p-values were detected.
Models used in these analyses: (a) ab_total ~ infestation + lineage, (b) biom_total ~ infestation + lineage, (c) count ~ infestation + lineage, (d) shannon ~ infestation + lineage, (e) simpson ~ infestation + lineage, and (f) pielou ~ infestation + lineage. Interactions were not significant in any of the models.

Source of variation	Sum of Squares	df	*F*-value	p-value
(a) Total infaunal abundance				
Infestation	743	1	0.268	0.613
Lineage	1580	1	0.571	0.463
Residuals	35987	13		
(b) Total infaunal biomass				
Infestation	164948	1	0.124	0.730
Lineage	346600	1	0.261	0.618
Residuals	17231935	13		
(c) Species richness				
Infestation	121	1	2.774	0.120
Lineage	9	1	0.206	0.657
Residuals	567	13		
(d) Shannon-Wiener index (*H'*)				
Infestation	0.713	1	2.805	0.118
Lineage	0.292	1	1.148	0.304
Residuals	3.303	13		
(e) Simpson's index (λ)				
Infestation	0.025	1	2.237	0.159
Lineage	0.012	1	1.074	0.319
Residuals	0.145	13		
(f) Pielou's index (J)				
Infestation	0.026	1	2.014	0.179
Lineage	0.019	1	1.523	0.239
Residuals	0.165	13		

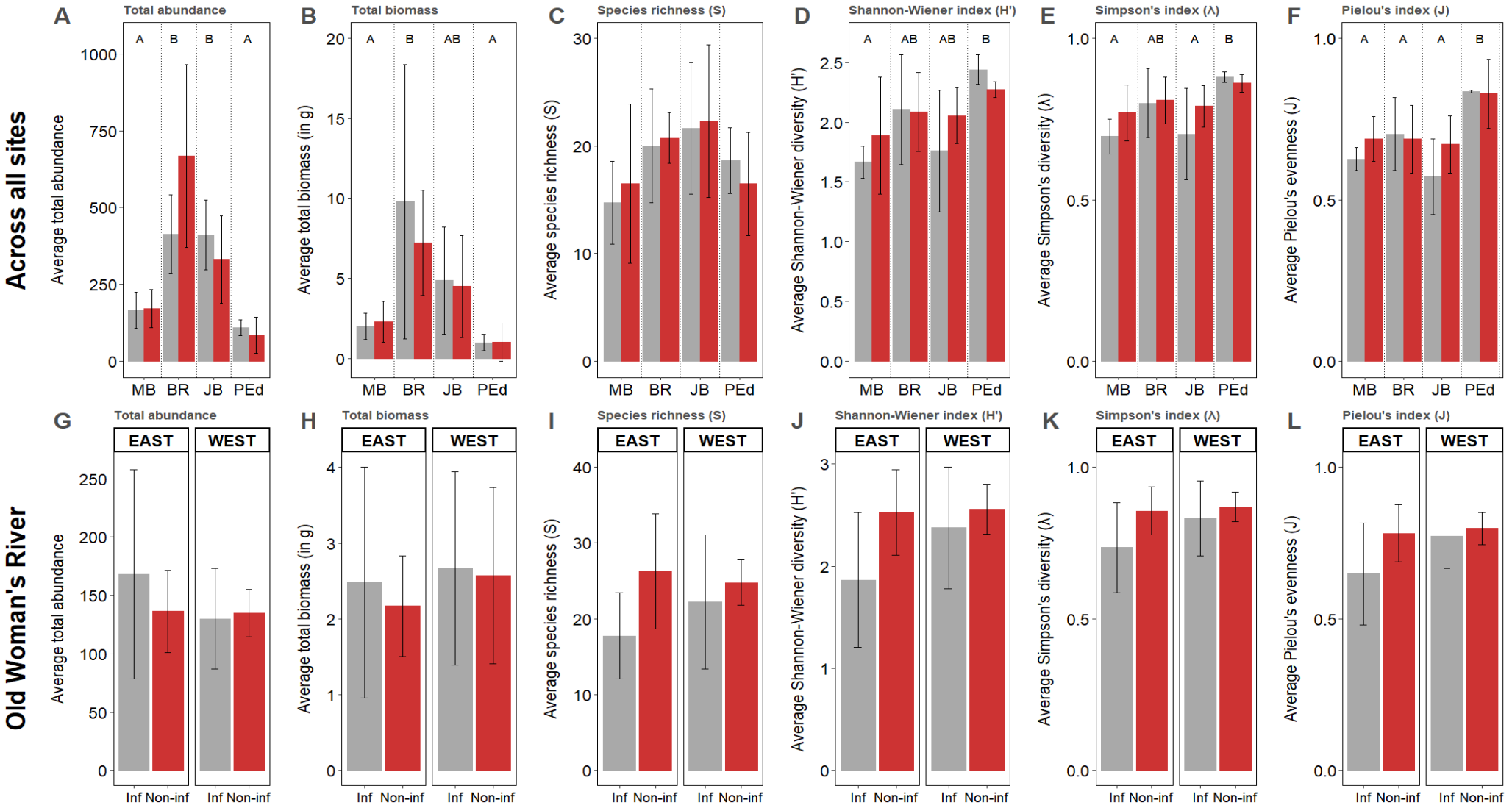

Figure 4.6. Barplots for (a,g) average infaunal abundance per quadrat (± SD), (b,h) average infaunal biomass (in g) per quadrat (± SD), (c,i) average species richness (S) per quadrat (± SD), (d,j) average Shannon-Wiener diversity index (*H'*) per quadrat (± SD), and (e,k) average Simpson's diversity index (λ) per quadrat (± SD), (f,l) average Pielou's evenness index (J) per quadrat (± SD). Across all sites (a,b,c,d,e,f), homogeneous groups are indicated by similar letters. MB: Mosselbaai; BR: Brenton-on-Sea; JB: Jeffreysbaai; PEd: Port Edward. At Old Woman's River (g,h,i,j,k,l), no significant differences were detected between infestation levels or *Perna perna* lineages (East and West). Infested and non-infested mussel beds are represented in grey and red respectively.

Across all sites (excluding Old Woman's River), infaunal communities in terms of abundance and biomass did not differ between the infested and non-infested mussel beds, although it did differ between sites (PERMANOVA, Figures 4.7a, 4.8a; Table 4.9a,b). nMDS plots, dispersion plots and hierarchical clustering analyses mirrored the PERMANOVA results and detected clear group separation by site but not by infestation level (Figures 4.7b,c, 4.8b,c, and 4.9a,b).

Table 4.9. PERMANOVA on the effect of euendolithic infestation and site on (a) infaunal abundance and (b) infaunal biomass per quadrat across all sites, excluding Old Woman's River. Significant p-values are underlined.

Source of variation	Sum of Squares	df	R^2	*F*-value	p-value
(a) **Infaunal abundance**					
Infestation	0.102	1	0.018	1.040	0.366
Site	3.381	3	0.597	11.549	<u>0.001</u>
Interaction	0.232	3	0.041	0.791	0.718
Residuals	1.951	20	0.344		
Total	5.665	27	1.000		
(b) Infaunal biomass					
Infestation	0.118	1	0.021	1.311	0.231
Site	3.501	3	0.618	12.945	<u>0.001</u>
Interaction	0.243	3	0.043	0.898	0.580
Residuals	1.803	20	0.318		
Total	5.666	27	1.000		

At Old Woman's River, total infaunal abundance and biomass did not differ with euendolithic infestation levels or *P. perna* lineage (PERMANOVA, Figures 4.7d,e,f, 4.8d,e,f, and 4.9c,d; Tables 4.29 and 4.30). While nMDS plots and dispersion plots showed a clear difference in the spread of the data between infested and non-infested mussel beds for both abundance and biomass, there was no such difference among the centroids (Figures 4.7e and 4.8e).

Table 4.10. PERMANOVA on the effect of euendolithic infestation and *Perna perna* lineage on (a) infaunal abundance and (b) infaunal biomass per quadrat across all sites per quadrat at Old Woman's River. No significant p-values were detected.

Source of variation	Sum of Squares	df	R^2	*F*-value	p-value
(a) Infaunal abundance					
Infestation	0.134	1	0.066	0.936	0.450
Lineage	0.103	1	0.051	0.723	0.650
Interaction	0.064	1	0.032	0.450	0.894
Residuals	1.716	12	0.851		
Total	2.017	15	1.000		
(b) Infaunal biomass					
Infestation	0.106	1	0.050	0.700	0.620
Lineage	0.122	1	0.058	0.809	0.544
Interaction	0.062	1	0.029	0.408	0.887
Residuals	1.811	12	0.862		
Total	2.101	15	1.000		

SIMPER analyses indicated that the following species collectively accounted for 50% of the dissimilarity between sites (excluding Old Woman's River): *Talorchestia* sp. Dana, 1852, unidentified Actiniaria species, *Burnupena lagenaria* (Lamarck, 1822), juvenile *Mytilus galloprovincialis*, *Parisocladus perforatus* (H. Milne Edwards, 1840), *Parvulastra exigua*, juvenile *Perna perna* and *Pseudonereis podocirra* (Schmarda, 1861) (formerly incorrectly synonymized as the widespread *Pseudonereis variegata* (Grube, 1857)) (Figure 4.10a, Table S4.2). In terms of biomass, dissimilarity between sites was largely driven by unidentified Actiniaria species, *Burnupena lagenaria*, juvenile *Mytilus galloprovincialis*, *Parvulastra exigua*, juvenile *P. perna*, *Ischyromene huttoni* (G. Thomson, 1879), *Pseudonereis podocirra* (Figure 4.10b; Table S4.3).

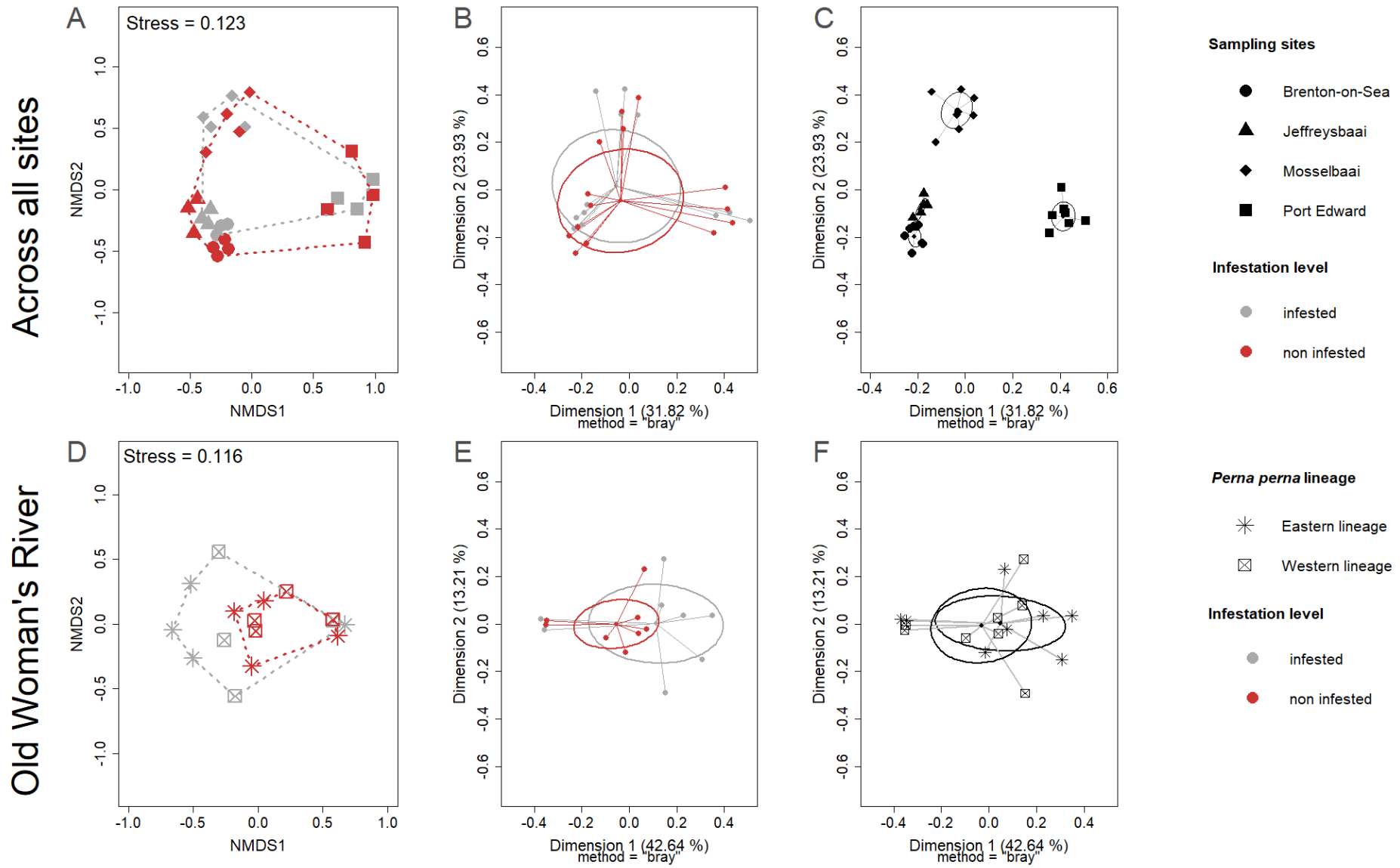

Figure 4.7. Similarity in infaunal species abundances for (a,b,c) the effect of euendolithic infestation of artificial mussel beds across all sites excluding Old Woman's River, and (c,d,e) the effect of euendolithic infestation and *Perna perna* lineages at Old Woman's River. (a,d) Non-metric multidimensional scaling (nMDS) plots, and dispersion plots for the effect of (b,e) euendolithic infestation, (c) sites, and (f) *Perna perna* lineages. Infested and non-infested mussel beds are represented in grey and red respectively.

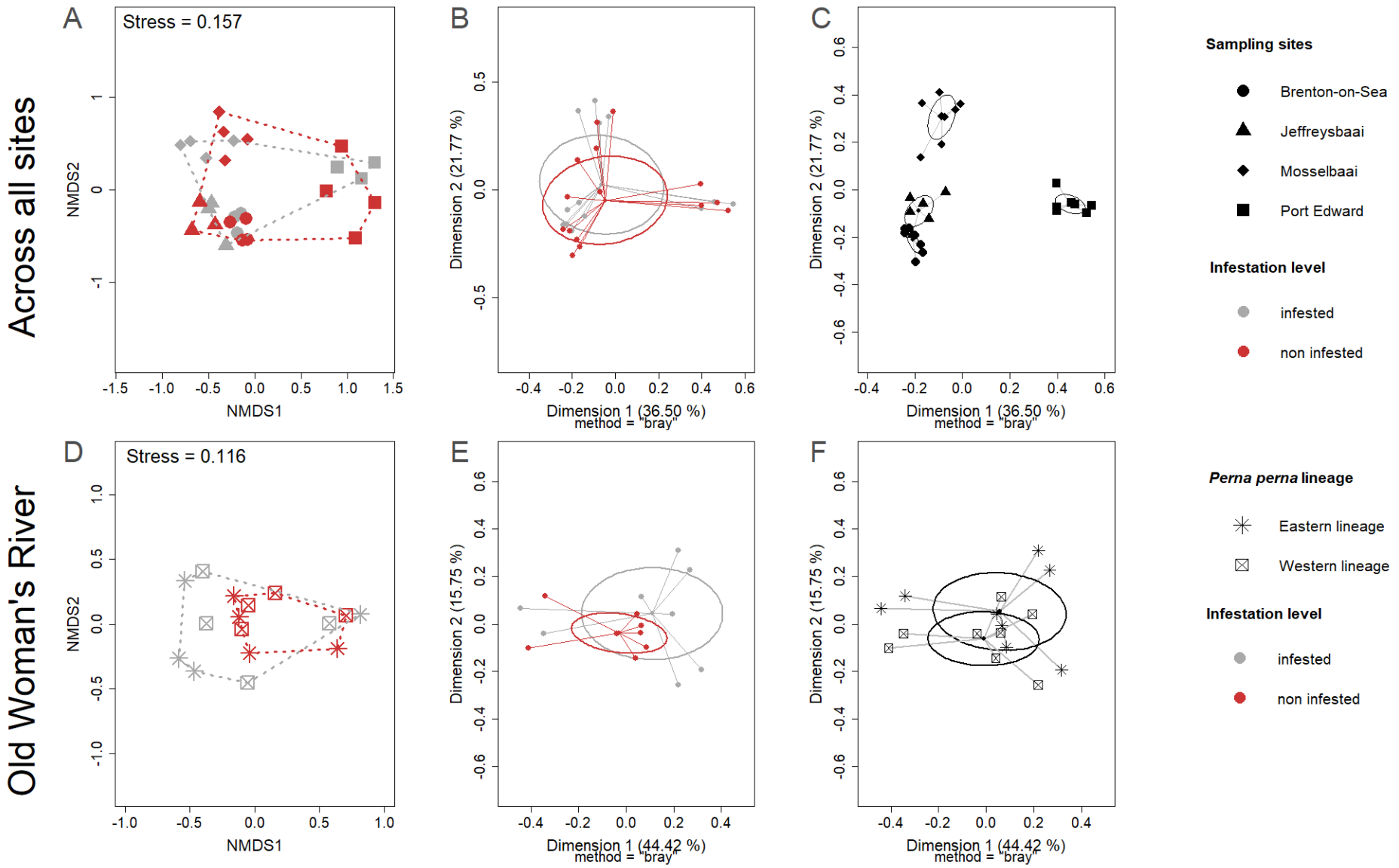

Figure 4.8. Similarity in infaunal species biomass for (a,b,c) the effect of euendolithic infestation of artificial mussel beds across all sites excluding Old Woman's River, and (c,d,e) the effect of euendolithic infestation and *Perna perna* lineages at Old Woman's River. (a,d) Non-metric multidimensional scaling (nMDS) plots, and dispersion plots for the effect of (b,e) euendolithic infestation, (c) sites, and (f) *Perna perna* lineages. Infested and non-infested mussel beds are represented in grey and red respectively.

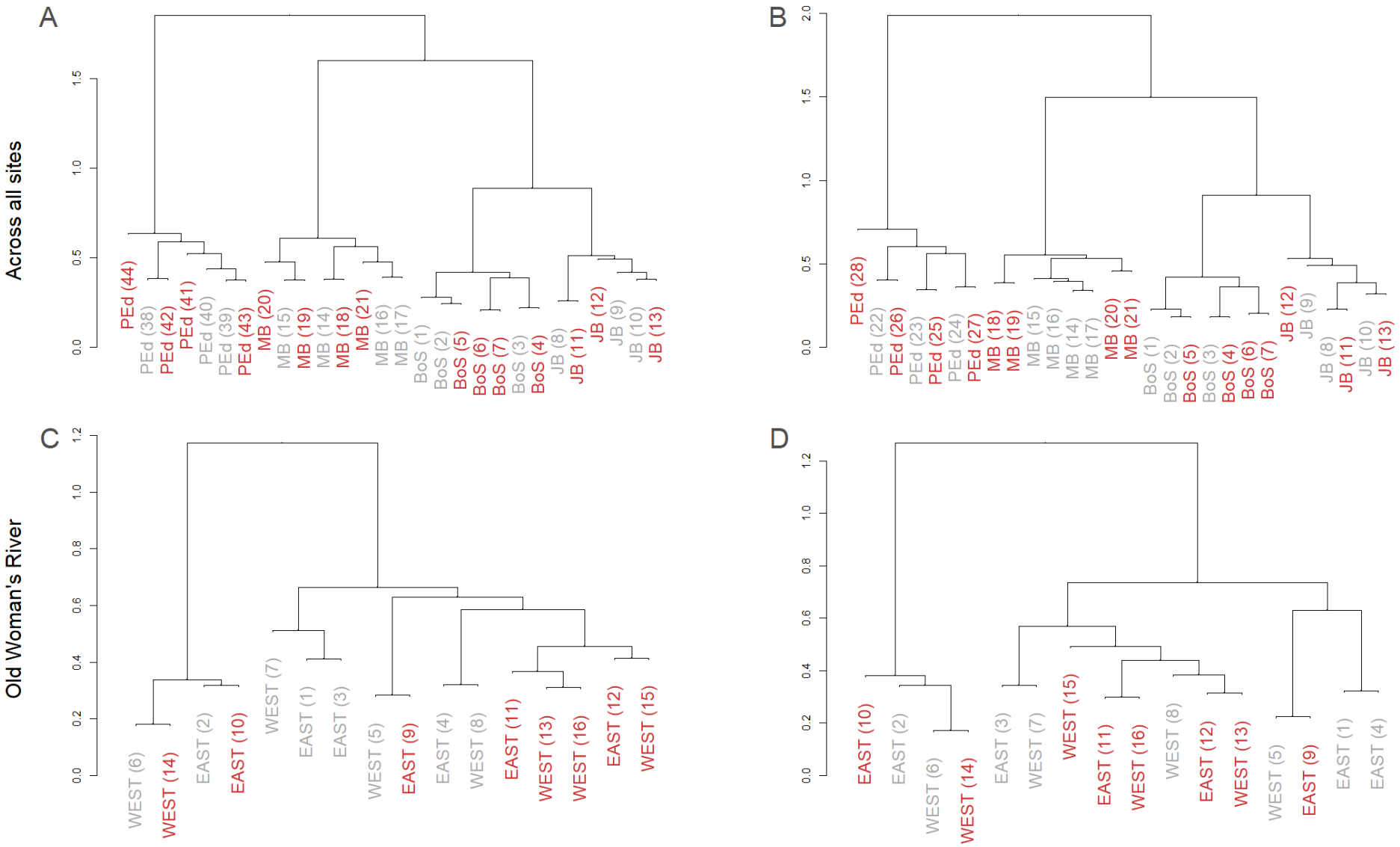

Figure 4.9. Dendrograms of the Ward linkage cluster analysis. Across all sites, infaunal (a) abundance and (b) biomass for each quadrat are clustered by sites. MB: Mosselbaai; BoS: Brenton-on-Sea; JB: Jeffreysbaai; PEd: Port Edward. At Old Woman's River, infaunal (c) abundance and (d) biomass for each quadrat are clustered by *Perna perna* lineages (i.e., eastern, or western). Infested and non-infested mussel beds are represented in grey and red respectively. Quadrat numbers are represented in brackets.

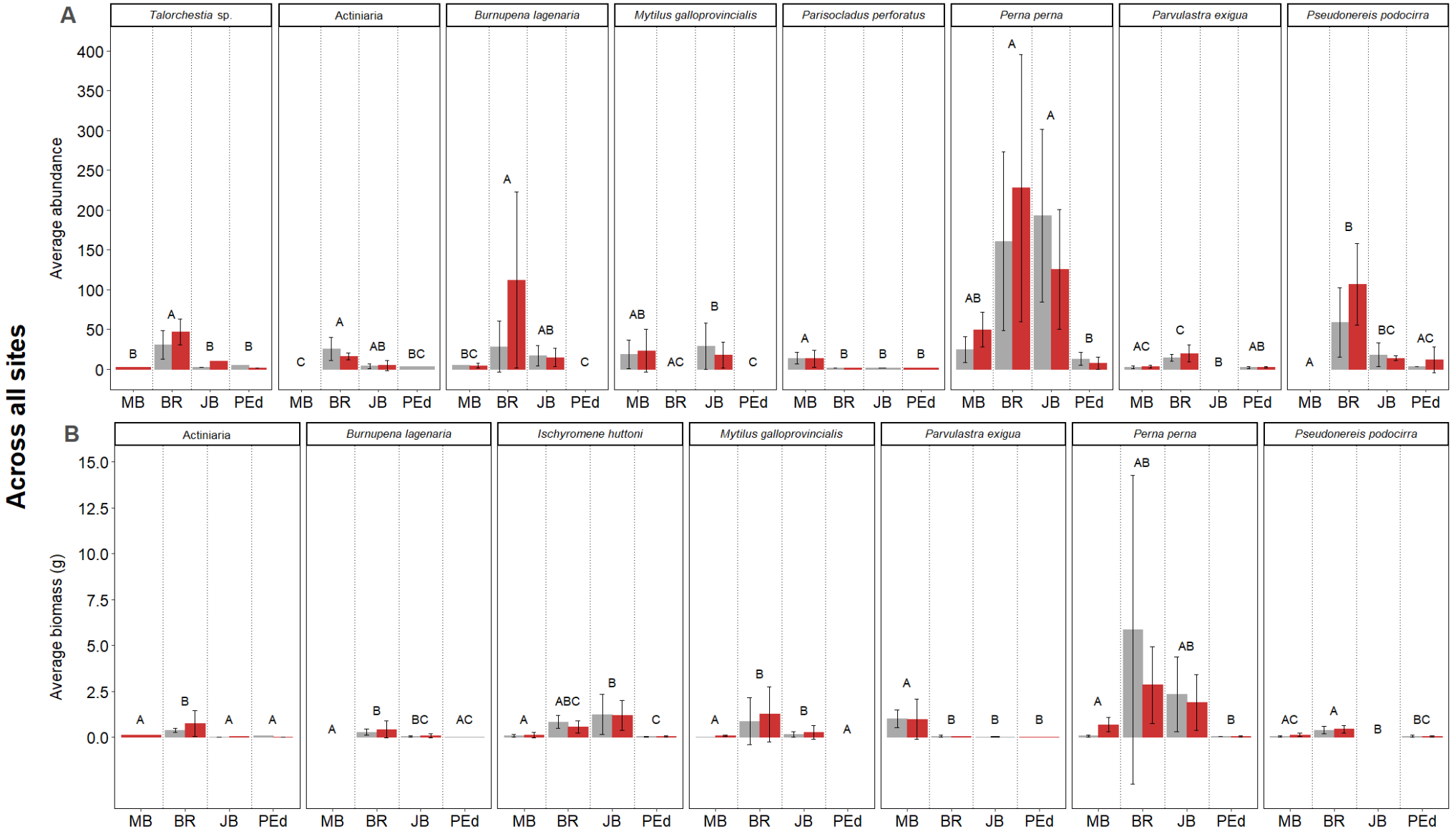

Figure 4.10. Average (a) abundance and (b) biomass per quadrat of species that contributed the most to dissimilarity between infaunal communities across sites. Significant differences between sites are indicated by the different letters. MB: Mosselbaai; BR: Brenton-on-Sea; JB: Jeffreysbaai; PEd: Port Edward. Infested and non-infested mussel beds are represented in grey and red respectively.

4.4. Discussion

It was anticipated that euendolithic infestation across all the sites would reduce the architectural complexity of the mussel beds by reducing byssal thread production, contributing to a less abundant and diverse infaunal community in the infested mussel beds. By contrast, the euendolith-induced improvements in the mussel bed microclimate, in terms of temperature and humidity, would influence the infaunal communities associated with the infested mussel beds, and would comprise species vulnerable to thermal and desiccation stress. At Old Woman's River, euendolithic infestation was hypothesized to interact with genetically-based differences in behaviour between the two lineages of *Perna perna*. Mussel beds composed of eastern lineage of *P. perna* were shown to be more benign for associated infaunal organisms, with lower within-bed temperatures and higher humidities, and thus supported higher infaunal abundances and biomass than mussel beds composed of western *P. perna*. It was expected that euendolith-induced improvements of mussel bed microclimate would counterbalance the influence of *P. perna* lineages on associated infaunal communities, with infested western mussel beds supporting similar infaunal communities than non-infested and infested eastern beds.

In this study, architectural complexity (i.e., number of byssal threads per mussel) did not differ significantly between infested and non-infested mussel beds across all sites, or between the eastern and western lineages of *P. perna* at Old Woman's River. General infaunal community descriptors, such as total abundance, species richness, diversity, and evenness indexes, followed the same pattern, as did infaunal communities. However, there was always a significant effect of site on the mussel bed architectural and structural complexity, community descriptors and infaunal communities associated with the mussel beds.

4.4.1. Within-bed structural complexity

Euendolithic infested mussels have been demonstrated to attach less strongly to the underlying substratum since they require significantly less force to be dislodged than non-infested mussels (Marquet et al., 2013; Ndhlovu et al., 2022; Zardi et al., 2009). The reduced attachment strength is thought to be the result of the lower production of byssal threads (Ndhlovu et al., 2022; Zardi et al., 2009). It is worth noting that the number, diameter and strength of byssal threads were not considered in these studies (as in Zardi et al., 2006). No evidence of the influence of euendolithic infestation on the average number of byssal threads per mussel was observed during the current investigation. Due to the corrosive activity of photoautotrophic euendoliths on their shells, infested mussels channel more energy towards shell repair, likely at the expenses of other key physiological processes, such as attachment strength (through byssal thread production) and reproduction (Alfaro et al., 2008; Kaehler and McQuaid, 1999; Ndhlovu et al., 2022, 2021a; Zardi et al., 2009). *Perna perna* has the capacity to channel energy towards the production of thicker byssal threads to cope with high hydrodynamic stress, without altering gonad production (Zardi et al., 2007a, 2006). A similar mechanism could thus be at play in *P. perna* individuals infested by euendoliths. In this context, even as more energy is required for shell repair, infested *P. perna* might be able to produce as many byssal threads as non-infested conspecifics to survive wave action. The lower attachment strength of infested mussels demonstrated in previous studies (Marquet et al., 2013; Ndhlovu et al., 2022; Zardi et al., 2009) could possibly be explained by a difference in the quality of byssal threads produced, in terms of diameter and strength.

The eastern lineage of *P. perna* has been demonstrated to attach more strongly to the substratum (Zardi et al., 2015) and produce more byssal threads (Nicastro et al., 2020)

than western lineage individuals. Interestingly, in a similar common-garden experiment conducted at the same site, the eastern lineage produced less byssal threads than the western lineage (Dievart, 2018). No evidence of the influence of either euendolithic infestation or genetic lineages on the number of byssal threads per mussel at Old Woman's River was observed during this study. The absence of any significant pattern in the number of byssal threads between genetic lineages could possibly be explained by the poor condition of eastern lineage mussels sourced for the current and previous experiments (Dievart, 2018). Indeed, eastern lineage mussels had a narrower shell and were lighter, considering flesh weight, than western lineage mussels. *Perna perna* demonstrate different spawning periods across bioregions in South Africa (van Erkom Schurink and Griffiths, 1991). In KwaZulu-Natal, *P. perna* spawn over an extended period, from May to December, while those in the Cape and Transkei have a well-marked winter spawning period (van Erkom Schurink and Griffiths, 1991). As reproduction is energetically expensive (Seed and Suchanek, 1992), the post-spawning eastern linage mussels collected from Port Edward in KwaZulu-Natal for these experiments might have not been able to channel as much energy towards byssal thread production.

Various environmental factors influence the quality and production of byssal threads in mussels, including hydrodynamic stress (Garner and Litvaitis, 2013; Nicastro et al., 2010; Zardi et al., 2007a), temperature, salinity, seasonality (Garner and Litvaitis, 2013; Moeser and Carrington, 2006; Young, 1985, but see Roberts and Carrington, 2023), ocean acidification (O'Donnell et al., 2013) and the presence of predators and epibionts (Côté, 1995; Garner and Litvaitis, 2013). The number of byssal threads per mussel was different between the experimental sites that spanned across the warm-temperate and the subtropical bioregions along the coastline of South Africa.

The wave activity and height within these two bioregions are not known to differ significantly (Zardi et al., 2015). During this investigation, the number of byssal threads per mussel was higher at Jeffreysbaai and Mosselbaai, two sites sheltered from wave action, compared to the other sites situated on the open coast. A number of mussel species produce more byssal threads at sites with low wave exposure (Garner and Litvaitis, 2013), although others showed higher attachment strength at wave exposed sites (Nicastro et al., 2010). In the laboratory, byssal thread formation was disrupted under medium to high water flow (25 – 50 $cm.s^{-1}$) in several mytilid species, but this was mitigated by the reduced flow velocity in mussel bed aggregations (Carrington et al., 2008). Similarly under laboratory conditions, juvenile *Perna canaliculus* (Gmelin, 1791) increase byssal thread production with a increase in water flow rates (Alfaro, 2006). Moreover, hydrodynamic stress may be influenced by microscale variations in the morphology of the site, and the presence of bioengineered structures (e.g., mussel beds, worm reefs; Carrington et al., 2008), thus hydrodynamic comparisons among different sites is extremely difficult.

4.4.2. Infaunal communities

It was hypothesised that euendolith-infested mussel beds would support higher species richness, diversity, and evenness, but lower total infaunal abundance and biomass per quadrat, than non-infested mussel beds across all sites. Moreover, euendolithic infestation would also contribute to variations in the abundance and biomass of the associated infaunal communities.

Infested mussel beds have been demonstrated to create a more benign habitat in terms of within-bed temperature and humidity when thermal and desiccation stress are high than non-infested mussel beds (Lourenço et al., 2017; Monsinjon et al., 2021; Zardi et al., 2021, 2016). Moreover, the architectural complexity of infested mussel beds

is influenced by the corrosive activity of euendoliths, which increases architectural complexity of mussel bed surfaces by inducing variations in shell microtopography (Nicastro et al., 2022) but potentially decreases structural complexity of the mussel bed matrix through a lower production of byssal threads (Marquet et al., 2013; Ndhlovu et al., 2022; Zardi et al., 2009). As the number of byssal threads per mussel was not different between infested and non-infested mussel beds, infested mussel beds would thus likely be more favourable to a wide array of associated infaunal species. However, no firm evidence of the influence of euendolithic infestation was found on species richness, species diversity (calculate with Shannon-Wiener and Simpson indexes) and species evenness of infauna during the current investigation. This was also the case for total infaunal abundance and biomass. Finally, infaunal communities were not different between the infested and non-infested mussel beds. The absence of any significant differences between the infested and non-infested beds may be the result of experimental set-up. Artificial mussel beds were covered by a mesh during the entire duration of the experiment to avoid any loss of mussels by storms or strong wave action. While this is a common practice in manipulative studies of mussel beds (Dievart, 2018; Nicastro et al., 2020; Zardi et al., 2011), the mesh might have modified the heat absorption properties of the mussel shells (i.e., through shading) akin to that of euendolithic infestation. The absence of any significant differences in the infaunal community structure and species diversity between the infested and non-infested mussel beds is, therefore, not surprising. This could be investigated in the laboratory by measuring within-bed temperatures and humidities of mussel beds, using data loggers, to assess potential differences between infested and non-infested mussel beds, either covered or not by a mesh.

Total infaunal abundance and biomass, species diversity and species evenness, as well as infaunal communities did differ significantly between sites. It is worth noting that the non-infested mussel beds and infested mussel beds at Brenton-on-Sea displayed the highest total abundance and biomass of infauna, respectively. Compared to other sites, Brenton-on-Sea is characterised by dense beds of *Perna perna* and *Mytilus galloprovincialis* mussel beds (pers. obs.) which are able to sustain high levels of overall infaunal biodiversity. Due to difficulty in accessibility, mussels at Brenton-on-Sea are subject to lower levels of exploitation than other sites, such as Mosselbaai or Port Edward, which are situated close to urban areas. In contrast, mussel beds at Port Edward displayed the lowest total abundance and biomass, but the highest species evenness, whereas species richness and diversity were not statistically different from the other sites. Overharvesting in KwaZulu-Natal dramatically reduced the mussel cover on the rocky shores within the region (Hammond and Griffiths, 2006; Lasiak, 1992), thus potentially reducing the pool of infaunal invertebrates that could colonize the experimental mussel beds in Port Edward.

Infaunal community structure was different between sites, which can in part be explained by the different distributions of infaunal species associated with mussel beds along the coast (inferred from Branch et al., 2016), as well as site-specific differences in the local infaunal species compostion as a result of habitat availability. The majority of those species responsible for dissimilarities between infaunal communities across sites were previously identified in natural and experimental mussel beds (Cole and McQuaid, 2010; Dievart, 2018; Hammond and Griffiths, 2006, 2004; Nicastro et al., 2020). Here, only the most influential species detected in this experiment will be discussed (Figure 4.10). Juvenile sea anemones (Actiniaria) were most abundant at Brenton-on-Sea. Juvenile sea anemones are common in mussel beds, especially the

sandy anemone *Bunodactis reynaudi* (Kruger and Griffiths, 1998), which was also highly abundant in rock pools and sand gullies in Brenton-on-Sea. The ridged burnupena, *Burnupena lagenaria*, was abundant in all south coast sites, but was absent from Mosselbaai and found only in infested mussel beds in Port Edward. *Burnupena lagenaria* is the commonest whelk on the south-east coast, where larger individuals are often observed, while KwaZulu-Natal is thought to be out of the distribution range for this species. Juvenile blue mussels, *Mytilus galloprovincialis*, were abundant on the south coast, but absent from Old Woman's River and Port Edward. *Mytilus galloprovincialis* invaded the coasts of South Africa from the west (Grant and Cherry, 1985), where it replaced native mussel species, and is now abundant on the south coast (Bownes and McQuaid, 2006). However, it becomes less abundant on the south-east coast and completely absent from the east coast, as warmer temperatures slow down its invasion (Ma et al., 2023). Juvenile brown mussels, *P. perna*, were the most abundant species and had the highest biomass detected across all sites, with variations depending on the recruitment rates (Harris et al., 1998; Reaugh-Flower et al., 2011). The mussel worm, *Pseudonereis podocirra*, was more abundant in all south coast sites, except for Jeffreysbaai, and was found in lower abundances in Port Edward. *Pseudonereis podocirra* is the largest and commonest worm on the rocky shores, living among seaweeds, reef worms, and mussel beds. Its absence from Jeffreysbaai was unexpected, as this rocky shore support all the mentioned habitats where *P. podocirra* is commonly found. The dwarf cushion star, *Parvulastra exigua*, showed higher biomass in Mosselbaai compared to the other sites. These rocky shores are flat and gently sloped compared to the other sites, which could potentially explain this disparity. The spike-back isopod, *Parisocladus perforatus*, was more abundant at Mosselbaai and Jeffreysbaai, but interestingly absent from Brenton-on-Sea, while the roll-tail isopod, *Ischyromene huttoni*, was more important at

both Brenton-on-Sea and Jeffreysbaai. Both isopods are common on the rocky shores, often in association with kelp holdfasts and algal tufts, although *Parisocladus perforatus* is not present on the East coast.

The majority of organisms associated with the mussel beds were juveniles or sub-adults. Mussel beds offer a protected habitat from stressful environmental conditions, but also from predators, which make them potential nurseries for a wide array of associated species (e.g., sea anemones, crabs, sea cucumbers, mussels, snails, and limpets). In South Africa, environmental conditions characteristic of each bioregion are known to influence the structure of mussel beds and their associated infaunal assemblages (Cole and McQuaid, 2010; Lathlean and McQuaid, 2017). On a given rocky shore, the importance of mussel beds as refuge is dependent on local environmental conditions (e.g., wave exposure, sand scour; Hammond and Griffiths, 2004; Zardi et al., 2008), often fluctuating at extremely small scale (Helmuth et al., 2006a), the configuration and specific composition of the mussel bed (Cole, 2010; Hammond and Griffiths, 2006; Nicastro et al., 2020), as well as the overall local biodiversity in presence. Seasonal and daily fluctuations in environmental conditions may also play a role in shaping mussel beds and their associated communities. The site-specific unique infaunal assemblages observed within the infested and non-infested mussel beds during this study is, therefore, not surprising.

Considering *P. perna* genetic lineages, eastern mussel beds were shown to be a more benign habitat for associated infaunal communities than western mussel beds at Old Woman's River (Nicastro et al., 2020). As *P. perna* eastern lineage produce more byssal threads and gape more than the western lineage, eastern mussel beds display higher structural complexity, lower within-bed temperature and higher within-bed humidity (Nicastro et al., 2020, 2012; Zardi et al., 2015). Thus, the eastern lineage

mussel beds were expected to host higher total infaunal abundance and biomass, as well as higher species richness, diversity, and evenness, than western mussel beds. There was no evidence of the influence of either euendolithic infestation or *P. perna* lineage on the total infaunal abundance and biomass, species richness, diversity, and evenness, as well as the composition of infaunal communities (abundance and biomass) at Old Woman's River. While this could be explained by the similar number of byssal threads for each infestation level and each lineage in this experiment, it is also plausible that the duration of the experiment influenced the establishment of infaunal communities. The common-garden experiment was left to be colonized for more than 6 months, potentially homogenising the infestation and lineage effects. In a similar experiment conducted at Old Woman's River, artificial mussel beds were left to colonize for 3 months (Dievart, 2018) after which an influence of *P. perna* lineages was detected on the number of byssal threads, on species richness and infaunal communities in terms of biomass (western > eastern; Dievart, 2018). Although the limited number of replicates in each aforementioned study does not allow for firm conclusions to be made (Lathlean et al., 2016b), environmental conditions at the time of measurements differed between the two studies, especially in terms of relative humidity and solar irradiance (Dievart, 2018; Nicastro et al., 2020).

4.5. Conclusions

In summary, infaunal communities were not different between infested and non-infested mussel beds across all sites, although site-specific differences were apparent. In addition, no differences in infaunal communities were observed between infested and non-infested mussel beds and between *P. perna* lineages at Old Woman's River. Below the species level, conspecific individuals differ in many obvious traits, such as sex, age, and size, but

also in more subtle traits, such as shape, colour, behaviour, or physiology. Intraspecific genotypic trait variation, resulting in within-species phenotypic variation, provides basis for any evolutionary change (Fisher, 1930) and thus stands for the most fundamental level of biodiversity (May, 1994). Abiotic and biotic interactions, such as predation or parasitism, can also modify individual phenotypes, thus increasing intraspecific phenotypic diversity (Mouritsen and Poulin, 2002; Poulin and Thomas, 1999; Reimer and Tedengren, 1997; Thomas et al., 2011; Zardi et al., 2023). In many ways, intraspecific trait variation has key ecological effects on ecosystem processes (Bolnick et al., 2003; Hughes et al., 2008), which effects are expected to be even greater in the case of ecosystems based on one or a few foundation species, such as mussel beds (Cook-Patton et al., 2011; Nicastro et al., 2020; Whitham et al., 2003). However, it is important to note that intraspecific trait variability occurs within individuals, between individuals of the same population, and across populations (Thomas et al., 2011), and thus its various effects are context-specific. Time also influences the detection and the magnitude of effects that intraspecific trait variation can have on ecosystem functioning (Kuppler et al., 2016). Indeed, the presence and activity of species interacting with the habitat-forming species of interest is highly variable over time, due to variable environmental conditions or species phenologies (Kuppler et al., 2016), as well as research methodologies, such as the duration of manipulative experiments and collection time (Fariñas-Franco and Roberts, 2014; Llewelyn et al., 2016; Palomo et al., 2007). Euendolithic infestation of the mussel shell has the potential to lead to differences in infaunal communities between infested and non-infested mussel beds, although mostly under stressful environmental conditions these parasites indirectly mediate. As the beneficial effects of euendolithic infestation are conditional, mobile species might be the most likely to migrate to more benign infested mussel beds when under stress.

CHAPTER 5

LIFE ON COLLAPSING SHELLS:

THE RELATIONSHIP BETWEEN EUENDOLITHIC

INFESTATION AND EPIBIOSIS

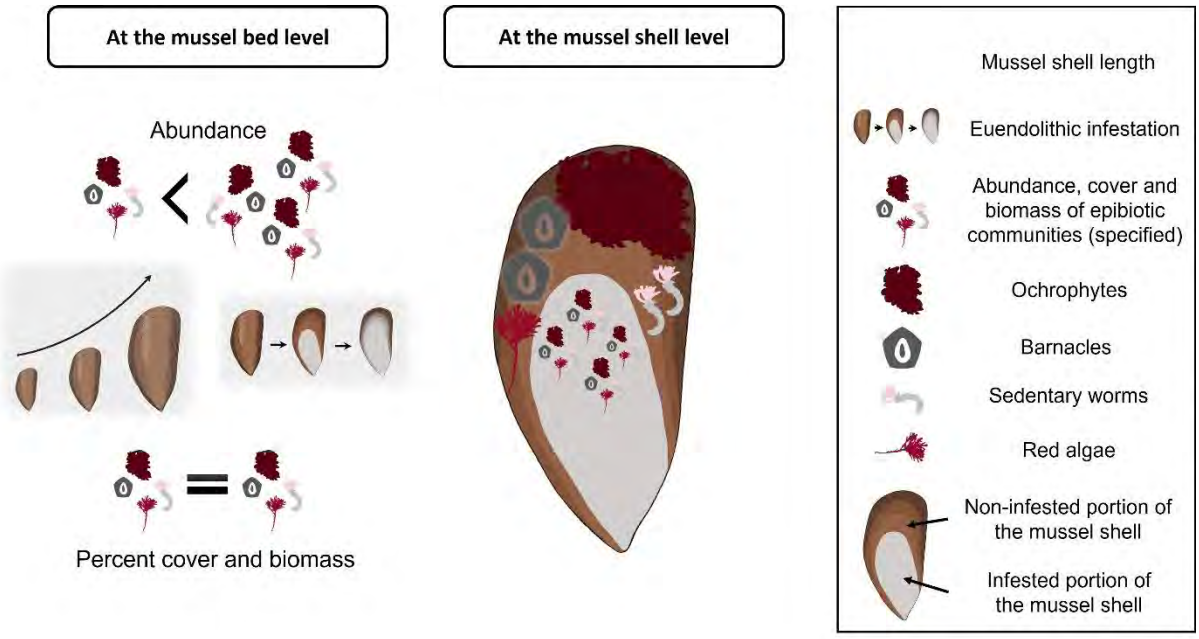

Figure 5.0. Graphical abstract summarizing the findings presented in Chapter 5. **Left panel**: graphical presentation of the survey results comparing the abundance, percent cover and biomass of epibitic organisms at the mussel bed level, considering the size of the mussel and their levels of euendolithic infestation; **right panel**: graphical presentation of the survey results comparing the abundance, percent cover and biomass of epibiotic organisms at the mussel shell level, considering the euendolithic-infested and the non-infested portion of the mussel shell.

5.1. Introduction

Space is the primary limiting resource in many marine systems, particularly on rocky shores (Connell, 1972, 1961; Dayton, 1971; Paine, 1974, 1966). While rocky shores display high physical heterogeneity, with a variety of habitats (Kostylev et al., 2005), intra- and interspecific competition for space is intense, for both sessile and mobile intertidal organisms (Connell, 1972, 1961; Dayton, 1971; Paine, 1974, 1966). Epibiosis is a common phenomenon in space-limited marine systems (Paine, 1974; Wahl, 2009, 1989) and is defined as the non-symbiotic, facultative spatial association between an organism (i.e., the 'epibiont', also called fouling organism) that lives on or attaches itself to the outer surface of a substrate organism (i.e., the 'basibiont'), without trophic interdependency (Wahl, 2009, 1989; Wahl and Mark, 1999). On rocky shores, mussel shells provide an important secondary space for the settlement of various epibionts (Bell, 2013; Dayton, 1971; Gutiérrez et al., 2003; Lohse, 1993; Paine, 1974). Lohse (1993) revealed that virtually all sessile organisms subject to competitive exclusion on the rock substratum along the US coasts were present on the shells of *Mytilus californianus*. Mussel beds are spatially more intricate structures than bare rock surfaces across several scales, displaying a heterogeneous distribution and within-bed patchiness, with smaller patches of mussels occurring within larger ones (Erlandsson and McQuaid, 2004; Kostylev and Erlandsson, 2001; Lawrie and McQuaid, 2001). Mussel beds thus act as a refuge for infaunal species (Palomo *et al.*, 2007), while also increasing the quantity of suitable substratum available for settlement by epibionts (Gutiérrez et al., 2003; Lohse, 1993).

Epibiosis is influenced in space and time by various abiotic factors, such as the physical and chemical properties of the substratum (Scardino et al., 2003; Steinberg et al., 2001)

or macro- and micro-scale hydrodynamics (Bertness et al., 1996; Crisp, 1955), and biotic factors, such as the seasonal variability in larval supply of epibionts (Buschbaum, 2000) or simple stochasticity as epibiosis is a facultative association (Wahl and Mark, 1999). In turn, epibiosis affects biological interactions within an ecological community by creating a new interface between the basibiont and its environment (Garner and Litvaitis, 2013; Laudien and Wahl, 2004, 1999; Wahl, 2008; Witman and Suchanek, 1984). As a result, epibiosis has both positive and negative effects on both the epibiont and the basibiont involved, the importance of which is context-specific and determined by both abiotic and biotic factors (Wahl, 1989). For the epibiont, colonizing an as yet unoccupied surface in a space-limited system is the main beneficial effect of living attached to another organism (Wahl, 1989). Depending on their position on the basibiont, epibionts can benefit from more favourable environmental conditions (Wahl, 1989), for example better hydrodynamic regimes, ensuring higher nutrient supply and efficient waste evacuation, or higher exposure to solar irradiation (Brouns and Heijs, 1986; Crisp, 1955; Laihonen and Furman, 1986). One major problem faced by epibionts is the instability of their living substratum, either due to the basibiont's mortality (i.e., either natural or through predation) or morphological and/or physiological changes (i.e., growth, shrinking, fission, shedding) during the life cycle of the basibiont. For the basibiont, beneficial effects of epibiosis include 'associational resistance', through the optical, tactile and chemical 'camouflage' of the host from predators and parasites (Laudien and Wahl, 2004, 1999; Wahl, 2009), the mitigation of environmental stresses, such as desiccation, temperature and solar irradiation by water-retaining and shading epibionts, respectively (Gutiérrez et al., 2019; Seaborn, 2014). Conversely, being overgrown by epibionts indirectly increases drag forces on the basibiont, and thus mortality rates through dislodgement (Bell, 2013;

Bers and Wahl, 2004; Garner and Litvaitis, 2013; Thieltges and Buschbaum, 2007; Witman and Suchanek, 1984). Epibiosis can also interfere with the basibiont's physiological processes, such as filter-feeding, reproduction or growth (Thieltges and Buschbaum, 2007; Wahl, 2008). Moreover, epibiosis can modulate ecological interactions between the basibiont and the ecological community, by increasing the basibiont's susceptibility to predators and parasites (i.e., 'shared doom'), favouring the recruitment of additional boring and fouling organisms (Thieltges and Buschbaum, 2007; Wahl, 2008; Wahl and Hay, 1995), and increasing overall habitat complexity for organisms associated with the basibiont (de Sá et al., 2007; Gutiérrez et al., 2019).

Although mussels have been demonstrate to be a secondary substratum of choice for epibionts on the rocky shores, mussel shells support fewer fouling organisms than adjacent non-biological substrata (Bell et al., 2015; Bers and Wahl, 2004; Wahl et al., 1998). More often than not, epibiosis is harmful to the host, thus basibionts have evolved a combination of behavioural, chemical, physical and mechanical defences against biofouling (Bers and Wahl, 2004; Krug, 2006; Scardino et al., 2003; Wahl, 1989; Wahl et al., 1998). Bivalve shells are protected by the periostracum, a well-defined external proteinaceous coating of variable thickness, which firstly provides a physical, and later a chemical defence against boring (Kaehler, 1999) and fouling organisms (Bell et al., 2015; Bers et al., 2010, 2006; Ma et al., 2023; Mao Che et al., 1996; Scardino et al., 2003; Wahl et al., 1998). Bivalves with an intact periostracum demonstrate increased fitness due to the antifouling properties of their shell microtopography (Bers et al., 2010; Scardino et al., 2003; Scardino and de Nys, 2004). Shell microtopography can be described in terms of the complexity of its texture (i.e., regular, well-defined surface structure smaller than the epibiont), roughness (i.e., random surface irregularities), or contour (i.e., irregularities larger than the

epibiont) (Carve et al., 2019; Scardino et al., 2009, 2008). Explained by the 'attachment point theory', epibionts settle and attach more successfully on microtextures (e.g., periostracum microtopography) slightly wider than themselves or their sensory settlement organ, as it maximizes the number of attachment points between the epibiont and its living substrata, thus providing maximum adhesion and hence resistance against drag forces (Carve et al., 2019; Scardino et al., 2009, 2008, 2006; Schumacher et al., 2007). For example, barnacles demonstrated reduced attachment success on textures designed within the range of their settlement organ (i.e., 40 μm; Schumacher *et al.*, 2007), while showing increased settlement on rougher surfaces (Berntsson et al., 2000).

Around the world, mussel shells are commonly infested by euendolithic boring microorganisms (reviewed in Dievart *et al.*, 2022). Euendolithic infestation of mussel shells is facilitated by the removal of the protective periostracum (Kaehler, 1999; Mao Che et al., 1996; Raghukumar et al., 1991; Scardino et al., 2003). Once the periostracum is removed, even on a small portion of the shell, the corrosive activity of euendoliths expands until the entire shell is degraded (Kaehler, 1999; Kaehler and McQuaid, 1999; Ndhlovu et al., 2021b). Increased shell degradation caused by euendolithic infestation destroys the mussel shell microtopography and increases shell roughness, ultimately contributing to diminished antifouling properties (Ma et al., 2023; Marquet et al., 2013). Marquet et al. (2013) and Ma et al. (2023) demonstrated that the percentage of barnacle cover of the shells of *Mytilus galloprovincialis* increased with growing levels of euendolithic infestation. It is worth noting that these studies observed that both the euendolithic and barnacle infestation increased in frequency and intensity with shell length, and thus mussel age (Bell, 2013; Kaehler, 1999; Ma et al., 2023; Marquet et al., 2013; Ndhlovu et al., 2019). Thus, it is plausible that the relationship

between shell degradation due to euendolithic infestation and epibiotic infestation is in fact an artefact of a longer exposure of mussels to both propagules, which reflects through mussel age and shell length. Moreover, the corrosive activity of euendoliths gradually weakens the whole structure of the mussel shell until the sudden collapse of the mussel shell and the subsequent death of the animal (Kaehler and McQuaid, 1999; Ndhlovu et al., 2019), making the mussel shell unfit to support epibiotic life.

Perna perna is, numerically and by biomass, the dominant mussel species on the east coast of South Africa, and co-occurs with the invasive blue mussel *Mytilus galloprovincialis* on the south coast (Bownes and McQuaid, 2009, 2006). The mussel forms extensive mono-layered mussel beds on the south coast that support a wide array of associated infaunal and epibiotic species (see Chapter 3; Bell, 2013). Here, the interactions between euendolithic and epibiotic infestation of the mussel shell were investigated using natural mussel beds made up by the native brown mussel *P. perna*, with a focus on the entire epibiotic community (e.g., barnacles, algae, sedentary worms, anemones). Specifically, it was expected that (1) shell degradation caused by euendolithic infestation would increase in intensity and cover with increasing mussel shell length (considered as a proxy of age) (Kaehler, 1999; Ma et al., 2023; Marquet et al., 2013; Ndhlovu et al., 2019), (2) occurrence, abundance, cover and biomass of epibionts would increase with mussel size, because (3) occurrence, abundance, cover and biomass of epibionts was expected to covary with euendolithic infestation and/or shell degradation (e.g., Marquet *et al.*, 2013; Ma *et al.*, 2023).

5.2. Materials and Methods

5.2.1. Collection procedure

Mussels were collected from two open-coast sites on the warm-temperate south coast of South Africa (Figure 5.1): Brenton-on-Sea (34°04'31.7"S, 23°01'28.1"E) and Kasouga (33°38'54.5"S, 26°45'35.2"E). These sites were selected due to the similar nature of the rocky shore substrate (i.e., sandstone) and structure (i.e., presence of platforms; Figure 5.2a,b), and the co-occurrence of *Perna perna* and *Mytilus galloprovincialis*, and the occurrence of epibionts on their mussel shells. Mussels are vertically distributed on both rocky shores, with *M. galloprovincialis* generally colonizing the high 'mussel zone', while *P. perna* dominates the low 'mussel zone'. Both species vertical distributions overlap in the mid-'mussel zone', forming mixed mussel beds (Bownes and McQuaid, 2009, 2006).

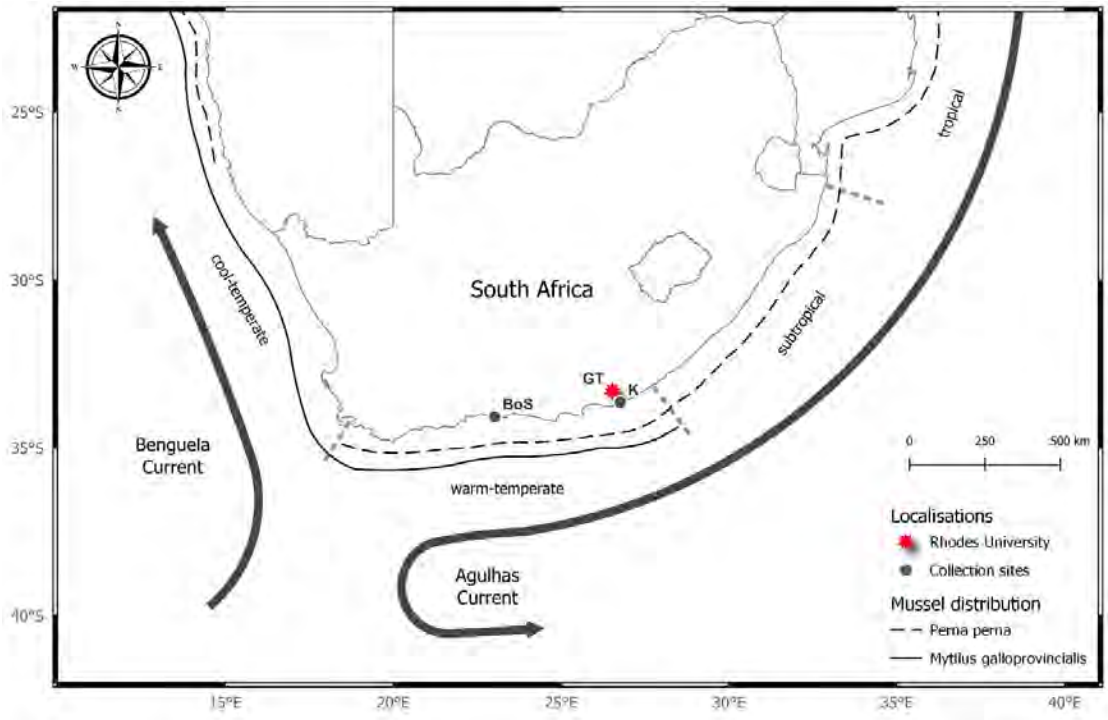

Figure 5.1. Map of the collection sites on the south coast of South Africa. Grey dots represent localities where the mussels were collected (BoS: Brenton-on-Sea and K: Kasouga). The distributional ranges of the dominant mussel species are represented by a continuous black line (*Mytilus galloprovincialis*) and a dashed black line (*Perna perna*) (according to Bownes and McQuaid, 2006; Cunha et al., 2014; Grant and Cherry, 1985). The three biogeographic regions along the South African coastline are delimited by grey dotted lines (according to Emanuel et al., 1992).

At each site, ten 25 x 25 cm quadrats were randomly sampled along a 50m-transect, parallel to the ocean, in a sun-exposed area of mid- 'mussel zone', on 75 to 100% mussel cover beds (Figure 5.2). Within each replicate (i.e., quadrat), all mussels were carefully scraped from the substrate to reduce the dislodgment of epibionts and preserved in 70% ethanol for further analyses in the laboratory.

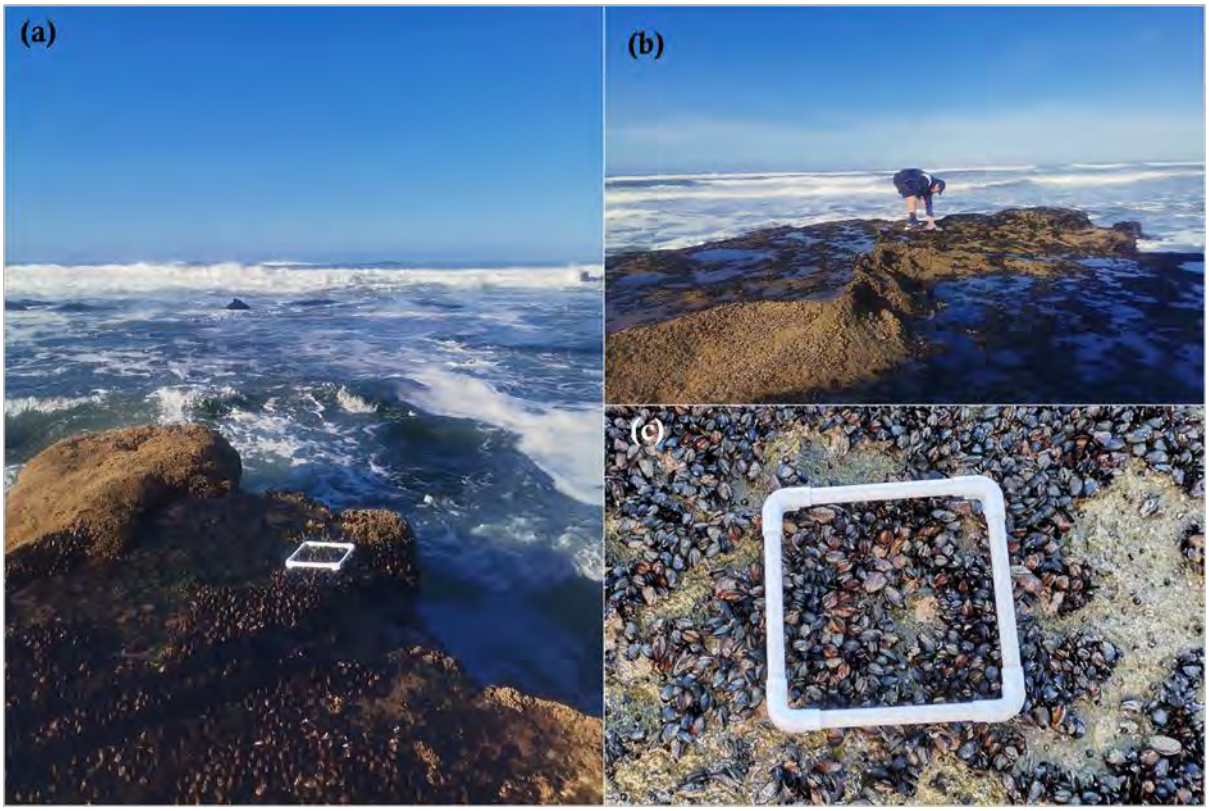

Figure 5.2. (a,b) Examples of replicate sampling at the edge of the sandstone platform, in the mid- 'mussel zone', in Brenton-on-Sea. (c) Example of a replicate, using a 25 x 25 cm quadrat, place on 75 to 100% mussel covered area. Pictures (a,b,c): © Alexia DIEVART.

5.2.2. Laboratory analyses

Samples were handled carefully, to ensure that any epibiotic organisms were not dislodged from the mussel shell. Due to time constraints, only adult mussels (> 30 mm in shell length; Bownes & McQuaid, 2006) were considered for the study.

For each replicate, each individual mussel was identified (i.e., *Perna perna* or *Mytilus galloprovincialis*) and shell length was measured (in mm) using a vernier calliper. Both valves of each individual mussel were then photographed (with a scale bar) to estimate the percentage cover of each epibiotic organism on each valve. Each epibiotic organism on each valve was sorted, counted, and where possible, identified to the lowest taxonomic level possible using the keys of Branch et al. (2016), Day (1969, 1967), Griffiths (1976), and Kensley (1978). The position of the epibiont on each valve and level of euendolithic infestation was also noted. Epibiotic organisms found unattached to the substrate (e.g., limpets, worms) were considered at the habitat scale (i.e., total number per quadrat). Once sorted, epibionts were separately dried in the oven at 60°C for 48 h, and their biomass expressed as dry weight determined using a Satorius microbalance. After processing the epibionts and revealing the mussel shell, the percentage of shell surface that exhibited euendolithic degradation was estimated visually and classified into one of six categories: 0%, > 0 to 25%, > 25 to 50%, > 50 to 75%, > 75 to 100%, and 100% according to Ma et al. (2023). In addition, the intensity of euendolithic infestation of each valve was classified according to Kaehler (1999) into one of five categories: A – shells with clean, intact periostracum and distinct outer growth lines, B – shells with central portion of surface eroding and turning pale purple with outer growth lines becoming indistinct, C – shells with erosion spreading past the central porting with grooves and pits appearing on shell surface, D – shells heavily pitted and becoming deformed with outer growth lines almost completely absent, and E – shells extremely pitted, deformed and brittle, eventually holed (e.g., Kaehler, 1999; Kaehler and McQuaid, 1999; Zardi et al., 2009; Marquet et al., 2013; Ndhlovu et al., 2019). Finally, each mussel was dissected to determine its sex and investigate the presence of internal parasites in relationship to the level of euendolithic infestation.

Photographs were processed using ImageJ (1.53e) software and properly scaled. For each valve of each individual mussel, the area of the shell and the cover area of each epibiotic species was determined by hand, using the polygon tool. For each valve, the percentage cover of each epibiotic species was calculated as follow:

$$\boldsymbol{Epifaunal\ cover} = \frac{\boldsymbol{epibiont\ area\ (mm^2)}}{\boldsymbol{whole\ shell\ area\ (mm^2)}} \times \mathbf{100} \qquad (5.1)$$

Prevalence of mussels infested by epibionts was calculated as the proportion of mussels with at least one epibiont attached to the shell (i.e., presence/absence).

5.2.3. Data analyses

As field sampling was particularly ambitious and laboratory analyses extremely time-consuming, only data recorded from seven replicates from Kasouga (Eastern Cape) were analysed for this chapter, for a total of 493 mussels (i.e., 986 valves). Due to the complexity of the dataset, epibionts recorded on the blue mussel *Mytilus galloprovincialis* were excluded from all statistical analyses, while mussel valves without epibionts and epibiotic organisms for which percent cover or biomass could not be determined were additionnaly excluded from the statistical analyses on epibiotic communities. Data never fitted the assumptions of normality and homogeneity of variances for parametric tests, so several types of models were employed to analyse the data.

All datasets and R scripts can be accessed and downloaded using the following link: https://github.com/AlexiaDievart/endolith_epibiosis.

5.2.3.1. Relationship between mussel shell condition and epibiosis

The relationship between euendolithic infestation levels and shell degradation indexes was examined using a Pearson's χ^2 test of independence. The effect of euendolithic infestation levels and shell degradation indexes on shell length (continuous, in mm) was

assessed using a Linear Model (LM). As euendolithic infestation and shell degradation both covaried with shell length, the predictive variables were used separately in the following analyses. Generalized Linear Models (GLMs) were used to assess either the effect of shell length (i.e., from $]30-40]$ to $]110-115]$ mm), or the effect of euendolithic infestation and shell degradation, on the occurrence of epibiosis (i.e., with or without epibionts, binomial).

5.2.3.2. Epibiotic community analyses

Separate models were used to assess the effect of shell length, and the effects of euendolithic infestation, shell degradation and/or position of the epibionts on the mussel shell in the following analyses.

First, epibiotic communities were described in terms of total abundance, percent cover and biomass of epibionts, species richness (S), species diversity, either calculated with Shannon-Wiener (*H'*) or Simpson (λ) diversity index, and species evenness, calculated with Pielou's evenness index (J). Species richness is the number of different species represented in an ecological community (Colwell, 2009). Shannon-Wiener diversity index emphasizes rare species, while Simpson diversity index emphasizes common species (Colwell, 2009; Fedor and Spellerberg, 2013; Nagendra, 2002). Pielou's evenness index indicates how evenly the individuals in an ecological community are distributed among the different species (Pielou, 1966).

A series of negative binomial GLMs were used to assess the relationship between the total abundance of epibionts and shell length (fixed, nine levels: from $]30-40]$ to $]110-115]$ mm), or euendolithic infestation (fixed, five levels: A to E) and shell degradation (fixed, six levels: 1 to 6), or position of the epibionts (fixed, 3 levels: non-infested, infested, secondary epibiosis) on the mussel shell. A series of zero-inflated Gamma GLMs were used to assess the relationship between the average

percent cover of epibionts and either shell length, or euendolithic infestation, shell degradation or position on the mussel shell, and the relationship between the total biomass of epibionts and either shell length, and euendolithic infestation and shell degradation, or position of the epibionts.

A series of GLMs were used to assess the relationship between the average epibiotic species richness and either shell length (Poisson GLM), or euendolithic infestation and shell degradation (negative binomial GLM), or position of the epibionts (Poisson GLM). A series of Linear Models (LM) and GLM were used to assess the relationship between the average Shannon-Wiener diversity index (*H'*) and either shell length (LM), or euendolithic infestation and shell degradation (LM), or position of the epibionts (zero-inflated Gamma GLM). A series of GLMs were used to assess the relationship between the average Simpson's diversity index (λ) and either shell length (zero-inflated Gaussian GLM), or euendolithic infestation and shell degradation (zero-inflated Gaussian GLM), or position of the epibionts (zero-inflated Gamma GLM). Finally, a series of LMs were used to assess the relationship between the average Pielou's evenness index (*J'*) and either shell length, or euendolithic infestation and shell degradation, or position of the epibionts. Model fits were assessed using residual diagnostic tools from the 'DHARMa' R package (Hartig, 2022), or using the 'appraise' function from the 'gratia' R package (Simpson, 2022). When an effect was significant, pairwise comparisons using Tukey's HSD were conducted.

Second, multivariate analyses were performed to assess the relationship between epibiotic communities and either shell length, or euendolithic infestation and shell degradation, and/or position of the epibionts on the mussel shell.

The relationships between abundance of both higher taxonomical groups and epibiotic species, and either shell length, or euendolithic infestation and shell degradation, were

assess using the 'mvabund' approach, that fits a single Generalized Linear Model (GLM) to each response variable with a common set of predictor variables (Wang *et al.*, 2012), followed by multivariate hypothesis tests (Warton, 2008; Warton et al., 2017). The effect of position of the epibionts on the shell could not be analysed as the models tested could not calculate coefficients. Univariate hypothesis tests were then used to determine which epibiotic higher taxonomical groups or species were driving the differences in epibiotic communities between the specific predictor variables.

The relationships between either percent cover or biomass of both higher taxonomical groups and epibiotic species, and shell length, euendolithic infestation, shell degradation, and position of the epibionts on the mussel shell, were assessed using a series of permutational multivariate analyses of variance (PERMANOVA) on Bray-Curtis dissimilarity matrices for square root transformed multivariate data, as raw data were heavily skewed (Lamy et al., 2015). Across all quadrats, PERMANOVA were performed with shell length (fixed, nine levels: from $]30-40]$ to $]110-115]$ mm), or euendolithic infestation (fixed, five levels: A to E), shell degradation (fixed, six levels: 1 to 6), and position of the epibionts on the mussel shell (fixed, two to three levels: non-infested and infested for percent cover, with the addition of secondary epibiosis for the biomass) as categorical parameters for both epibiotic percent cover and biomass. Significance of F-ratios was determined from 9,999 randomizations (Anderson, 2005). Permutation tests of multivariate dispersion (PERMDISP; Anderson, 2004) were used to check the homogeneity in the average dissimilarities of samples from the central location of their group. Similarity percentage analyses (SIMPER; Clarke and Ainsworth, 1993) were then used to determine the percentage contribution of each variable made to the Bray-Curtis dissimilarities. Epibiotic higher taxonomical groups or epibiotic species were ranked by their contribution to overall dissimilarity and included up to a cumulative total of 70% of

average dissimilarity. Differences between assemblages were visualized using: (1) non-metric multidimensional scaling (nMDS) ordination plots, and (2) dispersion plots. All methods were based on Bray-Curtis similarity matrices of either percent cover or biomass of epibiotic higher taxonomical groups or epibiotic species.

Finally, a series of GLM were used to assess the relationship between either abundance (Poisson or negative binomial GLM), percent cover (Gamma GLM), or biomass (Gamma GLM), and either shell length, or euendolithic infestation, shell degradation and position of the epibionts, for each epibiotic higher taxonomical group and epibiotic species that significantly contributed to the differences between epibiotic communities. Model fits were assessed using residual diagnostic tools from the 'DHARMa' R package (Hartig, 2022), or using the 'appraise' function from the 'gratia' R package (Simpson, 2022). When an effect was significant, pairwise comparisons using Tukey's HSD were conducted.

5.3. Results

5.3.1. Relationship between mussel shell condition and epibiosis

There was a significant relationship between euendolithic infestation levels and shell degradation index (χ^2 (20, N = 899) = 938.7, $p < 0.001$) (Figure 5.3a). Proportionally, mussel valves demonstrated low shell degradation indexes (i.e., 1 and 2, 0 and $]0-25]$ %) at low levels of euendolithic infestation (i.e. A and B). Similarly, the highest shell degradation indexes (i.e., 5 and 6, $]75-100]$ and 100 %) were associated with highest levels of euendolithic infestation (i.e., D and E).

Euendolithic infestation levels (as defined in Kaehler, 1999) and shell degradation index (as defined in Ma *et al.*, 2023) were significantly correlated to mussel shell length, with no significant interaction (Table 5.1, Figure 5.3a,b,c). Heavily euendolith-infested

mussels (i.e., D and E) were significantly larger (in shell length, mm) than the less infested mussels (i.e., A to C) (Table S5.1, Figure 5.3b). Similarly, mussels were significantly larger as the area of degraded shell increased (i.e., between 1 and 4, 0 % to]50 – 75] %), except between the two highest indexes (i.e., 5 and 6,]75 – 100] and 100 %) (Table S5.2, Figure 5.3c).

Table 5.1. Type II two-way ANOVA (unbalanced design) on the Linear Model (LM) of the effect of euendolithic infestation levels (from A to E, as defined in Kaehler, 1999) and shell degradation index (from 1 to 6, as defined in Ma *et al.*, 2023) on mussel shell length. Significant p-values are underlined.
Model used in this analysis: shell_length ~ inf.lvl + inf.percent. Interaction was not significant.

Source of variation	Type II Sum of Squares	df	*F*-value	p-value
Infestation level	14960	4	20.857	$< 2.00 \times 10^{-16}$
Shell degradation	31483	5	35.114	$< 2.00 \times 10^{-16}$
Residuals	159415	889		

The prevalence of epibiotic infestation significantly increased with shell length (Table 5.2) and was significantly lower for smaller shell length sizes (i.e.,]30 – 40] and]40 – 50] mm) than for larger shell length sizes (i.e.,]50 – 110] mm) (Table S5.3, Figure 5.3d). All mussels > 95 mm were infested by epibionts (Figure 5.3d). Similarly, the prevalence of epibiosis was significantly different between euendolithic infestation levels and shell degradation indexes (Table 5.3, Figure 5.3e,f).

Table 5.2. One-way ANOVA on the Generalized Linear Model (LM) on the relationship between the prevalence of epibiosis and shell length range (from]30 – 40] to]110 – 120] in mm). Significant p-values are underlined.
Model used in this analysis: epibiosis ~ length_range, family = "binomial".

Source of variation	df	Deviance	Resid. df	Resid. Dev	p (> Chi)
Null			898	606.59	
Length range	8	108.14	890	498.45	$< 2.2 \times 10^{-16}$

The prevalence of epibiosis at euendolithic infestation level D was significantly higher than at level C (Table S5.4, Figure 5.3e), as well as at shell degradation indexes 3 and 5 (i.e., $]25-50]$ and $]75-100]$ %) than when shell was not degraded (i.e., 1, 0 %) (Table S5.5, Figure 5.3f).

Table 5.3. Type II two-way ANOVA (unbalanced design) on the Generalized Linear Model (GLM) of the effect of euendolithic infestation levels (from A to E, as defined in Kaehler, 1999) and shell degradation index (from 1 to 6, as defined in Ma *et al.*, 2023) on the prevalence of epibiosis. Significant p-values are underlined.
Model used in this analysis: epibiosis ~ inf.lvl + inf.percent, family = "binomial". Interaction was not significant.

Source of variation	df	Deviance	Resid. df	Resid. Dev	P(> Chi)
Null			898	606.59	
Infestation levels	4	49.346	894	557.25	$\underline{4.944 \times 10^{-10}}$
Shell degradation	5	14.068	889	543.18	<u>0.015</u>

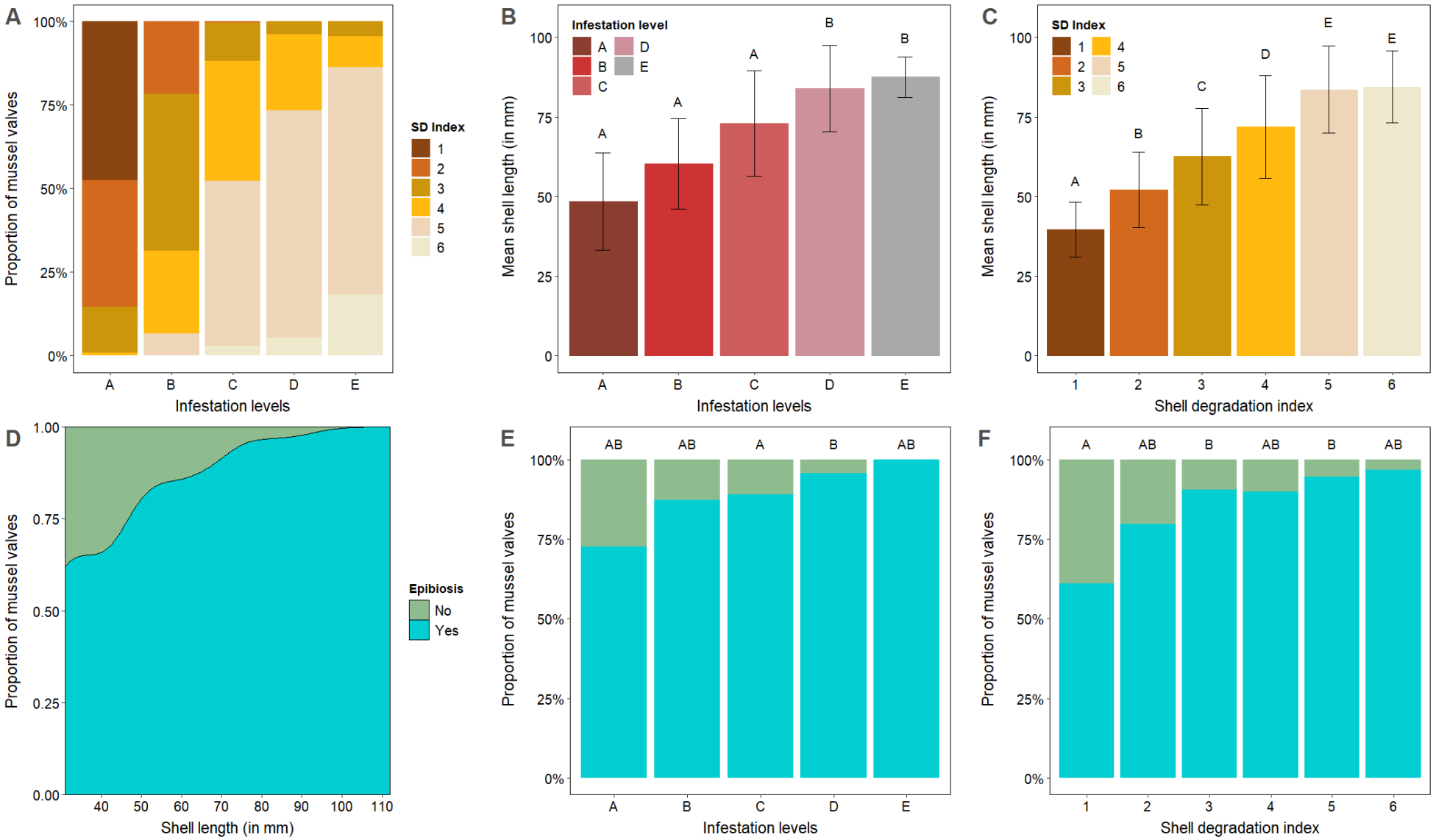

Figure 5.3. (a) Proportions of mussel valves affected to each shell degradation index for each euendolithic infestation levels; (b) Average mussel shell length (in mm, ± SD) for each euendolithic infestation level; (c) Average mussel shell length (in mm, ±SD) for each shell degradation index. Proportion of mussel valves with and without epibionts (d) depending on mussel shell length (in mm), (e) for each euendolithic infestation levels, and (f) for each shell degradation index. Homogeneous groups are indicated by similar letters.

5.3.2. Epibiotic communities

5.3.2.1. Epibiotic community descriptors

Firstly, epibiotic communities were considered in terms of average total abundance, percent cover and biomass per mussel valve (Figure 5.4), as well as species richness (S), species diversity, either calculated with Shannon-Wiener (*H'*) or Simpson (λ) diversity index, and species evenness, calculated with Pielou's evenness index (J) (Figure 5.5).

5.3.2.1.1. Total abundance of epibionts

Average total abundance of epibionts per mussel increased with shell length (Table 5.4) and was significantly lower for small shell length sizes (i.e., $]30-70]$ mm) than the large shell length sizes (i.e., $]80-110]$ mm) (Table S5.6, Figure 5.4a).

Table 5.4. Type II one-way ANOVA on the Generalized Linear Model (GLM) on the relationship between the total abundance of epibionts per mussel and shell length range (from $]30-40]$ to $]110-120]$ in mm). Significant p-values are underlined.
Model used in this analysis: abundance ~ length_range, family = "negative binomial".

Source of variation	LR Chisq	df	p (> Chisq)
Length range	184.310	8	$\underline{< 2.2 \times 10^{-16}}$
Residual deviance	483.850	450	

The average total epibiotic abundance per mussel valve was significantly different between euendolithic infestation levels, and close to significantly different between shell degradation indexes (Table 5.5, Figure 5.4b,c). Average total abundance per mussel valve was significantly higher at euendolithic infestation levels C and D than at level B (Table S5.7, Figure 5.4b). Although not significant in the previous analysis (Table 5.5), average total epibiotic abundance was significantly higher at shell degradation indexes 4 and 5 (i.e., $]50-75]$ to $]75-100]$ %) than at the lowest index 1 (i.e., 0 %) (Table S5.8, Figure 5.4c).

Table 5.5. Type II two-way ANOVA on the Generalized Linear Model (GLM) on the relationship between the total abundance of epibionts per valve and euendolithic infestation levels (from A to E, as defined in Kaehler, 1999) and shell degradation index (from 1 to 6, as defined in Ma *et al.*, 2023). Significant p-values are underlined.
Model used in this analysis: abundance ~ inf.lvl + inf.percent, family = "negative binomial". Interaction was not significant.

Source of variation	LR Chisq	df	p (> Chisq)
Infestation level	11.365	4	0.023
Shell degradation	10.439	5	0.064
Residual deviance	837.40	794	

Finally, average total abundance of epibionts per mussel valve was significantly different depending on where epibionts settled on the mussel shell (Table 5.6), with the lowest abundances on the non-infested part of the shell, median abundances on the infested part of the shell and highest abundances for secondary epibiosis (Table S5.9, Figure 5.4d).

Table 5.6. Type II one-way ANOVA on the Generalized Linear Model (GLM) on the relationship between the total abundance of epibionts per mussel and position on the shell (i.e., infested, non-infested, or secondary epibiosis). Significant p-values are underlined.
Model used in this analysis: abundance ~ position, family = "negative binomial".

Source of variation	LR Chisq	df	p (> Chisq)
Position	43.031	2	4.529×10^{-10}
Residual deviance	1281.8	1290	

5.3.2.1.2. Percent cover of epibionts

Average epibiotic percent cover was significantly different between shell length ranges (Table 5.7a, Figure 5.4e), and position with a significant interaction with shell degradation indexes, but not between euendolithic infestation levels (Table 5.7b, Figure 5.4f,g). Average epibiotic percent cover was significantly lower for small shell length sizes (i.e., $]30 - 50]$ mm) than larger shell length sizes (i.e., $]50 - 100]$ mm), with a non-significant drop for the most extreme shell length size (i.e., > 110 mm) (Table S5.10, Figure 5.4e). Average epibiotic percent cover was significantly higher on

the non-infested part of the shell for shell degradation indexes 2 to 4 (i.e.,]0 – 25] to]50 – 75] %) (Table S5.11, Figure 5.4g).

Table 5.7. Type II Wald χ^2 test on the Generalized Linear Mixed Model (GLMM) on the relationship between the percent cover of epibionts per mussel and (a) shell length range (from]30 – 40] to]110 – 120] in mm), and (b) euendolithic infestation levels (from A to E, as defined in Kaehler, 1999), shell degradation index (from 1 to 6, as defined in Ma et al., 2023) and position on the shell (i.e., infested, non-infested). Significant p-values are underlined.
Models used in these analyses: (a) cover ~ length_range, family = "ziGamma(link = "log")", and (b) cover ~ inf.lvl + inf.percent + position + inf.percent:position, family = "ziGamma(link = "log")".

Source of variation	LR Chisq	df	p (> Chisq)
(a) Shell length range			
Length range	53.336	8	$\underline{9.285 \times 10^{-9}}$
Residual deviance	2971.0	432	
(b) Infestation level, shell degradation and position on the shell			
Infestation level	7.765	4	0.101
Shell degradation	69.909	9	$\underline{1.586 \times 10^{-11}}$
Position	88.906	5	$\underline{< 2.2 \times 10^{-16}}$
Shell degradation x Position	30.244	5	$\underline{1.321 \times 10^{-5}}$

5.3.2.1.3. Total biomass of epibionts

Average total biomass of epibionts per mussel increased with shell length (Table 5.8a, Figure 5.4h), and was significantly lower for small shell length sizes (i.e.,]30 – 60] mm) than the median shell length sizes (i.e.,]70 – 90] mm), with a non-significant drop for the larger shell length sizes (i.e.,]90 – 120] mm) (Table S5.12, Figure 5.4h).

The average epibiotic total biomass per mussel valve was significantly different between euendolithic infestation levels and shell degradation indexes, with no significant interaction (Table 5.8b, Figure 5.4i,j). Average total biomass of epibionts was not significantly different between euendolithic infestation level A and levels B to D but increased significantly between euendolithic infestation levels B to D, with a non-significant drop at level E (Table S5.13, Figure 5i). Similarly, average epibiotic total biomass was significantly lower when the mussel shell was not degraded (i.e., index 1, 0 %) than at medium levels of shell degradation (i.e., indexes 2 to 4,]0 – 25] to

]50 − 75] %) but was not significantly different than at the highest levels of shell degradation (i.e., indexes 5 and 6,]75 − 100] and 100 %) (Table S5.14, Figure 5.4j). In addition, average epibiotic total biomass was significantly lower at the highest shell degradation indexes (i.e., indexes 5 and 6,]75 − 100] and 100 %) than at shell degradation index 3 (i.e.,]25 − 50] %) but was not significantly different at shell degradation indexes 2 and 4 (i.e.,]0 − 25] and]50 − 75] %) (Table S5.14, Figure 5.4j).

Finally, average total biomass of epibionts per mussel valve was significantly different depending on where epibionts settled on the mussel shell (Table 5.8c), with the lowest biomass on the infested part of the shell (Table S5.15, Figure 5.4k).

Table 5.8. Type II Wald χ^2 test on the Generalized Linear Mixed Model (GLMM) on the relationship between the total biomass of epibionts per mussel and (a) shell length range (from]30 − 40] to]110 − 120] in mm), (b) euendolithic infestation levels (from A to E, as defined in Kaehler, 1999) and shell degradation index (from 1 to 6, as defined in Ma *et al.*, 2023), and (c) position on the shell (i.e., infested, non-infested, or secondary epibiosis). Significant p-values are underlined.
Models used in these analysese: (a) biomass ~ length_range, family = "ziGamma(link = "log")", (b) biomass ~ inf.lvl + inf.percent, family = "ziGamma(link = "log")" (interaction was not significant), and (c) biomass ~ position, family = "ziGamma(link = "log")".

Source of variation	LR Chisq	df	p (> Chisq)
(a) Shell length range			
Length range	100.85	8	$\underline{< 2.2 \times 10^{-16}}$
Residual deviance	4118.7	428	
(b) Infestation level and shell degradation			
Infestation level	35.379	4	$\underline{3.883 \times 10^{-7}}$
Shell degradation	53.437	5	$\underline{2.735 \times 10^{-10}}$
Residual deviance	6285.0	749	
(c) Position on the shell			
Position	83.748	2	$\underline{< 2.2 \times 10^{-16}}$
Residual deviance	8533.8	1202	

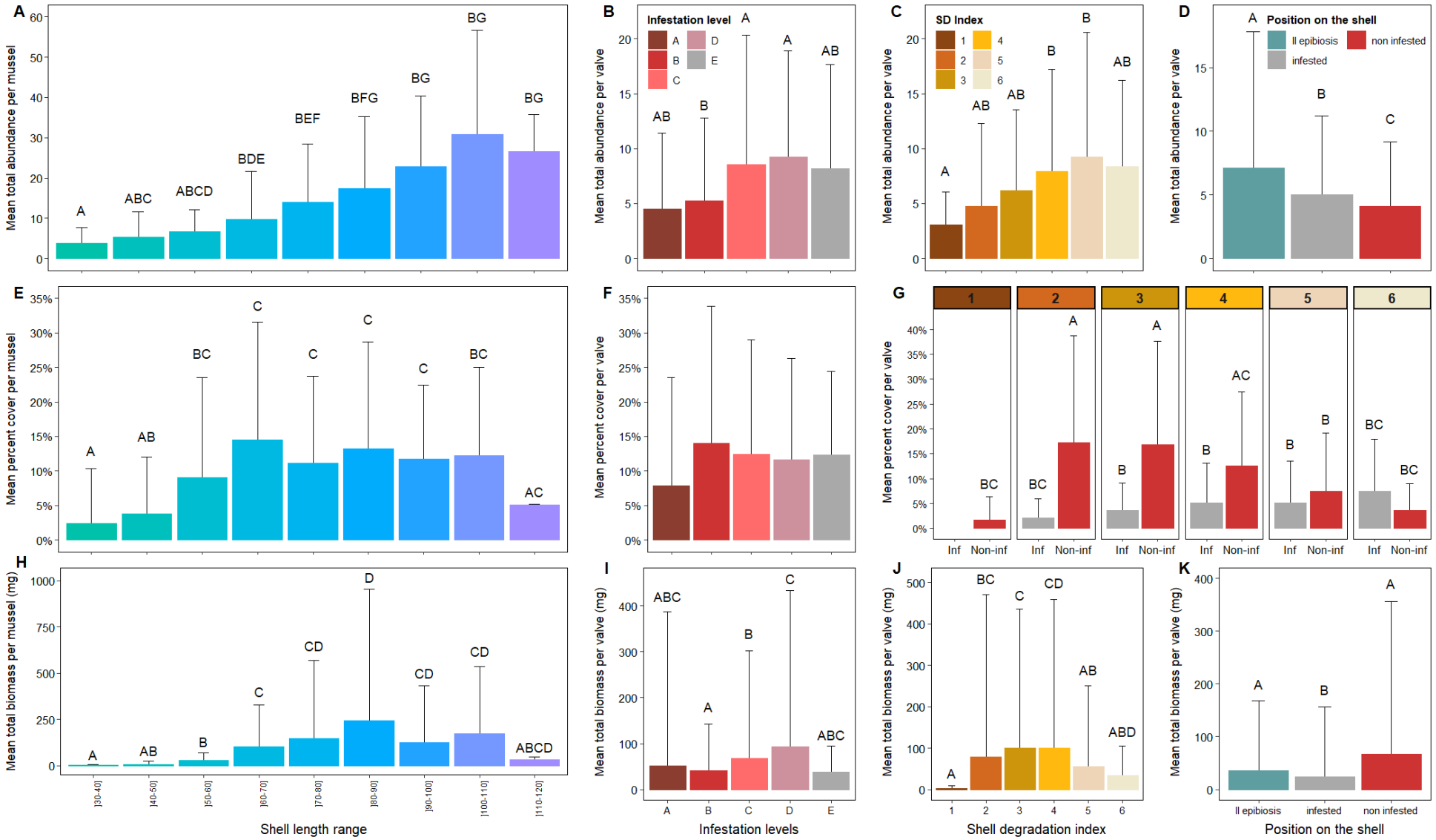

Figure 5.4. Average total abundance (± SD) in epibionts for each (a) shell length range, (b) euendolithic infestation level, (c) shell degradation index, and (d) position of the epibionts on the mussel shell. Average percent cover (± SD) in epibionts for each (e) shell length range, (f) euendolithic infestation level, and (g) position of the epibionts on the mussel shell for each shell degradation index. Average total biomass (± SD) in epibionts for each (h) shell length range, (i) euendolithic infestation level, (j) shell degradation index, and (k) position of the epibionts on the mussel shell. Homogeneous groups are indicated by similar letters.

5.3.2.1.4. Species richness (S)

A total of 55 epibiotic taxa were recorded on the mussels collected and processed for this investigation (Table S5.16). Among the epibionts, 19 taxa could only be identified to phylum, order, class, or family levels, while four taxa could only be identified to the genus level. The number of unique epibiotic taxa recorded increased with euendolithic infestation levels and shell degradation indexes (i.e., A = 25, B = 30, C = 36, D = 47, and 0% = 11,]0 − 25]% = 23,]25 − 50]% = 26,]50 − 75]% = 39,]75 − 100]% = 48) with a marked drop off at the most extreme levels (i.e., E = 18, and 100% = 18). Considering the position of epibionts on the mussel shell, a total of 28 taxa were associated with secondary epibiosis, 48 taxa with the infested part of the shell, and 39 taxa with the non-infested part of the shell. A total of 13 taxa were common at all euendolithic infestation levels, while the same four taxa were common to all shell degradation indexes and position on the mussel shell.

Average species richness per mussel increased significantly with shell length (Table 5.9a, Figure 5.5a) and was significantly lower for small shell length sizes (i.e.,]30 − 60] mm) than the median and larger shell length sizes (i.e.,]70 − 90] and]90 − 120] mm, respectively) (Table S5.17, Figure 5.5a). Average species richness per mussel valve was significantly different between euendolithic infestation levels, but not between shell degradation indexes, with no significant interaction observed (Tables 5.9b and S5.19, Figure 5.5b,c). Average species richness per mussel valve increased with euendolithic infestation levels and was significantly lower at level B than at levels C and D (Table S5.18, Figure 5.5b). Average species richness per mussel valve at the most extreme levels of euendolithic infestation (i.e., A and E) were, however, not significantly different from one another and compared to the other euendolithic infestation levels (i.e., B to D). Average species richness per mussel valve was significantly different

depending on where epibionts settled on the mussel shell (Table 5.9c), with the highest species richness on the infested part of the shell (Table S5.20, Figure 5.5d).

Table 5.9. Type II ANOVA on the Generalized Linear Model (GLM) on the relationship between the epibiotic species richness per mussel and (a) shell length range (from]30 – 40] to]110 – 120] in mm), (b) euendolithic infestation levels (from A to E, as defined in Kaehler, 1999) and shell degradation index (from 1 to 6, as defined in Ma *et al.*, 2023), and (c) position on the shell (i.e., infested, non-infested, or secondary epibiosis). Significant p-values are underlined.
Models used in these analyses: (a) count ~ length_range, family = "poisson", (b) count ~ inf.lvl + inf.percent, family = "negative binomial" (interaction was not significant), and (c) count ~ position, family = "poisson".

Source of variation	LR Chisq	df	p (> Chisq)
(a) Shell length range			
Length range	178.28	8	$\underline{< 2.2 \times 10^{-16}}$
Residual deviance	367.29	450	
(b) Infestation level and shell degradation index			
Infestation	21.40	4	$\underline{2.637 \times 10^{-4}}$
Degradation	8.337	5	0.139
Residual deviance	568.23	794	
(c) Position on the shell			
Position	18.258	2	$\underline{1.085 \times 10^{-4}}$
Residual deviance	591.33	1290	

5.3.2.1.5. Shannon–Wiener diversity index (*H'*)

Average Shannon-Wiener diversity index (*H'*) values significantly increased with shell length (Table 5.10, Figure 5.5e) and was significantly lower for small shell length sizes (i.e.,]30 – 60] mm) than the median and larger shell length sizes (i.e.,]70 – 100] mm), with a non-significant drop for the most extreme shell length size (i.e.]100 – 120] mm) (Table S5.21, Figure 5.5e).

Table 5.33. Type II one-way ANOVA on the Linear Model (LM) on the relationship between the average Shannon-Wiener diversity index per mussel and shell length range (from]30 – 40] to]110 – 120] in mm). Significant p-values are underlined.
Model used in this analysis: shannon_length ~ length_range.

Source of variation	Type II Sum of Square	df	F-value	p-value
Length range	36.498	8	20.95	$\underline{< 2.2 \times 10^{-16}}$
Residuals	97.996	450		

Average Shannon-Wiener diversity index (*H'*) values significantly differed between euendolithic infestation levels, but not between shell degradation indexes, with no significant interaction observed (Tables 5.11 and S5.23, Figure 5.5f,g). Average Shannon-Wiener diversity index (*H'*) values per mussel valve significantly increased with euendolithic infestation levels and was significantly higher at levels C and D than at level B, with a non-significant drop at level E (Table S5.22, Figure 5.5f).

Table 5.11. Type II two-way ANOVA on the Linear Model (LM) on the relationship between the average Shannon-Wiener diversity index per mussel and euendolithic infestation levels (from A to E, as defined in Kaehler, 1999) and shell degradation index (from 1 to 6, as defined in Ma *et al.*, 2023). Significant p-values are underlined.
Model used in this analysis: shannon_inf ~ inf.lvl + inf.percent. Interaction was not significant.

Source of variation	Type II Sum of Square	df	F-value	p-value
Infestation	7.848	4	9.141	$\underline{3.194 \times 10^{-7}}$
Degradation	1.840	5	1.714	0.129
Residuals	170.430	794		

Average Shannon-Wiener diversity index (*H'*) value per mussel valve was significantly different depending on where epibionts settled on the mussel shell (Table 5.12), with higher diversity on the infested than for secondary epibiosis and on the non-infested parts of the shell (Table S5.24, Figure 5.5h).

Table 5.12. Type II Wald χ^2 test on the Generalized Linear Mixed Model (GLMM) on the relationship between the average Shannon-Wiener diversity index (*H'*) per mussel valve and position on the shell (i.e., infested, non-infested, or secondary epibiosis). Significant p-values are underlined.
Model used in this analysis: shannon_pos ~ position, family = "ziGamma(link = "log")".

Source of variation	LR Chisq	df	p (> Chisq)
Position	7.362	2	<u>0.025</u>
Residual deviance	1900.7	1286	

5.3.2.1.6. Simpson's diversity index (λ)

Average Simpson's diversity index (λ) values increased significantly with shell length (Table 5.13a), with lower diversity at lower shell length sizes (i.e., $]30-70]$ mm) than at median and larger shell length sizes (i.e., $]70-120]$ mm) (Table S5.25, Figure 5.5i).

The average Simpson's diversity index (λ) values differed significantly between euendolithic infestation levels, but not between shell degradation indexes, with no significant interaction recorded (Tables 5.13b and S5.27, Figure 5.5j,k). Average Simpson's diversity index (λ) value per mussel valve significantly increased with euendolithic infestation levels and was significantly higher at levels C and D than at level B, with a non-significant drop at level E (Table S5.26, Figure 5.5j). Average Simpson's diversity index (λ) per mussel valve at euendolithic infestation level A was significantly lower than at level D but was not significantly different from levels B, C and E (Table S5.26, Figure 5.5j). Similarly, average Simpson's diversity index (λ) value per mussel valve at euendolithic infestation level E was not significantly different from the other euendolithic infestation levels (Table S5.26, Figure 5.5j).

Average Simpson's diversity index (λ) per mussel valve did not significantly differ depending on where epibionts settled on the mussel shell (Table 5.13c, Figure 5.5l).

5.3.2.1.7. Pielou's evenness index (*J'*)

Average Pielou's evenness index (*J'*) values did not significantly differ between shell length sizes (Table 5.14a, Figure 5.5m), euendolithic infestation levels and shell degradation indexes (Table 5.14b, Figure 5.5n,o), or depending on where epibionts settled on the mussel shell (Table 5.14c, Figure 5.5p).

Table 5.13. Type II Wald χ^2 test on the Generalized Linear Mixed Model (GLMM) on the relationship between the average Simpson's diversity index (λ) per mussel and (a) shell length range (from]30 − 40] to]110 − 120] in mm), (b) euendolithic infestation levels (from A to E, as defined in Kaehler, 1999) and shell degradation index (from 1 to 6, as defined in Ma *et al.*, 2023), and (c) position on the shell (i.e., infested, non-infested, or secondary epibiosis). Significant p-values are underlined.
Models used in these analyses: (a) simpson_length ~ length_range, family = "gaussian(link = "identity")", (b) simpson_inf ~ inf.lvl + inf.percent, family = "gaussian(link = "identity")" (interaction was not significant), and (c) shannon_pos ~ position, family = "ziGamma(link = "log")".

Source of variation	LR Chisq	df	p (> Chisq)
(a) Shell length range			
Length range	154.16	8	$< 2.2 \times 10^{-16}$
Residual deviance	− 28.0	448	
(b) Infestation level and shell degradation			
Infestation	37.661	4	$< 1.316 \times 10^{-7}$
Degradation	8.491	5	0.131
Residual deviance	79.4	788	
(c) Position on the shell			
Position	3.088	2	0.214
Residual deviance	1345.7	1286	

Table 5.14. Type II ANOVAs on the Linear Model (LM) on the relationship between the average Pielou's evenness index (*J'*) per mussel and (a) shell length range (from]30 − 40] to]110 − 120] in mm), (b) euendolithic infestation levels (from A to E, as defined in Kaehler, 1999) and shell degradation index (from 1 to 6, as defined in Ma *et al.*, 2023), and (c) mussel position on the shell (i.e., infested, non-infested, or secondary epibiosis). No significant p-values were detected.
Models used in these analyses: (a) pielou_length ~ length_range, (b) pielou_inf ~ inf.lvl + inf.percent (interaction was not significant), and (c) pielou_pos ~ position.

Source of variation	Type II Sum of Square	df	F-value	p-value
(a**) Shell length range**				
Length range	0.446	8	1.516	0.150
Residuals	12.714	346		
(b) Infestation level and shell degradation index				
Infestation	0.021	4	0.123	0.974
Degradation	0.139	5	0.653	0.659
Residuals	21.488	503		
(c) Position on the shell				
Position	0.059	2	0.781	0.458
Residuals	21.685	576		

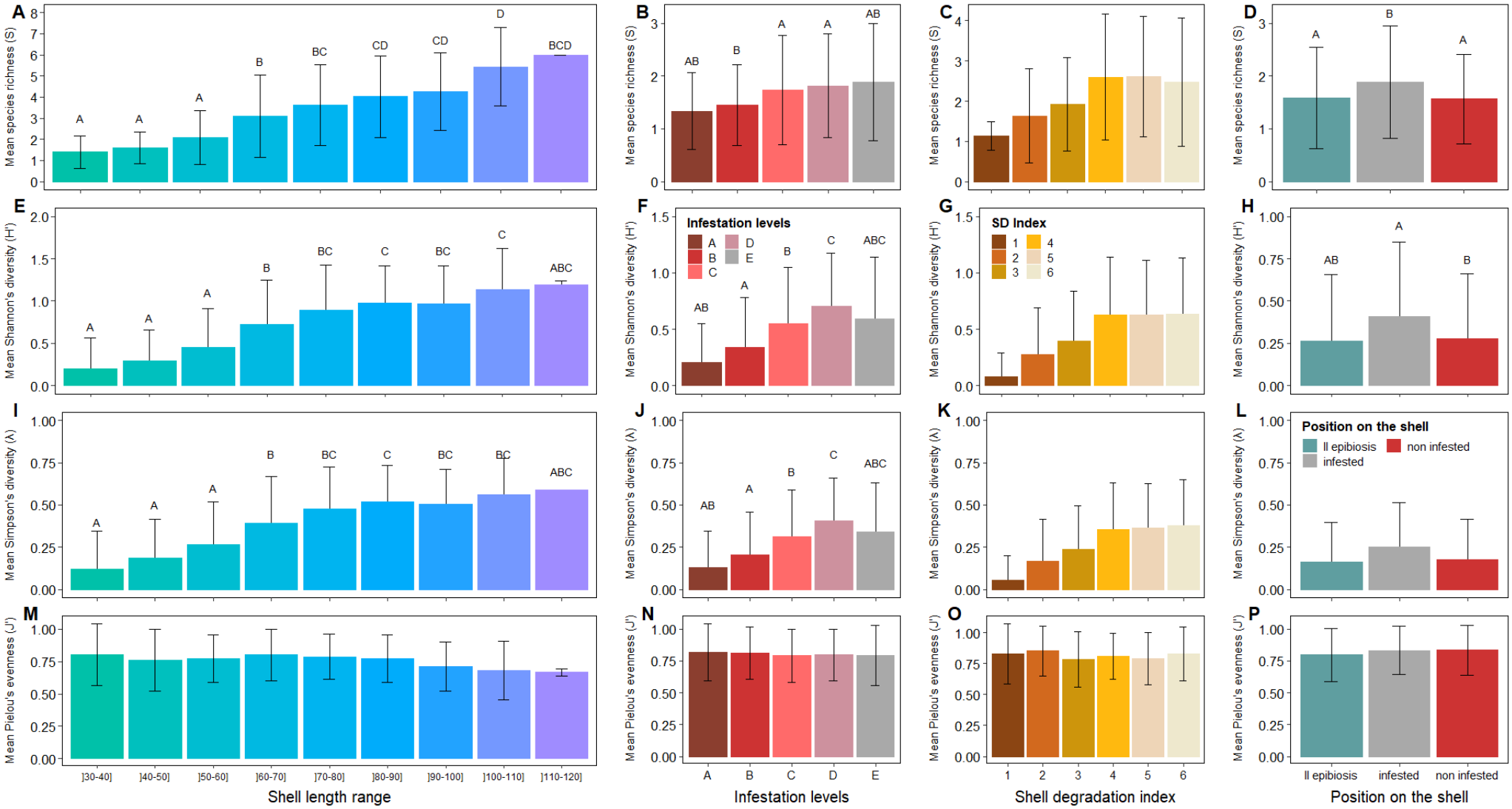

Figure 5.5. Average species richness (S, ± SD) in epibionts for each (a) shell length range, (b) euendolithic infestation level, (c) shell degradation index, and (d) position of the epibionts on the mussel shell. Average Shannon-Wiener diversity index (*H'*, ± SD) in epibionts for each (e) shell length range, (f) euendolithic infestation level, (g) shell degradation index, and (h) position of the epibionts on the mussel shell. Average Simpson's diversity index (λ, ± SD) in epibionts for each (i) shell length range, (j) euendolithic infestation level, (k) shell degradation index, and (l) position of the epibionts on the mussel shell. Average Pielou's evenness index (*J'*, ± SD) in epibionts for each (m) shell length range, (n) euendolithic infestation level, (o) shell degradation index, and (p) position of the epibionts on the mussel shell. Homogeneous groups are indicated by similar letters.

5.3.2.2. Multivariate analyses on epibiotic communities

5.3.2.2.1. Abundance of epibiotic communities

5.3.2.2.1.1. Shell length size

In terms of abundance, epibiotic community structure was significantly affected by shell length sizes for both the epibiotic higher taxonomical groups and epibiotic species (Table 5.15, Figures 5.6a and 5.6b).

Table 5.15. ANOVA (Wald-like test) on the many Generalized Linear Model (GLM) on the relationship between the abundance of (a) higher taxonomical groups or (b) epibiotic species, and shell length range (from $]30-40]$ to $]110-120]$ in mm). Significant p-values are underlined.
Models used in these analysese: (a) sp_mva_group ~ abund_wide_group$length_range, family = "negative binomial", and (b) sp_mva_sp ~ abund_wide_sp$length_range, family = "negative binomial".

Source of variation	Res. df	df	Wald	Pr(>Wald)
(a) **Higher taxonomical groups**				
(Intercept)	1310			
Length range	1302	8	17.05	<u>0.001</u>
(b) Epibiotic species				
(Intercept)	1310			
Length range	1302	8	19.45	<u>0.001</u>

Bryozoans (i.e., Bryozoa), barnacles (i.e., Cirripedia), ochrophytes (i.e., Ochrophyta), sedentary worms (i.e., Sedentaria), bivalves (i.e., Bivalvia) and red algae (i.e. Rhodophyta) were largely responsible for driving the community differences in terms of abundance between shell length sizes (Table S5.28, Figure 5.6a). Among the higher taxonomical groups, species driving epibiotic community differences included: *Tetraclita serrata* and juvenile barnacles (Cirripedia), *Ralfsia verrucosa* (Areschoug) Areschoug, 1845 (Ochrophyta), *Spirorbis* sp. Daudin, 1800 (Sedentaria) and encrusting coralline algae (Rhodophyta) (Table S5.29, Figure 5.6b).

Barnacles were significantly less abundant on the smaller shell length sizes (i.e., $]30-70]$ mm) than on the larger shell length sizes (i.e., $]90-110]$ mm) (Tables 5.16a and S5.30, Figure 5.6a). Abundances of *Tetraclita serrata* and juvenile

barnacles differed significantly between shell length sizes (Table 5.16b,c). *Tetraclita serrata* was absent from the shell of the smallest mussels (i.e., $]30-40]$ mm) and subsequent pairwise comparisons did not detect significant differences in abundance between shell length sizes (Table S5.31, Figure 5.6b). However, juvenile barnacles were significantly less abundant at smaller shell length sizes (i.e., $]30-40]$ and $]50-70]$ mm) than at larger shell length sizes (i.e., $]80-100]$ mm) (Table S5.32, Figure 5.6b).

Sedentary worm abundances increased significantly increased with shell length (Table 5.16d), with lower abundances at smaller shell length sizes (i.e., $]30-50]$ mm) than at median and larger shell length sizes (i.e., $]50-110]$ mm), with a non-significant drop at the most extreme shell length size (i.e., > 110 mm) (Table S5.33, Figure 5.6a). *Spirorbis* sp. abundances increased significantly with shell length (Table 5.16e), with lower abundances at smaller shell length sizes (i.e., $]30-60]$ mm) than at larger shell length sizes (i.e., $]60-110]$ mm) (Table S5.34, Figure 5.6b).

Abundances in red algae (i.e., number of separate patches) differed significantly between shell length sizes (Table 5.16f), however this was not detected in the subsequent pairwise comparisons (Table S5.35, Figure 5.6a). While encrusting coralline algae were detected to drive epibiotic community differences, their abundances did not differ significantly between shell length sizes (Table 5.16g, Figure 5.6b).

Conversely, abundances of bryozoans, bivalves and ochrophytes did not differ significantly between shell length sizes (Tables 5.16h,i,j, Figure 5.6a). Although *Ralfsia verrucosa* was largely responsible for driving the changes in epibiotic communities, its abundances did not differ significantly between shell length sizes (Table 5.16k). It is, however, worth noting it was absent from the largest mussel shells (i.e., $]110-120]$ mm) (Figure 5.6b).

Table 5.16. Type II one-way ANOVA on the Generalized Linear Model (GLM) on the relationship between shell length range (from]30 – 40] to]110 – 120] in mm) and the abundance in (a) Cirripedia (barnacles), (b) *Tetraclita serrata* (Cirripedia), (c) juvenile Cirripedia, (d) Sedentaria (sedentary worms), (e) *Spirorbis* spp. (Sedentaria), (f) Rhodophyta (red algae), (g) Corallinales (encrusting coralline algae), (h) Bryozoa, (i) Bivalvia, (j) Ochrophyta, and (k) *Ralfsia verrucosa* (Ochrophyta), per mussel valve. Significant p-values are underlined.
Models used in these analyses were coded as follow: abundance ~ length_range, family = "negative binomial", except for (h) Bryozoa and (i) Bivalvia models for which family = "poisson".

Source of variation	LR Chisq	df	p (> Chisq)
(a) Cirripedia			
Length range	184.31	8	$\underline{< 2.2 \times 10^{-16}}$
Residual deviance	483.85	450	
(b) Cirripedia – *Tetraclita serrata*			
Length range	22.98	7	<u>0.002</u>
Residual deviance	121.17	121	
(b) Cirripedia (juvenile)			
Length range	30.559	8	$\underline{1.683 \times 10^{-4}}$
Residual deviance	293.03	278	
(d) Sedentaria			
Length range	29.613	8	$\underline{2.474 \times 10^{-4}}$
Residual deviance	220.67	196	
(e) Sedentaria – *Spirorbis* spp.			
Length range	28.882	8	$\underline{3.325 \times 10^{-4}}$
Residual deviance	173.72	152	
(f) Rhodophyta			
Length range	18.604	8	<u>0.017</u>
Residual deviance	155.81	173	
(g) Rhodophyta – Corallinales			
Length range	14.903	8	0.061
Residual deviance	92.253	121	
(h) Bryozoa			
Length range	2.905	8	0.940
Residual deviance	30.106	91	
(i) Bivalvia			
Length range	3.117	7	0.874
Residual deviance	20.350	37	
(j) Ochrophyta			
Length range	3.566	7	0.828
Residual deviance	107.99	123	
(k) Ochrophyta – *Ralfsia verrucosa*			
Length range	3.333	7	0.853
Residual deviance	108.59	122	

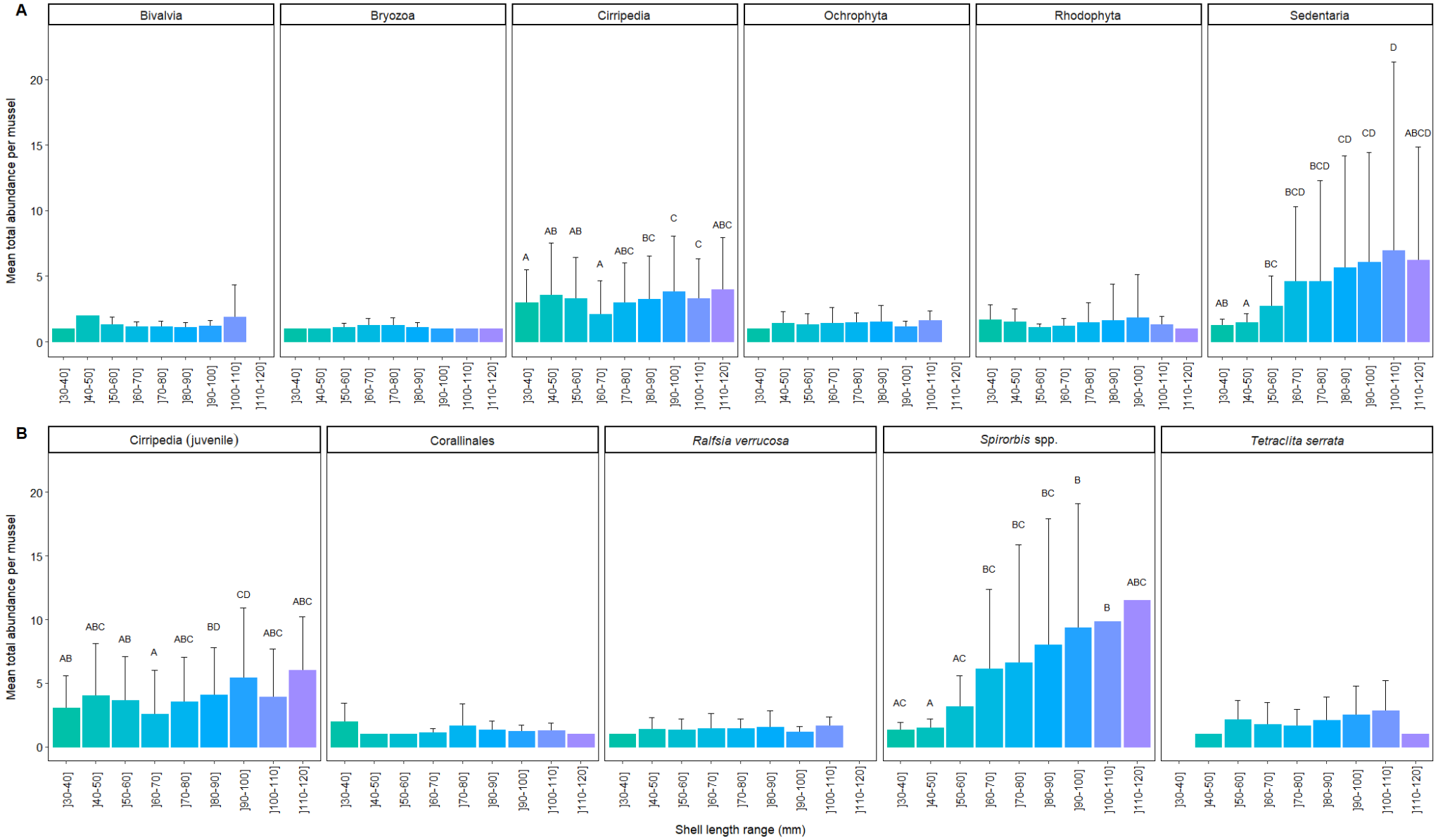

Figure 5.6. Average abundance (± SD) for each shell length range (in mm) for (a) significant epibiotic higher taxonomical groups and (b) significant epibiotic species driving differences in community. Homogeneous groups are indicated by similar letters.

5.3.2.2.1.2. Euendolithic infestation and shell degradation

In terms of abundance, the epibiotic community structure was significantly affected by euendolithic infestation levels and shell degradation indexes at both the higher taxonomical group and species levels (Table 5.17).

Table 5.17. ANOVA (Wald-like test) on the many Generalized Linear Model (GLM) on the relationship between the abundance of (a) higher taxonomical groups or (b) epibiotic species and euendolithic infestation levels (from A to E, as defined in Kaehler, 1999) and shell degradation index (from 1 to 6, as defined in Ma *et al.*, 2023). Significant p-values are underlined.
Models used in these analyses: (a) sp_mva_group ~ abund_wide_group$inf.lvl + inf.percent, family = "negative binomial", and (b) sp_mva_sp ~ abund_wide_sp$inf.lvl + inf.percent, family = "negative binomial".

Source of variation	Res. df	df	Wald	Pr(>Wald)
(a) Higher taxonomical groups				
(Intercept)	1310			
Infestation	1306	4	10.22	0.001
Degradation	1301	5	12.51	0.001
(b) Epibiotic species				
(Intercept)	1310			
Infestation	1306	4	13.43	0.001
Degradation	1301	5	14.85	0.001

Barnacle, ochrophyte and red algae abundances were largely responsible for driving the community differences at the different euendolithic infestation levels and shell degradation indexes (Table S5.36, Figure 5.7a,b,c). Among the higher taxonomical groups, species responsible for driving the epibiotic community differences included: *Tetraclita serrata* (Cirripedia) and Corallinales (Rhodophyta) for euendolithic infestation levels, juvenile barnacles (Cirripedia) and *Hildenbrandia lecannellieri* Hariot, 1887 (Rhodophyta) for shell degradation indexes, and *Ralfsia verrucosa* (Ochrophyta) for both euendolithic infestation levels and shell degradation indexes (Table S5.37, Figure 5.7d,e).

Abundances of ochrophytes and red algae significantly differed between euendolithic infestation levels and shell degradation indexes (Table 5.18a, Figure 5.7a,b), with a

significant interaction in the case of the red algae (Table 5.18b, Figure 5.7c). Ochrophytes were significantly less abundant at euendolithic infestation level A than at level E (Table S5.38, Figure 5.7a), and significantly more abundant at shell degradation index 2 (i.e., $]0-25]$ %) than at index 5 (i.e., $]75-100]$ %) (Table S5.39, Figure 5.7b). *Ralfsia verrucosa* abundances did not significantly differ between euendolithic infestation levels and shell degradation indexes (Table 5.18c, Figure 5.7d,e). However, subsequent pairwise comparisons demonstrated that *R. verrucosa* was less abundant at euendolithic infestation level A than at levels D and E, although this was not significant (Table S5.40, Figure 5.7d), and significantly more abundant at shell degradation index 2 (i.e., $]0-25]$ %) than at index 5 (i.e., $]75-100]$ %) (Table S5.41, Figure 5.7e). Conversely, abundances of red algae significantly differed between euendolithic infestation levels for shell degradation index 4 (i.e., $]50-75]$ %), and were significantly higher at level E than at other levels of euendolithic infestation (Table S5.18, Figure 5.7c). While Corallinales and *Hildenbrandia lecannellieri* were largely responsible for driving epibiotic community differences, their abundances did not differ significantly between euendolithic infestation levels and shell degradation indexes (Table 5.18d,e, Figure 5.7d,e). It is worth noting that *H. lecannellieri* was absent at the most extreme shell degradation indexes (i.e., 1 and 6, 0 % and 100 %) (Figure 5.7e).

Although detected as driving epibiotic community differences, abundances in Cirripedia, mainly represented by *Tetraclita serrata* and juvenile barnacles, did not differ significantly between euendolithic infestations levels and shell degradation indexes (Table 5.18f,g,h, Figure 5.7a,b,d,e). *Tetraclita serrata* was absent from the lowest shell degradation index (i.e., 1, 0 %) (Figure 5.7e).

Table 5.18. Type II two-way ANOVA on the Generalized Linear Model (GLM) on the relationship between euendolithic infestation levels (from A to E, as defined in Kaehler, 1999) and shell degradation index (from 1 to 6, as defined in Ma *et al.*, 2023) and the abundance in (a) Ochrophyta, (b) Rhodophyta, (c) *Ralfsia verrucosa* (Ochrophyta), (d) Corallinales (Rhodophyta), (e) *Hildenbrandia lecannelleri* (Rhodophyta), (f) Cirripedia, (g) *Tetraclita serrata* (Cirripedia), and (h) juvenile Cirripedia per mussel valve. Models used in these analyses were coded as follow : abundance ~ inf.lvl + inf.percent, family = "negative binomial", except for (c) *Ralfsia verrucosa*, (d) Corallinales, (e) *Hildenbrandia lecannellieri* model for which family = "poisson". Interaction was significant only for (b) Rhodophyta model.

Source of variation	LR Chisq	df	p (> Chisq)
(a) Ochrophyta			
Infestation	10.192	4	0.037
Degradation	11.190	5	0.048
Residual deviance	111.30	175	
(b) Rhodophyta			
Infestation	15.808	4	3.288×10^{-3}
Degradation	11.382	5	0.044
Interaction	21.942	9	9.066×10^{-3}
Residual deviance	185.52	236	
(c) Ochrophyta – *Ralfsia verrucosa*			
Infestation	8.330	4	0.080
Degradation	10.309	5	0.067
Residual deviance	97.728	174	
(d) Rhodophyta – Corallinales			
Infestation	5.908	4	0.206
Degradation	4.451	5	0.487
Residual deviance	85.10	163	
(e) Rhodophyta – *Hildenbrandia lecannellieri*			
Infestation	1.222	4	0.875
Degradation	1.122	3	0.772
Residual deviance	19.443	75	
(f) Cirripedia			
Infestation	6.524	4	0.163
Degradation	5.047	5	0.410
Residual deviance	495.26	482	
(g) Cirripedia – *Tetraclita serrata*			
Infestation	8.820	4	0.066
Degradation	4.512	4	0.341
Residual deviance	145.22	150	
(h) Cirripedia (juvenile)			
Infestation	3.613	4	0.461
Degradation	3.765	5	0.584
Residual deviance	383.12	377	

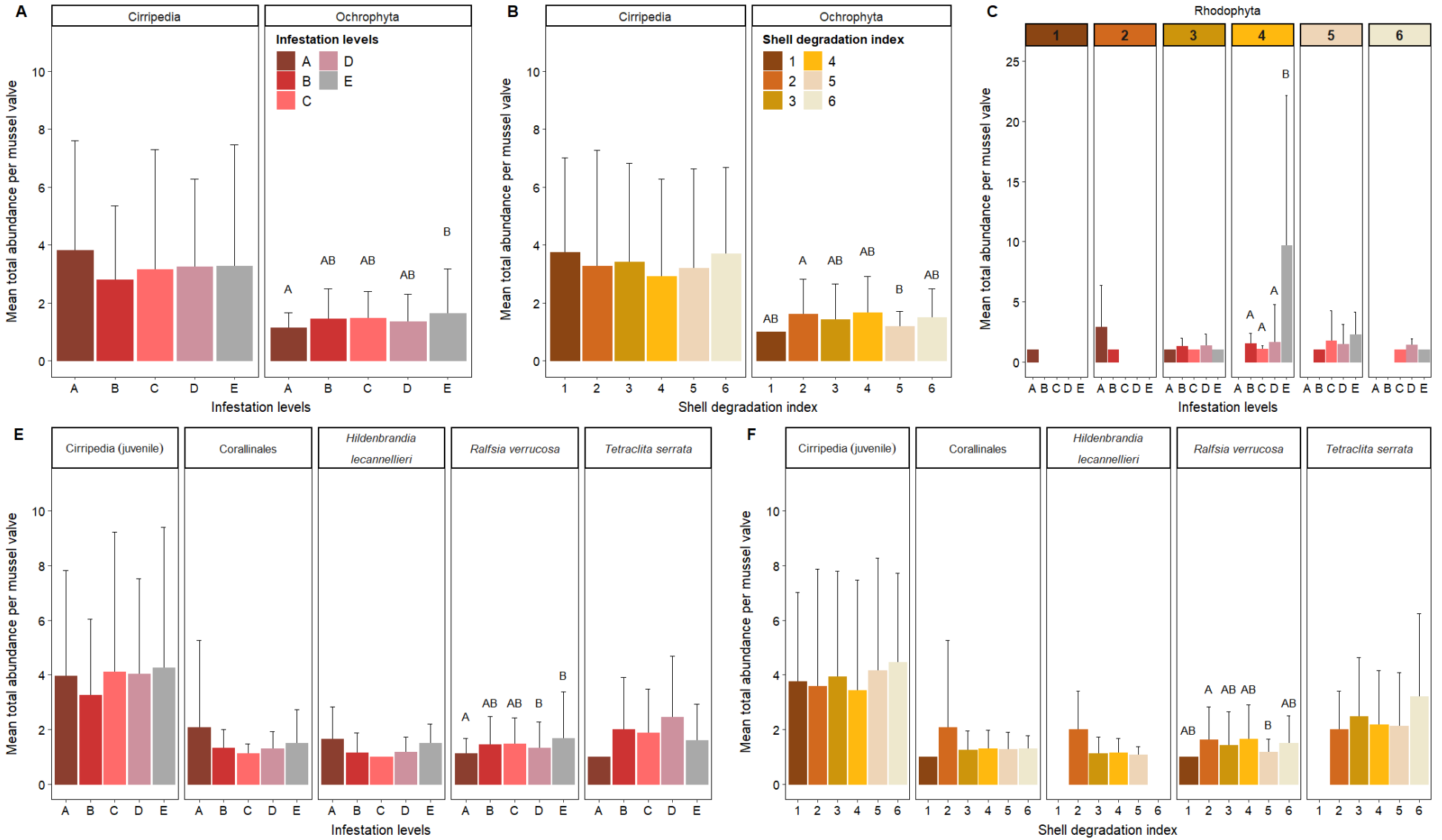

Figure 5.7. Average total abundance per mussel valve (± SD) for (a,b,c) significant epibiotic higher taxonomical groups for each (a) euendolithic infestation levels and (b) shell degradation index for Cirripedia and Ochrophyta, and for (c) each euendolithic infestation levels per shell degradation index for Rhodophyta. Average total abundance per mussel valve (± SD) for (d,e) significant epibiotic species driving differences in community for each (e) euendolithic infestation levels and (f) shell degradation index. Homogeneous groups are indicated by similar letters.

5.3.2.2.2. Percent cover of epibiotic communities

In terms of percent cover, epibiotic community structure was significantly affected by shell length size, euendolithic infestation levels, shell degradation indexes and, the position of the epibionts on the mussel shell, with a significant interaction between shell degradation index and position, for epibiotic higher taxonomical groups and epibiotic species (Table 5.19). nMDS plots and dispersion plots mirrored the PERMANOVA results and detected clear group separation between the mussel's biological variables (i.e., shell length, euendolithic infestation level and degree of shell degradation) (Figures 5.8 and 5.9).

Table 5.19. PERMANOVA on the effect of environmental variables on the percent cover of (a) epibiotic higher taxonomical groups and (b) epibiotic species. Significant p-values are underlined.

Source of variation	Sum of Squares	df	R^2	*F*-value	p-value
(a) Higher taxonomical groups					
Length range	17.720	8	0.042	6.453	0.001
Infestation	3.710	4	0.009	2.703	0.001
Degradation	10.460	5	0.025	6.096	0.001
Position	15.510	1	0.037	45.187	0.001
Infestation x Position	1.660	4	0.004	1.208	0.212
Degradation x Position	2.050	4	0.005	1.494	0.045
Residual	371.090	1081	0.879		
Total	422.210	1107	1.000		
(b) Epibiotic species					
Length range	18.370	8	0.039	5.893	0.001
Infestation	3.310	4	0.007	2.126	0.001
Degradation	8.380	5	0.018	4.300	0.001
Position	14.610	1	0.031	37.477	0.001
Infestation x Position	1.530	4	0.003	0.980	0.500
Degradation x Position	2.080	4	0.004	1.332	0.078
Residual	421.310	1081	0.897		
Total	469.590	1107	1.000		

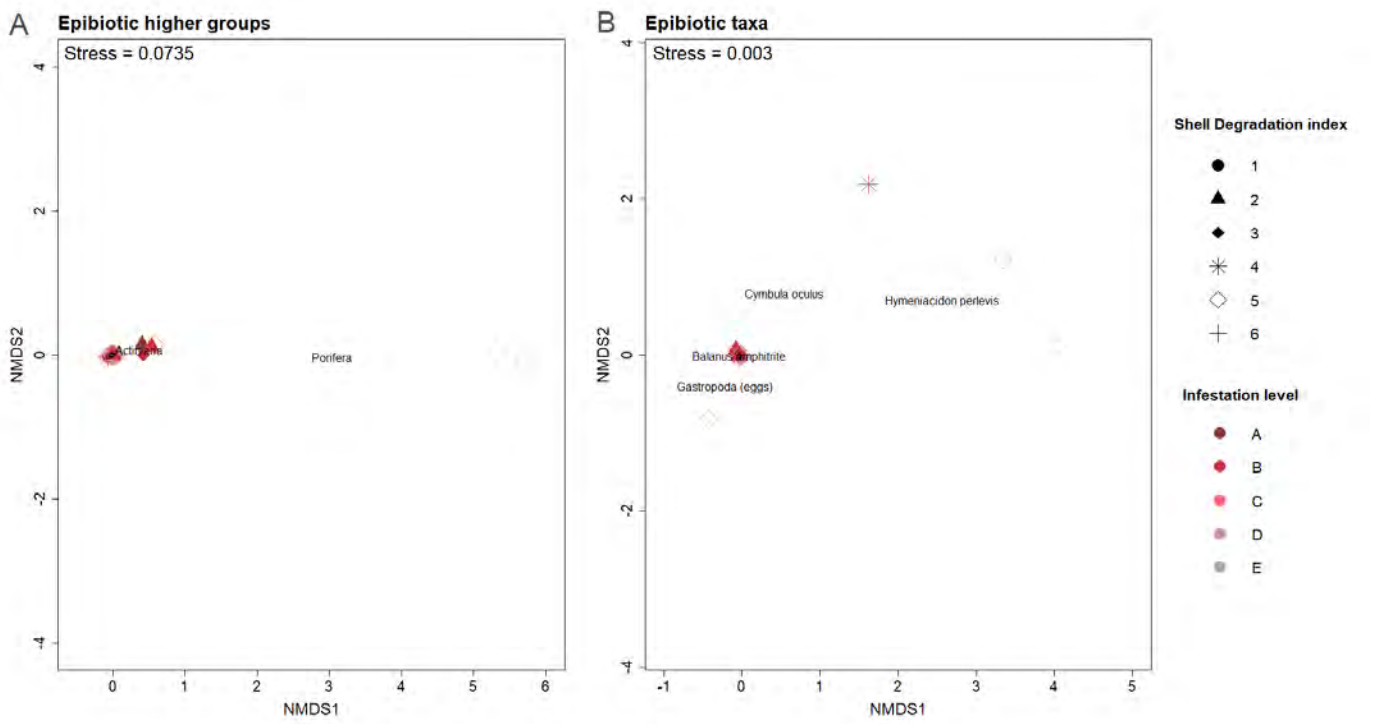

Figure 5.8. Similarity in percent cover of epibiotic communities, with non-metric multidimensional scaling (nMDS) plots for (a) higher epibiotic functional groups, and (b) epibiotic species.

In terms of percent cover, SIMPER analyses indicated that the following higher epibiotic taxonomical groups collectively accounted for 70% of the dissimilarity between shell length sizes, euendolithic infestation levels, shell degradation indexes and position of the epibionts on the mussel shell: Cirripedia, Ochrophyta, Rhodophyta and Sedentaria (Tables S5.43, S5.44, S5.45 and S5.46, Figures 5.10a and 5.11). In particular, the following epibiotic species or taxa collectively accounted for 70% of the dissimilarity: *Tetraclita serrata, Chthamalus dentatus* and juvenile barnacle (Cirripedia), *Ralfsia verrucosa* (Ochrophyta), *Hildenbrandia lecannellieri* and Corallinales (Rhodophyta), and *Spirorbis* sp. and *Spirobranchus kraussii* (Baird, 1864) (Sedentaria) (Tables S5.47, S5.48, S5.49 and S5.50, Figures 5.10b and 5.12).

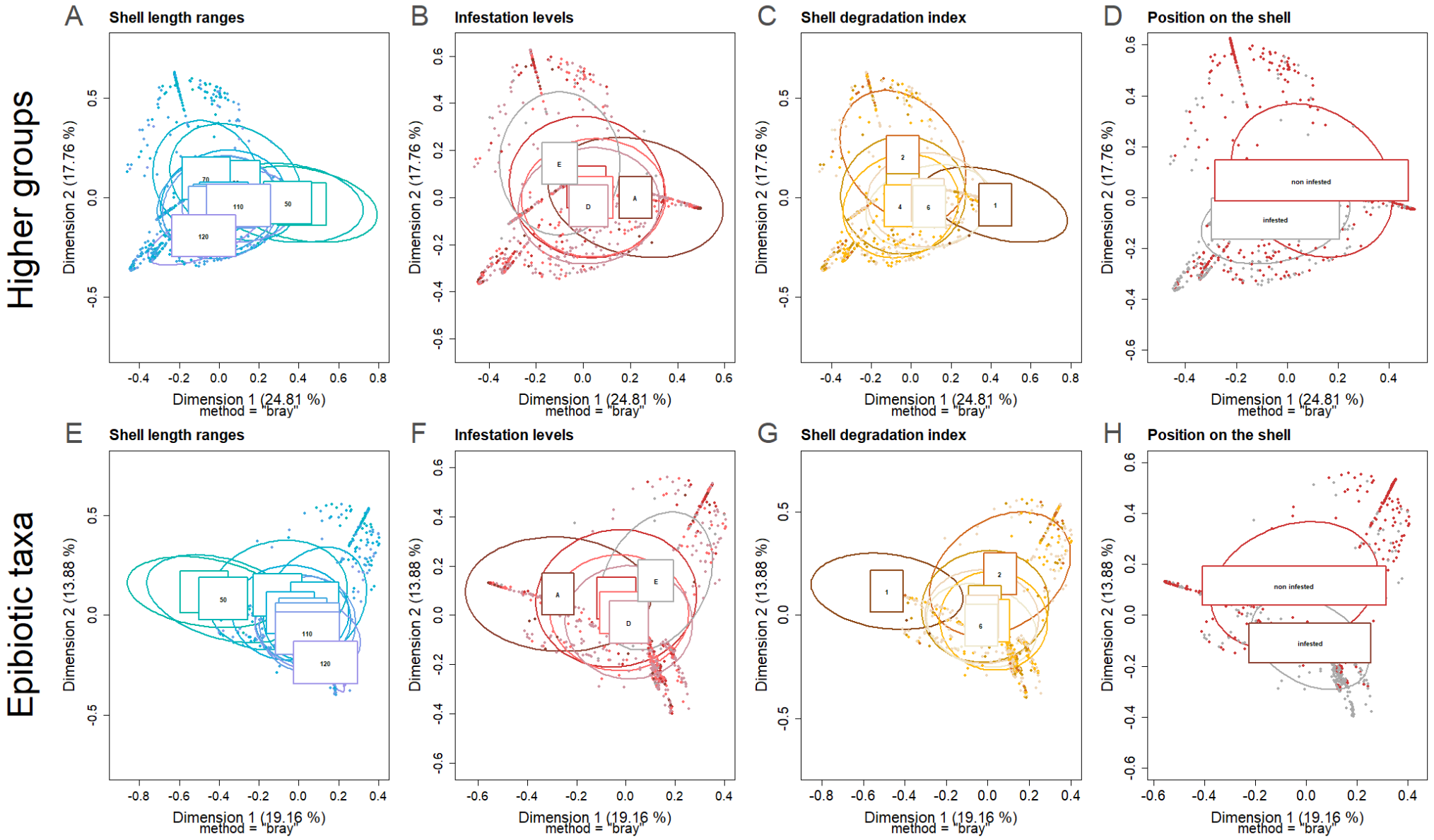

Figure 5.9. Similarity in percent cover of epibiotic communities with dispersion plots for the effect of (a,e) shell length size, (b,f) euendolithic infestation levels, (c,g) shell degradation indexes, and (d,h) position of the epibionts on the mussel shell, for either (a,b,c,d) higher epibiotic functional groups or (e,f,g,h) epibiotic species.

5.3.2.2.2.1. Shell length size

Percent cover of barnacles was significantly different between shell length sizes (Table 5.20a), but subsequent pairwise comparisons did not detect any differences (Table S5.51, Figure 5.10a). *Tetraclita serrata* and *Chthamalus dentatus* covers did not differ significantly between shell length sizes (Table 5.20b,c), while juvenile barnacle cover was significantly higher at larger shell length sizes (i.e., $]100-110]$ mm) than at smaller and median shell length sizes (i.e., $]30-100]$ mm) (Tables 5.20d and S5.52, Figure 5.10b). *Tetraclita serrata* was absent from the smallest shell length size (i.e., $]30-40]$ mm) (Figure 5.10b). The percentage cover of ochrophytes, represented by *Ralfsia verrucosa*, was significantly lower for a larger shell length size (i.e., $]80-90]$ mm) than for the smallest shell length size (i.e., $]30-40]$ mm) (Table 5.20e,f, S5.53 and S5.54, Figure 5.10a,b). Percent cover of red algae was significantly different between shell length sizes (Table 5.20g), but subsequent pairwise comparisons did not detect any differences (Table S5.55, Figure 5.10a). While *Hildenbrandia lecannellieri* cover did not significantly differ between shell length sizes (Table 5.20h, Figure 5.10b), the encrusting Corallinale cover were significantly lower at a larger shell length size (i.e., $]90-100]$ mm) than at a median shell length size (i.e., $]70-80]$ mm) (Tables 5.20i and S5.56, Figure 5.10b). *Hildenbrandia lecannellieri* was absent from the most extreme shell length sizes (i.e., $]30-40]$ and $]110-120]$ mm) (Figure 5.10b). The percentage cover of encrusting worms was significantly different between shell length sizes (Table 5.20j), but subsequent pairwise comparisons did not detect any differences (Table S5.57, Figure 5.10a). *Spirobranchus kraussii* cover was significantly different between shell length sizes (Table 5.20k), however this was not detected in subsequent pairwise comparisons (Table S5.58, Figure 5.10b). *Spirobranchus kraussii* was absent from the smallest shell length sizes (i.e., $]30-50]$ mm) (Figure 5.10b).

Conversely, percent cover of *Spirorbis* sp. did not significantly differ between shell length sizes (Table 5.20l, Figure 5.10b).

Table 5.20. Type II one-way ANOVA on the Generalized Linear Model (GLM) on the relationship between shell length ranges (from]30 – 40] to]110 – 120] in mm) and the average percent cover of (a) Cirripedia (barnacles), (b) *Tetraclita serrata* (Cirripedia), (c) *Chthamalus dentatus* (Cirripedia), (d) Cirripedia (juvenile), (e) Ochrophyta, (f) *Ralfsia verrucosa* (Ochrophyta), (g) Rhodophyta (red algae), (h) *Hildenbrandia lecannellieri* (Rhodophyta), (i) Corallinales (Rhodophyta), (j) Sedentaria (sedentary worms), (k) *Spirobranchus kraussii* (Sedentaria), and (l) *Spirorbis* spp. (Sedentaria). Significant p-values are underlined.
Models used in these analyses were coded as follow: cover ~ length_range, family = "Gamma".

Source of variation	LR Chisq	df	p (> Chisq)
(a) Cirripedia			
Length range	51.475	8	$\underline{2.125 \times 10^{-8}}$
Residual deviance	1121.6	324	
(b) Cirripedia – *Tetraclita serrata*			
Length range	12.624	7	0.082
Residual deviance	121.68	121	
(c) Cirripedia – *Chthamalus dentatus*			
Length range	7.170	8	0.518
Residual deviance	54.540	60	
(d) Cirripedia (juvenile)			
Length range	109.780	8	$\underline{< 2.2 \times 10^{-16}}$
Residual deviance	432.700	259	
(e) Ochrophyta			
Length range	19.580	7	<u>0.007</u>
Residual deviance	159.120	121	
(f) Ochrophyta – *Ralfsia verrucosa*			
Length range	19.286	7	<u>0.007</u>
Residual deviance	143.920	121	
(g) Rhodophyta			
Length range	23.733	8	<u>0.003</u>
Residual deviance	340.42	165	
(h) Rhodophyta – *Hildenbrandia lecannellieri*			
Length range	8.391	6	0.211
Residual deviance	56.987	56	
(i) Rhodophyta - Corallinales			
Length range	27.938	8	$\underline{4.863 \times 10^{-4}}$
Residual deviance	177.900	121	
(j) Sedentaria			
Length range	22.566	8	<u>0.004</u>
Residual deviance	501.950	194	
(k) Sedentaria – *Spirobranchus kraussii*			
Length range	17.498	6	<u>0.008</u>
Residual deviance	57.424	69	
(l) Sedentaria – *Spirorbis* spp.			
Length range	9.339	8	0.315
Residual deviance	189.030	144	

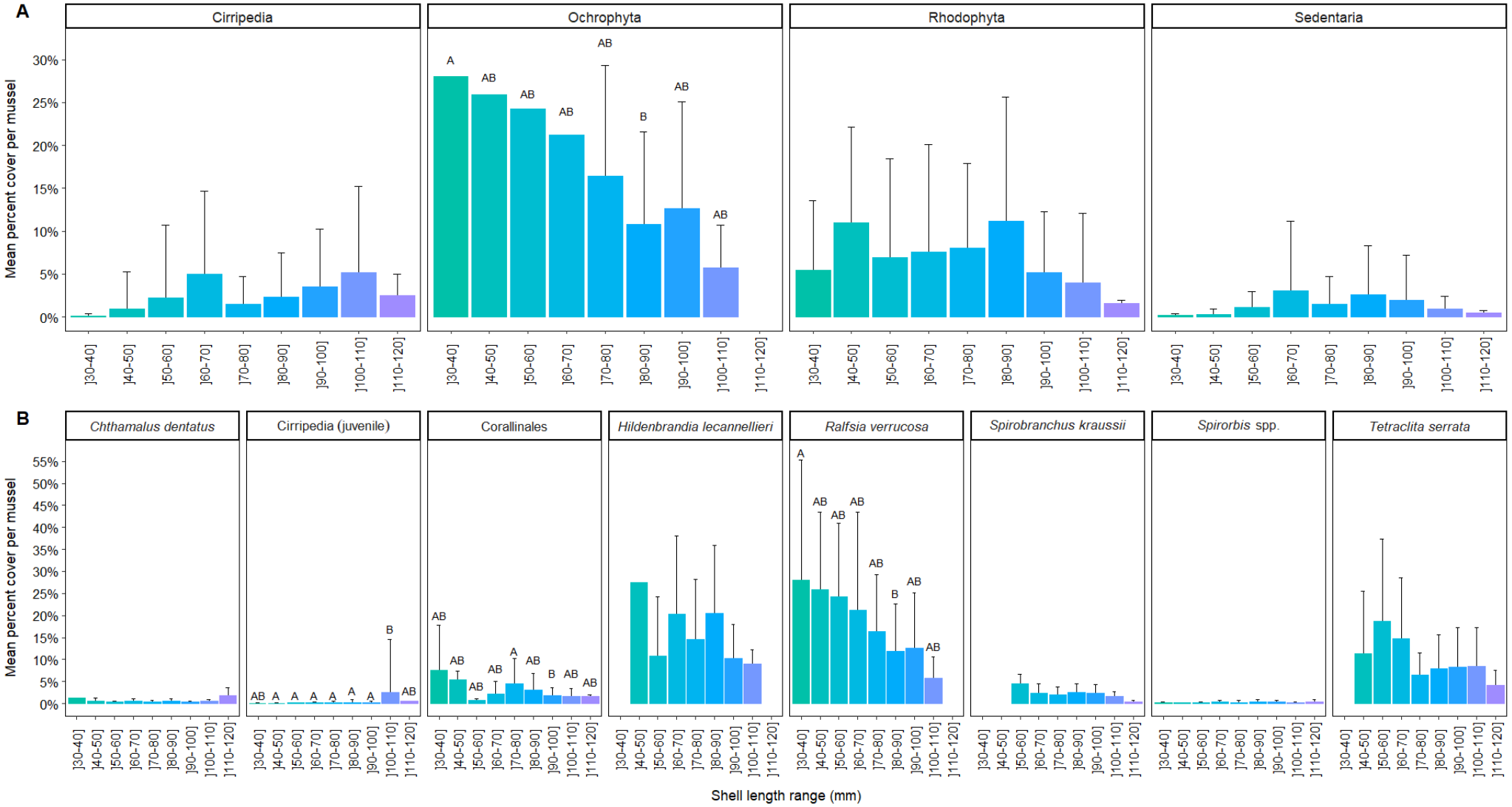

Figure 5.10. Average percent cover (± SD) for each shell length range (in mm) for (a) significant epibiotic higher taxonomical groups and (b) significant epibiotic species driving differences in community. Homogeneous groups are indicated by similar letters.

5.3.2.2.2.2. Euendolithic infestation, shell degradation and position

The percentage cover of barnacles was significantly different between shell degradation indexes, but not between euendolithic infestation levels and position of the epibionts on the mussel shell (Table 5.21a, Figure 5.11a,b,c). Percent cover in barnacles was significantly higher at median shell degradation index (i.e., 3, $]25-50]$ %) than at higher shell degradation index (i.e., 5, $]75-100]$ %) (Table S5.59, Figure 5.11b). Juvenile barnacle percentage cover was significantly different between euendolithic infestation levels and shell degradation indexes, with a significant interaction, but not between position of the epibionts on the mussel shell (Table 5.21b, Figure 5.12c,d). Juvenile barnacle percentage cover was significantly lower at euendolithic infestation level B than at levels C and D, for a median shell degradation index (i.e., 4, $]50-75]$ %) (Table S5.60, Figure 5.12d). Percent cover in juvenile barnacles peaked at euendolithic infestation level C for a median shell degradation index (i.e., 3, $]25-50]$ %), however this was not detected as significant (Figure 5.12d). Conversely, percent cover in *Tetraclita serrata* did not significantly differ between euendolithic infestation levels and shell degradation indexes, and between the infested and non-infested portions of the mussel shell (Table 5.21c, Figure 5.12a,b,c).

The percentage cover of ochrophytes was significantly different between position of the epibionts on the mussel shell, with a significant interaction with shell degradation indexes, but not between euendolithic infestation levels (Table 5.21d, Figure 5.11a,d). The percent cover of ochrophytes on the non-infested portion was significantly higher than on the infested portion of the mussel shell at the median shell degradation index (i.e., 4, $]50-75]$ %) (Table S5.61, Figure 5.11d). Surprisingly, the percent cover of *R. verrucosa* was significantly different between position of the epibionts on the mussel shell, with a significant interaction with euendolithic infestation levels, but not between

shell degradation indexes (Table 5.21e, Figure 5.12b,e). *Ralfsia verrucosa* percentage cover was significantly higher on the non-infested portion than on the infested portion of the mussel shell for euendolithic infestation level B (Table S5.62, Figure 5.12e).

Red algae cover, expressed as a percentage, were significantly different between shell degradation indexes and position of the epibionts on the mussel shell, but not between euendolithic infestation levels (Table 5.21f, Figure 5.11a,b,c). While there were no significant differences between the shell degradation indexes (Table S5.63, Figure 5.11b), the percentage cover of red algae was significantly higher on the non-infested part of the shell than on the infested part (Table S5.64, Figure 5.11c). Percent cover in *H. lecannellieri* was significantly different between interacting shell degradation indexes and position of the epibionts on the mussel shell, but not between euendolithic infestation levels (Table 5.21g, Figure 5.12a,f). However, the subsequent pairwise comparisons did not detect any differences in the percent cover of *H. lecannellieri* (Table S5.65, Figure 5.12f). Percent cover of encrusting Corallinales was significantly different between euendolithic infestation levels (Table 5.21h), however this was not detected in subsequent pairwise comparisons (Table S5.66, Figure 5.12a), and between shell degradation indexes, with a significant interaction with position of the epibionts on the shell (Table 5.21h, Figure 5.12g). The percentage cover of corallinales was significantly higher on the infested part than on the non-infested part of the mussel shell for both shell degradation indexes 2 and 5 (i.e., 2, $]0-25]$ and $]75-100]$ %) (Table S5.67, Figure 5.12g).

The percentage cover of the encrusting worms was significantly different between the interacting shell degradation indexes and position of the epibionts on the mussel shell, but not between euendolithic infestation levels (Table 5.21i, Figure 5.11a,e). Subsequent pairwise comparisons did not detect significant differences in percent cover of encrusting worms (Table S5.68, Figure 5.11e). Percent cover of *Spirobranchus kraussii* was

significantly different between position of the epibionts on the mussel shell, but not between the different euendolithic infestation levels or shell degradation indexes (Table 5.21j, Figure 5.11a,b,c). Percent cover of *S. kraussii* was significantly higher on the infested than on the non-infested part of the mussel shell (Table S5.69, Figure 5.12c). However, percent cover of *Spirorbis* sp. was extremely low (i.e., < 1%) compared to other epibiotic species and did not significantly differ between euendolithic infestation levels, shell degradation indexes and position of the epibionts on the mussel shell (Table 5.21k, Figure 5.12a,b,c).

Table 5.21. Type II three-way ANOVA on the Generalized Linear Model (GLM) on the relationship between euendolithic infestation levels (from A to E, as defined in Kaehler, 1999), shell degradation index (from 1 to 6, as defined in Ma *et al.*, 2023) and position of the epibionts on the shell (i.e., infested, non-infested) and the average percent cover of (a) Cirripedia (barnacles), (b) Cirripedia (juvenile), (c) *Tetraclita serrata* (Cirripedia), (d) Ochrophyta, (e) *Ralfsia verrucosa* (Ochrophyta), (f) Rhodophyta (red algae), (g) *Hildenbrandia lecannellieri* (Rhodophyta), (h) Corallinales (Rhodophyta), (i) Sedentaria (sedentary worms), (j) *Spirobranchus kraussii* (Sedentaria), and (k) *Spirorbis* spp. Significant p-values are underlined. Models used in these analyses were coded as follow: (a),(c),(f),(j) cover ~ inf.lvl + inf.percent + position, family = "Gamma", (b),(k) cover ~ inf.lvl * inf.percent + position, family = "Gamma", (d),(g),(h),(i) cover ~ inf.lvl + inf.percent * position, family = "Gamma", (e) cover ~ inf.lvl * position + inf.percent, family = "Gamma". Interactions were not significant for (a),(c),(f),(j),(k) models.

Source of variation	LR Chisq	df	p (> Chisq)
(a) Cirripedia			
Infestation	6.672	4	0.154
Degradation	19.250	5	<u>0.002</u>
Position	1×10^{-4}	1	0.994
Residual deviance	2139.300	574	
(b) Cirripedia (juvenile)			
Infestation	34.883	4	<u>4.909×10^{-7}</u>
Degradation	41.796	5	<u>6.477×10^{-8}</u>
Position	0.336	1	0.562
Infestation x Degradation	78.527	10	<u>9.753×10^{-13}</u>
Residual deviance	671.380	401	
(c) Cirripedia – *Tetraclita serrata*			
Infestation	1.538	4	0.820
Degradation	7.765	4	0.101
Position	2×10^{-4}	1	0.989
Residual deviance	148.180	176	
(d) Ochrophyta			
Infestation	6.832	4	0.145
Degradation	3.675	5	0.597
Position	17.114	1	<u>3.520×10^{-5}</u>

Table 5.21 (continued).

Source of variation	LR Chisq	df	p (> Chisq)
(d) Ochrophyta (continued)			
Degradation x Position	12.911	4	0.012
Residual deviance	219.920	187	
(e) Ochrophyta – *Ralfsia verrucosa*			
Infestation	4.238	4	0.375
Degradation	5.392	5	0.370
Position	11.777	1	5.996×10^{-4}
Infestation x Position	12.353	3	6.266×10^{-3}
Residual deviance	198.610	186	
(f) Rhodophyta			
Infestation	3.317	4	0.506
Degradation	13.905	5	0.016
Position	28.088	1	1.159×10^{-7}
Residual deviance	477.420	287	
(g) Rhodophyta – *Hildenbrandia lecannellieri*			
Infestation	8.313	4	0.081
Degradation	3.711	3	0.294
Position	3.581	1	0.058
Degradation x Position	10.241	2	0.006
Residual deviance	64.744	82	
(h) Rhodophyta - Corallinales			
Infestation	11.984	4	0.017
Degradation	12.435	5	0.029
Position	0.224	1	0.636
Degradation x Position	18.017	4	0.001
Residual deviance	217.660	178	
(i) Sedentaria			
Infestation	3.781	4	0.436
Degradation	6.152	5	0.103
Position	2.576	1	0.109
Degradation x Position	10.100	3	0.018
Residual deviance	880.410	316	
(j) Sedentaria – *Spirobranchus kraussii*			
Infestation	4.957	4	0.292
Degradation	8.384	4	0.078
Position	14.873	1	1.150×10^{-4}
Residual deviance	59.143	74	
(k) Sedentaria – *Spirorbis* spp.			
Infestation	6.575	4	0.160
Degradation	8.137	5	0.149
Position	1.504	1	0.220
Infestation x Degradation	2.798	7	0.903
Residual deviance	255.370	224	

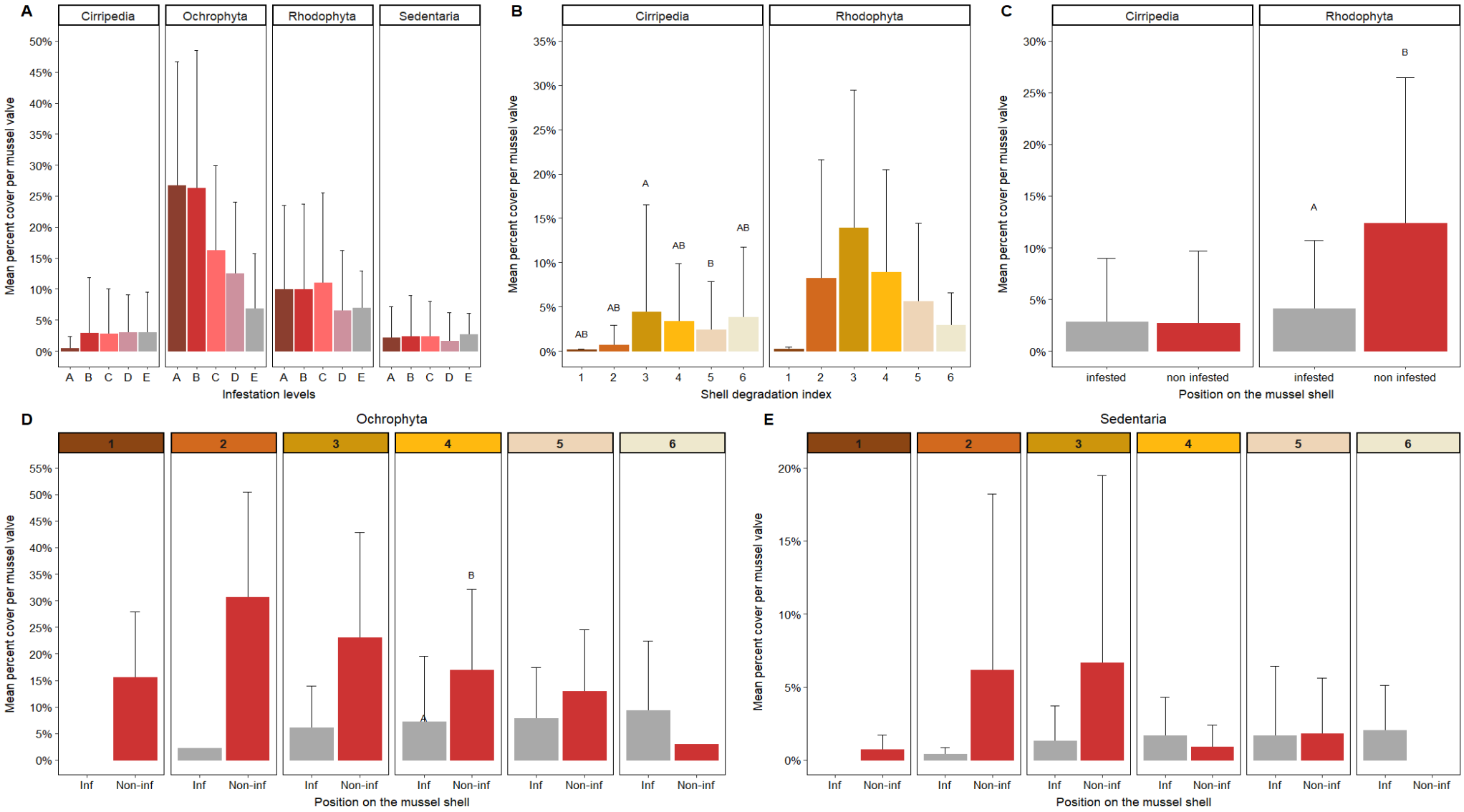

Figure 5.11. Average percent cover per mussel valve (± SD) of significant epibiotic higher taxonomical groups for (a) euendolithic infestation levels for all significant epibiotic higher taxonomical groups, (b) shell degradation indexes and (c) position of the epibionts on the mussel shell for Cirripedia and Rhodophyta, and position of the epibionts on the mussel for each shell degradation index for (d) Ochrophyta and (e) Sedentaria. Homogeneous groups are indicated by similar letters. Inf: infested; Non-inf: non-infested portion of the mussel shell.

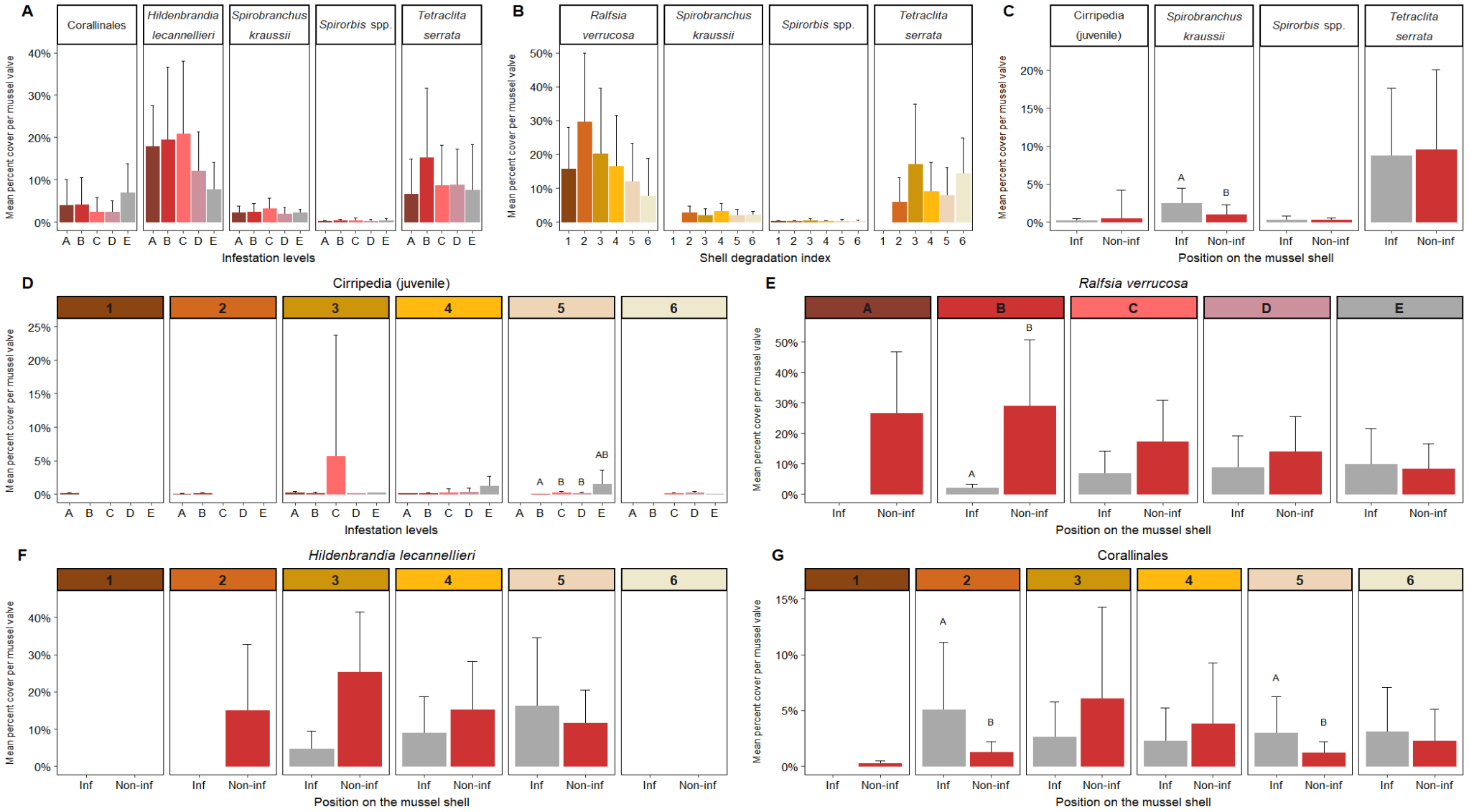

Figure 5.12. Average percent cover per mussel valve (± SD) of significant epibiotic species for (a) euendolithic infestation levels, (b) shell degradation indexes and (c) position of the epibionts on the mussel shell, as well as for (d) euendolithic infestation levels for each shell degradation index for juvenile barnacles, and position of the epibionts on the mussel shell for (e) each euendolithic infestation level for *Ralfsia verrucosa*, and each shell degradation index for (f) *Hildenbrandia lecannellieri* and (g) Corallinales. Homogeneous groups are indicated by similar letters. Inf: infested; Non-inf: non-infested portion of the mussel shell.

5.3.2.2.3. Biomass of epibiotic communities

In terms of biomass, the epibiotic community structure was significantly affected by shell length size, euendolithic infestation levels, shell degradation indexes, and position of the epibionts on the mussel shell, with a significant interaction between euendolithic infestation levels and position, for epibiotic higher taxonomical groups and epibiotic taxa (Table 5.22). nMDS plots and dispersion plots mirrored the PERMANOVA results and detected clear group separation between mussel's biological variables (i.e., shell length, euendolithic infestation levels, shell degradation indexes and position of the epibionts on the mussel shell) (Figures 5.13 and 5.14).

Table 5.22. PERMANOVA on the effect of environmental variables on the biomass of (a) epibiotic higher taxonomical groups and (b) epibiotic species. Significant p-values are underlined.

Source of variation	Sum of Squares	df	R^2	*F*-value	p-value
(a) Higher taxonomical groups					
Length range	13.351	8	0.047	4.82	0.001
Infestation	3.970	4	0.014	2.880	0.001
Degradation	9.606	5	0.034	5.574	0.001
Position	19.233	2	0.067	27.902	0.001
Infestation x Position	4.275	8	0.015	1.550	0.009
Degradation x Position	2.665	7	0.009	1.105	0.275
Residual	233.683	678	0.815		
Total	286.783	712	1.000		
(b) Epibiotic species					
Length range	13.330	8	0.045	4.536	0.001
Infestation	3.848	4	0.013	2.619	0.001
Degradation	8.773	5	0.029	4.777	0.001
Position	15.839	2	0.053	21.561	0.001
Infestation x Position	4.399	8	0.015	1.497	0.011
Degradation x Position	2.775	7	0.009	1.079	0.327
Residual	249.041	678	0.836		
Total	298.004	712	1.000		

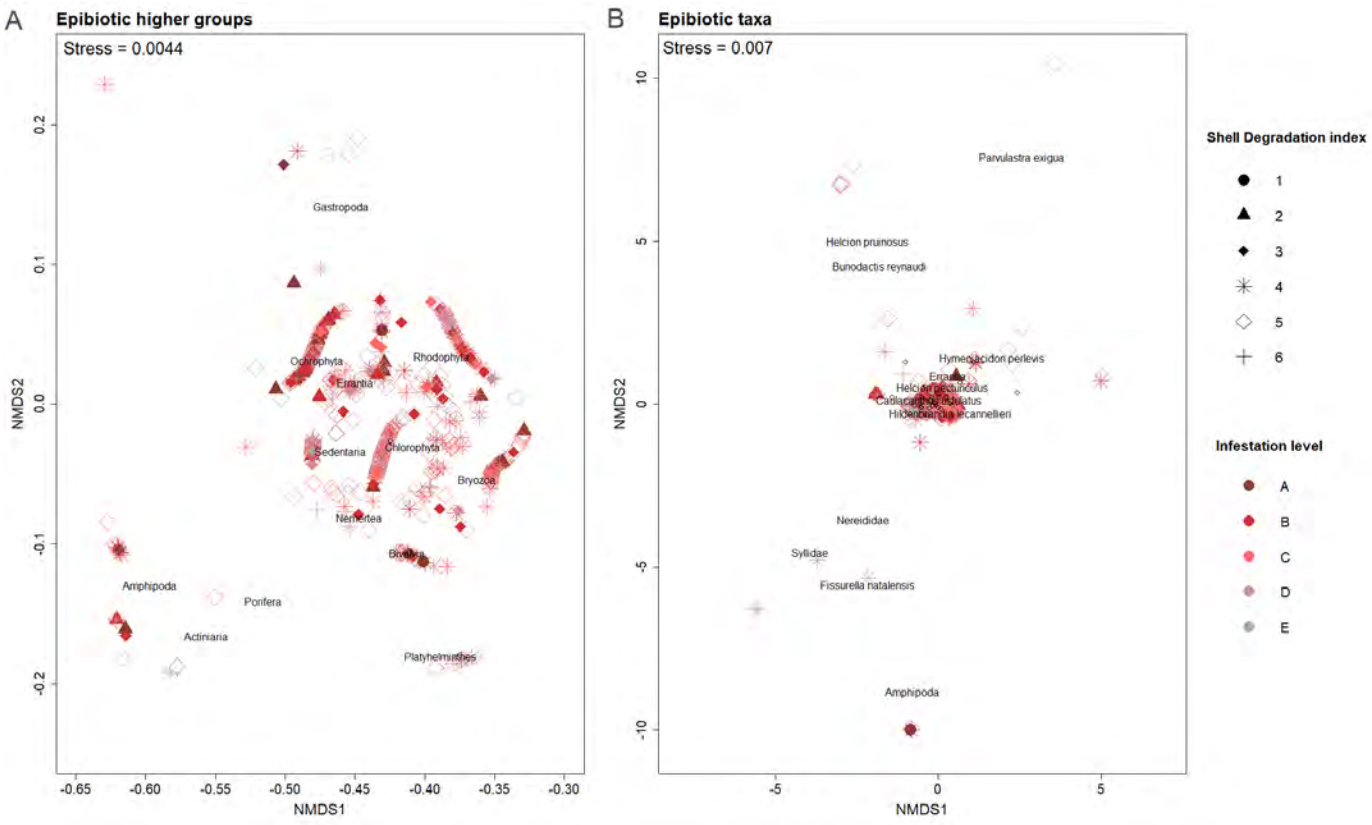

Figure 5.13. Similarity in biomass of epibiotic communities, with non-metric multidimensional scaling (nMDS) plots for (a) higher epibiotic functional groups, and (b) epibiotic species.

In terms of biomass, SIMPER analyses indicated that the broad taxonomic groups, Cirripedia, Ochrophyta, Rhodophyta and Bryozoa, accounted for 70% of the dissimilarity between shell length sizes, euendolithic infestation levels, shell degradation indexes and position of the epibionts on the mussel shell: (Tables S5.70, S5.71, S5.72 and S5.73, Figures 5.15 and 5.16). In particular, the following epibiotic species or taxa collectively accounted for 70% of the dissimilarity: *Tetraclita serrata* (Cirripedia), *Ralfsia verrucosa* (Ochrophyta), *Hildenbrandia lecannellieri* and *Gelidium pristoides* (Rhodophyta), and *Electra verticillata* (Ellis & Solander, 1786) and unidentified bryozoans (Bryozoa) (Tables S5.74, S5.75, S5.76 and S5.77, Figures 5.15 and 5.17).

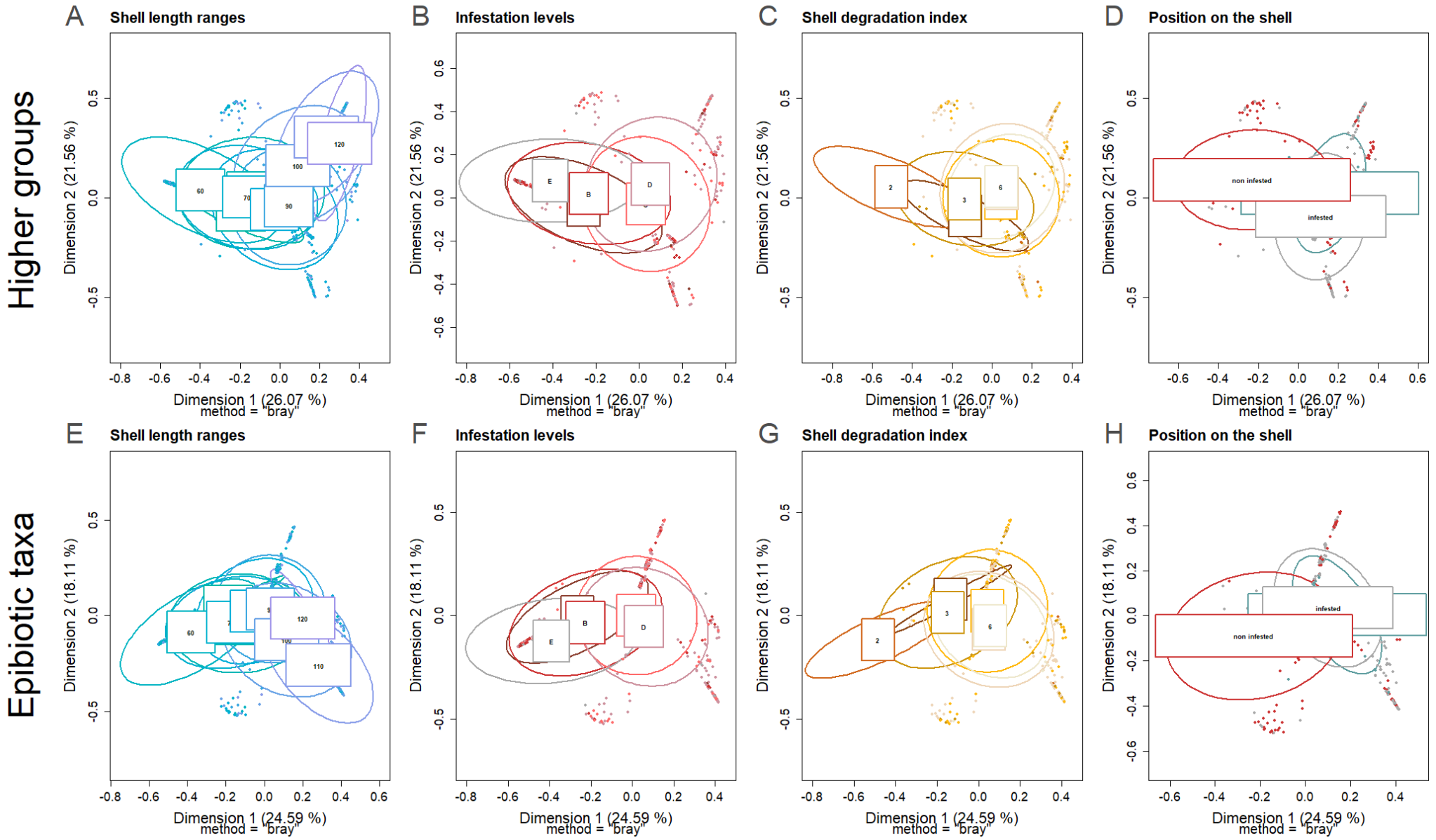

Figure 5.14. Similarity in biomass of epibiotic communities with dispersion plots for the effect of (a,e) shell length size, (b,f) euendolithic infestation levels, (c,g) shell degradation indexes, and (d,h) position of the epibionts on the mussel shell, for either (a,b,c,d) higher epibiotic functional groups or (e,f,g,h) epibiotic species.

5.3.2.2.3.1. Shell length size

Biomass of barnacles, and especially *Tetraclita serrata*, was significantly different between shell length sizes (Table 5.23a,b), although subsequent pairwise comparisons did not detect any differences (Table S5.78 and S5.79, Figure 5.15). *Tetraclita serrata* was absent from the mussel shell at the smallest shell length size (i.e., $]30-40]$ mm, Figure 5.15b).

Biomass of ochrophytes, red algae and bryozoans, respectively represented by *Ralfsia verrucosa*, *Hildenbrandia lecannellieri*, and *Electra verticillata* and unidentified bryozoans, did not differ significantly between shell length sizes (Table 5.23c,d,e,f,g,h, Figure 5.15a,b). *Ralfsia verrucosa* was absent from the mussel shell at the highest shell length size (i.e.,$]110-120]$ mm), while red algae, especially *Hildenbrandia lecannellieri*, were absent from the most extreme shell length sizes (i.e., $]30-40]$ and $]110-120]$ mm) (Figure 5.15a,b). Amongst the bryozoans, *Electra verticillata* was absent from the largest shell length sizes (i.e., $]90-120]$ mm) (Figure 5.15a,b).

Table 5.23. Type II one-way ANOVA on the Generalized Linear Model (GLM) on the relationship between shell length range (from]30 – 40] to]110 – 120] in mm) and the average biomass in (a) Cirripedia, (b) *Tetraclita serrata* (Cirripedia), (c) Ochrophyta, (d) *Ralfsia verrucosa* (Ochrophyta), (e) Rhodophyta, (f) *Hildenbrandia lecannellieri* (Rhodophyta), (g) Bryozoa, and (h) *Electra verticillata* (Bryozoa) per mussel. Significant p-values are underlined.
Models used in these analyses were coded as follow: biomass ~ length_range, family = "Gamma".

Source of variation	LR Chisq	df	p (> Chisq)
(a) Cirripedia			
Length range	16.011	7	<u>0.025</u>
Residual deviance	232.200	121	
(b) Cirripedia – *Tetraclita serrata*			
Length range	14.493	7	<u>0.043</u>
Residual deviance	221.660	118	
(c) Ochrophyta			
Length range	8.145	7	0.320
Residual deviance	190.210	118	
(d) Ochrophyta – *Ralfsia verrucosa*			
Length range	8.111	7	0.323
Residual deviance	190.310	119	
(e) Rhodophyta			
Length range	10.103	6	0.120
Residual deviance	229.740	81	
(f) Rhodophyta – *Hildenbrandia lecannellieri*			
Length range	10.008	6	0.124
Residual deviance	70.640	56	
(g) Bryozoa			
Length range	8.166	8	0.418
Residual deviance	69.075	91	
(h) Bryozoa – *Electra verticillata*			
Length range	2.280	5	0.809
Residual deviance	42.473	40	

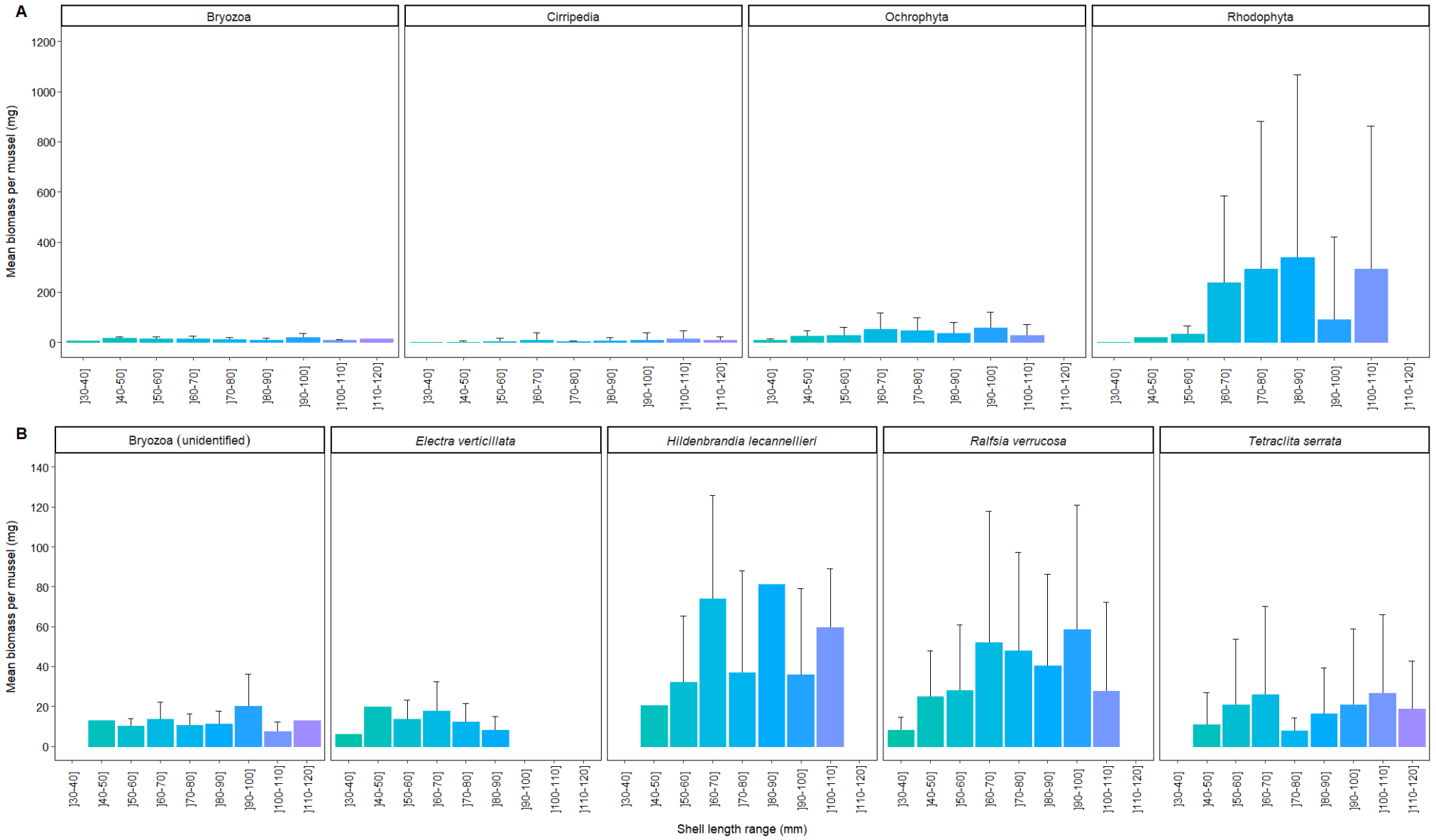

Figure 5.15. Average biomass (in mg, ± SD) for each shell length range (in mm) for (a) significant epibiotic higher taxonomical groups and (b) significant epibiotic species driving differences in community. Homogeneous groups are indicated by similar letters.

5.3.2.2.3.2. Euendolithic infestation, shell degradation and position

Biomass of barnacles, especially *Tetraclita serrata*, was significantly different between the interacting euendolithic infestation levels and shell degradation indexes, but not between position of the epibionts on the mussel shell (Table 5.24a,b, Figures 5.16c,d and 5.17c,d). However, subsequent pairwise comparisons did not detect any significant differences between euendolithic infestation levels for each shell degradation index (Tables S5.80 and S5.81, Figures 5.16c,d and 5.17c,d).

Red algae biomass was significantly different between euendolithic infestation levels, but not between shell degradation indexes or position of the epibionts on the mussel shell (Table 5.24c, Figure 5.16a,b,c). Biomass of the red algae was significantly higher at euendolithic infestation level D than at levels A and B (Table S5.82, Figure 5.16a). Biomass of *Hildenbrandia lecannellieri* was significantly different between euendolithic infestation levels, and shell degradation indexes in interaction with position (Table 5.24d, Figure 5.17a,f). The biomass of *Gelidium pristoides* was significantly different between euendolithic infestation levels, shell degradation indexes and position, with significant interactions (Table 5.24e, Figure 5.17e,g). Biomass of *H. lecannellieri* was significantly higher at euendolithic infestation level C than at level D (Table S5.83, Figure 5.17a), while biomass in *G. pristoides* as a secondary epibiont was significantly lower than on the non-infested and infested parts of the mussel shell for euendolithic infestation level D (Table S5.86, Figure 5.17g). Subsequent pairwise comparisons between position for each shell degradation index for *H. lecannellieri*, and between euendolithic infestation levels for each shell degradation index for *G. pristoides*, did not detect any significant differences (Tables S5.84 and S5.85, Figure 5.17e,f).

The biomass of ochrophytes and bryozoans, and their specific representatives, did not differ significantly between mussel's biological parameters, with no significant interactions observed (Table 5.24f,g,h,j, Figures 5.16a,b,c and 5.17a,b,c). Surprisingly, biomass of the bryozoan *Electra verticillata* was significantly higher at euendolithic infestation level B than at level D (Tables 5.24i and S5.87, Figure 5.17a).

Table 5.24. Type II three-way ANOVA on the Generalized Linear Model (GLM) on the relationship betweeneuendolithic infestation levels (from A to E, as defined in Kaehler, 1999), shell degradation index (from 1 to 6, as defined in Ma *et al.*, 2023) and position of the epibionts on the shell (i.e., infested, non-infested) and the average biomass of (a) Cirripedia, (b) *Tetraclita serrata* (Cirripedia), (c) Rhodophyta, (d) *Hildenbrandia lecannellieri* (Rhodophyta), (e) *Gelidium pristoides* (Rhodophyta), (f) Ochrophyta, (g) Bryozoa, (h) *Ralfsia verrucosa* (Ochrophyta), (i) *Electra verticillata* (Bryozoa), and (j) unidentified Bryozoa per mussel valve. Significant p-values are underlined.
Models used in these analyses were coded as follow: (a),(b),(c) biomass ~ inf.lvl * inf.percent + position, family = "Gamma", (d) biomass ~ inf.lvl + inf.percent * position, family = "Gamma", (e) biomass ~ inf.lvl * inf.percent + position + inf.lvl:position, family = "Gamma", (f),(g),(h),(i),(j) biomass ~ inf.lvl + inf.percent + position, family = "Gamma". Interactions were not significant for the (f(,(g),(h),(i), and (j) models.

Source of variation	LR Chisq	df	p (> Chisq)
(a) Cirripedia			
Infestation	1.799	4	0.773
Degradation	6.534	4	0.163
Position	1.752	2	0.416
Infestation x Degradation	15.460	7	<u>0.044</u>
Residual deviance	291.810	187	
(b) Cirripedia – *Tetraclita serrata*			
Infestation	1.693	4	0.792
Degradation	6.623	4	0.157
Position	1.230	2	0.541
Infestation x Degradation	15.285	4	<u>0.033</u>
Residual deviance	273.060	179	
(c) Rhodophyta			
Infestation	11.017	4	<u>0.026</u>
Degradation	3.457	4	0.485
Position	2.217	2	0.330
Residual deviance	375.790	119	
(d) Rhodophyta – *Hildenbrandia lecannellieri*			
Infestation	18.235	4	<u>0.001</u>
Degradation	1.269	3	0.736
Position	2.896	2	0.235
Degradation x Position	6.475	2	<u>0.039</u>
Residual deviance	105.940	86	

Table 5.24 (continued).

Source of variation	LR Chisq	df	p (> Chisq)
(e) Rhodophyta – *Gelidium pristoides*			
Infestation	11.604	3	0.009
Degradation	31.483	3	6.727×10^{-7}
Position	14.584	2	6.810×10^{-4}
Infestation x Degradation	11.181	3	0.011
Infestation x Position	7.330	2	0.026
Residual deviance	7.328	15	
(f) Ochrophyta			
Infestation	2.022	4	0.732
Degradation	2.096	5	0.836
Position	4.599	2	0.100
Residual deviance	317.230	187	
(g) Bryozoa			
Infestation	7.205	3	0.066
Degradation	2.342	3	0.505
Position	0.452	2	0.798
Residual deviance	72.548	113	
(h) Ochrophyta – *Ralfsia verrucosa*			
Infestation	1.993	4	0.737
Degradation	2.039	5	0.844
Position	4.429	2	0.109
Residual deviance	317.920	188	
(i) Bryozoa – *Electra verticillata*			
Infestation	6.706	2	0.035
Degradation	6.639	3	0.084
Position	0.578	2	0.749
Residual deviance	33.887	52	
(j) Bryozoa – unidentified Bryozoa			
Infestation	2.033	3	0.566
Degradation	0.179	2	0.914
Position	0.100	2	0.951
Residual deviance	31.283	53	

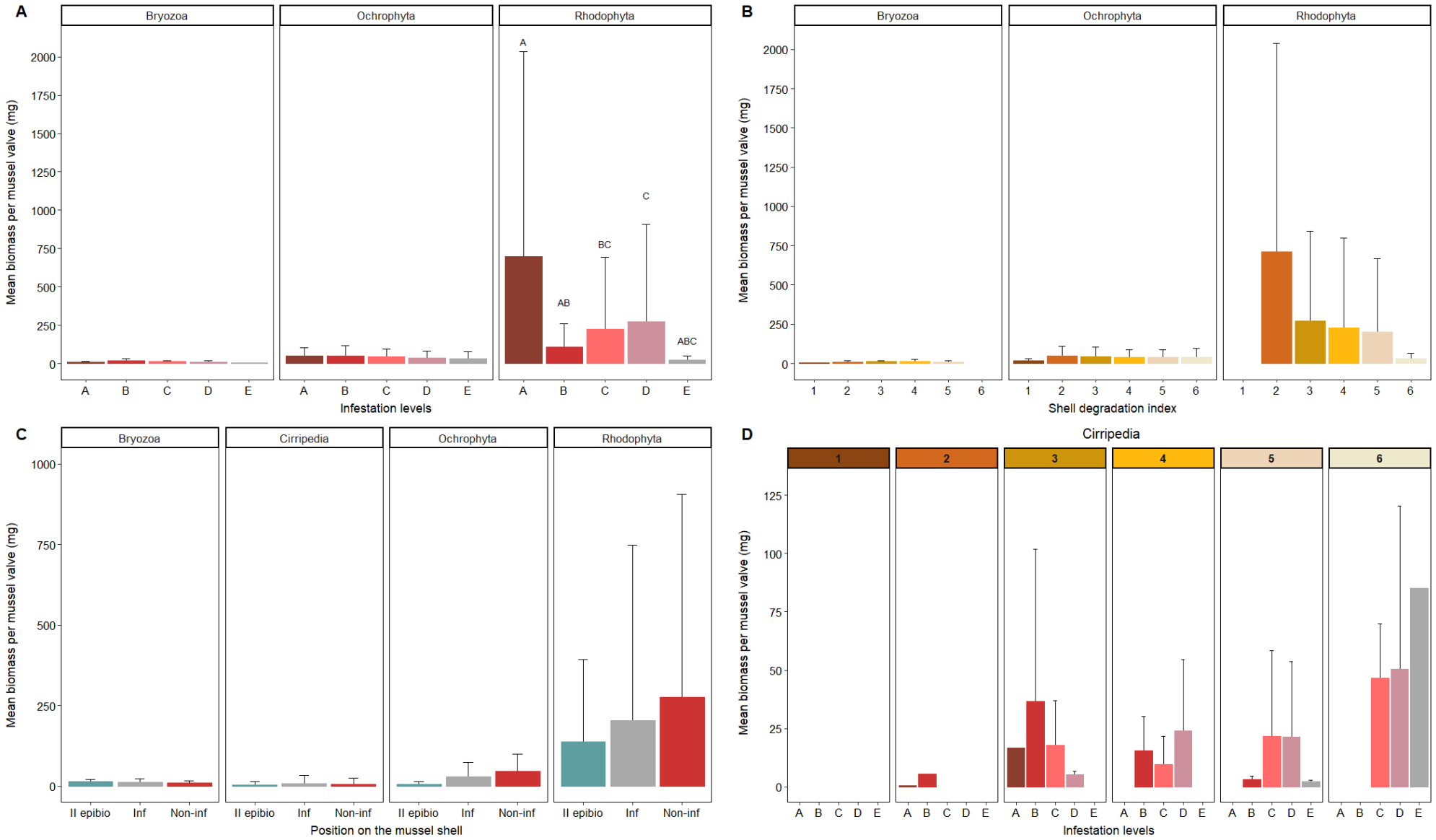

Figure 5.16. Average biomass per mussel valve (± SD) of significant epibiotic higher taxonomical groups for (a) euendolithic infestation levels, (b) shell degradation indexes and (c) position of the epibionts on the mussel shell for all significant epibiotic higher taxonomical groups (except Cirripedia for a,b), and euendolithic infestation level for each shell degradation index for (d) Cirripedia. Homogeneous groups are indicated by similar letters. Inf: infested; Non-inf: non-infested portion of the mussel shell.

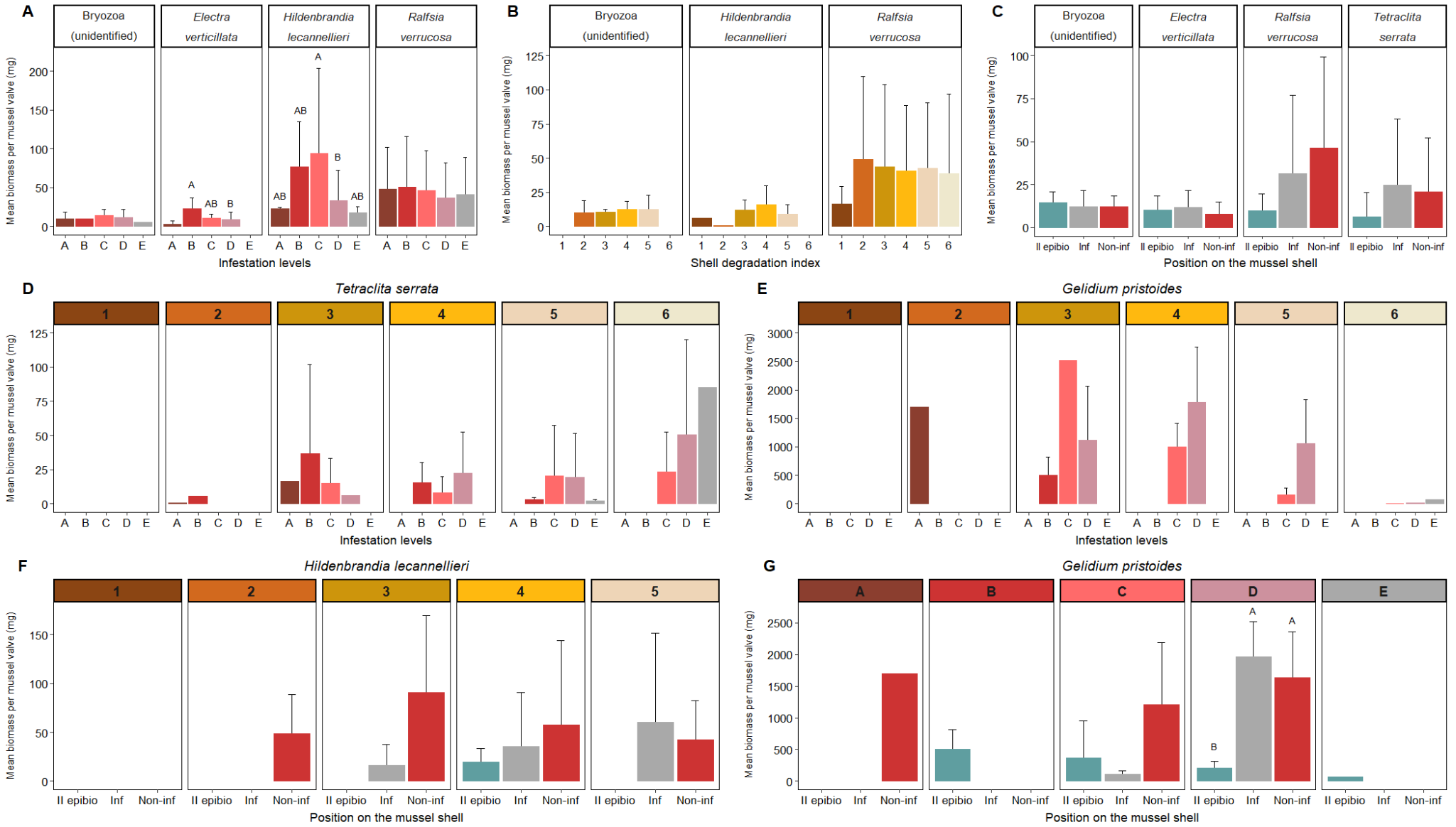

Figure 5.17. Average biomass per mussel valve (± SD) of significant epibiotic species for (a) euendolithic infestation levels, (b) shell degradation indexes and (c) position of the epibionts on the mussel shell, as well as for euendolithic infestation levels for each shell degradation index for (d) *Tetraclita serrata*, (e) *Gelidium pristoides* and (f) *Hildenbrandia lecannellieri*, and for (g) position of the epibionts on the mussel shell for each euendolithic infestation level for *Gelidium pristoides*. Homogeneous groups are indicated by similar letters. II epibio: secondary epibiosis; Inf: infested; Non-inf: non-infested portion of the mussel shell.

5.4. Discussion

It was anticipated that euendolithic infestation would increase in intensity and cover with mussel shell length, which would in turn influence the associated epibiotic communities in terms of occurrence, abundance, cover, and biomass. As the corrosive activity of euendolithic infestation destroys the antifouling properties of the mussel shell and increases its roughness, epibionts were expected to be more prevalent and more abundant with increasing levels of euendolithic infestation. However, the continual euendolith-induced weakening of the mussel shell could increase the instability of the mussel shell as a substratum, thus the cover and biomass of epibionts was expected to increase from low to medium levels of euendolithic infestation and shell degradation, and to decrease at the highest levels of euendolithic infestation.

5.4.1. General relationship between mussel shell condition and epibiosis

Euendolithic infestation levels and the area of degraded shell both increased significantly with mussel shell length (and thus, mussel age), which is consistent with previous studies (Kaehler, 1999; Lourenço et al., 2017; Ma et al., 2023; Marquet et al., 2013; Ndhlovu et al., 2021b; Webb, 1999; Zardi et al., 2009). Kaehler (1999) evaluated the degree of euendolith-induced damage on the mussel shell using both the area of degraded shell and the depth of penetration of euendoliths (i.e., erosion of outer growth lines, formation of grooves and pits). Euendolithic infestation categories defined by Kaehler (1999) were subsequently used in later studies (e.g., Zardi et al., 2009; Marquet et al., 2013; Ndhlovu et al., 2021). Recently, Ma et al. (2023) proposed to solely use the area of shell exhibiting euendolithic degradation, rather than the overall degree of damage, to investigate barnacle epibiosis on the mussel *Mytilus galloprovincialis*. Here, both euendolithic infestation levels (i.e., degree of shell damage) and the

percentage of degraded shell were recorded to investigate how they relate to each other. While the percentage of degraded shell tended to increase with euendolithic infestation levels, these two scales did not converge as expected. For example, high levels of euendolithic infestation as defined by Kaehler (1999) are characterized by heavily pitted and deformed shells, with almost completely or completely absent outer growth lines and euendolith-induced erosion spreading past the central portions of the mussel shell. On occasions, these characteristics (i.e., heavy pits, deformations, absence of outer growth lines) were recorded in mussels for which less than 50 % of the shell was degraded. The classification of euendolith-induced damages based solely on the surface of degraded shell (as in Ma et al., 2023) may overlook how corroded and irregular the mussel shell surface is. When investigating epibiosis, the correct definition of the substratum conditions (e.g., texture, available space) is critical, as it directly and indirectly influences the possible settlement and survival of epibionts. Considering mussel shell as a substratum, euendolithic infestation levels offer specific insights on the texture and roughness of the mussel shell and can be further refined by the area of degraded shell, making both scales complementary.

Prevalence, abundance, percent cover and biomass of epibiotic organisms generally increased with shell length, levels of euendolithic infestation and the area of degraded shell, before diminishing at the highest ranges (i.e., > 100 mm in shell length, infestation level E, and > 75 % of degraded shell). Similarly, species richness and diversity (Shannon-Wiener and Simpson's indexes) of epibonts, increased with shell length, euendolithic infestation levels and the area of degraded shell, although the relationship with the latter was not always significant. In addition, abundance, species richness and Shannon-Wiener diversity index values were higher on the infested than on the non-infested part of the mussel shell. The positive relationship between the occurrence,

abundance, species richness and species diversity of epibiotic organisms and mussel shell length is not unexpected, as larger, thus older, mussels would be exposed to propagules of epibiotic organisms for longer periods of time (Creed, 2000; Smyth and Roberts, 2010; Thomason et al., 2002). As mussel beds are naturally densely packed, larger mussels would also present a larger shell surface exposed for epibiotic colonisation (Keough, 1983). Prolonged exposure of the mussel shell may also explain higher levels of euendolithic infestation, and thus the subsequent expansion of the area of degraded shell (Kaehler, 1999; Marquet et al., 2013; Ndhlovu et al., 2021b; Webb, 1999; Zardi et al., 2009). The corrosive activity of euendoliths creates pits and grooves on the mussel shell, further destroying its microtopography and its antifouling properties (Bers et al., 2010; Bers and Wahl, 2004; Scardino et al., 2003; Scardino and de Nys, 2004). This influences the texture of the mussel shell by increasing its roughness, which has been demonstrated to favour the attachment of selected epibionts, such as barnacles (Berntsson et al., 2000; Köhler et al., 1999), and can be explained by the 'attachment point' theory (Scardino et al., 2009, 2008, 2006). Moreover, the presence of pits and grooves in the mussel shell may further provide a refuge for epibionts during their settling stage (Crisp, 1955; Walters and Wethey, 1996). The positive relationship between occurrence, abundance, species richness and species diversity of epibiotic organisms with euendolithic infestation levels (i.e., degree of shell damage), and the higher abundance of epibionts on the degraded portion of the mussel shell, can possibly be explained by the increased settlement success and the selection of a favourable microhabitat on the mussel shell by epibiotic larvae and spores. Moreover, the abundance of epibionts was highest for secondary epibionts (i.e., epibionts settling on epibionts already attached to the mussel shell), which could be explained by the gregariousness of many epibiotic species, which settlement is favoured by the presence of

conspecifics. On the other hand, the corrosive activity of euendoliths on the mussel shell is continuous and will ultimately expand to the entire shell, therefore increasing substratum instability (i.e., risks of sudden shell collapse). Living attached on an unstable substratum could potentially reduce the attachment strength of the epibionts to the substratum, increasing its susceptibility to drag forces or predation, and slow down its growth, delaying its maturation and reproduction (Wahl, 1989). Indeed, the percent cover and biomass of epibiotic organisms increased with shell length, although for mussels > 60 mm in length, values were highly variable. Epibiotic communities on smaller mussels are driven by the settlement and attachment of epibionts, as smaller mussels have been exposed to colonisation for shorter periods of time and the available space for colonisation is not limited. Later, direct, and indirect interactions among epibionts, and between the epibionts and the basibiont, as well as fluctuating environmental conditions, drive the dynamics of the epibiotic community, which could explain their observed variability in percent cover and biomass on larger mussels. Similarly, percent cover, biomass, species richness and species diversity of epibonts reached a plateau when the area of degraded shell exceeded 50 %. In contrast with abundance, percent cover and biomass of epibionts was higher on the non-infested part of the mussel. The observed pattern can likely be explained by a lower growth and survival rates of epibionts on the infested, unstable portions of the mussel shell. Species evenness was not significantly different between the above-mentioned shell characteristics, although consistently high ($J' > 0.75$), indicating that epibiotic species are similarly abundant between shell length sizes, euendolithic infestation levels, shell degradation indexes and position of the epibionts on the mussel shell.

5.4.2. Epibiotic communities associated with the mussel shell

By and large, sessile organisms, such as barnacles, encrusting ochrophytes and rhodophytes, sedentary worms and bryozoans, were the main drivers of the differences in the epibiotic community found on mussel shells of different sizes and levels of euendolithic infestation. It should be noted, however, that the epibiotic community composition recorded on the mussel shells during this study was highly variable, which made the interpretation of the results difficult. The composition of the epibiotic community displayed marked differences in abundance, percent cover and biomass and was significantly influenced by shell length, euendolithic infestation level, shell degradation index and position of the epibionts on the mussel shell.

5.4.2.1. Mussel shells as a refuge for a diverse epibiotic community

On marine hard substrates, the relative composition of epibiotic communities fluctuates in space and time and is influenced by a wide array of abiotic and biotic factors, including the life-history traits of both basibiont and epibionts, seasonality in the recruitment and mortality of epibionts, the biological interactions within and between species (i.e., intra- and interspecific competition for space, predation), and the size and stability of the substratum, amongst others (Dayton, 1971; Keough, 1984, 1983; Osman, 1977; Smyth and Roberts, 2010; Vance, 1988; Wahl, 2009, 1989; Ward and Thorpe, 1991).

During this study, barnacles and sedentary worms generally increased in abundance with an increase in mussel shell length. As larger, thus older, mussels were exposed to colonisation by epibionts for longer periods of time, it is logical to observe an increase in the abundance of newly settled epibiotic organisms with length. In addition, barnacles and sedentary worms were recorded on specific portions of the mussel shell, often in groups of conspecifics. Juvenile barnacles were also common secondary epibionts of

larger barnacles. The early colonisation of the mussel shell by barnacles and sedentary worms favour the later settlement of conspecifics until the area is overcrowded, which is a well-known gregarious behaviour for these organisms (Grosberg, 1982; Kent et al., 2003; Knight-Jones, 1951). Barnacles mostly settled and developed near the mussel siphonal apertures on the posterior portion of the shell, whereas *Spirorbis* sp. were mostly recorded on the ventral and anterior portion of the shell, where the byssus naturally exits. In the case of barnacles, two hypotheses could explain their position on the mussel shell. Firstly, mussels can be too densely packed for the entire mussel shell to be equally available for colonisation, so much that either the posterior portion of the shell constituted the only exposed site available for colonisation by barnacle cyprids or the cyprids settling on the anterior portions of the shell were eliminated by unfavourable conditions at early stages of development (Laihonen and Furman, 1986). Secondly, the settlement of barnacle cyprids is an active process and is favoured by strong currents (Crisp, 1955), in this case near the mussel siphonal apertures (Laihonen and Furman, 1986). As for *Spirorbis* sp., recruits are attracted to dark-coloured or shaded substratum (James and Underwood, 1994; Knight-Jones, 1951), explaining their concentrations at the antero-ventral portion of the mussel shell, which is orientated towards the underlying substrate and thus almost always shaded.

Percentage cover of encrusting algae, mainly *Ralfsia verrucosa* (Ochrophyta) and *Hildenbrandia lecannellieri* and Corallinales (Rhodophyta), generally decreased with mussel shell length, although it was variable for the red algae. By contrast, the biomass of both encrusting ochrophytes and rhodophytes, represented solely by *H. lecannellieri*, tended to increase with mussel shell length. Encrusting algae, such as ochrophytes and red algae, are considered as inferior competitors for the occupation of primary space due to their slow growth rates, their susceptibility to grazers and given that they are easily

overgrown by foliose macroalgae (Steneck, 1986; Steneck et al., 1991). Competition for space intensifies on the mussel shell as the epibiotic community develops and covers more surface area, often to the detriment of encrusting algae. While their percentage cover on the shell proportionally diminishes, the overall biomass of encrusting algae increases as they grow thicker, which ultimately lowers their growth rates and fecundity but increases their resistance to grazing and their competitive abilities (Bertness et al., 1983; Maneveldt and Keats, 2008; Steneck, 1986; Zeeman et al., 2013). Indeed, a competitive hierarchy exists between encrusting algae, with thicker thalli generally overgrowing thinner ones (i.e., interference competition) and thinner thalli growing faster, thus occupying more space, than thicker ones (i.e., exploitation competition) (Keats et al., 1994; Maneveldt and Keats, 2008; Steneck, 1986; Steneck et al., 1991). On rock surfaces, the less palatable *Hildenbrandia* sp. was commonly overgrown by large patches of *Ralfsia verrucosa* or foliose macroalgae in the absence of grazers, though this overgrowth was not always lethal (Bertness et al., 1983; Madikiza, 2006; Underwood, 2006). During this investigation, competition between *R. verrucosa* and *H. lecannellieri* was not observed as these encrusting algae were seldom recorded on the same mussel shell. *Ralfsia verrucosa* has not been observed settling directly on established *Hildenbrandia* sp. patches on rock surfaces (Bertness et al., 1983), which is rarely fouled by other opportunistic epibionts (Madikiza, 2006). The presence of *Hildenbrandia* sp. thus likely inhibits the settlement of *R. verrucosa*, and potentially other epibiotic organisms (Bertness et al., 1983; Madikiza, 2006), which may explain why both encrusting algae were not simultaneously observed on the same mussel shell during the current study. Similarly, Corallinales crusts remains largely free of epibiotic organisms owing to the antifouling properties of their epithallial layer (Steneck, 1986).

The percentage cover and biomass of barnacles were not influenced by mussel shell length, although the percentage cover of *Tetraclita serrata* tended to decrease, and its biomass to increase, with mussel size. Biomass of the foliar *Gelidium pristoides* (Rhodophyta) also tended to increase with mussel shell length. It is worth noting that encrusting Corallinales were mostly recorded around the umbo of shell, while *R. verrucosa, H. lecannellieri* and the foliar *G. pristoides* were all recorded on the posterior portion of the mussel shell, where barnacles concentrated, and often as secondary epibionts on barnacle plates. The encrusting algae appeared to inhibit barnacle settlement, as few newly settled barnacles were observed to recruit on encrusting algae (Bertness et al., 1983). Conversely, the presence of encrusting and foliose algae was strongly associated with large barnacles, which agrees with previous observations (Bertness et al., 1983). Barnacles appears to represent areas of reduced grazing pressure as their plates are not easily traversible by macrograzers (Bertness et al., 1983; Carter and Anderson, 1991). This is especially true for tall specimens such as *Tetraclita serrata*. Moreover, in the case of *G. pristoides*, encrusting algae appeared to enhance recruitment of the foliose macroalgae and barnacles to provide better attachment than other substrata (Carter and Anderson, 1991; Jernakoff, 1986). In addition to their susceptibility to grazers, foliose macroalgae, such as *G. pristoides*, and crustose coralline algae are also susceptible to desiccation and sun damage (Carter and Anderson, 1991; Steneck, 1986).

In addition to being a secondary substratum for epibiotic settlement (Lohse, 1993), mussel shells may represent a refuge for algae from direct consumption by macrograzers, and from bulldozing as a by-product of grazing activity for other epibionts. Mussel shells are less easily traversible than bare rocks, especially in association with epibiotic barnacles (Bertness et al., 1983; Carter and Anderson, 1991). However, mussels beds are commonly inhabited by a wide array of associated species, including predators and

grazers (Seed and Suchanek, 1992; Suchanek, 1985). As a consequence, mussel beds are an inefficient refuge for most epibionts in the face of common macrograzers, such as sea urchins and gastropods (O'Connor and Crowe, 2007; Witman, 1985). Not all encrusting and foliose algae are equally susceptible to grazing, which could explain the persistence of less palatable algal species on mussel shells, such as *Ralfsia verrucosa* and *Hildenbrandia lecannellieri* (Bertness et al., 1983). Besides space, a large set of interactions arises from the intricate structure of the mussel beds that could influence epibiotic assemblages. Amongst others, the physical and biological properties of mussel beds increase water retention and shading, thus providing a protection against desiccation and solar irradiance for associated infaunal and epibiotic communities (Gutiérrez et al., 2019; Lathlean and McQuaid, 2017; Lawrie and McQuaid, 2001; Nicastro et al., 2010; Nicastro et al., 2020; Santelices and Martínez, 1988). Furthermore, during incoming tides, mussels eject faecal materials that are rich in ammonium and other nutrients, which could benefit epibiotic algae and barnacles (Laihonen and Furman, 1986; Santelices and Martínez, 1988). Fully understanding the relationship between mussel beds and their epibiotic communities would thus require investigating many interacting physical and biological components of this bioengineered ecosystem.

5.4.2.2. Living attached on a degrading substratum

Amongst previously mentioned abiotic and biotic factors influencing epibiosis, substratum size and stability through time is an essential aspect for the survival and success of epibionts which ultimately shapes the development of epibiotic assemblages (Osman, 1977; Wahl, 2009). According to the intermediate disturbance hypothesis, mildly disturbed substratum of intermediate size would support the highest diversity of epibionts but would be disturbed before dominance occurs (Osman, 1977; Petraitis et al., 1989). Meanwhile, small and often disturbed substrata support reduced

epibiotic diversity and their epibiotic assemblages would reflect immediate settlement whereas large substrata that remains stable for long periods of time are the theatre of an epibiotic succession, that achieves the dominance of one or a few species (Osman, 1977; Petraitis et al., 1989). As mussels grow larger and older, the corrosive activity of photoautotrophic euendoliths infesting the superficial layer of the mussel shell weakens the whole structure of the shell (i.e., disturbance) for associated epibionts. Both the depth and the area of degraded shell increases as euendolithic infestation progresses, potentially influencing epibiotic communities until the mussel ultimately dies as a consequence of shell dismantlement (Kaehler and McQuaid, 1999; Ma et al., 2023; Marquet et al., 2013; Ndhlovu et al., 2021b). As a by-product of their corrosive activity, photoautotrophic euendoliths cause the whitening of the mussel shell on the degraded area, which is in stark contrast to the naturally occurring dark-coloured periostracum. Substratum colour may influence the settlement, attachment strength, growth and survival of epibiotic organisms (Dobretsov et al., 2013; James and Underwood, 1994; Richmond and Seed, 1991; Siddik and Satheesh, 2021; Yule and Walker, 1984). In this way, the influence of this continuous disturbance (i.e., corrosive activity of euendolithic infestation) and its consequences on the properties of the mussel shell (i.e., texture, stability, colour) on the associated epibiotic community might be subtle, as its outcome is dependent on the local biotic and abiotic conditions (Mackey and Currie, 2000; Svensson et al., 2009).

Barnacles, especially *Tetraclita serrata*, and encrusting algae (i.e., ochrophytes and red algae) generally increased in abundance (i.e., number of isolated patches) with increasing shell degradation, until such time that the mussel shell was too degraded to support epibiotic colonization. By creating pits and grooves through their corrosive activity, photoautotrophic euendoliths modify the microtopography of the mussel shell and its

physical antifouling properties (Bers et al., 2010; Bers and Wahl, 2004; Scardino et al., 2003; Scardino and de Nys, 2004), and increase the shell roughness (Thieltges and Buschbaum, 2007). According to the 'attachment point' theory, rougher surfaces display topographic features larger than the epibiont's body or attachment organ dimension and therefore that provide more attachment points for adhesion (Scardino et al., 2009, 2008, 2006). Rougher surfaces favour the attachment of selected epibionts, such as barnacles (Berntsson et al., 2000; Köhler et al., 1999) and some algae (Fletcher and Callow, 1992; Harlin and Lindbergh, 1977), which was demonstrated on mussel shells in this study. In addition to maximizing adhesion, rougher surfaces may provide a refuge against dislodgment, predation and environmental stressors, such as desiccation and high solar irradiance, for epibionts in their settling stage (Crisp, 1955; Raimondi, 1990; Walters and Wethey, 1996; Zeeman et al., 2013). For example, barnacle cyprids settled in octopus drill holes in the shells of live kelp snails or in grooves of various experimental substrata (Crisp and Barnes, 1954; Schmitt et al., 1983). Although this was not assessed at the species level during the current investigation, the overall abundance of epibionts was higher on the infested portion than on the non-infested portion of the mussel shell. Juvenile barnacles were often observed in the grooves and cracks on the infested portion of the mussel shell. Substratum colour may also have played a role in the preference for epibionts to settle on the light-coloured infested portion of the mussel shell. Larvae and spores of most epibionts preferentially settle on dark substrata (James and Underwood, 1994; Swain et al., 2006; Thorson, 1964; Yule and Walker, 1984). However, in the intertidal, surfaces remain emersed from the water and are being exposed to high solar irradiance for extended periods of time. As they absorb more light, exposed dark surfaces are warmer than light surfaces, which is true for non-infested and infested mussel shells (Zardi et al., 2016). Substratum colour can thus indirectly

influence associated organisms, as intertidal molluscs displayed lower body temperatures on the light-coloured infested mussels than on the dark-coloured non-infested mussels (Chapter 3 published as Dievart et al., 2023; Zardi et al., 2023). This is potentially the case for epibionts at a finer scale, which could reinforce the preference for settlement on the infested portion of the mussel shell.

By contrast, the percentage cover and biomass of barnacles, largely represented by *Tetraclita serrata*, and algae (i.e., ochrophytes represented by *Ralfsia verrucosa*, and red algae, represented by the encrusting *Hildenbrandia lecannellieri* and either Corallinales for percentage cover, or the foliar *Gelidium pristoides* for biomass) generally increased from low to mild levels of shell degradation. Although variable, the cover and biomass generally decreased at higher levels of shell degradation. The large barnacle *Tetraclita serrata* was absent from mussel shells that were not degraded, while the encrusting red algae *Hildenbrandia lecannellieri* was absent at the most extreme levels of shell degradation (i.e., lowest, and highest). Mild levels of shell degradation imply that the substratum is still relatively stable, which could have allowed enough time for the barnacles and encrusting algae to grow and thus increase their survival rates. Meanwhile, lower levels of shell degradation comprised of mostly smaller (i.e., < 50 mm), thus younger, mussels, which could explain the lower cover and biomass of barnacles and encrusting algae, as these mussels might have been less exposed to colonization and overgrowth by epibionts. Ultimately, the higher levels of shell degradation may have rendered the substratum too instable to support large numbers of epibionts. This pattern is akin to the intermediate disturbance hypothesis (Mackey and Currie, 2000; Petraitis et al., 1989; Svensson et al., 2009, 2007). Although this was not the case for barnacles, the percentage cover and biomass of algae was generally higher on the non-infested than on the infested portion of the mussel shell. Once the non-infested portion of

the mussel shell was entirely covered, algae were observed to grow towards the only available spaces, that is the infested portion of the mussel shell and large barnacles. Considering algae, *Ralfsia verrucosa* (Ochrophyta) and *Hildenbrandia lecannellieri* (Rhodophyta) were observed to settle predominantly around barnacles, although they are both resistant to grazers (Bertness et al., 1983) and seemingly strongly attached to the substratum (Keats et al., 1994). This was also the case for *Gelidium pristoides* (Rhodophyta), which has a greater attachment strength on barnacles and mollusc shells than on other substrata (Carter and Anderson, 1991). Barnacles settle predominantly on the posterior part of the mussel shell, which is also where the last portion of the shell degraded by the activity of photoautotrophic euendoliths. Encrusting and foliose algae thus settle and grow on the non-infested portion of the mussel shell. Moreover, partially-detached *Ralfsia* crusts appear to enhance recruitment of *G. pristoides* (Carter and Anderson, 1991), further concentrating the settlement of algal epibionts towards the non-infested portion of the mussel shell. As the mussel shell becomes increasingly unstable, algae increase their cover area towards the infested portion of the mussel shell up to a certain point thanks to their vegetative means of propagation and their regenerative capabilities (Bertness et al., 1983; Fletcher and Callow, 1992; Keats et al., 1994).

Depending on the epibiotic species considered, different strategies allow for the growth and survival of epibionts after their settlement on a continuously degrading substratum. As euendolithic infestation progresses, the diversity of the epibiotic community increases until the mussel shell is too unstable to support epibiotic life. After this point, the attachment of epibionts to the mussel shell is insufficient to avoid dislodgement and ensure their survival on large, heavily infested mussels.

5.4.3. Interactions between euendolithic infestation and epibiosis

Epibionts are limited by the amount of stable space available for colonization and subsequent survival and growth, and can benefit from better environmental conditions depending on their position on the mussel shell (Wahl, 1989). The intensity and cover of euendolithic infestation increased with mussel shell length, as did the abundance of epibionts (Ma et al., 2023; Marquet et al., 2013). Using mussel length as a proxy of age, larger, older, mussels are exposed to potential colonization by epibionts for longer periods of time, which likely explains higher epibiotic abundance on the larger shells. Since the corrosive activity of photoautotrophic euendoliths destroys the shell microtopography and its physical antifouling properties (Bers et al., 2010; Scardino et al., 2003), the increased roughness of the infested mussel shell favours the settlement of epibionts, especially barnacles (Ma et al., 2023; Marquet et al., 2013). Abundance of epibionts was higher on the infested than on the non-infested part of the mussel shell, whereas the inverse was true for the percentage cover and biomass of epibionts. Besides the modification of the mussel shell properties by the activity of euendolithic infestation (i.e., texture, stability, colour), species-specific patterns of abundance could also reflect the level of shell roughness (Berntsson et al., 2000; Schumacher et al., 2007), or an artefact of the different survival of epibionts on the different region of the shell where they settled (Laihonen and Furman, 1986) or by mortality due to the settlement and growth of other epibionts (Denley and Underwood, 1979). As euendolithic infestation progresses, the amount of stable space available for epibiotic survival and growth decreases. According to the intermediate disturbance hypothesis, the percentage cover and biomass of epibiotic community on the mussel shell increased from low to mild levels of shell degradation, and subsequently decreased at the highest levels of shell degradation. Indeed, as epibionts grow, they are

subject to increased drag forces, which increases their risk of dislodgement. This is particularly true for those epibionts that grow tall, have a hard shell and a limited number of attachment points to the substratum (e.g., barnacles). This phenomenon is less relevant for encrusting organisms (e.g., corallinales, encrusting ochrophytes) or organisms that can modulate their susceptibility to drag forces (i.e., algae attached with a holdfast) or their attachment strength (e.g., bivalves). On the contrary, the main competitive risk for encrusting algae would be the overgrowth or shading by barnacles or foliose algae, which impede growth (Keats et al., 1994; Zeeman et al., 2013). However, the unshaded portions of encrusting algae can support the shaded portions if connected (Underwood, 2006), and it was observed that encrusting and foliose algae often overgrow barnacles.

Epibionts can have both negative and positive effects on their basibiont. Overgrowth by epibionts indirectly increases drag forces on the basibiont contributing to increased mortality through dislodgement (Bell, 2013; Bers and Wahl, 2004; Garner and Litvaitis, 2013; Thieltges and Buschbaum, 2007; Witman and Suchanek, 1984). Epibiosis can also interfere with the basibiont's physiological processes (Thieltges and Buschbaum, 2007; Wahl, 2008). Mussels overgrown by epibionts have a reduced condition index (Bell, 2013; de Sá et al., 2007), lower reproductive output (Dittman and Robles, 1991) and in some cases, lower growth (Dittman & Robles, 1991; Buschbaum and Saier, 2001, but see Laihonen & Furman, 1986; Bell, 2013; Garner and Litvaitis, 2013), and increased production of byssal threads and attachment strength (Garner and Litvaitis, 2013). In the scope of euendolithic infestation, the greater the level of infestation, the less strongly the mussel attaches to the underlying rocky substratum as it allocates more energy towards shell repair (Kaehler, 1999; Marquet et al., 2013; Ndhlovu et al., 2022; Zardi et al., 2009). Epibiotic overgrowth of euendolith-infested

mussels may thus increase their susceptibility to drag forces, on already weakened attachment points. That said, the presence of epibionts may influence the energetic budget allocation of the mussel towards a higher production of byssal threads (Garner and Litvaitis, 2013) in response to the increase risk of dislodgement, at the expense of other important processes, such as shell repair and reproductive output. Indeed, euendolithic infestation of the mussel already negatively affect its shell strength, condition index, reproduction and scope of growth, amongst others (Kaehler and McQuaid, 1999; Ndhlovu et al., 2022, 2021a; Zardi et al., 2009). With the additional load on the mussel shell, epibiotic and euendolithic infestations may have synergetic detrimental effects on the fitness of mussels. Whereas specific epibionts can induce 'associational resistance' for their basibiont by reducing susceptibility to predation, for example of starfish on mussels (Laudien and Wahl, 2004, 1999; Wahl, 2009), others can trigger a 'shared doom' scenario by attracting predators, parasites and other epibionts (Enderlein, 2003; Wahl, 2008; Wahl and Hay, 1995). Euendolith-infested mussels are more susceptible to crushing predators, such as crabs and lobsters, as the strength of their shell is weakened by the corrosive activity of euendoliths (Kaehler and McQuaid, 1999; Zardi et al., 2009). Being overgrown by epibionts could not only attract predators, but also improve their handling of the mussels (Enderlein, 2003), with potential detrimental consequences on mussel populations on the rocky shores. It is worth noting that the portion of the mussel shell situated directly under the base of barnacles was often intact, although the barnacles were surrounded by degraded shell. Despite the negative effects of epibiosis on the mussel basibiont, epibionts have the potential to protect the shell from euendolithic infestation, since they reduce light availability to the photoautotrophic euendoliths (Cho et al., 2022). It, therefore, follows that epibionts might also reduce the beneficial effects of euendolithic infestation on mussel temperatures during heatwaves

(Lourenço et al., 2017; Monsinjon et al., 2021; Zardi et al., 2021, 2016), although epibionts can themselves protect the mussel beds from temperature and desiccation stress (Gutiérrez et al., 2019). Further studies are, however, required to test this hypothesis.

5.5. Conclusions

Through their corrosive boring activity, photoautotrophic euendoliths influence the quantity and quality of habitat provided by mussel shells for epibiotic organisms on the rocky shores. Euendolithic infestation tended to favour the settlement of epibionts, but the continuous degradation of the mussel ultimately impeded their survival and growth. There is a complex trade-off between the development of euendolithic infestation on the mussel shells and colonization by epibionts which is further influenced by species interactions within the epibiotic community. This investigation represents a first attempt to explore the relationship between euendolithic infestation and epibiosis on mussel shells. A more detailed analysis will be critical to disentangle the interactive effects of mussel shell condition on the epibiotic community fitness and structure.

CHAPTER 6

SYNTHESIS AND CONCLUSION

Understanding the influence of parasitism on ecosystems has been rooted in the common agreement that being parasitized is detrimental to the host organism (Price, 1977). In other words, non-infested hosts have a higher fitness than their infested conspecifics. While many studies have documented cases where parasites benefit their hosts (Michalakis et al., 1992; Thomas et al., 2000), the benefits they provide exist only under specific conditions and depend on abiotic and biotic factors. Parasites influence ecosystem properties and functions, by indirectly altering species coexistence, ecosystem engineering, trophic interactions and biogeochemical cycles (Hatcher et al., 2012; Wood and Johnson, 2015). In the case of ecosystem engineers, parasites can indirectly interfere with the host's engineering capacities (Pascal et al., 2020; Thomas et al., 1999, 1998), and thus influence the associated ecological communities by altering the provision of habitat and facilitative interactions from which they depend, especially in stressful environments (Bertness and Callaway, 1994; Bruno et al., 2003; Crain and Bertness, 2006). Global climate change and habitat modification challenge the roles of ecosystem engineers (Coggan et al., 2018; Wernberg et al., 2016; Wild et al., 2011), while emphasizing their importance as a refuge from increasing abiotic stress for a wide array of associated species (Cartwright and Williams, 2014; Jurgens and Gaylord, 2018; Lathlean and McQuaid, 2017; Wright et al., 2006; Wright and Gribben, 2017). Assessing the indirect influence of parasites on ecosystem engineers by investigating their associated ecological communities is critical to predicting the response of of ecological systems to global climate change.

6.1. Ecosystem engineering mediated by euendolithic infestation in mussels

Bivalves act as both autogenic and allogenic ecosystem engineers in aquatic habitats worldwide (Gutiérrez et al., 2003; Hammond and Griffiths, 2006; Lathlean and McQuaid, 2017). On the rocky shores, mussel beds provide a physical habitat for both infaunal and epibiotic species (Gutiérrez et al., 2003; Palomo et al., 2007; Suchanek, 1985) and a refuge against predators (Lintas and Seed, 1994; Thiel and Dernedde, 1994; Witman, 1985). In addition to their autogenic engineering capacities, mussel beds mitigate both temperature and desiccation stress under extreme environmental conditions (Gutiérrez et al., 2019; Helmuth, 1998; Jurgens and Gaylord, 2018; Nicastro et al., 2020; Stephens and Bertness, 1991), prevent the physical erosion of sediments (Bertness, 1984b; Widdows et al., 2002) and participate in the transport of solutes and organic particles (Crooks and Khim, 1999; Tsuchiya and Nishihira, 1985).

Because the engineering properties of mussel beds are affected by individual trait variations (Cole, 2010; Nicastro et al., 2020; Palomo et al., 2007; Tsuchiya and Nishihira, 1986; Zardi et al., 2015), as well as abiotic and biotic factors (Garner and Litvaitis, 2017; Kaehler and McQuaid, 1999; Nicastro et al., 2019; Reimer and Tedengren, 1997; Tummon Flynn et al., 2020), infestation by diverse parasites can have a dramatic effect on the ecological communities associated with mussel beds. Most studies investigating photoautotrophic euendoliths in ecosystem engineers have focused on the taxonomic identification of the microorganisms involved, as well as the influence of abiotic conditions on the prevalence and intensity of euendolithic infestation (reviewed in Chapter 2, published as Dievart et al., 2022). While the negative and

positive impacts of euendolithic infestation have been demonstrated at the individual and patch level (Kaehler and McQuaid, 1999; Lourenço et al., 2017; Ndhlovu et al., 2022, 2021a; Zardi et al., 2016), few studies have investigated if these are manifested on the associated ecological communities (Chapter 3 published as Dievart et al., 2023; Zardi et al., 2023). Using a combination of manipulative *in situ* and laboratory-based experiments, the current study investigated the indirect influence of shell-boring microscopic parasites (i.e., photoautotrophic euendoliths), through the alteration of mussels' life-history traits, on the infaunal and epibiotic communities associated with *Perna perna* mussel beds along the south-east coast of South Africa.

6.1.1. Shell colour polymorphism and indirect thermal benefits

Notwithstanding their lethal and sub-lethal effects, the beneficial effect of euendolithic infestation, through the whitening of the shell, has been demonstrated on the body temperatures of infested mussels, and their survival rates to heatwaves, within aggregations and in solitary individuals (Gehman and Harley, 2019; Zardi et al., 2016). The thermal benefit of euendolithic infestation extends to neighbouring mussels, so that the interstitial spaces in infested mussel beds were cooler and more humid than in non-infested mussel beds (Lourenço et al., 2017). Interestingly, the indirect influence of euendolithic infestation on the temperature and relative humidity of mussel beds is comparable to the direct influence of genetically-based behaviours (i.e., gaping) in mussel beds comprising of different mussel species or genetic lineages (Nicastro et al., 2020, 2012). Indeed, within-bed temperature and relative humidity were lower and higher respectively in *Perna perna* mussel beds, a gaping (i.e., periodic valve movement during emersion) mussel, than in *Mytilus galloprovincialis*, a non-gaping mussel (Nicastro et al., 2012). Similarly, eastern lineage *P. perna* mussel beds were more structurally complex (i.e., number of byssal threads) and provided a more benign

microscale environment (i.e., temperature and relative humidity) than beds made up of western lineage *P. perna* or *M. galloprovincialis* (Nicastro et al., 2020). Thermal buffering by euendoliths is, however, context-dependent and restricted in space and time to stressful environmental conditions (i.e., high solar irradiance, no overcast, low wind speed) (Gehman and Harley, 2019; Lourenço et al., 2017; Monsinjon et al., 2021; Zardi et al., 2021, 2016). In their quality of ecosystem engineers, the protection against heat and desiccation stresses offered by mussel beds to associated intertidal organisms was expected to be enhanced by euendolith-induced improvements in temperature and humidity (Lourenço et al., 2017), in a similar fashion than such improvements arose from genetically-based differences in behaviours (Nicastro et al., 2020, 2012).

Colour polymorphism (i.e., body colour and pattern) is a common phenomenon in a range of terrestrial and aquatic species, including intertidal bivalves and gastropods (Roulin, 2004; Williams, 2017). Although the body colour and pattern of individuals are genetically-based, colour polymorphism has an adaptive function related to abiotic and biotic factors in the habitat (Roulin, 2004; Schilthuizen, 2013; Williams, 2017). In the case of shelled molluscs, the frequency of shell colours and patterns is influenced by physical stressors, such as exposition to solar irradiance, salinity, and desiccation (Etter, 1988; Johnson, 2011; Mitton, 1977), and by biotic stressors, such as predation (Manríquez et al., 2009; Nagarajan et al., 2002). In Chapter 3 (published as Dievart et al., 2023), the benefit of euendolithic infestation on the body temperatures of mussels was highlighted. In agreement with previous studies (Gehman and Harley, 2019; Lourenço et al., 2017; Monsinjon et al., 2021; Zardi et al., 2021, 2016), the shell temperatures of infested biomimetic mussels (i.e., lighter-coloured shell) were always lower than non-infested biomimetic mussels (i.e., darker-coloured shell). Natural variations in the shell colour of *Mytilus edulis* Linnaeus, 1758 yielded similar

results, as pale striped individuals attained lower temperatures when exposed to sunlight and suffered less mortality from heat stress than uniformly blue-black individuals (Mitton, 1977). Parasite-induced change in shell colour alone was thus sufficient to alter the mussel body temperature (Gehman and Harley, 2019). Infection by endoparasites (i.e., living inside the host's tissues) have been demonstrated to influence the host's thermal tolerance and subsequent survival to heat stress (Bates et al., 2011; Encomio and Chu, 2007). In the marine snail, *Zeacumantus subcarinatus* (G. B. Sowerby II, 1855), infection by trematodes can either increase or decrease thermal tolerance depending on the species involved (Bates et al., 2011), whereas in the eastern oyster *Crassostrea virginica* (Gmelin, 1791), infection by a protozoan did not influence thermal tolerance (Encomio and Chu, 2007). It is worth noting that none of these endoparasites alter the host's shell colour. Although the mechanisms involved varied greatly, other endoparasites have been demonstrated to alter their host body colour, which influenced predation and parasite infection risks (Bakker et al., 1997; Cook and Lofton, 1973; Hechtel et al., 1993). Infestation by photoautotrophic euendoliths, which can be considered as ectoparasites, causes a permanent and extended discoloration of the mussel shell, similar to that induced by shell-boring macro-organisms, such as sponges (Kumar and Thomas, 2011), or ocean acidification (Bressan et al., 2014). However, the thermal effects of changes in the host body or shell colour induced by either endoparasites, shell-boring organisms or physical factors, appear to be understudied. In this way, the demonstration of the indirect thermal benefits of euendolithic infestation to mussels could motivate increasing research investigating the influence of induced colour alteration on organisms' thermal biology.

Furthermore, the thermal benefit of euendolithic infestation on mussels improved within-bed abiotic conditions, which extended to associated intertidal organisms

(Dievart et al., 2023; Zardi et al., 2023). Indeed, lighter-coloured molluscs displayed lower body temperatures on infested mussel beds than on non-infested mussel beds when exposed to extreme solar irradiation and low wind speed, which is in agreement with recent findings of Zardi et al. (2023). While this investigation solely focused on intertidal molluscs sensitive to the substratum temperature, mussel recruits (0.5 to 1.5 mm in shell length) also displayed lower body temperatures on infested mussel beds (Zardi et al., 2023). This was not the case for the darker-coloured molluscs or when environmental conditions were less stressful (i.e., cloud cover, lower solar irradiance, high wind speed). Since rocky shore organisms live close to or at the upper end of their thermal tolerance (Somero, 2010, 2002; Stillman and Somero, 1996; Stillman, 2002), intertidal organisms are particularly susceptible to local extinction events due to anormal heat and desiccation stress (Harley, 2008; Helmuth et al., 2002; Paine and Levin, 1981). Amongst other behavioural thermal adaptations (Muñoz et al., 2005; Williams et al., 2005), intertidal organisms often seek thermal refuges in more favourable microhabitats (Cartwright and Williams, 2014; Lathlean et al., 2016a; Moisez et al., 2020). Substratum temperatures underpin the body temperatures for both sessile and mobile intertidal organisms that maintain a direct contact with the substratum (Bertness, 1989; Chapperon et al., 2017; Chapperon and Seuront, 2011b, 2011a; Hayworth and Quinn, 1990; Kordas et al., 2015). Intertidal organisms exhibit a preference for cooler substratum when exposed to heat and desiccation stress. For example, the polymorphic snail *Littoraria scabra* (Linnaeus, 1758) and the dark-coloured *Nerita atramentosa* Reeve, 1855 actively seek thermal refuge on the underside of roots, boulders, or rocks (Chapperon and Seuront, 2011b, 2011a).

As a by-product of their corrosive activity, photoautotrophic euendoliths cause the whitening of the mussel shell on the degraded area, in contrast with the dark-coloured

periostracum naturally present, which could influence the dynamics of settlement of epibiotic organisms on the mussel shell at a fine scale. Indeed, substratum colour has been demonstrated to influence the settlement, attachment strength, growth and survival of a variety of epibiotic organisms (Dobretsov et al., 2013; James and Underwood, 1994; Richmond and Seed, 1991; Siddik and Satheesh, 2021; Yule and Walker, 1984). Larvae and spores of most epibionts are attracted to dark substratum (James and Underwood, 1994; Swain et al., 2006; Thorson, 1964; Yule and Walker, 1984). This is the case for encrusting worms, such as *Spirorbis* sp. (James and Underwood, 1994; Knight-Jones, 1951; Swain et al., 2006), which explains their preference for the non-degraded and shaded antero-ventral portion of the mussel shell during this investigation (Chapter 5). Similarly, barnacle cyprids have been demonstrated to have a greater attachment strength on dark-coloured than light-coloured panels in an experimental laboratory setting (Yule and Walker, 1984), although other factors such as current flow and larvae orientation influence settlement (Crisp, 1955; Crisp and Barnes, 1954). Finally, substratum colour can influence the germination, growth, size, and attachment strength of algae (Finlay et al., 2008; Swain et al., 2006). For example, sporelings of the green alga *Ulva* sp. showed higher settlement rates, but lower germination rates and slower growth on dark-coloured than on light-coloured panels, indirectly increasing their resistance to drag forces (Finlay et al., 2008; Swain et al., 2006). However, while substratum colour appears to play an important role in the settlement choice of epibionts, its influence on epibiotic communities decreases over time as the relative influence of other abiotic and biotic factors increases (Dobretsov et al., 2013). Although attracted to dark-coloured surfaces at the larval stage (James and Underwood, 1994; Swain et al., 2006; Yule and Walker, 1984), epibionts can later benefit from higher growth and survival rates when settled on light-coloured

surfaces, as these reflect more light and are thus cooler, especially under stressful environmental conditions (Bertness, 1989; Finlay et al., 2008; Kordas et al., 2015; Swain et al., 2006). As such, in the field, barnacles were found to be more abundant on cooler light-coloured panels, where their potential to survive heat and desiccation stress is increased, than on warmer dark-coloured panels (Bertness, 1989; Kordas et al., 2015). In Chapter 5, epibiotic communities of well-established mussel beds were investigated, thus the influence of substratum colour is suspected to be relatively low compared to other abiotic (e.g., temperature, rugosity and degradation state of the mussel shell, current flows) and biotic (e.g., presence of grazers, intra- and interspecific interactions between epibionts) factors.

Although the thermal responses of intertidal organisms to environmental stress is species-specific (Kordas et al., 2015) and the dynamics of epibiotic communities on the mussel shell is dependent of a wide array of interacting factors, euendolithic infestation of the mussel shell has potential to further mediate environmental stress of invertebrates. As it was effectively demonstrated that euendolithic infestation indirectly improved the thermal buffering offered by mussel beds to associated molluscs under controlled conditions (Chapter 3 as Dievart et al., 2023; Zardi et al., 2023), it was expected that infaunal and epibiotic communities associated with euendolith-infested mussel beds (i.e., lower within-bed temperatures and higher humidities) would be more abundant and more diverse than those associated with non-infested mussel beds. While parasite-induced shell colour polymorphism has thermal benefits for the mussels and associated organisms, the continuous shell degradation resulting from the corrosive activity of euendoliths appears to influence the permanently associated ecological communities.

6.1.2. Architectural complexity of the mussel bed habitat to associated communities

Amongst the sub-lethal effects, euendolithic infestation ultimately degrades the mussel shell, destroying its microtopography and rendering its surface rougher, and subsequently reduces the scope for growth, mussel shell strength, and mussel attachment strength to the underlying substratum, by increasing maintenance costs (Kaehler and McQuaid, 1999; Marquet et al., 2013; Ndhlovu et al., 2022, 2021a; Zardi et al., 2009). Mussel attachment strength is largely mediated by the production of numerous and thick byssal threads, which contribute to the architectural and structural complexity of the mussel beds, which in turn influence the associated infaunal communities in terms of both abundance and biomass (Nicastro et al., 2020). Similarly, euendolith-infested mussels demonstrate lower growth rates than non-infested mussels (Ndhlovu et al., 2021b), and an increasingly rougher shell (Kaehler and McQuaid, 1999; Marquet et al., 2013), which could further influence the architectural complexity of the mussel beds and the amount of available space for infaunal and epibiotic organisms (Commito and Rusignuolo, 2000; Kostylev and Erlandsson, 2001; Kostylev et al., 2005; Lawrie and McQuaid, 2001; Nicastro et al., 2022). Finally, the sub-lethal effects of euendolithic infestation of the mussel shell directly impede the perennity of mussel beds. Indeed, euendolith-infested mussels are more susceptible to dislodgement due to reduced attachment strength (Marquet et al., 2013; Ndhlovu et al., 2022; Zardi et al., 2009), and to mortality by crushing predators or anthropogenic disturbances (i.e., trampling) due to reduced shell strength (Nicastro et al., 2019). The quality of habitat offered by infested mussel beds was thus anticipated to be reduced in terms of structural complexity (i.e., byssal thread production) for associated infaunal communities, although it was expected this would be counterbalanced by the greater complexity of infested mussel bed surfaces (Nicastro et al., 2022) and the thermal benefits of euendolithic infestation.

Moreover, the continuous degradation of the mussel shell, increasing its roughness, was expected to result in increased abundances, percentage cover and biomass of epibionts (Ma et al., 2023; Marquet et al., 2013).

Mussel beds comprise a physical matrix of living and dead mussel shells, interconnected by a complex network of byssal threads, that attaches to the underlying substratum and retains sediments, coarse shell fragments, and mussel faeces and pseudofaeces, which create a habitat for a wide array of associated species (Hammond and Griffiths, 2004; Lintas and Seed, 1994; Seed and Suchanek, 1992; Suchanek, 1985). Along with live and dead mussel shells, byssal threads thus play an important part in the development of a structurally complex mussel bed, supporting an abundant and productive infaunal community (Nicastro et al., 2020). Indeed, genetically-driven differences in the number of byssal threads produced by different mussel lineages and species have been demonstrated to influence mussel bed architectural complexity and microclimate, which influences the abundance and biomass of associated infaunal communities (Nicastro et al., 2010; Nicastro et al., 2020, 2012; Zardi et al., 2015). In addition to genetics, several biotic (e.g., mussel age, infestation by parasites and epibionts, presence of predators) and abiotic (e.g., temperature, salinity, wave exposure, pollution) factors are known to affect byssal thread production in mussels (Alfaro, 2006; Garner and Litvaitis, 2017, 2013; Moles and Hale, 2003; Reimer and Tedengren, 1997; Roberts and Carrington, 2023; Webb, 1999; Young, 1985). Endoparasites influence byssal thread production in *Mytilus edulis* in contrasting ways. For example, mussels infected by the trematode *Proctoeces maculatus* (Looss, 1901) Odhner, 1911 produce more but lower quality byssal threads than non-infected mussels (Liang, 2020), while mussels heavily infected by other trematodes, *Himasthla elongata* (Mehlis, 1831) Dietz, 1909 and *Renicola parvicaudatus* (Stunkard & Shaw, 1931) Galaktionov, Solovyeva, Blakeslee &

Skírnisson, 2022, produce less byssal threads than non-infected mussels (Lauckner, 1984). Euendolithic infestation has been demonstrated to reduce mussel attachment strength (Marquet et al., 2013; Ndhlovu et al., 2022; Zardi et al., 2009), which is thought to be the result of the lower production of byssal threads. During this investigation (Chapter 4), the number of byssal threads per mussel was not statistically different between euendolith-infested and non-infested mussels ($p > 0.05$). Moreover, there was no apparent influence of euendolithic infestation on the community structure of their associated infaunal communities. While euendolithic infestation of mussels may not necessarily lower byssal thread production, it could reduce the quality of byssal thread produced (i.e., diameter, tensile strength), which could explain the lower attachment strength of infested mussels (Marquet et al., 2013; Ndhlovu et al., 2022; Zardi et al., 2009). By contrast, geographical site influenced the number of byssal threads per mussel, as well as the associated infaunal communities, although in different manners. At the end of the experiment, transplanted mussels generally produced less byssal threads on exposed rocky shores than at more sheltered sites, which is in agreement with Garner and Litvaitis (2013). Byssal thread production has been demonstrated to increase with water flow and agitation (Alfaro, 2006; Young, 1985) and to decrease above a certain water flow threshold (Carrington et al., 2008; Moeser et al., 2006). Meanwhile, the abundance and biomass of associated infaunal communities for each site did not correlate with either byssal thread production or wave exposure but could potentially be explained by the local communities present on the different rocky shores (Chapter 4). The indirect effect of euendolithic infestation of mussels on their associated infaunal communities, mediated through the production of byssal threads (i.e., architectural complexity), was not detected in this investigation. Moreover, it was expected that infested mussel beds would represent a more favourable

habitat against heat and desiccation stress, especially for mobile invertebrates. While euendolithic infestation has been demonstrated to thermally benefit infested mussels, this effect is highly variable in space and time (Gehman and Harley, 2019; Lourenço et al., 2017; Monsinjon et al., 2021; Zardi et al., 2021, 2016). Despite the conditional beneficial effect of euendolithic infestation on mussel bed microclimate, there was no differences in the composition of associated infaunal communities between the infested and non-infested mussels during this investigation. The absence of any difference suggests that differences in ecological communities associated with mussel beds is complex and driven by a suite of factors, including architectural and structural complexity (Cole, 2010; Cole and McQuaid, 2010; Nicastro et al., 2020) and site-specific availability of propagules.

While the matrix formed by byssal threads contributes to mussel bed structural complexity for infaunal communities, the condition of the mussel shell (e.g., size, texture, colour, degree of erosion) dramatically influences epibiotic communities (Bell, 2013; Berntsson et al., 2000; Dobretsov et al., 2013; Ma et al., 2023; Marquet et al., 2013; Scardino et al., 2009). Living strictly attached to the underlying substratum, space and substratum stability are the main factors limiting epibiotic settlement, development, and long-term survival (Paine, 1974; Wahl, 2009, 1989). It was hypothesized that the corrosive activity of photoautotrophic euendoliths, which destroys mussel shell microtopography and its antifouling properties, would facilitate the settlement and survival of epibionts, especially barnacles, on their shells (Ma et al., 2023; Marquet et al., 2013). In Chapter 5, the prevalence and severity of epibiosis (i.e., abundances, percentage cover, biomass) increased with mussel shell length. Larger, older mussels were shown to have more degraded shells (Kaehler, 1999; Ndhlovu et al., 2021b; Zardi et al., 2009) and more epibionts (Ma et al., 2023;

Marquet et al., 2013). These findings are not unexpected since larger mussels would have been exposed to continuous shell degradation by photoautotrophic euendoliths and potential colonization by epibionts, as well as infestation by endoparasites, for longer periods of time than smaller mussels (Ambariyanto and Seed, 1991; Bell, 2013; Calvo-Ugarteburu and McQuaid, 1998; Lauckner, 1983; Ma et al., 2023; Marquet et al., 2013). Moreover, as mussel beds are often densely packed, larger mussels would proportionally provide more space for the settlement and development of epibionts (Bell, 2013; Laihonen and Furman, 1986), which could be indirectly influenced by the effects of parasitism on mussel shell growth. Molluscs infested by castrating trematodes demonstrated both growth increases (i.e., gigantism) or reductions, or no apparent effect on molluscan shell growth (see Lafferty and Kuris, 2009; Minchella, 1985 and references therein). To account for these contrasting results, it was argued that shell gigantism in some infested long-lasting molluscan species could compromise the reproduction of endoparasites and improve host survival and fitness, in the hopes of outlasting the parasitic infection and its negative effects (Lafferty and Kuris, 2009; Minchella, 1985). In mussels, trematode parasites have been demonstrated to both increase or reduce mussel growth rates depending on the mussel host species and the trematode parasites involved in the interaction, as well as the environmental conditions (Calvo-Ugarteburu and McQuaid, 1998; García-Huidobro et al., 2019; Thieltges, 2006). For example, multi-specific trematode infection resulted in increased shell growth, which agrees with the shell gigantism hypothesis, but was linked to reduced shell thickness in *Perumytilus purpuratus* (Lamarck, 1819) (García-Huidobro et al., 2019). By contrast, infection by the trematode *Proctoeces* sp. reduced growth only in the smaller *Perna perna* individuals, as these would allocate more energy towards growth under normal conditions (Calvo-Ugarteburu and McQuaid, 1998). Similarly, infection by the

trematode *Renicola parvicaudatus* reduced growth in *Mytilus edulis*, although abiotic environmental factors (i.e., tidal height) had a stronger effect on mussel growth rates (Thieltges, 2006). Infestation by photoautotrophic euendoliths have been demonstrated to reduce mussel growth rates, by inducing a re-arrangement of the mussel energetic budget towards shell repair at the expenses of growth and other physiological processes (Kaehler and McQuaid, 1999; Ndhlovu et al., 2022, 2021a). Over time, it is possible that the euendolith-infested mussels will attain a smaller overall size than non-infested mussels, which will ultimately contribute to a reduction in the absolute amount of available space for epibiotic communities. Strikingly visible, euendolithic infestation corrodes the mussel shell, increasing its roughness and creating fine-scale irregularities, which favours epibiotic settlement on the short term but impede their growth and survival on the long term by increasing substratum instability. In Chapter 5, the prevalence and severity of epibiosis (i.e., abundances, percentage cover, biomass) increased with mussel shell degradation (i.e., degree of shell damage and area of degraded shell), although this relationship was variable when considering the epibiotic percentage cover and biomass. Furthermore, the epibiotic community structure on the mussel shells were also influenced by the nature of the mussel shell substratum (i.e., infested, or non-infested portion of the mussel shell). In agreement with the attachment point theory (Scardino et al., 2008, 2006), the increased roughness of the infested mussel shells appeared to facilitate the settlement of some epibionts, especially sessile organisms such as barnacles, encrusting algae (i.e., rhodophytes and ochrophytes) and sedentary worms (Berntsson et al., 2000; Knight-Jones, 1951; Le Tourneux and Bourget, 1988; Warner, 1997). Also, total epibiotic abundances were higher on the infested (i.e., rougher) than on the non-infested portion of the mussel shell during this study. In molluscs, boring macroorganisms, which have a comparable effect than

euendolithic infestation on the mussel shell, have been demonstrated to facilitate the settlement of epibionts (Thieltges and Buschbaum, 2007; Warner, 1997). For example, the boring polychaete *Polydora* Bosc, 1802 have been demonstrated to facilitate barnacle settlement on the shell of the snail *Littorina littorea*, while the presence of barnacles increased shell irregularities, thus facilitating the infestation by the polychaete (Thieltges and Buschbaum, 2007; Warner, 1997). Ultimately, however, the euendolithic infestation of the mussel shells would contribute to a collapse of the epibiotic community, as the increasing instability associated with its spread might be detrimental to the survival of epibionts (Lambert et al., 2011; Osman, 1977; Yorke and Metaxas, 2012). It is important to note that mussel shell length and shell degradation covaried, which could have influenced the current conclusions of this investigation, and that a more detailed analysis into each species constituting the epibiotic communities recorded in this study is needed to identify potential inter- and intraspecific interactions within the epibiotic communities.

6.1.3. An evaluation of the methodologies

This explorative study is amongst the firsts to assess the nature and magnitude of the indirect effects of external parasites (i.e., photoautotrophic euendoliths) on the ecosystem engineering capacities of the host (i.e., marine mussels) by focusing on the associated infaunal and epibiotic communities. In this context, it is necessary to reflect on the methodologies employed during this study and the improvements that could be made for future research.

Infrared thermography (IRT) is a portable non-invasive tool that allow the rapid detection and measurement of small-scale temperature variability *in situ* without disturbing the animals' behaviour or thermoregulatory capacities (Lathlean and Seuront, 2014; Lathlean et al., 2017). In Chapter 3, IRT was employed to simultaneously

measure the shell temperatures of intertidal molluscs and of biomimetic euendolith-infested and non-infested mussels. Shell temperatures of intertidal molluscs measured by IRT have been shown to be strongly correlated with internal body temperatures (Caddy-Retalic et al., 2011; Chapperon and Seuront, 2011b; Seuront et al., 2018). Unfortunately, the IRT methodology employed during this study was restricted to organisms at the surface of the mussel beds and could therefore, not assess the effect of euendolithic infestation on the infaunal community as a whole (e.g., organisms hiding beneath mussels). Alternative methods used to measure an organism's temperature *in situ* include the insertion of a thermocouple tip into the organism itself (Williams et al., 2005), and the deployment of biomimetic organisms, which are objects containing temperature data loggers that mimic the morphological characteristics of the organism of interest (Harley et al., 2009; Helmuth et al., 2016). Embedding a miniature temperature data logger within a large intertidal mollusc (> 50 mm in length) is theoretically possible, as the smallest data loggers available are approx. 17 mm long and 6 mm wide (e.g. DST nano-T, Star-Oddi). These alternative methods involve either the direct manipulation of the organisms of interest, which could increase the organisms' stress and thus influence the estimation of the body temperatures. In this way, IRT can be considered as a useful tool to monitor the actual temperatures experienced by targeted organisms within their natural microhabitats at small and larger scales.

Other technological innovations are gaining attention for the identification of invertebrates, such as image-based approaches (Høye et al., 2022, 2021; Lürig et al., 2021). Computer vision tools can provide a well-needed help for the taxonomic identification of invertebrates, as well as morphological information, such as body size (Wilson et al., 2022), although their accuracy depends on the level of training and the image quality (Høye et al., 2022). Once trained with manually annotated

images, deep learning models can automatically provide estimates of invertebrate abundance, biomass, and diversity (Høye et al., 2021). Image-based methods for species identification could provide a cost-efficient solution for analysing large data sets and biomonitoring (Høye et al., 2022). This was the case in Chapter 4, for which > 10 000 individual invertebrate specimens were sorted, identified, counted, and weighed, whereas in Chapter 5, the number of mussel shells photographed processed reached > 1000, for > 8000 individual invertebrates sorted, identified, counted, scraped from the shell, and weighed, from seven quadrats out of the 20 samples. Image-based methods and deep learning offers an automated perspective to the process of bulk invertebrate samples, and their usefulness is worth investigating for the process of the large sample collections.

Finally, at the theoretical level, predictions of how ecological communities respond to changing abiotic and biotic environmental conditions have been increasingly challenging due to the limitations of species-based approaches (Lavergne et al., 2010; Wisz et al., 2013). By treating species as qualitative entities, one needs to study each species separately, which is often logistically impossible. This was the case in Chapters 4 and 5, in which the diverse infaunal and epibiotic communities associated with mussel beds and shells could not be investigated at the species level. Trait-based, or functional, approaches could potentially provide a simpler and more generic framework to model species interactions, dispersal ability and physiological tolerance across large spatial scales (Green et al., 2008). Using trait-based approaches to interpret the taxonomical data obtained in Chapters 4 and 5 could thus provide information on the influence of euendolithic infestation on ecological communities associated with mussel beds and shells that were not detected by solely using taxonomical-based approaches (Gusha, 2022).

6.2. How can parasites become your ally?

6.2.1. Photoautotrophic euendoliths as conditionally helpful parasites

Conditionally helpful parasites refer to parasites that are beneficial to their host only under specific environmental conditions (Fellous and Salvaudon, 2009). Parasites can benefit their host by providing the host with a function that it cannot perform alone, or by modifying a host life-history trait, which becomes beneficial in a particular environment. In the first case, infestation by parasites can benefit the hosts' physiological performances or survival (e.g., Munger and Holmes, 1988), or help the host compete against conspecifics, for example through the production of toxins (Kusch et al., 2002). The presence of the parasite may also facilitate the hosts' ability to deal with adverse abiotic conditions, such as pollution by heavy metals (Sures et al., 2003). In the latter case, parasites can cause a plastic change in a life-history trait of the host, for example by increasing its survival to temperature stress (Clay and Schardl, 2002; Zardi et al., 2016) or provide resistance to infestation by other parasites (Barton et al., 2007; Haine et al., 2005). It is worth noting that the majority of conditionally helpful parasites are endoparasites (i.e., living within the body of its host) (Fellous and Salvaudon, 2009; Weinersmith and Earley, 2016).

Photoautotrophic euendoliths can be considered as conditionally beneficial parasites in marine bioengineered ecosystems (Dievart et al., 2022). Euendolithic infestation is not limited to mussels, but rather to any other intertidal organisms with a shell or calcified structures, and its overall ecological effects in marine calcifiers is negative. In corals and coralline algae, euendolithic infestation alters calcification patterns, resulting in a thicker but more porous skeletal structure, reduced vertical growth and reproduction, and enhanced skeletal deformations (Hassenrück et al., 2013; Le Campion-Alsumard

et al., 1995b). In bivalves, euendolithic infestation reduces shell and attachment strength, growth and reproduction (Kaehler and McQuaid, 1999; Marquet et al., 2013; Ndhlovu et al., 2022, 2021a). However, under stressful environmental conditions, such as heatwaves, euendoliths have been demonstrated to mitigate the temperature stress experienced by marine calcifiers. In corals, euendolithic communities can sustain coral survival during bleaching events through a critical supply of organic carbon and nutrients (Fine et al., 2006, 2005, 2004; Odum and Odum, 1955). In coralline algae, euendolithic infestation can reduce the susceptibility of skeletons to dissolution, through the preferential removal of highly soluble skeletal components (Diaz-Pulido et al., 2014; Nash et al., 2013; Reyes-Nivia et al., 2013), which is especially favourable under ocean acidification and global climate change. In bivalves, euendolithic activity causes the whitening of the shell, which increases its albedo, which in turns increases survival rates of infested bivalves and their associated communities in the face of heat stress (Dievart et al., 2023; Lourenço et al., 2017; Monsinjon et al., 2021; Zardi et al., 2023, 2021, 2016).

6.2.2. From parasitism to mutualism: a continuum

As long as the adverse effects of infestation remain more important than the conditional benefits to the host, photoautotrophic euendoliths can be considered as parasites. Euendolithic infestation provide their host mussels with a key innovation (i.e., thermal buffering) under environmental extremes, that potentially offers an ecological opportunity for the future. Key innovations (Miller, 1949) are traits that influence how a species interacts with its environment and thus may provide the capacity to exploit previously unavailable resources (Hunter, 1998; Rabosky, 2014). Mainly investigated in an evolutionary context, key innovations are described as essential for adaptive radiation (Rabosky, 2014) and can be obtained through slow microevolutionary

steps, or even through faster non-evolutionary routes. This is the case for the alteration of a host's life-history traits triggered by parasites, such as the modification of the phenotype of the mussel shell caused by the corrosive activity of euendoliths.

Under certain environmental conditions, the presence of photoautotrophic euendoliths fast-track the host mussel to higher fitness levels that would otherwise be inaccessible through evolutionary steps (Fellous and Salvaudon, 2009). Indeed, although shell colour in intertidal mussels is plastic, the distinctive shell discolouration caused by euendoliths extends beyond the range of such plasticity (Zardi et al., 2016). The pronounced intraspecific phenotypic variation provides infested mussels with a higher degree of resistance to heat stress, that would probably not be reached through classic evolutionary processes (Gehman and Harley, 2019; Zardi et al., 2021, 2016). Such conditionally helpful parasites illustrate the existence of a continuum between parasitism and mutualism (Bronstein, 1994). Parasites could metamorphose into real mutualists if infested hosts display a higher average fitness than non-infested hosts across all possible environments, as a result of environmental change (Fellous and Salvaudon, 2009; Lesser et al., 2013).

6.3. Parasite-mediated ecosystem engineering, present and future

6.3.1. Photoautotrophic euendoliths and mussels: a contribution to the field

Although previously overlooked, parasites have been recognized to dramatically influence ecosystem properties, both negatively and positively, through their cascading effects at the individual, community and ecosystem level (Dobson and Hudson, 1986; Hatcher et al., 2012; Poulin, 1999; Frédéric Thomas et al., 2000). For instance, parasites can influence the dynamics of competition, predation, and herbivory, thus modifying intra- and interspecific interactions, and alter the physical and chemical properties of

ecosystems, thus influencing ecosystem processes (reviewed in Hatcher et al., 2012). At the individual level, parasites can modify multiple physiological, behavioural, and morphological traits of the infested hosts (Calvo-Ugarteburu and McQuaid, 1998; Poulin and Thomas, 1999; Thomas et al., 2010; Zardi et al., 2016). In the case of ecosystem engineers, the parasite-mediated alteration of life-history traits, if involved in the host's engineering processes, is argued to affect the properties of the bioengineered habitat, which in turn influence associated ecological communities (Thomas et al., 1999). In the marine environment, most examples of parasite-mediated ecosystem engineering concern endoparasites (e.g., trematodes, crustaceans) that infects the host's body (Fellous and Salvaudon, 2009; Mouritsen and Poulin, 2002; Thomas et al., 1999; Weinersmith and Earley, 2016). The influence of ectoparasites on engineering capabilities has not received as much attention. Moreover, while the influence of parasites on the individual hosts is well-documented, studies investigating their indirect influence on their associated ecological communities are limited (but see Pascal et al., 2020; Thomas et al., 1998, 1999). In this context, the investigation on the indirect effects of euendolithic infestation on the ecological communities associated with mussel beds presented in this thesis represents a step towards a more comprehensive picture of parasite-mediated ecosystem engineering in the intertidal environment.

Euendoliths are difficult to observe, isolate and identify due to their complex life histories, successional patterns and responses to environmental variables that occur on live carbonate substrates. Given this complexity, it is logical that studies investigating the ecological consequences of euendolithic infestation in marine calcifiers lies beyond the individual level. Recently, there has been an increase in the interest of researchers in studying the relationships between euendolithic infestation of marine calcifiers and interacting components of the marine bioengineered ecosystems they create

(e.g., coral reefs, coralline algal mats, bivalve beds). In corals and coralline algae, the presence of photoautotrophic euendoliths within their skeleton has been demonstrated to positively influence excavating invertebrates and vertebrates (Chazottes et al., 1995; Tribollet and Golubic, 2005). For example, the presence of a bivalve macroborer positively influence euendolithic infestation within the coral skeleton, *via* nitrogen enrichment through bivalve excretion, the reduction of the energetic costs of boring from the presence of both macro- and microborers, and the increase in irradiance from the open hole in the skeleton created by the bivalve, which promotes the settlement and development of euendoliths (Fordyce et al., 2020). Photoautotrophic euendoliths can also represent an important source of food for larger organisms within the bioengineered ecosystem, such as parrotfishes, which are themselves considered as ecosystem engineers within coral reefs, removing algal turf, macroalgae and sediments (Nicholson and Clements, 2020). In bivalves, both negative and positive effects of euendolithic infestation on individual mussels have been demonstrated to influence the quality of habitat provided by mussel beds to their associated organisms. Indeed, the corrosive activity of euendoliths influence the mussel bed microclimate by reducing within-bed temperatures and increasing humidities, thereby creating a favourable environment for the associated intertidal organisms under stressful conditions (Lourenço et al., 2017; Monsinjon et al., 2021; Zardi et al., 2023, 2021, 2016). The thermal benefits of euendolithic infestation for *Perna perna* and the associated infauna was highlighted in Chapter 3 of the thesis (published as Dievart et al., 2023). Although it was expected that euendolith-infested mussel beds would host a more abundant and diverse infaunal communities, no differences in infaunal abundances and biomasses were detected between infested and non-infested manipulated mussel beds made of *Perna perna* at selected sites along the South African coastline (see Chapter 4). Finally, euendolithic

infestation of the mussel, through the modification of the characteristics of the shell (i.e., destruction of antifouling properties and increased roughness) has been demonstrated to positively influence barnacle epibiosis on *Mytilus galloprovincialis* in both Portugal and South Africa (Ma et al., 2023; Marquet et al., 2013). In Chapter 5, the survey of epibiotic communities from natural mussel beds confirmed that euendolithic infestation positively influences the settlement of epibionts, particularly sessile organisms. However, the continuous degradation of the mussel shell would likely increase shell instability over time, which would ultimately impede epibiotic growth and survival. Because each intertidal ecosystem can be considered unique, transferring the results presented in this thesis to other geographical areas and other mytilid species will require to conduct local replicates. In conclusion, this thesis represents a first attempt to comprehensively understand the direct and indirect effects of euendolithic infestation on mussel bed architectural complexity and its influence on associated infaunal and epibiotic communities along the South African coastline, using the native brown mussel *Perna perna* as a focal species.

6.3.2. Predicting the future of euendolithic infestation on mussel beds

The incidence of euendolithic infestation by photoautotrophs, especially in living calcifying organisms, is anticipated to increase in response to global climate change (Enochs et al., 2016; Marcelino et al., 2017; Monsinjon et al., 2021; Reyes-Nivia et al., 2014, 2013; Zardi et al., 2021). Consequently, the detrimental and beneficial effects of euendolithic infestation in marine calcifiers are both expected to be magnified with global climate change and ocean acidification. Under global climate change, the thermal buffering provided by euendoliths to the mussels is likely to become increasingly important to the survival of mussel beds (Gehman and Harley, 2019; Lourenço et al., 2017; Monsinjon et al., 2021; Zardi et al., 2021, 2016) and associated

molluscs (Dievart et al., 2023; Zardi et al., 2023), especially under stressful conditions (i.e., high solar radiation, low to no wind speed, no cloud cover). Although not observed in this study (Chapter 4), it is possible that infaunal communities will associate more readily with euendolith-infested mussel beds in the future, since they provide a thermal refuge on rocky shores. By contrast, it is likely that epibiotic communities will be negatively impacted from the expected increase in mussel shell corrosion by euendoliths under global climate change and ocean acidification scenarios (Chapter 5).

Parasite-host relationships have only recently been incorporated into global climate change and ocean acidification research, although parasites have been demonstrated to alter their hosts' responses to changing abiotic conditions (Burge et al., 2014; Byers, 2020) and their interactions with other biotic components of the ecosystem through competition, predation or facilitation (Dievart et al., 2023; Hatcher et al., 2012; Zardi et al., 2023). In marine ecosystems, parasites and hosts' responses to global climate change and ocean acidification is, more often than not, species-specific and context-dependent (Clements et al., 2017; Harland et al., 2015; MacLeod and Poulin, 2015). For example, the cercarial longevity and survival of the trematode *Maritremas* sp. were reduced under low pH conditions but was compensated by the high numbers of cercariae produced by infested snails, so their prevalence was not affected (MacLeod and Poulin, 2015). Meanwhile, the transmission success of this trematode increased, potentially due to an increase of the host's susceptibility, under low pH conditions (Harland et al., 2015). By contrast, lower pH conditions were associated with a reduction in recruitment of the shell-boring worm *Polydora* sp. on oysters as a result of the increasing instability of the shell substratum (Clements et al., 2017). In a rapidly changing environment, parasites have the potential to increase their hosts' survival, beyond the natural hosts' plasticity (Gehman and Harley, 2019; MacLeod and

Poulin, 2016; Zardi et al., 2021, 2016). For example, the castrative trematode infection in snails have been demonstrated to increases their survival rates at low pH, as infested snails have more energy to compensate higher metabolic rates of calcification (MacLeod and Poulin, 2016). While it has been suggested that euendolith-induced thermal buffering in mussels might indicate a transition from parasitism to mutualism (Gehman and Harley, 2019; Zardi et al., 2021, 2016), the outcomes of the euendolith-mussel relationship remain difficult to predict. Ultimately, the ecological disadvantages and advantages of euendolithic infestation on mussels will vary spatially and temporally. The influence of many abiotic and biotic factors, such as seawater pH and the presence of pollutants, on euendolithic infestation and its ecological consequences on individual mussels and mussel beds still needs to be investigated. Disentangling the effects of euendolithic infestation on the engineering properties of mussels is not an easy task, especially when considering large biogeographical areas. As an increasing number of studies investigate these effects worldwide, this field of research would benefit from a theoretical and methodological framework, which would allow to compare research outcomes. In conclusion, this thesis, along with other studies (e.g., Clements et al., 2017; Harland et al., 2015; MacLeod and Poulin, 2016), advocate the need for the inclusion of parasitic infestation in experimental designs to accurately assess the influence of both abiotic and biotic factors on investigated organisms, and especially in the context of global climate change and ocean acidification.

SUPPLEMENTARY MATERIALS

Chapter 3

Table S3.1. Summary outputs of the Generalized Additive Model (GAM) on the effect of euendolithic infestation on biomimetic mussel shell temperatures (data pooled for all experimental dates).
Model used in this analysis: shell_temp ~ infestation + s(time, bs = "cr", by = infestation, k = 4) + s(id, bs = "re").

Component	Term	Estimate	Std Error	*F*-value	p-value
A. Parametric coefficients	(intercept)	34.08	0.34	-	-
	Non-infested	3.12	0.14	496.6	< 0.001
Component	**Term**	**edf**	**Ref.df**	***F*-value**	**p-value**
B. Smooth terms	s(time):Infested	2.986	3	1081.55	< 0.001
	s(time):Non-infested	2.990	3	1496.45	< 0.001
	s(id)	84.903	89	19.83	< 0.001

* Significant parameters are underlined. Parameter significance was assessed for parametric coefficients using standard F-tests, while the significance of smoothed terms were assessed using adapted Wald's-like tests (Wood, 2013).
Adjusted R-squared: 0.919, Deviance explained: 0.927.
REML: 2097.6, Scale est: 4.4228, N: 900.

Table S3.2. Results of Wald's-like test to assess whether the non-linear relationship between infestation and biomimetic mussel shell temperatures differ over time (data pooled for all experimental dates).

Model	Resid.df	Resid.dev	df	Deviance	Pr(>Chi)
Model 1 (ref) shell_temp ~ infestation + s(time, bs = "cr", k = 4) + s(id, bs = "re")	806.10	3796.00	-	-	-
Model 2 shell_temp ~ infestation + s(time, bs = "cr", by = infestation, k = 4) + s(id, bs = "re")	803.06	3569.70	3.03	226.28	< 0.001

* Significant parameters are underlined. Parameter significance was assessed for parametric coefficients using standard F-tests, while the significance of smoothed terms were assessed using adapted Wald's-like tests (Wood, 2013).

Table S3.3. Results of Wald's-like test to assess whether the non-linear relationship between infestation and biomimetic mussel shell temperatures over time differ between experimental dates.

Model	Resid.df	Resid.dev	df	Deviance	*F*-value	p-value
Model 1 (ref) shell_temp ~ infestation + s(time, bs = "cr", by = infestation, k = 4) + s(id, bs = "re")	803.06	3569.70	-	-	-	-
Model 2 shell_temp ~ infestation + date + s(time, bs = "cr", by = infestation, k = 4) + s(id, bs = "re")	816.06	3680.80	12.996	111.04	1.93	< 0.01

* Significant parameters are underlined. Parameter significance was assessed for parametric coefficients using standard F-tests, while the significance of smoothed terms were assessed using adapted Wald's-like tests (Wood, 2013).

Table S3.4. Summary outputs of the Generalized Additive Model (GAM) on the effect of euendolithic infestation of the biomimetic mussels on the shell temperatures of the spiny chiton, *Acanthochitona garnoti* (data pooled for all experimental dates).
Model used in this analysis: shell_temp ~ infestation + s(time, bs = "cr", by = infestation, k = 6) + s(id, bs = "re").

Component	Term	Estimate	Std Error	*F*-value	p-value
A. Parametric coefficients	(intercept)	32.85	0.23	-	-
	Infestation	1.73	0.16	86.73	< 0.001
Component	**Term**	**edf**	**Ref.df**	***F*-value**	**p-value**
B. Smooth terms	s(time):Infested	4.57	4.90	177.356	< 0.001
	s(time):Non-infested	4.45	4.85	248.17	< 0.001
	s(id)	30.89	41.00	4.34	< 0.001

* Significant parameters are underlined. Parameter significance was assessed for parametric coefficients using standard F-tests, while the significance of smoothed terms were assessed using adapted Wald's-like tests (Wood, 2013).
Adjusted R-squared: 0.849, Deviance explained: 0.863.
REML: 958.91, Scale est: 3.5744, N: 445.

Table S3.5. Results of Wald's-like test to assess whether the non-linear relationship between infestation and shell temperatures of the spiny chiton, *Acanthochitona garnoti*, differ over time (data pooled for all experimental dates).

Model	Resid.df	Resid.dev	df	Deviance	Pr(>Chi)
Model 1 (ref) shell_temp ~ infestation + s(time, bs = "cr", k = 6) + s(id, bs = "re")	399.94	1476.20	-	-	-
Model 2 shell_temp ~ infestation + s(time, bs = "cr", by = infestation, k = 6) + s(id, bs = "re")	394.75	1440.80	5.19	35.38	0.09

* No significant parameters were detected. Parameter significance was assessed for parametric coefficients using standard F-tests, while the significance of smoothed terms were assessed using adapted Wald's-like tests (Wood, 2013).

Table S3.6. Results of Wald's-like test to assess whether the non-linear relationship between infestation and shell temperatures of the spiny chiton, *Acanthochitona garnoti*, over time differ between experimental dates.

Model	Resid.df	Resid.dev	df	Deviance	*F*-value	p-value
Model 1 (ref) shell_temp ~ infestation + s(time, bs = "cr", by = infestation, k = 6) + s(id, bs = "re")	394.75	1440.80	-	-	-	-
Model 2 shell_temp ~ infestation + date + s(time, bs = "cr", by = infestation, k = 6) + s(id, bs = "re")	394.99	1442.60	0.24	1.78	2.08	0.13

* No significant parameters were detected. Parameter significance was assessed for parametric coefficients using standard F-tests, while the significance of smoothed terms were assessed using adapted Wald's-like tests (Wood, 2013).

Table S3.7. Summary outputs of the Generalized Additive Model (GAM) on the effect of euendolithic infestation on the biomimetic mussel shell temperatures and on the shell temperatures of the spiny chiton, *Acanthochitona garnoti* (data pooled for all experimental dates).
Model used in this analysis: shell_temp ~ infestation + species + s(time, bs = "cr", by = infestation, k = 6) + s(id, bs = "re").

Component	Term	Estimate	Std Error	*F*-value	p-value
A. Parametric coefficients	(intercept)	32.95	0.30	-	-
	Infestation	2.31	0.27	74.43	< 0.001
	Species	3.66	0.37	95.36	< 0.001
Component	**Term**	**edf**	**Ref.df**	***F*-value**	**p-value**
B. Smooth terms	s(time):Infested	4.45	4.84	182.61	< 0.001
	s(time):Non-infested	4.36	4.79	264.60	< 0.001
	s(id)	44.64	70.00	1.99	< 0.001

* Significant parameters are underlined. Parameter significance was assessed for parametric coefficients using standard F-tests, while the significance of smoothed terms were assessed using adapted Wald's-like tests (Wood, 2013).
Adjusted R-squared: 0.874, Deviance explained: 0.890.
REML: 993.99, Scale est: 4.6414, N: 432.

Table S3.8. Summary outputs of the Generalized Additive Model (GAM) on the effect of euendolithic infestation of the biomimetic mussels on the shell temperatures of the granular limpet, *Scutellastra granularis* (data pooled for all experimental dates).
Model used in this analysis: shell_temp ~ infestation + s(time, bs = "cr", by = infestation, k = 4) + s(id, bs = "re").

Component	Term	Estimate	Std Error	*F*-value	p-value
A. Parametric coefficients	(intercept)	29.05	0.39	-	-
	Infestation	1.77	0.29	37.92	< 0.001
Component	**Term**	**edf**	**Ref.df**	***F*-value**	**p-value**
B. Smooth terms	s(time):Infested	2.87	2.99	233.20	< 0.001
	s(time):Non-infested	2.92	3.00	255.54	< 0.001
	s(id)	30.76	38.00	5.66	< 0.001

* Significant parameters are underlined. Parameter significance was assessed for parametric coefficients using standard F-tests, while the significance of smoothed terms were assessed using adapted Wald's-like tests (Wood, 2013).
Adjusted R-squared: 0.883, Deviance explained: 0.902.
REML: 535.13, Scale est: 4.4892, N: 228.

Table S3.9. Results of Wald's-like test to assess whether the non-linear relationship between infestation and shell temperatures of the granular limpet, *Scutellastra granularis*, differ over time (data pooled for all experimental dates).

Model	Resid.df	Resid.dev	df	Deviance	Pr(>Chi)
Model 1 (ref) shell_temp ~ infestation + s(time, bs = "cr", k = 4) + s(id, bs = "re")	186.51	888.24	-	-	-
Model 2 shell_temp ~ infestation + s(time, bs = "cr", by = infestation, k = 4) + s(id, bs = "re")	183.24	850.48	3.27	37.76	< 0.05

* Significant parameters are underlined. Parameter significance was assessed for parametric coefficients using standard F-tests, while the significance of smoothed terms were assessed using adapted Wald's-like tests (Wood, 2013).

Table S3.10. Results of Wald's-like test to assess whether the non-linear relationship between infestation and shell temperatures of the granular limpet, *Scutellastra granularis*, over time differ between experimental dates.

Model	Resid.df	Resid.dev	df	Deviance	*F*-value	p-value
Model 1 (ref) shell_temp ~ infestation + s(time, bs = "cr", by = infestation, k = 4) + s(id, bs = "re")	183.24	850.48	-	-	-	-
Model 2 shell_temp ~ infestation + date + s(time, bs = "cr", by = infestation, k = 4) + s(id, bs = "re")	200.81	927.60	17.57	77.12	0.98	0.49

* No significant parameters were detected. Parameter significance was assessed for parametric coefficients using standard F-tests, while the significance of smoothed terms were assessed using adapted Wald's-like tests (Wood, 2013).

Table S3.11. Summary outputs of the Generalized Additive Model (GAM) on the effect of euendolithic infestation on the biomimetic mussel shell temperatures and on the shell temperatures of the granular limpet, *Scutellastra granularis* (data pooled for all experimental dates).
Model used in this analysis: shell_temp ~ infestation + species + s(time, bs = "cr", by = infestation, k = 4) + s(id, bs = "re").

Component	Term	Estimate	Std Error	*F*-value	p-value
A. Parametric coefficients	(intercept)	32.32	0.45	-	-
	Infestation	1.97	0.37	28.27	< 0.001
	Species	2.50	0.58	18.68	< 0.001
Component	**Term**	**edf**	**Ref.df**	***F*-value**	**p-value**
B. Smooth terms	s(time):Infested	2.90	2.99	274.81	< 0.001
	s(time):Non-infested	2.95	3.00	361.15	< 0.001
	s(id)	45.95	63.00	2.99	< 0.001

* Significant parameters are underlined. Parameter significance was assessed for parametric coefficients using standard F-tests, while the significance of smoothed terms were assessed using adapted Wald's-like tests (Wood, 2013).
Adjusted R-squared: 0.912, Deviance explained: 0.932.
REML: 553.03, Scale est: 4.2857, N: 234.

Table S3.12. Summary outputs of the Generalized Additive Model (GAM) on the effect of euendolithic infestation on the biomimetic mussels and on the shell temperatures of the prickly limpet, *Helcion pectunculus*, and the variegated topshell, *Oxystele antoni* (data pooled for all experimental dates). Model used in this analysis: shell_temp ~ infestation + s(time, bs = "cr", by = infestation, k = 4) + s(id, bs = "re").

Component	Term	Estimate	Std Error	*F*-value	p-value
A. Parametric coefficients	(intercept)	33.46	0.96	-	-
	Infestation	0.56	0.38	2.18	0.14
	Oxystele antoni	0.24	1.33	0.60	0.55
	Perna perna	1.03	1.25	0.60	0.55
Component	**Term**	**edf**	**Ref.df**	***F*-value**	**p-value**
B. Smooth terms	s(time):Infested	2.96	3.00	305.70	< 0.001
	s(time):Non-infested	2.96	3.00	309.80	< 0.001
	s(id)	68.16	75.00	11.80	< 0.001

* Significant parameters are underlined. Parameter significance was assessed for parametric coefficients using standard F-tests, while the significance of smoothed terms were assessed using adapted Wald's-like tests (Wood, 2013).
Adjusted R-squared: 0.903, Deviance explained: 0.928.
REML: 797.67, Scale est: 6.2238, N: 299.

Table S3.13. Results of Wald's-like test to assess whether the non-linear relationship between infestation and shell temperatures of prickly limpet, *Helcion pectunculus*, and the variegated topshell, *Oxystele antoni*, differ over time (data pooled for all experimental dates).

Model	Resid.df	Resid.dev	df	Deviance	Pr(>Chi)
Model 1 (ref) shell_temp ~ infestation + species + s(time, bs = "cr", k = 4) + s(id, bs = "re")	217.47	1377.30	-	-	-
Model 2 shell_temp ~ infestation + species + s(time, bs = "cr", by = infestation, k = 4) + s(id, bs = "re")	214.45	1375.00	3.02	2.24	0.95

* No significant parameters were detected. Parameter significance was assessed for parametric coefficients using standard F-tests, while the significance of smoothed terms were assessed using adapted Wald's-like tests (Wood, 2013).

Table S3.14. Results of Wald's-like test to assess whether the non-linear relationship between infestation and shell temperatures of the prickly limpet, *Helcion pectunculus*, and the variegated topshell, *Oxystele antoni*, over time differ between experimental dates.

Model	Resid.df	Resid.dev	df	Deviance	*F*-value	p-value
Model 1 (ref) shell_temp ~ infestation + species + s(time, bs = "cr", by = infestation, k = 4) + s(id, bs = "re")	214.45	1375.00	-	-	-	-
Model 2 shell_temp ~ infestation + date + species + s(time, bs = "cr", by = infestation, k = 4) + s(id, bs = "re")	239.20	1639.10	24.75	264.07	1.71	< 0.05

* Significant parameters are underlined. Parameter significance was assessed for parametric coefficients using standard F-tests, while the significance of smoothed terms were assessed using adapted Wald's-like tests (Wood, 2013).

Table S3.15. Summary outputs of the Generalized Additive Model (GAM) on the effect of euendolithic infestation on the wet weight of infaunal invertebrates (data pooled for all species and experimental dates). Model used in this analysis: log(wet_wgt) ~ infestation * species + s(time, bs = "cr", by = infestation, k = 5) + s(id, bs = "re")

Component	Term	Estimate	Std Error	*F*-value	p-value
A. Parametric coefficients	(intercept)	7.69	0.06	-	-
	Infestation	0.09	0.09	1.02	0.31
	Species			239.74	< 0.001
	Infestation x Species			0.98	0.40
Component	**Term**	**edf**	**Ref.df**	***F*-value**	**p-value**
B. Smooth terms	s(time):Infested	1.19	1.36	19.51	< 0.001
	s(time):Non-infested	2.01	2.46	7.16	< 0.001
	s(id)	1.02	32.00	0.03	0.42

* Significant parameters are underlined. Parameter significance was assessed for parametric coefficients using standard F-tests, while the significance of smoothed terms were assessed using adapted Wald's-like tests (Wood, 2013).
Adjusted R-squared: 0.799, Deviance explained: 0.805.
REML: 202.87, Scale est: 0.16678, N: 359.

Table S3.16. Results of Wald's-like test to assess whether the non-linear relationship between infestation and wet weight of infaunal invertebrates (data pooled for all species and experimental dates) differ over time between species (data pooled for all experimental dates).

Model	Resid.df	Resid.dev	df	Deviance	Pr(>Chi)
Model 1 (ref) log(wet_wgt) ~ infestation + species + s(time, bs = "cr", by = infestation, k = 5) + s(id, bs = "re")	346.34	58.30	-	-	-
Model 2 log(wet_wgt) ~ infestation * species + s(time, bs = "cr", by = infestation, k = 5) + s(id, bs = "re")	343.59	57.84	2.75	0.46	0.38

* No significant parameters were detected. Parameter significance was assessed for parametric coefficients using standard F-tests, while the significance of smoothed terms were assessed using adapted Wald's-like tests (Wood, 2013).

Table S4.1. List of the infaunal taxa recorded in the infested and non-infested experimental mussel beds (made up of *Perna perna* mussel shells) deployed in this study. Presence of each taxon is indicated by a 'X' in the corresponding column for each level of euendolithic infestation and *P. perna* genetic lineages at each experimental site. NI: non-infested mussel bed, I: infested mussel bed, E: *P. perna* eastern lineage, and W: *P. perna* genetic lineage.

	Mosselbaai		**Brenton-on-Sea**		**Jeffreysbaai**		**Old Woman's River**				**Port Edward**	
Taxon	**NI – W**	**I – W**	**NI – W**	**I -W**	**NI – W**	**I – W**	**NI – W**	**I – W**	**NI – E**	**I – E**	**NI – E**	**I – E**
ACTINIARIA												
Actiniaria	X		X	X	X	X	X	X	X	X	X	X
PLATYHELMINTHES												
Notocomplana erythrotoaenia	X		X	X	X	X	X	X	X			
Planocera gilchristi			X		X		X		X	X		
Platyhelminthes									X			
ANNELIDA												
HIRUDINEA												
Hirudinea								X		X		
ERRANTIA												
Arabella iricolor							X	X	X			
Lepidonotus clava		X										
Lepidonotus durbanensis					X	X	X	X	X	X		
Nereididae			X	X	X	X	X	X	X	X		
Phyllodocidae	X				X	X			X			
Pseudonereis podocirra	X	X	X	X			X	X	X	X	X	X
Scoletoma tetraura		X	X	X	X	X	X	X	X	X		
Syllidae	X	X	X	X	X		X	X	X	X	X	X
Errantia	X	X							X		X	
SEDENTARIA												
Cirriformia sp.							X					
Gunnarea gaimardi								X	X	X		
Orbinidae					X							
Spirobranchus kraussii											X	
Thelepus sp.		X						X		X		
Sedentaria											X	

Table S4.1 (continued).

	Mosselbaai		Brenton-on-Sea		Jeffreysbaai		Old Woman's River				Port Edward	
Taxon	**NI – W**	**I – W**	**NI – W**	**I -W**	**NI – W**	**I – W**	**NI – W**	**I – W**	**NI – E**	**I – E**	**NI – E**	**I – E**
NEMERTEA												
Cerebratulus fuscus									X			
Nemertea	X		X	X	X	X	X		X			
SIPUNCULIDA												
Sipunculida						X	X	X	X	X		
ARTHROPODA												
ARACHNIDA												
Desis formidabilis	X	X					X	X	X			
PYCNOGONIDA												
Nymphopsis cuspidata	X											
Tanystylum brevipes					X							
Pycnogonida			X					X				
HEXAPODA												
Telmatogeton minor	X	X	X	X	X			X	X	X		
DECAPODA												
Cyclograpsus punctatus	X	X		X	X	X						
Guinusia chabrus			X			X	X	X	X			
Leucisca squalina					X	X					X	
Metopograpsus messor												X
Plagusia squamosa											X	
AMPHIPODA												
Paramoera capensis	X	X						X	X	X	X	X
Talorchestia sp.			X	X	X	X	X	X	X	X	X	X
Amphipoda							X	X				X
ISOPODA												
Cirolana cranchii		X			X		X					
Cirolana hirtipes	X											
Cirolana venusticauda	X											
Cirolana sp.	X		X	X		X			X			
Exosphaeroma truncatitelson	X		X									
Iais pubescens	X	X	X	X		X	X	X	X	X		
Ischyromene huttoni	X	X	X	X	X	X	X	X	X	X	X	X
Janira sp.							X	X				

Table S4.1 (continued).

	Mosselbaai		Brenton-on-Sea		Jeffreysbaai		Old Woman's River				Port Edward	
	NI – W	I – W	NI – W	I -W	NI – W	I – W	NI – W	I – W	NI – E	I – E	NI – E	I – E
ISOPODA (suite)												
Joeropsis stebbingi					X		X	X	X	X		
Mesanthura catenula	X	X							X			
Parisocladus perforatus	X	X			X	X	X		X	X		
Sphaeramene polytylotos			X	X			X	X	X	X		
Stenetrium sp.		X										
Isopoda	X			X				X	X	X		
TANAIDACEA												
Zeuxoides helleri		X			X				X			
CIRRIPEDIA												
Chthamalus dentatus	X								X		X	X
Octomeris angulosa	X										X	X
Solidobalanus elizabethae												X
Tetraclita serrata								X	X		X	X
Cirripedia	X										X	
ECHINODERMATA												
ASTEROIDEA												
Parvulastra exigua	X	X		X	X	X	X	X	X	X	X	
ECHINOIDEA												
Parechinus angulosus	X		X	X	X	X	X	X	X	X		
OPHIUROIDEA												
Amphipholis squamata	X	X			X		X	X	X	X		
HOLOTHUROIDEA												
Neostichopus grammatus										X		
Pentacta doliolum										X		
Pseudocnella sykion					X	X		X			X	X
Roweia stephensoni				X								
Holothuroidea		X					X	X	X			
MOLLUSCA												
BIVALVIA												
Brachidontes variabilis											X	X
Choromytilus meridionalis			X									
Mytilus galloprovincialis	X	X	X	X	X	X						

Table S4.1 (continued).

	Mosselbaai		Brenton-on-Sea		Jeffreysbaai		Old Woman's River				Port Edward	
	NI – W	I – W	NI – W	I -W	NI – W	I – W	NI – W	I – W	NI – E	I – E	NI – E	I – E
BIVALVIA (suite)												
Perna perna	X	X	X	X	X	X	X	X	X	X	X	X
Venerupis corrugata			X									
Bivalvia			X									
GASTROPODA												
Afrolittorina africana												X
Afrolittorina knysnaensis						X						
Anachis kraussii subsp. *Kraussii*											X	
Burnupena cincta				X								
Burnupena lagenaria			X	X	X	X	X	X	X	X		X
Cellana capensis											X	X
Crepidula porcellana										X		
Cymbula granatina							X	X	X			
Cymbula oculus					X	X	X	X	X	X	X	
Cymbula sanguinans											X	X
Eoacmaea albonotata											X	
Fissurella mutabilis			X	X	X							
Fissurella natalensis							X	X	X	X	X	X
Gibbula cicer					X		X	X	X	X		
Gibbula multicolor											X	X
Helcion concolor											X	X
Helcion dunkeri							X					X
Helcion pruinosus	X	X		X			X	X	X	X	X	X
Heliacus variegatus		X						X				
Mancinella capensis		X										
Nucella dubia	X	X	X		X	X	X	X			X	X
Nucella squamosa			X	X	X	X	X	X	X			
Oxystele antoni	X	X	X	X	X	X	X	X	X	X		
Oxystele impervia		X		X			X	X	X	X		
Oxystele tabularis							X		X		X	X
Purpura panama												X
Scutellastra granularis	X	X	X	X	X	X	X	X	X	X	X	X
Scutellastra longicosta						X						

Table S4.1 (continued).

	Mosselbaai		Brenton-on-Sea		Jeffreysbaai		Old Woman's River				Port Edward	
	NI – W	I – W	NI – W	I -W	NI – W	I – W	NI – W	I – W	NI – E	I – E	NI – E	I – E
GASTROPODA (suite)												
Scutellastra natalensis												X
Scutellastra obtecta											X	X
Siphonaria capensis	X	X	X	X	X	X						
Siphonaria concinna	X	X			X							
Siphonaria oculus						X						
Siphonaria serrata									X			
Tricolia capensis			X		X	X		X	X	X		
Tricolia kochii				X	X			X	X	X		
Tricolia neritina			X	X	X	X						
Tubo cidaris subsp. *Cidaris*	X											
Gastropoda	X		X					X			X	X
POLYPLACOPHORA												
Acanthochitona garnoti	X	X	X	X	X	X	X	X	X	X		
Ischnochiton oniscus	X					X		X		X		
Onithochiton literatus											X	X
Rhyssoplax polita							X	X		X		
OSTEICHTHYES												
Clinus sp.									X			

Table S4.2. Results of the SIMPER analysis on infaunal abundances showing the most influential species discriminating among sites. Cut-off for low contribution: 50%. Significant p-values indicating difference in average species abundance between sites are underlined.

Species	Average a	Average b	Cumulative contribution (%)
Brenton-on-Sea *vs* Mosselbaai			
Talorchestia sp.	2.947	0.000	7.397
Paramoera capensis	0.000	2.776	14.369
Actiniaria	2.468	0.149	20.243
Burnupena lagenaria	2.070	0.000	25.427
Mytilus galloprovincialis	2.569	0.702	30.242
Sphaeramene phylotylotos	1.542	0.000	34.106
Ischyromene huttoni	2.281	0.954	37.545
Parisocladus perforatus	0.000	1.416	40.927
Tricolia neritina	1.284	0.000	44.116
Parvulastra exigua	0.571	1.844	47.244
Perna perna	3.596	2.373	50.363
Brenton-on-Sea *vs* Jeffreysbaai			
Parisocladus perforatus	0.000	1.998	5.929
Pseudonereis podocirra	1.996	0.000	11.827
Actiniaria	2.468	0.693	17.205
Sphaeramene polytylotos	1.542	0.000	21.740
Nucella dubia	0.143	1.412	25.540
Tricolia neritina	1.284	0.333	28.611
Talorchestia sp.	2.947	1.948	31.581
Mytilus galloprovincialis	2.569	1.879	34.377
Notocomplona erythrotaenia	1.070	0.402	37.051
Burnupena lagenaria	2.070	1.301	39.407
Nereididae	1.090	0.960	41.727
Acanthochitona garnoti	1.156	1.298	44.020
Fissurella mutabilis	0.733	0.198	46.193
Scoletoma tetraura	0.345	0.731	48.346
Siphonaria capensis	0.474	0.709	50.478
Brenton-on-Sea *vs* Port Edward			
Mytilus galloprovincialis	2.569	0.000	5.701
Actiniaria	2.468	0.499	10.165
Oxystele tabularis	0.000	2.005	14.569
Perna perna	3.596	1.643	18.959
Oxystele antoni	1.976	0.000	23.335
Talorchestia sp.	2.947	1.041	27.574
Burnupena lagenaria	2.070	0.188	31.804
Sphaeramene polytylotos	1.542	0.000	35.233
Tricolia neritina	1.284	0.000	38.100

Table S4.2 (continued).

Species	Average a	Average b	Cumulative contribution (%)
Brenton-on-Sea *vs* Port Edward (suite)			
Pseudonereis podocirra	1.996	0.832	40.717
Helcion concolor	0.000	1.149	43.319
Acanthochitona garnoti	1.156	0.000	45.857
Helcion pruinosus	0.000	1.201	48.369
Nereididae	1.090	0.000	50.771
Jeffreysbaai *vs* Mosselbaai			
Paramoera capensis	0.000	2.776	7.677
Talorchestia sp.	1.948	0.000	13.056
Ischyromene huttoni	2.842	0.954	18.394
Parvulastra exigua	0.333	1.844	22.559
Mytilus galloprovincialis	1.879	0.702	26.074
Burnupena lagenaria	1.301	0.000	29.576
Perna perna	3.433	2.373	32.669
Nucella dubia	1.412	0.561	35.690
Pseudonereis podocirra	0.000	1.093	38.659
Parisocladus perforatus	1.998	1.416	41.558
Acanthochitona garnoti	1.298	0.500	44.240
Nereididae	0.960	0.000	46.784
Siphonaria capensis	0.709	0.274	48.766
Scutellastra granularis	1.494	0.939	50.703
Jeffreysbaai *vs* Port Edward			
Parisocladus perforatus	1.998	0.000	4.668
Oxystele tabularis	0.000	2.005	9.243
Oxystele antoni	1.974	0.000	13.726
Mytilus galloprovincialis	1.879	0.000	18.102
Perna perna	3.433	1.643	22.308
Acanthochitona garnoti	1.298	0.000	25.283
Ischyromene huttoni	2.842	1.676	28.094
Helcion concolor	0.000	1.149	30.801
Burnupena lagenaria	1.301	0.188	33.453
Helcion pruinosus	0.167	1.201	35.932
Fissurella natalensis	0.000	1.090	38.383
Nucella dubia	1.412	0.429	40.768
Talorchestia sp.	1.948	1.041	43.103
Nereididae	0.960	0.000	45.235
Gastropoda	0.000	0.905	47.305
Pseudonereis podocirra	0.000	0.832	49.182
Cymbula sanguinans	0.000	0.767	50.963

Table S4.2 (continued).

Species	Average a	Average b	Cumulative contribution (%)
Mosselbaai *vs* Port Edward			
Paramoera capensis	2.776	0.493	6.748
Oxystele tabularis	0.000	2.005	12.398
Parvulastra exigua	1.844	0.143	17.237
Oxystele antoni	1.639	0.000	21.931
Parisocladus perforatus	1.416	0.000	25.736
Helcion concolor	0.000	1.149	29.108
Talorchestia sp.	0.000	1.041	32.123
Fisurella natalensis	0.000	1.090	35.137
Ischyromene huttoni	0.954	1.676	38.071
Helcion pruinosus	0.274	1.201	40.994
Scutellastra granularis	0.939	1.491	43.491
Gastropoda	0.125	0.905	45.914
Perna perna	2.373	1.643	48.180
Cymbula sanguinans	0.000	0.767	50.389

Table S4.3. Results of the SIMPER analysis on infaunal biomasses showing the most influential species discriminating among sites. Cut-off for low contribution: 50%. Significant p-values indicating difference in average species biomass between sites are underlined.

Species	Average a	Average b	Cumulative contribution (%)
Brenton-on-Sea *vs* Mosselbaai			
Actiniaria	4.655	0.400	7.197
Burnupena lagenaria	4.068	0.000	13.927
Mytilus galloprovincialis	5.026	1.253	20.387
Parvulastra exigua	1.470	5.338	26.819
Perna perna	7.169	3.721	32.789
Ischyromene huttoni	4.921	1.753	38.074
Sphaeramene polytylotos	3.074	0.000	43.119
Talorchestia sp.	2.881	0.000	47.907
Paramoera capensis	0.000	2.478	52.015
Brenton-on-Sea *vs* Jeffreysbaai			
Pseudonereis podocirra	4.422	0.000	8.587
Actiniaria	4.655	0.819	16.115
Sphaeramene polytylotos	3.074	0.000	22.007
Parisocladus perforatus	0.000	2.686	27.201
Perna perna	7.169	6.152	31.974
Nucella dubia	0.174	2.521	36.460
Acanthochitona garnoti	2.830	3.454	40.848
Mytilus galloprovincialis	5.026	3.286	45.113
Burnupena lagenaria	4.068	2.340	48.634
Parvulastra exigua	1.470	0.538	51.339
Brenton-on-Sea *vs* Port Edward			
Perna perna	7.169	2.182	7.170
Mytilus galloprovincialis	5.026	0.000	14.331
Actiniaria	4.655	0.665	20.136
Burnupena lagenaria	4.068	0.245	25.586
Pseudonereis podocirra	4.422	1.410	30.030
Sphaeramene polytylotos	3.074	0.000	34.336
Ischyromene huttoni	4.922	1.972	38.523
Onithochiton literatus	0.000	3.067	42.566
Oxystele tabularis	0.000	2.904	46.594
Acanthochitona garnoti	2.830	0.000	50.504
Jeffreysbaai *vs* Mosselbaai			
Parvulastra exigua	0.538	5.338	9.215
Ischyromene huttoni	5.603	1.753	16.526
Perna perna	6.152	3.721	21.986
Acanthochitona garnoti	3.454	1.401	26.928
Paramoera capensis	0.000	2.478	31.696
Pseudonereis podocirra	0.000	2.503	36.426

Table S4.3 (continued).

Species	Average a	Average b	Cumulative contribution (%)
Jeffreysbaai *vs* Mosselbaai (suite)			
Mytilus galloprovincialis	3.286	1.253	40.851
Burnupena lagenaria	2.340	0.000	45.236
Cyclograpsus punctatus	1.254	1.927	49.180
Nucella dubia	2.521	0.944	52.928
Jeffreysbaai *vs* Port Edward			
Perna perna	6.152	2.182	6.184
Ischyromene huttoni	5.603	1.972	11.956
Acanthochitona garnoti	3.454	0.000	17.181
Mytilus galloprovincialis	3.286	0.000	22.288
Oxystele antoni	3.198	0.000	27.377
Oxystele tabularis	0.000	2.904	31.926
Onithochiton literatus	0.000	3.067	36.455
Parisocladus perforatus	2.686	0.000	40.760
Fissurella natalensis	0.000	2.548	44.694
Burnupena lagenaria	2.340	0.245	48.067
Nucella dubia	2.521	0.506	51.309
Mosselbaai *vs* Port Edward			
Parvulastra exigua	5.338	0.210	9.909
Oxystele antoni	3.190	0.000	16.188
Oxystele tabularis	0.000	2.904	21.647
Onithochiton literatus	0.000	3.067	27.005
Fissurella natalensis	0.000	2.548	31.717
Paramoera capensis	2.478	0.613	35.619
Parisocladus perforatus	2.109	0.000	39.447
Cyclograpsus punctatus	1.927	0.000	43.217
Perna perna	3.721	2.182	46.688
Pseudonereis podocirra	2.503	1.410	49.878
Helcion concolor	0.000	1.528	52.773

Chapter 5

This supplementary material comprises of separate sections corresponding to the subtitles in the 'Results' section of this chapter to facilitate navigation.

5.3.1. Relationship between mussel shell condition and epibiosis

Table S5.1. Results of the TukeySD post-hoc pairwise comparisons on the relationship between shell length (in mm) and euendolithic infestation levels (from A to E, as defined in Kaehler, 1999). Significant p-values are underlined.

Infestation level (a)	Infestation level (b)	Estimate	Std Error	*t*-value	p-value
A	B	– 3.722	2.232	– 1.668	0.420
	C	– 0.317	2.609	– 0.122	0.999
	D	8.301	2.642	3.142	0.013
	E	10.887	3.857	2.832	0.033
B	C	3.405	1.653	2.060	0.213
	D	12.023	1.688	7.123	< 0.001
	E	14.609	3.281	4.453	< 0.001
C	D	8.618	1.154	7.468	< 0.001
	E	11.204	3.029	3.699	0.002
D	E	2.586	2.963	0.873	0.894

Table S5.2. Results of the TukeySD post-hoc pairwise comparisons on the relationship between shell length (in mm) and shell degradation index (from 1 to 6, as defined in Ma *et al.*, 2023). Significant p-values are underlined.

Shell degradation index (a)	Shell degradation index (b)	Estimate	Std Error	*t*-value	p-value
1	2	13.923	2.477	5.621	< 0.001
	3	24.097	2.857	8.434	< 0.001
	4	29.704	3.114	9.537	< 0.001
	5	38.465	3.166	12.150	< 0.001
	6	38.087	3.973	9.586	< 0.001
2	3	10.174	2.119	4.802	< 0.001
	4	15.781	2.380	6.631	< 0.001
	5	24.542	2.454	10.003	< 0.001
	6	24.164	3.434	7.036	< 0.001
3	4	5.607	1.670	3.358	0.009
	5	14.368	1.718	8.366	< 0.001
	6	13.990	2.948	4.745	< 0.001
4	5	8.762	1.207	7.261	< 0.001
	6	8.383	2.671	3.138	0.019
5	6	– 0.379	2.555	– 0.148	1.000

Table S5.3. Results of the TukeySD post-hoc pairwise comparisons on the relationship between the prevalence of epibiosis and shell length range (from]30 − 40] to]110 − 120] in mm). Significant p-values are underlined.

Shell length range (a)	Shell length range (b)	Estimate	Std Error	z-value	p(> |z|)
]30 − 40]	]40 − 50]	− 0.420	0.355	− 1.181	0.961
	]50 − 60]	− 1.341	0.365	− 3.672	<u>0.007</u>
	]60 − 70]	− 1.501	0.363	− 4.131	<u>0.001</u>
	]70 − 80]	− 2.749	0.522	− 5.261	<u>< 1 x 10^{-4}</u>
	]80 − 90]	− 2.887	0.461	− 6.259	<u>< 1 x 10^{-4}</u>
	]90 − 100]	− 4.230	1.036	− 4.082	<u>0.002</u>
	]100 − 110]	− 17.069	610.452	− 0.028	1.000
	]110 − 120]	− 17.069	1978.090	− 0.009	1.000
]40 − 50]	]50 − 60]	− 0.921	0.360	− 2.558	0.205
	]60 − 70]	− 1.081	0.358	− 3.017	0.064
	]70 − 80]	− 2.329	0.519	− 4.488	<u>2 x 10^{-4}</u>
	]80 − 90]	− 2.468	0.457	− 5.395	<u>< 0.001</u>
	]90 − 100]	− 3.811	1.035	− 3.683	<u>0.007</u>
	]100 − 110]	− 16.676	610.452	− 0.027	1.000
	]110 − 120]	− 16.676	1978.090	− 0.008	1.000
]50 − 60]	]60 − 70]	− 0.160	0.368	− 0.434	1.000
	]70 − 80]	− 1.408	0.526	− 2.677	0.156
	]80 − 90]	− 1.546	0.465	− 3.325	<u>0.025</u>
	]90 − 100]	− 2.889	1.038	− 2.783	0.120
	]100 − 110]	− 15.755	610.452	− 0.026	1.000
	]110 − 120]	− 15.755	1978.090	− 0.008	1.00
]60 − 70]	]70 − 80]	− 1.248	0.524	− 2.380	0.295
	]80 − 90]	− 1.387	0.464	− 2.991	0.069
	]90 − 100]	− 2.730	1.037	− 2.631	0.174
	]100 − 110]	− 15.595	610.452	− 0.026	1.000
	]110 − 120]	− 15.595	1978.090	− 0.008	1.000
]70 − 80]	]80 − 90]	− 0.139	0.597	− 0.232	1.000
	]90 − 100]	− 1.482	1.103	− 1.343	0.9184
	]100 − 110]	− 14.347	610.452	− 0.024	1.000
	]110 − 120]	− 14.347	1978.090	− 0.007	1.000
]80 − 90]	]90 − 100]	− 1.343	1.076	− 1.249	0.946
	]100 − 110]	− 14.209	610.452	− 0.023	1.000
	]110 − 120]	− 14.209	1978.090	− 0.007	1.000
]90 − 100]	]100 − 110]	− 12.866	610.453	− 0.021	1.000
	]110 − 120]	− 12.866	1978.090	− 0.007	1.000
]100 − 110]	]110 − 120]	0.000	2070.143	0.000	1.000

Table S5.4. Results of the TukeySD post-hoc pairwise comparisons on the relationship between the prevalence of epibiosis and euendolithic infestation levels (from A to E, as defined in Kaehler, 1999). Significant p-values are underlined.

Infestation level (a)	Infestation level (b)	Estimate	Std Error	z-value	P (> z)
A	B	– 0.161	0.474	– 0.340	0.996
	C	– 0.297	0.588	– 0.505	0.982
	D	0.648	0.634	1.023	0.807
	E	13.997	510.129	0.027	1.000
B	C	– 0.137	0.399	– 0.342	0.996
	D	0.809	0.460	1.759	0.334
	E	14.158	510.128	0.028	1.000
C	D	0.945	0.343	2.754	0.033
	E	14.295	510.128	0.028	1.000
D	E	13.349	510.128	0.026	1.000

Table S5.5. Results of the TukeySD post-hoc pairwise comparisons on the relationship between the prevalence of epibiosis and shell degradation index (from 1 to 6, as defined in Ma *et al.*, 2023). Significant p-values are underlined.

Shell degradation index (a)	Shell degradation index (b)	Estimate	Std Error	z-value	P (> z)
1	2	1.074	0.444	2.419	0.126
	3	1.908	0.579	3.295	0.010
	4	1.703	0.638	2.671	0.068
	5	2.119	0.674	3.145	0.017
	6	2.467	1.211	2.037	0.284
2	3	0.845	0.457	1.826	0.407
	4	0.630	0.513	1.226	0.797
	5	1.046	0.559	1.871	0.379
	6	1.393	1.151	1.210	0.805
3	4	– 0.205	0.418	– 0.492	0.996
	5	0.211	0.458	0.460	0.999
	6	0.559	1.105	0.506	0.995
4	5	0.416	0.338	1.232	0.793
	6	0.764	1.057	0.722	0.975
5	6	0.348	1.049	0.331	0.999

5.3.2. Epibiotic communities

5.3.2.1. Epibiotic community descriptors

5.3.2.1.1. Total abundance of epibionts

Table S5.6. Results of the TukeySD post-hoc pairwise comparisons on the relationship between the total abundance of epibionts per mussel and shell length range (from]30 − 40] to]110 − 120] in mm). Significant p-values are underlined.

Shell length range (a)	Shell length range (b)	Estimate	Std Error	z-value	p(> |z|)
]30 − 40]	]40 − 50]	0.321	0.231	1.389	0.887
	]50 − 60]	0.553	0.208	2.660	0.142
	]60 − 70]	0.940	0.205	4.597	< 0.010
	]70 − 80]	1.306	0.205	6.386	< 0.010
	]80 − 90]	1.525	0.194	7.868	< 0.010
	]90 − 100]	1.790	0.208	8.603	< 0.010
	]100 − 110]	2.094	0.253	8.279	< 0.010
	]110 − 120]	1.942	0.618	3.145	0.038
]40 − 50]	]50 − 60]	0.232	0.187	1.245	0.937
	]60 − 70]	0.619	0.183	3.388	0.017
	]70 − 80]	0.986	0.183	5.389	< 0.010
	]80 − 90]	1.204	0.171	7.052	< 0.010
	]90 − 100]	1.469	0.187	7.866	< 0.010
	]100 − 110]	1.774	0.236	7.522	< 0.010
	]110 − 120]	1.621	0.611	2.655	0.143
]50 − 60]	]60 − 70]	0.387	0.153	2.537	0.189
	]70 − 80]	0.753	0.153	4.934	< 0.010
	]80 − 90]	0.972	0.138	7.047	< 0.010
	]90 − 100]	1.237	0.157	7.862	< 0.010
	]100 − 110]	1.541	0.213	7.229	< 0.010
	]110 − 120]	1.389	0.602	2.306	0.305
]60 − 70]	]70 − 80]	0.366	0.148	2.474	0.218
	]80 − 90]	0.585	0.133	4.404	< 0.010
	]90 − 100]	0.850	0.153	5.561	< 0.010
	]100 − 110]	1.154	0.210	2.499	< 0.010
	]110 − 120]	1.002	0.601	1.667	0.738
]70 − 80]	]80 − 90]	0.218	0.133	1.645	0.752
	]90 − 100]	0.484	0.153	3.164	0.035
	]100 − 110]	0.788	0.210	3.754	< 0.001
	]110 − 120]	0.636	0.601	1.058	0.976
]80 − 90]	]90 − 100]	0.265	0.139	1.920	0.563
	]100 − 110]	0.570	0.200	2.857	0.085
	]110 − 120]	0.418	0.598	0.699	0.999
]90 − 100]	]100 − 110]	0.305	0.213	1.428	0.870
	]110 − 120]	0.152	0.602	0.253	1.000
]100 − 110]	]110 − 120]	− 0.152	0.619	− 0.246	1.000

Table S5.7. Results of the TukeySD post-hoc pairwise comparisons on the relationship the total abundance of epibionts per mussel valve and euendolithic infestation levels (from A to E, as defined in Kaehler, 1999). Significant p-values are underlined.

Infestation level (a)	Infestation level (b)	Estimate	Std Error	z-value	P (> z)
A	B	– 0.181	0.181	– 0.997	0.839
	C	0.185	0.208	0.891	0.887
	D	0.241	0.209	1.152	0.754
	E	0.139	0.292	0.474	0.988
B	C	0.366	0.130	2.821	0.033
	D	0.422	0.131	3.228	0.009
	E	0.319	0.243	1.315	0.651
C	D	0.056	0.087	0.641	0.963
	E	– 0.046	0.222	– 0.209	1.000
D	E	– 0.102	0.216	– 0.474	0.988

Table S5.8. Results of the TukeySD post-hoc pairwise comparisons on the relationship between the total abundance of epibionts per mussel valve and shell degradation index (from 1 to 6, as defined in Ma *et al.*, 2023). Significant p-values are underlined.

Shell degradation index (a)	Shell degradation index (b)	Estimate	Std Error	z-value	P (> z)
1	2	0.499	0.231	2.158	0.227
	3	0.708	0.254	2.785	0.051
	4	0.796	0.273	2.918	0.035
	5	0.890	0.275	3.234	0.013
	6	0.787	0.328	2.402	0.135
2	3	0.209	0.174	1.204	0.810
	4	0.297	0.194	1.534	0.604
	5	0.391	0.198	1.979	0.318
	6	0.288	0.266	1.083	0.870
3	4	0.088	0.130	0.676	0.981
	5	0.182	0.132	1.379	0.706
	6	0.079	0.221	0.357	0.999
4	5	0.094	0.091	1.030	0.892
	6	– 0.009	0.199	– 0.046	1.000
5	6	– 0.103	0.189	– 0.547	0.993

Table S5.9. Results of the TukeySD post-hoc pairwise comparisons on the relationship between the total abundance of epibionts per mussel and position on the shell (i.e., infested, non-infested, or secondary epibiosis). Significant p-values are underlined.

Position (a)	Position (b)	Estimate	Std Error	z-value	P (> z)
II epibiosis	Infested	– 0.346	0.088	– 3.927	2.510×10^{-4}
	Non-infested	– 0.546	0.088	– 6.230	$< 1 \times 10^{-4}$
Non-infested	Infested	– 0.200	0.058	– 3.467	0.001

5.3.2.1.2. Percent cover of epibionts

Table S5.10. Results of the TukeySD post-hoc pairwise comparisons on the relationship between the percent cover of epibionts per mussel and shell length range (from]30 − 40] to]110 − 120] in mm). Significant p-values are underlined.

Shell length range (a)	Shell length range (b)	Estimate	Std Error	z-value	p(> |z|)
]30 − 40]	]40 − 50]	0.493	0.362	1.363	0.897
	]50 − 60]	1.312	0.317	4.133	< 0.001
	]60 − 70]	1.779	0.316	5.631	< 0.001
	]70 − 80]	1.514	0.317	4.771	< 0.001
	]80 − 90]	1.690	0.298	5.663	< 0.001
	]90 − 100]	1.565	0.326	4.806	< 0.001
	]100 − 110]	1.612	0.406	3.969	0.002
	]110 − 120]	0.735	1.030	0.713	0.998
]40 − 50]	]50 − 60]	0.819	0.300	2.729	0.120
	]60 − 70]	1.286	0.299	4.308	< 0.001
	]70 − 80]	1.021	0.300	3.405	0.016
	]80 − 90]	1.197	0.280	4.276	< 0.001
	]90 − 100]	1.073	0.309	3.473	0.013
	]100 − 110]	1.120	0.393	2.850	0.087
	]110 − 120]	0.242	1.025	0.236	1.000
]50 − 60]	]60 − 70]	0.468	0.243	1.923	0.562
	]70 − 80]	0.203	0.245	0.828	0.995
	]80 − 90]	0.378	0.220	1.720	0.703
	]90 − 100]	0.254	0.256	0.993	0.984
	]100 − 110]	0.301	0.353	0.853	0.994
	]110 − 120]	− 0.577	1.010	− 0.571	1.000
]60 − 70]	]70 − 80]	− 0.265	0.243	− 1.089	0.971
	]80 − 90]	− 0.089	0.218	− 0.410	1.000
	]90 − 100]	− 0.214	0.254	− 0.842	0.995
	]100 − 110]	− 0.167	0.351	− 0.475	1.000
	]110 − 120]	− 1.045	1.010	− 1.035	0.979
]70 − 80]	]80 − 90]	0.0176	0.220	0.798	0.996
	]90 − 100]	0.051	0.256	0.200	1.000
	]100 − 110]	0.098	0.353	0.278	1.000
	]110 − 120]	− 0.780	1.010	− 0.772	0.997
]80 − 90]	]90 − 100]	− 0.124	0.232	− 0.537	1.000
	]100 − 110]	− 0.077	0.336	− 0.231	1.000
	]110 − 120]	− 0.955	1.004	− 0.951	0.988
]90 − 100]	]100 − 110]	0.047	0.360	0.130	1.000
	]110 − 120]	− 0.831	1.013	− 0.820	0.995
]100 − 110]	]110 − 120]	− 0.878	1.041	− 0.843	0.995

Table S5.11. Results of the TukeySD post-hoc pairwise comparisons on the relationship between the mean percent cover in epibionts (in mm^2) and shell degradation index (from 1 to 6, as defined in Ma *et al.*, 2023) interacting with position on the shell (i.e., infested, non-infested). Significant p-values are underlined.

Shell degradation index – Position on the shell (a)	Shell degradation index – Position on the shell (b)	Estimate	Std Error	*t*-value	p-value
1 – infested	2 – infested	– 0.292	689284.7	0.000	1.000
	3 – infested	– 0.504	689284.7	0.000	1.000
	4 – infested	– 0.679	689284.7	0.000	1.000
	5 – infested	– 0.634	689284.7	0.000	1.000
	6 – infested	– 0.915	689284.7	0.000	1.000
	1 – non-infested	– 0.275	689284.7	0.000	1.000
	2 – non-infested	– 2.336	689284.7	0.000	1.000
	3 – non-infested	– 2.066	689284.7	0.000	1.000
	4 – non-infested	– 1.568	689284.7	0.000	1.000
	5 – non-infested	– 1.008	689284.7	0.000	1.000
	6 – non-infested	– 0.295	689284.7	0.000	1.000
2 – infested	3 – infested	– 0.212	0.5	– 0.450	1.000
	4 – infested	– 0.386	0.5	– 0.825	1.000
	5 – infested	– 0.341	0.5	– 0.735	1.000
	6 – infested	– 0.623	0.5	– 1.152	0.992
	1 – non-infested	0.017	0.5	0.037	1.000
	2 – non-infested	– 2.044	0.4	– 4.757	$\underline{1 \times 10^{-4}}$
	3 – non-infested	– 1.774	0.5	– 3.939	<u>0.005</u>
	4 – non-infested	– 1.276	0.5	– 2.731	0.213
	5 – non-infested	– 0.716	0.5	– 1.536	0.930
	6 – non-infested	– 0.003	0.8	– 0.004	1.000
3 – infested	4 – infested	– 0.175	0.3	– 0.643	1.000
	5 – infested	– 0.130	0.3	– 0.498	1.000
	6 – infested	– 0.412	0.4	– 1.087	0.995
	1 – non-infested	0.229	0.4	0.542	1.000
	2 – non-infested	– 1.833	0.3	– 5.937	$\underline{< 1 \times 10^{-4}}$
	3 – non-infested	– 1.563	0.3	– 5.872	$\underline{< 1 \times 10^{-4}}$
	4 – non-infested	– 1.064	0.3	– 3.958	<u>0.005</u>
	5 – non-infested	– 0.504	0.3	– 1.906	0.756
	6 – non-infested	0.208	0.7	0.292	1.000
4 – infested	5 – infested	0.045	0.2	0.282	1.000
	6 – infested	– 0.237	0.3	– 0.742	1.000
	1 – non-infested	0.404	0.4	0.949	0.999
	2 – non-infested	– 1.658	0.3	– 5.691	$\underline{< 1 \times 10^{-4}}$
	3 – non-infested	– 1.388	0.2	– 6.624	$\underline{< 1 \times 10^{-4}}$
	4 – non-infested	– 0.890	0.2	– 4.918	$\underline{1 \times 10^{-4}}$
	5 – non-infested	– 0.329	0.2	– 1.966	0.716
	6 – non-infested	0.383	0.7	0.562	1.000

Table S5.11 (continued).

Shell degradation index – Position on the shell (a)	Shell degradation index – Position on the shell (b)	Estimate	Std Error	*t*-value	p-value
5 – infested	6 – infested	– 0.282	0.3	– 0.938	0.999
	1 – non-infested	0.359	0.4	0.851	1.000
	2 – non-infested	– 1.703	0.3	– 5.938	$< 1 \times 10^{-4}$
	3 – non-infested	– 1.433	0.2	– 7.254	$< 1 \times 10^{-4}$
	4 – non-infested	– 0.935	0.2	– 6.202	$< 1 \times 10^{-4}$
	5 – non-infested	– 0.374	0.1	– 2.864	0.156
	6 – non-infested	0.338	0.7	0.502	1.000
6 – infested	1 – non-infested	0.604	0.5	1.271	0.983
	2 – non-infested	– 1.421	0.4	– 3.564	0.020
	3 – non-infested	– 1.151	0.3	– 3.365	0.038
	4 – non-infested	– 0.653	0.3	– 2.068	0.646
	5 – non-infested	– 0.093	0.3	– 0.302	1.000
	6 – non-infested	0.620	0.7	0.850	1.000
1 – non-infested	2 – non-infested	– 2.061	0.4	– 5.571	$< 1 \times 10^{-4}$
	3 – non-infested	– 1.791	0.4	– 4.446	6×10^{-4}
	4 – non-infested	– 1.293	0.4	– 3.046	0.097
	5 – non-infested	– 0.733	0.4	– 1.738	0.850
	6 – non-infested	– 0.020	0.8	– 0.026	1.000
2 – non-infested	3 – non-infested	0.270	0.3	1.017	0.997
	4 – non-infested	0.768	0.3	2.649	0.254
	5 – non-infested	1.328	0.3	4.597	3×10^{-4}
	6 – non-infested	2.041	0.7	2.825	0.171
3 – non-infested	4 – non-infested	0.498	0.2	2.415	0.397
	5 – non-infested	1.058	0.2	5.225	$< 1 \times 10^{-4}$
	6 – non-infested	1.771	0.7	2.557	0.306
4 – non-infested	5 – non-infested	0.560	0.2	3.511	0.023
	6 – non-infested	1.273	0.7	1.872	0.777
5 – non-infested	6 – non-infested	0.713	0.7	1.053	0.996

5.3.2.1.3. Total biomass of epibionts

Table S5.12. Results of the TukeySD post-hoc pairwise comparisons on the relationship between the total biomass of epibionts per mussel and shell length range (from]30 − 40] to]110 − 120] in mm). Significant p-values are underlined.

Shell length range (a)	Shell length range (b)	Estimate	Std Error	z-value	p(> |z|)
]30 − 40]	]40 − 50]	0.952	0.687	1.387	0.884
	]50 − 60]	1.887	0.613	3.080	0.043
	]60 − 70]	2.879	0.594	4.847	< 0.001
	]70 − 80]	3.286	0.596	5.509	< 0.001
	]80 − 90]	3.706	0.582	6.372	< 0.001
	]90 − 100]	3.002	0.599	5.015	< 0.001
	]100 − 110]	3.231	0.647	4.991	< 0.001
	]110 − 120]	1.563	1.189	1.315	0.912
]40 − 50]	]50 − 60]	0.935	0.467	2.001	0.497
	]60 − 70]	1.927	0.442	4.355	< 0.001
	]70 − 80]	2.333	0.446	5.235	< 0.001
	]80 − 90]	2.753	0.425	6.471	< 0.001
	]90 − 100]	2.050	0.448	4.570	< 0.001
	]100 − 110]	2.278	0.512	4.452	< 0.001
	]110 − 120]	0.611	1.121	0.545	1.000
]50 − 60]	]60 − 70]	0.992	0.316	3.141	0.036
	]70 − 80]	1.398	0.320	4.365	< 0.001
	]80 − 90]	1.818	0.292	6.236	< 0.001
	]90 − 100]	1.115	0.324	3.438	0.014
	]100 − 110]	1.343	0.407	3.299	0.022
	]110 − 120]	− 0.324	1.077	− 0.301	1.000
]60 − 70]	]70 − 80]	0.406	0.283	1.436	0.862
	]80 − 90]	0.826	0.250	3.306	0.021
	]90 − 100]	0.123	0.287	0.428	1.000
	]100 − 110]	0.352	0.379	0.929	0.989
	]110 − 120]	− 1.316	1.067	− 1.233	0.938
]70 − 80]	]80 − 90]	0.420	0.256	1.642	0.728
	]90 − 100]	− 0.284	0.292	− 0.970	0.986
	]100 − 110]	− 0.055	0.382	− 0.144	1.000
	]110 − 120]	− 1.722	1.068	− 1.612	0.767
]80 − 90]	]90 − 100]	− 0.704	0.261	− 2.700	0.124
	]100 − 110]	− 0.475	0.359	− 1.324	0.909
	]110 − 120]	− 2.142	1.060	− 2.021	0.484
]90 − 100]	]100 − 110]	0.229	0.386	0.593	1.000
	]110 − 120]	− 1.439	1.070	− 1.345	0.901
]100 − 110]	]110 − 120]	− 1.667	1.098	− 1.519	0.820

Table S5.13. Results of the TukeySD post-hoc pairwise comparisons on the relationship the total biomass of epibionts per mussel valve and euendolithic infestation levels (from A to E, as defined in Kaehler, 1999). Significant p-values are underlined.

Infestation level (a)	Infestation level (b)	Estimate	Std Error	z-value	P (> z)
A	B	– 0.918	0.462	– 1.984	0.240
	C	0.043	0.521	0.082	1.000
	D	0.486	0.521	0.932	0.866
	E	– 0.182	0.662	– 0.275	0.998
B	C	0.960	0.258	3.720	0.001
	D	1.403	0.257	5.458	< 0.001
	E	0.736	0.483	1.524	0.506
C	D	0.443	0.162	2.730	0.041
	E	– 0.225	0.433	– 0.519	0.983
D	E	– 0.668	0.427	– 1.564	0.479

Table S5.14. Results of the TukeySD post-hoc pairwise comparisons on the relationship between the total biomass of epibionts per mussel valve and shell degradation index (from 1 to 6, as defined in Ma *et al.*, 2023). Significant p-values are underlined.

Shell degradation index (a)	Shell degradation index (b)	Estimate	Std Error	z-value	P (> z)
1	2	2.611	0.645	4.048	< 0.001
	3	2.845	0.754	3.772	0.002
	4	2.165	0.772	2.803	0.045
	5	1.477	0.775	1.907	0.347
	6	1.365	0.869	1.570	0.567
2	3	0.234	0.417	0.560	0.992
	4	– 0.446	0.447	– 0.997	0.900
	5	– 1.134	0.451	– 2.513	0.097
	6	– 1.247	0.600	– 2.079	0.255
3	4	– 0.680	0.252	– 2.702	0.060
	5	– 1.368	0.251	– 5.449	< 0.001
	6	– 1.480	0.466	– 3.175	0.015
4	5	– 0.688	0.166	– 4.151	< 0.001
	6	– 0.800	0.428	– 1.871	0.369
5	6	– 0.113	0.413	– 0.273	1.000

Table S5.15. Results of the TukeySD post-hoc pairwise comparisons on the relationship between the total biomass of epibionts per mussel valve and position on the shell (i.e., infested, non-infested, or secondary epibiosis). Significant p-values are underlined.

Position (a)	Position (b)	Estimate	Std Error	z-value	P (> z)
II epibiosis	Infested	– 0.845	0.222	– 3.800	3.950×10^{-4}
	Non-infested	0.240	0.221	1.086	0.511
Non-infested	Infested	1.085	0.120	9.055	$< 1 \times 10^{-5}$

5.3.2.1.4. Species richness (S)

Table S5.16. Preliminary list of the epibiotic taxa recorded on *Perna* perna mussel shells collected in Kasouga (Eastern Cape, South Africa). Presence of each taxon for each level of euendolithic infestation of the mussel shell (according to Kaehler, 1999), shell degradation index (according to Ma et al., 2023) and position of the epibionts on the mussel shell are indicated by a 'X' in the corresponding column. For the position on the shell, NI: non-infested portion, I: infested portion, and II-E: secondary epibiosis.

	Euendolithic infestation level					Shell degradation index						Position on the shell		
Taxon	**A**	**B**	**C**	**D**	**E**	**0%**	**0-25%**	**25-50%**	**50-75%**	**75-100%**	**100%**	**NI**	**I**	**II-E**
CHLOROPHYTA														
Chlorophyta				X					X	X		X		X
Ulva spp	X	X	X	X	X		X	X	X	X	X	X	X	X
RHODOPHYTA														
Caulacanthus ustulatus		X		X			X			X		X	X	
Corallinales	X	X	X	X	X	X	X	X	X	X	X	X	X	X
Gelidium pristoides	X	X	X	X	X		X	X	X	X	X	X	X	X
Hildenbrandia lecannellieri	X	X	X	X	X		X	X	X	X		X	X	X
Rhodophyta		X	X	X	X			X	X	X		X	X	X
OCHROPHYTA														
Ralfsia verrucosa	X	X	X	X	X	X	X	X	X	X	X	X	X	X
Splachnidium rugosum			X	X	X				X	X		X	X	X
BRYOZOA														
Bryozoa	X	X	X	X	X		X	X	X	X		X	X	X
Electra verticillata	X	X	X	X		X	X	X	X	X		X	X	X
PORIFERA														
Hymeniacidon perlevis				X	X					X	X	X	X	
Porifera				X	X					X	X		X	
ACTINIARIA														
Actiniaria	X	X	X	X			X	X	X	X		X	X	
Bunodactis reynaudi			X	X						X			X	
PLATYHELMINTHES														
Notocomplana erythrotaenia			X	X					X	X	X	X	X	
Platyhelminthes		X								X			X	
NEMERTEA														
Cerebratulus sp.				X						X		X	X	
Nemertea		X	X	X				X	X	X			X	X

Table S5.16 (continued).

	Euendolithic infestation level					Shell degradation index						Position on the shell		
Taxon	**A**	**B**	**C**	**D**	**E**	**0%**	**0-25%**	**25-50%**	**50-75%**	**75-100%**	**100%**	**NI**	**I**	**II-E**
ANNELIDA – POLYCHAETA														
ERRANTIA														
Errantia	X	X	X	X		X	X		X	X	X	X	X	X
Nereididae				X					X				X	X
Phyllodocidae			X						X				X	
Pseudonereis podocirra	X	X	X	X			X	X	X	X		X	X	X
Scoletoma tetraura	X	X	X	X		X		X	X	X	X	X	X	X
Syllidae	X	X	X	X		X	X		X	X	X	X	X	X
SEDENTARIA														
Gunnarea gaimardi	X	X	X	X	X		X	X	X	X	X	X	X	
Orbinidae	X			X			X		X	X	X	X	X	
Sedentaria	X	X	X	X	X	X	X	X	X	X		X	X	X
Spirobranchus kraussii	X	X	X	X	X		X	X	X	X	X	X	X	
Spirorbis spp	X	X	X	X	X	X	X	X	X	X	X	X	X	X
ARTHROPODA														
AMPHIPODA														
Amphipoda	X	X	X	X		X		X	X	X		X	X	
Paramoera capensis	X	X	X	X			X		X	X		X	X	X
Talorchestia sp.				X						X		X		
COPEPODA														
Copepoda				X						X		X		
CIRRIPEDIA														
Balanus amphitrite				X						X			X	
Chthamalus dentatus		X	X	X	X		X	X	X	X	X	X	X	X
Cirripedia (juvenile)	X	X	X	X	X	X	X	X	X	X	X	X	X	X
Notomegabalanus algicola				X						X			X	
Octomeris angulosa			X	X					X	X		X	X	X
Tetraclita serrata	X	X	X	X	X		X	X	X	X	X	X	X	X
ISOPODA														
Cirolana spp		X	X					X	X			X	X	
Ischyromene huttoni				X						X				X

Table S5.16 (continued).

	Euendolithic infestation level					Shell degradation index						Position on the shell		
Taxon	**A**	**B**	**C**	**D**	**E**	**0%**	**0-25%**	**25-50%**	**50-75%**	**75-100%**	**100%**	**NI**	**I**	**II-E**
ECHINODERMATA														
ASTEROIDEA														
Parvulastra exigua			X	X					X	X			X	X
HOLOTHUROIDEA														
Holothuroidea		X						X						X
MOLLUSCA														
BIVALVIA														
Mytilus galloprovincialis	X						X						X	
Perna perna	X	X	X	X	X	X		X	X	X	X	X	X	X
GASTROPODA														
Cymbula granatina	X							X					X	
Cymbula oculus		X		X				X	X	X		X	X	X
Fissurella natalensis				X					X				X	
Gastropoda (eggs)			X	X					X	X		X		
Helcion pectunculus			X							X		X		
Helcion pruinosus		X	X	X					X	X		X	X	
POLYPLACOPHORA														
Acanthochitona garnoti				X						X			X	

Table S5.17. Results of the TukeySD post-hoc pairwise comparisons on the relationship between the epibiotic species richness per mussel and shell length range (from]30 − 40] to]110 − 120] in mm). Significant p-values are underlined.

Shell length range (a)	Shell length range (b)	Estimate	Std Error	z-value	p(> |z|)
]30 − 40]	]40 − 50]	0.137	0.201	0.682	0.999
	]50 − 60]	0.394	0.176	2.233	0.347
	]60 − 70]	0.795	0.169	4.716	< 0.001
	]70 − 80]	0.952	0.167	5.696	< 0.001
	]80 − 90]	1.057	0.162	6.540	< 0.001
	]90 − 100]	1.109	0.167	6.637	< 0.001
	]100 − 110]	1.355	0.181	7.508	< 0.001
	]110 − 120]	1.455	0.327	4.446	< 0.001
]40 − 50]	]50 − 60]	0.257	0.154	1.670	0.734
	]60 − 70]	0.658	0.145	4.541	< 0.001
	]70 − 80]	0.815	0.143	5.692	< 0.001
	]80 − 90]	0.920	0.137	6.729	< 0.001
	]90 − 100]	0.973	0.143	6.789	< 0.001
	]100 − 110]	1.218	0.159	7.680	< 0.001
	]110 − 120]	1.318	0.316	4.175	< 0.001
]50 − 60]	]60 − 70]	0.401	0.109	3.676	0.006
	]70 − 80]	0.558	0.107	5.223	< 0.001
	]80 − 90]	0.663	0.098	6.766	< 0.001
	]90 − 100]	0.716	0.107	6.693	< 0.001
	]100 − 110]	0.961	0.127	7.583	< 0.001
	]110 − 120]	1.061	0.301	3.526	0.010
]60 − 70]	]70 − 80]	0.157	0.093	1.681	0.727
	]80 − 90]	0.262	0.083	3.150	0.036
	]90 − 100]	0.314	0.093	3.364	0.018
	]100 − 110]	0.560	0.116	4.844	< 0.001
	]110 − 120]	0.660	0.297	2.227	0.350
]70 − 80]	]80 − 90]	0.105	0.080	1.309	0.916
	]90 − 100]	0.158	0.091	1.734	0.691
	]100 − 110]	0.403	0.114	3.553	0.009
	]110 − 120]	0.503	0.296	1.702	0.713
]80 − 90]	]90 − 100]	0.053	0.080	0.657	0.999
	]100 − 110]	0.298	0.105	2.837	0.089
	]110 − 120]	0.399	0.293	1.362	0.896
]90 − 100]	]100 − 110]	0.246	0.114	2.164	0.390
	]110 − 120]	0.346	0.296	1.169	0.955
]100 − 110]	]110 − 120]	0.100	0.303	0.330	1.000

Table S5.18. Results of the TukeySD post-hoc pairwise comparisons on the relationship the epibiotic species richness per mussel valve and euendolithic infestation levels (from A to E, as defined in Kaehler, 1999). Significant p-values are underlined.

Infestation level (a)	Infestation level (b)	Estimate	Std Error	z-value	P (> z)
A	B	– 0.032	0.137	– 0.234	0.999
	C	0.246	0.153	1.611	0.455
	D	0.371	0.153	2.421	0.095
	E	0.286	0.203	1.413	0.586
B	C	0.278	0.091	3.064	0.016
	D	0.403	0.091	4.450	< 0.001
	E	0.319	0.161	1.980	0.247
C	D	0.125	0.056	2.221	0.151
	E	0.040	0.144	0.281	0.998
D	E	– 0.084	0.140	– 0.604	0.970

Table S5.19. Results of the TukeySD post-hoc pairwise comparisons on the relationship between the average epibiotic species richness per mussel valve and shell degradation index (from 1 to 6, as defined in Ma *et al.*, 2023). No significant p-values were detected.

Shell degradation index (a)	Shell degradation index (b)	Estimate	Std Error	z-value	P (> z)
1	2	0.369	0.192	1.921	0.347
	3	0.443	0.208	2.132	0.236
	4	0.572	0.218	2.626	0.076
	5	0.508	0.219	2.319	0.159
	6	0.445	0.248	1.795	0.425
2	3	0.073	0.132	0.556	0.992
	4	0.203	0.143	1.417	0.679
	5	0.139	0.145	0.954	0.918
	6	0.075	0.186	0.405	0.998
3	4	0.129	0.089	1.449	0.658
	5	0.065	0.090	0.726	0.974
	6	0.002	0.146	0.015	1.000
4	5	– 0.064	0.058	– 1.108	0.856
	6	– 0.127	0.129	– 0.990	0.906
5	6	– 0.063	0.123	– 0.514	0.995

Table S5.20. Results of the TukeySD post-hoc pairwise comparisons on the relationship between the average epibiotic species richness per mussel valve and position on the shell (i.e., infested, non-infested, or secondary epibiosis). Significant p-values are underlined.

Position (a)	Position (b)	Estimate	Std Error	z-value	P (> z)
II epibiosis	Infested	0.171	0.073	2.342	0.048
	Non-infested	– 0.015	0.074	– 0.204	0.977
Non-infested	Infested	– 0.186	0.045	– 4.117	1.100×10^{-4}

5.3.2.1.5. Shannon–Wiener diversity index (*H'*)

Table S5.21. Results of the TukeySD post-hoc pairwise comparisons on the relationship between the Shannon-Wiener diversity index per mussel and shell length range (from]30 − 40] to]110 − 120] in mm). Significant p-values are underlined.

Shell length range (a)	Shell length range (b)	Estimate	Std Error	*t*-value	p-value
]30 − 40]	]40 − 50]	0.097	0.114	0.852	0.994
	]50 − 60]	0.253	0.103	2.466	0.225
	]60 − 70]	0.525	0.102	5.153	< 0.01
	]70 − 80]	0.700	0.103	6.835	< 0.01
	]80 − 90]	0.780	0.096	8.102	< 0.01
	]90 − 100]	0.774	0.105	7.354	< 0.01
	]100 − 110]	0.945	0.133	7.117	< 0.01
	]110 − 120]	0.999	0.341	2.932	0.072
]40 − 50]	]50 − 60]	0.156	0.095	1.645	0.752
	]60 − 70]	0.428	0.094	4.548	< 0.01
	]70 − 80]	0.603	0.095	6.366	< 0.01
	]80 − 90]	0.683	0.088	7.762	< 0.01
	]90 − 100]	0.677	0.098	6.927	< 0.01
	]100 − 110]	0.848	0.127	6.682	< 0.01
	]110 − 120]	0.902	0.339	2.665	0.143
]50 − 60]	]60 − 70]	0.271	0.080	3.389	0.018
	]70 − 80]	0.447	0.081	5.523	< 0.01
	]80 − 90]	0.527	0.073	7.227	< 0.01
	]90 − 100]	0.521	0.084	6.171	< 0.01
	]100 − 110]	0.692	0.117	5.915	< 0.01
	]110 − 120]	0.746	0.335	2.227	0.356
]60 − 70]	]70 − 80]	0.176	0.080	2.202	0.372
	]80 − 90]	0.256	0.072	3.569	< 0.01
	]90 − 100]	0.249	0.083	2.995	0.060
	]100 − 110]	0.420	0.116	3.619	< 0.01
	]110 − 120]	0.475	0.335	1.418	0.874
]70 − 80]	]80 − 90]	0.080	0.073	1.101	0.969
	]90 − 100]	0.074	0.084	0.877	0.993
	]100 − 110]	0.245	0.117	2.096	0.442
	]110 − 120]	0.299	0.335	0.893	0.992
]80 − 90]	]90 − 100]	– 0.006	0.076	– 0.081	1.000
	]100 − 110]	0.165	0.111	1.480	0.845
	]110 − 120]	0.219	0.333	0.658	0.999
]90 − 100]	]100 − 110]	0.171	0.119	1.435	0.867
	]110 − 120]	0.225	0.336	0.671	0.999
]100 − 110]	]110 − 120]	0.054	0.345	0.157	1.000

Table S5.22. Results of the TukeySD post-hoc pairwise comparisons on the relationship the average Shannon-Wiener diversity index (*H'*) per mussel valve and euendolithic infestation levels (from A to E, as defined in Kaehler, 1999). Significant p-values are underlined.

Infestation level (a)	Infestation level (b)	Estimate	Std Error	z-value	P (> z)
A	B	0.005	0.083	0.056	1.000
	C	0.185	0.096	1.929	0.274
	D	0.349	0.097	3.605	0.003
	E	0.249	0.137	1.817	0.333
B	C	0.181	0.061	2.985	0.021
	D	0.345	0.061	5.640	< 0.001
	E	0.245	0.115	2.130	0.185
C	D	0.164	0.042	3.930	< 0.001
	E	0.064	0.105	0.606	0.970
D	E	– 0.100	0.103	– 0.974	0.850

Table S5.23. Results of the TukeySD post-hoc pairwise comparisons on the relationship between the average Shannon-Wiener diversity (*H'*) per mussel valve and shell degradation index (from 1 to 6, as defined in Ma *et al.*, 2023). No significant p-values were detected.

Shell degradation index (a)	Shell degradation index (b)	Estimate	Std Error	z-value	P (> z)
1	2	0.189	0.102	1.847	0.398
	3	0.237	0.114	2.090	0.262
	4	0.328	0.123	2.678	0.069
	5	0.263	0.124	2.125	0.245
	6	0.249	0.150	1.662	0.518
2	3	0.048	0.079	0.611	0.988
	4	0.140	0.089	1.570	0.581
	5	0.075	0.091	0.819	0.957
	6	0.061	0.124	0.488	0.996
3	4	0.091	0.061	1.492	0.633
	5	0.026	0.062	0.420	0.998
	6	0.012	0.105	0.116	1.000
4	5	– 0.065	0.043	– 1.495	0.632
	6	– 0.079	0.095	– 0.835	0.953
5	6	– 0.014	0.090	– 0.155	1.000

Table 5.24. Results of the TukeySD post-hoc pairwise comparisons on the relationship between the average Shannon-Wiener diversity index (*H'*) per mussel valve and position on the shell (i.e., infested, non-infested, or secondary epibiosis). Significant p-values are underlined.

Position (a)	Position (b)	Estimate	Std Error	z-value	P (> z)
II epibiosis	Infested	0.068	0.058	1.163	0.466
	Non-infested	– 0.024	0.059	– 0.398	0.914
Non-infested	Infested	– 0.092	0.034	– 2.671	0.019

5.3.2.1.6. Simpson's diversity index (λ)

Table S5.25. Results of the TukeySD post-hoc pairwise comparisons on the relationship between the Simpson's diversity index (λ) per mussel and shell length range (from]30 − 40] to]110 − 120] in mm). Significant p-values are underlined.

Shell length range (a)	Shell length range (b)	Estimate	Std Error	z-value	p-value
]30 − 40]	]40 − 50]	0.065	0.057	1.134	0.963
	]50 − 60]	0.144	0.052	2.780	0.104
	]60 − 70]	0.275	0.051	5.364	< 0.01
	]70 − 80]	0.356	0.052	6.899	< 0.01
	]80 − 90]	0.400	0.048	8.252	< 0.01
	]90 − 100]	0.385	0.053	7.272	< 0.01
	]100 − 110]	0.439	0.067	6.574	< 0.01
	]110 − 120]	0.469	0.171	2.738	0.116
]40 − 50]	]50 − 60]	0.079	0.048	1.646	0.752
	]60 − 70]	0.210	0.047	4.435	< 0.01
	]70 − 80]	0.291	0.048	6.099	< 0.01
	]80 − 90]	0.335	0.044	7.561	< 0.01
	]90 − 100]	0.320	0.049	6.510	< 0.01
	]100 − 110]	0.374	0.064	5.860	< 0.01
	]110 − 120]	0.404	0.170	2.375	0.267
]50 − 60]	]60 − 70]	0.131	0.040	3.254	0.026
	]70 − 80]	0.212	0.041	5.209	< 0.01
	]80 − 90]	0.256	0.037	6.982	< 0.01
	]90 − 100]	0.241	0.042	5.686	< 0.01
	]100 − 110]	0.295	0.059	5.022	< 0.01
	]110 − 120]	0.326	0.168	1.933	0.554
]60 − 70]	]70 − 80]	0.081	0.040	2.018	0.494
	]80 − 90]	0.125	0.036	3.470	0.013
	]90 − 100]	0.110	0.042	2.633	0.152
	]100 − 110]	0.164	0.058	2.813	0.096
	]110 − 120]	0.195	0.168	1.156	0.959
]70 − 80]	]80 − 90]	0.044	0.037	1.206	0.947
	]90 − 100]	0.029	0.042	0.692	0.999
	]100 − 110]	0.083	0.059	1.419	0.874
	]110 − 120]	0.114	0.168	0.675	0.999
]80 − 90]	]90 − 100]	− 0.015	0.038	− 0.383	1.000
	]100 − 110]	0.039	0.056	0.702	0.999
	]110 − 120]	0.070	0.167	0.416	1.000
]90 − 100]	]100 − 110]	0.054	0.060	0.901	0.991
	]110 − 120]	0.084	0.169	0.500	1.000
]100 − 110]	]110 − 120]	0.030	0.174	0.175	1.000

Table S5.26. Results of the TukeySD post-hoc pairwise comparisons on the relationship the average Simpson's diversity index (λ) per mussel valve and euendolithic infestation levels (from A to E, as defined in Kaehler, 1999). Significant p-values are underlined.

Infestation level (a)	Infestation level (b)	Estimate	Std Error	z-value	P (> z)
A	B	– 0.000	0.046	– 0.005	1.000
	C	0.095	0.053	1.801	0.341
	D	0.190	0.053	3.565	0.003
	E	0.128	0.075	1.707	0.397
B	C	0.095	0.033	2.864	0.029
	D	0.190	0.034	5.660	< 0.001
	E	0.129	0.063	2.042	0.220
C	D	0.095	0.023	4.133	< 0.001
	E	0.033	0.058	0.579	0.975
D	E	– 0.061	0.056	– 1.084	0.793

Table S5.27. Results of the TukeySD post-hoc pairwise comparisons on the relationship between the average Simpson's diversity index (λ) per mussel valve and shell degradation index (from 1 to 6, as defined in Ma *et al.*, 2023). No significant p-values were detected.

Shell degradation index (a)	Shell degradation index (b)	Estimate	Std Error	z-value	P (> z)
1	2	0.113	0.056	2.006	0.304
	3	0.143	0.062	2.292	0.173
	4	0.185	0.067	2.757	0.055
	5	0.154	0.068	2.268	0.182
	6	0.160	0.082	1.943	0.339
2	3	0.030	0.043	0.696	0.979
	4	0.073	0.049	1.495	0.631
	5	0.042	0.050	0.836	0.953
	6	0.047	0.068	0.696	0.979
3	4	0.043	0.034	1.274	0.771
	5	0.011	0.034	0.337	0.999
	6	0.017	0.058	0.300	1.000
4	5	– 0.031	0.024	– 1.308	0.752
	6	– 0.025	0.052	– 0.491	0.996
5	6	0.006	0.049	0.117	1.000

5.3.2.2. Multivariate analyses on epibiotic communities

5.3.2.2.1. Abundance of epibiotic communities

5.3.2.2.1.1. Shell length size

Table S5.28. Detailed results of the ANOVA (Wald-like test) on the many Generalized Linear Model (GLM) on the relationship between the abundance of each higher taxonomical group and shell length range (from $]30-40]$ to $]110-120]$ in mm). Significant p-values are underlined.

Higher taxonomical group	Source of variation	Wald	Pr(>Wald)
Bryozoa	Length range	5.002	0.006
Cirripedia	Length range	7.706	0.001
Gastropoda	Length range	2.521	0.829
Ochrophyta	Length range	4.588	0.029
Sedentaria	Length range	7.503	0.001
Errantia	Length range	3.239	0.492
Copepoda	Length range	0.273	0.953
Bivalvia	Length range	4.363	0.048
Platyhelminthes	Length range	1.869	0.829
Rhodophyta	Length range	8.407	0.001
Chlorophyta	Length range	2.833	0.742
Amphipoda	Length range	3.360	0.423
Isopoda	Length range	1.452	0.829
Nemertea	Length range	0.403	0.953
Actiniaria	Length range	2.160	0.829
Porifera	Length range	1.415	0.829
Holothuroidea	Length range	0.315	0.953
Asteroidea	Length range	0.294	0.953
Polyplacophora	Length range	0.315	0.953

Table S5.29. Detailed results of the ANOVA (Wald-like test) on the many Generalized Linear Model (GLM) on the relationship between the abundance of each epibiotic species and shell length range (from $]30-40]$ to $]110-120]$ in mm). Significant p-values are underlined.

Epibiotic species	Source of variation	Wald	Pr(>Wald)
Bryozoa			
Electra verticillata	Length range	2.400	0.950
Bryozoa	Length range	3.175	0.598
Cirripedia			
Balanus amphitrite	Length range	0.273	1.000
Chthamalus dentatus	Length range	4.064	0.098
Notomegabalanus algicola	Length range	0.315	1.000
Octomeris angulosa	Length range	2.253	0.955
Tetraclita serrata	Length range	8.947	0.001
Cirripedia (juvenile)	Length range	6.141	0.001
Cirripedia (traces)	Length range	2.718	0.826
Gastropoda			
Cymbula granatina	Length range	0.273	1.000
Cymbula oculus	Length range	0.653	0.999
Fissurella natalensis	Length range	0.314	1.000
Helcion pectunculus	Length range	0.273	1.00
Helcion pruinosus	Length range	0.854	0.999
Gastropoda (eggs)	Length range	0.353	1.000
Ochrophyta			
Ralfsia verrucosa	Length range	4.559	0.031
Splachnidium rugosum	Length range	0.346	1.000
Sedentaria			
Gunnarea gaimardi	Length range	1.463	0.998
Spirobranchus kraussii	Length range	3.739	0.208
Spirorbis sp.	Length range	6.320	0.001
Orbinidae	Length range	1.549	0.998
Sedentaria	Length range	2.053	0.981
Errantia			
Scoletoma tetraura	Length range	2.211	0.967
Pseudonereis podocirra	Length range	1.054	0.999
Nereididae	Length range	1.021	0.999
Phyllodocidae	Length range	0.337	1.000
Syllidae	Length range	1.852	0.986
Errantia	Length range	2.13	0.973
Copepoda	Length range	0.273	1.000
Bivalvia			
Mytilus galloprovincialis	Length range	0.394	1.000
Perna perna	Length range	4.302	0.062
Platyhelminthes			
Notocomplana erythrotaenia	Length range	1.946	0.985
Platyhelminthes	Length range	0.315	1.000

Table S5.29 (continued).

Epibiotic species	Source of variation	Wald	Pr(>Wald)
Rhodophyta			
Caulacanthus ustulatus	Length range	0.564	1.000
Gelidium pristoides	Length range	1.565	0.998
Hildenbrandia lecannellieri	Length range	3.360	0.495
Corallinales	Length range	6.245	0.001
Rhodophyta	Length range	2.889	0.826
Chlorophyta			
Chlorophyta	Length range	0.753	0.999
Ulva sp.	Length range	2.845	0.826
Amphipoda			
Paramoera capensis	Length range	2.691	0.826
Talorchestia sp.	Length range	0.273	1.000
Amphipoda	Length range	2.209	0.967
Isopoda			
Cirolana sp.	Length range	0.363	1.000
Ischyromene huttoni	Length range	1.196	0.998
Nemertea			
Cerebratulus sp.	Length range	0.294	1.000
Nemertea	Length range	1.048	0.999
Actiniaria			
Bunodactis reynaudi	Length range	0.876	0.999
Actiniaria	Length range	1.757	0.986
Porifera			
Hymeniacidon perlevis	Length range	0.306	1.000
Porifera	Length range	1.894	0.985
Holothuroidea	Length range	0.315	1.000
Asteroidea			
Parvulastra exigua	Length range	0.294	1.000
Polyplacophora			
Acanthochitona garnoti	Length range	0.315	1.000

Table S5.30. Results of the TukeySD post-hoc pairwise comparisons on the relationship between the abundance in Cirripedia per mussel and shell length range (from]30 − 40] to]110 − 120] in mm). Significant p-values are underlined.

Shell length range (a)	Shell length range (b)	Estimate	Std Error	z-value	p-value
]30 − 40]	]40 − 50]	0.306	0.278	1.101	0.970
	]50 − 60]	0.333	0.258	1.293	0.923
	]60 − 70]	0.115	0.265	0.433	1.000
	]70 − 80]	0.612	0.249	2.458	0.227
	]80 − 90]	0.817	0.236	3.466	0.013
	]90 − 100]	1.142	0.249	4.580	< 0.001
	]100 − 110]	1.316	0.297	4.438	< 0.001
	]110 − 120]	0.122	0.677	1.658	0.747
]40 − 50]	]50 − 60]	0.027	0.230	0.116	1.000
	]60 − 70]	− 0.192	0.239	− 0.803	0.996
	]70 − 80]	0.305	0.221	1.385	0.890
	]80 − 90]	0.510	0.206	2.482	0.216
	]90 − 100]	0.835	0.221	3.779	0.004
	]100 − 110]	1.010	0.273	3.695	0.006
	]110 − 120]	0.815	0.667	1.223	0.944
]50 − 60]	]60 − 70]	− 0.218	0.214	− 1.019	0.981
	]70 − 80]	0.279	0.194	1.437	0.868
	]80 − 90]	0.483	0.177	2.737	0.119
	]90 − 100]	0.809	0.194	4.158	< 0.001
	]100 − 110]	0.983	0.252	3.896	0.003
	]110 − 120]	0.788	0.658	1.197	0.950
]60 − 70]	]70 − 80]	0.497	0.204	2.440	0.236
	]80 − 90]	0.702	0.187	3.749	0.005
	]90 − 100]	1.027	0.204	5.031	< 0.001
	]100 − 110]	1.201	0.260	4.624	< 0.001
	]110 − 120]	1.007	0.661	1.522	0.826
]70 − 80]	]80 − 90]	0.205	0.164	1.251	0.936
	]90 − 100]	0.530	0.183	2.899	0.077
	]100 − 110]	0.704	0.243	2.894	0.078
	]110 − 120]	0.510	0.655	0.778	0.997
]80 − 90]	]90 − 100]	0.325	0.164	1.980	0.525
	]100 − 110]	0.500	0.230	2.174	0.390
	]110 − 120]	0.305	0.650	0.469	1.000
]90 − 100]	]100 − 110]	0.174	0.244	0.716	0.998
	]110 − 120]	− 0.020	0.655	− 0.031	1.000
]100 − 110]	]110 − 120]	− 0.195	0.675	− 0.289	1.000

Table S5.31. Results of the TukeySD post-hoc pairwise comparisons on the relationship between the abundance in *Tetraclita serrata* (Cirripedia) per mussel and shell length range (from]40 − 50] to]110 − 120] in mm). No significant p-values were detected.

Shell length range (a)	Shell length range (b)	Estimate	Std Error	z-value	p-value
]40 − 50]	]50 − 60]	0.865	0.798	1.084	0.951
	]60 − 70]	1.204	0.766	1.572	0.730
	]70 − 80]	0.956	0.760	1.257	0.896
	]80 − 90]	1.179	0.733	1.608	0.707
	]90 − 100]	1.591	0.734	2.166	0.327
	]100 − 110]	1.903	0.746	2.551	0.146
	]110 − 120]	-7.564×10^{-16}	1.135	0.000	1.000
]50 − 60]	]60 − 70]	0.339	0.438	0.774	0.993
	]70 − 80]	0.091	0.428	0.212	1.000
	]80 − 90]	0.314	0.377	0.831	0.989
	]90 − 100]	0.726	0.380	1.909	0.497
	]100 − 110]	1.038	0.403	2.579	0.137
	]110 − 120]	− 0.865	0.946	− 0.915	0.981
]60 − 70]	]70 − 80]	− 0.249	0.364	− 0.682	0.997
	]80 − 90]	− 0.025	0.303	− 0.083	1.000
	]90 − 100]	0.387	0.307	1.260	0.895
	]100 − 110]	0.699	0.334	2.093	0.373
	]110 − 120]	− 1.204	0.919	− 1.310	0.874
]70 − 80]	]80 − 90]	0.223	0.289	0.772	0.993
	]90 − 100]	0.635	0.293	2.171	0.325
	]100 − 110]	0.948	0.321	2.951	0.050
	]110 − 120]	− 0.956	0.914	− 1.045	0.959
]80 − 90]	]90 − 100]	0.412	0.212	1.945	0.472
	]100 − 110]	0.724	0.250	2.901	0.058
	]110 − 120]	− 1.179	0.892	− 1.322	0.867
]90 − 100]	]100 − 110]	0.313	0.254	1.231	0.906
	]110 − 120]	− 1.591	0.893	− 1.782	0.587
]100 − 110]	]110 − 120]	− 1.903	0.903	− 2.109	0.363

Table S5.32. Results of the TukeySD post-hoc pairwise comparisons on the relationship between the abundance of juvenile Cirripedia (barnacles) per mussel and shell length range (from]30 − 40] to]110 − 120] in mm). Significant p-values are underlined.

Shell length range (a)	Shell length range (b)	Estimate	Std Error	z-value	p-value
]30 − 40]	]40 − 50]	0.267	0.278	0.959	0.987
	]50 − 60]	0.183	0.258	0.709	0.998
	]60 − 70]	− 0.071	0.288	− 0.248	1.000
	]70 − 80]	0.427	0.255	1.674	0.734
	]80 − 90]	0.618	0.240	2.574	0.174
	]90 − 100]	0.894	0.256	3.492	0.012
	]100 − 110]	0.754	0.317	2.380	0.265
	]110 − 120]	1.087	0.914	1.189	0.951
]40 − 50]	]50 − 60]	− 0.084	0.231	− 0.364	1.000
	]60 − 70]	− 0.338	0.263	− 1.284	0.925
	]70 − 80]	0.160	0.227	0.705	0.998
	]80 − 90]	0.351	0.210	1.670	0.737
	]90 − 100]	0.628	0.228	2.747	0.114
	]100 − 110]	0.487	0.295	1.652	0.748
	]110 − 120]	0.820	0.907	0.904	0.991
]50 − 60]	]60 − 70]	− 0.254	0.242	− 1.050	0.977
	]70 − 80]	0.244	0.202	1.207	0.947
	]80 − 90]	0.435	0.183	2.379	0.265
	]90 − 100]	0.711	0.203	3.496	0.012
	]100 − 110]	0.571	0.276	2.069	0.458
	]110 − 120]	0.904	0.901	1.003	0.983
]60 − 70]	]70 − 80]	0.498	0.239	2.086	0.447
	]80 − 90]	0.689	0.223	3.095	0.043
	]90 − 100]	0.966	0.240	4.025	0.001
	]100 − 110]	0.825	0.304	2.716	0.124
	]110 − 120]	1.158	0.910	1.273	0.928
]70 − 80]	]80 − 90]	0.191	0.179	1.067	0.974
	]90 − 100]	0.467	0.200	2.339	0.288
	]100 − 110]	0.326	0.273	1.195	0.950
	]110 − 120]	0.660	0.900	0.733	0.998
]80 − 90]	]90 − 100]	0.277	0.180	1.538	0.815
	]100 − 110]	0.136	0.259	0.525	1.000
	]110 − 120]	0.469	0.896	0.254	1.000
]90 − 100]	]100 − 110]	− 0.141	0.274	− 0.514	1.000
	]110 − 120]	0.192	0.900	0.214	1.000
]100 − 110]	]110 − 120]	0.333	0.919	0.362	1.000

Table S5.33. Results of the TukeySD post-hoc pairwise comparisons on the relationship between the abundance in Sedentaria per mussel and shell length range (from]30 − 40] to]110 − 120] in mm). Significant p-values are underlined.

Shell length range (a)	Shell length range (b)	Estimate	Std Error	z-value	p-value
]30 − 40]	]40 − 50]	0.470	0.838	0.561	1.000
	]50 − 60]	1.396	0.749	1.864	0.596
	]60 − 70]	2.125	0.731	2.905	0.071
	]70 − 80]	2.121	0.731	2.903	0.072
	]80 − 90]	2.308	0.718	3.214	0.029
	]90 − 100]	2.197	0.724	3.034	0.049
	]100 − 110]	2.660	0.755	3.525	0.010
	]110 − 120]	2.303	1.058	2.177	0.376
]40 − 50]	]50 − 60]	0.926	0.527	1.759	0.670
	]60 − 70]	1.655	0.501	3.302	0.021
	]70 − 80]	1.651	0.500	3.302	0.022
	]80 − 90]	1.838	0.482	3.816	0.003
	]90 − 100]	1.727	0.490	3.523	0.010
	]100 − 110]	2.190	0.534	4.098	0.001
	]110 − 120]	1.833	0.914	2.066	0.493
]50 − 60]	]60 − 70]	0.729	0.333	2.190	0.368
	]70 − 80]	0.824	0.331	2.190	0.368
	]80 − 90]	0.912	0.303	3.014	0.053
	]90 − 100]	0.801	0.316	2.533	0.185
	]100 − 110]	1.264	0.381	3.317	0.020
	]110 − 120]	0.906	0.833	1.088	0.970
]60 − 70]	]70 − 80]	− 0.005	0.288	− 0.016	1.000
	]80 − 90]	0.183	0.256	0.717	0.998
	]90 − 100]	0.072	0.272	0.266	1.000
	]100 − 110]	0.535	0.345	1.552	0.801
	]110 − 120]	0.178	0.817	0.217	1.000
]70 − 80]	]80 − 90]	0.188	0.253	0.743	0.998
	]90 − 100]	0.077	0.269	0.285	1.000
	]100 − 110]	0.540	0.343	1.574	0.789
	]110 − 120]	0.182	0.816	0.223	1.000
]80 − 90]	]90 − 100]	− 0.111	0.234	− 0.476	1.000
	]100 − 110]	0.352	0.316	1.113	0.966
	]110 − 120]	− 0.006	0.806	− 0.007	1.000
]90 − 100]	]100 − 110]	0.463	0.329	1.408	0.875
	]110 − 120]	0.105	0.811	0.130	1.000
]100 − 110]	]110 − 120]	− 0.358	0.838	− 0.427	1.000

Table S5.34. Results of the TukeySD post-hoc pairwise comparisons on the relationship between the abundance of *Spirorbis* spp. (Sedentaria) per mussel and shell length range (from]30 − 40] to]110 − 120] in mm). Significant p-values are underlined.

Shell length range (a)	Shell length range (b)	Estimate	Std Error	z-value	p-value
]30 − 40]	]40 − 50]	0.474	0.917	0.517	1.000
	]50 − 60]	1.390	0.833	1.669	0.732
	]60 − 70]	2.153	0.815	2.640	0.145
	]70 − 80]	2.226	0.818	2.722	0.118
	]80 − 90]	0.284	0.802	2.849	0.085
	]90 − 100]	2.480	0.816	3.039	<u>0.049</u>
	]100 − 110]	2.731	0.840	3.250	<u>0.026</u>
	]110 − 120]	2.155	1.101	1.957	0.530
]40 − 50]	]50 − 60]	0.916	0.548	1.672	0.730
	]60 − 70]	1.678	0.521	3.220	<u>0.028</u>
	]70 − 80]	1.751	0.525	3.336	<u>0.020</u>
	]80 − 90]	1.809	0.499	3.624	<u>0.007</u>
	]90 − 100]	2.005	0.522	3.840	<u>0.003</u>
	]100 − 110]	2.256	0.559	4.035	<u>0.001</u>
	]110 − 120]	1.680	0.905	1.857	0.603
]50 − 60]	]60 − 70]	0.763	0.351	2.0172	0.382
	]70 − 80]	0.386	0.357	2.343	0.278
	]80 − 90]	0.894	0.318	2.814	0.093
	]90 − 100]	1.090	0.353	3.090	<u>0.042</u>
	]100 − 110]	1.341	0.405	3.307	<u>0.022</u>
	]110 − 120]	0.765	0.819	0.934	0.989
]60 − 70]	]70 − 80]	0.073	0.315	0.232	1.000
	]80 − 90]	0.131	0.270	0.486	1.000
	]90 − 100]	0.327	0.310	1.054	0.976
	]100 − 110]	0.578	0.369	1.566	0.795
	]110 − 120]	0.002	0.801	0.002	1.000
]70 − 80]	]80 − 90]	0.058	0.277	0.210	1.000
	]90 − 100]	0.254	0.316	0.803	0.996
	]100 − 110]	0.505	0.374	1.350	0.900
	]110 − 120]	− 0.071	0.804	− 0.088	1.000
]80 − 90]	]90 − 100]	0.196	0.271	0.722	0.998
	]100 − 110]	0.447	0.337	1.326	0.908
	]110 − 120]	− 0.129	0.787	− 0.164	1.000
]90 − 100]	]100 − 110]	0.251	0.370	0.678	0.999
	]110 − 120]	− 0.325	0.802	− 0.405	1.000
]100 − 110]	]110 − 120]	− 0.576	0.827	− 0.697	0.998

Table S5.35. Results of the TukeySD post-hoc pairwise comparisons on the relationship between the abundance in Rhodophyta (red algae) per mussel and shell length range (from]30 − 40] to]110 − 120] in mm). No significant p-values were detected.

Shell length range (a)	Shell length range (b)	Estimate	Std Error	z-value	p-value
]30 − 40]	]40 − 50]	0.182	0.826	0.221	1.000
	]50 − 60]	– 0.270	0.687	– 0.393	1.000
	]60 − 70]	0.131	0.638	0.205	1.000
	]70 − 80]	0.658	0.618	1.065	0.972
	]80 − 90]	0.757	0.609	1.243	0.932
	]90 − 100]	0.720	0.614	1.174	0.951
	]100 − 110]	0.215	0.649	0.331	1.00
	]110 − 120]	– 0.105	0.963	– 0.109	1.000
]40 − 50]	]50 − 60]	– 0.452	0.662	– 0.683	0.999
	]60 − 70]	– 0.051	0.612	– 0.084	1.000
	]70 − 80]	0.476	0.590	0.806	0.996
	]80 − 90]	0.575	0.581	0.989	0.982
	]90 − 100]	0.538	0.586	0.918	0.989
	]100 − 110]	0.033	0.623	0.053	1.000
	]110 − 120]	– 0.288	0.945	– 0.304	1.000
]50 − 60]	]60 − 70]	0.401	0.405	0.989	0.983
	]70 − 80]	0.928	0.373	2.490	0.197
	]80 − 90]	1.027	0.358	2.872	0.076
	]90 − 100]	0.990	0.365	2.710	0.116
	]100 − 110]	0.485	0.422	1.149	0.956
	]110 − 120]	0.164	0.827	0.199	1.000
]60 − 70]	]70 − 80]	0.527	0.273	1.933	0.536
	]80 − 90]	0.626	0.252	2.487	0.197
	]90 − 100]	0.589	0.263	2.243	0.326
	]100 − 110]	0.084	0.337	0.249	1.000
	]110 − 120]	– 0.236	0.787	– 0.300	1.000
]70 − 80]	]80 − 90]	0.099	0.195	0.508	1.000
	]90 − 100]	0.062	0.209	0.298	1.000
	]100 − 110]	– 0.443	0.297	– 1.492	0.828
	]110 − 120]	– 0.764	0.771	– 0.991	0.982
]80 − 90]	]90 − 100]	– 0.037	0.180	– 0.204	1.000
	]100 − 110]	– 0.542	0.278	– 1.951	0.522
	]110 − 120]	– 0.862	0.764	– 1.130	0.960
]90 − 100]	]100 − 110]	– 0.505	0.288	– 1.755	0.663
	]110 − 120]	– 0.826	0.767	– 1.076	0.970
]100 − 110]	]110 − 120]	– 0.320	0.796	– 0.403	1.000

5.3.2.2.1.2. Euendolithic infestation and shell degradation

Table S5.36. Detailed results of the ANOVA (Wald-like test) on the many Generalized Linear Model (GLM) on the relationship between the abundance of each higher taxonomical group and euendolithic infestation levels (from A to E, as defined in Kaehler, 1999) and shell degradation index (from 1 to 6, as defined in Ma *et al.*, 2023). Significant p-values are underlined.

Higher taxonomic group	Source of variation	Wald	Pr(>Wald)
Bryozoa	Infestation	3.108	0.307
	Degradation	3.066	0.199
Cirripedia	Infestation	3.843	0.069
	Degradation	4.526	<u>0.028</u>
Gastropoda	Infestation	1.839	0.952
	Degradation	1.693	0.871
Ochrophyta	Infestation	4.793	<u>0.014</u>
	Degradation	7.204	<u>0.001</u>
Sedentaria	Infestation	2.051	0.941
	Degradation	3.539	0.162
Errantia	Infestation	1.340	0.952
	Degradation	3.123	0.194
Copepoda	Infestation	0.220	0.967
	Degradation	0.214	0.942
Bivalvia	Infestation	1.564	0.952
	Degradation	2.784	0.297
Platyhelminthes	Infestation	1.486	0.952
	Degradation	1.945	0.791
Rhodophyta	Infestation	5.455	<u>0.014</u>
	Degradation	4.952	<u>0.028</u>
Chlorophyta	Infestation	2.193	0.905
	Degradation	1.476	0.895
Amphipoda	Infestation	1.653	0.952
	Degradation	2.617	0.327
Isopoda	Infestation	0.812	0.967
	Degradation	0.517	0.942
Nemertea	Infestation	0.511	0.967
	Degradation	0.443	0.942
Actiniaria	Infestation	0.802	0.967
	Degradation	1.059	0.895
Porifera	Infestation	1.935	0.941
	Degradation	1.597	0.871
Holothuroidea	Infestation	0.318	0.967
	Degradation	0.290	0.942
Asteroidea	Infestation	0.423	0.967
	Degradation	0.513	0.942
Polyplacophora	Infestation	0.220	0.967
	Degradation	0.214	0.942

Table S5.37. Detailed results of the ANOVA (Wald-like test) on the many Generalized Linear Model (GLM) on the relationship between the abundance of each epibiotic species and euendolithic infestation levels (from A to E, as defined in Kaehler, 1999) and shell degradation index (from 1 to 6, as defined in Ma *et al.*, 2023). Significant p-values are underlined.

Epibiotic species	Source of variation	Wald	Pr(>Wald)
Bryozoa			
Electra verticillata	Infestation	1.556	1.000
	Degradation	2.464	0.888
Bryozoa	Infestation	3.022	0.440
	Degradation	1.907	0.985
Cirripedia			
Balanus amphitrite	Infestation	0.220	1.000
	Degradation	0.214	1.000
Chthamalus dentatus	Infestation	2.535	0.781
	Degradation	3.273	0.357
Notomegabalanus algicola	Infestation	0.220	1.000
	Degradation	0.214	1.000
Octomeris angulosa	Infestation	1.323	1.000
	Degradation	0.349	1.000
Tetraclita serrata	Infestation	5.871	<u>0.001</u>
	Degradation	2.249	0.961
Juvenile barnacle	Infestation	2.596	0.766
	Degradation	4.019	<u>0.042</u>
Cirripedia (traces)	Infestation	1.267	1.000
	Degradation	1.578	0.998
Gastropoda			
Cymbula granatina	Infestation	0.353	1.000
	Degradation	0.226	1.000
Cymbula oculus	Infestation	1.166	1.000
	Degradation	0.583	1.000
Fissurella natalensis	Infestation	0.220	1.000
	Degradation	0.317	1.000
Helcion pectunculus	Infestation	0.276	1.000
	Degradation	0.267	1.000
Helcion pruinosus	Infestation	0.721	1.000
	Degradation	1.384	1.000
Gastropoda (eggs)	Infestation	0.532	1.000
	Degradation	0.771	1.000
Ochrophyta			
Ralfsia verrucosa	Infestation	4.049	<u>0.027</u>
	Degradation	7.322	<u>0.001</u>
Splachnidium rugosum	Infestation	3.501	0.140
	Degradation	0.772	1.000

Table S5.37 (continued).

Epibiotic species	Source of variation	Wald	Pr(>Wald)
Sedentaria			
Gunnarea gaimardi	Infestation	0.621	1.000
	Degradation	1.785	0.993
Spirobranchus kraussii	Infestation	2.144	0.968
	Degradation	2.164	0.963
Spirorbis sp.	Infestation	2.856	0.575
	Degradation	3.051	0.533
Orbinidae	Infestation	0.375	1.000
	Degradation	1.444	1.000
Sedentaria	Infestation	2.683	0.680
	Degradation	1.581	0.997
Errantia			
Scoletoma tetraura	Infestation	1.093	1.000
	Degradation	1.248	1.000
Pseudonereis podocirra	Infestation	0.463	1.000
	Degradation	1.259	1.000
Nereididae	Infestation	0.249	1.000
	Degradation	0.384	1.000
Phyllodocidae	Infestation	0.297	1.000
	Degradation	0.397	1.000
Syllidae	Infestation	1.473	1.000
	Degradation	2.746	0.736
Errantia	Infestation	1.760	0.999
	Degradation	2.401	0.915
Copepoda	Infestation	0.220	1.000
	Degradation	0.214	1.000
Bivalvia			
Mytilus galloprovincialis	Infestation	0.353	1.000
	Degradation	0.191	1.000
Perna perna	Infestation	1.449	1.000
	Degradation	2.274	0.961
Platyhelminthes			
Notocomplana erythrotaenia	Infestation	0.256	1.000
	Degradation	2.116	0.963
Platyhelminthes	Infestation	0.318	1.000
	Degradation	0.395	1.000

Table S5.37 (continued).

Epibiotic species	Source of variation	Wald	Pr(>Wald)
Rhodophyta			
Caulacanthus ustulatus	Infestation	0.835	1.000
	Degradation	0.346	1.000
Gelidium pristoides	Infestation	1.913	0.995
	Degradation	2.829	0.694
Hildenbrandia lecannellieri	Infestation	1.689	0.999
	Degradation	6.573	0.001
Corallinales	Infestation	4.447	0.009
	Degradation	2.763	0.736
Rhodophyta	Infestation	1.836	0.996
	Degradation	0.583	1.000
Chlorophyta			
Ulva sp.	Infestation	2.194	0.968
	Degradation	1.432	1.000
Chlorophyta	Infestation	0.239	1.000
	Degradation	0.760	1.000
Amphipoda			
Paramoera capensis	Infestation	1.096	1.000
	Degradation	2.056	0.963
Talorchestia sp.	Infestation	0.220	1.000
	Degradation	0.214	1.000
Amphipoda	Infestation	2.612	0.752
	Degradation	0.800	1.000
Isopoda			
Cirolana sp.	Infestation	0.490	1.000
	Degradation	0.360	1.000
Ischyromene huttoni	Infestation	0.263	1.000
	Degradation	0.295	1.000
Nemertea			
Cerebratulus sp.	Infestation	0.239	1.000
	Degradation	0.248	1.000
Nemertea	Infestation	0.818	1.000
	Degradation	0.532	1.000
Actiniaria			
Bunodactis reynaudi	Infestation	0.697	1.000
	Degradation	0.255	1.000
Actiniaria	Infestation	1.350	1.000
	Degradation	0.836	1.000

Table S5.37 (continued).

Epibiotic species	Source of variation	Wald	Pr(>Wald)
Porifera			
Hymeniacidon perlevis	Infestation	2.974	0.475
	Degradation	0.265	1.000
Porifera	Infestation	0.986	1.000
	Degradation	1.368	1.000
Holothuroidea	Infestation	0.318	1.000
	Degradation	0.290	1.000
Asteroidea			
Parvulastra exigua	Infestation	0.423	1.000
	Degradation	0.513	1.000
Polyplacophora			
Acanthochitona garnoti	Infestation	0.220	1.000
	Degradation	0.214	1.000

Table S5.38. Results of the TukeySD post-hoc pairwise comparisons on the relationship the average abundance in Ochrophyta per mussel valve and euendolithic infestation levels (from A to E, as defined in Kaehler, 1999). Significant p-values are underlined.

Infestation level (a)	Infestation level (b)	Estimate	Std Error	z-value	P (> z)
A	B	0.488	0.313	1.562	0.494
	C	0.797	0.371	2.150	0.180
	D	0.972	0.376	2.587	0.064
	E	1.219	0.417	2.926	<u>0.025</u>
B	C	0.309	0.226	1.366	0.623
	D	0.484	0.231	2.095	0.202
	E	0.731	0.293	2.495	0.082
C	D	0.175	0.154	1.137	0.767
	E	0.423	0.238	1.775	0.361
D	E	0.248	0.224	1.105	0.785

Table S5.39. Results of the TukeySD post-hoc pairwise comparisons on the relationship between the average abundance in Ochrophyta per mussel valve and shell degradation index (from 1 to 6, as defined in Ma *et al.*, 2023). Significant p-values are underlined.

Shell degradation index (a)	Shell degradation index (b)	Estimate	Std Error	z-value	P (> z)
1	2	0.179	0.756	0.237	1.000
	3	– 0.174	0.788	– 0.220	1.000
	4	– 0.242	0.801	– 0.302	1.000
	5	– 0.597	0.802	– 0.744	0.970
	6	– 0.724	0.909	– 0.797	0.960
2	3	– 0.353	0.238	– 1.484	0.625
	4	– 0.421	0.276	– 1.529	0.594
	5	– 0.776	0.277	– 2.802	<u>0.045</u>
	6	– 0.903	0.510	– 1.772	0.429
3	4	– 0.068	0.198	– 0.346	1.000
	5	– 0.423	0.196	– 2.154	0.217
	6	– 0.550	0.469	– 1.173	0.818
4	5	– 0.355	0.150	– 2.372	0.135
	6	– 0.482	0.454	– 1.063	0.872
5	6	– 0.127	0.446	– 0.286	1.000

Table S5.40. Results of the TukeySD post-hoc pairwise comparisons on the relationship the average abundance of *Ralfsia verrucosa* (Ochrophyta) per mussel valve and euendolithic infestation levels (from A to E, as defined in Kaehler, 1999). No significant p-values were detected.

Infestation level (a)	Infestation level (b)	Estimate	Std Error	z-value	P (> z)
A	B	0.488	0.313	1.560	0.494
	C	0.809	0.371	2.183	0.168
	D	0.955	0.376	2.541	0.072
	E	1.107	0.431	2.570	0.067
B	C	0.321	0.226	1.420	0.587
	D	0.468	0.231	2.2020	0.234
	E	0.620	0.313	1.979	0.252
C	D	0.146	0.154	0.947	0.865
	E	0.299	0.263	1.135	0.767
D	E	0.152	0.252	0.604	0.971

Table S5.41. Results of the TukeySD post-hoc pairwise comparisons on the relationship between the average abundance of *Ralfsia verrucosa* (Ochrophyta) per mussel valve and shell degradation index (from 1 to 6, as defined in Ma *et al.*, 2023). Significant p-values are underlined.

Shell degradation index (a)	Shell degradation index (b)	Estimate	Std Error	z-value	P (> z)
1	2	0.179	0.756	0.237	1.000
	3	– 0.168	0.788	– 0.213	1.000
	4	– 0.268	0.801	– 0.335	0.999
	5	– 0.596	0.802	– 0.744	0.970
	6	– 0.635	0.912	– 0.697	0.977
2	3	– 0.346	0.238	– 1.459	0.642
	4	– 0.447	0.276	– 1.622	0.530
	5	– 0.775	0.278	– 2.790	<u>0.046</u>
	6	– 0.814	0.516	– 1.579	0.560
3	4	– 0.101	0.198	– 0.508	0.995
	5	– 0.429	0.198	– 2.161	0.214
	6	– 0.468	0.476	– 0.983	0.905
4	5	– 0.328	0.151	– 2.180	0.206
	6	– 0.367	0.461	– 0.797	0.959
5	6	– 0.039	0.456	– 0.085	1.000

Table S5.42. Results of the TukeySD post-hoc pairwise comparisons on the relationship between the mean abundance in Rhodophyta and shell degradation index (from 1 to 6, as defined in Ma *et al.*, 2023) interacting with euendolithic infestation levels (from A to E, as defined in Kaehler, 1999). Significant p-values are underlined.

Shell degradation index	Infestation levels (contrast)	Estimate	Std Error	*z*-value	p-value
1	NA	NA	NA	NA	NA
2	A – B	1.239	0.538	2.304	0.144
3	A – B	– 0.312	0.560	– 0.558	0.9810
	A – C	– 0.396	0.630	– 0.628	0.971
	A – D	– 0.470	0.641	– 0.734	0.949
	A – E	– 0.470	1.040	– 0.452	0.991
	B – C	– 0.084	0.397	– 0.210	1.000
	B – D	– 0.158	0.414	– 0.381	0.996
	B – E	– 0.158	0.918	– 0.172	1.000
	C – D	– 0.074	0.505	– 0.147	1.000
	C – E	– 0.074	0.962	– 0.077	1.000
	D – E	0.000	0.969	0.000	1.000
4	B – C	0.462	0.403	1.146	0.782
	B – D	– 0.208	0.353	– 0.589	0.977
	B – E	– 1.912	0.545	– 3.056	<u>0.004</u>
	C – D	– 0.670	0.259	– 2.591	0.072
	C – E	– 2.374	0.489	– 4.851	<u>< 0.001</u>
	D – E	– 1.704	0.449	– 3.794	<u>0.001</u>
5	B – C	– 0.693	1.156	– 0.600	0.975
	B – D	– 0.611	1.147	– 0.532	0.984
	B – E	– 0.811	1.222	– 0.664	0.964
	C – D	0.083	0.230	0.406	0.994
	C – E	– 0.118	0.467	– 0.252	0.999
	D – E	– 0.200	0.445	– 0.451	0.992
6	C – D	– 0.560	1.190	– 0.470	0.990
	C – E	0.000	1.399	0.000	1.000
	D – E	0.560	0.873	0.641	0.968

5.3.2.2.2. Percent cover of epibiotic communities

Table S5.43. Results of the SIMPER analysis on epibiotic percent cover showing the most influential higher taxonomical groups discriminating among shell length sizes (from]30 − 40] to]110 − 120] in mm). Cut-off for low contribution: 70%. Significant p-values are underlined.

Higher taxonomical group	Average a	Average b	Cumulative contr. (%)	p-value
[30 − 40[*vs* [40 − 50[				
Cirripedia	0.253	0.366	33.3	0.234
Ochrophyta	0.380	0.419	51.5	0.906
Rhodophyta	0.149	0.217	64.7	1.000
Sedentaria	0.050	0.88	77.9	0.932
[30 − 40[*vs* [50 − 60[				
Ochrophyta	0.380	1.198	30.1	0.040
Cirripedia	0.253	0.403	54.0	0.886
Sedentaria	0.050	0.209	70.1	0.528
[30 − 40[*vs* [60 − 70[				
Ochrophyta	0.380	1.074	26.8	0.026
Cirripedia	0.253	0.628	51.0	0.620
Sedentaria	0.050	0.436	66.8	0.339
Rhodophyta	0.149	0.377	78.8	0.999
[30 − 40[*vs* [70 − 80[				
Rhodophyta	0.149	0.815	24.2	0.403
Cirripedia	0.253	0.484	47.0	0.926
Ochrophyta	0.380	0.621	66.1	0.767
Sedentaria	0.050	0.287	78.6	0.928
[30 − 40[*vs* [80 − 90[				
Cirripedia	0.253	0.611	25.9	0.464
Rhodophyta	0.149	0.974	51.4	0.164
Ochrophyta	0.380	0.495	67.7	0.921
Sedentaria	0.050	0.349	79.8	0.924
[30 − 40[*vs* [90 − 100[				
Cirripedia	0.253	0.936	30.6	0.042
Rhodophyta	0.149	0.711	53.7	0.423
Ochrophyta	0.380	0.502	70.8	0.886
[30 − 40[*vs* [100 − 110[				
Cirripedia	0.253	1.477	42.3	0.001
Sedentaria	0.050	0.350	58.8	0.355
Rhodophyta	0.149	0.454	73.2	0.990
[30 − 40[*vs* [110 − 120[				
Cirripedia	0.253	1.180	38.7	0.048
Rhodophyta	0.149	0.746	64.9	0.296
Sedentaria	0.050	0.395	82.4	0.274
[40 − 50[*vs* [50 − 60[				
Ochrophyta	0.419	1.198	30.2	0.007
Cirripedia	0.366	0.403	57.0	0.586
Sedentaria	0.088	0.209	75.3	0.159

Table S5.43 (continued).

Higher taxonomical group	Average a	Average b	Cumulative contribution (%)	p-value
[40 − 50[*vs* [60 − 70[				
Ochrophyta	0.419	1.074	27.3	0.014
Cirripedia	0.366	0.628	53.0	0.381
Sedentaria	0.088	0.436	70.1	0.115
[40 − 50[*vs* [70 − 80[				
Cirripedia	0.366	0.484	25.2	0.729
Rhodophyta	0.217	0.815	50.0	0.265
Ochrophyta	0.419	0.621	69.6	0.761
Sedentaria	0.088	0.287	84.1	0.735
[40 − 50[*vs* [80 − 90[				
Cirripedia	0.366	0.611	27.6	0.186
Rhodophyta	0.217	0.974	540	0.068
Ochrophyta	0.419	0.495	70.7	0.939
[40 − 50[*vs* [90 − 100[				
Cirripedia	0.366	0.936	32.4	0.003
Rhodophyta	0.217	0.711	56.4	0.299
Ochrophyta	0.419	0.502	74.0	0.882
[40 − 50[*vs* [100 − 110[				
Cirripedia	0.366	1.477	0.439	0.001
Sedentaria	0.088	0.350	61.5	0.225
Rhodophyta	0.217	0.454	76.9	0.997
[40 − 50[*vs* [110 − 120[				
Cirripedia	0.366	1.180	40.1	0.031
Rhodophyta	0.217	0.746	67.9	0.255
Sedentaria	0.088	0.395	85.6	0.302
[50 − 60[*vs* [60 − 70[				
Ochrophyta	1.198	1.074	33.6	0.001
Cirripedia	0.403	0.628	55.0	0.996
Sedentaria	0.209	0.436	72.3	0.056
[50 − 60[*vs* [70 − 80[				
Ochrophyta	0.621	1.198	28.1	0.001
Rhodophyta	0.815	0.217	49.8	0.757
Cirripedia	0.484	0.403	70.2	1.000
[50 − 60[*vs* [80 − 90[				
Ochrophyta	1.198	0.495	25.4	0.003
Rhodophyta	0.217	0.974	48.4	0.296
Cirripedia	0.403	0.611	71.4	0.968
[50 − 60[*vs* [90 − 100[				
Cirripedia	0.403	0.936	27.6	0.132
Ochrophyta	1.198	0.502	53.6	0.005
Rhodophyta	0.217	0.711	74.5	0.855

Table S5.43 (continued).

Higher taxonomical group	Average a	Average b	Cumulative contribution (%)	p-value
[50 − 60[*vs* [100 − 110[				
Cirripedia	0.403	1.477	37.2	0.001
Ochrophyta	1.198	0.259	59.6	0.358
Sedentaria	0.209	0.350	76.3	0.204
[50 − 60[*vs* [110 − 120[				
Cirripedia	0.403	1.180	34.2	0.088
Rhodophyta	0.217	0.746	57.8	0.421
Ochrophyta	1.198	0.000	75.9	0.541
[60 − 70[*vs* [70 − 80[				
Ochrophyta	1.074	0.621	25.9	0.002
Cirripedia	0.628	0.484	47.0	0.999
Rhodophyta	0.377	0.815	67.2	0.915
Sedentaria	0.436	0.287	82.5	0.367
[60 − 70[*vs* [80 − 90[				
Ochrophyta	1.074	0.495	23.6	0.022
Cirripedia	0.628	0.611	46.7	0.980
Rhodophyta	0.377	0.974	68.1	0.719
Sedentaria	0.436	0.349	83.2	0.368
[60 − 70[*vs* [90 − 100[				
Cirripedia	0.628	0.936	26.9	0.194
Ochrophyta	1.074	0.502	51.2	0.041
Rhodophyta	0.377	0.711	70.5	0.971
[60 − 70[*vs* [100 − 110[				
Cirripedia	0.628	1.477	34.9	0.001
Ochrophyta	1.074	0.259	56.0	0.451
Sedentaria	0.436	0.350	72.3	0.265
[60 − 70[*vs* [110 − 120[				
Cirripedia	0.628	1.180	32.1	0.207
Rhodophyta	0.377	0.746	53.8	0.537
Ochrophyta	1.074	0.000	71.8	0.559
[70 − 80[*vs* [80 − 90[				
Rhodophyta	0.815	0.974	29.2	0.001
Cirripedia	0.484	0.611	51.9	0.999
Ochrophyta	0.621	0.495	70.0	0.987
[70 − 80[*vs* [90 − 100[				
Rhodophyta	0.815	0.711	26.8	0.013
Cirripedia	0.484	0.936	53.5	0.471
Ochrophyta	0.621	0.502	0.723	0.924
[70 − 80[*vs* [100 − 110[				
Cirripedia	0.484	1.477	35.1	0.001
Rhodophyta	0.815	0.454	56.8	0.768
Sedentaria	0.287	0.350	72.2	0.533

Table S5.43 (continued).

Higher taxonomical group	Average a	Average b	Cumulative contribution (%)	p-value
[70 − 80[*vs* [110 − 120[				
Cirripedia	0.484	1.181	33.4	0.172
Rhodophyta	0.815	0.746	61.7	0.274
Sedentaria	0.287	0.395	77.7	0.475
[80 − 90[*vs* [90 − 100[				
Cirripedia	0.612	0.936	27.9	0.141
Rhodophyta	0.974	0.711	55.7	0.001
Ochrophyta	0.495	0.502	72.6	1.000
[80 − 90[*vs* [100 − 110[				
Cirripedia	0.611	1.477	35.7	0.001
Rhodophyta	0.974	0.453	59.0	0.546
Sedentaria	0.349	0.350	74.5	0.569
[80 − 90[*vs* [110 − 120[				
Cirripedia	0.611	1.180	33.8	0.203
Rhodophyta	0.974	0.746	63.2	0.250
Sedentaria	0.349	0.395	79.5	0.442
[90 − 100[*vs* [100 − 110[				
Cirripedia	0.936	1.477	38.7	0.001
Rhodophyta	0.711	0.454	60.2	0.905
Sedentaria	0.392	0.350	77.2	0.384
[90 − 100[*vs* [110 − 120[				
Cirripedia	0.936	1.180	37.0	0.144
Rhodophyta	0.711	0.746	64.5	0.397
Sedentaria	0.392	0.395	81.6	0.461
[100 − 110[*vs* [110 − 120[				
Cirripedia	1.477	1.180	43.5	0.074
Rhodophyta	0.454	0.746	68.2	0.552
Sedentaria	0.350	0.395	85.2	0.505

Table S5.44. Results of the SIMPER analysis on epibiotic percent cover showing the most influential higher taxonomical groups discriminating among euendolithic infestation levels (from A to E, as defined by Kaehler, 1999). Cut-off for low contribution: 70%. Significant p-values are underlined.

Higher taxonomical group	Average a	Average b	Cumulative contribution (%)	p-value
A *vs* B				
Ochrophyta	0.746	1.086	29.6	<u>0.002</u>
Rhodophyta	0.455	0.649	51.0	0.801
Cirripedia	0.243	0.413	70.5	1.000
A *vs* C				
Cirripedia	0.243	0.692	24.5	0.813
Ochrophyta	0.746	0.600	46.6	0.307
Rhodophyta	0.455	0.586	65.4	0.991
Sedentaria	0.231	0.404	82.1	0.141
A *vs* D				
Cirripedia	0.243	0.773	26.0	0.448
Rhodophyta	0.455	0.696	49.0	0.405
Ochrophyta	0.746	0.497	69.7	0.555
Sedentaria	0.231	0.295	83.9	0.728
A *vs* E				
Ochrophyta	0.746	1.120	33.7	<u>0.005</u>
Rhodophyta	0.455	0.725	53.7	0.710
Cirripedia	0.243	0.602	73.4	0.964
B *vs* C				
Ochrophyta	1.086	0.600	25.6	<u>0.001</u>
Cirripedia	0.413	0.692	48.7	0.987
Rhodophyta	0.649	0.586	69.9	0.886
Sedentaria	0.279	0.404	86.4	0.071
B *vs* D				
Cirripedia	0.413	0.773	24.7	0.872
Ochrophyta	1.086	0.497	49.0	<u>0.012</u>
Rhodophyta	0.649	0.696	73.3	0.068
B *vs* E				
Ochrophyta	1.086	1.120	34.5	<u>0.002</u>
Rhodophyta	0.649	0.725	56.6	0.584
Cirripedia	0.413	0.602	75.8	0.988
C *vs* D				
Cirripedia	0.692	0.773	27.8	<u>0.010</u>
Rhodophyta	0.586	0.696	50.6	0.622
Ochrophyta	0.600	0.497	68.7	1.000
Sedentaria	0.404	0.295	84.7	0.165
C *vs* E				
Ochrophyta	0.600	1.120	28.9	<u>0.023</u>
Cirripedia	0.692	0.602	51.4	0.889
Rhodophyta	0.586	0.725	71.8	0.761

Table S5.44 (continued).

Higher taxonomical group	Average a	Average b	Cumulative contribution (%)	p-value
D *vs* E				
Ochrophyta	0.497	1.120	27.8	0.029
Cirripedia	0.773	0.602	51.5	0.797
Rhodophyta	0.696	0.725	74.4	0.469

Table S5.45. Results of the SIMPER analysis on epibiotic percent cover showing the most influential higher taxonomical groups discriminating among shell degradation indexes (from 1 to 6, as defined by Ma et al., 2023). Cut-off for low contribution: 70%. Significant p-values are underlined.

Higher taxonomical group	Average a	Average b	Cumulative contribution (%)	p-value
1 *vs* 2				
Ochrophyta	0.280	1.861	40.2	<u>0.001</u>
Cirripedia	0.261	0.184	60.5	0.977
Sedentaria	0.103	0.292	74.2	0.723
1 *vs* 3				
Rhodophyta	0.037	1.055	24.8	0.328
Ochrophyta	0.280	0.907	48.8	0.264
Cirripedia	0.261	0.535	71.6	0.879
1 *vs* 4				
Cirripedia	0.261	0.672	25.7	0.496
Rhodophyta	0.037	0.902	49.9	0.308
Sedentaria	0.103	0.351	66.9	0.212
Ochrophyta	0.280	0.589	83.6	0.850
1 *vs* 5				
Cirripedia	0.261	0.734	31.7	0.070
Ochrophyta	0.280	0.477	49.2	0.880
Sedentaria	0.103	0.301	65.4	0.408
Rhodophyta	0.037	0.4555	80.7	0.997
1 *vs* 6				
Cirripedia	0.261	1.022	34.4	<u>0.040</u>
Rhodophyta	0.037	0.440	52.6	0.880
Sedentaria	0.103	0.407	69.4	0.398
Ochrophyta	0.280	0.275	83.1	0946
2 *vs* 3				
Ochrophyta	1.861	0.907	37.8	<u>0.001</u>
Rhodophyta	0.447	1.055	61.2	0.374
Cirripedia	0.184	0.535	77.3	1.000
2 *vs* 4				
Ochrophyta	1.861	0.589	33.1	<u>0.001</u>
Rhodophyta	0.447	0.902	55.5	0.440
Cirripedia	0.184	0.672	74.1	1.000
2 *vs* 5				
Ochrophyta	1.861	0.477	34.7	<u>0.001</u>
Cirripedia	0.184	0.734	57.3	0.966
Rhodophyta	0.447	0.455	73.5	0.999
2 *vs* 6				
Ochrophyta	1.861	0.275	31.8	<u>0.004</u>
Cirripedia	0.184	1.022	57.0	0.481
Rhodophyta	0.447	0.440	74.3	0.935

Table S5.45 (continued).

Higher taxonomical group	Average a	Average b	Cumulative contribution (%)	p-value
3 *vs* 4				
Rhodophyta	1.055	0.902	29.6	0.001
Ochrophyta	0.907	0.589	51.8	0.237
Cirripedia	0.535	0.672	73.2	1.000
3 *vs* 5				
Rhodophyta	1.055	0.455	25.2	0.022
Cirripedia	0.535	0.734	50.2	0.743
Ochrophyta	0.907	0.477	72.7	0.120
3 *vs* 6				
Cirripedia	0.535	1.022	27.7	0.239
Rhodophyta	1.055	0.440	53.4	0.151
Ochrophyta	0.907	0.275	73.1	0.646
4 *vs* 5				
Cirripedia	0.672	0.734	26.8	0.177
Rhodophyta	0.902	0.455	51.4	0.019
Ochrophyta	0.589	0.477	68.9	1.000
Sedentaria	0.351	0.301	84.7	0.217
4 *vs* 6				
Cirripedia	0.672	1.022	29.4	0.136
Rhodophyta	0.902	0.440	54.3	0.251
Sedentaria	0.351	0.407	70.7	0.340
5 *vs* 6				
Cirripedia	0.734	1.022	33.2	0.012
Rhodophyta	0.455	0.440	53.0	0.888
Sedentaria	0.301	0.407	69.2	0.377
Ochrophyta	0.477	0.275	83.8	0.988

Table S5.46. Results of the SIMPER analysis on epibiotic percent cover showing the most influential higher taxonomical groups discriminating among position of the epibionts on the mussel shell (i.e., infested, non-infested). Cut-off for low contribution: 70%. Significant p-values are underlined.

Higher taxonomical group	Average a	Average b	Cumulative contribution (%)	p-value
Infested *vs* Non-infested				
Cirripedia	0.600	0.694	25.6	0.004
Rhodophyta	0.507	0.764	48.2	0.029
Ochrophyta	0.157	1.111	69.5	0.001
Sedentaria	0.470	0.180	85.4	0.001

Table S5.47. Results of the SIMPER analysis on epibiotic percent cover showing the most influential species discriminating among shell length sizes (from]30 − 40] to]110 − 120] in mm). Cut-off for low contribution: 70%. Significant p-values are underlined.

Species	Average a	Average b	Cumulative contribution (%)	p-value
[30 − 40[*vs* [40 − 50[				
Cirripedia (juvenile)	0.223	0.195	26.747	<u>0.001</u>
Ralfsia verrucosa	0.380	0.419	44.255	0.893
Spirorbis sp.	0.035	0.062	54.588	0.081
Corallinales	0.121	0.123	63.869	0.920
Perna perna	0.062	0.043	70.259	<u>0.038</u>
[30 − 40[*vs* [50 − 60[				
Ralfsia verrucosa	1.198	0.380	29.289	<u>0.021</u>
Cirripedia (juvenile)	0.143	0.223	47.486	<u>0.001</u>
Spirorbis sp.	0.089	0.035	57.995	<u>0.013</u>
Corallinales	0.032	0.121	63.586	1.000
Electra verticillata	0.089	0.085	68.842	0.270
Hildenbrandia lecannellieri	0.185	0.000	73.725	0.964
[30 − 40[*vs* [60 − 70[				
Ralfsia verrucosa	0.380	1.074	25.829	<u>0.032</u>
Cirripedia (juvenile)	0.223	0.075	38.703	<u>0.005</u>
Spirorbis sp.	0.035	0.149	47.728	<u>0.032</u>
Tetraclita serrata	0.000	0.429	55.446	1.000
Corallinales	0.121	0.147	62.870	0.964
Perna perna	0.062	0.103	68.708	<u>0.008</u>
Bryozoa	0.000	0.151	73.811	0.058
[30 − 40[*vs* [70 − 80[				
Ralfsia verrucosa	0.380	0.651	18.228	0.714
Cirripedia (juvenile)	0.223	0.146	32.837	<u>0.001</u>
Corallinales	0.121	0.414	47.337	0.104
Electra verticillata	0.085	0.132	0.541	<u>0.049</u>
Hildenbrandia lecannellieri	0.000	0.296	60.364	0.912
Tetraclita serrata	0.000	0.267	66.509	1.000
Spirorbis sp.	0.035	0.088	0.724	0.746
[30 − 40[*vs* [80 − 90[				
Ralfsia verrucosa	0.380	0.495	15.239	0.907
Cirripedia (juvenile)	0.223	0.154	28.639	<u>0.001</u>
Corallinales	0.121	0.306	40.586	0.303
Tetraclita serrata	0.000	0.425	51.102	0.967
Hildenbrandia lecannellieri	0.000	0.515	60.357	0.452
Electra verticillata	0.085	0.072	66.115	0.104
Spirorbis sp.	0.035	0.102	71.069	0.905

Table S5.47 (continued).

Species	Average a	Average b	Cumulative contribution (%)	p-value
[30 − 40[*vs* [90 − 100[				
Tetraclita serrata	0.000	0.774	18.167	0.097
Ralfsia verrucosa	0.380	0.502	0.340	0.857
Cirripedia (juvenile)	0.223	0.152	46.148	0.014
Corallinales	0.121	0.275	58.225	0.287
Hildenbrandia lecannellieri	0.000	0.375	66.550	0.632
Spirorbis sp.	0.035	0.123	73.880	0.252
[30 − 40[*vs* [100 − 110[				
Tetraclita serrata	0.000	1.257	29.548	0.001
Cirripedia (juvenile)	0.223	0.237	41.988	0.012
Ralfsia verrucosa	0.380	0.259	52.628	0.993
Corallinales	0.121	0.275	62.314	0.719
Spirobranchus kraussii	0.000	0.213	70.373	0.049
[30 − 40[*vs* [110 − 120[				
Corallinales	0.121	0.746	23.595	0.026
Tetraclita serrata	0.000	0.787	39.160	0.393
Chtamalus dentatus	0.030	0.502	52.940	0.003
Cirripedia (juvenile)	0.223	0.152	64.866	0.109
Spirobranchus kraussii	0.00	0.239	76.599	0.079
[40 − 50[*vs* [50 − 60[				
Ralfsia verrucosa	0.419	1.198	29.206	0.006
Cirripedia (juvenile)	0.195	0.143	47.746	0.001
Spirorbis sp.	0.062	0.089	59.993	0.001
Tetraclita serrata	0.152	0.254	68.013	0.999
Corallinales	0.123	0.032	74.369	1.000
[40 − 50[*vs* [60 − 70[				
Ralfsia verrucosa	0.419	1.074	26.244	0.009
Cirripedia (juvenile)	0.195	0.075	38.525	0.004
Tetraclita serrata	0.152	0.429	49.023	0.981
Spirorbis sp.	0.062	0.149	59.042	0.001
Corallinales	0.123	0.147	67.040	0.968
Bryozoa	0.009	0.151	72.597	0.015
[40 − 50[*vs* [70 − 80[				
Ralfsia verrucosa	0.419	0.651	18.519	0.733
Corallinales	0.123	0.414	33.286	0.031
Cirripedia (juvenile)	0.195	0.146	47.834	0.001
Tetraclita serrata	0.152	0.267	57.026	0.999
Spirorbis sp.	0.062	0.088	64.709	0.176
Hildenbrandia lecannellieri	0.094	0.296	72.267	0.839

Table S5.47 (continued).

Species	Average a	Average b	Cumulative contribution (%)	p-value
[40 − 50[*vs* [80 − 90[				
Ralfsia verrucosa	0.419	0.495	15.718	0.942
Tetraclita serrata	0.152	0.425	28.774	0.806
Cirripedia (juvenile)	0.195	0.154	41.765	0.001
Corallinales	0.123	0.306	54.107	0.196
Hildenbrandia lecannellieri	0.094	0.515	64.486	0.288
Spirorbis sp.	0.062	0.102	70.845	0.552
[40 − 50[*vs* [90 − 100[				
Tetraclita serrata	0.152	0.774	20.295	0.013
Ralfsia verrucosa	0.419	0.502	36.708	0.884
Corallinales	0.123	0.275	49.229	0.196
Cirripedia (juvenile)	0.195	0.152	61.186	0.006
Hildenbrandia lecannellieri	0.094	0.375	70.708	0.484
[40 − 50[*vs* [100 − 110[				
Tetraclita serrata	0.152	1.257	31.067	0.001
Cirripedia (juvenile)	0.195	0.237	43.698	0.008
Ralfsia verrucosa	0.419	0.259	54.982	0.999
Corallinales	0.123	0.275	65.158	0.709
Spirobranchus kraussii	0.000	0.213	0.732	0.020
[40 − 50[*vs* [110 − 120[				
Corallinales	0.123	0.746	23.818	0.023
Tetraclita serrata	0.152	0.787	42.345	0.296
Chtamalus dentatus	0.024	0.502	54.902	0.003
Spirobranchus kraussii	0.000	0.239	67.025	0.058
Cirripedia (juvenile)	0.195	0.152	77.904	0.180
[50 − 60[*vs* [60 − 70[				
Ralfsia verrucosa	1.198	1.074	32.177	0.001
Tetraclita serrata	0.254	0.429	41.906	1.000
Spirorbis sp.	0.089	0.149	51.097	0.001
Cirripedia (juvenile)	0.143	0.075	59.797	0.622
Hildenbrandia lecannellieri	0.185	0.180	65.700	0.993
Corallinales	0.032	0.147	71.205	1.000
[50 − 60[*vs* [70 − 80[				
Ralfsia verrucosa	0.198	0.651	26.617	0.001
Corallinales	0.032	0.414	37.938	0.457
Cirripedia (juvenile)	0.143	0.146	48.371	0.035
Hildenbrandia lecannellieri	0.185	0.296	57.041	0.722
Tetraclita serrata	0.254	0.267	65.236	1.000
Spirorbis sp.	0.089	0.088	72.932	0.083

Table S5.47 (continued).

Species	Average a	Average b	Cumulative contribution (%)	p-value
[50 − 60[*vs* [80 − 90[				
Ralfsia verrucosa	1.198	0.495	23.910	0.004
Tetraclita serrata	0.254	0.425	35.549	0.992
Hildenbrandia lecannellieri	0.185	0.515	46.630	0.087
Cirripedia (juvenile)	0.143	0.154	56.168	0134
Corallinales	0.032	0.306	65.369	0.950
Spirorbis sp.	0.089	0.102	71.916	0.462
[50 − 60[*vs* [90 − 100[				
Ralfsia verrucosa	1.198	0.502	24.408	0.006
Tetraclita serrata	0.254	0.774	42.365	0.036
Hildenbrandia lecannellieri	0.185	0.375	52.514	0.304
Corallinales	0.032	0.275	61.804	0.908
Cirripedia (juvenile)	0.143	0.152	70.695	0.469
[50 − 60[*vs* [100 − 110[				
Tetraclita serrata	0.254	1.257	27.057	0.001
Ralfsia verrucosa	1.198	0.259	47.635	0.378
Cirripedia (juvenile)	0.143	0.237	57.092	0.271
Spirobranchus kraussii	0.102	0.213	65.722	0.003
Corallinales	0.032	0.275	73.060	0.987
[50 − 60[*vs* [110 − 120[				
Corallinales	0.032	0.746	19.414	0.054
Ralfsia verrucosa	1.198	0.000	35.282	0.563
Tetraclita serrata	0.254	0.787	51.057	0.385
Chthamalus dentatus	0.032	0.502	62.854	0.003
Spirobranchus kraussii	0.102	0.239	74.091	0.084
[60 − 70[*vs* [70 − 80[				
Ralfsia verrucosa	1.074	0.651	24.424	0.001
Corallinales	0.147	0.414	35.664	0.376
Tetraclita serrata	0.429	0.267	45.886	1.000
Spirorbis sp.	0.149	0.088	52.999	0.176
Cirripedia (juvenile)	0.075	0.146	60.020	0.998
Hildenbrandia lecannellieri	0.180	0.296	66.888	0.957
Bryozoa	0.151	0.065	71.855	0.005
[60 − 70[*vs* [80 − 90[				
Ralfsia verrucosa	1.074	0.495	22.086	0.024
Tetraclita serrata	0.429	0.425	34.954	0.938
Corallinales	0.147	0.306	44.306	0.948
Hildenbrandia lecannellieri	0.180	0.515	53.582	0.472
Cirripedia (juvenile)	0.075	0.154	60.075	1.000
Spirorbis sp.	0.149	0.102	66.431	0.504
Bryozoa	0.151	0.071	71.380	0.003

Table S5.47 (continued).

Species	Average a	Average b	Cumulative contribution (%)	p-value
[60 − 70[*vs* [90 − 100[				
Ralfsia verrucosa	1.074	0.502	22.516	0.048
Tetraclita serrata	0.429	0.774	40.453	0.022
Corallinales	0.147	0.275	49.769	0.931
Hildenbrandia lecannellieri	0.180	0.375	0.582	0.719
Spirorbis sp.	0.149	0.123	65.399	0.132
Cirripedia (juvenile)	0.075	0.152	71.645	1.000
[60 − 70[*vs* [100 − 110[				
Tetraclita serrata	0.429	1.257	25.401	0.001
Ralfsia verrucosa	1.074	0.259	44.693	0.497
Corallinales	0.147	0.275	52.660	0.967
Cirripedia (juvenile)	0.075	0.237	59.653	0.978
Spirorbis sp.	0.149	0.109	66.457	0.375
Spirobranchus kraussii	0.051	0.213	72.781	0.084
[60 − 70[*vs* [110 − 120[				
Corallinales	0.147	0.746	17.479	0.110
Tetraclita serrata	0.429	0.787	34.110	0.366
Ralfsia verrucosa	1.074	0.000	0.498	0.579
Chthamalus dentatus	0.033	0.502	60.520	0.015
Spirobranchus kraussii	0.051	0.239	68.624	0.215
Spirorbis sp.	0.149	0.254	75.719	0.369
[70 − 80[*vs* [80 − 90[				
Ralfsia verrucosa	0.651	0.495	16.689	0.980
Corallinales	0.414	0.306	30.699	0.004
Tetraclita serrata	0.267	0.425	42.576	0.996
Hildenbrandia lecannellieri	0.296	0.515	54.294	0.013
Juvenile barnacle	0.146	0.154	62.448	0.890
Electra verticillata	0.132	0.072	68.431	0.001
Spirorbis sp.	0.088	0.102	73.264	0.999
[70 − 80[*vs* [90 − 100[				
Tetraclita serrata	0.267	0.774	17.279	0.039
Ralfsia verrucosa	0.651	0.502	34.451	0.928
Corallinales	0.414	0.275	0.483	0.010
Hildenbrandia lecannellieri	0.296	0.375	59.047	0.139
Cirripedia (juvenile)	0.146	0.152	66.736	0.965
Spirorbis sp.	0.088	0.123	72.938	0.705

Table S5.47 (continued).

Species	Average a	Average b	Cumulative contribution (%)	p-value
[70 − 80[*vs* [100 − 110[				
Tetraclita serrata	0.267	1.257	25.352	0.001
Ralfsia verrucosa	0.651	0.259	38.636	0.996
Corallinales	0.414	0.275	51.108	0.173
Cirripedia (juvenile)	0.146	0.237	59.412	0.732
Spirobranchus kraussii	0.072	0.213	66.380	0.035
Hildenbrandia lecannellieri	0.296	0.088	72.170	0.971
[70 − 80[*vs* [110 − 120[				
Corallinales	0.414	0.746	20.929	0.065
Tetraclita serrata	0.267	0.787	37.016	0.428
Chthamalus dentatus	0.064	0.502	48.975	0.013
Ralfsia verrucosa	0.651	0.000	58.453	0.940
Spirobranchus kraussii	0.072	0.239	67.620	0.146
Cirripedia (juvenile)	0.146	0.152	74.550	0.694
[80 − 90[*vs* [90 − 100[				
Tetraclita serrata	0.425	0.774	18.963	0.002
Ralfsia verrucosa	0.495	0.502	34.159	0.999
Hildenbrandia lecannellieri	0.515	0.375	47.087	0.001
Corallinales	0.306	0.275	59.008	0.159
Cirripedia (juvenile)	0.154	0.152	66.314	0.999
Spirobranchus kraussii	0.126	0.167	72.13	0.059
[80 − 90[*vs* [100 − 110[				
Tetraclita serrata	0.425	0.257	26.166	0.001
Ralfsia verrucosa	0.495	0.259	37.591	1.000
Corallinales	0.306	0.275	48.343	0.574
Hildenbrandia lecannellieri	0.515	0.088	56.802	0.689
Cirripedia (juvenile)	0.154	0.237	64.930	0.818
Spirobranchus kraussii	0.126	0.213	72.627	0.006
[80 − 90[*vs* [110 − 120[				
Corallinales	0.306	0.746	19.056	0.079
Tetraclita serrata	0.425	0.787	36.899	0.327
Chthamalus dentatus	0.063	0.502	48.559	0.015
Spirobranchus kraussii	0.126	0.239	57.830	0.174
Ralfsia verrucosa	0.495	0.000	65.566	0.993
Hildenbrandia lecannellieri	0.515	0.000	72.784	0.372
[90 − 100[*vs* [100 − 110[				
Tetraclita serrata	0.775	1.257	29.449	0.001
Ralfsia verrucosa	0.502	0.259	41.788	1.000
Corallinales	0.275	0.275	52.710	0.641
Spirobranchus kraussii	0.167	0.213	61.082	0.003
Juvenile barnacle	0.152	0.237	69.115	0.905
Hildenbrandia lecannellieri	0.375	0.088	76.845	0.843

Table S5.47 (continued).

Species	Average a	Average b	Cumulative contribution (%)	p-value
$[90-100[$ *vs* $[110-120[$				
Tetraclita serrata	0.774	0.787	21.657	0.180
Corallinales	0.275	0.746	40.487	0.122
Chtamalus dentatus	0.048	0.502	51.923	0.012
Spirobranchus kraussii	0.167	0.239	61.373	0.145
Ralfsia verrucosa	0.502	0.000	69.891	0.980
Spirorbis sp.	0.123	0.254	76.991	0.377
$[100-110[$ *vs* $[110-120[$				
Tetraclita serrata	1.257	0.787	27.690	0.084
Corallinales	0.275	0.746	0.466	0.149
Chthamalus dentatus	0.051	0.502	58.314	0.023
Spirobranchus kraussii	0.213	0.239	69.213	0.120
Cirripedia (juvenile)	0.237	0.152	76.967	0.665

Table S5.48. Results of the SIMPER analysis on epibiotic percent cover showing the most influential species discriminating among euendolithic infestation levels (from A to E, as defined in Kaehler, 1999). Cut-off for low contribution: 70%. Significant p-values are underlined.

Species	Average a	Average b	Cumulative contribution (%)	p-value
A *vs* B				
Ralfsia verrucosa	0.746	1.086	28.5	0.001
Cirripedia (juvenile)	0.164	0.104	41.0	0.001
Corallinales	0.210	0.257	52.1	0.572
Hildenbrandia lecannellieri	0.140	0.409	61.2	0.619
Spirorbis sp.	0.058	0.102	69.2	0.071
Tetraclita serrata	0.049	0.295	75.7	1.000
A *vs* C				
Ralfsia verrucosa	0.746	0.599	20.8	0.300
Cirripedia (juvenile)	0.164	0.178	33.0	0.001
Tetraclita serrata	0.049	0.462	43.6	1.000
Hildenbrandia lecannellieri	0.140	0.376	52.2	0.715
Corallinales	0.210	0.140	60.1	0.994
Spirorbis sp.	0.058	0.129	66.9	0.357
Bryozoa	0.063	0.113	71.5	0.026
A *vs* D				
Ralfsia verrucosa	0.746	0.510	19.5	0.508
Tetraclita serrata	0.049	0.580	32.6	0.879
Corallinales	0.210	0.308	45.0	0.140
Cirripedia (juvenile)	0.164	0.140	55.9	0.008
Hildenbrandia lecannellieri	0.140	0.267	63.4	0.889
Spirorbis sp.	0.058	0.103	69.9	0.553
Perna perna	0.064	0.053	73.5	0.039
A *vs* E				
Ralfsia verrucosa	0.746	1.092	31.5	0.001
Corallinales	0.210	0.472	43.7	0.278
Cirripedia (juvenile)	0.164	0.241	55.1	0.052
Tetraclita serrata	0.049	0.392	63.9	0.977
Hildenbrandia lecannellieri	0.140	0.175	69.6	0.874
Spirorbis sp.	0.058	0.51	74.5	0.873
B *vs* C				
Ralfsia verrucosa	1.086	0.599	24.0	0.002
Tetraclita serrata	0.295	0.462	36.2	0.992
Hildenbrandia lecannellieri	0.409	0.376	47.1	0.083
Cirripedia (juvenile)	0.104	0.178	56.2	0.336
Corallinales	0.257	0.140	65.2	0.986
Spirorbis sp.	0.102	0.129	72.6	0.063

Table S5.48 (continued).

Species	Average a	Average b	Cumulative contribution (%)	p-value
B *vs* D				
Ralfsia verrucosa	1.086	0.510	22.9	0.003
Tetraclita serrata	0.295	0.580	37.3	0.756
Corallinales	0.257	0.308	49.8	0.029
Hildenbrandia lecannellieri	0.409	0.267	59.8	0.273
Cirripedia (juvenile)	0.104	0.140	67.9	0.938
Spirorbis sp.	0.102	0.103	74.9	0.141
B *vs* E				
Ralfsia verrucosa	1.086	1.092	32.0	0.001
Corallinales	0.257	0.472	44.8	0.226
Tetraclita serrata	0.295	0.392	55.4	0.938
Cirripedia (juvenile)	0.104	0.241	64.2	0.549
Hildenbrandia lecannellieri	0.409	0.175	72.5	0.634
C *vs* D				
Tetraclita serrata	0.462	0.580	16.7	0.006
Ralfsia verrucosa	0.599	0.510	33.3	1.000
Corallinales	0.140	0.308	45.3	0.959
Hildenbrandia lecannellieri	0.376	0.267	53.1	0.290
Cirripedia (juvenile)	0.178	0.140	61.6	0.893
Spirorbis sp.	0.129	0.103	68.0	0.711
Spirobranchus kraussii	0.134	0.097	73.1	0.122
C *vs* E				
Ralfsia verrucosa	0.599	1.092	26.2	0.032
Tetraclita serrata	0.462	0.392	39.1	0.753
Corallinales	0.140	0.472	49.6	0.545
Cirripedia (juvenile)	0.178	0.241	58.6	0.377
Hildenbrandia lecannellieri	0.376	0.175	66.5	0.631
Spirobranchus kraussii	0.134	0.197	72.4	0.223
D *vs* E				
Ralfsia verrucosa	0.510	1.092	25.1	0.050
Tetraclita serrata	0.580	0.392	39.7	0.507
Corallinales	0.308	0.472	53.2	0.113
Cirripedia (juvenile)	0.140	0.241	61.5	0.629
Hildenbrandia lecannellieri	0.267	0.175	68.5	0.779
Spirobranchus kraussii	0.097	0.197	73.7	0.373

Table S5.49. Results of the SIMPER analysis on epibiotic percent cover showing the most influential species discriminating among shell degradation indexes (from 1 to 6, as defined in Ma et al., 2023). Cut-off for low contribution: 70%. Significant p-values are underlined.

Species	Average a	Average b	Cumulative contribution (%)	p-value
1 *vs* 2				
Ralfsia verrucosa	0.280	1.861	39.3	0.001
Cirripedia (juvenile)	0.261	0.083	57.1	0.001
Corallinales	0.037	0.216	65.1	0.904
Spirorbis sp.	0.048	0.075	72.8	0.306
1 *vs* 3				
Ralfsia verrucosa	0.280	0.907	23.4	0.237
Cirripedia (juvenile)	0.261	0.169	39.9	0.001
Hildenbrandia lecannellieri	0.000	0.695	52.0	0.222
Corallinales	0.037	0.307	63.3	0.546
Spirorbis sp.	0.048	0.117	72.1	0.106
1 *vs* 4				
Ralfsia verrucosa	0.280	0.612	16.2	0.837
Cirripedia (juvenile)	0.261	0.124	30.8	0.001
Tetraclita serrata	0.000	0.518	42.3	0.903
Hildenbrandia lecannellieri	0.000	0.533	53.4	0.278
Corallinales	0.037	0.244	63.1	0.706
Spirorbis sp.	0.048	0.112	71.0	0.200
1 *vs* 5				
Cirripedia (juvenile)	0.261	0.159	16.8	0.001
Ralfsia verrucosa	0.280	0.476	32.9	0.872
Tetraclita serrata	0.000	0.518	46.4	0.731
Corallinales	0.037	0.244	56.1	0.787
Spirorbis sp.	0.048	0.105	63.6	0.317
Electra verticillata	0.117	0.077	69.8	0.114
Perna perna	0.121	0.050	75.6	0.024
1 *vs* 6				
Corallinales	0.037	0.440	17.0	0.046
Tetraclita serrata	0.000	0.824	33.9	0.390
Cirripedia (juvenile)	0.261	0.168	48.3	0.011
Ralfsia verrucosa	0.280	0.275	60.9	0.944
Perna perna	0.121	0.161	69.2	0.005
Spirorbis sp.	0.048	0.092	75.1	0.665
2 *vs* 3				
Ralfsia verrucosa	1.861	0.907	36.4	0.001
Corallinales	0.216	0.307	47.3	0.587
Hildenbrandia lecannellieri	0.087	0.695	58.1	0.266
Cirripedia (juvenile)	0.083	0.169	67.0	0.567
Spirorbis sp.	0.075	0.117	74.1	0.327

Table S5.49 (continued).

Species	Average a	Average b	Cumulative contribution (%)	p-value
2 *vs* 4				
Ralfsia verrucosa	1.861	0.612	31.7	0.001
Hildenbrandia lecannellieri	0.087	0.533	41.5	0.396
Tetraclita serrata	0.053	0.518	51.3	0.998
Corallinales	0.216	0.244	61.0	0.827
Cirripedia (juvenile)	0.083	0.124	68.4	0.964
Spirorbis sp.	0.075	0.112	74.8	0.533
2 *vs* 5				
Ralfsia verrucosa	1.861	0.476	32.8	0.001
Tetraclita serrata	0.053	0.518	43.9	0.994
Corallinales	0.216	0.244	53.7	0.825
Cirripedia (juvenile)	0.083	0.159	62.6	0.482
Spirorbis sp.	0.075	0.105	68.9	0.608
Hildenbrandia lecannellieri	0.087	0.141	72.7	1.000
2 *vs* 6				
Ralfsia verrucosa	1.861	0.275	30.2	0.003
Corallinales	0.216	0.440	44.5	0.091
Tetraclita serrata	0.053	0.824	58.2	0.664
Cirripedia (juvenile)	0.083	0.168	66.2	0.683
Spirorbis sp.	0.075	0.092	71.5	0.787
3 *vs* 4				
Ralfsia verrucosa	0.907	0.612	20.8	0.202
Hildenbrandia lecannellieri	0.695	0.533	37.2	0.001
Tetraclita serrata	0.342	0.518	49.6	0.974
Corallinales	0.307	0.244	60.8	0.415
Cirripedia (juvenile)	0.169	0.124	68.7	0.960
Spirorbis sp.	0.117	0.112	75.5	0.331
3 *vs* 5				
Ralfsia verrucosa	0.907	0.476	20.9	0.144
Tetraclita serrata	0.342	0.518	34.5	0.883
Hildenbrandia lecannellieri	0.695	0.141	46.2	0.011
Corallinales	0.307	0.244	57.8	0.254
Cirripedia (juvenile)	0.169	0.159	66.9	0.272
Spirorbis sp.	0.117	0.105	73.8	0.262
3 *vs* 6				
Ralfsia verrucosa	0.907	0.275	18.2	0.660
Tetraclita serrata	0.342	0.824	34.4	0.317
Corallinales	0.307	0.440	49.8	0.031
Hildenbrandia lecannellieri	0.695	0.000	59.2	0.452
Cirripedia (juvenile)	0.169	0.168	67.6	0.617
Spirorbis sp.	0.117	0.092	73.6	0.608

Table S5.49 (continued).

Species	Average a	Average b	Cumulative contribution (%)	p-value
4 *vs* 5				
Tetraclita serrata	0.518	0.518	16.6	0.008
Ralfsia verrucosa	0.612	0.476	32.8	1.000
Hildenbrandia lecannellieri	0.533	0.141	43.7	0.005
Corallinales	0.244	0.244	54.3	0.746
Cirripedia (juvenile)	0.124	0.159	62.4	0.996
Spirorbis sp.	0.112	0.105	68.8	0.582
Spirobranchus kraussii	0.140	0.109	74.1	0.042
4 *vs* 6				
Tetraclita serrata	0.518	0.824	18.9	0.087
Corallinales	0.244	0.440	33.2	0.060
Ralfsia verrucosa	0.612	0.275	46.7	0.973
Hildenbrandia lecannellieri	0.533	0.000	55.4	0.559
Cirripedia (juvenile)	0.124	0.168	62.9	0.866
Spirobranchus kraussii	0.140	0.171	68.7	0.237
Spirorbis sp.	0.112	0.092	74.4	0.750
5 *vs* 6				
Tetraclita serrata	0.518	0.824	20.8	0.024
Corallinales	0.244	0.440	36.1	0.028
Ralfsia verrucosa	0.476	0.275	49.3	0.987
Cirripedia (juvenile)	0.159	0.168	58.0	0.556
Spirobranchus kraussii	0.109	0.171	63.8	0.248
Chtamalus dentatus	0.074	0.112	69.5	0.012
Spirorbis sp.	0.105	0.092	75.1	0.769

Table S5.50. Results of the SIMPER analysis on epibiotic percent cover showing the most influential species discriminating among position of the epibionts on the mussel shell (i.e., infested, non-infested). Cut-off for low contribution: 70%. Significant p-values are underlined.

Species	Average a	Average b	Cumulative contribution (%)	p-value
Infested *vs* Non-infested				
Ralfsia verrucosa	0.166	1.112	19.8	0.001
Tetraclita serrata	0.449	0.464	34.5	0.387
Corallinales	0.378	0.135	45.7	0.001
Hildenbrandia lecannellieri	0.092	0.504	54.9	0.072
Cirripedia (juvenile)	0.120	0.176	63.7	0.001
Spirorbis sp.	0.166	0.049	70.6	0.001

5.3.2.2.2.1. Shell length size

Table S5.51. Results of the TukeySD post-hoc pairwise comparisons on the relationship between the mean percent cover of Cirripedia per mussel and shell length range (from]30 − 40] to]110 − 120] in mm). No significant p-values were detected.

Shell length range (a)	Shell length range (b)	Estimate	Std Error	z-value	p-value
]30 − 40]	]40 − 50]	− 4.064	2.081	− 1.953	0.480
	]50 − 60]	− 4.448	2.066	− 2.153	0.345
	]60 − 70]	− 4.610	2.065	− 2.232	0.296
	]70 − 80]	− 4.430	2.066	− 2.144	0.350
	]80 − 90]	− 4.543	2.065	− 2.200	0.315
	]90 − 100]	− 4.609	2.065	− 2.232	0.297
	]100 − 110]	− 4.664	2.065	− 2.259	0.281
	]110 − 120]	− 4.561	2.077	− 2.196	0.318
]40 − 50]	]50 − 60]	− 0.384	0.271	− 1.419	0.842
	]60 − 70]	− 0.546	0.260	− 2.100	0.378
	]70 − 80]	− 0.366	0.270	− 1.356	0.873
	]80 − 90]	− 0.478	0.260	− 1.837	0.566
	]90 − 100]	− 0.544	0.259	− 2.099	0.379
	]100 − 110]	− 0.600	0.259	− 2.317	0.250
	]110 − 120]	− 0.497	0.341	− 1.455	0.823
]50 − 60]	]60 − 70]	− 0.162	0.090	− 1.798	0.594
	]70 − 80]	0.018	0.115	0.160	1.000
	]80 − 90]	− 0.094	0.092	− 1.031	0.972
	]90 − 100]	− 0.161	0.089	− 1.811	0.585
	]100 − 110]	− 0.216	0.087	− 2.488	0.171
	]110 − 120]	− 0.113	0.239	− 0.472	1.000
]60 − 70]	]70 − 80]	0.180	0.087	2.069	0.400
	]80 − 90]	0.068	0.053	1.282	0.904
	]90 − 100]	0.001	0.047	0.031	1.000
	]100 − 110]	− 0.054	0.044	− 1.229	0.923
	]110 − 120]	0.049	0.227	0.217	1.000
]70 − 80]	]80 − 90]	− 0.113	0.089	− 1.271	0.909
	]90 − 100]	− 0.179	0.086	− 2.087	0.387
	]100 − 110]	− 0.234	0.084	− 2.798	0.078
	]110 − 120]	− 0.131	0.238	− 0.552	1.000
]80 − 90]	]90 − 100]	− 0.066	0.050	− 1.316	0.891
	]100 − 110]	− 0.121	0.047	− 2.600	0.131
	]110 − 120]	− 0.018	0.228	− 0.081	1.000
]90 − 100]	]100 − 110]	− 0.055	0.041	− 1.358	0.872
	]110 − 120]	0.048	0.226	0.211	1.000
]100 − 110]	]110 − 120]	0.103	0.226	0.456	1.000

Table S5.52. Results of the TukeySD post-hoc pairwise comparisons on the relationship between the mea percent cover in Cirripedia (juvenile) per mussel and shell length range (from]30 − 40] to]110 − 120] in mm). Significant p-values are underlined.

Shell length range (a)	Shell length range (b)	Estimate	Std Error	z-value	p-value
]30 − 40]	]40 − 50]	− 0.472	2.742	− 0.172	1.000
	]50 − 60]	− 0.168	2.556	− 0.066	1.000
	]60 − 70]	− 1.776	2.506	− 0.708	0.998
	]70 − 80]	− 3.293	2.218	− 1.484	0.819
	]80 − 90]	− 4.191	2.148	− 1.951	0.505
	]90 − 100]	− 3.629	2.211	− 1.641	0.723
	]100 − 110]	− 5.950	2.116	− 2.811	0.085
	]110 − 120]	− 4.430	3.390	− 1.307	0.902
]40 − 50]	]50 − 60]	0.304	2.261	0.134	1.000
	]60 − 70]	− 1.304	2.205	− 0.591	0.999
	]70 − 80]	− 2.821	1.871	− 1.508	0.806
	]80 − 90]	− 3.719	1.786	− 2.082	0.413
	]90 − 100]	− 3.157	1.862	− 1.696	0.687
	]100 − 110]	− 5.478	1.748	− 3.133	0.033
	]110 − 120]	− 3.958	3.173	− 1.247	0.923
]50 − 60]	]60 − 70]	− 1.607	1.968	− 0.817	0.994
	]70 − 80]	− 3.125	1.585	− 1.971	0.490
	]80 − 90]	− 4.022	1.485	− 2.708	0.111
	]90 − 100]	− 3.461	1.575	− 2.197	0.339
	]100 − 110]	− 5.781	1.439	− 4.018	0.001
	]110 − 120]	− 4.261	3.014	− 1.414	0.855
]60 − 70]	]70 − 80]	− 1.517	1.503	− 1.009	0.978
	]80 − 90]	− 2.415	1.397	− 1.728	0.664
	]90 − 100]	− 1.854	1.493	− 1.242	0.925
	]100 − 110]	− 4.174	1.348	− 3.096	0.038
	]110 − 120]	− 2.654	2.972	− 0.893	0.990
]70 − 80]	]80 − 90]	− 0.898	0.769	− 1.167	0.947
	]90 − 100]	− 0.336	0.931	− 0.361	1.000
	]100 − 110]	− 2.657	0.676	− 3.930	0.003
	]110 − 120]	− 1.137	2.733	− 0.416	1.000
]80 − 90]	]90 − 100]	0.561	0.749	0.750	0.997
	]100 − 110]	− 1.759	0.387	− 4.546	< 0.001
	]110 − 120]	− 0.239	2.676	− 0.089	1.000
]90 − 100]	]100 − 110]	− 2.321	0.652	− 3.557	0.008
	]110 − 120]	− 0.800	2.727	− 0.293	1.000
]100 − 110]	]110 − 120]	1.520	2.651	0.573	1.000

Table S5.53. Results of the TukeySD post-hoc pairwise comparisons on the relationship between the mean percent cover in Ochrophyta per mussel and shell length range (from]30 − 40] to]110 − 120] in mm). Significant p-values are underlined.

Shell length range (a)	Shell length range (b)	Estimate	Std Error	z-value	p-value
]30 − 40]	]40 − 50]	0.019	0.019	1.026	0.964
	]50 − 60]	0.015	0.013	1.202	0.917
	]60 − 70]	0.018	0.013	1.411	0.826
	]70 − 80]	0.025	0.014	1.827	0.557
	]80 − 90]	0.046	0.015	3.104	0.033
	]90 − 100]	0.041	0.016	2.505	0.165
	]100 − 110]	0.097	0.047	2.036	0.413
	]110 − 120]	NA	NA	NA	NA
]40 − 50]	]50 − 60]	− 0.004	0.016	− 0.244	1.000
	]60 − 70]	− 0.001	0.016	− 0.084	1.000
	]70 − 80]	0.006	0.017	0.384	1.000
	]80 − 90]	0.027	0.017	1.526	0.762
	]90 − 100]	0.022	0.019	1.167	0.929
	]100 − 110]	0.078	0.048	1.605	0.711
	]110 − 120]	NA	NA	NA	NA
]50 − 60]	]60 − 70]	0.003	0.008	0.303	1.000
	]70 − 80]	0.010	0.010	1.040	0.961
	]80 − 90]	0.030	0.011	2.785	0.082
	]90 − 100]	0.026	0.013	1.972	0.456
	]100 − 110]	0.081	0.046	1.754	0.609
	]110 − 120]	NA	NA	NA	NA
]60 − 70]	]70 − 80]	0.008	0.010	0.794	0.992
	]80 − 90]	0.028	0.011	2.578	0.138
	]90 − 100]	0.023	0.013	1.791	0.583
	]100 − 110]	0.079	0.046	1.701	0.646
	]110 − 120]	NA	NA	NA	NA
]70 − 80]	]80 − 90]	0.020	0.012	1.621	0.701
	]90 − 100]	0.016	0.014	1.803	0.951
	]100 − 110]	0.071	0.047	1.521	0.765
	]110 − 120]	NA	NA	NA	NA
]80 − 90]	]90 − 100]	− 0.005	0.015	− 0.301	1.000
	]100 − 110]	0.051	0.047	1.086	0.951
	]110 − 120]	NA	NA	NA	NA
]90 − 100]	]100 − 110]	0.056	0.048	1.169	0.928
	]110 − 120]	NA	NA	NA	NA
]100 − 110]	]110 − 120]	NA	NA	NA	NA

Table S5.54. Results of the TukeySD post-hoc pairwise comparisons on the relationship between the mean percent cover in *Ralfsia verrucosa* (Ochrophyta) per mussel and shell length range (from]30 − 40] to]110 − 120] in mm). Significant p-values are underlined.

Shell length range (a)	Shell length range (b)	Estimate	Std Error	z-value	p-value
]30 − 40]	]40 − 50]	0.019	0.018	1.042	0.960
	]50 − 60]	0.015	0.012	1.222	0.910
	]60 − 70]	0.018	0.012	1.435	0.814
	]70 − 80]	0.025	0.014	1.853	0.540
	]80 − 90]	0.044	0.014	3.053	0.038
	]90 − 100]	0.041	0.016	2.546	0.149
	]100 − 110]	0.097	0.047	2.069	0.391
	]110 − 120]	NA	NA	NA	NA
]40 − 50]	]50 − 60]	– 0.004	0.015	– 0.248	1.000
	]60 − 70]	– 0.001	0.015	– 0.085	1.000
	]70 − 80]	0.006	0.016	0.372	1.000
	]80 − 90]	0.025	0.017	1.455	0.803
	]90 − 100]	0.022	0.019	1.187	0.922
	]100 − 110]	0.078	0.048	1.631	0.694
	]110 − 120]	NA	NA	NA	NA
]50 − 60]	]60 − 70]	0.003	0.008	0.329	1.000
	]70 − 80]	0.010	0.010	1.045	0.960
	]80 − 90]	0.029	0.011	2.698	0.103
	]90 − 100]	0.026	0.013	2.004	0.434
	]100 − 110]	0.081	0.046	1.783	0.589
	]110 − 120]	NA	NA	NA	NA
]60 − 70]	]70 − 80]	0.007	0.009	0.789	0.992
	]80 − 90]	0.026	0.011	2.485	0.172
	]90 − 100]	0.023	0.013	1.821	0.562
	]100 − 110]	0.079	0.046	1.729	0.627
	]110 − 120]	NA	NA	NA	NA
]70 − 80]	]80 − 90]	0.019	0.012	1.570	0.734
	]90 − 100]	0.016	0.014	1.138	0.937
	]100 − 110]	0.072	0.046	1.555	0.743
	]110 − 120]	NA	NA	NA	NA
]80 − 90]	]90 − 100]	– 0.003	0.015	– 0.188	1.000
	]100 − 110]	0.053	0.046	1.143	0.936
	]110 − 120]	NA	NA	NA	NA
]90 − 100]	]100 − 110]	0.056	0.047	1.188	0.922
	]110 − 120]	NA	NA	NA	NA
]100 − 110]	]110 − 120]	NA	NA	NA	NA

Table S5.55. Results of the TukeySD post-hoc pairwise comparisons on the relationship between the mean percent cover in Rhodophyta per mussel and shell length range (from]30 − 40] to]110 − 120] in mm). No significant p-values were detected.

Shell length range (a)	Shell length range (b)	Estimate	Std Error	z-value	p-value
]30 − 40]	]40 − 50]	– 0.116	0.148	– 0.748	0.995
	]50 − 60]	– 0.062	0.147	– 0.424	1.000
	]60 − 70]	– 0.103	0.141	– 0.730	0.997
	]70 − 80]	– 0.126	0.139	– 0.908	0.987
	]80 − 90]	– 0.142	0.139	– 1.022	0.974
	]90 − 100]	– 0.077	0.141	– 0.545	1.000
	]100 − 110]	– 0.015	0.151	– 0.100	1.000
	]110 − 120]	0.242	0.416	0.581	0.999
]40 − 50]	]50 − 60]	0.054	0.070	0.762	0.996
	]60 − 70]	0.013	0.057	0.228	1.000
	]70 − 80]	– 0.011	0.053	– 0.200	1.000
	]80 − 90]	– 0.026	0.052	– 0.499	1.000
	]90 − 100]	0.039	0.057	0.695	0.998
	]100 − 110]	0.101	0.078	1.288	0.903
	]110 − 120]	0.358	0.396	0.904	0.988
]50 − 60]	]60 − 70]	– 0.041	0.054	– 0.750	0.997
	]70 − 80]	– 0.064	0.050	– 1.291	0.901
	]80 − 90]	– 0.080	0.049	– 1.641	0.709
	]90 − 100]	– 0.014	0.053	– 0.268	1.000
	]100 − 110]	0.047	0.076	0.621	0.999
	]110 − 120]	0.304	0.396	0.769	0.996
]60 − 70]	]70 − 80]	– 0.024	0.028	– 0.835	0.993
	]80 − 90]	– 0.039	0.026	– 1.495	0.801
	]90 − 100]	0.026	0.034	0.766	0.996
	]100 − 110]	0.088	0.064	1.370	0.867
	]110 − 120]	0.345	0.394	0.876	0.990
]70 − 80]	]80 − 90]	– 0.015	0.015	– 1.006	0.976
	]90 − 100]	0.050	0.027	1.855	0.555
	]100 − 110]	0.111	0.060	1.844	0.562
	]110 − 120]	0.369	0.393	0.983	0.985
]80 − 90]	]90 − 100]	0.065	0.025	2.659	0.115
	]100 − 110]	0.127	0.059	2.134	0.359
	]110 − 120]	0.384	0.393	0.977	0.980
]90 − 100]	]100 − 110]	0.061	0.063	0.969	0.981
	]110 − 120]	0.319	0.393	0.810	0.994
]100 − 110]	]110 − 120]	0.257	0.397	0.648	0.999

Table S5.56. Results of the TukeySD post-hoc pairwise comparisons on the relationship between the mean percent cover in Corallinales (Rhodophyta) per mussel and shell length range (from]30 − 40] to]110 − 120] in mm). No significant p-values were detected.

Shell length range (a)	Shell length range (b)	Estimate	Std Error	z-value	p-value
]30 − 40]	]40 − 50]	− 0.008	0.155	− 0.055	1.000
	]50 − 60]	1.366	0.824	1.658	0.708
	]60 − 70]	0.218	0.160	1.361	0.878
	]70 − 80]	− 0.002	0.117	− 0.018	1.000
	]80 − 90]	0.063	0.120	0.527	1.000
	]90 − 100]	0.300	0.148	2.021	0.449
	]100 − 110]	0.353	0.199	1.774	0.627
	]110 − 120]	0.295	0.384	0.768	0.996
]40 − 50]	]50 − 60]	1.374	0.823	1.671	0.700
	]60 − 70]	0.227	0.155	1.459	0.830
	]70 − 80]	0.006	0.110	0.058	1.000
	]80 − 90]	0.072	0.113	0.635	0.999
	]90 − 100]	0.308	0.143	2.158	0.358
	]100 − 110]	0.361	0.195	1.855	0.568
	]110 − 120]	0.304	0.382	0.794	0.995
]50 − 60]	]60 − 70]	− 1.147	0.824	− 1.393	0.863
	]70 − 80]	− 1.368	0.816	− 1.676	0.696
	]80 − 90]	− 1.303	0.817	− 1.595	0.749
	]90 − 100]	− 1.066	0.821	− 1.298	0.904
	]100 − 110]	− 1.013	0.832	− 1.217	0.932
	]110 − 120]	− 1.071	0.895	− 1.197	0.938
]60 − 70]	]70 − 80]	− 0.220	0.118	− 1.866	0.560
	]80 − 90]	− 0.155	0.120	− 1.290	0.907
	]90 − 100]	0.081	0.149	0.546	1.000
	]100 − 110]	0.135	0.199	0.675	0.999
	]110 − 120]	0.077	0.385	0.200	1.000
]70 − 80]	]80 − 90]	0.065	0.050	1.30	0.903
	]90 − 100]	0.302	0.101	2.991	0.050
	]100 − 110]	0.355	0.167	2.131	0.375
	]110 − 120]	0.297	0.369	0.806	0.995
]80 − 90]	]90 − 100]	0.237	0.103	2.286	0.281
	]100 − 110]	0.290	0.168	1.723	0.663
	]110 − 120]	0.232	0.370	0.628	0.999
]90 − 100]	]100 − 110]	0.053	0.190	0.281	1.000
	]110 − 120]	− 0.004	0.380	− 0.012	1.000
]100 − 110]	]110 − 120]	− 0.058	0.402	− 0.144	1.000

Table S5.57. Results of the TukeySD post-hoc pairwise comparisons on the relationship between the mean percent cover in Sedentaria per mussel and shell length range (from]30 − 40] to]110 − 120] in mm). No significant p-values were detected.

Shell length range (a)	Shell length range (b)	Estimate	Std Error	z-value	p-value
]30 − 40]	]40 − 50]	− 1.815	3.849	− 0.472	1.000
	]50 − 60]	− 3.539	3.589	− 0.986	0.977
	]60 − 70]	− 3.937	3.583	− 1.099	0.956
	]70 − 80]	− 3.765	3.584	− 1.050	0.966
	]80 − 90]	− 3.879	3.583	− 1.082	0.960
	]90 − 100]	− 3.792	3.584	− 1.058	0.965
	]100 − 110]	− 3.575	3.590	− 0.996	0.976
	]110 − 120]	− 2.932	3.856	− 0.760	0.996
]40 − 50]	]50 − 60]	− 1.724	1.423	− 1.212	0.924
	]60 − 70]	− 2.122	1.407	− 1.507	0.781
	]70 − 80]	− 1.950	1.410	− 1.383	0.852
	]80 − 90]	− 2.063	1.407	− 1.466	0.806
	]90 − 100]	− 1.977	1.409	− 1.403	0.841
	]100 − 110]	− 1.760	1.424	− 1.236	0.916
	]110 − 120]	− 1.117	2.004	− 0.557	1.000
]50 − 60]	]60 − 70]	− 0.398	0.218	− 1.823	0.559
	]70 − 80]	− 0.226	0.235	− 0.960	0.981
	]80 − 90]	− 0.339	0.218	− 1.554	0.752
	]90 − 100]	− 0.253	0.228	− 1.111	0.953
	]100 − 110]	− 0.036	0.308	− 0.116	1.000
	]110 − 120]	0.607	1.443	0.421	1.000
]60 − 70]	]70 − 80]	0.172	0.110	1.557	0.750
	]80 − 90]	0.058	0.068	0.862	0.990
	]90 − 100]	0.144	0.094	1.536	0.763
	]100 − 110]	0.362	0.227	1.592	0.726
	]110 − 120]	1.005	1.428	0.704	0.998
]70 − 80]	]80 − 90]	− 0.114	0.111	− 1.023	0.971
	]90 − 100]	− 0.028	0.129	− 0.214	1.000
	]100 − 110]	0.190	0.244	0.779	0.995
	]110 − 120]	0.833	1.430	0.582	0.999
]80 − 90]	]90 − 100]	0.086	0.095	0.909	0.986
	]100 − 110]	0.304	0.228	1.334	0.875
	]110 − 120]	0.946	1.428	0.663	0.998
]90 − 100]	]100 − 110]	0.217	0.237	0.919	0.985
	]110 − 120]	0.860	1.429	0.602	0.999
]100 − 110]	]110 − 120]	0.643	1.444	0.445	1.000

Table S5.58. Results of the TukeySD post-hoc pairwise comparisons on the relationship between the mean percent cover in *Spirobranchus kraussii* (Sedentaria) per mussel and shell length range (from]30 − 40] to]110 − 120] in mm). No significant p-values were detected.

Shell length range (a)	Shell length range (b)	Estimate	Std Error	z-value	p-value
]30 − 40]	Others	NA	NA	NA	NA
]40 − 50]	Others	NA	NA	NA	NA
]50 − 60]	]60 − 70]	0.220	0.144	1.530	0.680
	]70 − 80]	0.323	0.133	2.433	0.150
	]80 − 90]	0.231	0.084	2.744	0.069
	]90 − 100]	0.268	0.096	2.787	0.061
	]100 − 110]	0.407	0.146	2.783	0.062
	]110 − 120]	2.419	1.461	1.656	0.593
]60 − 70]	]70 − 80]	0.103	0.178	0.578	0.997
	]80 − 90]	0.011	0.145	0.073	1.000
	]90 − 100]	0.048	0.152	0.313	1.000
	]100 − 110]	0.186	0.188	0.993	0.943
	]110 − 120]	2.199	1.466	1.500	0.699
]70 − 80]	]80 − 90]	– 0.092	0.134	– 0.689	0.991
	]90 − 100]	– 0.055	0.142	– 0.390	1.000
	]100 − 110]	0.084	0.179	0.467	0.999
	]110 − 120]	2.096	1.464	1.431	0.744
]80 − 90]	]90 − 100]	0.037	0.097	0.379	1.000
	]100 − 110]	0.176	0.147	1.196	0.871
	]110 − 120]	2.188	1.461	1.498	0.701
]90 − 100]	]100 − 110]	0.139	0.154	0.901	0.964
	]110 − 120]	2.151	1.462	1.472	0.718
]100 − 110]	]110 − 120]	2.012	1.466	1.373	0.779

5.3.2.2.2.2. Euendolithic infestation, shell degradation and position

Table S5.59. Results of the TukeySD post-hoc pairwise comparisons on the relationship between the average percent cover of Cirripedia per mussel valve and shell degradation index (from 1 to 6, as defined in Ma *et al.*, 2023). Significant p-values are underlined.

Shell degradation index (a)	Shell degradation index (b)	Estimate	Std Error	z-value	P (> z)
1	2	– 4.777	2.963	– 1.612	0.509
	3	– 5.477	2.946	– 1.859	0.347
	4	– 5.360	2.946	– 1.819	0.371
	5	– 5.271	2.946	– 1.789	0.390
	6	– 5.424	2.947	– 1.840	0.358
2	3	– 0.700	0.474	– 1.478	0.603
	4	– 0.583	0.477	– 1.222	0.773
	5	– 0.494	0.478	– 1.034	0.873
	6	– 0.647	0.483	– 1.340	0.697
3	4	0.117	0.066	1.768	0.404
	5	0.206	0.066	3.111	<u>0.014</u>
	6	0.053	0.098	0.536	0.992
4	5	0.089	0.059	1.510	0.580
	6	– 0.065	0.092	– 0.701	0.974
5	6	– 0.015	0.086	– 1.793	0.388

Table S5.60. Results of the TukeySD post-hoc pairwise comparisons on the relationship between the average percent cover of Cirripedia (juvenile) per mussel valve and euendolithic infestation levels (from A to E, as defined in Kaehler, 1999) for each shell degradation index (from 1 to 6, as defined in Ma *et al.*, 2023). Significant p-values are underlined.

Infestation level (a)	Infestation level (b)	Estimate	Std Error	t-value	p-value
Shell degradation 1		NA	NA	NA	NA
Shell degradation 2					
A	B	– 0.038	0.063	– 0.601	0.975
Shell degradation 3					
A	B	0.082	0.115	0.717	0.953
	C	– 5.412	2.351	– 2.303	0.146
	D	0.113	0.129	0.871	0.907
	E	0.043	0.283	0.153	1.000
B	C	– 5.494	2.348	– 2.340	0.135
	D	0.031	0.083	0.370	0.996
	E	– 0.039	0.265	– 0.147	1.000
C	D	5.525	2.349	2.352	0.131
	E	5.456	2.363	2.309	0.144
D	E	– 0.069	0.272	– 0.255	0.999
Shell degradation 4					
A	B	0.038	0.184	0.207	1.000
	C	– 0.108	0.190	– 0.572	0.979
	D	– 0.148	0.195	– 0.762	0.941
	E	– 1.081	1.205	– 0.898	0.898
B	C	– 0.147	0.069	– 2.140	0.206
	D	– 0.186	0.082	– 2.276	0.155
	E	– 1.119	1.192	– 0.939	0.881
C	D	– 0.040	0.093	– 0.429	0.993
	E	– 0.973	1.193	– 0.816	0.926
D	E	– 0.933	1.193	– 0.782	0.936
Shell degradation 5					
A	Others	NA	NA	NA	NA
B	C	– 0.171	0.046	– 3.700	<u>0.002</u>
	D	– 0.132	0.034	– 3.907	<u>0.001</u>
	E	– 1.419	0.907	– 1.564	0.522
C	D	0.039	0.043	0.906	0.895
	E	– 1.248	0.908	– 1.375	0.644
D	E	– 1.286	0.907	– 1.418	0.616
Shell degradation 6					
A	Others	NA	NA	NA	NA
B	Others	NA	NA	NA	NA
C	D	– 0.089	0.129	– 0.684	0.960
	E	0.109	0.084	1.297	0.693
D	E	0.197	0.103	1.920	0.308

Table S5.61. Results of the TukeySD post-hoc pairwise comparisons on the relationship between the average percent cover of Ochrophyta per mussel valve and position of the epibionts on the mussel shell (i.e., infested, non-infested) for each shell degradation index (from 1 to 6, as defined in Ma *et al.*, 2023). Significant p-values are underlined.

Position on the shell (a)	Position on the shell (b)	Estimate	Std Error	t-value	p-value
Shell degradation 1		NA	NA	NA	NA
Shell degradation 2					
Infested	Non-infested	0.418	0.407	1.027	0.306
Shell degradation 3					
Infested	Non-infested	0.120	0.061	1.957	0.052
Shell degradation 4					
Infested	Non-infested	0.378	0.181	2.092	<u>0.038</u>
Shell degradation 5					
Infested	Non-infested	0.045	0.026	1.760	0.080
Shell degradation 6					
Infested	Non-infested	– 0.294	0.312	– 0.944	0.347

Table S5.62. Results of the TukeySD post-hoc pairwise comparisons on the relationship between the average percent cover of *Ralfsia verrucosa* (Ochrophyta) per mussel valve and position of the epibionts on the mussel shell (i.e., infested, non-infested) for each euendolithic infestation levels (from A to E, as defined in Kaehler, 1999). Significant p-values are underlined.

Position on the shell (a)	Position on the shell (b)	Estimate	Std Error	t-value	p-value
Infestation level A		NA	NA	NA	NA
Infestation level B					
Infested	Non-infested	0.440	0.208	2.116	<u>0.036</u>
Infestation level C					
Infested	Non-infested	0.090	0.075	1.206	0.229
Infestation level D					
Infested	Non-infested	0.039	0.022	1.807	0.072
Infestation level E					
Infested	Non-infested	– 0.051	0.058	– 0.880	0.380

Table S5.63. Results of the TukeySD post-hoc pairwise comparisons on the relationship between the average percent cover of Rhodophyta per mussel valve and shell degradation index (from 1 to 6, as defined in Ma *et al.*, 2023). No significant p-values were detected.

Shell degradation index (a)	Shell degradation index (b)	Estimate	Std Error	z-value	P (> z)
1	2	– 3.632	3.815	– 0.952	0.902
	3	– 3.652	3.815	– 0.957	0.900
	4	– 3.631	3.815	– 0.952	0.9902
	5	– 3.585	3.815	– 0.940	0.907
	6	– 3.461	3.818	– 0.906	0.919
2	3	– 0.020	0.043	– 0.470	0.995
	4	0.001	0.047	0.027	1.000
	5	0.047	0.051	0.924	0.913
	6	0.172	0.161	1.065	0.852
3	4	0.022	0.020	1.073	0.847
	5	0.067	0.028	2.433	0.098
	6	0.192	0.156	1.234	0.756
4	5	0.046	0.025	1.794	0.376
	6	0.170	0.155	1.100	0.834
5	6	0.125	0.155	0.804	0.950

Table S5.64. Results of the TukeySD post-hoc pairwise comparisons on the relationship between the average percent cover of Rhodophyta per mussel valve and position of the epibionts on the mussel shell (i.e., infested, non-infested). Significant p-values are underlined.

Position on the shell (a)	Position on the shell (b)	Estimate	Std Error	z-value	P (> z)
Non-infested	Infested	– 0.129	0.059	– 4.512	$\underline{6.430 \times 10^{-6}}$

Table S5.65. Results of the TukeySD post-hoc pairwise comparisons on the relationship between the average percent cover of *Hildenbrandia lecannellieri* (Rhodophyta) per mussel valve and position of the epibionts on the mussel shell (i.e., infested, non-infested) for each shell degradation index (from 1 to 6, as defined in Ma *et al.*, 2023). No significant p-values were detected.

Position on the shell (a)	Position on the shell (b)	Estimate	Std Error	t-value	p-value
Shell degradation 1		NA	NA	NA	NA
Shell degradation 2					
Infested	Non-infested	NA	NA	NA	NA
Shell degradation 3					
Infested	Non-infested	0.192	0.101	1.908	0.060
Shell degradation 4					
Infested	Non-infested	0.042	0.033	1.266	0.209
Shell degradation 5					
Infested	Non-infested	– 0.030	0.025	– 1.189	0.238
Shell degradation 6		NA	NA	NA	NA

Table S5.66. Results of the TukeySD post-hoc pairwise comparisons on the relationship between the average percent cover of Corallinales (Rhodophyta) per mussel valve and euendolithic infestation levels (from A to E, as defined in Kaehler, 1999). No significant p-values were detected.

Infestation level (a)	Infestation level (b)	Estimate	Std Error	t-value	p-value
A	B	0.358	0.455	0.786	0.934
	C	0.844	0.545	1.548	0.533
	D	0.893	0.531	1.683	0.447
	E	– 0.313	0.653	– 0.479	0.989
B	C	0.487	0.351	1.387	0.637
	D	0.536	0.326	1.644	0.472
	E	– 0.671	0.508	– 1.320	0.679
C	D	0.049	0.225	0.217	1.000
	E	– 1.158	0.486	– 2.382	0.125
D	E	– 1.206	0.462	– 2.609	0.073

Table S5.67. Results of the TukeySD post-hoc pairwise comparisons on the relationship between the average percent cover of Corallinales (Rhodophyta) per mussel valve and position of the epibionts on the mussel shell (i.e., infested, non-infested) for each shell degradation index (from 1 to 6, as defined in Ma et al., 2023). Significant p-values are underlined.

Position on the shell (a)	Position on the shell (b)	Estimate	Std Error	t-value	p-value
Shell degradation 1					
Infested	Non-infested	NA	NA	NA	NA
Shell degradation 2					
Infested	Non-infested	1.268	0.625	2.030	<u>0.044</u>
Shell degradation 3					
Infested	Non-infested	– 0.710	0.420	– 1.688	0.093
Shell degradation 4					
Infested	Non-infested	– 0.648	0.357	– 1.817	0.071
Shell degradation 5					
Infested	Non-infested	0.859	0.275	3.121	<u>0.002</u>
Shell degradation 6					
Infested	Non-infested	NA	NA	NA	NA

Table S5.68. Results of the TukeySD post-hoc pairwise comparisons on the relationship between the average percent cover of Sedentaria per mussel valve and position of the epibionts on the mussel shell (i.e., infested, non-infested) for each shell degradation index (from 1 to 6, as defined in Ma *et al.*, 2023). No significant p-values were detected.

Position on the shell (a)	Position on the shell (b)	Estimate	Std Error	t-value	p-value
Shell degradation 1					
Infested	Non-infested	NA	NA	NA	NA
Shell degradation 2					
Infested	Non-infested	2.068	1.759	1.176	0.240
Shell degradation 3					
Infested	Non-infested	0.505	0.291	1.737	0.083
Shell degradation 4					
Infested	Non-infested	– 0.522	0.414	– 1.262	0.208
Shell degradation 5					
Infested	Non-infested	0.022	0.213	0.103	0.918
Shell degradation 6					
Infested	Non-infested	NA	NA	NA	NA

Table S5.69. Results of the TukeySD post-hoc pairwise comparisons on the relationship between the average percent cover of *Spirobranchus kraussii* (Sedentaria) per mussel valve and position of the epibionts on the mussel shell (i.e., infested, non-infested). Significant p-values are underlined.

Position on the shell (a)	Position on the shell (b)	Estimate	Std Error	z-value	P (> z)
Non-infested	Infested	– 1.509	0.300	– 5.028	<u>4.970×10^{-7}</u>

5.3.2.2.3. Biomass of epibiotic communities

Table S5.70. Results of the SIMPER analysis on epibiotic biomass showing the most influential higher taxonomical groups discriminating among shell length sizes (from]30 − 40] to]110 − 120] in mm). Cut-off for low contribution: 70%. Significant p-values are underlined.

Higher taxonomical group	Average a	Average b	Cumulative contribution (%)	p-value
[30 − 40[*vs* [40 − 50[				
Ochrophyta	0.544	0.648	29.9	0.128
Bivalvia	0.332	0.161	45.7	0.045
Bryozoa	0.175	0.267	59.5	0.438
Cirripedia	0.000	0.297	70.9	0.929
[30 − 40[*vs* [50 − 60[				
Ochrophyta	0.544	1.091	35.6	0.013
Bivalvia	0.332	0.098	48.9	0.052
Bryozoa	0.175	0.277	62.0	0.529
Rhodophyta	0.000	0.259	69.9	0.970
Amphipoda	0.164	0.057	77.8	0.015
[30 − 40[*vs* [60 − 70[				
Ochrophyta	0.544	0.815	29.0	0.110
Bivalvia	0.332	0.286	44.4	0.018
Bryozoa	0.175	0.336	57.9	0.431
Cirripedia	0.000	0.407	68.3	0.995
Amphipoda	0.164	0.061	75.4	0.013
[30 − 40[*vs* [70 − 80[				
Ochrophyta	0.544	0.660	24.8	0.271
Bryozoa	0.175	0.433	40.9	0.200
Rhodophyta	0.000	0.682	55.1	0.678
Bivalvia	0.332	0.124	66.9	0.061
Cirripedia	0.000	0.353	76.4	0.995
[30 − 40[*vs* [80 − 90[				
Ochrophyta	0.544	0.485	21.4	0.461
Rhodophyta	0.000	0.767	36.3	0.592
Bryozoa	0.175	0.358	50.1	0.354
Cirripedia	0.000	0.460	62.3	0.944
Bivalvia	0.332	0.090	73.7	0.073
[30 − 40[*vs* [90 − 100[				
Ochrophyta	0.544	0.582	22.8	0.338
Cirripedia	0.000	0.846	44.2	0.163
Rhodophyta	0.000	0.578	57.0	0.756
Bivalvia	0.332	0.115	68.0	0.090
Bryozoa	0.175	0.142	75.9	0.855

Table S5.70 (continued).

Higher taxonomical group	Average a	Average b	Cumulative contribution (%)	p-value
[30 − 40[*vs* [100 − 110[				
Cirripedia	0.000	1.236	30.7	0.002
Ochrophyta	0.544	0.271	47.8	0.778
Bivalvia	0.332	0.210	60.6	0.028
Sedentaria	0.000	0.268	68.9	0.416
Bryozoa	0.175	0.134	76.6	0.865
[30 − 40[*vs* [110 − 120[				
Cirripedia	0.000	1.281	33.9	0.006
Sedentaria	0.000	0.683	52.1	0.051
Ochrophyta	0.544	0.000	66.2	0.764
Bryozoa	0.175	0.472	77.6	0.532
[40 − 50[*vs* [50 − 60[				
Ochrophyta	0.648	1.091	36.3	0.002
Bryozoa	0.267	0.277	50.8	0.420
Cirripedia	0.297	0.236	64.9	0.961
Rhodophyta	0.142	0.259	75.5	0.975
[40 − 50[*vs* [60 − 70[				
Ochrophyta	0.648	0.815	29.9	0.053
Cirripedia	0.297	0.407	46.4	0.841
Bryozoa	0.267	0.336	61.1	0.333
Bivalvia	0.161	0.286	71.2	0.091
[40 − 50[*vs* [70 − 80[				
Ochrophyta	0.648	0.660	26.4	0.172
Bryozoa	0.267	0.433	43.7	0.110
Rhodophyta	0.142	0.682	59.9	0.626
Cirripedia	0.297	0.353	75.1	0.889
[40 − 50[*vs* [80 − 90[				
Ochrophyta	0.648	0.485	23.3	0.403
Cirripedia	0.297	0.460	40.6	0.699
Rhodophyta	0.142	0.767	57.5	0.502
Bryozoa	0.267	0.358	72.8	0.220
[40 − 50[*vs* [90 − 100[				
Ochrophyta	0.648	0.582	25.2	0.257
Cirripedia	0.297	0.846	49.3	0.062
Rhodophyta	0.142	0.578	64.5	0.718
Bryozoa	0.267	0.142	74.5	0.824
[40 − 50[*vs* [100 − 110[				
Cirripedia	0.297	1.236	31.6	0.001
Ochrophyta	0.648	0.271	51.5	0.708
Bryozoa	0.267	0.134	61.3	0.824
Rhodophyta	0.142	0.366	70.1	0.978

Table S5.70 (continued).

Higher taxonomical group	Average a	Average b	Cumulative contribution (%)	p-value
[40 − 50[*vs* [110 − 120[				
Cirripedia	0.297	1.281	33.9	0.014
Sedentaria	0.000	0.683	52.9	0.042
Ochrophyta	0.648	0.000	70.3	0.713
Bryozoa	0.267	0.472	84.0	0.449
[50 − 60[*vs* [60 − 70[				
Ochrophyta	1.091	0.815	34.0	0.001
Bryozoa	0.277	0.336	48.3	0.448
Cirripedia	0.236	0.407	61.6	1.000
Rhodophyta	0.259	0.355	73.5	0.998
[50 − 60[*vs* [70 − 80[				
Ochrophyta	1.091	0.660	31.9	0.001
Rhodophyta	0.259	0.682	50.0	0.577
Bryozoa	0.277	0.433	66.7	0.055
Cirripedia	0.236	0.353	79.0	1.000
[50 − 60[*vs* [80 − 90[				
Ochrophyta	1.091	0.485	29.9	0.001
Rhodophyta	0.259	0.767	48.6	0.401
Bryozoa	0.277	0.360	63.0	0.200
Cirripedia	0.236	0.460	77.4	1.000
[50 − 60[*vs* [90 − 100[				
Ochrophyta	1.091	0.582	30.9	0.001
Cirripedia	0.236	0.846	53.0	0.066
Rhodophyta	0.259	0.578	69.6	0.752
Bryozoa	0.277	0.142	79.1	0.988
[50 − 60[*vs* [100 − 110[				
Cirripedia	0.236	1.236	29.1	0.001
Ochrophyta	1.091	0.271	56.2	0.012
Rhodophyta	0.259	0.366	67.2	0.989
Sedentaria	0.141	0.268	77.3	0.158
[50 − 60[*vs* [110 − 120[				
Cirripedia	0.236	1.281	31.7	0.024
Ochrophyta	1.091	0.000	58.1	0.237
Sedentaria	0.141	0.683	76.0	0.055
Bryozoa	0.277	0.472	88.6	0.471
[60 − 70[*vs* [70 − 80[				
Ochrophyta	0.815	0.660	26.4	0.031
Rhodophyta	0.355	0.682	43.1	0.776
Bryozoa	0.336	0.433	59.3	0.020
Cirripedia	0.407	0.353	73.7	1.000

Table S5.70 (continued).

Higher taxonomical group	Average a	Average b	Cumulative contribution (%)	p-value
[60 − 70[*vs* [80 − 90[				
Ochrophyta	0.815	0.485	24.0	0.134
Rhodophyta	0.355	0.767	41.3	0.604
Cirripedia	0.407	0.460	57.5	0.998
Bryozoa	0.336	0.358	72.0	0.090
[60 − 70[*vs* [90 − 100[				
Ochrophyta	0.815	0.582	25.4	0.071
Cirripedia	0.407	0.846	47.6	0.013
Rhodophyta	0.355	0.578	63.2	0.902
Bryozoa	0.336	0.142	73.6	0.982
[60 − 70[*vs* [100 − 110[				
Cirripedia	0.407	1.236	28.6	0.001
Ochrophyta	0.815	0.271	50.0	0.765
Rhodophyta	0.355	0.366	60.2	1.000
Bryozoa	0.337	0.134	70.4	0.954
[60 − 70[*vs* [110 − 120[				
Cirripedia	0.407	1.281	30.9	0.038
Ochrophyta	0.815	0.000	50.5	0.634
Sedentaria	0.165	0.683	68.1	0.049
Bryozoa	0.336	0.472	81.7	0.437
[70 − 80[*vs* [80 − 90[				
Rhodophyta	0.682	0.767	22.7	0.003
Ochrophyta	0.660	0.485	43.9	0.929
Bryozoa	0.433	0.358	60.7	0.003
Cirripedia	0.353	0.460	76.3	1.000
[70 − 80[*vs* [90 − 100[				
Ochrophyta	0.660	0.582	22.6	0.692
Cirripedia	0.353	0.846	44.0	0.113
Rhodophyta	0.682	0.578	64.6	0.109
Bryozoa	0.433	0.142	78.1	0.513
[70 − 80[*vs* [100 − 110[				
Cirripedia	0.353	1.236	27.7	0.001
Ochrophyta	0.660	0.271	45.3	0.993
Rhodophyta	0.682	0.366	61.9	0.696
Bryozoa	0.433	0.134	75.0	0.552
[70 − 80[*vs* [110 − 120[				
Cirripedia	0.353	1.281	30.1	0.042
Sedentaria	0.179	0.683	47.8	0.053
Bryozoa	0.433	0.472	64.1	0.324
Ochrophyta	0.660	0.000	79.6	0.830

Table S5.70 (continued).

Higher taxonomical group	Average a	Average b	Cumulative contribution (%)	p-value
[80 − 90[*vs* [90 − 100[				
Cirripedia	0.460	0.846	22.8	0.001
Rhodophyta	0.767	0.578	44.6	0.009
Ochrophyta	0.485	0.582	64.4	0.998
Bryozoa	0.358	0.142	76.1	0.943
[80 − 90[*vs* [100 − 110[				
Cirripedia	0.460	0.236	29.1	0.001
Rhodophyta	0.366	0.767	46.8	0.576
Ochrophyta	0.271	0.485	61.1	1.000
Bryozoa	0.134	0.358	72.5	0.899
[80 − 90[*vs* [110 − 120[				
Cirripedia	0.460	1.281	31.8	0.045
Sedentaria	0.205	0.683	50.6	0.051
Bryozoa	0.358	0.472	65.8	0.409
Rhodophyta	0.767	0.000	80.2	0.564
[90 − 100[*vs* [100 − 110[				
Cirripedia	0.846	1.236	31.6	0.001
Ochrophyta	0.582	0.271	49.1	1.000
Rhodophyta	0.578	0.366	66.1	0.803
Sedentaria	0.230	0.268	78.0	0.068
[90 − 100[*vs* [110 − 120[				
Cirripedia	0.846	1.281	32.8	0.077
Sedentaria	0.230	0.683	53.1	0.064
Ochrophyta	0.582	0.000	679	0.907
Rhodophyta	0.578	0.000	81.2	0.685
[100 − 110[*vs* [110 − 120[				
Cirripedia	1.236	1.281	38.8	0.061
Sedentaria	0.268	0.683	61.7	0.045
Bryozoa	0.134	0.472	74.6	0.607

Table S5.71. Results of the SIMPER analysis on epibiotic biomass showing the most influential higher taxonomical groups discriminating among euendolithic infestation levels (from A to E, as defined by Kaehler, 1999). Cut-off for low contribution: 70%. Significant p-values are underlined.

Higher taxonomical group	Average a	Average b	Cumulative contribution (%)	p-value
A *vs* B				
Ochrophyta	0.876	0.883	32.0	<u>0.001</u>
Rhodophyta	0.494	0.581	50.0	0.535
Bryozoa	0.251	0.173	60.5	0.919
Cirripedia	0.078	0.326	70.1	1.000
A *vs* C				
Ochrophyta	0.876	0.550	26.5	<u>0.050</u>
Rhodophyta	0.494	0.570	43.0	0.684
Bryozoa	0.251	0.447	58.5	0.111
Cirripedia	0.078	0.519	71.8	1.000
A *vs* D				
Ochrophyta	0.876	0.514	25.9	0.060
Cirripedia	0.078	0.665	42.5	0.909
Rhodophyta	0.494	0.550	58.7	0.688
Bryozoa	0.251	0.278	70.8	0.661
A *vs* E				
Ochrophyta	0.876	1.278	38.2	<u>0.001</u>
Rhodophyta	0.494	0.331	53.6	0.786
Cirripedia	0.078	0.380	64.5	0.994
Bryozoa	0.251	0.073	73.2	0.928
B *vs* C				
Ochrophyta	0.884	0.550	26.7	<u>0.001</u>
Rhodophyta	0.581	0.570	45.5	0.297
Cirripedia	0.326	0.519	61.7	0.999
Bryozoa	0.173	0.447	75.7	0.278
B *vs* D				
Ochrophyta	0.884	0.514	26.2	<u>0.005</u>
Cirripedia	0.326	0.665	45.3	0.657
Rhodophyta	0.581	0.550	64.1	0.272
Bryozoa	0.173	0.278	74.4	0.999
B *vs* E				
Ochrophyta	0.884	1.278	38.1	<u>0.001</u>
Rhodophyta	0.581	0.331	56.5	0.600
Cirripedia	0.326	0.380	71.4	0.983
C *vs* D				
Cirripedia	0.519	0.665	21.0	<u>0.013</u>
Ochrophyta	0.550	0.514	40.9	1.000
Rhodophyta	0.570	0.550	59.2	0.503
Bryozoa	0.447	0.278	74.8	<u>0.001</u>

Table S5.71 (continued).

Higher taxonomical group	Average a	Average b	Cumulative contribution (%)	p-value
C *vs* E				
Ochrophyta	0.550	1.278	33.6	0.006
Cirripedia	0.519	0.380	50.5	0.841
Rhodophyta	0.570	0.331	66.7	0.709
Bryozoa	0.447	0.073	79.5	0.603
D *vs* E				
Ochrophyta	0.514	1.278	33.5	0.003
Cirripedia	0.665	0.380	53.4	0.466
Rhodophyta	0.550	0.331	69.6	0.698
Bryozoa	0.278	0.073	78.2	0.975

Table S5.72. Results of the SIMPER analysis on epibiotic biomass showing the most influential higher taxonomical groups discriminating among shell degradation indexes (from 1 to 6, as defined by Ma et al., 2023). Cut-off for low contribution: 70%. Significant p-values are underlined.

Higher taxonomical group	Average a	Average b	Cumulative contribution (%)	p-value
1 *vs* 2				
Ochrophyta	0.559	1.534	42.7	0.003
Bivalvia	0.600	0.000	59.7	0.037
Bryozoa	0.225	0.179	71.3	0.657
1 *vs* 3				
Ochrophyta	0.559	0.793	26.7	0.192
Rhodophyta	0.000	1.003	46.4	0.334
Bivalvia	0.600	0.097	62.9	0.021
Bryozoa	0.225	0.125	72.4	0.748
1 *vs* 4				
Ochrophyta	0.559	0.507	21.4	0.501
Bivalvia	0.600	0.144	38.2	0.017
Rhodophyta	0.000	0.807	54.6	0.463
Cirripedia	0.000	0.524	67.4	0.910
Bryozoa	0.225	0.524	79.9	0.484
1 *vs* 6				
Bivalvia	0.600	0.446	20.3	0.005
Ochrophyta	0.559	0.370	40.2	0.590
Cirripedia	0.000	0.765	55.6	0.698
Sedentaria	0.000	0.291	64.8	0.379
Errantia	0.188	0.046	72.1	0.033
2 *vs* 3				
Ochrophyta	0.793	1.534	39.1	0.001
Rhodophyta	1.003	0.452	63.5	0.052
Cirripedia	0.341	0.055	72.5	1.000
2 *vs* 4				
Ochrophyta	1.534	0.507	37.0	0.001
Rhodophyta	0.452	0.807	56.8	0.228
Cirripedia	0.055	0.524	69.5	1.000
Bryozoa	0.179	0.316	80.3	0.914
2 *vs* 5				
Ochrophyta	1.534	0.538	38.3	0.001
Cirripedia	0.055	0.653	54.5	0.974
Bryozoa	0.179	0.383	67.8	0.503
Rhodophyta	0.452	0.316	79.0	0.999
2 *vs* 6				
Ochrophyta	1.534	0.370	35.9	0.001
Cirripedia	0.765	0.055	50.8	0.905
Rhodophyta	0.282	0.452	62.1	0.933
Sedentaria	0.291	0.145	72.0	0.271

Table S5.72 (continued).

Higher taxonomical group	Average a	Average b	Cumulative contribution (%)	p-value
3 *vs* 4				
Rhodophyta	1.003	0.807	27.6	0.001
Ochrophyta	0.793	0.507	51.7	0.301
Cirripedia	0.341	0.524	67.7	0.999
Bryozoa	0.125	0.316	77.6	0.999
3 *vs* 5				
Ochrophyta	0.793	0.538	25.6	0.070
Rhodophyta	1.003	0.316	46.3	0.002
Cirripedia	0.341	0.653	64.8	0.753
Bryozoa	0.125	0.383	76.9	0.865
3 *vs* 6				
Ochrophyta	0.793	0.370	22.3	0.516
Rhodophyta	1.003	0.282	43.6	0.144
Cirripedia	0.341	0.765	61.6	0.649
Sedentaria	0.182	0.291	72.5	0.163
4 *vs* 5				
Cirripedia	0.524	0.653	20.9	0.014
Ochrophyta	0.507	0.538	40.4	1.000
Rhodophyta	0.807	0.316	59.8	0.066
Bryozoa	0.316	0.383	74.6	0.010
4 *vs* 6				
Cirripedia	0.765	0.524	20.6	0.281
Rhodophyta	0.282	0.807	39.5	0.347
Ochrophyta	0.370	0.507	56.1	0.981
Sedentaria	0.291	0.183	66.8	0.136
Bivalvia	0.446	0.144	77.4	0.024
5 *vs* 6				
Cirripedia	0.765	0.653	23.1	0.046
Ochrophyta	0.370	0.538	40.7	0.960
Sedentaria	0.291	0.206	52.5	0.072
Rhodophyta	0.282	0.316	63.5	0.987
Bivalvia	0.446	0.150	74.4	0.027

Table S5.73. Results of the SIMPER analysis on epibiotic biomass showing the most influential higher taxonomical groups discriminating among position of the epibionts on the mussel shell (i.e., infested, non-infested, secondary epibiosis). Cut-off for low contribution: 70%. Significant p-values are underlined.

Higher taxonomical group	Average a	Average b	Cumulative contribution (%)	p-value
Infested *vs* Non-infested				
Ochrophyta	0.220	1.080	26.0	<u>0.001</u>
Cirripedia	0.527	0.540	44.6	0.637
Rhodophyta	0.187	0.833	61.9	0.465
Bryozoa	0.560	0.074	76.0	<u>0.001</u>
Infested *vs* II epibiosis				
Cirripedia	0.527	0.548	19.7	0.196
Rhodophyta	0.187	0.895	37.3	0.420
Bryozoa	0.560	0.234	54.6	<u>0.002</u>
Sedentaria	0.354	0.000	63.8	0.264
Bivalvia	0.236	0.194	72.1	<u>0.035</u>
Non-infested *vs* II epibiosis				
Ochrophyta	1.080	0.089	25.2	0.065
Rhodophyta	0.833	0.895	50.1	<u>0.001</u>
Cirripedia	0.540	0.548	69.0	0.541
Bryozoa	0.074	0.234	76.7	1.000

Table S5.74. Results of the SIMPER analysis on epibiotic biomass showing the most influential taxa discriminating among shell length sizes (from]30 − 40] to]110 − 120] in mm). Cut-off for low contribution: 70%. Significant p-values are underlined.

Species	Average a	Average b	Cumulative contribution (%)	p-value
[30 − 40[*vs* [40 − 50[				
Ralfsia verrucosa	0.544	0.548	0.291	0.117
Perna perna	0.332	0.161	44.467	0.028
Tetraclita serrata	0.000	0.297	55.532	0.911
Electra verticillata	0.175	0.171	65.458	0.268
Paramoera capensis	0.062	0.168	73.624	0.003
[30 − 40[*vs* [50 − 60[				
Ralfsia verrucosa	0.544	1.091	35.130	0.015
Perna perna	0.332	0.098	48.281	0.061
Electra verticillata	0.175	0.221	59.753	0.165
Hildenbrandia lecannellieri	0.000	0.259	67.572	0.832
Tetraclita serrata	0.000	0.235	73.189	1.000
[30 − 40[*vs* [60 − 70[				
Ralfsia verrucosa	0.544	0.815	28.367	0.123
Perna perna	0.332	0.286	43.507	0.009
Tetraclita serrata	0.000	0.380	53.096	0.996
Electra verticillata	0.175	0.117	60.739	0.415
Bryozoa	0.000	0.219	67.543	0.450
Errantia	0.146	0.054	73.437	0.002
[30 − 40[*vs* [70 − 80[				
Ralfsia verrucosa	0.544	0.685	24.634	0.261
Electra verticillata	0.175	0.274	36.953	0.091
Perna perna	0.332	0.124	48.651	0.070
Hildenbrandia lecannellieri	0.000	0.357	58.399	0.704
Tetraclita serrata	0.000	0.339	67.514	0.997
Actiniaria	0.119	0.033	72.487	0.028
[30 − 40[*vs* [80 − 90[				
Ralfsia verrucosa	0.544	0.484	21.143	0.475
Tetraclita serrata	0.000	0.445	32.859	0.937
Perna perna	0.332	0.090	44.108	0.066
Hildenbrandia lecannellieri	0.000	0.478	55.311	0.570
Electra verticillata	0.175	0.192	65.378	0.165
Errantia	0.146	0.008	70.031	0.015
[30 − 40[*vs* [90 − 100[				
Ralfsia verrucosa	0.544	0.582	22.588	0.324
Tetraclita serrata	0.000	0.832	43.503	0.183
Perna perna	0.332	0.115	54.428	0.067
Hildenbrandia lecannellieri	0.000	0.398	64.192	0.665
Electra verticillata	0.175	0.000	69.062	0.618
Errantia	0.146	0.000	73.464	0.034

Table S5.74 (continued).

Species	Average a	Average b	Cumulative contribution (%)	p-value
[30 − 40[*vs* [100 − 110[				
Tetraclita serrata	0.000	1.231	29.679	0.001
Ralfsia verrucosa	0.544	0.271	46.376	0.764
Perna perna	0.332	0.210	58.905	0.039
Spirobranchus kraussii	0.000	0.244	66.596	0.181
Electra verticillata	0.175	0.000	71.379	0.640
[30 − 40[*vs* [110 − 120[				
Chthamalus dentatus	0.000	0.706	19.163	0.001
Spirobranchus kraussii	0.000	0.683	37.120	0.020
Tetraclita serrata	0.000	0.901	0.536	0.501
Ralfsia verrucosa	0.544	0.000	66.730	0.808
Perna perna	0.332	0.000	75.414	0.251
[40 − 50[*vs* [50 − 60[				
Ralfsia verrucosa	0.648	1.091	35.835	0.006
Tetraclita serrata	0.297	0.235	49.738	0.936
Hildenbrandia lecannellieri	0.142	0.259	30.201	0.756
Electra verticillata	0.141	0.221	70.087	0.214
[40 − 50[*vs* [60 − 70[				
Ralfsia verrucosa	0.648	0.815	29.285	0.053
Tetraclita serrata	0.297	0.380	45.002	0.810
Perna perna	0.161	0.286	54.886	0.109
Bryozoa	0.126	0.219	64.178	0.217
Hildenbrandia lecannellieri	0.142	0.167	70.811	0.959
[40 − 50[*vs* [70 − 80[				
Ralfsia verrucosa	0.648	0.685	25.988	0.143
Tetraclita serrata	0.297	0.339	40.665	0.890
Hildenbrandia lecannellieri	0.142	0.357	52.494	0.604
Electra verticillata	0.141	0.274	63.753	0.086
Bryozoa	0.126	0.159	71.048	0.408
[40 − 50[*vs* [80 − 90[				
Ralfsia verrucosa	0.648	0.484	22.896	0.368
Tetraclita serrata	0.297	0.445	39.634	0.674
Hildenbrandia lecannellieri	0.142	0.478	52.941	0.407
Electra verticillata	0.141	0.192	61.979	0.219
Bryozoa	0.126	0.166	69.208	0.388
Perna perna	0.161	0.090	75.048	0.413
[40 − 50[*vs* [90 − 100[				
Ralfsia verrucosa	0.648	0.582	25.005	0.250
Tetraclita serrata	0.297	0.831	48.676	0.064
Hildenbrandia lecannellieri	0.142	0.398	60.895	0.550
Bryozoa	0.126	0.142	67.561	0.501
Perna perna	0.161	0.115	73.368	0.448

Table S5.74 (continued).

Species	Average a	Average b	Cumulative contribution (%)	p-value
[40 − 50[*vs* [100 − 110[				
Tetraclita serrata	0.297	1.231	30.586	0.001
Ralfsia verrucosa	0.648	0.271	50.123	0.734
Perna perna	0.161	0.210	58.270	0.223
Spirobranchus kraussii	0.000	0.244	66.037	0.224
Bryozoa	0.126	0.134	72.451	0.525
[40 − 50[*vs* [110 − 120[				
Tetraclita serrata	0.297	0.901	19.946	0.330
Chthamalus dentatus	0.000	0.706	0.390	0.001
Spirobranchus kraussii	0.000	0.683	56.813	0.031
Ralfsia verrucosa	0.648	0.000	72.267	0.749
[50 − 60[*vs* [60 − 70[				
Ralfsia verrucosa	1.091	0.815	33.156	0.001
Tetraclita serrata	0.235	0.380	45.620	0.999
Hildenbrandia lecannellieri	0.259	0.167	55.157	0.961
Perna perna	0.098	0.286	63.359	0.089
Electra verticillata	0.221	0.117	71.202	0.442
[50 − 60[*vs* [70 − 80[				
Ralfsia verrucosa	1.091	0.685	31.244	0.001
Hildenbrandia lecannellieri	0.259	0.357	45.143	0.434
Electra verticillata	0.221	0.274	57.301	0.003
Tetraclita serrata	0.235	0.339	69.084	1.000
Bryozoa	0.055	0.159	74.509	0.887
[50 − 60[*vs* [80 − 90[				
Ralfsia verrucosa	1.091	0.484	29.254	0.001
Hildenbrandia lecannellieri	0.259	0.478	44.393	0.112
Tetraclita serrata	0.235	0.445	58.205	1.000
Electra verticillata	0.221	0.192	68.217	0.022
Spirobranchus kraussii	0.141	0.130	75.170	0.178
[50 − 60[*vs* [90 − 100[				
Ralfsia verrucosa	1.091	0.582	30.416	0.001
Tetraclita serrata	0.235	0.831	51.899	0.052
Hildenbrandia lecannellieri	0.259	0.398	65.819	0.352
Spirobranchus kraussii	0.141	0.158	73.006	0.190
[50 − 60[*vs* [100 − 110[				
Tetraclita serrata	0.235	1.231	28.099	0.001
Ralfsia verrucosa	1.091	0.271	54.515	0.018
Spirobranchus kraussii	0.141	0.244	64.014	0.009
Hildenbrandia lecannellieri	0.259	0.142	72.087	0.970

Table S5.74 (continued).

Species	Average a	Average b	Cumulative contribution (%)	p-value
[50 − 60[*vs* [110 − 120[				
Ralfsia verrucosa	1.091	0.000	24.150	0.297
Chthamalus dentatus	0.000	0.706	41.826	0.001
Tetraclita serrata	0.235	0.901	59.242	0.442
Spirobranchus kraussii	0.141	0.683	76.269	0.024
[60 − 70[*vs* [70 − 80[				
Ralfsia verrucosa	0.815	0.685	25.566	0.012
Tetraclita serrata	0.380	0.339	38.968	1.000
Hildenbrandia lecannellieri	0.167	0.357	49.743	0.914
Electra verticillata	0.117	0.274	58.916	0.040
Bryozoa	0.219	0.159	67.416	0.089
Perna perna	0.286	0.124	75.135	0.053
[60 − 70[*vs* [80 − 90[				
Ralfsia verrucosa	0.815	0.484	23.200	0.153
Tetraclita serrata	0.380	0.445	38.341	0.997
Hildenbrandia lecannellieri	0.167	0.478	50.461	0.687
Bryozoa	0.219	0.166	58.900	0.036
Perna perna	0.286	0.090	66.200	0.041
Electra verticillata	0.117	0.192	73.367	0.461
[60 − 70[*vs* [90 − 100[				
Ralfsia verrucosa	0.815	0.582	24.837	0.067
Tetraclita serrata	0.380	0.831	46.245	0.014
Hildenbrandia lecannellieri	0.167	0.398	57.374	0.872
Bryozoa	0.219	0.142	65.433	0.178
Perna perna	0.286	0.115	72.760	0.087
[60 − 70[*vs* [100 − 110[				
Tetraclita serrata	0.380	1.231	27.399	0.001
Ralfsia verrucosa	0.815	0.271	48.051	0.761
Perna perna	0.286	0.210	57.237	0.012
Bryozoa	0.219	0.134	65.036	0.255
Spirobranchus kraussii	0.063	0.244	72.663	0.083
[60 − 70[*vs* [110 − 120[				
Tetraclita serrata	0.380	0.901	18.314	0.400
Ralfsia verrucosa	0.815	0.000	35.760	0.675
Chthamalus dentatus	0.012	0.706	52.522	0.001
Spirobranchus kraussii	0.063	0.683	68.362	0.028
Bryozoa	0.219	0.472	79.218	0.197

Table S5.74 (continued).

Species	Average a	Average b	Cumulative contribution (%)	p-value
[70 − 80[*vs* [80 − 90[				
Ralfsia verrucosa	0.685	0.484	20.435	0.940
Hildenbrandia lecannellieri	0.357	0.478	36.307	0.013
Tetraclita serrata	0.339	0.445	50.957	1.000
Electra verticillata	0.274	0.192	62.034	0.001
Bryozoa	0.159	0.166	69.048	0.434
Gelidium pristoides	0.325	0.275	75.628	0.056
[70 − 80[*vs* [90 − 100[				
Ralfsia verrucosa	0.685	0.582	22.069	0.640
Tetraclita serrata	0.339	0.831	24.484	0.099
Hildenbrandia lecannellieri	0.357	0.398	57.186	0.159
Electra verticillata	0.274	0.000	64.599	0.465
Bryozoa	0.159	0.142	71.112	0.652
[70 − 80[*vs* [100 − 110[				
Tetraclita serrata	0.339	1.231	26.285	0.001
Ralfsia verrucosa	0.685	0.271	43.389	0.989
Hildenbrandia lecannellieri	0.357	0.142	53.372	0.902
Spirobranchus kraussii	0.066	0.244	60.932	0.107
Electra verticillata	0.274	0.000	68.194	0.436
Gelidium pristoides	0.325	0.224	74.716	0.159
[70 − 80[*vs* [110 − 120[				
Tetraclita serrata	0.339	0.901	17.697	0.469
Chthamalus dentatus	0.000	0.706	34.274	0.001
Spirobranchus kraussii	0.066	0.683	49.863	0.028
Ralfsia verrucosa	0.685	0.000	63.411	0.857
Bryozoa	0.159	0.472	73.089	0.241
[80 − 90[*vs* [90 − 100[				
Tetraclita serrata	0.445	0.831	21.905	0.003
Ralfsia verrucosa	0.484	0.582	41.175	0.991
Hildenbrandia lecannellieri	0.478	0.398	57.469	0.014
Bryozoa	0.166	0.142	64.048	0.681
Spirobranchus kraussii	0.130	0.158	70.623	0.209
[80 − 90[*vs* [100 − 110[				
Tetraclita serrata	0.445	1.231	27.661	0.001
Ralfsia verrucosa	0.484	0.271	41.357	1.000
Hildenbrandia lecannellieri	0.478	0.142	53.079	0.743
Spirobranchus kraussii	0.130	0.244	62.144	0.008
Bryozoa	0.166	0.134	68.535	0.674
Perna perna	0.090	0.210	74.605	0.428

Table S5.74 (continued).

Species	Average a	Average b	Cumulative contribution (%)	p-value
[80 − 90[*vs* [110 − 120[				
Tetraclita serrata	0.445	0.901	19.541	0.333
Chthamalus dentatus	0.007	0.706	36.741	0.001
Spirobranchus kraussii	0.130	0.683	53.271	0.035
Bryozoa	0.166	0.472	63.259	0.237
Ralfsia verrucosa	0.484	0.000	72.966	0.994
[90 − 100[*vs* [100 − 110[				
Tetraclita serrata	0.831	1.231	30.298	0.001
Ralfsia verrucosa	0.582	0.271	47.240	1.000
Hildenbrandia lecannellieri	0.398	0.142	58.558	0.886
Spirobranchus kraussii	0.158	0.244	68.417	0.008
Perna perna	0.115	0.210	74.866	0.446
[90 − 100[*vs* [110 − 120[				
Tetraclita serrata	0.831	0.901	23.656	0.185
Chthamalus dentatus	0.000	0.706	41.357	0.001
Spirobranchus kraussii	0.158	0.683	58.342	0.025
Ralfsia verrucosa	0.582	0.000	70.739	0.946
[100 − 110[*vs* [110 − 120[				
Tetraclita serrata	1.231	0.901	29.657	0.083
Chthamalus dentatus	0.000	0.706	48.769	0.001
Spirobranchus kraussii	0.244	0.683	67.206	0.025
Bryozoa	0.134	0.472	77.772	0.247

Table S5.75. Results of the SIMPER analysis on epibiotic biomass showing the most influential taxa discriminating among euendolithic infestation levels (from A to E, as defined by Kaehler, 1999). Cut-off for low contribution: 70%. Significant p-values are underlined.

Higher taxonomical group	Average a	Average b	Cumulative contribution (%)	p-value
A *vs* B				
Ralfsia verrucosa	0.876	0.884	31.3	<u>0.002</u>
Hildenbrandia lecannellieri	0.177	0.467	44.6	0.479
Tetraclita serrata	0.078	0.326	53.9	1.000
Perna perna	0.225	0.112	62.1	0.135
Bryozoa	0.186	0.034	67.6	0.793
Electra verticillata	0.065	0.139	73.0	0.533
A *vs* C				
Ralfsia verrucosa	0.876	0.550	25.7	0.056
Tetraclita serrata	0.078	0.499	38.3	0.998
Hildenbrandia lecannellieri	0.177	0.368	49.4	0.747
Bryozoa	0.186	0.252	58.9	0.052
Perna perna	0.225	0.137	66.9	0.074
Electra verticillata	0.065	0.195	73.8	0.510
A *vs* D				
Ralfsia verrucosa	0.876	0.522	25.2	0.055
Tetraclita serrata	0.078	0.643	40.8	0.913
Hildenbrandia lecannellieri	0.177	0.297	51.0	0.879
Perna perna	0.225	0.154	59.4	0.069
Bryozoa	0.186	0.140	66.6	0.386
Gelidium pristoides	0.317	0.248	72.6	0.240
A *vs* E				
Ralfsia verrucosa	0.876	1.278	37.7	<u>0.002</u>
Tetraclita serrata	0.078	0.380	48.5	0.994
Hildenbrandia lecannellieri	0.177	0.193	57.4	0.886
Perna perna	0.225	0.123	65.7	0.266
Gelidium pristoides	0.317	0.138	72.6	0.299
B *vs* C				
Ralfsia verrucosa	0.884	0.550	26.1	<u>0.010</u>
Tetraclita serrata	0.326	0.499	41.6	0.995
Hildenbrandia lecannellieri	0.467	0.368	56.8	0.063
Electra verticillata	0.139	0.195	64.6	0.289
Spirobranchus kraussii	0.155	0.155	71.8	0.052
B *vs* D				
Ralfsia verrucosa	0.884	0.522	25.7	<u>0.004</u>
Tetraclita serrata	0.326	0.643	43.8	0.663
Hildenbrandia lecannellieri	0.467	0.297	58.4	0.110
Electra verticillata	0.139	0.138	64.9	0.770
Spirobranchus kraussii	0.155	0.115	71.3	0.265

Table S5.75 (continued).

Higher taxonomical group	Average a	Average b	Cumulative contribution (%)	p-value
B *vs* E				
Ralfsia verrucosa	0.884	1.278	37.4	0.004
Tetraclita serrata	0.326	0.380	52.1	0.969
Hildenbrandia lecannellieri	0.467	0.193	66.2	0.496
Gelidium pristoides	0.088	0.138	70.9	0.543
C *vs* D				
Tetraclita serrata	0.499	0.643	19.7	0.017
Ralfsia verrucosa	0.550	0.522	38.9	1.000
Hildenbrandia lecannellieri	0.368	0.297	51.8	0.497
Bryozoa	0.252	0.140	60.4	0.002
Electra verticillata	0.195	0.138	68.5	0.035
Spirobranchus kraussii	0.155	0.115	74.9	0.155
C *vs* E				
Ralfsia verrucosa	0.550	1.278	33.0	0.005
Tetraclita serrata	0.499	0.380	49.4	0.821
Hildenbrandia lecannellieri	0.368	0.193	60.7	0.713
Bryozoa	0.252	0.073	67.9	0.440
Electra verticillata	0.195	0.000	73.4	0.747
D *vs* E				
Ralfsia verrucosa	0.522	1.278	32.9	0.002
Tetraclita serrata	0.643	0.380	51.9	0.465
Hildenbrandia lecannellieri	0.297	0.193	62.4	0.809
Gelidium pristoides	0.248	0.138	68.4	0.317
Perna perna	0.154	0.123	73.4	0.609

Table S5.76. Results of the SIMPER analysis on epibiotic biomass showing the most influential taxa discriminating among shell degradation indexes (from 1 to 6, as defined by Ma et al., 2023). Cut-off for low contribution: 70%. Significant p-values are underlined.

Higher taxonomical group	Average a	Average b	Cumulative contribution (%)	p-value
1 *vs* 2				
Ralfsia verrucosa	0.559	1.534	41.9	0.003
Perna perna	0.600	0.000	58.5	0.026
Electra verticillata	0.225	0.020	66.4	0.415
Errantia	0.188	0.073	73.9	0.004
1 *vs* 3				
Ralfsia verrucosa	0.559	0.793	26.5	0.202
Perna perna	0.600	0.097	43.0	0.017
Hildenbrandia lecannellieri	0.000	0.676	58.3	0.281
Electra verticillata	0.225	0.071	66.6	0.363
Tetraclita serrata	0.000	0.339	74.4	0.996
1 *vs* 4				
Ralfsia verrucosa	0.559	0.521	21.0	0.508
Perna perna	0.600	0.144	37.5	0.013
Hildenbrandia lecannellieri	0.000	0.565	50.6	0.377
Tetraclita serrata	0.000	0.516	63.0	0.873
Electra verticillata	0.225	0.164	72.4	0.239
1 *vs* 5				
Ralfsia verrucosa	0.559	0.538	22.2	0.427
Perna perna	0.600	0.150	39.3	0.021
Tetraclita serrata	0.000	0.624	54.8	0.665
Electra verticillata	0.225	0.182	65.7	0.125
Errantia	0.188	0.004	71.8	0.003
1 *vs* 6				
Perna perna	0.600	0.446	20.2	0.003
Ralfsia verrucosa	0.559	0.370	40.0	0.580
Tetraclita serrata	0.000	0.765	55.2	0.663
Gelidium pristoides	0.000	0.282	62.1	0.289
Electra verticillata	0.225	0.000	68.6	0.488
Errantia	0.188	0.000	74.6	0.016
2 *vs* 3				
Ralfsia verrucosa	1.534	0.793	38.1	0.001
Hildenbrandia lecannellieri	0.118	0.676	55.0	0.182
Tetraclita serrata	0.055	0.339	63.8	1.000
Gelidium pristoides	0.273	0.327	71.0	0.194

Table S5.76 (continued).

Higher taxonomical group	Average a	Average b	Cumulative contribution (%)	p-value
2 *vs* 4				
Ralfsia verrucosa	1.534	0.521	36.1	0.001
Hildenbrandia lecannellieri	0.118	0.565	49.9	0.339
Tetraclita serrata	0.055	0.516	62.1	1.000
Bryozoa	0.160	0.152	69.1	0.513
Gelidium pristoides	0.273	0.245	74.6	0.358
2 *vs* 5				
Ralfsia verrucosa	1.534	0.538	37.4	0.001
Tetraclita serrata	0.055	0.624	52.5	0.980
Bryozoa	0.160	0.201	60.7	0.212
Electra verticillata	0.020	0.182	66.5	0.829
Hildenbrandia lecannellieri	0.118	0.157	72.2	1.000
2 *vs* 6				
Ralfsia verrucosa	1.534	0.370	35.5	0.001
Tetraclita serrata	0.055	0.765	50.1	0.874
Gelidium pristoides	0.273	0.282	58.8	0.098
Perna perna	0.000	0.446	67.0	0.155
Gunnarea gaimardi	0.145	0.132	72.5	0.070
3 *vs* 4				
Ralfsia verrucosa	0.793	0.521	23.5	0.288
Hildenbrandia lecannellieri	0.676	0.565	45.0	0.001
Tetraclita serrata	0.339	0.516	60.6	0.998
Gelidium pristoides	0.327	0.245	67.1	0.080
Spirobranchus kraussii	0.092	0.139	72.5	0.696
3 *vs* 5				
Ralfsia verrucosa	0.793	0.538	24.0	0.070
Tetraclita serrata	0.339	0.624	41.5	0.780
Hildenbrandia lecannellieri	0.676	0.157	57.8	0.010
Electra verticillata	0.071	0.182	64.4	0.703
Bryozoa	0.054	0.201	70.2	0.865
3 *vs* 6				
Ralfsia verrucosa	0.793	0.370	21.6	0.518
Tetraclita serrata	0.339	0.765	39.0	0.581
Hildenbrandia lecannellieri	0.676	0.000	52.5	0.343
Perna perna	0.097	0.446	61.9	0.047
Gelidium pristoides	0.327	0.282	71.4	0.043

Table S5.76 (continued).

Higher taxonomical group	Average a	Average b	Cumulative contribution (%)	p-value
4 *vs* 5				
Tetraclita serrata	0.516	0.624	19.8	0.015
Ralfsia verrucosa	0.521	0.538	38.8	1.000
Hildenbrandia lecannellieri	0.565	0.157	53.4	0.013
Electra verticillata	0.164	0.182	61.4	0.062
Bryozoa	0.152	0.201	69.1	0.091
Spirobranchus kraussii	0.139	0.140	75.4	0.134
4 *vs* 6				
Tetraclita serrata	0.516	0.765	19.8	0.196
Ralfsia verrucosa	0.521	0.370	36.0	0.983
Hildenbrandia lecannellieri	0.565	0.000	47.8	0.569
Perna perna	0.144	0.446	58.1	0.033
Gelidium pristoides	0.245	0.282	66.5	0.069
Spirobranchus kraussii	0.139	0.113	72.6	0.360
5 *vs* 6				
Tetraclita serrata	0.624	0.765	22.1	0.050
Ralfsia verrucosa	0.538	0.370	39.3	0.966
Perna perna	0.150	0.446	49.9	0.019
Gelidium pristoides	0.148	0.282	57.7	0.112
Spirobranchus kraussii	0.140	0.113	64.3	0.262
Electra verticillata	0.182	0.000	69.4	0.835
Gunnarea gaimardi	0.057	0.132	74.2	0.096

Table S5.77. Results of the SIMPER analysis on epibiotic biomass showing the most influential taxa discriminating among position of the epibionts on the mussel shell (i.e., infested, non-infested, secondary epibiosis). Cut-off for low contribution: 70%. Significant p-values are underlined.

Higher taxonomical group	Average a	Average b	Cumulative contribution (%)	p-value
Infested *vs* Non-infested				
Ralfsia verrucosa	0.229	1.080	25.6	0.001
Tetraclita serrata	0.520	0.521	43.4	0.531
Hildenbrandia lecannellieri	0.113	0.563	57.0	0.001
Electra verticillata	0.274	0.041	64.4	0.003
Bryozoa	0.286	0.032	71.3	0.259
Infested *vs* II epibiosis				
Tetraclita serrata	0.520	0.494	18.3	0.310
Gelidium pristoides	0.062	0.716	29.2	0.001
Bryozoa	0.286	0.173	39.3	0.010
Electra verticillata	0.274	0.061	47.5	0.146
Perna perna	0.236	0.194	55.6	0.022
Ralfsia verrucosa	0.229	0.089	62.2	1.000
Spirobranchus kraussii	0.262	0.000	68.8	0.171
Hildenbrandia lecannellieri	0.113	0.179	75.3	1.000
Non-infested *vs* II epibiosis				
Ralfsia verrucosa	1.080	0.089	24.0	0.065
Tetraclita serrata	0.521	0.494	41.3	0.605
Hildenbrandia lecannellieri	0.563	0.179	55.5	0.174
Gelidium pristoides	0.264	0.716	67.8	0.001
Ulva sp.	0.051	0.341	74.3	0.001

5.3.2.2.3.1. Shell length size

Table S5.78. Results of the TukeySD post-hoc pairwise comparisons on the relationship between the mean biomass of Cirripedia per mussel and shell length range (from]30 − 40] to]110 − 120] in mm). No significant p-values were detected.

Shell length range (a)	Shell length range (b)	Estimate	Std Error	z-value	p-value
]30 − 40]	Others	NA	NA	NA	NA
]40 − 50]	]50 − 60]	– 0.049	0.078	– 0.632	0.998
	]60 − 70]	– 0.072	0.076	– 0.957	0.971
	]70 − 80]	– 0.007	0.081	– 0.084	1.000
	]80 − 90]	– 0.054	0.076	– 0.709	0.995
	]90 − 100]	– 0.069	0.075	– 0.910	0.978
	]100 − 110]	– 0.076	0.075	– 1.013	0.961
	]110 − 120]	– 0.048	0.087	– 0.553	0.999
]50 − 60]	]60 − 70]	– 0.023	0.023	– 1.010	0.962
	]70 − 80]	0.043	0.037	1.153	0.923
	]80 − 90]	– 0.004	0.023	– 0.186	1.000
	]90 − 100]	– 0.019	0.022	– 0.870	0.983
	]100 − 110]	– 0.027	0.022	– 1.227	0.897
	]110 − 120]	0.001	0.049	0.026	1.000
]60 − 70]	]70 − 80]	0.066	0.031	2.102	0.341
	]80 − 90]	0.019	0.012	1.595	0.692
	]90 − 100]	0.004	0.010	0.375	1.000
	]100 − 110]	– 0.004	0.010	– 0.412	1.000
	]110 − 120]	0.024	0.045	0.544	0.999
]70 − 80]	]80 − 90]	– 0.047	0.031	– 1.495	0.757
	]90 − 100]	– 0.062	0.031	– 2.013	0.399
	]100 − 110]	– 0.070	0.031	– 2.271	0.246
	]110 − 120]	– 0.042	0.053	– 0.775	0.992
]80 − 90]	]90 − 100]	– 0.015	0.010	– 1-436	0.793
	]100 − 110]	– 0.023	0.010	– 2.243	0.261
	]110 − 120]	0.006	0.045	0.124	1.000
]90 − 100]	]100 − 110]	– 0.008	0.008	– 0.964	0.970
	]110 − 120]	0.021	0.044	0.463	1.000
]100 − 110]	]110 − 120]	0.028	0.044	0.638	0.997

Table S5.79. Results of the TukeySD post-hoc pairwise comparisons on the relationship between the mean biomass of *Tetraclita serrata* (Cirripedia) per mussel and shell length range (from]30 − 40] to]110 − 120] in mm). No significant p-values were detected.

Shell length range (a)	Shell length range (b)	Estimate	Std Error	z-value	p-value
]30 − 40]	Others	NA	NA	NA	NA
]40 − 50]	]50 − 60]	− 0.049	0.078	− 0.632	0.998
	]60 − 70]	− 0.072	0.076	− 0.951	0.972
	]70 − 80]	− 0.010	0.081	− 0.123	1.000
	]80 − 90]	− 0.055	0.076	− 0.729	0.994
	]90 − 100]	− 0.068	0.075	− 0.907	0.979
	]100 − 110]	− 0.076	0.075	− 1.009	0.962
	]110 − 120]	− 0.039	0.092	− 0.421	1.000
]50 − 60]	]60 − 70]	− 0.023	0.023	− 0.986	0.966
	]70 − 80]	0.039	0.037	1.072	0.947
	]80 − 90]	− 0.006	0.023	− 0.252	1.000
	]90 − 100]	− 0.019	0.022	− 0.861	0.984
	]100 − 110]	− 0.027	0.022	− 1.212	0.902
	]110 − 120]	0.011	0.057	0.185	1.000
]60 − 70]	]70 − 80]	0.062	0.031	1.993	0.410
	]80 − 90]	0.017	0.012	1.423	0.800
	]90 − 100]	0.003	0.010	0.341	1.000
	]100 − 110]	− 0.004	0.010	− 0.421	1.000
	]110 − 120]	0.033	0.054	0.615	0.998
]70 − 80]	]80 − 90]	− 0.045	0.031	− 1.451	0.783
	]90 − 100]	− 0.059	0.031	− 1.913	0.465
	]100 − 110]	− 0.066	0.030	− 2.168	0.300
	]110 − 120]	− 0.029	0.061	− 0.471	1.000
]80 − 90]	]90 − 100]	− 0.013	0.010	− 1.284	0.872
	]100 − 110]	− 0.021	0.010	− 2.076	0.355
	]110 − 120]	0.016	0.054	0.304	1.000
]90 − 100]	]100 − 110]	− 0.008	0.008	− 0.939	0.974
	]110 − 120]	0.030	0.054	0.554	0.999
]100 − 110]	]110 − 120]	0.037	0.054	0.696	0.996

5.3.2.2.3.2. Euendolithic infestation, shell degradation and position

Table S5.80. Results of the TukeySD post-hoc pairwise comparisons on the relationship between the average biomass of Cirripedia per mussel valve and euendolithic infestation levels (from A to E, as defined in Kaehler, 1999) for each shell degradation index (from 1 to 6, as defined in Ma *et al.*, 2023). No significant p-values were detected.

Infestation level (a)	Infestation level (b)	Estimate	Std Error	t-value	p-value
Shell degradation 1		NA	NA	NA	NA
Shell degradation 2					
A	B	1.742	2.690	0.647	0.967
Shell degradation 3					
A	B	0.034	0.085	0.404	0.994
	C	0.005	0.091	0.057	1.000
	D	– 0.067	0.151	– 0.446	0.992
	E	NA	NA	NA	NA
B	C	– 0.029	0.037	– 0.793	0.932
	D	– 0.101	0.126	– 0.806	0.929
	E	NA	NA	NA	NA
C	D	– 0.072	0.130	– 0.556	0.981
	E	NA	NA	NA	NA
D	E	NA	NA	NA	NA
Shell degradation 4					
A	Others	NA	NA	NA	NA
B	C	– 0.043	0.050	– 0.875	0.906
	D	0.019	0.038	0.506	0.987
	E	NA	NA	NA	NA
C	D	0.063	0.035	1.797	0.379
	E	NA	NA	NA	NA
D	E	NA	NA	NA	NA
Shell degradation 5					
A	Others	NA	NA	NA	NA
B	C	0.274	0.312	0.876	0.905
	D	0.273	0.312	0.876	0.905
	E	– 0.105	0.428	– 0.246	0.999
C	D	-1.940×10^{-4}	0.013	– 0.015	1.000
	E	– 0.379	0.293	– 1.294	0.695
D	E	– 0.379	0.293	– 1.294	0.695
Shell degradation 6					
A	Others	NA	NA	NA	NA
B	Others	NA	NA	NA	NA
C	D	-1.780×10^{-4}	0.023	– 0.008	1.000
	E	0.008	0.024	0.330	0.997
D	E	0.008	0.023	0.352	0.997

Table S5.81. Results of the TukeySD post-hoc pairwise comparisons on the relationship between the average biomass of *Tetraclita serrata* (Cirripedia) per mussel valve and euendolithic infestation levels (from A to E, as defined in Kaehler, 1999) for each shell degradation index (from 1 to 6, as defined in Ma *et al.*, 2023). No significant p-values were detected.

Infestation level (a)	Infestation level (b)	Estimate	Std Error	t-value	p-value
Shell degradation 1		NA	NA	NA	NA
Shell degradation 2					
A	B	1.742	2.658	0.655	0.966
Shell degradation 3					
A	B	0.035	0.084	0.413	0.994
	C	0.006	0.090	0.062	1.000
	D	– 0.105	0.181	– 0.582	0.978
	E	NA	NA	NA	NA
B	C	– 0.029	0.036	– 0.798	0.931
	D	– 0.140	0.161	– 0.867	0.909
	E	NA	NA	NA	NA
C	D	– 0.111	0.164	– 0.674	0.962
	E	NA	NA	NA	NA
D	E	NA	NA	NA	NA
Shell degradation 4					
A	Others	NA	NA	NA	NA
B	C	– 0.041	0.049	– 0.841	0.917
	D	0.020	0.038	0.522	0.985
	E	NA	NA	NA	NA
C	D	0.061	0.035	1.767	0.396
	E	NA	NA	NA	NA
D	E	NA	NA	NA	NA
Shell degradation 5					
A	Others	NA	NA	NA	NA
B	C	0.276	0.308	0.895	0.899
	D	0.275	0.308	0.892	0.900
	E	– 0.105	0.423	– 0.248	0.999
C	D	– 0.001	0.013	– 0.084	1.000
	E	– 0.381	0.289	– 1.316	0.682
D	E	– 0.380	0.289	– 1.313	0.684
Shell degradation 6					
A	Others	NA	NA	NA	NA
B	Others	NA	NA	NA	NA
C	D	3.460×10^{-4}	0.023	0.015	1.000
	E	0.008	0.024	0.356	0.997
D	E	0.008	0.023	0.356	0.997

Table S5.82. Results of the TukeySD post-hoc pairwise comparisons on the relationship between the average biomass of Rhodophyta per mussel valve and euendolithic infestation levels (from A to E, as defined in Kaehler, 1999). Significant p-values are underlined.

Infestation level (a)	Infestation level (b)	Estimate	Std Error	z-value	p-value
A	B	81.280	59.430	1.368	0.621
	C	257.850	95.720	3.694	0.049
	D	414.510	106.640	3.887	< 0.001
	E	293.490	122.64	2.393	0.105
B	C	176.560	84.800	2.082	0.208
	D	333.230	93.810	3.552	0.003
	E	212.210	114.220	1.858	0.315
C	D	156.67	94.230	1.663	0.429
	E	35.640	78.840	0.454	0.990
D	E	– 121.020	120.340	– 1.006	0.837

Table S5.83. Results of the TukeySD post-hoc pairwise comparisons on the relationship between the average biomass of *Hildenbrandia lecannellieri* (Rhodophyta) per mussel valve and euendolithic infestation levels (from A to E, as defined in Kaehler, 1999). Significant p-values are underlined.

Infestation level (a)	Infestation level (b)	Estimate	Std Error	z-value	p-value
A	B	0.032	0.028	1.140	0.785
	C	0.038	0.028	1.356	0.657
	D	0.020	0.028	0.708	0.954
	E	– 0.007	0.051	– 0.137	1.000
B	C	0.006	0.004	1.458	0.592
	D	– 0.012	0.006	– 1.833	0.362
	E	– 0.039	0.043	– 0.888	0.901
C	D	– 0.018	0.005	– 3.373	0.010
	E	– 0.045	0.043	– 1.032	0.840
D	E	– 0.027	0.043	– 0.620	0.972

Table S5.84. Results of the TukeySD post-hoc pairwise comparisons on the relationship between the average percent cover of *Hildenbrandia lecannellieri* (Rhodophyta) per mussel valve and position of the epibionts on the mussel shell (i.e., infested, non-infested, secondary epibiosis) for each shell degradation index (from 1 to 6, as defined in Ma *et al.*, 2023). No significant p-values were detected.

Position on the shell (a)	Position on the shell (b)	Estimate	Std Error	t-value	p-value
Shell degradation 1		NA	NA	NA	NA
Shell degradation 2		NA	NA	NA	NA
Shell degradation 3					
II epibiosis	Infested	NA	NA	NA	NA
II epibiosis	Non-infested	NA	NA	NA	NA
Infested	Non-infested	0.057	0.039	1.459	0.316
Shell degradation 4					
II epibiosis	Infested	0.018	0.027	0.671	0.781
II epibiosis	Non-infested	0.025	0.025	1.005	0.576
Infested	Non-infested	0.007	0.011	0.693	0.768
Shell degradation 5					
II epibiosis	Infested	NA	NA	NA	NA
II epibiosis	Non-infested	NA	NA	NA	NA
Infested	Non-infested	– 0.008	0.008	– 0.994	0.582
Shell degradation 6		NA	NA	NA	NA

Table S5.85. Results of the TukeySD post-hoc pairwise comparisons on the relationship between the average biomass of *Gelidium pristoides* (Rhodophyta) per mussel valve and euendolithic infestation levels (from A to E, as defined in Kaehler, 1999) for each shell degradation index (from 1 to 6, as defined in Ma et al., 2023). No significant p-values were detected.

Infestation level (a)	Infestation level (b)	Estimate	Std Error	t-value	p-value
Shell degradation 1		NA	NA	NA	NA
Shell degradation 2		NA	NA	NA	NA
Shell degradation 3					
A	Others	NA	NA	NA	NA
B	Others	NA	NA	NA	NA
C	D	-1.420×10^{-4}	0.001	– 0.096	1.000
	E	NA	NA	NA	NA
D	E	NA	NA	NA	NA
Shell degradation 4					
A	Others	NA	NA	NA	NA
B	Others	NA	NA	NA	NA
C	D	4.530×10^{-4}	0.004	0.311	0.998
	E	NA	NA	NA	NA
D	E	NA	NA	NA	NA
Shell degradation 5					
A	Others	NA	NA	NA	NA
B	Others	NA	NA	NA	NA
C	D	0.005	0.002	2.516	0.139
	E	NA	NA	NA	NA
D	E	NA	NA	NA	NA
Shell degradation 6					
A	Others	NA	NA	NA	NA
B	Others	NA	NA	NA	NA
C	D	0.023	0.078	0.297	0.998
	E	NA	NA	NA	NA
D	E	NA	NA	NA	NA

Table S5.86. Results of the TukeySD post-hoc pairwise comparisons on the relationship between the average percent cover of *Gelidium pristoides* (Rhodophyta) per mussel valve and position of the epibionts on the mussel shell (i.e., infested, non-infested, secondary epibiosis) for each euendolithic infestation level (from A to E, as defined in Kaehler, 1999). Significant p-values are underlined.

Position on the shell (a)	Position on the shell (b)	Estimate	Std Error	t-value	p-value
Infestation level A		NA	NA	NA	NA
Infestation level B		NA	NA	NA	NA
Infestation level C					
II epibiosis	Infested	-3.330×10^{-3}	0.004	– 0.819	0.698
II epibiosis	Non-infested	1.480×10^{-4}	7.180×10^{-4}	0.207	0.977
Infested	Non-infested	3.470×10^{-3}	0.004	0.856	0.675
Infestation level D					
II epibiosis	Infested	3.490×10^{-3}	0.001	2.965	<u>0.025</u>
II epibiosis	Non-infested	3.400×10^{-3}	0.001	2.971	<u>0.024</u>
Infested	Non-infested	-9.680×10^{-5}	2.840×10^{-4}	– 0.341	0.9381
Infestation level E		NA	NA	NA	NA

Table S5.87. Results of the TukeySD post-hoc pairwise comparisons on the relationship between the average biomass of *Electra verticillata* (Bryozoa) per mussel valve and euendolithic infestation levels (from A to E, as defined in Kaehler, 1999). No significant p-values were detected.

Infestation level (a)	Infestation level (b)	Estimate	Std Error	z-value	p-value
A	Others	NA	NA	NA	NA
B	C	– 0.047	0.021	– 2.284	0.115
	D	– 0.059	0.024	– 2.507	0.071
	E	NA	NA	NA	NA
C	D	– 0.012	0.022	– 0.530	0.951
	E	NA	NA	NA	NA
D	E	NA	NA	NA	NA

REFERENCES

Adler, F.R., Harvell, C.D., 1990. Inducible defenses, phenotypic variability and biotic environments. Trends Ecol. Evol. 5, 407–410. https://doi.org/10.1016/0169-5347(90)90025-9

Aeby, G.S., Williams, G.J., Franklin, E.C., Haapkyla, J., Harvell, C.D., Neale, S., Page, C.A., Raymundo, L., Vargas-Ángel, B., Willis, B.L., Work, T.M., Davy, S.K., 2011. Growth anomalies on the coral genera *Acropora* and *Porites* are strongly associated with host density and human population size across the Indo-Pacific. PLoS ONE 6, e16887. https://doi.org/10.1371/journal.pone.0016887

Akpan, E.B., 1990. Bioerosion of oyster shells in brackish modern mangrove swamps, Nigeria. Ichnos Int. J. Plant Anim. Traces 1, 125–132. https://doi.org/10.1080/10420949009386341

Akpan, E.B., Farrow, G.E., 1984. Shell-boring algae on the Scottish continental shelf: identification, distribution, bathymetric zonation. Trans. R. Soc. Edinb. Eart Sci. 75, 1–12. https://doi.org/10.1017/S0263593300009743

Alexanderson, E.T., 1975. Marks of unknown carbonate-decomposing organelles in cyanophyte borings. Nature 254, 236–238. https://doi.org/10.1038/254212b0

Alfaro, A.C., 2006. Byssal attachment of juvenile mussels, *Perna canaliculus*, affected by water motion and air bubbles. Aquaculture 255, 357–361. https://doi.org/10.1016/j.aquaculture.2005.11.059

Alfaro, A.C., Webb, S.C., Barnaby, C., 2008. Variability of growth, health, and population turnover within mussel beds of *Perna canaliculus* in northern New Zealand. Mar. Biol. Res. 4, 376–383. https://doi.org/10.1080/17451000802022879

Al-Thukair, A.A., 2011. Calculating boring rate of endolithic cyanobacteria *Hyella immanis* under laboratory conditions. Int. Biodeterior. Biodegrad. 65, 664–667. https://doi.org/10.1016/j.ibiod.2011.03.009

Al-Thukair, A.A., 2002. Effect of oil pollution on euendolithic cyanobacteria of the Arabian Gulf. Environ. Microbiol. 4, 125–129. https://doi.org/10.1046/j.1462-2920.2002.00276.x

Al-Thukair, A.A., Golubic, S., Rosen, G., 1994. New euendolithic cyanobacteria from the Bahama Bank and the Arabian Gulf: *Hyella racemus* sp. nov. 1. J. Phycol. 30, 764–769. https://doi.org/10.1111/j.0022-3646.1994.00764.x

Amarelle, V., Carrasco, V., Fabiano, E., 2019. The hidden life of Antarctic rocks, in: Castro-Sowinski, S. (Ed.), The Ecological Role of Micro-Organisms in the Antarctic Environment, Springer Polar Sciences. Springer International Publishing, Cham, pp. 221–237. https://doi.org/10.1007/978-3-030-02786-5_10

Ambariyanto, A., Seed, R., 1991. The infestation of *Mytilus edulis* Linnaeus by *Polydora ciliata* (Johnston) in the Conwy Estuary, North Wales. J. Molluscan Stud. 57, 413–424. https://doi.org/10.1093/mollus/57.4.413

Anderson, M.J., 2005. PERMANOVA: a FORTRAN computer program for permutational multivariate analysis of variance. Department of Statistics, University of Auckland, Auckland.

Anderson, M.J., 2004. PERMDISP: a FORTRAN computer program for permutational analysis of multivariate dispersions (for any two-factor ANOVA design) using permutation tests. Department of Statistics, University of Auckland, New Zealand.

Andersson, A.J., 2005. Coastal ocean and carbonate systems in the high CO_2 world of the Anthropocene. Am. J. Sci. 305, 875–918.
https://doi.org/10.2475/ajs.305.9.875

Ascaso, C., Wierzchos, J., Castello, R., 1998. Study of the biogenic weathering of calcareous litharenite stones caused by lichen and endolithic microorganisms. Int. Biodeterior. Biodegrad. 42, 29–38. https://doi.org/10.1016/S0964-8305(98)00043-2

Badano, E.I., Cavieres, L.A., 2006. Ecosystem engineering across ecosystems: do engineer species sharing common features have generalized or idiosyncratic effects on species diversity? J. Biogeogr. 33, 304–313.
https://doi.org/10.1111/j.1365-2699.2005.01384.x

Badano, E.I., Marquet, P.A., 2008. Ecosystem engineering affects ecosystem functioning in high-Andean landscapes. Oecologia 155, 821–829.
https://doi.org/10.1007/s00442-007-0953-2

Bakker, T.C.M., Mazzi, D., Zala, S., 1997. Parasite-induced changes in behavior and color make *Gammarus pulex* more prone to fish predation. Ecology 78, 1098–1104. https://doi.org/10.1890/0012-9658(1997)078[1098:PICIBA]2.0.CO;2

Balvanera, P., Siddique, I., Dee, L., Paquette, A., Isbell, F., Gonzalez, A., Byrnes, J., O'Connor, M.I., Hungate, B.A., Griffin, J.N., 2014. Linking biodiversity and ecosystem services: Current uncertainties and the necessary next steps. BioScience 64, 49–57. https://doi.org/10.1093/biosci/bit003

Bangert, R.K., Lonsdorf, E.V., Wimp, G.M., Shuster, S.M., Fischer, D., Schweitzer, J.A., Allan, G.J., Bailey, J.K., Whitham, T.G., 2008. Genetic structure of a foundation species: scaling community phenotypes from the individual to the region. Heredity 100, 121–131. https://doi.org/10.1038/sj.hdy.6800914

Bangert, R.K., Slobodchikoff, C.N., 2006. Conservation of prairie dog ecosystem engineering may support arthropod beta and gamma diversity. J. Arid Environ. 67, 100–115. https://doi.org/10.1016/j.jaridenv.2006.01.015

Barker, C., 2021. Phylogeography and reproductive isolation of the brown mussel, *Perna perna*, on the South African coastline (Master of Science). Rhodes University, Grahamstown, South Africa.

Barnosky, A.D., Matzke, N., Tomiya, S., Wogan, G.O.U., Swartz, B., Quental, T.B., Marshall, C., McGuire, J.L., Lindsey, E.L., Maguire, K.C., Mersey, B., Ferrer, E.A., 2011. Has the Earth's sixth mass extinction already arrived? Nature 471, 51–57. https://doi.org/10.1038/nature09678

Barton, E.S., White, D.W., Cathelyn, J.S., Brett-McClellan, K.A., Engle, M., Diamond, M.S., Miller, V.L., Virgin, H.W., 2007. Herpesvirus latency confers symbiotic protection from bacterial infection. Nature 447, 326–329.
https://doi.org/10.1038/nature05762

Bates, A.E., Leiterer, F., Wiedeback, M.L., Poulin, R., 2011. Parasitized snails take the heat: a case of host manipulation? Oecologia 167, 613–621.
https://doi.org/10.1007/s00442-011-2014-0

Bathurst, R.G.C., 1966. Boring algae, micrite envelopes and lithification of molluscan biosparites. Geol. J. 5, 15–32.
https://doi.org/10.1002/gj.3350050104

Behrendt, L., Larkum, A.W., Norman, A., Qvortrup, K., Chen, M., Ralph, P., Sørensen, S.J., Trampe, E., Kühl, M., 2011. Endolithic chlorophyll *d*-containing phototrophs. ISME J. 5, 1072–1076.
https://doi.org/10.1038/ismej.2010.195

Bell, C., McQuaid, C.D., Porri, F., 2015. Barnacle settlement on rocky shores: Substratum preference and epibiosis on mussels. J. Exp. Mar. Biol. Ecol. 473, 195–201. https://doi.org/10.1016/j.jembe.2015.09.006

Bell, C.M., 2013. The epibiotic relationship between mussels and barnacles (Master of Science). Rhodes University, Grahamstown, South Africa.

Bellard, C., Bertelsmeier, C., Leadley, P., Thuiller, W., Courchamp, F., 2012. Impacts of climate change on the future of biodiversity. Ecol. Lett. 15, 365–377. https://doi.org/10.1111/j.1461-0248.2011.01736.x

Bentis, C.J., Kaufman, L., Golubic, S., 2000. Endolithic fungi in reef-building corals (Order: Scleractinia) are common, cosmopolitan, and potentially pathogenic. Biol. Bull. 198, 254–260. https://doi.org/10.2307/1542528

Berntsson, K.M., Andreasson, H., Tonsson, P.R., Larsson, L., Ring, K., Petronis, S., Gatenholm, P., 2000. Reduction of barnacle recruitment on micro-textured surfaces: Analysis of effective topographic characteristics and evaluation of skin friction. Biofouling 16, 245–261. https://doi.org/10.1080/08927010009378449

Bers, A.V., Díaz, E.R., da Gama, B.A.P., Vieira-Silva, F., Dobretsov, S., Valdivia, N., Thiel, M., Scardino, A.J., McQuaid, C.D., Sudgen, H.E., Thomason, J.C., Wahl, M., 2010. Relevance of mytilid shell microtopographies for fouling defence – a global comparison. Biofouling 26, 367–377. https://doi.org/10.1080/08927011003605888

Bers, A.V., D'Souza, F., Klijnstra, J.W., Willemsen, P.R., Wahl, M., 2006. Chemical defence in mussels: antifouling effect of crude extracts of the periostracum of the blue mussel *Mytilus edulis*. Biofouling 22, 251–259.
https://doi.org/10.1080/08927010600901112

Bers, A.V., Wahl, M., 2004. The influence of natural surface microtopographies on fouling. Biofouling 20, 43–51. https://doi.org/10.1080/08927010410001655533

Bertness, M., Gaines, S., Wahle, R., 1996. Wind-driven settlement patterns in the acorn barnacle *Semibalanus balanoides*. Mar. Ecol. Prog. Ser. 137, 103–110.
https://doi.org/10.3354/meps137103

Bertness, M.D., 1989. Intraspecific competition and facilitation in a northern acorn barnacle population. Ecology 70, 257–268. https://doi.org/10.2307/1938431

Bertness, M.D., 1984a. Habitat and community modification by an introduced herbivorous snail. Ecology 65, 370–381. https://doi.org/10.2307/1941400

Bertness, M.D., 1984b. Ribbed mussels and *Spartina alterniflora* production in a New England salt marsh. Ecology 65, 1794–1807. https://doi.org/10.2307/1937776

Bertness, M.D., Callaway, R., 1994. Positive interactions in communities. Trends Ecol. Evol. 9, 191–193. https://doi.org/10.1016/0169-5347(94)90088-4

Bertness, M.D., Yund, P.O., Brown, A.F., 1983. Snail grazing and the abundance of algal crusts on a sheltered New England rocky beach. J. Exp. Mar. Biol. Ecol. 71, 147–164. https://doi.org/10.1016/0022-0981(93)90070-5

Bishop, M.J., Fraser, J., Gribben, P.E., 2013. Morphological traits and density of foundation species modulate a facilitation cascade in Australian mangroves. Ecology 94, 1927–1936. https://doi.org/10.1890/12-1847.1

Bolnick, D.I., Amarasekare, P., Araújo, M.S., Bürger, R., Levine, J.M., Novak, M., Rudolf, V.H.W., Schreiber, S.J., Urban, M.C., Vasseur, D.A., 2011. Why intraspecific trait variation matters in community ecology. Trends Ecol. Evol. 26, 183–192. https://doi.org/10.1016/j.tree.2011.01.009

Bolnick, D.I., Svanbäck, R., Fordyce, J.A., Yang, L.H., Davis, J.M., Hulsey, C.D., Forister, M.L., 2003. The ecology of individuals: Incidence and implications of individual specialization. Am. Nat. 161, 1–28. https://doi.org/10.1086/343878

Boogert, N.J., Paterson, D.M., Laland, K.N., 2006. The implications of niche construction and ecosystem engineering for conservation biology. BioScience 56, 570–578. https://doi.org/10.1641/0006-3568(2006)56[570:TIONCA]2.0.CO;2

Bornet, M.E., Flahault, C., 1889. Sur quelques plantes vivant dans le test calcaire des mollusques. Bull. Société Bot. Fr. 36, CXLVII–CLXXVI. https://doi.org/10.1080/00378941.1889.10835893

Borsje, B.W., van Wesenbeeck, B.K., Dekker, F., Paalvast, P., Bouma, T.J., van Katwijk, M.M., de Vries, M.B., 2011. How ecological engineering can serve in coastal protection. Ecol. Eng. 37, 113–122. https://doi.org/10.1016/j.ecoleng.2010.11.027

Bownes, S.J., McQuaid, C.D., 2009. Mechanisms of habitat segregation between an invasive and an indigenous mussel: settlement, post-settlement mortality and recruitment. Mar. Biol. 156, 991–1006. https://doi.org/10.1007/s00227-009-1143-z

Bownes, S.J., McQuaid, C.D., 2006. Will the invasive mussel *Mytilus galloprovincialis* Lamarck replace the indigenous *Perna perna* L. on the south coast of South Africa? J. Exp. Mar. Biol. Ecol. 338, 140–151. https://doi.org/10.1016/j.jembe.2006.07.006

Branch, G., Branch, M., 2018. Living Shores: Interacting with Southern Africa's marine ecosystems. Struik Nature, Cape Town.

Branch, G.M., Griffiths, C.L., Branch, M.L., Beckley, L.E., 2016. Two Oceans: A guide to the marine life of southern Africa, 4th edition. ed. Struik Nature, Cape Town.

Bressan, M., Chinellato, A., Munari, M., Matozzo, V., Manci, A., Marčeta, T., Finos, L., Moro, I., Pastore, P., Badocco, D., Marin, M.G., 2014. Does seawater acidification affect survival, growth and shell integrity in bivalve juveniles? Mar. Environ. Res. 99, 136–148. https://doi.org/10.1016/j.marenvres.2014.04.009

Bronstein, J.L., 1994. Conditional outcomes in mutualistic interactions. Trends Ecol. Evol. 9, 214–217. https://doi.org/10.1016/0169-5347(94)90246-1

Brouns, J.J.W.M., Heijs, F.M.L., 1986. Production and biomass of the seagrass *Enhalus acoroides* (L.f.) Royle and its epiphytes. Aquat. Bot. 25, 21–45. https://doi.org/10.1016/0304-3770(86)90038-0

Brown, B.E., Tudhope, A.W., Le Tissier, M.D.A., Scoffin, T.P., 1991. A novel mechanism for iron incorporation into coral skeletons. Coral Reefs 10, 211–215. https://doi.org/10.1007/BF00336776

Brundtland, G.H., 1987. Our common future - Call for action. Environ. Conserv. 14, 291–294. https://doi.org/10.1017/S0376892900016805

Bruno, J.F., Stachowicz, J.J., Bertness, M.D., 2003. Inclusion of facilitation into ecological theory. Trends Ecol. Evol. 18, 119–125. https://doi.org/10.1016/S0169-5347(02)00045-9

Burge, C.A., Mark Eakin, C., Friedman, C.S., Froelich, B., Hershberger, P.K., Hofmann, E.E., Petes, L.E., Prager, K.C., Weil, E., Willis, B.L., Ford, S.E., Harvell, C.D., 2014. Climate change influences on marine infectious diseases: Implications for management and society. Annu. Rev. Mar. Sci. 6, 249–277. https://doi.org/10.1146/annurev-marine-010213-135029

Buschbaum, C., 2000. Direct and indirect effects of *Littorina littorea* (L.) on barnacles growing on mussel beds in the Wadden Sea. Hydrobiologia 440, 119–128. https://doi.org/10.1023/A:1004142306396

Buschbaum, C., Dittmann, S., Hong, J.-S., Hwang, I.-S., Strasser, M., Thiel, M., Valdivia, N., Yoon, S.-P., Reise, K., 2009. Mytilid mussels: global habitat engineers in coastal sediments. Helgol. Mar. Res. 63, 47–58. https://doi.org/10.1007/s10152-008-0139-2

Buschbaum, C., Saier, B., 2001. Growth of the mussel *Mytilus edulis* L. in the Wadden Sea affected by tidal emergence and barnacle epibionts. J. Sea Res. 45, 27–36. https://doi.org/10.1016/S1385-1101(00)00061-7

Bush, A.O., Fernández, J.C., Esch, Seed, J.R., 2001. Parasitism: the diversity and ecology of animal parasites. Cambridge University Press, Cambridge, UK ; New York, NY.

Bustamante, R.H., Branch, G.M., 1996. Large scale patterns and trophic structure of southern African rocky shores: the roles of geographic variation and wave exposure. J. Biogeogr. 23, 339–351. https://doi.org/10.1046/j.1365-2699.1996.00026.x

Byers, J.E., 2020. Effects of climate change on parasites and disease in estuarine and nearshore environments. PLOS Biol. 18, e3000743. https://doi.org/10.1371/journal.pbio.3000743

Cabioch, G., Montaggioni, L.F., Faure, G., Ribaud-Laurenti, A., 1999. Reef coralgal assemblages as recorders of paleobathymetry and sea level changes in the Indo-Pacific province. Quat. Sci. Rev. 18, 1681–1695. https://doi.org/10.1016/S0277-3791(99)00014-1

Caddy-Retalic, S., Benkendorff, K., Faireweather, P.G., 2011. Visualizing hotspots: Applying thermal imaging to monitor internal temperatures in intertidal gastropods. Molluscan Res. 31, 106–113.

Caldeira, K., Wickett, M.E., 2003. Anthropogenic carbon and ocean pH. Nature 425, 365–365. https://doi.org/10.1038/425365a

Calvo-Ugarteburu, G., McQuaid, C., 1998. Parasitism and invasive species: effects of digenetic trematodes on mussels. Mar. Ecol. Prog. Ser. 169, 149–163. https://doi.org/10.3354/meps169149

Campbell, S.E., 1983. The modern distribution and geological history of calcium carbonate boring microorganisms, in: Westbroek, P., de Jong, E.W. (Eds.), Biomineralization and Biological Metal Accumulation. Springer Netherlands, Dordrecht, pp. 99–104. https://doi.org/10.1007/978-94-009-7944-4

Caraco, N., Cole, J., Findlay, S., Wigand, C., 2006. Vascular plants as engineers of oxygen in aquatic systems. BioScience 56, 219. https://doi.org/10.1641/0006-3568(2006)056[0219:VPAEOO]2.0.CO;2

Cardinale, B.J., Duffy, J.E., Gonzalez, A., Hooper, D.U., Perrings, C., Venail, P., Narwani, A., Mace, G.M., Tilman, D., Wardle, D.A., Kinzig, A.P., Daily, G.C., Loreau, M., Grace, J.B., Larigauderie, A., Srivastava, D., Naeem, S., 2012. Biodiversity loss and its impact on humanity. Nature 486, 59–67. https://doi.org/10.1038/nature11148.

Carpenter, W., 1845. On the microscopic structure of shells. Rep. Br. Assoc. Adv. Sci. 14, 1–24.

Carreiro-Silva, M., Kiene, W.E., Golubic, S., McClanahan, T.R., 2012. Phosphorus and nitrogen effects on microbial euendolithic communities and their bioerosion rates. Mar. Pollut. Bull. 64, 602–613. https://doi.org/10.1016/j.marpolbul.2011.12.013

Carreiro-Silva, M., McClanahan, T., Kiene, W., 2009. Effects of inorganic nutrients and organic matter on microbial euendolithic community composition and microbioerosion rates. Mar. Ecol. Prog. Ser. 392, 1–15. https://doi.org/10.3354/meps08251

Carreiro-Silva, M., McClanahan, T.R., Kiene, W.E., 2005. The role of inorganic nutrients and herbivory in controlling microbioerosion of carbonate substratum. Coral Reefs 24, 214–221. https://doi.org/10.1007/s00338-004-0445-3

Carrington, E., Moeser, G.M., Thompson, S.B., Coutts, L.C., Craig, C.A., 2008. Mussel attachment on rocky shores: the effect of flow on byssus production. Integr. Comp. Biol. 48, 801–807. https://doi.org/10.1093/icb/icn078

Carter, A.R., Anderson, R.J., 1991. Biological and physical factors controlling the spatial distribution of the intertidal alga *Gelidium pristoides* in the Eastern Cape, South Africa. J. Mar. Biol. Assoc. U. K. 71, 555–568. https://doi.org/10.1017/S0025315400053145

Cartwright, S.R., Williams, G.A., 2014. How hot for how long? The potential role of heat intensity and duration in moderating the beneficial effects of an ecosystem engineer on rocky shores. Mar. Biol. 161, 2097–2105. https://doi.org/10.1007/s00227-014-2489-4

Carve, M., Scardino, A., Shimeta, J., 2019. Effects of surface texture and interrelated properties on marine biofouling: a systematic review. Biofouling 35, 597–617. https://doi.org/10.1080/08927014.2019.1636036

Cerrano, C., Bavestrello, G., Calcinai, B., Cattaneo-Vietti, R., Chiantore, M., Guidetti, M., Sarà, A., 2001. Bioerosive processes in Antarctic seas. Polar Biol. 24, 790–792. https://doi.org/10.1007/s003000100294

Chacón, E., Berrendero, E., Garcia-Pichel, F., 2006. Biogeological signatures of microboring cyanobacterial communities in marine carbonates from Cabo Rojo, Puerto Rico. Sediment. Geol. 185, 215–228. https://doi.org/10.1016/j.sedgeo.2005.12.014

Chapperon, C., Seuront, L., 2011a. Behavioral thermoregulation in a tropical gastropod: links to climate change scenarios. Glob. Change Biol. 17, 1740–1749. https://doi.org/10.1111/j.1365-2486.2010.02356.x

Chapperon, C., Seuront, L., 2011b. Space-time variability in environmental thermal properties and snail thermoregulatory behaviour. Funct. Ecol. 25, 1040–1050. https://doi.org/10.1111/j.1365-2435.2011.01859.x

Chapperon, C., Studerus, K., Clavier, J., 2017. Mitigating thermal effect of behaviour and microhabitat on the intertidal snail *Littorina saxatilis* (Olivi) over summer. J. Therm. Biol. 67, 40–48. https://doi.org/10.1016/j.jtherbio.2017.03.017

Chazottes, V., Cabioch, G., Golubic, S., Radtke, G., 2009. Bathymetric zonation of modern microborers in dead coral substrates from New Caledonia — Implications for paleodepth reconstructions in Holocene corals. Palaeogeogr. Palaeoclimatol. Palaeoecol. 280, 456–468. https://doi.org/10.1016/j.palaeo.2009.06.033

Chazottes, V., Campion-Alsumard, T.L., Peyrot-Clausade, M., 1995. Bioerosion rates on coral reefs: interactions between macroborers, microborers and grazers (Moorea, French Polynesia). Palaeogeogr. Palaeoclimatol. Palaeoecol. 113, 189–198. https://doi.org/10.1016/0031-0182(95)00043-L

Chazottes, V., Le Campion-Alsumard, T., Peyrot-Clausade, M., Cuet, P., 2002. The effects of eutrophication-related alterations to coral reef communities on agents and rates of bioerosion (Reunion Island, Indian Ocean). Coral Reefs 21, 375–390. https://doi.org/10.1007/s00338-002-0259-0

Cherchi, A., Buosi, C., Zuddas, P., De Giudici, G., 2012. Bioerosion by microbial euendoliths in benthic foraminifera from heavy metal-polluted coastal environments of Portovesme (South-Western Sardinia, Italy). Biogeosciences 9, 4607–4620. https://doi.org/10.5194/bg-9-4607-2012

Cherchi, A., Da Pelo, S., Ibba, A., Mana, D., Buosi, C., Floris, N., 2009. Benthic foraminifera response and geochemical characterization of the coastal environment surrounding the polluted industrial area of Portovesme (South-Western Sardinia, Italy). Mar. Pollut. Bull. 59, 281–296. https://doi.org/10.1016/j.marpolbul.2009.09.016

Cho, B., Bae, H., Kim, T., 2022. The symbiotic relationship between the Antarctic limpet, *Nacella concinna*, and epibiont coralline algae. J. Mar. Sci. Eng. 10, 496. https://doi.org/10.3390/jmse10040496

Clarke, K.R., Ainsworth, M., 1993. A method of linking multivariate community structure to environmental variables. Mar. Ecol. Prog. Ser. 92, 205–219. https://doi.org/10.3354/meps092205

Clay, K., Schardl, C., 2002. Evolutionary origins and ecological consequences of endophyte symbiosis with grasses. Am. Nat. 160, S99–S127. https://doi.org/10.1086/342161

Clements, J.C., Bourque, D., McLaughlin, J., Stephenson, M., Comeau, L.A., 2017. Extreme ocean acidification reduces the susceptibility of eastern oyster shells to a polydorid parasite. J. Fish Dis. 40, 1573–1585. https://doi.org/10.1111/jfd.12626

Coastal Research Group, 2022. Vertical zonation on rocky shores around the coast of South Africa. https://doi.org/10.13140/RG.2.2.33897.26729/1

Cockell, C.S., Herrera, A., 2007. Why are some microorganisms boring? Trends Microbiol. 16, 101–106. https://doi.org/10.1016/j.tim.2007.12.007

Coggan, N.V., Hayward, M.W., Gibb, H., 2018. A global database and "state of the field" review of research into ecosystem engineering by land animals. J. Anim. Ecol. 87, 974–994. https://doi.org/10.1111/1365-2656.12819

Cole, V., 2010. Alteration of the configuration of bioengineers affects associated taxa. Mar. Ecol. Prog. Ser. 416, 127–136. https://doi.org/10.3354/meps08772

Cole, V.J., McQuaid, C.D., 2010. Bioengineers and their associated fauna respond differently to the effects of biogeography and upwelling. Ecology 91, 3549–3562. https://doi.org/10.1890/09-2152.1

Colwell, R.K., 2009. Biodiversity: Concepts, patterns, and measurement, in: Levin, S.A. (Ed.), The Princeton Guide to Ecology. Princeton University Press, New Jersey, USA, pp. 257–263.

Commito, J.A., Rusignuolo, B.R., 2000. Structural complexity in mussel beds: the fractal geometry of surface topography. J. Exp. Mar. Biol. Ecol. 255, 133–152. https://doi.org/10.1016/S0022-0981(00)00285-9

Connell, J.H., 1972. Community interactions on marine rocky intertidal shores. Annu. Rev. Ecol. Syst. 3, 169–192. https://doi.org/10.1146/annurev.es.03.110172.001125

Connell, J.H., 1961. The influence of interspecific competition and other factors on the distribution of the barnacle *Chthamalus stellatus*. Ecology 42, 710–723. https://doi.org/10.2307/1933500

Cook, D.W., Lofton, S.R., 1973. Chitinoclastic bacteria associated with shell disease in *Penaeus* shrimp and the blue Ccab (*Callinectes sapidus*). J. Wildl. Dis. 9, 154–159. https://doi.org/10.7589/0090-3558-9.2.154

Cook-Patton, S.C., McArt, S.H., Parachnowitsch, A.L., Thaler, J.S., Agrawal, A.A., 2011. A direct comparison of the consequences of plant genotypic and species diversity on communities and ecosystem function. Ecology 92, 915–923. https://doi.org/10.1890/10-0999.1

Côté, I.M., 1995. Effects of predatory crab effluent on byssus production in mussels. J. Exp. Mar. Biol. Ecol. 188, 233–241. https://doi.org/10.1016/0022-0981(94)00197-L

Couradeau, E., Roush, D., Guida, B.S., Garcia-Pichel, F., 2017. Diversity and mineral substrate preference in endolithic microbial communities from marine intertidal outcrops (Isla de Mona, Puerto Rico). Biogeosciences 14, 311–324. https://doi.org/10.5194/bg-14-311-2017

Crain, C.M., Bertness, M.D., 2006. Ecosystem engineering across environmental gradients: Implications for conservation and management. BioScience 56, 211–218. https://doi.org/10.1641/0006-3568(2006)056[0211:EEAEGI]2.0.CO;2

Creed, J.C., 2000. Epibiosis on cerith shells in a seagrass bed: correlation of shell occupant with epizoite distribution and abundance. Mar. Biol. 137, 775–782. https://doi.org/10.1007/s002270000429

Crisp, D.J., 1955. The behaviour of barnacle cyprids in relation to water movement over a surface. J. Exp. Biol. 32, 569–590.

Crisp, D.J., Barnes, H., 1954. The orientation and distribution of barnacles at settlement with particular reference to surface contour. J. Anim. Ecol. 23, 142–162. https://doi.org/10.2307/1664

Crooks, J.A., 2002. Characterizing ecosystem-level consequences of biological invasions: the role of ecosystem engineers. Oikos 97, 153–166. https://doi.org/10.1034/j.1600-0706.2002.970201.x

Crooks, J.A., Khim, H.S., 1999. Architectural vs. biological effects of a habitat-altering, exotic mussel, *Musculista senhousia*. J. Exp. Mar. Biol. Ecol. 240, 53–75. https://doi.org/10.1016/S0022-0981(99)00041-6

Cunha, R.L., Nicastro, K.R., Costa, J., McQuaid, C.D., Serrão, E.A., Zardi, G.I., 2014. Wider sampling reveals a non-sister relationship for geographically contiguous lineages of a marine mussel. Ecol. Evol. 11, 2070–2081. https://doi.org/10.1002/ece3.1033

Cunningham, J.A., Rahman, I.A., Lautenschlager, S., Rayfield, E.J., Donoghue, P.C.J., 2014. A virtual world of paleontology. Trends Ecol. Evol. 29, 347–357. https://doi.org/10.1016/j.tree.2014.04.004

Ćurin, M., Peharda, M., Calcinai, B., Golubić, S., 2014. Incidence of damaging endolith infestation of the edible mytilid bivalve *Modiolus barbatus*. Mar. Biol. Res. 10, 179–189. https://doi.org/10.1080/17451000.2013.814793

Curry, G.B., 1983. Microborings in recent brachiopods and the functions of caeca. Lethaia 16, 119–127. https://doi.org/10.1111/j.1502-3931.1983.tb01707.x

Day, E.G., Branch, G.M., Viljoen, C., 2000. How costly is molluscan shell erosion? A comparison of two patellid limpets with contrasting shell structures. J. Exp. Mar. Biol. Ecol. 243, 185–208. https://doi.org/10.1016/S0022-0981(99)00120-3

Day, J.H., 1969. A guide to marine life on South African shores. A. A. Balkemia, Cape Town.

Day, J.H., 1967. A monograph on the Polychaeta of Southern Africa. Part 1, Errantia: Part 2, Sedentaria. Trustees of the British Museum (Natural History), London.

Dayton, P.K., 1971. Competition, disturbance, and community organization: The provision and subsequent utilization of space in a rocky intertidal community. Ecol. Monogr. 41, 351–389. https://doi.org/10.2307/1948498

De Greef, K., Griffiths, C.L., Zeeman, Z., 2013. Deja vu? A second mytilid mussel, *Semimytilus algosus*, invades South Africa's west coast. Afr. J. Mar. Sci. 35, 307–313. https://doi.org/10.2989/1814232X.2013.829789

de Sá, F.S., Nalesso, R.C., Paresque, K., 2007. Fouling organisms on *Perna perna* mussels: is it worth removing them? Braz. J. Oceanogr. 55, 155–161. https://doi.org/10.1590/S1679-87592007000200008

del Campo, J., Pombert, J.-F., Šlapeta, J., Larkum, A., Keeling, P.J., 2017. The 'other' coral symbiont: *Ostreobium* diversity and distribution. ISME J. 11, 296–299. https://doi.org/10.1038/ismej.2016.101

Delvoye, L., 1992. Endolithic algae in living stony corals: algal concentrations under influence of depth-dependent light conditions and coral tissue fluorescence in *Agaricia agaricites* (L.) and *Meandrina meandrites* (L.) (Scleractinia, Anthozoa). Stud. Nat. Hist. Caribb. Reg. 71, 24–41.

Denley, E.J., Underwood, A.J., 1979. Experiments on factors influencing settlement, survival, and growth of two species of barnacles in New South Wales. J. Exp. Mar. Biol. Ecol. 36, 269–293. https://doi.org/10.1016/0022-0981(79)90122-9

Denny, M.W., Harley, C.D.G., 2006. Hot limpets: predicting body temperature in a conductance-mediated thermal system. J. Exp. Biol. 209, 2409–2419. https://doi.org/10.1242/jeb.02257

Denoël, M., Winandy, L., 2015. The importance of phenotypic diversity in conservation: Resilience of palmate newt morphotypes after fish removal in Larzac ponds (France). Biol. Conserv. 192, 402–408. https://doi.org/10.1016/j.biocon.2015.10.018

Diaz-Pulido, G., Anthony, K.R.N., Kline, D.I., Dove, S., Hoegh-Guldberg, O., 2012. Interactions between ocean acidification and warming on the mortality and dissolution of coralline algae. J. Phycol. 48, 32–39. https://doi.org/10.1111/j.1529-8817.2011.01084.x

Diaz-Pulido, G., Nash, M.C., Anthony, K.R.N., Bender, D., Opdyke, B.N., Reyes-Nivia, C., Troitzsch, U., 2014. Greenhouse conditions induce mineralogical changes and dolomite accumulation in coralline algae on tropical reefs. Nat. Commun. 5, 3310. https://doi.org/10.1038/ncomms4310

Dievart, A.M., 2018. Influence of intraspecific diversity on ecosystem functioning: does genetically-based behaviour in the brown mussel *Perna perna* shape the quality of habitat offered to associated fauna. (Master of Science). Université de La Réunion, La Réunion, France.

Dievart, A.M., McQuaid, C.D., Zardi, G.I., Nicastro, K.R., Froneman, P.W., 2023. Euendolithic infestation of mussel shells indirectly improves the thermal buffering offered by mussel beds to associated molluscs, but one size does not fit all. Diversity 15, 239. https://doi.org/10.3390/d15020239

Dievart, A.M., McQuaid, C.D., Zardi, G.I., Nicastro, K.R., Froneman, P.W., 2022. Photoautotrophic euendoliths and their complex ecological effects in marine bioengineered ecosystems. Diversity 14, 737. https://doi.org/10.3390/d14090737

Dittman, D., Robles, C., 1991. Effect of algal epiphytes on the mussel *Mytilus californianus*. Ecology 72, 286–296. https://doi.org/10.2307/1938922

Dobretsov, S., Abed, R.M.M., Voolstra, C.R., 2013. The effect of surface colour on the formation of marine micro and macrofouling communities. Biofouling 29, 617–627. https://doi.org/10.1080/08927014.2013.784279

Dobson, A.P., Hudson, P.J., 1986. Parasites, disease and the structure of ecological communities. Trends Ecol. Evol. 1, 11–15. https://doi.org/10.1016/0169-5347(86)90060-1

Dominik, C., Seppelt, R., Horgan, F.G., Marquez, L., Settele, J., Václavík, T., 2017. Regional-scale effects override the influence of fine-scale landscape heterogeneity on rice arthropod communities. Agric. Ecosyst. Environ. 246, 269–278. https://doi.org/10.1016/j.agee.2017.06.011

Drew, K.M., 1958. Studies in the Bangiophycidae. IV. The *Conchocelis*-phase of *Bangia fuscopurpurea* (Dillw.) Lyngbye in culture. Pubblicazioni Della Stazione Zool. Napoli 30, 358–372.

Drew, K.M., 1954. Studies in the Bangioideae. III. The life-history of *Porphyra umbilicalis* (L.) Kütz. var. *laciniata* (Lighf.) J. Ag. A. The *Conchocelis*-phase in culture. Ann. Bot. XVIII, 183–211.

Duerden, J.E., 1902. Boring algae as agents in the disintegration of corals. Bull. Am. Mus. Nat. Hist. 16, 323–332.

Eakin, C.M., 1996. Where have all the carbonates gone? A model comparison of calcium carbonate budgets before and after the 1982-1983 El Niño at Uva Island in the eastern Pacific. Coral Reefs 15, 109–119. https://doi.org/10.1007/BF01771900

Ehlers, A., Worm, B., Reusch, T., 2008. Importance of genetic diversity in eelgrass *Zostera marina* for its resilience to global warming. Mar. Ecol. Prog. Ser. 355, 1–7. https://doi.org/10.3354/meps07369

Emanuel, B.P., Bustamante, R.H., Branch, G.M., Eekhout, S., Odendaal, F.J., 1992. A zoogeographic and functional approach to the selection of marine reserves on the west coast of South Africa. South Afr. J. Mar. Sci. 12, 341–354. https://doi.org/10.2989/02577619209504710

Emery, S.M., Rudgers, J.A., 2014. Biotic and abiotic predictors of ecosystem engineering traits of the dune building grass, *Ammophila breviligulata*. Ecosphere 5, 87. https://doi.org/10.1890/ES13-00331.1

Encomio, V., Chu, F., 2007. Heat shock protein (hsp70) expression and thermal tolerance in sublethally heat-shocked eastern oysters *Crassostrea virginica* infected with the parasite *Perkinsus marinus*. Dis. Aquat. Organ. 76, 251–260. https://doi.org/10.3354/dao076251

Enderlein, P., 2003. Optimal foraging versus shared doom effects: interactive influence of mussel size and epibiosis on predator preference. J. Exp. Mar. Biol. Ecol. 292, 231–242. https://doi.org/10.1016/S0022-0981(03)00199-0

Enochs, I.C., Manzello, D.P., Tribollet, A., Valentino, L., Kolodziej, G., Donham, E.M., Fitchett, M.D., Carlton, R., Price, N.N., 2016. Elevated colonization of microborers at a volcanically acidified coral reef. PLOS ONE 11, e0159818. https://doi.org/10.1371/journal.pone.0159818

Ercegović, A., 1932. Études écologiques et sociologiques des cyanophycées lithophytes de la côte Yougoslave de l'Adriatique. Bull. Int. Académie Yougosl. Sci. B.-arts 26, 33–56.

Erlandsson, J., McQuaid, C., 2004. Spatial structure of recruitment in the mussel *Perna perna* at local scales: effects of adults, algae and recruit size. Mar. Ecol. Prog. Ser. 267, 173–185. https://doi.org/10.3354/meps267173

Etter, R.J., 1988. Physiological stress and color polymorphism in the intertidal snail *Nucella lapillus*. Evolution 42, 660–680. https://doi.org/10.1111/j.1558-5646.1988.tb02485.x

Fariñas-Franco, J.M., Roberts, D., 2014. Early faunal successional patterns in artificial reefs used for restoration of impacted biogenic habitats. Hydrobiologia 727, 75–94. https://doi.org/10.1007/s10750-013-1788-y

Fedor, P.J., Spellerberg, I.F., 2013. Shannon–Wiener index, in: Reference Module in Earth Systems and Environmental Sciences. Elsevier, pp. 1–4. https://doi.org/10.1016/B978-0-12-409548-9.00602-3

Fellous, S., Salvaudon, L., 2009. How can your parasites become your allies? Trends Parasitol. 25, 62–66. https://doi.org/10.1016/j.pt.2008.11.010

Fine, M., Loya, Y., 2002. Endolithic algae: an alternative source of photoassimilates during coral bleaching. Proc. R. Soc. Lond. B Biol. Sci. 269, 1205–1210. https://doi.org/10.1098/rspb.2002.1983

Fine, M., Meroz-Fine, E., Hoegh-Guldberg, O., 2005. Tolerance of endolithic algae to elevated temperature and light in the coral *Montipora monasteriata* from the southern Great Barrier Reef. J. Exp. Biol. 208, 75–81. https://doi.org/10.1242/jeb.01381

Fine, M., Roff, G., Ainsworth, T.D., Hoegh-Guldberg, O., 2006. Phototrophic microendoliths bloom during coral "white syndrome." Coral Reefs 25, 577–581. https://doi.org/10.1007/s00338-006-0143-4

Fine, M., Steindler, L., Loya, Y., 2004. Endolithic algae photoacclimate to increased irradiance during coral bleaching. Mar. Freshw. Res. 55, 115–121. https://doi.org/10.1071/MF03120

Fine, M., Zibrowius, H., Loya, Y., 2001. *Oculina patagonica*: a non-lessepsian scleractinian coral invading the Mediterranean Sea. Mar. Biol. 138, 1195–1203. https://doi.org/10.1007/s002270100539

Finlay, J.A., Fletcher, B.R., Callow, M.E., Callow, J.A., 2008. Effect of background colour on growth and adhesion strength of *Ulva* sporelings. Biofouling 24, 219–225. https://doi.org/10.1080/08927010802040693

Fisher, R.A., 1930. The genetical theory of natural selection. Dover Publications, Ind, New York.

Fitzhenry, T., Halpin, PatriciaM., Helmuth, B., 2004. Testing the effects of wave exposure, site, and behavior on intertidal mussel body temperatures: applications and limits of temperature logger design. Mar. Biol. 145, 339–349. https://doi.org/10.1007/s00227-004-1318-6

Fletcher, R.L., Callow, M.E., 1992. The settlement, attachment and establishment of marine algal spores. Br. Phycol. J. 27, 303–329. https://doi.org/10.1080/00071619200650281

Fordyce, A.J., Ainsworth, T.D., Leggat, W., 2020. Microalgae, a boring bivalve and a coral - A newly described association between two coral reef bioeroders within their coral host. Integr. Org. Biol. 2, 1–10. https://doi.org/10.1093/iob/obaa035

Försterra, G., Beuck, L., Häussermann, V., Freiwald, A., 2005. Shallow-water *Desmophyllum dianthus* (Scleractinia) from Chile: characteristics of the biocoenoses, the bioeroding community, heterotrophic interactions and (paleo)bathymetric implications, in: Freiwald, A., Roberts, J.M. (Eds.), Cold-Water Corals and Ecosystems, Erlangen Earth Conference Series. Springer-Verlag, Berlin/Heidelberg, pp. 937–977. https://doi.org/10.1007/3-540-27673-4_48

Försterra, G., Häussermann, V., 2008. Unusual symbiotic relationships between microendolithic phototrophic organisms and azooxanthellate cold-water corals from Chilean fjords. Mar. Ecol. Prog. Ser. 370, 121–125. https://doi.org/10.3354/meps07630

Fox, G.A., Kendall, B.E., 2002. Demographic stochasticity and the variance reduction effect. Ecology 83, 1928–1934.
https://doi.org/10.1890/0012-9658(2002)083[1928:DSATVR]2.0.CO;2

Fraser, D.J., Bernatchez, L., 2001. Adaptative evolutionary conservation: towards a unified concept for defining conservation units. Mol. Ecol. 10, 2741–2752.

Fredd, C.N., Fogler, H.S., 1998. The influence of chelating agents on the kinetics of calcite dissolution. J. Colloid Interface Sci. 204, 187–197.
https://doi.org/10.1006/jcis.1998.5535

Frémy, P., 1945. Contribution à la physiologie des thallophytes marines perforant et cariant les roches calcaires et les coquilles. Ann. Inst. Océan. 22, 107–144.

Friedmann, I.E., Hua, M., Ocampo-Friedmann, R., 1988. Cryptoendolithic lichen and cyanobacterial communities of the Ross Desert, Antarctica. Polarforschung 58, 251–259.

Frölicher, T.L., Fischer, E.M., Gruber, N., 2018. Marine heatwaves under global warming. Nature 560, 360–364. https://doi.org/10.1038/s41586-018-0383-9

Gaines, S.D., Denny, M.W., 1993. The largest, smallest, highest, lowest, longest, and shortest: Extremes in ecology. Ecology 74, 1677–1692.
https://doi.org/10.2307/1939926

Galindo-Martínez, C.T., Weber, M., Avila-Magaña, V., Enríquez, S., Kitano, H., Medina, M., Iglesias-Prieto, R., 2022. The role of the endolithic alga *Ostreobium* spp. during coral bleaching recovery. Sci. Rep. 12, 2977. https://doi.org/10.1038/s41598-022-07017-6

García-Huidobro, M.R., Varas, O., George-Nascimento, M., Pulgar, J., Aldana, M., Lardies, M.A., Lagos, N.A., 2019. Role of temperature and carbonate system variability on a host-parasite system: Implications for the gigantism hypothesis. Int. J. Parasitol. Parasites Wildl. 9, 7–15. https://doi.org/10.1016/j.ijppaw.2019.03.016

Garcia-Pichel, F., 2006. Plausible mechanisms for the boring on carbonates by microbial phototrophs. Sediment. Geol. 185, 205–213. https://doi.org/10.1016/j.sedgeo.2005.12.013

Garcia-Pichel, F., Ramirez-Reinat, E., Gao, Q., 2010. Microbial excavation of solid carbonates powered by P-type ATPase-mediated transcellular Ca^{2+} transport. Proc. Natl. Acad. Sci. 107, 21749–21754. https://doi.org/10.1073/pnas.1011884108

Gardner, J., Thomas, M., 1987. Growth, mortality and production of organic matter by a rocky intertidal population of *Mytilus edulis* in the Quoddy Region of the Bay of Fundy. Mar. Ecol. Prog. Ser. 39, 31–36. https://doi.org/10.3354/meps039031

Garner, Y.L., Litvaitis, M.K., 2017. Effects of artificial epibionts on byssogenesis, attachment strength, and movement in two size classes of the blue mussel, *Mytilus edulis*. Invertebr. Biol. 136, 15–21. https://doi.org/10.1111/ivb.12144

Garner, Y.L., Litvaitis, M.K., 2013. Effects of wave exposure, temperature and epibiont fouling on byssal thread production and growth in the blue mussel, *Mytilus edulis*, in the Gulf of Maine. J. Exp. Mar. Biol. Ecol. 446, 52–56. https://doi.org/10.1016/j.jembe.2013.05.001

Gary, M., McAfee, R., Wolf, C.L., 1973. Glossary of Geology. American Geological Institute, Washington, USA.

Gaspard, D., 2011. Endolithic algae, fungi and bacterial activity in Holocene and Cretaceous brachiopod shells – diagenetic consequences. Mem. Assoc. Australas. Palaeontol. 41, 327–337.

Gattuso, J.-P., Allemand, D., Frankignoulle, M., 1999. Photosynthesis and calcification at cellular, organismal and community levels in coral reefs: A review on interactions and control by carbonate chemistry. Am. Zool. 39, 160–183. https://doi.org/10.1093/icb/39.1.160

Gaylarde, P.M., Jungblut, A.-D., Gaylarde, C.C., Neilan, B.A., 2006. Endolithic phototrophs from an active geothermal region in New Zealand. Geomicrobiol. J. 23, 579–587. https://doi.org/10.1080/01490450600897401

Geen, M.R.S., Johnston, G.R., 2014. Coloration affects heating and cooling in three color morphs of the Australian bluetongue lizard, *Tiliqua scincoides*. J. Therm. Biol. 43, 54–60. https://doi.org/10.1016/j.jtherbio.2014.04.004

Gehman, A.M., Harley, C.D.G., 2019. Symbiotic endolithic microbes alter host morphology and reduce host vulnerability to high environmental temperatures. Ecosphere 10, e02683. https://doi.org/10.1002/ecs2.2683

Gektidis, M., 1999. Development of microbial euendolithic communities: the influence of light and time. Bull. Geol. Soc. Den. 45, 147–150.

Gektidis, M., Dubinsky, Z., Goffredo, S., 2007. Microendoliths of the Shallow Euphotic Zone in open and shaded habitats at 30°N – Eilat, Israel – paleoecological implications. Facies 53, 43–55. https://doi.org/10.1007/s10347-006-0091-z

Gerstenmaier, C., Krueger-Hadfield, S., Sotka, E., 2016. Genotypic diversity in a non-native ecosystem engineer has variable impacts on productivity. Mar. Ecol. Prog. Ser. 556, 79–89. https://doi.org/10.3354/meps11809

Ghirardelli, L.A., 2002. Endolithic microorganisms in live and dead thalli of coralline red algae (Corallinales, Rhodophyta) in the northern Adriatic Sea. Acta Geol. Hisp. 37, 53–60.

Ghirardelli, L.A., 1998. An endolithic cyanophyte in the cell wall of calcareous algae. Bot. Mar. 41, 367–373. https://doi.org/10.1515/botm.1998.41.1-6.367

Glaub, I., Vogel, K., Gektidis, M., 2001. The role of modern and fossil cyanobacterial borings in bioerosion and bathymetry. Ichnos 8, 185–195. https://doi.org/10.1080/10420940109380186

Glynn, P.W., 1994. State of coral reefs in the Galápagos islands: Natural vs anthropogenic impacts. Mar. Pollut. Bull. 29, 131–140.

Godinot, C., Tribollet, A., Grover, R., Ferrier-Pagès, C., 2012. Bioerosion by euendoliths decreases in phosphate-enriched skeletons of living corals. Biogeosciences Discuss. 9, 2425–2444. https://doi.org/10.5194/bgd-9-2425-2012

Goff, L.J., 1982. Symbiosis and parasitism: Another viewpoint. BioScience 32, 255–256. https://doi.org/10.2307/1308531

Goldberg, W.M., Makemson, J.C., Colley, S.B., 1984. *Entocladia endozoica* sp. nov., a pathogenic chlorophyte: structure, life history, physiology, and effect on its coral host. Biol. Bull. 166, 368–383. https://doi.org/10.2307/1541223

Golubic, S., 1969. Distribution, taxonomy, and boring patterns of marine endolithic algae. Am. Zool. 9, 747–751. https://doi.org/10.1093/icb/9.3.747

Golubic, S., Brent, G., Le Campion, T., 1970. Scanning electron microscopy of endolithic algae and fungi using a multipurpose casting-embedding technique. Lethaia 3, 203–209. https://doi.org/10.1111/j.1502-3931.1970.tb01858.x

Golubic, S., Campbell, S.E., Drobne, K., Cameron, B., Balsam, W.L., Cimerman, F., Dubois, L., 1984. Microbial endoliths: A benthic overprint in the sedimentary record, and a paleobathymetric cross-reference with foraminifera. J. Paleontol., Trace Fossils and Paleoenvironments: Marine Carbonate, Marginal Marine Terrigenous and Continental Terrigenous Settings 58, 351–361.

Golubic, S., Friedmann, I., Schneider, J., 1981. The lithobiontic ecological niche, with special reference to microorganisms. J. Sediment. Petrol. 51, 475–478. https://doi.org/10.1306/212F7CB6-2B24-11D7-8648000102C1865D

Golubic, S., Perkins, R.D., Lukas, K.J., 1975. Boring microorganisms and microborings in carbonate substrates, in: Frey, R.W. (Ed.), The Study of Trace Fossils. Springer Berlin Heidelberg, Berlin, Heidelberg, pp. 229–259. https://doi.org/10.1007/978-3-642-65923-2_12

Golubic, S., Radtke, G., Campion-Alsumard, T.L., 2005. Endolithic fungi in marine ecosystems. Trends Microbiol. 13, 229–235. https://doi.org/10.1016/j.tim.2005.03.007

Golubic, S., Schneider, J., 2003. Microbial endoliths as internal biofilms, in: Krumbein, W.E., Paterson, D.M., Zavarzin, G.A. (Eds.), Fossil and Recent Biofilms: A Natural History of Life on Earth. Springer Netherlands, Dordrecht, pp. 249–263. https://doi.org/10.1007/978-94-017-0193-8

Golubic, S., Schneider, J., 1979. Carbonate dissolution. Stud. Environ. Sci. 3, 107–129. https://doi.org/10.1016/S0166-1116(08)71056-2

Golubic, S., Schneider, J., Le Campion-Alsumard, T., Campbell, S.E., Hook, J.E., Radtke, G., 2019. Approaching microbial bioerosion. Facies 65, 25. https://doi.org/10.1007/s10347-019-0568-1

Golubic, S., Seong-Joo, L., Browne, K.M., 2000. Cyanobacteria: architects of sedimentary structures, in: Riding, R.E., Awramik, S.M. (Eds.), Microbial Sediments. Springer Berlin Heidelberg, Berlin, Heidelberg, pp. 57–67. https://doi.org/10.1007/978-3-662-04036-2

Gonzalez-Zapata, F.L., Gómez-Osorio, S., Sánchez, J.A., 2018. Conspicuous endolithic algal associations in a mesophotic reef-building coral. Coral Reefs 37, 705–709. https://doi.org/10.1007/s00338-018-1695-9

Grange, J.S., Rybarczyk, H., Tribollet, A., 2015. The three steps of the carbonate biogenic dissolution process by microborers in coral reefs (New Caledonia). Environ. Sci. Pollut. Res. 22, 13625–13637. https://doi.org/10.1007/s11356-014-4069-z

Grant, W.S., Cherry, M.I., 1985. *Mytilus galloprovincialis* Lmk. in Southern Africa. J. Exp. Mar. Biol. Ecol. 90, 179–191. https://doi.org/10.1016/0022-0981(85)90119-4

Green, J.L., Bohannan, B.J.M., Whitaker, R.J., 2008. Microbial biogeography: From taxonomy to traits. Science 320, 1039–1043. https://doi.org/10.1126/science.1153475

Gribben, P.E., Byers, J.E., Clements, M., McKenzie, L.A., Steinberg, P.D., Wright, J.T., 2009. Behavioural interactions between ecosystem engineers control community species richness. Ecol. Lett. 12, 1127–1136. https://doi.org/10.1111/j.1461-0248.2009.01366.x

Gribben, P.E., Byers, J.E., Wright, J.T., Glasby, T.M., 2013. Positive versus negative effects of an invasive ecosystem engineer on different components of a marine ecosystem. Oikos 122, 816–824. https://doi.org/10.1111/j.1600-0706.2012.20868.x

Griffiths, C.L., 1976. Guide to the benthic marine amphipods of Southern Africa. Trustees of the South African Museum, Cape Town.

Griffiths, C.L., King, J.A., 1979. Energy expended on growth and gonad output in the ribbed mussel *Aulacomya ater*. Mar. Biol. 53, 217–222. https://doi.org/10.1007/BF00952429

Griffiths, C.L., Robinson, T.B., Lange, L., Mead, A., 2010. Marine biodiversity in South Africa: An evaluation of current states of knowledge. PLoS ONE 5, e12008. https://doi.org/10.1371/journal.pone.0012008

Grosberg, R.K., 1982. Intertidal zonation of barnacles: The influence of planktonic zonation of larvae on vertical distribution of adults. Ecology 63, 894–899. https://doi.org/10.2307/1937228

Gruber, N., Sarmiento, J.L., Stocker, T.F., 1996. An improved method for detecting anthropogenic CO_2 in the oceans. Glob. Biogeochem. Cycles 10, 809–837. https://doi.org/10.1029/96GB01608

Gründlingh, M.L., 1983. On the course of the Agulhas current. South Afr. Geogr. J. 65, 49–57. https://doi.org/10.1080/03736245.1983.10559671

Guida, B.S., 2016. Unique cellular, physiological, and metabolic adaptations to the euendolithic lifestyle in a boring cyanobacterium (Doctor of Philosophy). Arizona State University.

Guida, B.S., Bose, M., Garcia-Pichel, F., 2017. Carbon fixation from mineral carbonates. Nat. Commun. 8, 1025. https://doi.org/10.1038/s41467-017-00703-4

Guida, B.S., Garcia-Pichel, F., 2016. Extreme cellular adaptations and cell differentiation required by a cyanobacterium for carbonate excavation. Proc. Natl. Acad. Sci. 113, 5712–5717. https://doi.org/10.1073/pnas.1524687113

Gupta, A.S., Thomsen, M., Benthuysen, J.A., Hobday, A.J., Oliver, E., Alexander, L.V., Burrows, M.T., Donat, M.G., Feng, M., Holbrook, N.J., Perkins-Kirkpatrick, S., Moore, P.J., Rodrigues, R.R., Scannell, H.A., Taschetto, A.S., Ummenhofer, C.C., Wernberg, T., Smale, D.A., 2020. Drivers and impacts of the most extreme marine heatwave events. Sci. Rep. 10, 19359. https://doi.org/10.1038/s41598-020-75445-3

Gusha, N.M., 2022. Functional biogeography: evaluating community assemblage patterns and ecosystem functioning in intertidal systems using trait-based approaches (Doctor of Philosophy). Rhodes University, Grahamstown, South Africa.

Gutiérrez, J., Bagur, M., Palomo, M., 2019. Algal epibionts as co-engineers in mussel beds: Effects on abiotic conditions and mobile interstitial invertebrates. Diversity 11, 17. https://doi.org/10.3390/d11020017

Gutiérrez, J.L., Jones, C.G., 2006. Physical ecosystem engineers as agents of biogeochemical heterogeneity. BioScience 56, 227–236. https://doi.org/10.1641/0006-3568(2006)056[0227:PEEAAO]2.0.CO;2

Gutiérrez, J.L., Jones, C.G., Strayer, D.L., Iribarne, O.O., 2003. Mollusks as ecosystem engineers: the role of shell production in aquatic habitats. Oikos 101, 79–90. https://doi.org/10.1034/j.1600-0706.2003.12322.x

Gutiérrez-Isaza, N., Espinoza-Avalos, J., León-Tejera, H.P., González-Solís, D., 2015. Endolithic community composition of *Orbicella faveolata* (Scleractinia) underneath the interface between coral tissue and turf algae. Coral Reefs 34, 625–630. https://doi.org/10.1007/s00338-015-1276-0

Gutner-Hoch, E., Fine, M., 2011. Genotypic diversity and distribution of *Ostreobium quekettii* within scleractinian corals. Coral Reefs 30, 643–650. https://doi.org/10.1007/s00338-011-0750-6

Haine, E.R., Boucansaud, K., Rigaud, T., 2005. Conflict between parasites with different transmission strategies infecting an amphipod host. Proc. R. Soc. B Biol. Sci. 272, 2505–2510. https://doi.org/10.1098/rspb.2005.3244

Halldal, P., 1968. Photosynthetic capacities and photosynthetic action spectra of endozoic algae of the massive coral *Favia*. Biol. Bull. 134, 411–424. https://doi.org/10.2307/1539860

Hammond, W., Griffiths, C., 2006. Biogeographical patterns in the fauna associated with southern African mussel beds. Afr. Zool. 41, 123–130. https://doi.org/10.1080/15627020.2006.11407342

Hammond, W., Griffiths, C.L., 2004. Influence of wave exposure on South African mussel beds and their associated infaunal communities. Mar. Biol. 144, 547–552. https://doi.org/10.1007/s00227-003-1210-9

Harland, H., MacLeod, C., Poulin, R., 2015. Non-linear effects of ocean acidification on the transmission of a marine intertidal parasite. Mar. Ecol. Prog. Ser. 536, 55–64. https://doi.org/10.3354/meps11416

Harley, C., 2008. Tidal dynamics, topographic orientation, and temperature-mediated mass mortalities on rocky shores. Mar. Ecol. Prog. Ser. 371, 37–46. https://doi.org/10.3354/meps07711

Harley, C.D.G., Denny, M.W., Mach, K.J., Miller, L.P., 2009. Thermal stress and morphological adaptations in limpets. Funct. Ecol. 23, 292–301. https://doi.org/10.1111/j.1365-2435.2008.01496.x

Harlin, M.M., Lindbergh, J.M., 1977. Selection of substrata by seaweeds: Optimal surface relief. Mar. Biol. 40, 33–40. https://doi.org/10.1007/BF00390625

Harmelin-Vivien, M.L., 1994. The effects of storms and cyclones on coral reefs: A review. J. Coast. Res. Spec. Issue, Coastal Hazards: Perception, Susceptibilitu and Mitigation 211–231.

Harper, K.D., Williams, G.A., 2001. Variation in abundance and distribution of the chiton *Acanthopleura japonica* and associated molluscs on a seasonal, tropical, rocky shore. J. Zool. 253, 293–300. https://doi.org/10.1017/S0952836901000279

Harrington, L., Fabricius, K., De'ath, G., Negri, A., 2004. Recognition and selection of settlement substrata determine post-settlement survival in corals. Ecology 85, 3428–3437. https://doi.org/10.1890/04-0298

Harris, J.M., Branch, G.M., Elliott, B.L., Currie, B., Dye, A.H., McQuaid, C.D., Tomalin, B.J., Velasquez, C., 1998. Spatial and temporal variability in recruitment of intertidal mussels around the coast of southern Africa. South Afr. J. Zool. 33, 1–11. https://doi.org/10.1080/02541858.1998.11448447

Hartig, F., 2022. DHARMa: Residual diagnostics for hierarchical (multi-level/mixed) regression models.

Hassenrück, C., Jantzen, C., Försterra, G., Häussermann, V., Willenz, P., 2013. Rates of apical septal extension of *Desmophyllum dianthus*: effect of association with endolithic photo-autotrophs. Mar. Biol. 160, 2919–2927.
https://doi.org/10.1007/s00227-013-2281-x

Hastings, A., Byers, J.E., Crooks, J.A., Cuddington, K., Jones, C.G., Lambrinos, J.G., Talley, T.S., Wilson, W.G., 2007. Ecosystem engineering in space and time. Ecol. Lett. 10, 153–164. https://doi.org/10.1111/j.1461-0248.2006.00997.x

Hatch, W.I., 1980. The implication of carbonic anhydrase in the physiological mechanism of penetration of carbonate substrata by the marine burrowing sponge *Cliona celata* (Demospongiae). Biol. Bull. 159, 135–147.
https://doi.org/10.2307/1541014

Hatcher, M.J., Dick, J.T., Dunn, A.M., 2012. Diverse effects of parasites in ecosystems: linking interdependent processes. Front. Ecol. Environ. 10, 186–194.
https://doi.org/10.1890/110016

Hayakawa, J., Kawamura, T., Ohashi, S., Horii, T., Watanabe, Y., 2008. Habitat selection of Japanese top shell (*Turbo cornutus*) on articulated coralline algae: combination of preferences in settlement and post-settlement stage.
J. Exp. Mar. Biol. Ecol. 363, 118–123. https://doi.org/10.1016/j.jembe.2008.06.033

Hayworth, A.M., Quinn, J.F., 1990. Temperature of limpets in the rocky intertidal zone: Effects of caging and substratum. Limnol. Oceanogr. 35, 967–970. https://doi.org/10.4319/lo.1990.35.4.0967

Hechtel, L.J., Johnson, C.L., Juliano, S.A., 1993. Modification of antipredator behavior of *Caecidotea intermedius* by its parasite *Acanthocephalus dirus*. Ecology 74, 710–713. https://doi.org/10.2307/1940798

Helmuth, B., Broitman, B.R., Blanchette, C.A., Gilman, S., Halpin, P., Harley, C.D.G., O'Donnell, M.J., Hofmann, G.E., Menge, B., Strickland, D., 2006a. Mosaic patterns of thermal stress in the rocky intertidal zone: implications for climate change. Ecol. Monogr. 76, 461–479. https://doi.org/10.1890/0012-9615(2006)076[0461:MPOTSI]2.0.CO;2

Helmuth, B., Broitman, B.R., Yamane, L., Gilman, S.E., Mach, K., Mislan, K.A.S., Denny, M.W., 2010. Organismal climatology: analyzing environmental variability at scales relevant to physiological stress. J. Exp. Biol. 213, 995–1003. https://doi.org/10.1242/jeb.038463

Helmuth, B., Choi, F., Matzelle, A., Torossian, J.L., Morello, S.L., Mislan, K.A.S., Yamane, L., Strickland, D., Szathmary, P.L., Gilman, S.E., Tockstein, A., Hilbish, T.J., Burrows, M.T., Power, A.M., Gosling, E., Mieszkowska, N., Harley, C.D.G., Nishizaki, M., Carrington, E., Menge, B., Petes, L., Foley, M.M., Johnson, A., Poole, M., Noble, M.M., Richmond, E.L., Robart, M., Robinson, J., Sapp, J., Sones, J., Broitman, B.R., Denny, M.W., Mach, K.J., Miller, L.P., O'Donnell, M., Ross, P., Hofmann, G.E., Zippay, M., Blanchette, C., Macfarlan, J.A., Carpizo-Ituarte, E., Ruttenberg, B., Peña Mejía, C.E., McQuaid, C.D., Lathlean, J., Monaco, C.J., Nicastro, K.R., Zardi, G., 2016. Long-term, high frequency in situ measurements of intertidal mussel bed temperatures using biomimetic sensors. Sci. Data 3, 160087. https://doi.org/10.1038/sdata.2016.87

Helmuth, B., Harley, C.D.G., Halpin, P.M., O'Donnell, M., Hofmann, G.E., Blanchette, C.A., 2002. Climate change and latitudinal patterns of intertidal thermal stress. Science 298, 1015–1017. https://doi.org/10.1126/science.1076814

Helmuth, B., Mieszkowska, N., Moore, P., Hawkins, S.J., 2006b. Living on the edge of two changing worlds: Forecasting the responses of rocky intertidal ecosystems to climate change. Annu. Rev. Ecol. Evol. Syst. 37, 373–404. https://doi.org/10.1146/annurev.ecolsys.37.091305.110149

Helmuth, B., Yamane, L., Lalwani, S., Matzelle, A., Tockstein, A., Gao, N., 2011. Hidden signals of climate change in intertidal ecosystems: What (not) to expect when you are expecting. J. Exp. Mar. Biol. Ecol. 400, 191–199. https://doi.org/10.1016/j.jembe.2011.02.004

Helmuth, B.S.T., 1998. Intertidal mussel microclimates: predicting the body temperature of a sessile invertebrate. Ecol. Monogr. 68, 51–74. https://doi.org/10.1890/0012-9615(1998)068[0051:IMMPTB]2.0.CO;2

Helmuth, B.S.T., Hofmann, G.E., 2001. Microhabitats, thermal heterogeneity, and patterns of physiological stress in the rocky intertidal zone. Biol. Bull. 201, 374–384. https://doi.org/10.2307/1543615

Hicks, D.W., McMahon, R.F., 2003. Temperature and relative humidity effects on water loss and emersion tolerance of *Perna perna* (L.) (Bivalvia: Mytilidae) from the Gulf of Mexico. Bull. Mar. Sci. 72, 135–150.

Highsmith, R.C., 1981. Lime-boring algae in hermatypic coral skeletons. J. Exp. Mar. Biol. Ecol. 55, 267–281. https://doi.org/10.1016/0022-0981(81)90117-9

Hines, A.H., Comtois, K.L., 1985. Vertical distribution of infauna in sediments of a subestuary of central Chesapeake Bay. Estuaries 8, 296. https://doi.org/10.2307/1351490

Hoegh-Guldberg, O., 1999. Climate change, coral bleaching and the future of the world's coral reefs. Mar. Freshw. Res. 50, 839–866. https://doi.org/10.1071/MF99078

Hooper, D.U., Adair, E.C., Cardinale, B.J., Byrnes, J.E.K., Hungate, B.A., Matulich, K.L., Gonzalez, A., Duffy, J.E., Gamfeldt, L., O'Connor, M.I., 2012. A global synthesis reveals biodiversity loss as a major driver of ecosystem change. Nature 486, 105–108. https://doi.org/10.1038/nature11118

Høye, T.T., Ärje, J., Bjerge, K., Hansen, O.L.P., Iosifidis, A., Leese, F., Mann, H.M.R., Meissner, K., Melvad, C., Raitoharju, J., 2021. Deep learning and computer vision will transform entomology. Proc. Natl. Acad. Sci. 118, e2002545117. https://doi.org/10.1073/pnas.2002545117

Høye, T.T., Dyrmann, M., Kjær, C., Nielsen, J., Bruus, M., Mielec, C.L., Vesterdal, M.S., Bjerge, K., Madsen, S.A., Jeppesen, M.R., Melvad, C., 2022. Accurate image-based identification of macroinvertebrate specimens using deep learning — How much training data is needed? PeerJ 10, e13837. https://doi.org/10.7717/peerj.13837

Huber, J., Jadin, F., 1892. Sur une algue perforante d'eau douce. C. r. Hebd. Séances L'Académie Sci. Paris 115, 262–264.

Hughes, A.R., 2014. Genotypic diversity and trait variance interact to affect marsh plant performance. J. Ecol. 102, 651–658. https://doi.org/10.1111/1365-2745.12244

Hughes, A.R., Johnson, M.T.J., Underwood, N., 2008. Ecological consequences of genetic diversity. Ecol. Lett. 11, 609–623. https://doi.org/10.1111/j.1461-0248.2008.01179.x

Hughes, A.R., Stachowicz, J.J., 2004. Genetic diversity enhances the resistance of a seagrass ecosystem to disturbance. Proc. Natl. Acad. Sci. 101, 8998–9002. https://doi.org/10.1073/pnas.0402642101

Hughes, R.N., Griffiths, C.L., 1988. Self-thinning in barnacles and mussels: The geometry of packing. Am. Nat. 132, 484–491. https://doi.org/10.1086/284866

Hunter, J.P., 1998. Key innovations and the ecology of macroevolution. Trends Ecol. Evol. 13, 31–36. https://doi.org/10.1016/S0169-5347(97)01273-1

Hutchings, L., Van Der Lingen, C.D., Shannon, L.J., Crawford, R.J.M., Verheye, H.M.S., Bartholomae, C.H., Van Der Plas, A.K., Louw, D., Kreiner, A., Ostrowski, M., Fidel, Q., Barlow, R.G., Lamont, T., Coetzee, J., Shillington, F., Veitch, J., Currie, J.C., Monteiro, P.M.S., 2009. The Benguela current: An ecosystem of four components. Prog. Oceanogr. 83, 15–32. https://doi.org/10.1016/j.pocean.2009.07.046

Hutchings, P.A., 1986. Biological destruction of coral reefs. Coral Reefs 4, 239–252. https://doi.org/10.1007/BF00298083

Iha, C., Dougan, K.E., Varela, J.A., Avila, V., Jackson, C.J., Bogaert, K.A., Chen, Y., Judd, L.M., Wick, R., Holt, K.E., Pasella, M.M., Ricci, F., Repetti, S.I., Medina, M., Marcelino, V.R., Chan, C.X., Verbruggen, H., 2021. Genomic adaptations to an endolithic lifestyle in the coral-associated alga *Ostreobium*. Curr. Biol. 31, 1393–1402. https://doi.org/10.1016/j.cub.2021.01.018

Isbell, F., Gonzalez, A., Loreau, M., Cowles, J., Díaz, S., Hector, A., Mace, G.M., Wardle, D.A., O'Connor, M.I., Duffy, J.E., Turnbull, L.A., Thompson, P.L., Larigauderie, A., 2017. Linking the influence and dependence of people on biodiversity across scales. Nature 546, 65–72. https://doi.org/10.1038/nature22899

James, R.J., Underwood, A.J., 1994. Influence of colour of substratum on recruitment of spirorbid tubeworms to different types of intertidal boulders. J. Exp. Mar. Biol. Ecol. 181, 105–115. https://doi.org/10.1016/0022-0981(94)90107-4

Jernakoff, P., 1986. Experimental investigation of interactions between the perennial red alga *Gelidium pusillum* and barnacles on a New South Wales rocky shore. Mar. Ecol. Prog. Ser. 28, 259–263. https://doi.org/10.3354/meps028259

Johnson, M.S., 2011. Thirty-four years of climatic selection in the land snail *Theba pisana*. Heredity 106, 741–748. https://doi.org/10.1038/hdy.2010.114

Jones, C.G., Gutiérrez, J.L., 2007. On the purpose, meaning, and usage of the physical ecosystem engineering concept, in: Cuddington, K. (Ed.), Ecosystem Engineers: Plants to Protists, Theoretical Ecology Series. Academic Press, Amsterdam; Boston, pp. 3–24.

Jones, C.G., Gutiérrez, J.L., Byers, J.E., Crooks, J.A., Lambrinos, J.G., Talley, T.S., 2010. A framework for understanding physical ecosystem engineering by organisms. Oikos 119, 1862–1869. https://doi.org/10.1111/j.1600-0706.2010.18782.x

Jones, C.G., Lawton, J.H., Shachak, M., 1997. Positive and negative effects of organisms as physical ecosystem engineers. Ecology 78, 1946–1957. https://doi.org/10.1890/0012-9658(1997)078[1946:PANEOO]2.0.CO;2

Jones, C.G., Lawton, J.H., Shachak, M., 1994. Organisms as ecosystem engineers. Oikos 69, 373–386. https://doi.org/10.2307/3545850

Jurgens, L.J., Gaylord, B., 2018. Physical effects of habitat-forming species override latitudinal trends in temperature. Ecol. Lett. 21, 190–196. https://doi.org/10.1111/ele.12881

Kaehler, S., 1999. Incidence and distribution of phototrophic shell-degrading endoliths of the brown mussel *Perna perna*. Mar. Biol. 135, 505–514. https://doi.org/10.1007/s002270050651

Kaehler, S., McQuaid, C.D., 1999. Lethal and sub-lethal effects of phototrophic endoliths attacking the shell of the intertidal mussel *Perna perna*. Mar. Biol. 135, 497–503. https://doi.org/10.1007/s002270050650

Kanwisher, J.W., Wainwright, S.A., 1967. Oxygen balance in some reef corals. Biol. Bull. 133, 378–390. https://doi.org/10.2307/1539833

Keats, D.W., Groener, A., Chamberlain, Y.M., 1993. Cell sloughing in the littoral zone coralline alga, *Spongites yendoi* (Foslie) Chamberlain (Corallinales, Rhodophyta). Phycologia 32, 143–150. https://doi.org/10.2216/i0031-8884-32-2-143.1

Keats, D.W., Matthews, I., Maneveldt, G., 1994. Competitive relationships and coexistence in a guild of crustose algae in the eulittoral zone, Cape Province, South Africa. South Afr. J. Bot. 60, 108–113. https://doi.org/10.1016/S0254-6299(16)30640-8

Kensley, B.F., 1978. Guide to the marine isopods of southern Africa. Trustees of the South African Museum, Cape Town.

Kent, A., Hawkins, S.J., Doncaster, C.P., 2003. Population consequences of mutual attraction between settling and adult barnacles. J. Anim. Ecol. 72, 941–952. https://doi.org/10.1046/j.1365-2656.2003.00762.x

Keough, M.J., 1984. Dynamics of the epifauna of the bivalve *Pinna bicolor*: Interactions among recruitment, predation, and competition. Ecology 65, 677–688. https://doi.org/10.2307/1938040

Keough, M.J., 1983. Patterns of recruitment of sessile invertebrates in two subtidal habitats. J. Exp. Mar. Biol. Ecol. 66, 213–245. https://doi.org/10.1016/0022-0981(83)90162-4

Key, R.M., Kozyr, A., Sabine, C.L., Lee, K., Wanninkhof, R., Bullister, J.L., Feely, R.A., Millero, F.J., Mordy, C., Peng, T.-H., 2004. A global ocean carbon climatology: Results from Global Data Analysis Project (GLODAP). Glob. Biogeochem. Cycles 18, GB4031. https://doi.org/10.1029/2004GB002247

Kiene, W.E., Hutchings, P.A., 1994. Bioerosion experiments at Lizard Island, Great Barrier Reef. Coral Reefs 13, 91–98. https://doi.org/10.1007/BF00300767

Kiene, W.E., Radtke, G., Gektidis, M., Golubic, S., Vogel, K., 1995. Factors controlling the distribution of microborers in Bahamian reef environments, in: Schumacher, H., Kiene, W.E., Dullo, W.-C. (Eds.), Factors Controlling Holocene Reef Growth: An Interdisciplinary Approach, Facies. pp. 174–188.

Knight-Jones, E.W., 1951. Gregariousness and some other aspects of the setting behaviour of *Spirorbis*. J. Mar. Biol. Assoc. U. K. 30, 201–222. https://doi.org/10.1017/S0025315400012716

Knoll, A.H., 2008. Cyanobacteria and Earth history, in: Herrero, A., Flores, E. (Eds.), The Cyanobacteria: Molecular Biology, Genomics, and Evolution. Caister Academic Press, U.K., pp. 1–19.

Knowlton, N., Brainard, R.E., Fisher, R., Moews, M., Plaisance, L., Caley, M.J., 2010. Coral reef biodiversity, in: McIntyre, A.D. (Ed.), Life in the World's Oceans. Wiley-Blackwell, Oxford, UK, pp. 65–78. https://doi.org/10.1002/9781444325508.ch4

Kobluk, D.R., Risk, M.J., 1977. Calcification of exposed filaments of endolithic algae, micrite envelope formation and sediment production. SEPM J. Sediment. Res. 47, 517–528. https://doi.org/10.1306/212F71C6-2B24-11D7-8648000102C1865D

Köhler, J., Hansen, P., Wahl, M., 1999. Colonization patterns at the substratum-water interface: How does surface microtopography influence recruitment patterns of sessile organisms? Biofouling 14, 237–248. https://doi.org/10.1080/08927019909378415

Koivisto, M.E., Westerbom, M., 2010. Habitat structure and complexity as determinants of biodiversity in blue mussel beds on sublittoral rocky shores. Mar. Biol. 157, 1463–1474. https://doi.org/10.1007/s00227-010-1421-9

Kölliker, A.V., 1860. On the frequent occurrence of vegetable parasites in the hard structures of animals. Proc. R. Soc. Lond. 10, 95–99. https://doi.org/10.1098/rspl.1859.0023

Kordas, R.L., Dudgeon, S., Storey, S., Harley, C.D.G., 2015. Intertidal community responses to field-based experimental warming. Oikos 124, 888–898. https://doi.org/10.1111/oik.00806

Kostylev, V., Erlandsson, J., 2001. A fractal approach for detecting spatial hierarchy and structure on mussel beds. Mar. Biol. 139, 497–506. https://doi.org/10.1007/s002270100597

Kostylev, V.E., Erlandsson, J., Ming, M.Y., Williams, G.A., 2005. The relative importance of habitat complexity and surface area in assessing biodiversity: Fractal application on rocky shores. Ecol. Complex. 2, 272–286. https://doi.org/10.1016/j.ecocom.2005.04.002

Krause, S., Liebetrau, V., Nehrke, G., Damm, T., Büsse, S., Leipe, T., Vogts, A., Gorb, S.N., Eisenhauer, A., 2019. Endolithic algae affect modern coral carbonate morphology and chemistry. Front. Earth Sci. 7, 304. https://doi.org/10.3389/feart.2019.00304

Kremen, C., 2005. Managing ecosystem services: what do we need to know about their ecology? Ecol. Lett. 8, 468–479. https://doi.org/10.1111/j.1461-0248.2005.00751.x

Krug, P.J., 2006. Defense of benthic invertebrates against surface colonization by larvae: A chemical arms race, in: Fusetani, N., Clare, A.S. (Eds.), Antifouling Compounds, Progress in Molecular and Subcellular Biology. Springer-Verlag, Berlin, Heidelberg, pp. 1–53.

Kruger, L.M., Griffiths, C.L., 1998. Sea anemones as secondary consumers on rocky shores in the south-western Cape, South Africa. J. Nat. Hist. 32, 629–644. https://doi.org/10.1080/00222939800770331

Kühl, M., Holst, G., Larkum, A.W.D., Ralph, P.J., 2008. Imaging of oxygen dynamics within the endolithic algal community of the massive coral *Porites lobata*. J. Phycol. 44, 541–550. https://doi.org/10.1111/j.1529-8817.2008.00506.x

Kumar, P.S., Thomas, P.A., 2011. Pathological manifestations of sponge infestation in *Perna indica* Kuriakose & Nair 1976. J. Mar. Biol. Assoc. India 53, 278–280. https://doi.org/10.6024/jmbai.2011.53.2.01619-21

Kuppler, J., Höfers, M.K., Wiesmann, L., Junker, R.R., 2016. Time-invariant differences between plant individuals in interactions with arthropods correlate with intraspecific variation in plant phenology, morphology and floral scent. New Phytol. 210, 1357–1368. https://doi.org/10.1111/nph.13858

Kusch, J., Czubatinski, L., Nachname, S., Hübner, M., Alter, M., Albrecht, P., 2002. Competitive advantages of *Caedibacter*-infected *Paramecia*. Protist 153, 47–58. https://doi.org/10.1078/1434-4610-00082

Laborel, J., Le Campion-Alsumard, T., 1979. Infestation massive du squelette de coraux vivants par des Rhodophycées de type *Conchocelis*. Comptes Rendus Académie Sci. Paris, D 288, 1575–1577.

Lafferty, K.D., Kuris, A.M., 2009. Parasitic castration: the evolution and ecology of body snatchers. Trends Parasitol. 25, 564–572. https://doi.org/10.1016/j.pt.2009.09.003

Lagerheim, G., 1886. Note sur le *Mastigocoleus*, nouveau genre des algues marines de l'ordre des Phycochromacées. Notarisia 1, 65–69.

Laihonen, P., Furman, E.R., 1986. The site of settlement indicates commensalism between blue mussel and its epibiont. Oecologia 71, 38–40. https://doi.org/10.1007/BF00377317

LaJeunesse, T.C., Parkinson, J.E., Gabrielson, P.W., Jeong, H.J., Reimer, J.D., Voolstra, C.R., Santos, S.R., 2018. Systematic revision of Symbiodiniaceae highlights the antiquity and diversity of coral endosymbionts. Curr. Biol. 28, 2570–2580. https://doi.org/10.1016/j.cub.2018.07.008

Lambert, G., Jennings, S., Kaiser, M., Hinz, H., Hiddink, J., 2011. Quantification and prediction of the impact of fishing on epifaunal communities. Mar. Ecol. Prog. Ser. 430, 71–86. https://doi.org/10.3354/meps09112

Lamy, T., Legendre, P., Chancerelle, Y., Siu, G., Claudet, J., 2015. Understanding the spatio-temporal response of coral reef fish communities to natural disturbances: Insights from beta-diversity decomposition. PLoS ONE 10, e0138696. https://doi.org/10.1371/journal.pone.0138696

Lasiak, T., 1992. Contemporary shellfish-gathering practices of indigenous coastal people in Transkei: some implications for interpretation of the archaeological record. South Afr. J. Sci. 88, 19–28. https://doi.org/10.10520/AJA00382353_9423

Lathlean, J., Seuront, L., 2014. Infrared thermography in marine ecology: methods, previous applications and future challenges. Mar. Ecol. Prog. Ser. 514, 263–277. https://doi.org/10.3354/meps10995

Lathlean, J.A., Ayre, D.J., Minchinton, T.E., 2011. Rocky intertidal temperature variability along the southeast coast of Australia: comparing data from in situ loggers, satellite-derived SST and terrestrial weather stations. Mar. Ecol. Prog. Ser. 439, 83–95. https://doi.org/10.3354/meps09317

Lathlean, J.A., McQuaid, C.D., 2017. Biogeographic variability in the value of mussel beds as ecosystem engineers on South African rocky shores. Ecosystems 20, 568–582. https://doi.org/10.1007/s10021-016-0041-8

Lathlean, J.A., Seuront, L., McQuaid, C.D., Ng, T.P.T., Zardi, G.I., Nicastro, K.R., 2016a. Cheating the locals: Invasive mussels steal and benefit from the cooling effect of indigenous mussels. PLOS ONE 11, e0152556. https://doi.org/10.1371/journal.pone.0152556

Lathlean, J.A., Seuront, L., McQuaid, C.D., Ng, T.P.T., Zardi, G.I., Nicastro, K.R., 2016b. Size and position (sometimes) matter: small-scale patterns of heat stress associated with two co-occurring mussels with different thermoregulatory behaviour. Mar. Biol. 163, 189. https://doi.org/10.1007/s00227-016-2966-z

Lathlean, J.A., Seuront, L., Ng, T.P.T., 2017. On the edge: The use of infrared thermography in monitoring responses of intertidal organisms to heat stress. Ecol. Indic. 81, 567–577. http://dx.doi.org/10.1016/j.ecolind.2017.04.057

Lauckner, G., 1984. Impact of trematode parasitism on the fauna of a North Sea tidal flat. Helgoländer Meeresunters. 37, 185–199. https://doi.org/10.1007/BF01989303

Lauckner, G., 1983. Diseases of Mollusca: Bivalvia, in: Kinne, O. (Ed.), Diseases of Marine Animals. Biologische Anstalt Helgoland., Hamburg, Germany, pp. 477–961.

Laudien, J., Wahl, M., 2004. Associational resistance of fouled blue mussels (*Mytilus edulis*) against starfish (*Asterias rubens*) predation: Relative importance of structural and chemical properties of the epibionts. Helgol. Mar. Res. 58, 162–167. https://doi.org/10.1007/s10152-004-0181-7

Laudien, J., Wahl, M., 1999. Indirect effects of epibiosis on host mortality: Seastar predation on differently fouled mussels. Mar. Ecol. 20, 35–47. https://doi.org/10.1046/j.1439-0485.1999.00063.x

Lavergne, S., Mouquet, N., Thuiller, W., Ronce, O., 2010. Biodiversity and climate change: Integrating evolutionary and ecological responses of species and communities. Annu. Rev. Ecol. Evol. Syst. 41, 321–350. https://doi.org/10.1146/annurev-ecolsys-102209-144628

Lawrie, S.M., McQuaid, C.D., 2001. Scales of mussel bed complexity: structure, associated biota and recruitment. J. Exp. Mar. Biol. Ecol. 257, 135–161. https://doi.org/10.1016/S0022-0981(00)00290-2

Lazier, A.V., Smith, J.E., Risk, M.J., Schwarcz, H.P., 1999. The skeletal structure of *Desmophyllum cristagalli*: The use of deep-water corals in sclerochronology. Lethaia 32, 119–130. https://doi.org/10.1111/j.1502-3931.1999.tb00530.x

Le Bris, S., Le Campion-Alsumard, T., Romano, J.-C., 1998. Caractéristiques du feutrage algal des récifs coralliens de Polynésie française soumis à différentes intensités de bioérosion. Oceanol. Acta 21, 695–708. https://doi.org/10.1016/S0399-1784(99)80025-5

Le Campion-Alsumard, T., 1979. Les Cyanophycées endolithes marines. Systématique, ultrastructure, écologie et biodestruction. Oceanol. Acta 2, 143–156.

Le Campion-Alsumard, T., Campbell, S.E., Golubic, S., 1982. Endoliths and the depth of the photic zone: Discussion. J. Sediment. Petrol. 52, 1333–1338.

Le Campion-Alsumard, T., Golubic, S., Hutchings, P., 1995a. Microbial endoliths in skeletons of live and dead corals: *Porites lobata* (Moorea, French Polynesia). Mar. Ecol. Prog. Ser. 117, 149–157. https://doi.org/10.3354/MEPS117149

Le Campion-Alsumard, T., Golubic, S., Priess, K., 1995b. Fungi in corals: symbiosis or disease? Interaction between polyps and fungi causes pearl-like skeleton biomineralization. Mar. Ecol. Prog. Ser. 117, 137–147.

Le Campion-Alsumard, T., Golubic, S., Priess, K., 1995c. Fungi in corals: symbiosis or disease? Interaction between polyps and fungi causes pearl-like skeleton biomineralization. Mar. Ecol. Prog. Ser. 117, 137–147. https://doi.org/10.3354/MEPS117137

Le Tourneux, F., Bourget, E., 1988. Importance of physical and biological settlement cues used at different spatial scales by the larvae of *Semibalanus balanoides*. Mar. Biol. 97, 57–66. https://doi.org/10.1007/BF00391245

Leggat, W.P., Camp, E.F., Suggett, D.J., Heron, S.F., Fordyce, A.J., Gardner, S., Deakin, L., Turner, M., Beeching, L.J., Kuzhiumparambil, U., Eakin, C.M., Ainsworth, T.D., 2019. Rapid coral decay is associated with marine heatwave mortality events on reefs. Curr. Biol. 29, 2723–2730. https://doi.org/10.1016/j.cub.2019.06.077

Lesser, M.P., Stat, M., Gates, R.D., 2013. The endosymbiotic dinoflagellates (*Symbiodinium* sp.) of corals are parasites and mutualists. Coral Reefs 32, 603–611. https://doi.org/10.1007/s00338-013-1051-z

Liang, V., 2020. Impacts of the trematode parasite *Proctoeces maculatus* on byssal thread production, byssal thread quality, and shell strength of the blue mussel *Mytilus edulis* (Master of Science). Hofstra University, New York, USA.

Lima, F.P., Ribeiro, P.A., Queiroz, N., Hawkins, S.J., Santos, A.M., 2007. Do distributional shifts of northern and southern species of algae match the warming pattern? Glob. Change Biol. 13, 2592–2604.
https://doi.org/10.1111/j.1365-2486.2007.01451.x

Lintas, C., Seed, R., 1994. Spatial variation in the fauna associated with *Mytilus edulis* on a wave-exposed rocky shore. J. Molluscan Stud. 60, 165–174.
https://doi.org/10.1093/mollus/60.2.165

Littler, M.M., Littler, D.S., 1995. Impact of CLOD pathogen on Pacific coral reefs. Science 267, 1356–1360. https://doi.org/10.1126/science.267.5202.1356

Llewelyn, J., Macdonald, S.L., Hatcher, A., Moritz, C., Phillips, B.L., 2016. Intraspecific variation in climate-relevant traits in a tropical rainforest lizard. Divers. Distrib. 22, 1000–1012. https://doi.org/10.1111/ddi.12466

Lohse, D.P., 1993. The importance of secondary substratum in a rocky intertidal community. J. Exp. Mar. Biol. Ecol. 166, 1–17.
https://doi.org/10.1016/0022-0981(93)90075-Y

Lombard, A.T., Strauss, T., Harris, J., Sink, K., Attwood, C., Hutchings, L., 2004. Volume 4: Marine Component (Technical Report), South African National Spatial Biodiversity Assessment 2004. South African National Biodiversity Institute, Pretoria, South Africa.

Lourenço, C.R., Nicastro, K.R., McQuaid, C.D., Sabour, B., Zardi, G.I., 2017. Latitudinal incidence of phototrophic shell-degrading endoliths and their effects on mussel bed microclimates. Mar. Biol. 164, 129–139.
https://doi.org/10.1007/s00227-017-3160-7

Lourenço, C.R., Nicastro, K.R., Serrão, E.A., Zardi, G.I., 2012. First record of the brown mussel (*Perna perna*) from the European Atlantic coast. Mar. Biodivers. Rec. 5, e39. https://doi.org/10.1017/S1755267212000280

Lukas, K.J., 1978. Depth distribution and form among common microboring algae from the Florida continental shelf, in: Proceedings of the Annual Meeting of the Geological Society of America. Presented at the Annual Meeting of the Geological Society of America, Boulder, p. 448.

Lukas, K.J., 1974. Two species of the Chlorophyte genus *Ostreobium* from skeletons of Atlantic and Caribbean reef corals. J. Phycol. 10, 331–335. https://doi.org/10.1111/j.1529-8817.1974.tb02722.x

Lukas, K.J., 1973. Taxonomy and ecology of the endolithic microflora of reef corals with a review of the literature on endolithic microphytes (Doctor of Philosophy). University of Rhode Island, Kingston.

Lürig, M.D., Donoughe, S., Svensson, E.I., Porto, A., Tsuboi, M., 2021. Computer vision, machine learning, and the promise of phenomics in ecology and evolutionary biology. Front. Ecol. Evol. 9, 642774. https://doi.org/10.3389/fevo.2021.642774

Lutjeharms, J.R.E., 1998. Coastal hydrography, in: Lubke, R., De Moor, I. (Eds.), Field Guide to the Eastern and Southern Cape Coasts. University of Cape Town Press, Cape Town, South Africa, pp. 50–61.

Ma, K.C.K., Monsinjon, J.R., Froneman, P.W., McQuaid, C.D., 2023. Thermal stress gradient causes increasingly negative effects towards the range limit of an invasive mussel. Sci. Total Environ. 865, 161184. https://doi.org/10.1016/j.scitotenv.2022.161184

Mace, G.M., Norris, K., Fitter, A.H., 2012. Biodiversity and ecosystem services: a multilayered relationship. Trends Ecol. Evol. 27, 19–26. https://doi.org/10.1016/j.tree.2011.08.006

Mackey, R.L., Currie, D.J., 2000. A re-examination of the expected effects of disturbance on diversity. Oikos 88, 483–493. https://doi.org/10.1034/j.1600-0706.2000.880303.x

MacLeod, C.D., Poulin, R., 2016. Parasitic infection: a buffer against ocean acidification? Biol. Lett. 12, 20160007. https://doi.org/10.1098/rsbl.2016.0007

MacLeod, C.D., Poulin, R., 2015. Differential tolerances to ocean acidification by parasites that share the same host. Int. J. Parasitol. 45, 485–493. https://doi.org/10.1016/j.ijpara.2015.02.007

Madikiza, L.O., 2006. The role of grazers and basal substrate cover in the control of intertidal algal (Master of Science). University of the Western Cape, Bellville, South Africa.

Magnusson, S., Fine, M., Kühl, M., 2007. Light microclimate of endolithic phototrophs in the scleractinian corals *Montipora monasteriata* and *Porites cylindrica*. Mar. Ecol. Prog. Ser. 332, 119–128. https://doi.org/10.3354/meps332119

Maneveldt, G., Keats, D., 2008. Effects of herbivore grazing on the physiognomy of the coralline alga *Spongites yendoi* and on associated competitive interactions. Afr. J. Mar. Sci. 30, 581–593. https://doi.org/10.2989/AJMS.2008.30.3.11.645

Manríquez, P.H., Lagos, N.A., Jara, M.E., Castilla, J.C., 2009. Adaptive shell color plasticity during the early ontogeny of an intertidal keystone snail. Proc. Natl. Acad. Sci. 106, 16298–16303. https://doi.org/10.1073/pnas.0908655106

Mao Che, L., Le Campion-Alsumard, T., Boury-Esnault, N., Payri, C., Golubic, S., Bézac, C., 1996. Biodegradation of shells of the black pearl oyster, *Pinctada margaritifera* var. *cumingii*, by microborers and sponges of French Polynesia. Mar. Biol. 126, 509–519. https://doi.org/10.1007/BF00354633

Marcelino, V.R., Morrow, K.M., Oppen, M.J.H., Bourne, D.G., Verbruggen, H., 2017. Diversity and stability of coral endolithic microbial communities at a naturally high pCO_2 reef. Mol. Ecol. 26, 5344–5357. https://doi.org/10.1111/mec.14268

Marcelino, V.R., Verbruggen, H., 2016. Multi-marker metabarcoding of coral skeletons reveals a rich microbiome and diverse evolutionary origins of endolithic algae. Sci. Rep. 6, 31508. https://doi.org/10.1038/srep31508

Marin, M., Feng, M., Phillips, H.E., Bindoff, N.L., 2021. A global, multiproduct analysis of coastal marine heatwaves: Distribution, characteristics, and long-term trends. J. Geophys. Res. Oceans 126, e2020JC016708. https://doi.org/10.1029/2020JC016708

Marquet, N., Nicastro, K.R., Gektidis, M., McQuaid, C.D., Pearson, G.A., Serrão, E.A., Zardi, G.I., 2013. Comparison of phototrophic shell-degrading endoliths in invasive and native populations of the intertidal mussel *Mytilus galloprovincialis*. Biol. Invasions 15, 1253–1272. https://doi.org/10.1007/s10530-012-0363-1

Marshall, A.T., 1996. Calcification in hermatypic and ahermatypic corals. Science 271, 637–639. https://doi.org/10.1126/science.271.5249.637

Marshall, D.J., McQuaid, C.D., Williams, G.A., 2010. Non-climatic thermal adaptation: implications for species' responses to climate warming. Biol. Lett. 6, 669–673. https://doi.org/10.1098/rsbl.2010.0233

Massé, A., Domart-Coulon, I., Golubic, S., Duché, D., Tribollet, A., 2018. Early skeletal colonization of the coral holobiont by the microboring Ulvophyceae *Ostreobium* sp. Sci. Rep. 8, 2293. https://doi.org/10.1038/s41598-018-20196-5

Massé, A., Tribollet, A., Meziane, T., Bourguet-Kondracki, M., Yéprémian, C., Sève, C., Thiney, N., Longeon, A., Couté, A., Domart-Coulon, I., 2020. Functional diversity of microboring *Ostreobium* algae isolated from corals. Environ. Microbiol. 22, 4825–4846. https://doi.org/10.1111/1462-2920.15256

May, R.M., 1994. Conceptual aspects of the quantification of the extent of biological diversity. Philos. Trans. Biol. Sci. 345, 13–20. https://doi.org/10.1098/rstb.1994.0082

Mbokodo, I., Bopape, M.-J., Chikoore, H., Engelbrecht, F., Nethengwe, N., 2020. Heatwaves in the future warmer climate of South Africa. Atmosphere 11, 712. https://doi.org/10.3390/atmos11070712

McClanahan, T.R., Weil, E., Maina, J., 2009. Strong relationship between coral bleaching and growth anomalies in massive *Porites*. Glob. Change Biol. 15, 1804–1816. https://doi.org/10.1111/j.1365-2486.2008.01799.x

McMahon, R.F., 1990. Thermal tolerance, evaporative water loss, air-water oxygen consumption and zonation of intertidal prosobranchs: a new synthesis. Hydrobiologia, Progress in Littorinid and Muricid Biology 193, 241–260. https://doi.org/10.1007/BF00028081

McQuaid, C.D., Branch, G.M., Frost, P.G.H., 1979. Aestivation behaviour and thermal relations of the pulmonate *Theba pisana* in a semi-arid environment. J. Therm. Biol. 4, 47–55. https://doi.org/10.1016/0306-4565(79)90045-7

McQuaid, C.D., Mostert, B.P., 2010. The effects of within-shore water movement on growth of the intertidal mussel *Perna perna*: An experimental field test of bottom-up control at centimetre scales. J. Exp. Mar. Biol. Ecol. 384, 119–123. https://doi.org/10.1016/j.jembe.2010.01.005

Meehl, G.A., Tebaldi, C., 2004. More intense, more frequent, and longer lasting heat waves in the 21st century. Science 305, 994–997. https://doi.org/10.1126/science.1098704

Mendoza, V., Pazos, M., Garduño, R., Mendoza, B., 2021. Thermodynamics of climate change between cloud cover, atmospheric temperature and humidity. Sci. Rep. 11, 21244. https://doi.org/10.1038/s41598-021-00555-5

Merz-Preiβ, M., 2000. Calcification in cyanobacteria, in: Riding, R.E., Awramik, S.M. (Eds.), Microbial Sediments. Springer, Berlin, Heidelberg, pp. 50–56. https://doi.org/10.1007/978-3-662-04036-2

Meyer, N., Wisshak, M., Freiwald, A., 2021. Bioerosion ichnodiversity in barnacles from the Ross Sea, Antarctica. Polar Biol. 44, 667–682. https://doi.org/10.1007/s00300-021-02825-4

Meyer, N., Wisshak, M., Freiwald, A., 2020. Ichnodiversity and bathymetric range of microbioerosion traces in polar barnacles of Svalbard. Polar Res. 39, 3766. https://doi.org/10.33265/polar.v39.3766

Michalakis, Y., Olivieri, I., Renaud, F., Raymond, M., 1992. Pleiotropic action of parasites: How to be good for the host. Trends Ecol. Evol. 7, 59–62. https://doi.org/10.1016/0169-5347(92)90108-N

Miller, A.H., 1949. Some ecologic and morphologic considerations in the evolution of higher taxonomic categories. Ornithol. Als Biol. Wiss. 28, 84–88.

Miller, A.W., Blackwelder, P., Al-Sayegh, H., Richardson, L.L., 2011. Fine-structural analysis of black band disease-infected coral reveals boring cyanobacteria and novel bacteria. Dis. Aquat. Organ. 93, 179–190. https://doi.org/10.3354/dao02305

Minchella, D.J., 1985. Host life-history variation in response to parasitism. Parasitology 90, 205–216. https://doi.org/10.1017/S0031182000049143

Mislan, K.A.S., Wethey, D.S., Helmuth, B., 2009. When to worry about the weather: role of tidal cycle in determining patterns of risk in intertidal ecosystems. Glob. Change Biol. 15, 3056–3065. https://doi.org/10.1111/j.1365-2486.2009.01936.x

Mitton, J.B., 1977. Shell color and pattern variation in *Mytilus edulis* and its adaptive significance. Chesap. Sci. 18, 387–390. https://doi.org/10.2307/1350595

Moeser, G.M., Carrington, E., 2006. Seasonal variation in mussel byssal thread mechanics. J. Exp. Biol. 209, 1996–2003. https://doi.org/10.1242/jeb.02234

Moeser, G.M., Leba, H., Carrington, E., 2006. Seasonal influence of wave action on thread production in *Mytilus edulis*. J. Exp. Biol. 209, 881–890. https://doi.org/10.1242/jeb.02050

Moisez, E., Spilmont, N., Seuront, L., 2020. Microhabitats choice in intertidal gastropods is species-, temperature- and habitat-specific. J. Therm. Biol. 94, 102785. https://doi.org/10.1016/j.jtherbio.2020.102785

Moles, A., Hale, N., 2003. Use of physiological responses in *Mytilus trossulus* as integrative bioindicators of sewage pollution. Mar. Pollut. Bull. 46, 954–958. https://doi.org/10.1016/S0025-326X(03)00108-5

Monsinjon, J.R., McQuaid, C.D., Nicastro, K.R., Seuront, L., Oróstica, M.H., Zardi, G.I., 2021. Weather and topography regulate the benefit of a conditionally helpful parasite. Funct. Ecol. 35, 2691–2706. https://doi.org/10.1111/1365-2435.13939

Morse, D.E., Morse, A., Duncan, H., 1977. Algal tumors in the Caribeean sea-fan, *Gorgonia ventalina*, in: Taylor, D.L. (Ed.), Proceeding of Third International Coral Reef Symposium. Rosenstiel School of Marine and Atmospheric Science, Miami, Florida, pp. 623–629.

Morse, D.E., Morse, A., Duncan, H., Trench, R.K., 1981. Algal tumors in the Caribbean octocorallian, *Gorgonia ventalina*: II. Biochemical characterization of the algae, and first epidemiological observations. Bull. Mar. Sci. 31, 399–409.

Mouritsen, K.N., Poulin, R., 2002. Parasitism, community structure and biodiversity in intertidal ecosystems. Parasitology 124, 101–117. https://doi.org/10.1017/S0031182002001476

Munger, J.C., Holmes, J.C., 1988. Benefits of parasitic infection: a test using a ground squirrel – trypanosome system. Can. J. Zool. 66, 222–227. https://doi.org/10.1139/z88-032

Muñoz, J.L.P., Finke, G.R., Camus, P.A., Bozinovic, F., 2005. Thermoregulatory behavior, heat gain and thermal tolerance in the periwinkle *Echinolittorina peruviana* in central Chile. Comp. Biochem. Physiol. 142, 92–98. https://doi.org/10.1016/j.cbpa.2005.08.002

Musso, B., 1994. Internal bioerosion *in situ* living and dead corals on the Great Barrier Reef (PhD Thesis). James Cook University, Townsville.

Myers, N., Knoll, A.H., 2001. The biotic crisis and the future of evolution. Proc. Natl. Acad. Sci. 98, 5389–5392. https://doi.org/10.1073/pnas.091092498

Nagarajan, R., Goss–Custard, J.D., Lea, S.E.G., 2002. Oystercatchers use colour preference to achieve longer-term optimality. Proc. R. Soc. Lond. B Biol. Sci. 269, 523–528. https://doi.org/10.1098/rspb.2001.1908

Nagelkerken, I., Connell, S.D., 2022. Ocean acidification drives global reshuffling of ecological communities. Glob. Change Biol. 28, 7038–7048. https://doi.org/10.1111/gcb.16410

Nagendra, H., 2002. Opposite trends in response for the Shannon and Simpson indices of landscape diversity. Appl. Geogr. 22, 175–186. https://doi.org/10.1016/S0143-6228(02)00002-4

Naiman, R.J., Johnston, C.A., Kelley, J.C., 1988. Alteration of North American streams by beaver. BioScience 38, 753–762. https://doi.org/10.2307/1310784

Nash, M.C., Opdyke, B.N., Troitzsch, U., Russell, B.D., Adey, W.H., Kato, A., Diaz-Pulido, G., Brent, C., Gardner, M., Prichard, J., Kline, D.I., 2013. Dolomite-rich coralline algae in reefs resist dissolution in acidified conditions. Nat. Clim. Change 3, 268–272. https://doi.org/10.1038/nclimate1760

Ndhlovu, A., McQuaid, C.D., Monaco, C.J., 2021a. Ectoparasites reduce scope for growth in a rocky-shore mussel (*Perna perna*) by raising maintenance costs. Sci. Total Environ. 753, 142020. https://doi.org/10.1016/j.scitotenv.2020.142020

Ndhlovu, A., McQuaid, C.D., Nicastro, K., Marquet, N., Gektidis, M., Monaco, C.J., Zardi, G., 2019. Biogeographical patterns of endolithic infestation in an invasive and an indigenous intertidal marine ecosystem engineer. Diversity 11, 75. https://doi.org/10.3390/d11050075

Ndhlovu, A., McQuaid, C.D., Nicastro, K.R., Zardi, G.I., 2022. Parasitism by endolithic cyanobacteria reduces reproductive output and attachment strength of intertidal ecosystem engineers. Mar. Biol. 169, 37. https://doi.org/10.1007/s00227-022-04023-0

Ndhlovu, A., McQuaid, C.D., Nicastro, K.R., Zardi, G.I., 2021b. Community succession in phototrophic shell-degrading endoliths attacking intertidal mussels. J. Molluscan Stud. 87, eyaa036. https://doi.org/10.1093/mollus/eyaa036

Nicastro, K.R., McQuaid, C.D., Dievart, A., Zardi, G.I., 2020. Intraspecific diversity in an ecological engineer functionally trumps interspecific diversity in shaping community structure. Sci. Total Environ. 743, 140723.
https://doi.org/10.1016/j.scitotenv.2020.140723

Nicastro, K.R., McQuaid, C.D., Zardi, G.I., 2019. Between a rock and a hard place: combined effect of trampling and phototrophic shell-degrading endoliths in marine intertidal mussels. Mar. Biodivers. 49, 1581–1586.
https://doi.org/10.1007/s12526-018-0924-3

Nicastro, K.R., Seuront, L., McQuaid, C.D., Zardi, G.I., 2022. Symbiont-induced intraspecific phenotypic variation enhances plastic trapping and ingestion in biogenic habitats. Sci. Total Environ. 826, 153922.
https://doi.org/10.1016/j.scitotenv.2022.153922

Nicastro, K. R., Zardi, G.I., McQuaid, C.D., 2010. Differential reproductive investment, attachment strength and mortality of invasive and indigenous mussels across heterogeneous environments. Biol. Invasions 12, 2165–2177.
https://doi.org/10.1007/s10530-009-9619-9

Nicastro, K.R., Zardi, G.I., McQuaid, C.D., Pearson, G.A., Serrão, E.A., 2012. Love thy neighbour: Group properties of gaping behaviour in mussel aggregations. PLoS ONE 7, e47382. https://doi.org/10.1371/journal.pone.0047382

Nicastro, Katy R., Zardi, G.I., McQuaid, C.D., Stephens, L., Radloff, S., Blatch, G.L., 2010. The role of gaping behaviour in habitat partitioning between coexisting intertidal mussels. BMC Ecol. 10, 17. https://doi.org/10.1186/1472-6785-10-17

Nicholson, G.M., Clements, K.D., 2020. Resolving resource partitioning in parrotfishes (Scarini) using microhistology of feeding substrata. Coral Reefs 39, 1313–1327. https://doi.org/10.1007/s00338-020-01964-0

Nolan, C.P., 1991. Size, shape and shell morphology in the Antarctic limpet *Nacella concinna* at Signy Island, South Orkney Islands. J. Molluscan Stud. 57, 225–238. https://doi.org/10.1093/mollus/57.2.225

Nothdurft, L.D., Webb, G.E., 2009. Earliest diagenesis in scleractinian coral skeletons: implications for palaeoclimate-sensitive geochemical archives. Facies 55, 161–201. https://doi.org/10.1007/s10347-008-0167-z

O'Connor, N.E., Crowe, T.P., 2007. Do mussel patches provide a refuge for algae from grazing gastropods? J. Molluscan Stud. 74, 75–78.
https://doi.org/10.1093/mollus/eym046

O'Donnell, M.J., George, M.N., Carrington, E., 2013. Mussel byssus attachment weakened by ocean acidification. Nat. Clim. Change 3, 587–590. https://doi.org/10.1038/nclimate1846

Odum, H.T., Odum, E.P., 1955. Trophic structure and productivity of a windward coral reef community on Eniwetok atoll. Ecol. Monogr. 25, 291–320. https://doi.org/10.2307/1943285

Oliver, E.C.J., Benthuysen, J.A., Darmaraki, S., Donat, M.G., Hobday, A.J., Holbrook, N.J., Schlegel, R.W., Gupta, A.S., 2021. Marine heatwaves. Annu. Rev. Mar. Sci. 13, 313–342. https://doi.org/10.1146/annurev-marine-032720-095144

Oliver, E.C.J., Burrows, M.T., Donat, M.G., Gupta, A.S., Alexander, L.V., Perkins-Kirkpatrick, S.E., Benthuysen, J.A., Hobday, A.J., Holbrook, N.J., Moore, P.J., Thomsen, M.S., Wernberg, T., Smale, D.A., 2019. Projected marine heatwaves in the 21st century and the potential for ecological impact. Front. Mar. Sci. 6, 734. https://doi.org/10.3389/fmars.2019.00734

Oliver, E.C.J., Donat, M.G., Burrows, M.T., Moore, P.J., Smale, D.A., Alexander, L.V., Benthuysen, J.A., Feng, M., Gupta, A.S., Hobday, A.J., Holbrook, N.J., Perkins-Kirkpatrick, S.E., Scannell, H.A., Straub, S.C., Wernberg, T., 2018. Longer and more frequent marine heatwaves over the past century. Nat. Commun. 9, 1324. https://doi.org/10.1038/s41467-018-03732-9

Oróstica, M.H., Wyness, A.J., Monsinjon, J.R., Nicastro, K.R., Zardi, G.I., Barker, C., McQuaid, C.D., 2022. Effects of habitat quality on abundance, size and growth of mussel recruits. Hydrobiologia 849, 4341–4356. https://doi.org/10.1007/s10750-022-04994-7

Osman, R.W., 1977. The establishment and development of a marine epifaunal community. Ecol. Monogr. 47, 37–63. https://doi.org/10.2307/1942223

Owen, G., Williams, A., 1969. The caecum of articulate Brachiopoda. Proc. R. Soc. Lond. B Biol. Sci. 172, 187–201. https://doi.org/10.1098/rspb.1969.0019

Paine, R.T., 1974. Intertidal community structure: Experimental studies on the relationship between a dominant competitor and its principal predator. Oecologia 15, 93–120. https://doi.org/10.1007/BF00345739

Paine, R.T., 1966. Food web complexity and species diversity. Am. Nat. 100, 65–75. https://doi.org/10.1086/282400

Paine, R.T., Levin, S.A., 1981. Intertidal landscapes: Disturbance and the dynamics of pattern. Ecol. Monogr. 51, 145–178. https://doi.org/10.2307/2937261

Palomo, M., People, J., Chapman, M., Underwood, A., 2007. Separating the effects of physical and biological aspects of mussel beds on their associated assemblages. Mar. Ecol. Prog. Ser. 344, 131–142. https://doi.org/10.3354/meps07002

Pantazidou, A., Louvrou, I., Economou-Amilli, A., 2006. Euendolithic shell-boring cyanobacteria and chlorophytes from the saline lagoon Ahivadolimni on Milos Island, Greece. Eur. J. Phycol. 41, 189–200. https://doi.org/10.1080/09670260600649420

Pari, N., Peyrot-Clausade, M., Hutchings, P.A., 2002. Bioerosion of experimental substrates on high islands and atoll lagoons (French Polynesia) during 5 years of exposure. J. Exp. Mar. Biol. Ecol. 276, 109–127. https://doi.org/10.1016/S0022-0981(02)00243-5

Pari, N., Peyrot-Clausade, M., Le Campion-Alsumard, T., Hutchings, P., Chazottes, V., Golubic, S., Le Campion, J., Fontaine, M., 1998. Bioerosion of experimental substrates on high islands and on atoll lagoons (French Polynesia) after two years of exposure. Mar. Ecol. Prog. Ser. 166, 119–130. https://doi.org/10.3354/meps166119

Parke, M.W., Moore, H.B., 1935. The biology of *Balanus balanoides*. II. Algal infection of the shell. J. Mar. Biol. Assoc. U. K. 20, 49–56. https://doi.org/10.1017/S002531540001002X

Parmesan, C., 2006. Ecological and evolutionary responses to recent climate change. Annu. Rev. Ecol. Evol. Syst. 37, 637–669. https://doi.org/10.1146/annurev.ecolsys.37.091305.110100

Parmesan, C., Yohe, G., 2003. A globally coherent fingerprint of climate change impacts across natural systems. Nature 421, 37–42. https://doi.org/10.1038/nature01286

Pascal, L., Grémare, A., Montaudouin, X., Deflandre, B., Romero-Ramirez, A., Maire, O., 2020. Parasitism in ecosystem engineer species: A key factor controlling marine ecosystem functioning. J. Anim. Ecol. 89, 2192–2205. https://doi.org/10.1111/1365-2656.13236

Pasella, M.M., Lee, M.-F.E., Marcelino, V.R., Willis, A., Verbruggen, H., 2022. Ten *Ostreobium* (Ulvophyceae) strains from Great Barrier Reef corals as a resource for algal endolith biology and genomics. Phycologia 61, 452–458. https://doi.org/10.1101/2021.08.16.453452

Peck, L.S., Clarke, A., Holmes, L.J., 1987. Size, shape and the distribution of organic matter in the recent Antarctic brachiopod *Liothyrella uva*. Lethaia 20, 33–40. https://doi.org/10.1111/j.1502-3931.1987.tb00757.x

Peebles, M.W., Lewis, R.D., 1988. Differential infestation of shallow-water benthic foraminifera by microboring organisms: Possible biases in preservation potential. PALAIOS 3, 345–351. https://doi.org/10.2307/3514663

Perkins, R.D., Halsey, S.D., 1971. Geologic significance of microboring fungi and algae in Carolina shelf sediments. J. Sediment. Res. 41, 843–853. https://doi.org/10.1306/74D72379-2B21-11D7-8648000102C1865D

Perry, C.T., 1998. Grain susceptibility to the effects of microboring: implications for the preservation of skeletal carbonates. Sedimentology 45, 39–51. https://doi.org/10.1046/j.1365-3091.1998.00134.x

Perry, C.T., Macdonald, I.A., 2002. Impacts of light penetration on the bathymetry of reef microboring communities: implications for the development of microendolithic trace assemblages. Palaeogeogr. Palaeoclimatol. Palaeoecol. 186, 101–113. https://doi.org/10.1016/S0031-0182(02)00446-7

Petes, L.E., Menge, B.A., Murphy, G.D., 2007. Environmental stress decreases survival, growth, and reproduction in New Zealand mussels. J. Exp. Mar. Biol. Ecol. 351, 83–91. https://doi.org/10.1016/j.jembe.2007.06.025

Petraitis, P.S., Latham, R.E., Niesenbaum, R.A., 1989. The maintenance of species diversity by disturbance. Q. Rev. Biol. 64, 393–418. https://doi.org/10.1086/416457

Piazza, B.P., Banks, P.D., La Peyre, M.K., 2005. The potential for created oyster shell reefs as a sustainable shoreline protection strategy in Louisiana. Restor. Ecol. 13, 499–506. https://doi.org/10.1111/j.1526-100X.2005.00062.x

Pielou, E.C., 1966. The measurement of diversity in different types of biological collections. J. Theor. Biol. 13, 131–144. https://doi.org/10.1016/0022-5193(66)90013-0

Pimm, S.L., 1998. Extinctions, in: Sutherland, W.J. (Ed.), Conservation Science and Action. Blackwell Science, Oxford ; Malden, MA, pp. 20–38.

Poulin, R., 1999. The functional importance of parasites in animal communities: many roles at many levels? Int. J. Parasitol. 29, 903–914. https://doi.org/10.1016/S0020-7519(99)00045-4

Poulin, R., Thomas, F., 1999. Phenotypic variability induced by parasites: Extent and evolutionary implications. Parasitol. Today 15, 28–32. https://doi.org/10.1016/S0169-4758(98)01357-X

Price, P.W., 1977. General concepts on the evolutionary biology of parasites. Evolution 31, 405–420. https://doi.org/10.2307/2407761

Prusina, I., Peharda, M., Ezgeta-Balic, D., Puljas, S., Glamuzina, B., Golubic, S., 2015. Life-history trait of the Mediterranean keystone species *Patella rustica*: growth and microbial bioerosion. Mediterr. Mar. Sci. 16, 393–401. https://doi.org/10.12681/mms.1121

R Core Team, 2022. R: A language and environment for statistical computing.

Rabosky, D.L., 2014. Automatic detection of key innovations, rate shifts, and diversity-dependence on phylogenetic trees. PLoS ONE 9, e89543. https://doi.org/10.1371/journal.pone.0089543

Radtke, G., Golubic, S., 2005. Microborings in mollusk shells, Bay of Safaga, Egypt: Morphometry and ichnology. Facies 51, 118–134.
https://doi.org/10.1007/s10347-005-0016-02

Raffaelli, D., Hawkins, S., 1996. Intertidal Ecology. Springer Netherlands, Dordrecht. https://doi.org/10.1007/978-94-009-1489-6

Raghukumar, C., Sharma, S., Lande, V., 1991. Distribution and biomass estimation of shell-boring algae in the intertidal at Goa, India. Phycologia 30, 303–309. https://doi.org/10.2216/i0031-8884-30-3-303.1

Raimondi, P.T., 1990. Patterns, mechanisms, consequences of variability in settlement and recruitment of an intertidal barnacle. Ecol. Monogr. 60, 283–309. https://doi.org/10.2307/1943059

Ralph, P.J., Larkum, A.W.D., Kühl, M., 2007. Photobiology of endolithic microorganisms in living coral skeletons: 1. Pigmentation, spectral reflectance and variable chlorophyll fluorescence analysis of endoliths in the massive corals *Cyphastrea serailia*, *Porites lutea* and *Goniastrea australensis*. Mar. Biol. 152, 395–404. https://doi.org/10.1007/s00227-007-0694-0

Ramírez-Reinat, E. L., Garcia-Pichel, F., 2012. Prevalence of Ca^{2+}-ATPase-mediated carbonate dissolution among cyanobacterial euendoliths. Appl. Environ. Microbiol. 78, 7–13. https://doi.org/10.1128/AEM.06633-11

Ramírez-Reinat, Edgardo L., Garcia-Pichel, F., 2012. Characterization of a marine cyanobacterium that bores into carbonates and the redescription of the genus *Mastigocoleus*. J. Phycol. 48, 740–749.
https://doi.org/10.1111/j.1529-8817.2012.01157.x

Raven, J.A., 2005. Ocean acidification due to increasing atmospheric carbon dioxide (Policy Document No. 12/05). The Royal Society, London.

Reaugh-Flower, K., Branch, G., Harris, J., McQuaid, C., Currie, B., Dye, A., Robertson, B., 2011. Scale-dependent patterns and processes of intertidal mussel recruitment around southern Africa. Mar. Ecol. Prog. Ser. 434, 101–119. https://doi.org/10.3354/meps09169

Reimer, O., Tedengren, M., 1997. Predator-induced changes in byssal attachment, aggregation and migration in the blue mussel, *Mytilus edulis*. Mar. Freshw. Behav. Physiol. 30, 251–266.
https://doi.org/10.1080/10236249709379029

Reinfelder, J.R., 2011. Carbon concentrating mechanisms in eukaryotic marine phytoplankton. Annu. Rev. Mar. Sci. 3, 291–315.
https://doi.org/10.1146/annurev-marine-120709-142720

Reusch, T.B.H., Ehlers, A., Hämmerli, A., Worm, B., 2005. Ecosystem recovery after climatic extremes enhanced by genotypic diversity. Proc. Natl. Acad. Sci. 102, 2826–2831. https://doi.org/10.1073/pnas.0500008102

Reyes-Nivia, C., Diaz-Pulido, G., Dove, S., 2014. Relative roles of endolithic algae and carbonate chemistry variability in the skeletal dissolution of crustose coralline algae. Biogeosciences Discuss. 11, 2993–3021. https://doi.org/10.5194/bgd-11-2993-2014

Reyes-Nivia, C., Diaz-Pulido, G., Kline, D., Guldberg, O.-H., Dove, S., 2013. Ocean acidification and warming scenarios increase microbioerosion of coral skeletons. Glob. Change Biol. 19, 1919–1929. https://doi.org/10.1111/gcb.12158

Reynolds, L.K., McGlathery, K.J., Waycott, M., 2012. Genetic diversity enhances restoration success by augmenting ecosystem services. PLoS ONE 7, e38397. https://doi.org/10.1371/journal.pone.0038397

Ricci, F., Fordyce, A., Leggat, W., Blackall, L.L., Ainsworth, T., Verbruggen, H., 2021. Multiple techniques point to oxygenic phototrophs dominating the *Isopora palifera* skeletal microbiome. Coral Reefs 40, 275–282. https://doi.org/10.1007/s00338-021-02068-z

Rice, M.M., Maher, R.L., Correa, A.M.S., Moeller, H.V., Lemoine, N.P., Shantz, A.A., Burkepile, D.E., Silbiger, N.J., 2020. Macroborer presence on corals increases with nutrient input and promotes parrotfish bioerosion. Coral Reefs 39, 409–418. https://doi.org/10.1007/s00338-020-01904-y

Richmond, M.D., Seed, R., 1991. A review of marine macrofouling communities with special reference to animal fouling. Biofouling 3, 151–168. https://doi.org/10.1080/08927019109378169

Roberts, E., Carrington, E., 2023. Byssal thread attachment and growth are not correlated across gradients of temperature and food availability for two congeneric mussel species. Mar. Ecol. Prog. Ser. 704, 35–54. https://doi.org/10.3354/meps14234

Roleda, M.Y., Dethleff, D., 2011. Storm-generated sediment deposition on rocky shores: Simulating burial effects on the physiology and morphology of *Saccharina latissima* sporophytes. Mar. Biol. Res. 7, 213–223. https://doi.org/10.1080/17451000.2010.497189

Rooney, W.S.J., Perkins, R.D., 1972. Distribution and geologic significance of microboring organisms within sediments of the Arlington Reef Complex, Australia. Geol. Soc. Am. Bull. 83, 1139–1150. https://doi.org/10.1130/0016-7606(1972)83[1139:DAGSOM]2.0.CO;2

Roulin, A., 2004. The evolution, maintenance and adaptive function of genetic colour polymorphism in birds. Biol. Rev. 79, 815–848. https://doi.org/10.1017/S1464793104006487

Roush, D., Giraldo-Silva, A., Garcia-Pichel, F., 2021. Cydrasil 3, a curated 16S rRNA gene reference package and web app for cyanobacterial phylogenetic placement. Sci. Data 8, 230. https://doi.org/10.1038/s41597-021-01015-5

Sabine, C.L., Feely, R.A., Gruber, N., Key, R.M., Lee, K., Bullister, J.L., Wanninkhof, R., Wong, C.S., Wallace, D.W.R., Tilbrook, B., Millero, F.J., Peng, T.-H., Kozyr, A., Ono, T., Rios, A.F., 2004. The oceanic sink for anthropogenic CO_2. Science 305, 367–371. https://doi.org/10.1126/science.1097403

Sánchez-Baracaldo, P., Bianchini, G., Wilson, J.D., Knoll, A.H., 2022. Cyanobacteria and biogeochemical cycles through Earth history. Trends Microbiol. 30, 143–157. https://doi.org/10.1016/j.tim.2021.05.008

Sanford, E., Sones, J.L., García-Reyes, M., Goddard, J.H.R., Largier, J.L., 2019. Widespread shifts in the coastal biota of northern California during the 2014–2016 marine heatwaves. Sci. Rep. 9, 4216. https://doi.org/10.1038/s41598-019-40784-3

Santelices, B., Martínez, E., 1988. Effects of filter-feeders and grazers on algal settlement and growth in mussel beds. J. Exp. Mar. Biol. Ecol. 118, 281–306. https://doi.org/10.1016/0022-0981(88)90079-2

Sauvage, T., Schmidt, W.E., Suda, S., Fredericq, S., 2016. A metabarcoding framework for facilitated survey of endolithic phototrophs with *tuf*A. BMC Ecol. 16, 8. https://doi.org/10.1186/s12898-016-0068-x

Scardino, A., de Nys, R., 2004. Fouling deterrence on the bivalve shell *Mytilus galloprovincialis* : A physical phenomenon? Biofouling 20, 249–257. https://doi.org/10.1080/08927010400016608

Scardino, A., De Nys, R., Ison, O., O'Connor, W., Steinberg, P., 2003. Microtopography and antifouling properties of the shell surface of the bivalve molluscs *Mytilus galloprovincialis* and *Pinctada imbricata*. Biofouling 19, 221–230. https://doi.org/10.1080/0892701021000057882

Scardino, A.J., Guenther, J., de Nys, R., 2008. Attachment point theory revisited: the fouling response to a microtextured matrix. Biofouling 24, 45–53. https://doi.org/10.1080/08927010701784391

Scardino, A.J., Harvey, E., De Nys, R., 2006. Testing attachment point theory: diatom attachment on microtextured polyimide biomimics. Biofouling 22, 55–60. https://doi.org/10.1080/08927010500506094

Scardino, A.J., Zhang, H., Cookson, D.J., Lamb, R.N., Nys, R. de, 2009. The role of nano-roughness in antifouling. Biofouling 25, 757–767. https://doi.org/10.1080/08927010903165936

Schilthuizen, M., 2013. Rapid, habitat-related evolution of land snail colour morphs on reclaimed land. Heredity 110, 247–252. https://doi.org/10.1038/hdy.2012.74

Schlegel, R.W., Oliver, E.C.J., Perkins-Kirkpatrick, S., Kruger, A., Smit, A.J., 2017. Predominant atmospheric and oceanic patterns during coastal marine heatwaves. Front. Mar. Sci. 4, 323. https://doi.org/10.3389/fmars.2017.00323

Schlichter, D., 1984. Cnidaria: Permability, epidermal transport and related phenomena, in: Bereiter-Hahn, J., Matoltsy, A.G., Richards, K.S. (Eds.), Biology of the Integument. Springer, Berlin, Heidelberg, pp. 79–95. https://doi.org/10.1007/978-3-642-51593-4

Schlichter, D., Kampmann, H., Conrady, S., 1997. Trophic potential and photoecology of endolithic algae living within coral skeletons. Mar. Ecol. 18, 299–317. https://doi.org/10.1111/j.1439-0485.1997.tb00444.x

Schlichter, D., Zscharnack, B., Krisch, H., 1995. Transfer of photoassimilates from endolithic algae to coral tissue. Naturwissenschaften 82, 561–564. https://doi.org/10.1007/BF01140246

Schmitt, R.J., Osenberg, C.W., Bercovitch, M.G., 1983. Mechanisms and consequences of shell fouling in the kelp snail, *Norrisia norrisi* (Sowerby) (Trochidae): Indirect effects of octopus drilling. J. Exp. Mar. Biol. Ecol. 69, 267–281. https://doi.org/10.1016/0022-0981(83)90074-6

Schneider, J., Le Campion-Alsumard, T., 1999. Construction and destruction of carbonates by marine and freshwater cyanobacteria. Eur. J. Phycol. 34, 417–426. https://doi.org/10.1080/09670269910001736472

Schneider, J., Torunski, H., 1983. Biokarst on limestone coasts, morphogenesis and sediment production. Mar. Ecol. 4, 45–63. https://doi.org/10.1111/j.1439-0485.1983.tb00287.x

Schönberg, C.H.L., Fang, J.K.H., Carreiro-Silva, M., Tribollet, A., Wisshak, M., 2017. Bioerosion: the other ocean acidification problem. ICES J. Mar. Sci. 74, 895–925. https://doi.org/10.1093/icesjms/fsw254

Schönberg, C.H.L., Wisshak, M., 2014. Marine bioerosion, in: Goffredo, S., Dubinsky, Z. (Eds.), The Mediterranean Sea. Springer Netherlands, Dordrecht, pp. 449–461. https://doi.org/10.1007/978-94-007-6704-1_26

Schroeder, J.H., 1972. Calcified filaments of an endolithic alga in Recent Bermuda reefs. Neues Jahrb. Geol. Palaontologie Monatshefte 1972, 16–33.

Schumacher, J.F., Aldred, N., Callow, M.E., Finlay, J.A., Callow, J.A., Clare, A.S., Brennan, A.B., 2007. Species-specific engineered antifouling topographies: correlations between the settlement of algal zoospores and barnacle cyprids. Biofouling 23, 307–317. https://doi.org/10.1080/08927010701393276

Schumann, E.H., 1987. The coastal ocean off the East coasts of South Africa. Trans. R. Soc. South Afr. 46, 215–229. https://doi.org/10.1080/00359198709520125

Scoffin, T.P., Alexandersson, E.T., Bowes, G.E., Clokie, J.J., Farrow, G.E., Milliman, J.D., 1980. Recent, temperate, sub-photic, carbonate sedimentation: Rockall Bank, Northeast Atlantic. J. Sediment. Petrol. 50, 331–356. https://doi.org/10.1306/212F7A04-2B24-11D7-8648000102C1865D

Seaborn, T., 2014. Limpets and their algal epibionts: Costs and benefits of *Acrosiphonia* spp and *Ulva lactuca* growth. J. Mar. Biol. 2014, 1–7. https://doi.org/10.1155/2014/891943

Seed, R., Suchanek, T.H., 1992. Population and community ecology of *Mytilus*, in: The Mussel *Mytilus*: Ecology, Physiology, Genetics and Culture. Elsevier, New York, pp. 87–169.

Seuront, L., Ng, T.P.T., Lathlean, J.A., 2018. A review of the thermal biology and ecology of molluscs, and of the use of infrared thermography in molluscan research. J. Molluscan Stud. 84, 203–232. https://doi.org/10.1093/mollus/eyy023

Shashar, N., Stambler, N., 1992. Endolithic algae within corals - life in an extreme environment. J. Exp. Mar. Biol. Ecol. 163, 277–286. https://doi.org/10.1016/0022-0981(92)90055-F

Shibata, K., Haxo, F.T., 1969. Light transmission and spectral distribution through epi- and endozoic algal layers in the brain coral, *Favia*. Biol. Bull. 136, 461–468. https://doi.org/10.2307/1539688

Shields, J.D., 1992. Parasites and symbionts of the crab *Portunus pelagicus* from Moreton Bay, Eastern Australia. J. Crustac. Biol. 12, 94–100. https://doi.org/10.2307/1548723

Siddik, A.A., Satheesh, S., 2021. Interactive effects of light and substrate colour on the recruitment of marine invertebrates on artificial materials. Community Ecol. 22, 69–78. https://doi.org/10.1007/s42974-020-00037-0

Silbiger, N., Guadayol, Ò., Thomas, F., Donahue, M., 2014. Reefs shift from net accretion to net erosion along a natural environmental gradient. Mar. Ecol. Prog. Ser. 515, 33–44. https://doi.org/10.3354/meps10999

Simpson, G.L., 2022. *gratia*: Graceful *ggplot*-based graphics and other functions for *GAM*s fitted using *mgcv*.

Singh, W., Hjorleifsson, E., Stefansson, G., 2011. Robustness of fish assemblages derived from three hierarchical agglomerative clustering algorithms performed on Icelandic groundfish survey data. ICES J. Mar. Sci. 68, 189–200. https://doi.org/10.1093/icesjms/fsq144

Sink, K., Holness, S., Harris, L., Majiedt, P., Atkinson, L., Robinson, T., Kirkman, S., Hutchings, L., Leslie, R., Lamberth, S., Kerwath, S., von der Heyden, S., Lombard, A.T., Attwood, C., Branch, G.M., Fairweather, T., Taljaard, S., Weerts, S., Cowley, P., Awad, A., Halpern, B.S., Grantham, H., Wold, T., 2012. Volume 4: Marine and coastal component (Technical Report), National Biodiversity Assessment 2011. South African National Biodiversity Institute, Pretoria, South Africa.

Smyth, D., Roberts, D., 2010. The European oyster (*Ostrea edulis*) and its epibiotic succession. Hydrobiologia 655, 25–36. https://doi.org/10.1007/s10750-010-0401-x

Somero, G.N., 2010. The physiology of climate change: how potentials for acclimatization and genetic adaptation will determine 'winners' and 'losers.' J. Exp. Biol. 213, 912–920. https://doi.org/10.1242/jeb.037473

Somero, G.N., 2002. Thermal physiology and vertical zonation of intertidal animals: Optima, limits, and costs of living. Integr. Comp. Biol. 42, 780–789. https://doi.org/10.1093/icb/42.4.780

Stal, L.J., Krumbein, W.E., 1987. Temporal separation of nitrogen fixation and photosynthesis in the filamentous, non-heterocystous cyanobacterium *Oscillatoria* sp. Arch. Microbiol. 149, 76–80. https://doi.org/10.1007/BF00423140

Steinberg, P., de Nys, R., Kjelleberg, S., 2001. Chemical mediation of surface colonization, in: McClinTOCk, J., Baker, B. (Eds.), Marine Chemical Ecology, Marine Science. CRC Press, pp. 355–387. https://doi.org/10.1201/9781420036602.ch10

Steneck, R.S., 1986. The Ecology of Coralline Algal Crusts: Convergent Patterns and Adaptative Strategies. Annu. Rev. Ecol. Syst. 17, 273–303.

Steneck, R.S., Hacker, S.D., Dethier, M.N., 1991. Mechanisms of competitive dominance between crustose coralline algae: An herbivore-mediated competitive reversal. Ecology 72, 938–950. https://doi.org/10.2307/1940595

Stephens, E.G., Bertness, M.D., 1991. Mussel facilitation of barnacle survival in a sheltered bay habitat. J. Exp. Mar. Biol. Ecol. 145, 33–48. https://doi.org/10.1016/0022-0981(91)90004-G

Stillman, J., Somero, G., 1996. Adaptation to temperature stress and aerial exposure in congeneric species of intertidal porcelain crabs (genus *Petrolisthes*): correlation of physiology, biochemistry and morphology with vertical distribution. J. Exp. Biol. 199, 1845–1855. https://doi.org/10.1242/jeb.199.8.1845

Stillman, J.H., 2002. Causes and consequences of thermal tolerance limits in rocky intertidal porcelain crabs, genus *Petrolisthes*. Integr. Comp. Biol. 42, 790–796. https://doi.org/10.1093/icb/42.4.790

Stobart, B., Mayfield, S., Mundy, C., Hobday, A.J., Hartog, J.R., 2016. Comparison of *in situ* and satellite sea surface-temperature data from South Australia and Tasmania: how reliable are satellite data as a proxy for coastal temperatures in temperate southern Australia? Mar. Freshw. Res. 67, 612–625. https://doi.org/10.1071/MF14340

Stolarski, J., 1996. *Gardineria* - a scleractinian living fossil. Acta Palaeontol. Pol. 41, 339–367.

Stumm, W., Morgan, J.J., 1996. Aquatic chemistry. Chemical equilibria and rates in natural waters, 3rd ed, Environmental Science and Technology. John Wiley & Sons, Inc, USA, Canada.

Suchanek, T.H., 1985. Mussels and their role in structuring rocky shore communities, in: Moore, P.G., Seed, R. (Eds.), The Ecology of Rocky Coasts. Hodder & Stoughton Press, London, Sydney, Auckland, Toronto, pp. 71–96.

Sures, B., Dezfuli, B.S., Krug, H.F., 2003. The intestinal parasite *Pomphorhynchus laevis* (Acanthocephala) interferes with the uptake and accumulation of lead (^{210}Pb) in its fish host chub (*Leuciscus cephalus*). Int. J. Parasitol. 33, 1617–1622. https://doi.org/10.1016/S0020-7519(03)00251-0

Sutton, M.D., 2008. Tomographic techniques for the study of exceptionally preserved fossils. Proc. R. Soc. B Biol. Sci. 275, 1587–1593. https://doi.org/10.1098/rspb.2008.0263

Svensson, J.R., Lindegarth, M., Pavia, H., 2009. Equal rates of disturbance cause different patterns of diversity. Ecology 90, 496–505. https://doi.org/10.1890/07-1628.1

Svensson, J.R., Lindegarth, M., Siccha, M., Lenz, M., Molis, M., Wahl, M., Pavia, H., 2007. Maximum species richness at intermediate frequencies of disturbance: Consistency among levels of productivity. Ecology 88, 830–838. https://doi.org/10.1890/06-0976

Swain, G., Herpe, S., Ralston, E., Tribou, M., 2006. Short-term testing of antifouling surfaces: the importance of colour. Biofouling 22, 425–429. https://doi.org/10.1080/08927010601037163

Swinchatt, J.P., 1969. Algal boring: A possible depth indicator in carbonate rocks and sediments. Geol. Soc. Am. Bull. 80, 1391–1396. https://doi.org/10.1130/0016-7606(1969)80[1391:ABAPDI]2.0.CO;2

Taberlet, P., Coissac, E., Pompanon, F., Brochmann, C., Willerslev, E., 2012. Towards next-generation biodiversity assessment using DNA metabarcoding. Mol. Ecol. 21, 2045–2050. https://doi.org/10.1111/j.1365-294X.2012.05470.x

Tagliarolo, M., Montalto, V., Sarà, G., Lathlean, J., McQuaid, C., 2016. Low temperature trumps high food availability to determine the distribution of intertidal mussels *Perna perna* in South Africa. Mar. Ecol. Prog. Ser. 558, 51–63. https://doi.org/10.3354/meps11876

Tandon, K., Pasella, M.M., Iha, C., Ricci, F., Hu, J., O'Kelly, C.J., Medina, M., Kühl, M., Verbruggen, H., 2023. Every refuge has its price: *Ostreobium* as a model for understanding how algae can live in rock and stay in business. Semin. Cell Dev. Biol. 134, 27–36. https://doi.org/10.1016/j.semcdb.2022.03.010

Thiel, M., Dernedde, T., 1994. Recruitment of shore crabs *Carcinus maenas* on tidal flats: mussel clumps as an important refuge for juveniles. Helgoländer Meeresunters. 48, 321–332. https://doi.org/10.1007/BF02367044

Thieltges, D.W., 2006. Effect of infection by the metacercarial trematode *Renicola roscovita* on growth in intertidal blue mussel *Mytilus edulis*. Mar. Ecol. Prog. Ser. 319, 129–134. https://doi.org/10.3354/meps319129

Thieltges, D.W., Buschbaum, C., 2007. Vicious circle in the intertidal: Facilitation between barnacle epibionts, a shell boring polychaete and trematode parasites in the periwinkle *Littorina littorea*. J. Exp. Mar. Biol. Ecol. 340, 90–95. https://doi.org/10.1016/j.jembe.2006.08.014

Thomas, C.D., Cameron, A., Green, R.E., Bakkenes, M., Beaumont, L.J., Collingham, Y.C., Erasmus, B.F.N., de Siqueira, M.F., Grainger, A., Hannah, L., Hughes, L., Huntley, B., van Jaarsveld, A.S., Midgley, G.F., Miles, L., Ortega-Huerta, M.A., Peterson, A.T., Phillips, O.L., Williams, S.E., 2004. Extinction risk from climate change. Nature 427, 145–148. https://doi.org/10.1038/nature02121

Thomas, F., Brodeur, J., Maure, F., Franceschi, N., Blanchet, S., Rigaud, T., 2011. Intraspecific variability in host manipulation by parasites. Infect. Genet. Evol. 11, 262–269. https://doi.org/10.1016/j.meegid.2010.12.013

Thomas, Frédéric, Guégan, J.-F., Michalakis, Y., Renaud, F., 2000. Parasites and host life-history traits: implications for community ecology and species co-existence. Int. J. Parasitol. 30, 669–674. https://doi.org/10.1016/S0020-7519(00)00040-0

Thomas, F., Poulin, R., Brodeur, J., 2010. Host manipulation by parasites: a multidimensional phenomenon. Oikos 119, 1217–1223. https://doi.org/10.1111/j.1600-0706.2009.18077.x

Thomas, F., Poulin, R., de Meeüs, T., Guégan, J.-F., Renaud, F., 1999. Parasites and ecosystem engineering: What roles could they play? Oikos 84, 167–171. https://doi.org/10.2307/3546879

Thomas, F, Poulin, R., Guégan, J.-F., Michalakis, Y., Renaud, F., 2000. Are there pros as well as cons to being parasitized? Parasitol. Today 16, 533–536. https://doi.org/10.1016/S0169-4758(00)01790-7

Thomas, F., Renaud, F., de Meeûs, T., Poulin, R., 1998. Manipulation of host behaviour by parasites: ecosystem engineering in the intertidal zone? Proc. R. Soc. Lond. B Biol. Sci. 265, 1091–1096. https://doi.org/10.1098/rspb.1998.0403

Thomason, J.C., Letissier, M.D.A., Thomason, P.O., Field, S.N., 2002. Optimising settlement tiles: The effects of surface texture and energy, orientation and deployment duration upon the fouling community. Biofouling 18, 293–304. https://doi.org/10.1080/0892701021000034409

Thorson, G., 1964. Light as an ecological factor in the dispersal and settlement of larvae of marine bottom invertebrates. Ophelia 1, 167–208. https://doi.org/10.1080/00785326.1964.10416277

Tilman, D., Fargione, J., Wolff, B., D'Antonio, C., Dobson, A., Howarth, R., Schindler, D., Schlesinger, W.H., Simberloff, D., Swackhamer, D., 2001. Forecasting agriculturally driven global environmental change. Science 292, 281–284. https://doi.org/10.1126/science.1057544

Tilman, D., Isbell, F., Cowles, J.M., 2014. Biodiversity and ecosystem functioning. Annu. Rev. Ecol. Evol. Syst. 45, 471–493. https://doi.org/10.1146/annurev-ecolsys-120213-091917

Tilman, D., Reich, P.B., Isbell, F., 2012. Biodiversity impacts ecosystem productivity as much as resources, disturbance, or herbivory. Proc. Natl. Acad. Sci. 109, 10394–10397. https://doi.org/10.1073/pnas.1208240109

Titlyanov, E.A., Kiyashko, S.I., Titlyanova, T.V., Kalita, T.L., Raven, J.A., 2008. $\delta^{13}C$ and $\delta^{15}N$ values in reef corals *Porites lutea* and *P. cylindrica* and in their epilithic and endolithic algae. Mar. Biol. 155, 353–361. https://doi.org/10.1007/s00227-008-1025-9

Tomimatsu, H., Nakano, K., Yamamoto, N., Suyama, Y., 2014. Effects of genotypic diversity of *Phragmites australis* on primary productivity and water quality in an experimental wetland. Oecologia 175, 163–172. https://doi.org/10.1007/s00442-014-2896-8

Tribollet, A., 2008a. The boring microflora in modern coral reef ecosystems: a review of its roles, in: Wisshak, M., Tapanila, L. (Eds.), Current Developments in Bioerosion. Springer Berlin Heidelberg, Berlin, Heidelberg, pp. 67–94. https://doi.org/10.1007/978-3-540-77598-0_4

Tribollet, A., 2008b. Dissolution of dead corals by euendolithic microorganisms across the northern Great Barrier Reef (Australia). Microb. Ecol. 55, 569–580. https://doi.org/10.1007/s00248-007-9302-6

Tribollet, A., Atkinson, M.J., Christopher, L., 2006. Effects of elevated pCO_2 on epilithic and endolithic metabolism of reef carbonates. Glob. Change Biol. 12, 2200–2208. https://doi.org/10.1111/j.1365-2486.2006.01249.x

Tribollet, A., Chauvin, A., Cuet, P., 2019. Carbonate dissolution by reef microbial borers: a biogeological process producing alkalinity under different pCO_2 conditions. Facies 65, 9. https://doi.org/10.1007/s10347-018-0548-x

Tribollet, A., Godinot, C., Atkinson, M., Langdon, C., 2009. Effects of elevated pCO_2 on dissolution of coral carbonates by microbial euendoliths. Glob. Biogeochem. Cycles 23, GB3008. https://doi.org/10.1029/2008GB003286

Tribollet, A., Golubic, S., 2011. Reef bioerosion: agents and processes, in: Dubinsky, Z., Stambler, N. (Eds.), Coral Reefs: An Ecosystem in Transition. Springer Netherlands, Dordrecht, pp. 435–450. https://doi.org/10.1007/978-94-007-0114-4

Tribollet, A., Golubic, S., 2005. Cross-shelf differences in the pattern and pace of bioerosion of experimental carbonate substrates exposed for 3 years on the northern Great Barrier Reef, Australia. Coral Reefs 24, 422–434.
https://doi.org/10.1007/s00338-005-0003-7

Tribollet, A., Golubic, S., Radtke, G., Reitner, J., 2011. On microbiocorrosion, in: Advances in Stromatolite Geobiology, Lecture Notes in Earth Sciences. Springer Berlin Heidelberg, Berlin, Heidelberg, pp. 265–276.
https://doi.org/10.1007/978-3-642-10415-2_17

Tribollet, A., Payri, C., 2001. Bioerosion of the coralline alga *Hydrolithon onkodes* by microborers in the coral reefs of Moorea, French Polynesia. Oceanol. Acta 24, 329–342. https://doi.org/10.1016/S0399-1784(01)01150-1

Tribollet, A., Pica, D., Puce, S., Radtke, G., Campbell, S.E., Golubic, S., 2018. Euendolithic *Conchocelis* stage (Bangiales, Rhodophyta) in the skeletons of live stylasterid reef corals. Mar. Biodivers. 48, 1855–1862. https://doi.org/10.1007/s12526-017-0684-5

Tribollet, A., Veinott, G., Golubic, S., Dart, R., 2008. Infestation of the North American freshwater mussel *Elliptio complanata* (Head Lake, Canada) by the euendolithic cyanobacterium *Plectonema terebrans* Bornet et Flahault. Algol. Stud. 128, 65–77. https://doi.org/10.1127/1864-1318/2008/0128-0065

Tsuchiya, M., Nishihira, M., 1986. Islands of *Mytilus edulis* as a habitat for small intertidal animals: effect of *Mytilus* age structure on the species composition of the associated fauna and community organization. Mar. Ecol. Prog. Ser. 31, 171–178. https://doi.org/10.3354/meps031171

Tsuchiya, M., Nishihira, M., 1985. Islands of *Mytilus* as a habitat for small intertidal animals: effect of island size on community structure. Mar. Ecol. Prog. Ser. 25, 71–81.

Tummon Flynn, P., McCarvill, K., Lynn, K.D., Quijón, P.A., 2020. The positive effect of coexisting ecosystem engineers: a unique seaweed-mussel association provides refuge for native mud crabs against a non-indigenous predator. PeerJ 8, e10540. https://doi.org/10.7717/peerj.10540

UNCED, 1993. Agenda 21: Program of Action for Sustainable Development; Rio Declaration on Environment and Development; Statement of Forest Principles: The Final Text of Agreements Negotiated by Governments at the United Nations Conference on Environment and Development (UNCED), 3-14 June 1992. Rio De Janeiro, Brazil. United Nations Dept. of Public Information, New York, NY.

Underwood, A.J., 2006. Why overgrowth of intertidal encrusting algae does not always cause competitive exclusion. J. Exp. Mar. Biol. Ecol. 330, 448–454. https://doi.org/10.1016/j.jembe.2005.09.005

Urban, M.C., 2015. Accelerating extinction risk from climate change. Science 348, 571–573. https://doi.org/10.1126/science.aaa4984

van Erkom Schurink, C., Griffiths, C., 1991. A comparison of reproductive cycles and reproductive output in four southern African mussel species. Mar. Ecol. Prog. Ser. 76, 123–134. https://doi.org/10.3354/meps076123

Van Rensburg, C., Robbins, A., Griffiths, C.L., 2021. Temperature cycles beneath, and adjacent to, intertidal boulders and associated differences in biotic composition. Afr. J. Mar. Sci. 43, 435–441. https://doi.org/10.2989/1814232X.2021.1979096

Vance, R., 1988. Ecological succession and the climax community on a marine subtidal rock wall. Mar. Ecol. Prog. Ser. 48, 125–136. https://doi.org/10.3354/meps048125

Verbruggen, H., 2014. Morphological complexity, plasticity, and species diagnosability in the application of old species names in DNA-based taxonomies. J. Phycol. 50, 26–31. https://doi.org/10.1111/jpy.12155

Verbruggen, H., Ashworth, M., LoDuca, S.T., Vlaeminck, C., Cocquyt, E., Sauvage, T., Zechman, F.W., Littler, D.S., Littler, M.M., Leliaert, F., 2009. A multi-locus time-calibrated phylogeny of the siphonous green algae. Mol. Phylogenet. Evol. 50, 642–653. https://doi.org/10.1016/j.ympev.2008.12.018

Vermeij, G.J., 1973. Morphological patterns in high-intertidal gastropods: Adaptive strategies and their limitations. Mar. Biol. 20, 319–346. https://doi.org/10.1007/BF00354275

Vogel, K., Gektidis, M., Golubic, S., Kiene, W.E., Radtke, G., 2000. Experimental studies on microbial bioerosion at Lee Stocking Island, Bahamas and One Tree Island, Great Barrier Reef, Australia: implications for paleoecological reconstructions. Lethaia 33, 190–204. https://doi.org/10.1080/00241160025100053

Wahl, M., 2009. Epibiosis, in: Wahl, M. (Ed.), Marine Hard Bottom Communities, Ecological Studies. Springer Berlin Heidelberg, Berlin, Heidelberg, pp. 61–72. https://doi.org/10.1007/b76710_4

Wahl, M., 2008. Ecological lever and interface ecology: epibiosis modulates the interactions between host and environment. Biofouling 24, 427–438. https://doi.org/10.1080/08927010802339772

Wahl, M., 1989. Marine epibiosis. I. Fouling and antifouling: some basic aspects. Mar. Ecol. Prog. Ser. 58, 175–189. https://doi.org/10.3354/meps058175

Wahl, M., Hay, M.E., 1995. Associational resistance and shared doom: effects of epibiosis on herbivory. Oecologia 102, 329–340. https://doi.org/10.1007/BF00329800

Wahl, M., Kröger, K., Lenz, M., 1998. Non-toxic protection against epibiosis. Biofouling 12, 205–226. https://doi.org/10.1080/08927019809378355

Wahl, M., Mark, O., 1999. The predominantly facultative nature of epibiosis: experimental and observational evidence. Mar. Ecol. Prog. Ser. 187, 59–66. https://doi.org/10.3354/meps187059

Walker, S.E., 1998. Endobionts on modern and fossil *Turritella* from the northern Gulf of California region. Ichnos 6, 99–115. https://doi.org/10.1080/10420949809386441

Walters, L., Wethey, D., 1996. Settlement and early post-settlement survival of sessile marine invertebrates on topographically complex surfaces: the importance of refuge dimensions and adult morphology. Mar. Ecol. Prog. Ser. 137, 161–171. https://doi.org/10.3354/meps137161

Wang, Y., Naumann, U., Wright, S.T., Warton, D.I., 2012. *mvabund* - an R package for model-based analysis of multivariate abundance data. Methods Ecol. Evol. 3, 471–474. https://doi.org/10.1111/j.2041-210X.2012.00190.x

Ward, M.A., Thorpe, J.P., 1991. Distribution of encrusting bryozoans and other epifauna on the subtidal bivalve *Chlamys opercularis*. Mar. Biol. 110, 253–259. https://doi.org/10.1007/BF01313711

Warner, G.F., 1997. Occurrence of epifauna on the periwinkle, *Littorina littorea* (L.), and interactions with the polychaete *Polydora ciliata* (Johnston), in: Naumov, A.D., Hummel, H., Sukhotin, A.A., Ryland, J.S. (Eds.), Interactions and Adaptation Strategies of Marine Organisms. Springer Netherlands, Dordrecht, pp. 41–47. https://doi.org/10.1007/978-94-017-1907-0_5

Warton, D.I., 2008. Penalized normal likelihood and ridge regularization of correlation and covariance matrices. J. Am. Stat. Assoc. 103, 340–349. https://doi.org/10.1198/016214508000000021

Warton, D.I., Thibaut, L., Wang, Y.A., 2017. The PIT-trap — A "model-free" bootstrap procedure for inference about regression models with discrete, multivariate responses. PLOS ONE 12, e0181790. https://doi.org/10.1371/journal.pone.0181790

Webb, S.C., 1999. Aspects of stress with particular reference to Mytilid mussels and their parasites. (Doctor of Philosophy). University of Cape Town, Cape Town.

Wedl, C., 1859. On the significance of the canals found in many mollusc and gastropod shells. Sitzungsberichte Kais. Akad. Wiss. 33, 451–472.

Weinersmith, K.L., Earley, R.L., 2016. Better with your parasites? Lessons for behavioural ecology from evolved dependence and conditionally helpful parasites. Anim. Behav. 118, 123–133. https://doi.org/10.1016/j.anbehav.2016.06.004

Wernberg, T., Arenas, F., Olabarria, C., Thomsen, M., Mohring, M., 2016. Threats to ecosystem engineering macrophytes: Climate change, in: Ólafsson, E. (Ed.), Marine Macrophytes as Foundation Species. CRC Press, Taylor & Francis Group, Boca Raton, USA, pp. 201–218. https://doi.org/10.4324/9781315370781-10

Wethey, D.S., 2002. Biogeography, competition, and microclimate: The barnacle *Chthamalus fragilis* in New England. Integr. Comp. Biol. 42, 872–880. https://doi.org/10.1093/icb/42.4.872

White, R., Anderson, S., Booth, J., Braich, G., Draeger, C., Fei, C., Harley, C., Henderson, S., Jakob, M., Lau, C.-A., Admasu, L.M., Narinesingh, V., Rodell, C., Roocroft, E., Weinberger, K., West, G., 2023. The unprecedented Pacific northwest heatwave of June 2021. Nat. Commun., Faculty Research and Publications 14, 727. https://doi.org/10.1038/s41467-023-36289-3

Whitham, T.G., Young, W.P., Martinsen, G.D., Gehring, C.A., Schweitzer, J.A., Shuster, S.M., Wimp, G.M., Fischer, D.G., Bailey, J.K., Lindroth, R.L., Woolbright, S., Kuske, C.R., 2003. Community and ecosystem genetics: A consequences of the extended phenotype. Ecology 84, 559–573.
https://doi.org/10.1890/0012-9658(2003)084[0559:CAEGAC]2.0.CO;2

Whitlock, R., Grime, J.P., Booth, R., Burke, T., 2007. The role of genotypic diversity in determining grassland community structure under constant environmental conditions. J. Ecol. 95, 895–907. https://doi.org/10.1111/j.1365-2745.2007.01275.x

Widdows, J., Lucas, J.S., Brinsley, M.D., Salkeld, P.N., Staff, F.J., 2002. Investigation of the effects of current velocity on mussel feeding and mussel bed stability using an annular flume. Helgol. Mar. Res. 56, 3–12. https://doi.org/10.1007/s10152-001-0100-0

Wieters, E., 2005. Upwelling control of positive interactions over mesoscales: A new link between bottom-up and top-down processes on rocky shores. Mar. Ecol. Prog. Ser. 301, 43–54. https://doi.org/10.3354/meps301043

Wild, C., Hoegh-Guldberg, O., Naumann, M.S., Colombo-Pallotta, M.F., Ateweberhan, M., Fitt, W.K., Iglesias-Prieto, R., Palmer, C., Bythell, J.C., Ortiz, J.-C., Loya, Y., van Woesik, R., 2011. Climate change impedes scleractinian corals as primary reef ecosystem engineers. Mar. Freshw. Res. 62, 205–215.
https://doi.org/10.1071/MF10254

Wilkinson, M., Burrows, E.M., 1972. The distribution of marine shell-boring green algae. J. Mar. Biol. Assoc. U. K. 52, 59–65.
https://doi.org/10.1017/S0025315400018579

Williams, G., De Pirro, M., Leung, K., Morritt, D., 2005. Physiological responses to heat stress on a tropical shore: the benefits of mushrooming behaviour in the limpet *Cellana grata*. Mar. Ecol. Prog. Ser. 292, 213–224. https://doi.org/10.3354/meps292213

Williams, S.T., 2017. Molluscan shell colour. Biol. Rev. 92, 1039–1058. https://doi.org/10.1111/brv.12268

Wilson, R.J., de Siqueira, A.F., Brooks, S.J., Price, B.W., Simon, L.M., van der Walt, S.J., Fenberg, P.B., 2022. Applying computer vision to digitised natural history collections for climate change research: Temperature-size responses in British butterflies. Methods Ecol. Evol. 14, 372–384. https://doi.org/10.1111/2041-210X.13844

Wisshak, M., 2012. Microbioerosion, in: Developments in Sedimentology. Elsevier, pp. 213–243. https://doi.org/10.1016/B978-0-444-53813-0.00008-3

Wisshak, M., Gektidis, M., Freiwald, A., Lundälv, T., 2005. Bioerosion along a bathymetric gradient in a cold-temperate setting (Kosterfjord, SW Sweden): an experimental study. Facies 51, 93–117. https://doi.org/10.1007/s10347-005-0009-1

Wisshak, M., Titschack, J., Kahl, W.-A., Girod, P., 2017. Classical and new bioerosion trace fossils in Cretaceous belemnite guards characterised via micro-CT. Foss. Rec. 20, 173–199. https://doi.org/10.5194/fr-20-173-2017

Wisshak, M., Tribollet, A., Golubic, S., Jakobsen, J., Freiwald, A., 2011. Temperate bioerosion: ichnodiversity and biodiversity from intertidal to bathyal depths (Azores). Geobiology 9, 492–520. https://doi.org/10.1111/j.1472-4669.2011.00299.x

Wisz, M.S., Pottier, J., Kissling, W.D., Pellissier, L., Lenoir, J., Damgaard, C.F., Dormann, C.F., Forchhammer, M.C., Grytnes, J., Guisan, A., Heikkinen, R.K., Høye, T.T., Kühn, I., Luoto, M., Maiorano, L., Nilsson, M., Normand, S., Öckinger, E., Schmidt, N.M., Termansen, M., Timmermann, A., Wardle, D.A., Aastrup, P., Svenning, J., 2013. The role of biotic interactions in shaping distributions and realised assemblages of species: implications for species distribution modelling. Biol. Rev. 88, 15–30. https://doi.org/10.1111/j.1469-185X.2012.00235.x

Witman, J., Suchanek, T., 1984. Mussels in flow: drag and dislodgement by epizoans. Mar. Ecol. Prog. Ser. 16, 259–268. https://doi.org/10.3354/meps016259

Witman, J.D., 1985. Refuges, biological disturbance, and rocky subtidal community structure in New England. Ecol. Monogr. 55, 421–445. https://doi.org/10.2307/2937130

Wood, C.L., Johnson, P.T., 2015. A world without parasites: exploring the hidden ecology of infection. Front. Ecol. Environ. 13, 425–434. https://doi.org/10.1890/140368

Wood, S.N., 2017. Generalized Additive Models: An introduction with R, 2nd ed. Chapman and Hall/CRC, New York. https://doi.org/10.1201/9781315370279

Wood, S.N., 2013. On *p*-values for smooth components of an extended generalized additive model. Biometrika 100, 221–228. https://doi.org/10.1093/biomet/ass048

Wright, J.P., Jones, C.G., Boeken, B., Shachak, M., 2006. Predictability of ecosystem engineering effects on species richness across environmental variability and spatial scales. J. Ecol. 94, 815–824. https://doi.org/10.1111/j.1365-2745.2006.01132.x

Wright, J.P., Jones, C.G., Flecker, A.S., 2002. An ecosystem engineer, the beaver, increases species richness at the landscape scale. Oecologia 132, 96–101. https://doi.org/10.1007/s00442-002-0929-1

Wright, J.T., Gribben, P.E., 2017. Disturbance-mediated facilitation by an intertidal ecosystem engineer. Ecology 98, 2425–2436. https://doi.org/10.1002/ecy.1932

Yáñez, B., Carballo, J.L., Olabarria, C., Barrón, J.J., 2008. Recovery of macrobenthic assemblages following experimental sand burial. Oceanologia 50, 391–420.

Yang, S.-H., Tandon, K., Lu, C.-Y., Wada, N., Shih, C.-J., Hsiao, S.S.-Y., Jane, W.-N., Lee, T.-C., Yang, C.-M., Liu, C.-T., Denis, V., Wu, Y.-T., Wang, L.-T., Huang, L., Lee, D.-C., Wu, Y.-W., Yamashiro, H., Tang, S.-L., 2019. Metagenomic, phylogenetic, and functional characterization of predominant endolithic green sulfur bacteria in the coral *Isopora palifera*. Microbiome 7, 3. https://doi.org/10.1186/s40168-018-0616-z

Yeakel, J.D., Pires, M.M., de Aguiar, M.A.M., O'Donnell, J.L., Guimarães, P.R., Gravel, D., Gross, T., 2020. Diverse interactions and ecosystem engineering can stabilize community assembly. Nat. Commun. 11, 3307. https://doi.org/10.1038/s41467-020-17164-x

Yorke, A., Metaxas, A., 2012. Relative importance of kelps and fucoids as substrata of the invasive epiphytic bryozoan Membranipora membranacea in Nova Scotia, Canada. Aquat. Biol. 16, 17–30. https://doi.org/10.3354/ab00419

Young, G.A., 1985. Byssus-thread formation by the mussel *Mytilus edulis*: effects of environmental factors. Mar. Ecol. Prog. Ser. 24, 261–271. https://doi.org/10.3354/meps024261

Yule, A.B., Walker, G., 1984. The temporary adhesion of barnacle cyprids: effects of some differing surface characteristics. J. Mar. Biol. Assoc. U. K. 64, 429–439. https://doi.org/10.1017/S0025315400030101

Zardi, G., McQuaid, C., Nicastro, K., 2007a. Balancing survival and reproduction: seasonality of wave action, attachment strength and reproductive output in indigenous *Perna perna* and invasive *Mytilus galloprovincialis* mussels. Mar. Ecol. Prog. Ser. 334, 155–163. https://doi.org/10.3354/meps334155

Zardi, G., McQuaid, C., Teske, P., Barker, N., 2007b. Unexpected genetic structure of mussel populations in South Africa: indigenous *Perna perna* and invasive *Mytilus galloprovincialis*. Mar. Ecol. Prog. Ser. 337, 135–144. https://doi.org/10.3354/meps337135

Zardi, G.I., Monsinjon, J.R., McQuaid, C.D., Seuront, L., Orostica, M., Want, A., Firth, L.B., Nicastro, K.R., 2021. Foul-weather friends: Modelling thermal stress mitigation by symbiotic endolithic microbes in a changing environment. Glob. Change Biol. 27, 2549–2560. https://doi.org/10.1111/gcb.15616

Zardi, G.I., Nicastro, K.R., McQuaid, C.D., Castilho, R., Costa, J., Serrão, E.A., Pearson, G.A., 2015. Intraspecific genetic lineages of a marine mussel show behavioural divergence and spatial segregation over a tropical/subtropical biogeographic transition. BMC Evol. Biol. 15. https://doi.org/10.1186/s12862-015-0366-5

Zardi, G.I., Nicastro, K.R., McQuaid, C.D., Erlandsson, J., 2008. Sand and wave induced mortality in invasive (*Mytilus galloprovincialis*) and indigenous (*Perna perna*) mussels. Mar. Biol. 153, 853–858. https://doi.org/10.1007/s00227-007-0857-z

Zardi, G.I., Nicastro, K.R., McQuaid, C.D., Gektidis, M., 2009. Effects of endolithic parasitism on invasive and indigenous mussels in a variable physical environment. PLoS ONE 4, e6560. https://doi.org/10.1371/journal.pone.0006560

Zardi, G.I., Nicastro, K.R., McQuaid, C.D., Hancke, L., Helmuth, B., 2011. The combination of selection and dispersal helps explain genetic structure in intertidal mussels. Oecologia 165, 947–958. https://doi.org/10.1007/s00442-010-1788-9

Zardi, G.I., Nicastro, K.R., McQuaid, C.D., Ng, T.P.T., Lathlean, J., Seuront, L., 2016. Enemies with benefits: parasitic endoliths protect mussels against heat stress. Sci. Rep. 6, 31413. https://doi.org/10.1038/srep31413

Zardi, G.I., Nicastro, K.R., McQuaid, C.D., Rius, M., Porri, F., 2006. Hydrodynamic stress and habitat partitioning between indigenous (*Perna perna*) and invasive (*Mytilus galloprovincialis*) mussels: constraints of an evolutionary strategy. Mar. Biol. 150, 79–88. https://doi.org/10.1007/s00227-006-0328-y

Zardi, G.I., Seuront, L., McQuaid, C.D., Froneman, W., Nicastro, K.R., 2023. Symbiont-induced phenotypic variation in an ecosystem engineer mediates thermal stress for the associated community. J. Therm. Biol. 112, 103428. https://doi.org/10.1016/j.jtherbio.2022.103428

Zeeman, Z., Branch, G.M., Farrell, D., Maneveldt, G.W., Robertson-Andersson, D., Pillay, D., 2013. Comparing community structure on shells of the abalone *Haliotis midae* and adjacent rock: implications for biodiversity. Mar. Biol. 160, 107–117. https://doi.org/10.1007/s00227-012-2067-6

Zhang, Y., Golubic, S., 1987. Endolithic microfossils (cyanophyta) from early Proterozoic stromatolites, Hebei, China. Acta Micropalaeontologica Sin. 4, 1–3.

Zubia, M., Peyrot-Clausade, M., 2001. Internal bioerosion of *Acropora formosa* in Réunion (Indian Ocean): microborer and macroborer activities. Oceanol. Acta 24, 251–262. https://doi.org/10.1016/S0399-1784(01)01144-6